



University
of Glasgow

Brown, Alison Margaret (2023) *Greenhouse gases from human-impacted rivers and estuaries - identifying 'hotspots' and their drivers: a source-to-sea study of the Clyde river and estuary*. PhD thesis.

<https://theses.gla.ac.uk/83915/>

Copyright and moral rights for this work are retained by the author

A copy can be downloaded for personal non-commercial research or study, without prior permission or charge

This work cannot be reproduced or quoted extensively from without first obtaining permission from the author

The content must not be changed in any way or sold commercially in any format or medium without the formal permission of the author

When referring to this work, full bibliographic details including the author, title, awarding institution and date of the thesis must be given

Enlighten: Theses

<https://theses.gla.ac.uk/>
research-enlighten@glasgow.ac.uk

Greenhouse gases from human-impacted rivers and
estuaries - identifying 'hotspots' and their drivers:
A source-to-sea study of the Clyde river and estuary

Alison Margaret Brown

Submitted in fulfilment of the requirements for the Degree of
Doctor of Philosophy

School of Geographical and Earth Sciences
College of Science and Engineering
University of Glasgow



University
of Glasgow

August 2023

Abstract

There is growing global concern that greenhouse gas (GHG) emissions from water bodies are increasing because of interactions between nutrient levels and climate warming. This thesis investigates three types of aquatic systems, rivers, estuaries and mine water outflows to determine key sources and controls on GHGs in these environments. Riverine systems were studied by consideration of land-cover, seasonal and hydrological controls of GHGs, by comparison of the semi-natural, agricultural and urban environments in a detailed source-to-sea study of the River Clyde, Scotland, home to one third of Scotland's population. Estuarine systems, some of the most sensitive ecosystems to ecological degradation, were investigated by consideration of GHGs from estuaries across the UK and by a detailed investigation of the urban, mesotidal, stratified Clyde estuary. Surveys of the Clyde estuary were made longitudinally, through tidal-cycles and across the river-estuary transition. Mine waters, which can be the dominant pollutant source in mining catchments, were studied by measurement of mine water outflows from sixteen sites across the Midland Valley, Scotland, including radiogenic and stable carbon isotopes measurements to determine the sources of dissolved methane (CH₄) and carbon dioxide (CO₂). GHG concentrations were consistently oversaturated with respect to the atmosphere. Concentrations of CH₄-C ranged from 0.1 to 44 µg l⁻¹ in the riverine environment, 1.2 to 132 µg l⁻¹ in estuarine waters and 20 to 215 µg l⁻¹ in mine waters. Concentrations of CO₂-C ranged from 0.1 to 2.6 mg l⁻¹ in the riverine environment and 30 to 120 mg l⁻¹ in mine waters. Concentrations of nitrous oxide (N₂O-N) ranged between 0.3 - 3.4 µg l⁻¹ in the riverine environment, 0.4 to 5.9 µg l⁻¹ in estuarine waters and 0.4 to 5.3 µg l⁻¹ in mine waters.

In the riverine environment high concentrations of CH₄ were primarily associated with point source inflows from urban wastewater (UWW) treatment, abandoned coal mines and lakes. Concentrations of CO₂ and N₂O were mainly driven by nitrogen concentrations, dominated by diffuse agricultural inputs in the upper catchment and supplemented by point source inputs from UWW in the lower urban catchment. Across the UK, estuarine GHG concentrations were highly correlated with UWW loading although the estuarine environment was highly variable. In the Clyde estuary persistent low river flows, increased freshwater flushing times, which impacted nutrient concentrations (primarily from UWW), salinity, and oxygen levels. Nitrogen processing in the upper freshwater layer occurred via nitrification, while in the lower saline layer denitrification dominated, quadrupling the N₂O per unit available nitrogen with a significant inverse exponential correlation with dissolved oxygen. Methanogenesis in the estuarine surface waters was stimulated by a small (0.5 ppt) increase in salinity and positively correlated with water turbidity, however CH₄ concentrations near the bed reduced exponentially with salinity persistence (continuously saline water > 5ppt) by about 50% after 10 days but were reinvigorated by freshwater flushing. Mine water CH₄ composition included 51% modern biogenic, 41% thermogenic and 8% from methanogenesis of coal. Biogenic CH₄ concentrations were inversely correlated with sulphate. Mine water CO₂ included 64% from the dissolution of limestone, 21% from terrestrial organic carbon and 15% from coal, with sulphate increasing the dissolution of limestone.

This study improves our understanding of aquatic GHG generation and dynamics, which contributes to our knowledge of their release to the atmosphere. GHGs were primarily associated with different sources of pollution including UWW, agriculture and legacy industry, and increased by interactions with physical conditions such as low river flow and low oxygen conditions with temperature a secondary cause. It identifies where actions could support reductions in aquatic GHG generation.

Table of Contents

Abstract	i
List of Tables.....	vii
List of Figures	viii
Acknowledgements.....	x
Author’s Declaration	xi
Statement of Originality.....	xii
Definitions and abbreviations	xiii
Definitions.....	xiii
Abbreviations	xiv
1 Introduction	1
1.1 Greenhouse gas emissions.....	1
1.2 Greenhouse gases and biogeochemical cycles	2
1.3 Greenhouse gases from inland waters.....	4
1.4 Greenhouse emission pathways from aquatic systems	5
1.5 Contrasting processes within different aquatic environments	8
1.6 Anthropogenic causes of GHGs in inland waters	9
1.7 Anthropogenic causes of GHG in estuarine waters.....	10
1.8 Hypotheses	11
1.9 Objectives.....	12
1.10 Scope of this thesis	13
2 Materials and methods	15
2.1 The Clyde catchment, river and estuary	15
2.2 Site descriptions and data collection	16
2.2.1 Riverine sampling.....	16
2.2.2 Mine water sampling	17
2.2.3 Estuarine sampling.....	19
2.3 Sampling regimes	23
2.4 Analytical methods	24
2.5 Gas partial pressures.....	26
2.6 Acknowledgements.....	27
3 Urban landscapes and legacy industry provide hotspots for riverine greenhouse gases: A source-to-sea study of the River Clyde.....	28
Graphical Abstract.....	28

Highlights	29
Abstract.....	29
Key Words	29
Authors.....	29
3.1 Introduction	30
3.2 Materials and methods.....	32
3.2.1 Study area	32
3.2.2 Sites description and data collections.....	33
3.2.3 Field sampling and laboratory measurements.....	35
3.2.4 Gas partial pressures.....	35
3.2.5 Data sources and processing.....	36
3.3 Results.....	38
3.3.1 GHG concentrations and water contamination from source-to-sea.....	38
3.3.2 Land cover relationship with and methane and nitrous oxide dynamics	39
3.3.3 GHG spatial heterogeneity.....	40
3.3.4 Seasonal GHG distribution by land use characteristics.....	43
3.3.5 GHGs, nutrient and contaminants correlations	45
3.3.6 Drivers for greenhouse gas concentrations	46
3.3.7 Carbon and nitrogen exports to the estuary.....	49
3.4 Discussion.....	51
3.4.1 Urban nutrients and climate warming increase GHG emissions	51
3.4.2 High nutrient-residence time interactions promote GHG generation	51
3.4.3 Main uncertainty in the causes of GHG variation	52
3.4.4 Carbon dioxide concentration variability reduced by carbonate buffering.....	53
3.4.5 Acid mine inflows are a major source of GHG and outgas directly to the atmosphere	54
3.4.6 Legacy industry is still detectable in our rivers	54
3.5 Conclusions	55
3.5.1 Benefits of a source-to-sea approach in interpreting riverine GHG data	55
3.5.2 Implications and ideas for policy makers	55
Declaration of Competing Interest.....	56
Acknowledgements.....	56
3.6 Supplementary information.....	57
4 Sources and controls of greenhouse gases and heavy metals in mine water: A continuing climate legacy.....	68
Graphical Abstract.....	68
Highlights	69
Abstract.....	69

Key words.....	69
Authors.....	69
4.1 Introduction	70
4.1.1 Acid mine drainage	70
4.1.2 Mine water treatment approaches.....	71
4.2 Materials and methods.....	74
4.2.1 Geology and study area	74
4.2.2 Gas partial pressures.....	77
4.2.3 Radiogenic and stable carbon isotopes.....	78
4.2.4 Analysis	79
4.3 Results.....	80
4.3.1 The Midland Valley’s mine water physicochemical properties.....	80
4.3.2 Sources of greenhouse gases in mine water.....	81
4.3.3 Greenhouse gas generation or consumption in reed pools.....	84
4.3.4 Impact of oxygenation by cascade on greenhouse gas concentrations.....	84
4.3.5 The effectiveness of reed pools for removing heavy metals	85
4.4 Discussion.....	87
4.4.1 Causes of and variation in carbon dioxide and methane in mine water	87
4.4.2 Causes of heavy metals in mine waters	89
4.4.3 Greenhouse gases from mine waters are all released to atmosphere	91
4.4.4 Estimates of the Global Warming Potential in the mine waters.....	91
4.5 Conclusions	93
Acknowledgements.....	94
5 Anthropogenic-estuarine interactions cause disproportionate greenhouse gas production: A review of the evidence base	95
Graphical Abstract.....	95
Highlights	96
Abstract.....	96
Key Words	96
Authors.....	96
5.1 Introduction	97
5.1.1 Objectives.....	98
5.2 Methods.....	99
5.3 Case studies considering the effect of urban waste and nutrients on GHG production	103
5.3.1 Wastewater loading is a primary driver of methane and nitrous oxide emissions.....	103
5.3.2 Nitrous oxide concentrations significantly increased by activation of denitrification	105
5.3.3 Methane dynamics driven by ammonium concentrations	106

5.3.4	Urban waste and nutrients summary	107
5.4	Estuarine processes as drivers of GHG production	108
5.4.1	Estuary stratification leading to near bed anoxia driving GHG production	108
5.4.2	Tidal range impacting sediment oxygen demand driving methane production	110
5.4.3	Estuarine processes summary.....	111
5.5	Conceptual model for methane and nitrous oxide within the estuary environment	111
5.6	Discussion and Conclusions	117
5.6.1	Are estuaries a net carbon source or sink?.....	119
5.6.2	The impact of survey design and areas of uncertainty	120
5.6.3	Opportunities to reduce estuarine GHG emissions	121
5.6.4	Considerations for policy makers:.....	121
	Declaration of interests.....	122
	Acknowledgments.....	122
5.7	Supplementary data.....	123
6	The impact of salinity and hypoxia on estuarine Greenhouse gases: A study of the stratified Clyde estuary.....	126
	Graphical Abstract.....	126
	Highlights	127
	Abstract	127
	Key words.....	127
	Authors.....	127
6.1	Introduction	128
6.2	Material and methods.....	130
6.2.1	Study Area	130
6.2.2	Site description and data collection.....	130
6.2.3	Field sampling and laboratory measurements.....	135
6.2.4	Data sources and processing.....	135
6.3	Results.....	137
6.3.1	Hydrological drivers on estuary flushing.....	137
6.3.2	The impact of estuary flushing on nutrients and greenhouse gases	138
6.3.3	Greenhouse gases across the riverine to estuary interface	140
6.3.4	Drivers of estuarine nitrous oxide.....	141
6.3.5	Estuarine methane generation	143
6.3.6	Short term tidal variability and GHG generation	145
6.3.7	Comparison with other estuaries.....	147
6.4	Discussion.....	149
6.4.1	Causes and controls of estuarine methane.....	149

6.4.2	Uncertainty in estuarine methane controls	150
6.4.3	Causes and controls of estuarine N ₂ O.....	151
6.4.4	High nutrients and low oxygen are driving N ₂ O	152
6.5	Conclusions	153
	Acknowledgement	154
6.6	Supplementary information	155
7	Discussion	157
7.1	GHG ‘hotspots’ in the Clyde catchment, river and estuary	157
7.2	GHG sources and controls (process understanding)	158
7.2.1	Greenhouse gas processes in freshwater.....	158
7.2.2	Greenhouse gas processes in mine water.....	160
7.2.3	Methane processes in estuaries.....	161
7.2.4	Nitrous oxide processes in estuaries.....	163
7.3	Implications for policy makers	164
8	Conclusions	167
8.1	Significance of this research.....	167
8.1.1	Novel research approaches.....	167
8.1.2	Increased process understanding	168
8.2	Suggestions for future work.....	169
	References.....	172
	Appendices.....	200
	Appendix 1 - Clyde river survey locations	200
	Appendix 2 - Mine water survey locations.....	211
	Appendix 3 - Estuarine survey locations	217
	Addendum 1 - Urban landscapes and legacy industry provide hotspots for riverine greenhouse gases: A source-to-sea study of the River Clyde	222
	Addendum 2 - Anthropogenic-estuarine interactions cause disproportionate greenhouse gas production: A review of the evidence base	241

List of Tables

Table 2.1 - Sampling locations in the Clyde catchment.....	17
Table 2.2 - Mine water outflow sampling locations.....	18
Table 2.3 - Sampling locations for the Clyde estuary transects (CET)	19
Table 2.4 - Sampling dates in the Clyde estuary - Estuary Transects (CET)	20
Table 2.5 - Sampling dates in the Clyde estuary - tidal cycle (CEP)	21
Table 3.1 - Pearson's Correlation Coefficient between nutrients and GHGs (EC, DO%, pH SUVA ₂₅₄ , TP, DOC, DIC, TDN, CH ₄ , N ₂ O and CO ₂) and percentage land-cover across Clyde tributaries and headwaters.....	40
Table 3.2 - Cluster analyses based on the measured water chemical properties (DOC, DIC, TDN, TP, Cl ⁻ , NO ₃ ⁻ , SO ₄ ²⁻ , Na ⁺ , NH ₄ ⁺ , K ⁺ , Ca ²⁺ and Mg ²⁺) distinguishes locations by position in the catchment.	43
Table 3.3 - GHG correlation (Pearson's R) with water physiochemical properties over the whole catchment	45
Table 3.4 - Categorisation of the dominant sources of GHG and nutrients between point and diffuse sources and their dependence on flow in upper and lower Clyde catchment	47
Table 3.5 - Flux of CO ₂ , CH ₄ , N ₂ O, TP, TDN, DOC, DIC, Cl ⁻ , NO ₃ ⁻ , SO ₄ ²⁻ , Na ⁺ , NH ₄ ⁺ , K ⁺ , Ca ²⁺ , Mg ²⁺ into the Clyde Estuary.....	49
Table 3.6 - Comparison of DIC and DOC export from UK Rivers as a function of catchment area	50
Table 3.A.1 - Sample locations on the River Clyde and flow gauging details	57
Table 3.A.2 - Average GHG and physiochemical concentrations for each survey location	58
Table 3.A.3 - Average dissolved ion concentrations for each survey location	59
Table 3.A.4 - Correlation between nutrients and GHG and percentage land-cover across all tributaries and Clyde headwater sampling points.....	60
Table 3.A.5 - GHG correlation with water physiochemical properties dissolved ion concentrations... ..	60
Table 4.1 - Mine water sampling location, treatment, geology and hydrology	76
Table 4.2 - Estimated concentrations of methane and carbon dioxide based on radiogenic and stable isotope ratios	83
Table 4.3 - Global warming potential from mine water in Scotland - High and low estimates are based on ±3 standard deviations from the mean for concentrations (shown as median).....	92
Table 5.1 - Summary of published data applied in this review	101
Table 5.2 - Summary of average methane and nitrous oxide concentrations measured	101
Table 5.3 - Physical characteristics of the estuarine systems.....	102
Table 5.4 - Clyde Estuary GHG concentrations associated with tidal, river, salinity and oxygen conditions.....	109
Table 5.5 - Tide and river condition associated with measurements occasions - Dart estuary.....	109
Table 5.A.1 - Average dissolved oxygen (DO) saturation data for several estuaries of interest.....	123
Table 5.A.2 - Percentage land cover for estuaries of interest	124
Table 6.1 - Sampling locations for the Clyde estuary transects	131
Table 6.2 - Sampling dates for the Clyde estuary transects	131
Table 6.3 - Sampling dates for the Clyde estuary tidal cycle measurements.....	132
Table 6.4 - Sampling locations for the Clyde river estuary transition	132
Table 6.5 - Comparison of annual CH ₄ and N ₂ O emissions in estuaries.....	148

List of Figures

Figure 1.1 - The causal chain from emissions to resulting warming of the climate system taken from .	1
Figure 1.2 - Simplified representation of the (a) the carbon cycle and (b) and the nitrogen cycle	3
Figure 1.3 - Flux pathways from aquatic systems	7
Figure 1.4 - Schematic diagram of sources of greenhouse gases within the Clyde catchment and the chapters which address them in this thesis	14
Figure 2.1 - Map of all locations for riverine, estuarine and mine water sampling	22
Figure 3.0 - Graphical Abstract - Urban landscapes and legacy industry provide hotspots for riverine greenhouse gases	28
Figure 3.1 - GHG generation, transport and loss	32
Figure 3.2 - Spatial plots of the River Clyde catchment	34
Figure 3.3 - River Clyde volumetric flow and contaminants inputs	37
Figure 3.4 - Radar plots of average dissolved GHGs and water chemical properties	39
Figure 3.5 - Spatial average of CH ₄ , CO ₂ , N ₂ O and SUVA at 254nm across the Clyde catchment.....	42
Figure 3.6 - Seasonal analysis of GHGs for the upper, middle and lower River Clyde and tributaries..	44
Figure 3.7 - Correlation (Peason's R) between GHGs and physiochemical water properties	46
Figure 3.8 - Average concentrations from point source and diffuse sources on the River Clyde	48
Figure 3.A.1 - Correlation between TP, TDN and DOC, and percentage land-cover across Clyde tributaries and headwaters	61
Figure 3.A.2 - Correlation between CH ₄ , N ₂ O and SUVA ₂₅₄ and percentage land-cover across Clyde tributaries and headwaters	62
Figure 3.A.3 - Spatial plots for Temperature, Dissolved Oxygen, Conductivity and pH	63
Figure 3.A.4 - Spatial plots for Total Dissolved Nitrogen, Total Phosphorous, Dissolved Organic and Carbon and Dissolved Inorganic Carbon.....	64
Figure 3.A.5 - Spatial plots for Potassium, Sulphate, and Calcium and Magnesium ions	65
Figure 3.A.6 - Spatial plots for Sodium, Chloride, Nitrate and Ammonium ions	66
Figure 3.A.7 - River Clyde Average concentrations for ion point source and diffuse sources	67
Figure 4.0 - Graphical Abstract - Sources and controls of greenhouse gases and heavy metals in mine water.....	68
Figure 4.1 - Schematic of main mine water treatment processes for measurement sites.....	73
Figure 4.2 - Sample site locations (MA1 to MA16) shown in the relation to the geology of the Midland Valley, Scotland.....	75
Figure 4.3 - Potential CO ₂ and CH ₄ sources in terms of their $\delta^{14}\text{C}$ and $\delta^{13}\text{C}$ signature.....	79
Figure 4.4 - Relationships between greenhouse gases and water chemical properties.....	81
Figure 4.5 - Relationships between $\delta^{13}\text{C}$ and $\delta^{14}\text{C}$ in mine water CH ₄ and CO ₂ (MA1 to MA16)	82
Figure 4.6 - Source to reed pool transition on $\delta^{14}\text{C}$ and $\delta^{13}\text{C}$ composition.....	84
Figure 4.7 - Changes in heavy metal concentrations in treatment reed pools.....	86
Figure 4.8 - Causal relationship for different CO ₂ and CH ₄ sources and metal concentration.....	90
Figure 5.0 - Graphical Abstract - Anthropogenic-estuarine interactions cause disproportionate greenhouse gas production.....	95
Figure 5.1 - Simplified nitrification-denitrification pathways in estuaries.....	98
Figure 5.2 - Outline of approach in this paper	99
Figure 5.3 - Map showing estuary catchments of the thirteen estuary systems considered	100

Figure 5.4 - UWW loading compared with GHG concentration data..... 104

Figure 5.5 - Relative relationships between DIN concentrations and N₂O saturation, 106

Figure 5.6 - Relationships between average methane concentration for each estuary 107

Figure 5.7 - Tyne estuary average relationships between methane concentration and tidal range... 111

Figure 5.8 - Longitudinal and cross-sectional profiles of a highly stratified salt-wedge 114

Figure 5.9 - Longitudinal and cross-sectional profiles of a fully-mixed estuary 116

Figure 5.A.1 - Average CH₄ and N₂O concentrations compared to urban and arable land cover 125

Figure 6.0 - Graphical Abstract - The impact of salinity and hypoxia on estuarine greenhouse gases
..... 126

Figure 6.1 - Sampling locations and land cover for the Clyde estuary 133

Figure 6.2 - River Clyde flow for survey period - 134

Figure 6.3 - Clyde estuary freshwater flushing time (*T_f*)..... 137

Figure 6.4 - Impact of freshwater flushing time (*T_f*) on estuary physiochemical properties..... 139

Figure 6.5 - Comparison of river and estuary transition - 140

Figure 6.6 - Relationship between [N₂O-N] and water physiochemical properties 142

Figure 6.7 - Relationship between [CH₄-C] and water physiochemical properties 144

Figure 6.8 - Methane concentrations vs. salinity persistence (time since last freshwater flushing) .. 145

Figure 6.9 - Impact of short-term (tidal) variation on GHG generations 146

Figure 6.10 - Relationship between observed UK estuarine N₂O saturations and TDN..... 152

Figure 6.A.1 - Clyde transect data for CET survey CET1 to CET8 for locations L1 to L10 155

Figure 6.A.2 - Clyde transect data for CET survey CET1 to CET8 for locations L1 to L10 156

Acknowledgements

The author would like to acknowledge and thank the following:

My supervisory committee for their support and guidance on my PhD project: Dr Amy E. Pickard and Prof. Ute Skiba from the UK Centre of Ecology & Hydrology and Dr Adrian Bass and Dr John MacDonald from the School of Geographical and Earth Sciences at University of Glasgow.

The Natural Environment Research Council (NERC), which financially supported this studentship through the IAPETUS Doctoral Training Partnership, Grant No. NE/S007431/1.

The National Environmental Isotope Facility (Part of the Natural Environmental Research Council), which financially supported the radiogenic and stable carbon isotope analysis, Grant Number 2513.0422.

The UK Centre for Ecology & Hydrology for their support with additional staff time and provision of the power boat for the estuary sampling work.

The Tall Ship Glenlee Trust, a registered charity limited by guarantee, and the wholly-owned subsidiary of the Trust, the Clyde Maritime Centre, which is responsible for the operation of Kelvin Harbour (Tall Ship Glenlee Trust, 2022), and supported the research work as access the Clyde estuary was via Kelvin Harbour.

Intu SGS, Global Mutual and Savills for allowing access to Braehead pontoon for the purpose of making these measurements.

The Glasgow City Council for allowing access to Govan pier for the purpose of making these measurements.

The Coal Authority and Severn Trent Services for allowing access to and supporting sampling respectively at several of the Coal Authorities Mine Water treatment sites for the purpose of making these measurements.

Dr. Mark Garnett for the training in taking samples for radiogenic and stable isotope measurement and for support with the grant proposal.

Dr. Lorna Eades at the University of Edinburgh for undertaking the ICP-MS analysis of the mine water samples

The Marine Alliance for Science and Technology for Scotland (MASTS) for a grant towards a HACH oxygen probe.

The Scottish Alliance for Geosciences Environment and Society (SAGES), for a grant for ICP-MS analysis although the data is not included herein.

Dr. Amy Pickard, Dr. Peter Heyes, Dr. Elliot Hurst, Stella White, Mairéad Corr, Alanna Grant, Dr. Justyna Olszewska, Galina Toteva, Ivan Simmons and Duncan Harvey for their help with the estuary field work.

Dr. Peter Heyes and Dr. Amy Pickard for their support with the riverine sampling work.

Dr. Amy Pickard, Stella White and Netty van Dijk for their training and support in the various laboratory measurement techniques used.

Author's Declaration

The material presented in this thesis is the result of research conducted between October 2019 and June 2023, under the supervision of Dr. Amy E. Pickard (primary) UK Centre of Ecology & Hydrology, Dr. Adrian M. Bass (secondary), the University of Glasgow; Prof. Ute Skiba, UK Centre of Ecology & Hydrology and Dr. John MacDonald University of Glasgow. This work is based on individual research carried out by myself, and any published or un-published material not of my own has been fully acknowledged in the text.

Statement of Originality

Name: Alison Margaret

Registration Number: Brown XXXXXXX

I certify that the thesis presented here for examination for PhD degree of the University of Glasgow is solely my own work other than where I have clearly indicated that it is the work of others (in which case the extent of any work carried out jointly by me and any other person is clearly identified in it) and that the thesis has not been edited by a third party beyond what is permitted by the University's PGR Code of Practice.

The copyright of this thesis rests with the author. No quotation from it is permitted without full acknowledgement.

I declare that the thesis does not include work forming part of a thesis presented successfully for another degree

I declare that this thesis has been produced in accordance with the University of Glasgow's Code of Good Practice in Research.

I acknowledge that if any issues are raised regarding good research practice based on review of the thesis, the examination may be postponed pending the outcome of any investigation of the issues.

Statement of conjoint work

I confirm that for Chapter 3, the data in this chapter was collected and analysed by the author of the thesis. Co-authors reviewed paper drafts and provided supervision, feedback, and guidance. The author of the thesis contributed > 90% of this work.

I confirm that for Chapter 4 the data in this chapter was collected and analysed by the author with support from one co-author during part of the data collection and one co-author in the analysis of the radiogenic and stable isotopes linked to the NEIF grant. Co-authors reviewed paper drafts and provided supervision, feedback, and guidance. Excluding the work undertaken by NEIF and funded by grant number 2513.0422, the author of the thesis contributed > 90% of this work.

I confirm that for Chapter 5, the data in this chapter was analysed by the author of the thesis. Co-authors reviewed paper drafts and provided supervision, feedback, and guidance. The author of the thesis contributed > 90% of this work.

I confirm that for Chapter 6 the data in this chapter were primarily collected by the author with support from some co-authors during the boat survey and was analysed by the author. Some co-authors reviewed paper drafts and provided supervision, feedback, and guidance. The author of the thesis contributed > 90% of this work.

Signature:

Date:13th July 2023.....

Definitions and abbreviations

The following are used within the text.

Definitions

Estuary residence time - The average time an initially existing water parcel resides in the estuary before being flushed out.

Freshwater flushing time - The time required to replace the existing freshwater in the estuary at a rate equal to the river discharge.

$\Delta^{14}\text{C}$ - The ratio of the isotopes of carbon ^{14}C and ^{12}C corrected for fractionation and age and referenced to the absolute international standard (base year 1950).

$\delta^{13}\text{C}$ - The ratio of the two stable isotopes of carbon ^{13}C and ^{12}C relative to the primary international standard for carbon-13 the Pee Dee Belemnite (PDB) reported in ppt (‰).

$$\delta^{13}\text{C} = \left(\frac{\left(\frac{^{13}\text{C}}{^{12}\text{C}} \right)_{\text{sample}}}{\left(\frac{^{13}\text{C}}{^{12}\text{C}} \right)_{\text{standard}}} - 1 \right) \times 1000$$

Percentage modern - The percentage of carbon from a modern source compared to a source where all the ^{14}C has decayed. 100% Modern is defined as 95% of the ^{14}C activity for AD 1950.

Inland waters - This includes rivers, streams, lakes, wetlands, ponds, ditches and reservoirs and inner estuaries (although not all estimates for GHGs from inland water account for all of these sources).

Aquatic - This includes inland water plus coastal waters, continental shelf and open ocean.

Marine - This includes coastal waters, continental shelf and open ocean.

Abbreviations

AMM	Abandoned mine methane
BOD	Biological oxygen demand
Ca ²⁺	Calcium ions
CH ₄	Methane
Cl ⁻	Chlorine ions
CO ₂	Carbon dioxide
Δp	Water-to-air partial pressure difference
DIC	Dissolved inorganic carbon
DOC	Dissolved organic carbon
DO (%)	Dissolved oxygen (saturation)
EC	Electrical conductivity
F	Sea-to-air flux
GHG	Greenhouse gas
IPC-MS	Inductively coupled plasma mass spectrometry
IPCC	Intergovernmental Panel on Climate Change
K ⁺	Potassium ions
K _w	Gas specific transfer velocity
L	Gas specific solubility
Mg ²⁺	Magnesium ions
MW	Mine water
Na ⁺	Sodium ions
N ₂ O	Nitrous oxide
NEDD	<i>N</i> - (1-naphthyl)-ethylenediamine dihydrochloride
NH ₄ ⁺	Ammonium ions
NO ₂ ⁻	Nitrite ions
NO ₃ ⁻	Nitrate ions
OC	Organic carbon (OC)
ppe	Per person equivalent
pppd	Per person per day
pH	Potential Hydrogen
<i>R</i> or <i>Q</i> ₀	River discharge
Sc	Gas specific Schmidt number
S _e	upper layer salinity (estuary)
S _o	sea water salinity (estuary)
SOD	Sediment oxygen demand
SO ₄ ²⁺	Sulphate ions
SRB	Sulphate reducing bacteria
SPM	Suspended particulate matter
SUVA ₂₅₄	Specific UV Absorbance at 254 nm
TDC	Total dissolved carbon
TDN	Total dissolved nitrogen
T _f	Fresh water flushing time
TMZ	Turbidity maximum zone
TP	Total phosphorus
T _{UR}	Turbidity
T _w	Water temperature
U	Wind velocity
UWW	Urban wastewater
UWWTP	Urban wastewater treatment plant
V	Low Tide Volume

1 Introduction

1.1 Greenhouse gas emissions

Human activities, causing emissions of greenhouse gases (GHGs), have according to the Intergovernmental Panel on Climate Change (IPCC) unequivocally caused global warming, with global surface temperature reaching 1.1°C above the 1850 - 1900 baseline in 2011 - 2020. Climate change is considered a threat to human well-being and planetary health with only deep, rapid and sustained mitigation and accelerated implementation of adaptation actions able to reduce projected losses and damages for humans and ecosystems (IPCC, 2023b). Emissions of GHGs have increased rapidly over recent decades (Figure 1.1).

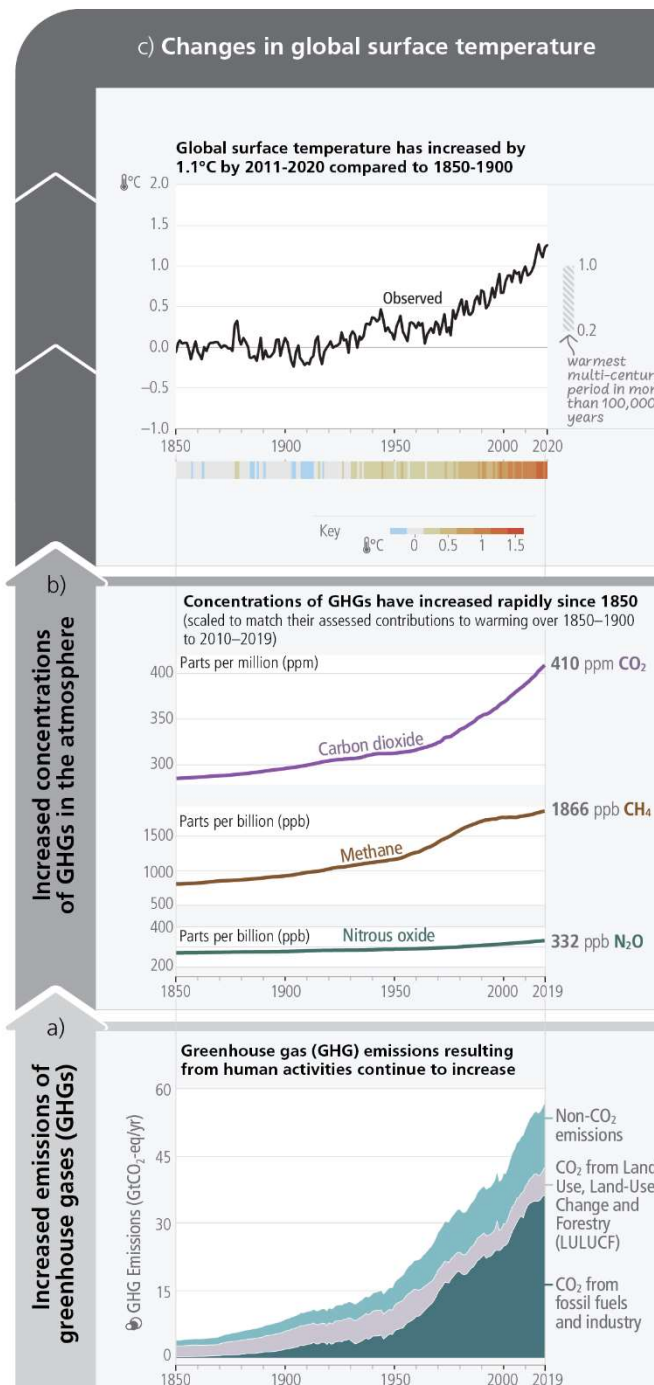


Figure 1.1 - The causal chain from emissions to resulting warming of the climate system taken from (IPCC, 2023a).

(a) Global net anthropogenic GHG emissions include CO₂ from fossil fuel combustion (CO₂-FFI) (dark green); net CO₂ from land use, land-use change and forestry (CO₂-LULUCF) (green); CH₄; N₂O; and fluorinated gases (light blue). These have led to increases in GHG atmospheric concentrations including CO₂, CH₄ and N₂O

(b) The vertical extent for CO₂, CH₄ and N₂O is scaled to match the assessed individual direct effect of historical emissions on temperature change from 1850 - 1900 to 2010 - 2019. This estimate arises from an assessment of effective radiative forcing and climate sensitivity. The global surface temperature (shown as annual anomalies from a 1850–1900 baseline) has increased by around 1.1°C since 1850–1900.

(c) Formal detection and attribution studies synthesise information from climate models and observations and show that the best estimate is that all the warming observed between 1850– 1900 and 2010–2019 is caused by humans.

Reaching net zero GHG emissions primarily requires reductions in emissions of carbon dioxide (CO₂), methane (CH₄) and other GHGs such as nitrous oxide (N₂O) (IPCC, 2023b). Research, into GHG sources, generation pathways and sinks, helps support actions needed to reduce GHG emission to the atmosphere and reduce global warming.

1.2 Greenhouse gases and biogeochemical cycles

Emissions of anthropogenically generated GHGs are causing the climate to warm with CO₂, CH₄ and N₂O having the largest impact (IPCC, 2023b). Anthropogenic impacts have resulted in the biogeochemical cycles governing these GHGs to become unbalanced with an increasing amount of the carbon and nitrogen lost to the atmosphere that was previously contained or absorbed within the lithosphere. The carbon and nitrogen cycles, with some of the anthropogenic influences impacting these cycles, are shown schematically in Fig. 1.2 (A the carbon cycle and B the nitrogen cycle). While the largest impact on global warming has been derived from fossil fuels (Fig 1.1a), agriculture, forestry and other land use activities accounted for around 13% of CO₂, 44% of CH₄, and 82% of N₂O emissions from human activities during 2007–2016, representing 23% (12.0 ± 3.0 Gt CO₂ equivalent yr⁻¹) of the total net anthropogenic emissions of GHGs (IPCC, 2021b).

Over the period 1750 to 2019, CO₂ increased by 131.6 ± 2.9 ppm (47.3%) with concentrations of CO₂ reaching 409.9 ± 0.3 ppm in 2019, with this the fastest rate of change over the last 56 million years. The increase of CH₄ since 1750 of 1137 ± 10 ppb (157.8%) far exceeds the range over the past 800,000 years, and concentrations of CH₄ reached 1866.3 ± 3.3 ppb by 2019. This recent growth of CH₄ was largely driven by fossil fuel exploitation, livestock, waste, wetlands and biomass burning. Since 1750, N₂O increased by 62.0 ± 6.0 ppb, reaching a level of 332.1 ± 0.4 ppb in 2019. This increase was largely driven by the intensification and expansion of global agriculture (IPCC, 2021b).

Over the past decade (2010 – 2019), 10.9 ± 0.9 Pg C yr⁻¹ were emitted from human activities, of which 46% accumulated in the atmosphere, 23% was taken up by the ocean and 31% was stored by vegetation in terrestrial ecosystems (IPCC., 2021). The ocean takes up CO₂ through photosynthesis by phytoplankton and by increased dissolution of CO₂ due to the rising atmospheric concentrations, increasing ocean acidity. The natural and anthropogenic transfers of carbon from soils to freshwater systems are also large ($2.4 - 5.1$ Pg C yr⁻¹), with a significant proportion of this carbon returned to the atmosphere via out-gassing from lakes, rivers and estuaries.

Estimates of CH₄ from Inland waters (lakes, rivers, streams, ponds, estuaries) range between $117 - 212$ Tg yr⁻¹ but these emissions are proportionally the largest source of uncertainty in the CH₄ budget, due to the large spatial and temporal variation in lake and river CH₄ fluxes. In natural ecosystems, N₂O is primarily produced as a by-product during the remineralisation of organic matter by nitrification and denitrification with the net N₂O production highly sensitive to local environmental conditions, causing strong spatial and temporal variability of N₂O. The use of fertilizers and manure, as well as nitrogen deposition resulting from land-based agriculture and fossil fuel burning has been the largest driver of the increase in atmospheric N₂O of 31.0 ± 0.5 ppb (10%) between 1980 and 2019 (IPCC., 2021).

1.3 Greenhouse gases from inland waters

Inland waters (rivers, streams, lakes and reservoirs) are significant net-sources of GHGs to the atmosphere, as they receive considerable organic matter and nitrogen compounds from the terrestrial ecosystem. Carbon received by inland waters is either stored, typically within the sediments, transported to the ocean or outgassed to the atmosphere, with the estimated carbon storage of 0.6 Pg C yr^{-1} and that transported to the ocean as 0.9 Pg C yr^{-1} (Drake et al., 2018). However, streams and rivers tend toward emission to atmosphere or transport downstream, compared to reservoirs and lakes, which exhibit higher accumulation rates (Vachon et al., 2021) (Gao et al., 2022), which can be rapid and significant (Mendonça et al., 2017). However, carbon stored in sediments may support anaerobic methanogenesis (Tittel et al., 2019). Global CO_2 evasion has been estimated as $1.8 \pm 0.25 \text{ Pg C yr}^{-1}$ from streams and rivers and $0.32 \pm 0.26 \text{ Pg C yr}^{-1}$ from lakes and reservoirs, resulting in a global evasion rate from inland waters of 2.1 Pg C yr^{-1} (Raymond et al., 2013). However historical underestimation of the amount of terrestrial carbon exported to inland waters has resulted in updated estimates of CO_2 evasion to 3.9 Pg C yr^{-1} (Drake et al., 2018). The contribution from streams and rivers is large relative to their surface area, acting as hotspots for the exchange of gases with the atmosphere. The major sources of CO_2 into inland waters are direct input via groundwater inflow, which transports CO_2 originating from soil respiration, and in-stream mineralization of organic carbon (OC) often from surface run-off (Winterdahl et al., 2016). Riparian wetlands also contribute disproportionately to CO_2 emissions (Abril and Borges, 2019). The relative importance of these mechanisms changes with stream order as headwater streams have a larger soil-water interface compared to lower reaches, resulting in the proportion of CO_2 produced from aquatic metabolism increasing with stream size (Marx et al., 2017; Hotchkiss et al., 2015). However the magnitude of the estimated CO_2 emissions from fresh waters are higher than those estimated both from in-water generation or transfer from soil and groundwater and are likely supported by carbonate buffering (Stets et al., 2017). The magnitude of CO_2 riverine emissions is highly dependent on hydrology (Gómez-Gener et al., 2016) and in urban areas CO_2 emissions are increased by significantly higher nutrients, organic matter content and riverine cyanobacteria (Salgado et al., 2022). Emissions of CO_2 from estuaries are complex and highly variable with the net mineralization of land-derived organic carbon estimated to lead to emissions between 44 to $44\,000 \text{ mg m}^{-2} \text{ d}^{-1}$ from inner estuarine waters. Outer estuarine plumes act as intense sources of primary production and can be both sources and sinks of CO_2 (Abril and Borges, 2005).

Atmospheric CH_4 is a potent GHG impacting the world's climate and accounting for an estimated 0.5°C of recent warming, although around 38% of this warming is masked by aerosol cooling (IPCC, 2021b). While CH_4 concentrations appeared to have stabilised in the period 2000 to 2006, since 2007 emissions have continued to increase with CH_4 emissions from natural and anthropogenic sources ranging between 538 and 884 Tg yr^{-1} (Saunio et al., 2016, 2020). The most important source of uncertainty is attributable to natural emissions, especially those from wetlands and other inland waters. Global CH_4 evasion from inland waters was estimated at $398.1 \pm 79.4 \text{ Tg CH}_4 \text{ yr}^{-1}$, with the total aquatic systems (including inland waters, coastal and open open) evading $431.3 \pm 87.9 \text{ Tg CH}_4 \text{ yr}^{-1}$. Aquatic ecosystems contributed about half of total global CH_4 emissions from anthropogenic and natural sources (Rosentreter et al., 2021). Rivers were estimated to evade $30.5 \pm 17.1 \text{ Tg CH}_4 \text{ yr}^{-1}$ and lakes

and reservoirs to evade 175.2 ± 81.0 Tg CH₄ yr⁻¹ with estuaries evading 0.90 ± 0.29 to 6.6 Tg CH₄ yr⁻¹. The level of CH₄ emissions varied by several orders of magnitude in all aquatic environments. Total CH₄ emissions were found to increase from natural to impacted and from marine to freshwater ecosystems. Emissions are expected to increase due to urbanization, eutrophication and positive climate feedbacks. However there is significant uncertainty in the production, transportation and consumption processes of aquatic CH₄ making future predictions challenging (Rosentreter et al., 2021, Stanley et al., 2016).

Atmospheric N₂O is a very potent GHG and considered the third most important GHG linked to global warming. Most N₂O is produced by microbial processes in both terrestrial and aquatic systems (Maavara et al., 2019). Anthropogenic nitrogen loading into inland waters is a significant source of N₂O via microbial nitrification and denitrification (the processes by which conversion from dissolved nitrogen to N₂O occurs), with the fraction of the available nitrogen converted to N₂O rather than N₂ important when considering the amount of N₂O produced (Beaulieu et al., 2011; Maavara et al., 2019). The production and emission of N₂O from aquatic systems are highly uncertain (0.3 - 2.1 Tg N₂O-N yr⁻¹) with large spatial and temporal variability in emission estimates (Seitzinger and Kroeze, 1998; Beaulieu et al., 2011; Ciais et al., 2013). However, N₂O emissions from rivers, reservoirs and estuaries have been estimated as 148 - 277 Gg N yr⁻¹ with anthropogenic perturbations to riverine systems resulting in a two- to four-fold increase in N₂O emissions from inland waters. The global emissions of N₂O from estuaries, estimated as 60.0 - 155.4 Gg N₂O-N yr⁻¹ was both higher and more variable than that of other inland waters (Maavara et al., 2019). The dominance of N₂O emissions from nitrification or denitrification in inland waters is considered partly dependent on residence time of the systems (Zarnetske et al., 2011). The proportion of denitrified N₂O has been found <1% of the nitrogen, with rate of nitrogen processing but not yield of N₂O increasing with water nitrate (NO₃⁻) concentrations (Beaulieu et al., 2011).

1.4 Greenhouse emission pathways from aquatic systems

The role of GHGs in climate change is recognised and GHG fluxes from aquatic systems have been identified as the most uncertain component of these GHG emissions. There is a need to understand these emissions and their variation over different timescales (inter-annually, seasonally and diurnally) at a national level. However, this is challenging due to their high spatial and temporal variability, which is further exacerbated by the different emission pathways. There are three main pathways for GHG fluxes from aquatic systems to reach the atmosphere, these include ebullitive, diffusive and plant mediated fluxes with available flux data dominated by diffusive measurements despite the recognized importance of ebullitive and plant-mediated CH₄ fluxes (Stanley et al., 2022). The various processes of aquatic GHG production and loss including diffusion, ebullition and plant mediated losses are shown schematically in Fig. 1.3.

Organic carbon is largely decomposed via microbial processes both within the water column and within the bed. In sediment microbial processes can result in ebullition or bubbling of gases from the sediment. Where this occurs in relatively shallow water, with low hydrostatic pressure, the travel time from the bed to the surface is small and these bubbles have little opportunity to dissolve or interact with other in-water processes before reaching the surface and escaping to the atmosphere (Wang et al., 2021a). Gases produced by ebullition are

typically episodic with high spatial variability and accurate estimates require both spatially intensive and near continuous temporal sampling (Davidson et al., 2018). Additionally ebullitive CH₄ may by-pass counteracting microbial processes such as oxidation compared to diffusive CH₄ (Dessandier et al., 2016).

Conversely diffusive fluxes are derived from dissolved gases that have become over- or super-saturated in the water column. The gases can be produced in the water column, at the sediment-water interface or within the sediments, but dissolve and diffuse through the water column, aligned to the concentration gradient, often towards the surface. The gases are emitted to atmosphere by diffusion across the air-water interface and are considered less spatially and temporally variable than ebullitive fluxes. The type of aquatic environment may impact the dominance of diffusive emissions, which have been found to produce 78 – 100% of the total CH₄ emissions in headwater streams (Robison et al., 2022). However, emissions are accelerated by increased turbulence such as that caused by a bed slope, wind, currents and waves, which impacts variability. Vegetation can impact the timing and location of GHG emissions, including acting as a conduit for gas release, providing carbon substrates for growth of microorganisms that produce GHGs and supplying oxygen to support CH₄ oxidation. Changes in vegetation including seasonal growth can therefore impact the timing and location of these emissions (Bansal et al., 2020).

Ebullitive CH₄ emission rates are significantly greater than diffusion-based estimates and estimating CH₄ budgets from only the diffusive term can be a significant risk (Zheng et al., 2022). Ebullitive fluxes for CO₂ and N₂O are less important (Davidson et al., 2018; Wang et al., 2021; Zheng et al., 2022). A further complication in estimating GHG fluxes from aquatic systems is that ebullitive, diffusive and plant mediated fluxes can be influenced differently by various physical processes such as water levels impacting pore pressure or temperature (Wang et al., 2021a). This multiplicity of processes and the high variability especially of ebullitive fluxes may make joint ebullitive and diffuse flux measurements more difficult to attribute to causal mechanisms.

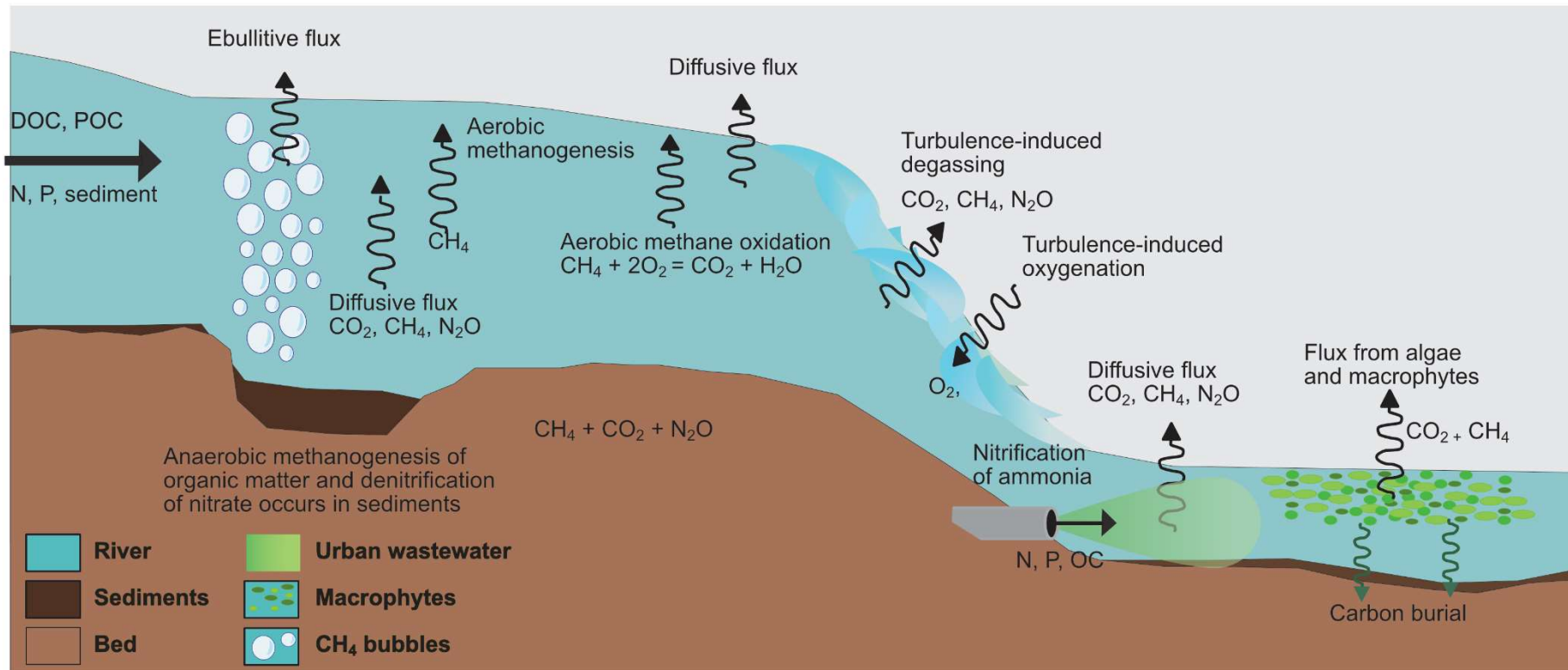


Figure 1.3 - Flux pathways from aquatic systems

Schematic diagram showing potential flux pathways for emission of greenhouse gases from aquatic systems, shown here for a riverine system with both placid and turbulent sections.

1.5 Contrasting processes within different aquatic environments

Understanding aquatic GHG emissions can be further complicated because of the range of different environments including wetlands, marshes, streams, ditches, rivers, lakes, ponds and estuaries. Different physical and chemical processes would be expected to dominate in these different environments and these systems will likely experience different physical conditions and pressures both natural and anthropogenic. For example, head-water streams can behave differently from rivers. In headwater streams the main source of stream CO₂ was inflowing groundwater transporting CO₂ originating from soil respiration. However in-stream mineralization of organic carbon (OC) to produce CO₂ becomes more important with increasing stream order compared to inputs from groundwater, as the connectivity to groundwater reduces compared to the flow (Winterdahl et al., 2016). Gas transfer from streams is influenced by turbulence and hence stream slope with most dissolved gases evaded over short distances (~100m) with steeper, often headwater, streams evading gases faster (Maurice et al., 2017). Steep small streams evading gases rapidly could be significant sources of GHGs, something that may not be reflected in their measured GHG concentrations, while larger, flat-water bodies could have higher GHG concentrations but result in lower emissions due to lower turbulence. This increased GHG residence time may increase opportunity for CO₂ buffering, CH₄ oxidation and other in water processes.

Emissions of CH₄, CO₂ and N₂O have all been correlated to land use with low emissions from natural systems and anthropogenically impacted systems exhibiting high GHG emissions (Hao et al., 2021). Catchment land cover can have a significant influence of water physicochemical properties, with urban and agricultural land increasing nutrient and GHG concentrations compared to, for example, forested systems (Borges et al., 2018; Dai et al., 2017; Li et al., 2009; Wan et al., 2014). The percent coverage of different land cover types has been found as a good indicator for estimating riverine pCO₂ (Tian et al., 2019). Rivers have been found to be impacted by their connectivity to wetlands (Borges et al., 2019) and the regions within 200 m of river banks were found to be key in dictating river water quality, when considering non-point source pollutants, nutrients and soil conservation (Dai et al., 2017).

Seasonal changes can also impact GHG generation, with positive correlations between temperature and all GHG concentrations routinely observed (Wang et al., 2021, Herrero Ortega et al., 2019 and Rosentreter et al., 2021). However the relationship between CH₄ emissions and temperature was not always consistent, with some studies finding temperature to be strongly correlated with CH₄ (Wang et al., 2021; Gulshin and Gogina, 2021; Macdonald et al., 1998; Borges et al., 2016; Campeau and Del Giorgio, 2014) while others found only a weak relationship (Dinsmore et al., 2013; Macias et al., 2014; Herrero Ortega et al., 2019) and in other studies no effect (Yu et al., 2017; Hope et al., 2001). This variability suggests that processes are complex and temperature correlations may be confounded with or influenced by other variables. Conversely in an investigation of N₂O concentrations upstream and downstream of wastewater treatment plants (WWTPs) in an urban river in Japan found lower N₂O concentrations were in summer (Zhou et al., 2022).

Variations in flows were found to have a greater influence than steep slopes on GHG evasion (Maurice et al., 2017). Droughts and low flows in both forested and agricultural watershed

had decreasing N₂O emissions with increasing low flow severity (Tonina et al., 2021), however this relationship might be impact dependent on whether nitrogen was derived from point or diffuse sources. Another physical impact on GHG concentrations and one that is under researched, due to survey practicalities, is that of diurnal variation which will likely influence to what extent rivers and estuaries are sources and sink of GHG (Tian et al., 2019). Diurnal variation has been reported to lead to lower DO during the night time as photosynthesis produces oxygen and consume CO₂ during the day, while aerobic respiration produces CO₂ and uses oxygen during the night resulting higher pN₂O and pCO₂, (Gong et al., 2021; Xia et al., 2013; Bass et al., 2013).

Our changing climate with both increasing temperature and variability in rainfall could change these stressors in the future (IPCC, 2021a). Natural CH₄ emissions from wetlands have increased, suggesting that a warmer, wetter climate could act as a positive feedback mechanism increasing CH₄ emissions (Peng et al., 2022). Similarly thawing of permafrost has led to a further increase CH₄ emission from cycling of organic carbon (Bogard et al., 2019; Cooper et al., 2017). These processes has resulted in changes to the carbon isotopic ($\delta^{13}\text{C}$) content of atmospheric CH₄ dominated by increasing biogenic sources, interpreted as wetland feedback (Nisbet, 2023). Climate impacts on river flow are predicted to result in more frequent flushing events in winter and longer periods of drought in summer (Robins et al., 2016), which could impact both diffuse and point sources. Rainfall has been found to increase water-to-air GHG fluxes by up to 780% due to increases in gas transfer velocity compared to still waters (Looman et al., 2017), although other studies have suggested rainfall has only a minor and short-term effect (Sieczko et al., 2023).

1.6 Anthropogenic causes of GHGs in inland waters

Urban rivers and lakes are potential hotspots for GHG emissions and there is an increasing body of literature concerned with quantifying their contribution to aquatic GHG emissions (Zhang et al., 2021; Wang et al., 2021; Gu et al., 2021; Herrero Ortega et al., 2019; Martinez-Cruz et al., 2017; Garnier et al., 2009; Hao et al., 2021; Ho et al., 2022). In Mexico City water quality indicators (such as trophic state index and phosphorous level) were positively correlated with CH₄ emissions, suggesting a reduction in untreated wastewater discharge could reduce GHG emissions. Fluxes of CH₄ were highly variable, both in and across ecosystem, locations and seasons (Martinez-Cruz et al., 2017) demonstrating the need for comprehensive studies to understand these temporal dynamics. Similarly in an urban river system in Ecuador the more polluted sites had higher dissolved GHG concentrations (Ho et al., 2022). In water bodies around the city of Berlin, a combination of high nutrient supply and shallow depth produced large CH₄ emissions. Dissolved oxygen and productivity were found to be poor predictors of CH₄ emissions, suggesting a complex combination of factors governed CH₄ fluxes from urban surface waters (Herrero Ortega et al., 2019). Conversely in rivers and lakes within the city of Beijing, high CH₄ emissions were attributed to high dissolved and sediment organic carbon, high aquatic primary production and shallow water depths, although results were again highly variable (Wang et al., 2021a). In the Chaohu Lake basin in eastern China, diffusive CH₄ and N₂O emissions from rivers were due to large nutrient supply and hypoxic environments, with CO₂ impacted by temperature-dependent rapid decomposition of organic matter (Zhang et al., 2021).

A further complication to estimating CH₄ emissions is CH₄ oxidation, with the balance between production and oxidation important for the final release to atmosphere. The percentage oxidation typically varies across waterbody types (Abril and Iversen, 2002) but CH₄ oxidation can deplete half of dissolved CH₄ in high oxygen environments (Robison et al., 2022). The presence of ammonia, entering inland water from agriculture or wastewater, can inhibit CH₄ oxidation resulting in elevated CH₄ concentrations compared to low nitrogen systems and high evasion to atmosphere (Dunfield and Knowles, 1995; Bosse et al., 1993; Cotovicz et al., 2021). Conversely in an investigation of N₂O concentrations upstream and downstream of wastewater treatment plants (UWWTPs) in an urban river in Japan found nitrate concentration increased downstream of the UWWTP with nitrate the crucial factor influencing N₂O saturation (Zhou et al., 2022). Downstream of nine WWTPs in Germany, the concentrations of dissolved CH₄ and CO₂ were enhanced and the atmospheric fluxes of both gases increased by a factor of 1.2 and 8.6, respectively (Alshboul et al., 2016)

Streams have been found to be a significant source of GHG, especially when draining agricultural landscapes (Beaulieu et al., 2008). Positive correlations between GHGs in surface waters and catchment agricultural land cover linked to higher levels of organic matter and dissolved inorganic nitrogen have been found significant, with increases in GHG levels during prolonged low water levels (Borges et al., 2018). While N₂O linked to agriculture is often attributed to run-off, agricultural reaches of rivers had higher N₂O emissions attributed to high nitrate concentrations even in low river flow conditions, but in forested reaches N₂O emissions remained constant or decreased, (Tonina et al., 2021). The combination of high denitrification rates and large anthropogenic DIN inputs has resulted in substantial anthropogenic N₂O emissions from river networks (Beaulieu et al., 2011).

1.7 Anthropogenic causes of GHG in estuarine waters

There is a larger range of uncertainty in estuarine and coastal GHG fluxes compared to those from inland waters, attributed to the paucity of data and the general more dynamic nature of these ecosystems. Human alterations to aquatic ecosystems such as urbanization, eutrophication and positive climate feedbacks act to increase CH₄ emissions (Rosentreter et al., 2021; Borges and Abril, 2012), but the type of estuarine environment may also be important. In fully mixed estuaries CH₄ concentrations are non-linearly correlated with salinity, with the highest CH₄ concentrations observed at low salinity and have been associated with the turbidity maximum zone (TMZ) (Upstill-Goddard et al., 2000; Upstill-Goddard and Barnes, 2016). Methane concentrations in salt wedge estuaries have been found considerably more variable (Middelburg et al., 2002), with distinct zones of elevated GHG concentrations at the tip of the salt wedge and in the anaerobic bottom waters, suggesting acetoclastic production in fresh surface waters and hydrogenotrophic production occurring in the saline bottom waters (Tait et al., 2017). The CH₄ production within the estuarine environment is highly dependent on both in-water and in-sediment processes, with methanogens competing for resources. For example, methanogens can be outcompeted by sulphate reducing bacteria (SRB) where the methanogenesis pathway is using H₂ and acetate, with rates of methanogenesis found to be two orders of magnitude lower than rates of sulphate reduction (Euler et al., 2020; Sela-Adler et al., 2017). Conversely the presence of ammonium may inhibit CH₄ oxidation increasing CH₄ evasion, (Dunfield and Knowles, 1995;

Bosse et al., 1993), especially as estuaries can become hypoxic. Decreased CH₄ concentrations have been observed in higher water flows and assumed to be linked to dilution under the assumption that the net CH₄ production does not change significantly (Bange et al., 2019). Conversely dissolved oxygen (DO) has been found the dominant factor influencing CH₄ fluxes with DO and dissolved organic carbon (DOC) explaining 60% of the variance, (Zheng et al., 2022), although estuarine CH₄ emission patterns need improved understanding.

Coastal ecosystems are recognized as significant carbon reservoirs because of their high carbon burial rates, although these ecosystems also emit CO₂ to the atmosphere. However estuarine and coastal areas often experience significant anthropogenic impact which may impact their efficiency as blue carbon stores, with human-dominated systems often characteristic of systems with higher net carbon uptake (Kuwaie et al., 2016). However arable and (sub)urban estuaries were found to export, on average, 50% more dissolved organic carbon (DOC) to coastal areas than they received from rivers due to net anthropogenic derived organic matter inputs within the estuary, with the bioavailability of this DOC promoting microbial production and degradation (García-martín et al., 2018).

Highly nutrified estuaries, with nutrients derived from run-off and wastewater can act as significant N₂O sources (Robinson et al., 1998; de Angelis and Gordon, 1985; Dong et al., 2005; Nguyen et al., 2022). The balance between nitrification and denitrification, is dependent on residence time, with nitrification dominating during short residence times and denitrification dominating at longer residence times. Denitrification is likely significant in estuaries where residence time can reach months or years (Zarnetske et al., 2011), and oxygen levels can be low (Tang et al., 2022; Li et al., 2022; Brase et al., 2017; Rosamond et al., 2012). Nitrification is reported to occur in both sediments and the water column with water column nitrification dominating in large river-estuary systems especially where there are long residence times associated with suspended sediments and particularly when turbidity maximums occur (Beaulieu et al., 2010; Barnes and Upstill-Goddard, 2011; Murray et al., 2015). Denitrification, a form of anaerobic respiration using NO₃⁻ occurs mostly in anoxic bed sediments and is generally a linear function of the nitrate concentration in the overlying water (Revsbech et al., 2005). Urban estuaries can experience eutrophication due to high nutrients and this can enhance phytoplankton abundance, leading to changes in GHG concentrations. For example the increase in eutrophication status along the dense urban area of the Saigon River Estuary, Vietnam was linearly correlated with increases in GHGs concentrations (Nguyen et al., 2022).

1.8 Hypotheses

GHG emissions from inland and coastal waters are difficult to attribute to sources due to multiple generation and consumption pathways and high spatial and temporal variability (Rosentreter et al., 2021). Their production results from the interplay of multiple drivers and is influenced by significant between and within-system variation. This variation can be especially difficult to predict in estuaries which form a meeting point between marine and freshwater environments, and where the mixing and residence times are influenced by the bathymetry, bed friction, rivers flows and tidal range. The variation in all inland and coastal water causes difficulties in up-scaling emissions from local-scale studies resulting in a need for more detailed studies measuring more in-water parameters across larger temporal and spatial

scales. It is hypothesised, in this research, the reasons for the high variation and poor predictability include:

- a) GHGs are not conserved like dissolved nutrients but readily out-gas especially in the riverine environment with flow intensity and high stream slopes the primary controls (Long et al., 2015; Maurice et al., 2017; Natchimuthu et al., 2017; Liu and Raymond, 2018).
- b) The large number of different source types within the riverine, lentic and estuarine environment, including; point, diffuse, in-water and in sediment generation, change with aquatic environment and present and legacy land-use.
- c) The concentration of nutrients is a partial driver of GHG generation, which changes with the availability of electron donors and acceptors, such that mixing of waters from different sources may stimulate GHG production (Wrage et al., 2001; Furukawa et al., 2004; Broder et al., 2012; Zhang et al., 2019).
- d) Different GHG sources and dynamics dominate in different types and sizes of water body dependent on: land-water interface, depth, hydraulic regime, sediments-water-air interfaces, residence time, land-use, physio-chemical properties, microbial communities, seasonality, salinity, stratification and mixing and anthropogenic impacts on seasonal patterns of changing water level and temperature.
- e) Urban and agricultural rivers and estuaries produce higher levels of GHGs due to the high levels of catchment-scale nutrients.
- f) In inland waters, but particularly in estuaries, the ability of methanogens and (de)nitrifying microorganisms to process carbon and nutrients and produce GHG is dependent not only on carbon and nutrient availability but on both short and long-term changes in estuarine physical conditions; including seasonal, tidal and river flow changes which impact residence time, salinity and mixing and impact the effectiveness of the microorganisms.

1.9 Objectives

Given the high natural variability of riverine and estuarine systems encompassing (1) topographical, bathymetrical and geomorphic variation, (2) hydrological variation including river flow, tidal dynamics and seasonal impacts and (3) variability introduced by urban, agricultural and legacy industry, GHG dynamics from these systems are difficult to predict. However, their significance but inadequate quantification and characterisation, suggest that further insight into the sources and mechanisms of riverine and estuarine GHG concentrations and dynamics could support improved interpretation and evasion estimates. To support increased insights, this study addressed the following key research questions:

- a) Does using a source-to-sea investigative approach allow quantification of how changes in the nature and size of the riverine and estuarine environment impact GHG concentrations?
- b) What are the key catchment-scale (land-cover, seasonal and hydrological) controls on GHG generation in the semi-natural, agricultural and urban environments?
- c) How does the balance between point source, diffuse source, in water and in-sediment generation of GHGs in the riverine and estuarine environments vary temporally and spatially?

- d) How do hydrological and physical drivers (river flow, temperature, tidal regime, salinity, level of stratification, mixing and sedimentation) affect GHG concentrations, fluxes and production mechanisms?
- e) How do anthropogenic changes, including the addition of nutrients from urban wastewater (UWW) and agriculture and the influence of legacy industry contamination, impact GHG generation and dynamics?

To investigate the above objectives a large temperate catchment, where land cover transitioned from semi-natural, through pastoral and arable agricultural to urban (including legacy industrial and coal mining), with a stratified estuary, the Clyde catchment in Scotland, was studied over three hydrological years.

1.10 Scope of this thesis

This introduction, Chapter 1 of this thesis, provides background into the problems of increasing GHG concentrations and focuses on GHGs from aquatic environments to provide context to the challenges of high uncertainty and high temporal and spatial variability in aquatic GHG emissions. It covers the knowledge gaps, hypotheses and the research questions investigated in this work. The second chapter of this thesis is dedicated to the study area under investigation and the methodologies used both within the field to collect the data and within the laboratory to analyse the samples.

Chapter 3 covers the study of the River Clyde and is titled: Urban landscapes and legacy industry provide hotspots for riverine greenhouse gases: a source-to-sea study of the River Clyde, and reports in detail riverine GHG mechanisms and controls. Chapter 4 covers a study of GHGs from mine water (MW) which form significant point sources in the Clyde catchment and is titled: Sources and controls of greenhouse gases and heavy metals in mine water: a continuing climate legacy. This study of MW spans the Midland Valley and is not restricted to the Clyde catchment. Chapter 5 reviews and analyses data on estuarine GHGs from across the UK from previously published work, as this is an area where there is less research compared to that of inland waters and is titled: Anthropogenic-estuarine interactions cause disproportionate greenhouse gas production: a review of the evidence base. Chapter 6 covers a focused and detailed study of the Clyde estuary to answer questions raised in the previous chapter about the mechanisms and controls linked to the high GHG concentrations in estuaries, with a specific focus on the variability of estuarine GHGs. This chapter is titled: The impact of salinity and hypoxia on estuarine greenhouse gases: a study of the stratified Clyde estuary. These four focus areas are shown schematically in Fig 1.4.

The final two chapters of this thesis (Chapters 7 and 8) are dedicated to the assessment and distillation of the key points from this research, building on information from the previous chapters to support the understanding of mechanisms of GHG production from inland waters. There is a focus on key drivers but also on novel aspects of the research and consideration for policy makers. These chapters consider how actions could be taken to support remediation and reduction of GHG emissions in the UK but also globally.

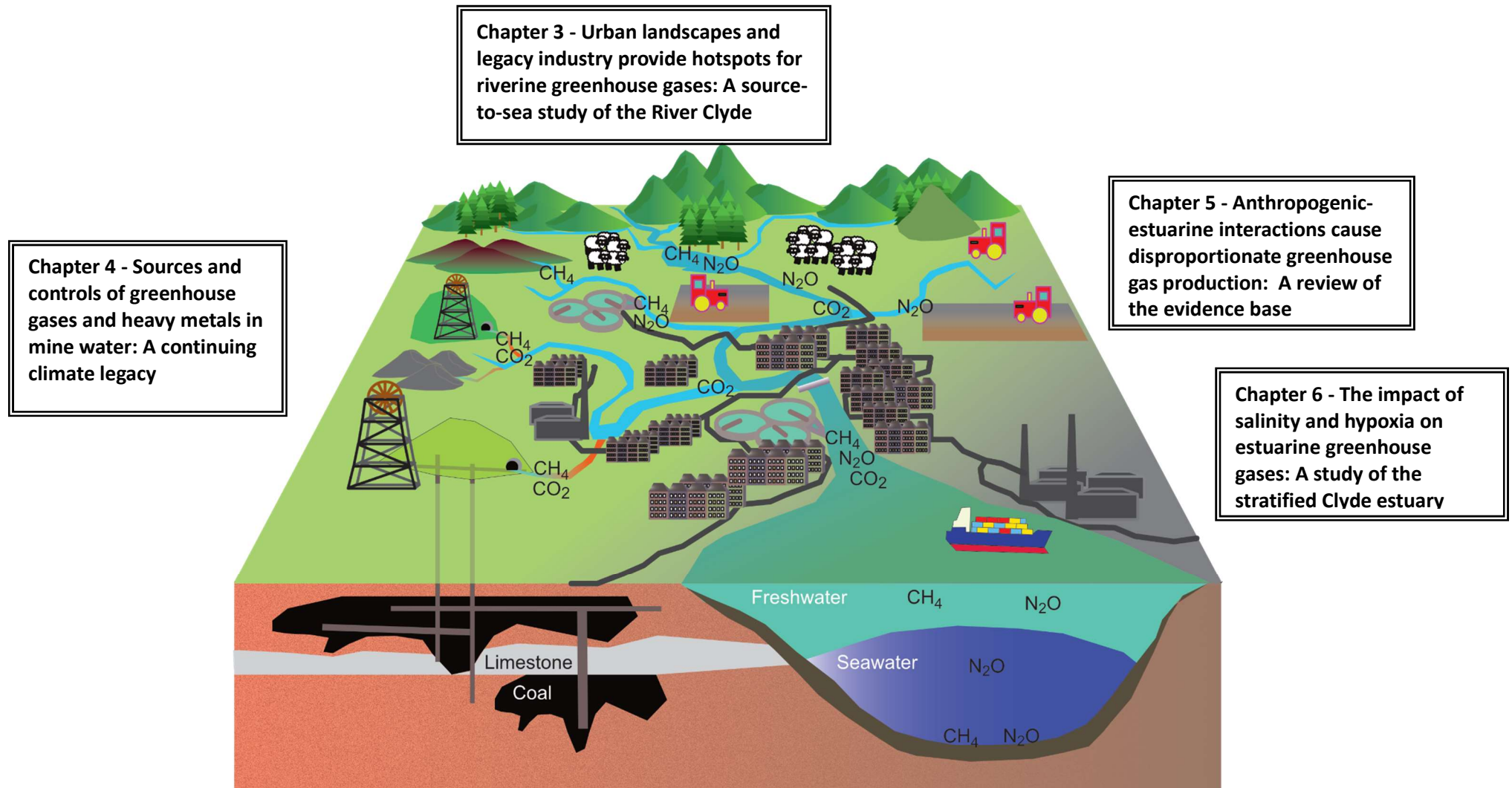


Figure 1.4 - Schematic diagram of sources of greenhouse gases within the Clyde catchment and the chapters which address them in this thesis
Potential sources of GHGs (CO_2 , CH_4 and N_2O) including urban wastewater (UWW), agriculture (pastoral and arable), peat, mine water from flooded coal mines, and in-water / in-sediment processing of nutrients in lakes, streams, rivers and the estuary. Other forms of pollution are likely to enter the streams, rivers and the estuary from roads, UWW, legacy industry (ship building, steel and paper making), legacy coal mining including both mines water and run-off from bings and current industry.

2 Materials and methods

2.1 The Clyde catchment, river and estuary

The River Clyde is the third longest river in Scotland (170 km) with a total river network length of 4,244 km and drains a catchment of 1903 km² (Clyde River Foundation, 2020). The River Clyde together with the rivers Kelvin, White Cart, Black Cart, Gryffe and Leven enter the Clyde estuary, with a catchment area of 3854 km² (Nedwell et al., 2002). The Clyde catchment is home to 33.8 % (1.79 million) of Scotland's total population (Clyde River Foundation, 2020). The River Clyde's mean annual discharge is 48.3 m³ s⁻¹ with the maximum of 560.5 m³ s⁻¹ (24th January 2018) as measured at Daldowie gauging station between 1963 and 2019 (UKCEH, 2020b). The average combined freshwater flow into the Clyde estuary was estimated as 110 m³ s⁻¹, with the 50-year extreme combined flow estimated as 1438 m³ s⁻¹ (Bekic et al., 2005).

The upper moorland catchment consists of steep rough ground with hill pasture and some forestry as the major land use. In the middle catchment there is mixed farming including arable and pastoral with some urban areas and significant urbanisation in the lower catchment. The soil type in the Clyde basin is predominantly controlled by the geology with non-calcareous gleys the dominate soil type over extensive till deposits. Peaty gleys have developed on poorly draining moor in upland areas resulting blanket peat bogs and peaty gley podzols have developed in the more freely draining southern uplands (Fordyce et al., 2017). Surface water quality in the River Clyde, as assessed in accordance with the European water framework directive, ranges from 'High' in some small tributaries to 'Bad' in some urban tributaries, with much of the River Clyde rated as 'Moderate' (SEPA, 2018 and Natural Scotland, 2015). The groundwater quality is also rated as 'Poor', both in the upper catchment in the Leadhills area and the lower urban catchment. A number of anthropogenic pressures affect the Clyde catchment, split into five categories: water quality point source pollution (20%), diffuse source pollution (17%), access for fish migration (46%), flows and levels (13%) and invasive non-native species (4%) (SEPA, 2017). Additionally a global study examining toxic levels of pharmaceuticals in rivers sufficient to pose a threat to the environmental and/or human health, found that the River Clyde was the most polluted in the UK with levels sufficient to cause a threat (Wilkinson et al., 2022).

The Clyde estuary enters the sea on the west coast of Scotland and is considered to have a highly contaminated estuarine environment due to its legacy industrial past, which peaked in the mid-19th century, and the increasing urban population of the City of Glasgow. The estuary has been continually dredged for around 200 years. It is constrained by seawalls and embankments to prevent flooding and estuarine flows are impacted by the construction of docks and jetties (Jones and Ahmed, 2000). Marked improvements in water quality have been seen with the estuary recovering ecologically since peak industrialisation ended. However estuarine sediments still contain high levels of contamination including heavy metals (Hursthouse et al., 2001), with the highest elemental concentrations of Cu, Pb, Co, Cr, Ni, Sb and Zn occurring in the urban estuary and with a large increase occurring between urban river and estuary sediments (Jones et al., 2019; Rodgers et al., 2020; Balls et al., 1997). The Clyde estuary exhibits anomalously high levels of polyaromatic hydrocarbons (PAHs) and polychlorinated biphenyls (PCBs) (Edgar et al., 2003; Edgar et al., 2006; Vane et al., 2007).

Further sources of pollution are linked to legacy industry. The River Clyde flows through the Midland Valley of Scotland, an area of coal bearing rocks that trend from southwest (covering the Ayrshire coast to Glasgow) to the northeast (covering the Edinburgh area and the Fife coast). These carboniferous rocks are bounded by the Highland Boundary Fault to the northwest and the Southern Upland Fault to the southeast (Leslie et al., 2016). The River Clyde and its tributaries below and including Douglas Water and the Clyde estuary are all within the area of coal bearing strata and the remains of an extensive coal mining industry are still evident in the catchment. Water pollution arising from abandoned coal mines is second only to sewage as a source of freshwater pollution in Scotland and in many coalfield catchments it is the dominant pollutant source. Mine water (MW) emerges via old adits (mine drainage passages), springs, seepage through the ground, and sometimes discharges into overlying aquifers polluting groundwater. Most MW pollution is from deep mines rather than opencast (Younger, 2001). Water from disused coal mines can contain high concentrations of Fe, Zn, Cu, Pb, Ca, Mn and Al (Dhir, 2018; Alhamed and Wohnlich, 2014; Stearns et al., 2005). These abandoned flooded coal mines and other legacy industrial activities including steel and paper making and shipbuilding in the estuary were also potential sources of legacy pollution. For example, the demolition and clean-up operation of Ravenscraig steel works has created the largest brownfield site in Europe (Canmore, 2022). The Clyde estuary has been reported to have high levels of GHGs but the sources are unknown (Pickard et al., 2021). A schematic of the potential sources of GHG in the Clyde catchment is shown in Fig. 1.4.

2.2 Site descriptions and data collection

Three major and some minor data collection campaigns were undertaken to quantify aquatic GHGs in the Clyde catchment, including primarily the riverine, estuarine and mine waters systems, with some overlap between the three sampling campaigns. These are described in the sections below.

2.2.1 Riverine sampling

Twenty-six measurement locations were selected on the River Clyde and its major tributaries and two locations within the upper Clyde estuary as part of a source-to-sea study. The source of the River Clyde is most likely the stream of Thick Cleuch, arising between Wedder Law and Gana Hill to the south of Dear reservoir, with the highest point in the Clyde catchment that of Lowther Hill at 725m. The Clyde reaches the estuary at the tidal weir, which separates the two distinct habitats of fresh and salt water and is designed to stabilise the upstream banks by maintaining the water level and preventing saline intrusion to the riverine environment. The twenty-six riverine locations were distributed along the River Clyde from near the source, on Daer Water above Daer reservoir, to Glasgow Green just above the Clyde tidal weir, with estuarine measurements made from the Govern and Breahead pontoons.

Sample locations on the River Clyde and its tributaries were aligned with the Scottish Environmental Protection Agency (SEPA) gauging stations where possible (Scottish Environment Protection Agency, 2020b); although not all measurements were made exactly at the gauging stations. In addition to the locations on the River Clyde all major tributaries and some minor tributaries were sampled, typically near to where they entered the main river. Sampling points on the River Clyde were selected to be between the locations where the major tributaries entered the river. Details of all the sample locations are included in Table

2.1 and Fig. 2.1 and photographs are included in Appendix 1. Samples were collected monthly between January 2020 and December 2021 at all locations. Twenty-one sampling campaigns were undertaken in total, as no sampling was permitted during the period April to June 2020 due to Covid-19 related working restrictions. Each sampling campaign was undertaken over two consecutive days with samples collected at the upper catchment sites on day 1 and in the lower catchment on day 2, with sample filtration and processing being undertaken on the same day the samples were collected. Sampling included water physical properties (temperature (T_w), conductivity (EC), pH and dissolved oxygen (DO)), GHG concentrations, dissolved organic carbon (DOC), dissolved inorganic carbon (DIC), total dissolved nitrogen (TDN), total phosphorus (TP), specific ultra violet absorption at 254nm ($SUVA_{254}$) and a range of anion and cation concentrations.

Table 2.1 - Sampling locations in the Clyde catchment

No.	Location code ⁽¹⁾	Latitude (N) (WGS84)	Longitude (W) (WGS84)	Distance (km) ⁽²⁾	River Name
1	T1	55°19'56.44"	3°38'08.02"	<i>0.0</i>	Rodger Cleuch
2	C2	55°20'00.96"	3°38'04.20"	0.2	Daer Water - reservoir inflow
3	C3	55°22'06.79"	3°37'34.25"	5.5	Daer Water - reservoir outflow
4	T4	55°28'28.53"	3°38'52.72"	<i>23.2</i>	Midlock Water
5	T5	55°28'29.37"	3°39'07.95"	<i>23.5</i>	Camps Water
6	T6	55°30'58.10"	3°41'18.84"	<i>31.5</i>	Duneaton Water at Maidencots
7	C7	55°31'20.99"	3°40'42.80"	32.4	Clyde at Abington
8	C8	55°36'33.59"	3°33'32.49"	46.7	Clyde at the Symington
9	C9	55°39'16.25"	3°43'34.40"	72.4	Clyde at Sills of Clyde
10	T10	55°34'49.81"	3°49'00.88"	<i>76.0</i>	Douglas Water at Happendon
11	C11	55°38'39.72"	3°45'41.24"	77.1	Clyde at Tulliford Mill
12	C12	55°40'31.87"	3°48'01.43"	82.4	Clyde at Kirkfieldbank
26	T13	55°40'40.62"	3°48'00.19"	<i>82.7</i>	Mouse Water
13	C14	55°41'51.18"	3°52'01.15"	88.1	Clyde at Hazelbank
14	T15	55°39'59.08"	3°53'55.87"	<i>89.0</i>	Nethan at Kirkmuirhill
15	C16	55°44'15.42"	3°55'22.74"	96.1	Clyde at Garrion bridge
16	T17	55°44'02.77"	3°59'17.37"	<i>107.6</i>	Avon Water at Fairholm
17	C18	55°47'00.03"	4°00'52.94"	108.0	Clyde at Hamilton
19	C19	55°48'28.82"	4°00'40.44"	<i>108.2</i>	South Calder Water
18	L20	55°47'08.93"	4°01'13.92"	<i>108.2</i>	Strathclyde Loch
20	C21	55°47'43.72"	4°03'28.24"	111.7	Clyde at Blairston
22	T22	55°50'12.02"	4°06'26.31"	<i>119.0</i>	North Calder at Calderpark
21	T23	55°49'05.51"	4°06'34.46"	<i>119.8</i>	Rotten Calder at Redless
23	C24	55°49'47.78"	4°07'19.11"	120.6	Clyde at Daldowie
24	C25	55°49'24.01"	4°10'16.21"	124.1	Clyde at Cambuslang
25	C26	55°51'00.14"	4°14'25.07"	134.0	Clyde at Glasgow Green
27	E27	55°51'51.01"	4°18'32.40"	138.7	Clyde estuary at Govan Pontoon
28	E28	55°52'33.40"	4°21'37.20"	142.2	Clyde estuary at Breahead Pontoon

Notes

1. The location code has the initial letter 'C' to indicate the River Clyde, 'T' to indicate a tributary, 'L' to indicate where the tributary is direct inflow to the River Clyde from a loch and 'E' to indicate the estuary.
2. Distance is the distance from the first measurements point nearest the source increasing towards the sea. Tributary distances are given as the distance at which they enter the River Clyde and are in italics.
3. Further details of each location are included in the chapter 3 supplementary information and Appendix 1.

2.2.2 Mine water sampling

Mine water locations identified in the Clyde catchment only (8 locations) were sampled quarterly between July 2021 and March 2021 as these locations were identified as interesting

point source locations for GHGs and other pollutants. This initial study resulted in information about the concentrations and variability of GHGs in MW and was developed into the more detailed study undertaken in the summer of 2022. In this study sixteen sites (MA1 - MA16), across the Midland Valley, Scotland were sampled for water physiochemical properties (T_w , EC, pH and DO), GHG concentrations, DOC, DIC, TDN and $SUVA_{254}$ and various ion concentrations. Additional sample collection was undertaken for carbon stable and radiogenic isotopes of the dissolved CO_2 and CH_4 , to help determine the GHG sources and for metal concentrations by inductively coupled plasma mass spectrometry (IPC-MS). Details of all the sample locations are included in Table 2.2 and Fig. 2.1 and photographs are included in Appendix 2. Additionally, four treatment locations, two using cascades (MA7 and MA10) and two using peroxide (MA11 and MA12), were sampled throughout their treatment reed pools to determine the impact of treatment on both GHG processing and heavy metal removal.

To understand out-gassing in the cascade systems, one system MA7, which had the most efficient oxygenation cascade, was sampled throughout the cascade. This cascade had 71 steps, each with a length of 0.76 m and a drop of 0.16 m (an overall drop of around 12m over 55m) with the water taking 65 seconds to traverse the cascade. Study of this system enabled the effect of oxygenation and out-gassing to be determined for GHG concentrations including changes to the carbonate balance and its impact CO_2 concentrations. Water samples could not be measured directly within the cascade but collected by bucket every 11 steps throughout the cascade. Sample collection caused some additional turbulence and likely caused more out-gassing, but it is assumed this effect was the same at each measurement point. Sampling included water physical properties (T_w , EC, pH and DO), GHG concentrations, DOC, DIC, TDN.

Table 2.2 - Mine water outflow sampling locations

No.	Location code (1)	Latitude (N) (WGS84)	Longitude (W) (WGS84)	Height (m asl)	Mine or mine water locations name
1	MA1	56°14'45.06"N	2°51'56.68"W	145m	Lathallan Mill
2	MA2	56° 9'30.24"N	3°38'36.52"W	35m	Mains of Blairingone
3	MA3	56° 8'20.60"N	3°16'51.52"W	75m	Minto - Adjacent Shaft
4	MA4	56° 8'1.15"N	3° 6'45.45"W	50m	Frances
5	MA5	56° 3'36.90"N	3°30'6.14"W	40m	Pitferrane
6	MA6	55°53'38.10"N	3° 3'40.39"W	35m	Bilston (Old Fordell)
7	MA7	55°50'53.67"N	3°36'49.78"W	175m	Cuthill
8	MA8	55°49'3.96"N	3°47'40.92"W	200m	Shotts
9	MA9	55°47'59.39"N	3°48'50.64"W	200m	East Allerton
10	MA10	55°47'43.31"N	3°49'40.28"W	200m	Kingshill
11	MA11	55°46'15.03"N	3°37'0.78"W	240m	Pool Farm
12	MA12	55°45'40.04"N	3°40'36.95"W	260m	Mousewater
13	MA13	55°36'57.91"N	3°52'49.97"W	210m	Johnhill burn
14	MA14	55°35'58.21"N	3°53'24.73"W	225	Muirburn
15	MA15	55°31'26.18"N	3°52'32.54"W	225	Glentaggart
16	MA16	55°30'43.73"N	4° 5'3.35"W	215m	Kames - Adjacent Shaft

Notes

1. Locations code: MA indicates this survey (Mine Adits) and the location number from 1 to 16 represents the position in this survey, with 1 furthest north and the 16 furthest south.
2. Further details of each location are included in the chapter 4 supplementary information and Appendix 2.

2.2.3 Estuarine sampling

Ten measurement locations were selected on the Clyde estuary (L1 to L10). These were distributed from near the tidal weir (L1), which separated the two distinct habitats of fresh and salt water (this enabled a definite location for the start of estuarine conditions to be identified independent of river flow and tidal conditions) and the location where the estuary widened as it joined the Irish Sea near Dumbarton (L10). Sample locations on the Clyde estuary were selected to provide an understanding of how location, salinity, river flow and stratification impacted the project objectives. As such, the spacing between sampling locations increased seawards as the estuary became more homogenised, enabling more detailed GHG concentration data to be collected in the lower salinity upper estuary. Details of all the sample locations are included in Table 2.3 and Fig. 2.1 and photographs are included in Appendix 3. Samples were collected on eight occasions between September 2021 and May 2022, with details in Table 2.4. Each survey was undertaken so that sampling started at high tide at the head of the estuary with sampling on the ebb tide. Sample filtration and processing was undertaken on the same day the samples were collected. Samples were collected at the surface using a 10 L bucket and 0.5m above the bed using a 5L water depth sampler, triggered by a dropped weight. The Clyde estuary is periodically dredged for shipping seawards of location L5, and locations were selected to be at the side of the main dredged channel, both to avoid the dredged area and for ease of handling the sampler, resulting in the maximum water depth sampled of 12m. The estuary landward the L3 typically had water depths less than 6m.

Table 2.3 - Sampling locations for the Clyde estuary transects (CET)

No.	Location code ⁽¹⁾	Latitude (N) (WGS84)	Longitude (W) (WGS84)	Distance from tidal weir (km)	Gaps between Locations (km)	Location Information
1	L1	55.853931°	-4.251681°	0.43	0.43	Most upstream point
2	L2	55.856082°	-4.273576°	1.85	1.42	Adjacent M8 motorway
3	L3	55.861379°	-4.297750°	3.51	1.66	Bend and restriction
4	L4	55.867974°	-4.318569°	5.00	1.49	Adjacent the SEPA Buoy
5	L5	55.868900°	-4.339734°	6.35	1.35	Shieldhall UWWTP
6	L6	55.876932°	-4.360132°	7.88	1.53	Breahead pontoon
7	L7	55.888767°	-4.390125°	10.2	2.14	Scrap metal working
8	L8	55.908154°	-4.444381°	14.35	4.14	Dalmuir UWWTP
9	L9	55.929253°	-4.487592°	18.0	3.65	Adjacent Bowling
10	L10	55.932344°	-4.575588°	23.5	5.50	Offshore from R. Leven

Notes

1. Distance is from the tidal weir to the measurements point, with distance between locations increasing seawards
2. Further details of each location are included in the supplementary information and Appendix 3.
3. The River Kelvin enters the estuary between L3 and L4
4. The Rivers White Cart and Black Cart enter the estuary between L7 and L8
5. The River Leven enters the estuary adjacent L10

Table 2.4 - Sampling dates in the Clyde estuary - Estuary Transects (CET)

No.	Survey code ⁽¹⁾	Date	Survey start time (GMT)	Surface Water Temperature ⁽²⁾ (°C)	Time of High tide (GMT)	Tidal range (m)	River Flow at high tide (m ³ /s)	Comments
1	CET1	21-Sep-21	13:00	16.4 - 15.6	13:10	3.86	10.8	All locations
2	CET2	15-Oct-21	08:50	11.7 - 12.1	08:10	1.73	16.0	All locations
3	CET3	21-Oct-21	12:40	11.2 - 11.5	13:20	3.82	29.0	All locations
4	CET4	22-Nov-21	12:51	7.3 - 8.7	14:20	3.45	26.6	All locations
5	CET5	29-Mar-22	10:50	10.4 - 9.8	11:00	3.29	17.4	All locations
6	CET6	13-Apr-22	10:20	9.2 - 10.4	10:30	2.29	22.3	Locations 1 to 8
7	CET7	25-May-22	09:30	14.7 - 15.4	08:50	3.09	13.1	Locations 1 to 4
8	CET8	31-May-22	12:40	15.4 - 14.5	13:30	3.45	10.5	Locations 1 to 8

Notes

1. The survey code has the letters CET, for Clyde Estuary Transect.
2. The sea water temperature is presented as that for L1 and then for L10 for the surface data only
3. The river flow data is taken at Daldowie SEPA gauge and is indicated for the time of the survey start, (UKCEH, 2020b)
4. The tidal range is taken from a harmonic analysis of the tidal data and Renfrew tide gauge which is located at Latitude 55.885812°N, Longitude -4.3828324 West (Scottish Environment Protection Agency, 2020b). This is closest to location L7.
5. The time of high tide was used as a guide for the start of the survey.
6. In the last three surveys, some locations could not be reached due to rough weather.

To understand the impact of short-term variation, measurements were made through a tidal cycle, from a single location, the Braehead pontoon (CEP), selected to be in the middle of the inner Clyde estuary where a range of salinities could be observed. Surveys were undertaken to cover a tidal cycle, but sampling times were changed relative to high tide to cover both ebb and flood tides when possible. Samples were collected at the surface, by a 10 L bucket and 0.5m above the bed using a 5 L water depth sampler, with sample filtrations and processing occurring on the day after the samples were collected due to the extended nature of the survey. The Braehead pontoon is 7.9 km from the tidal weir and located on the south bank of the estuary and extends about 25m into the estuary, which is about 150m wide at this location. Measurements were made from the north side in the middle of the pontoon (latitude 55.876932°N and longitude 4.360132°W). The Braehead pontoon is the same location as CET L6 in the estuary transects survey (Table 2.3) and the most seaward estuary location measured in the source-to-sea survey (E28) (Table 2.1), making a larger number of independent data points available for this location. The water depth at this location varied between 3m and 7m (dependent on the tidal cycle). The estuary is periodically dredged, and the last known dredging activity occurred in the summer of 2020, and was ongoing during the first survey (August 2020) reported here. Samples were collected on seven occasions between August 2020 and May 2022. Details of the survey dates and river and tidal conditions on these dates are included in Table 2.5 with photographs of the location and adjacent outfall in Appendix 3. Estuarine sampling included water physical properties (T_w , EC, pH and DO), GHG concentrations, DOC, DIC, TDN, TP, NO_3^- , NO_2^- and NH_4^+ and SUVA_{254} . CO_2 and CH_4 evasion data were measured using an ABB Microportable Gas Analyser GLA131 Series (GGA) in the CEP6 and CEP7 surveys.

Table 2.5 - Sampling dates in the Clyde estuary - tidal cycle (CEP)

No.	Survey code ⁽¹⁾	Date	Survey time (GMT)	Average Surface Temp ⁽²⁾ (°C)	Time of High tide (GMT)	Tidal range (m)	River Flow at mid survey (m ³ /s)	Comments
1	CEP1	13-Aug-20	06:00 - 18:30	18.1	06:30	2.23	33.8	Surface only
2	CEP2	25-Feb-21	06:15 - 16:00	7.3	11:50	2.94	106.6	Surface and bed
3	CEP3	28-Mar-21	06:15 - 15:15	8.2	12:50	4.40	56.8	Surface and bed
4	CEP4	29-Jun-21	06:00 - 16:30	19.0	16:10	4.35	8.1	Surface and bed
5	CEP5	24-Aug-21	05:30 - 15:30	17.9	14:10	4.06	10.0	Surface and bed
6	CEP6	15-Mar-22	08:00 - 17:00	7.5	11:20	2.63	99.8	Surface, bed, evasion
7	CEP7	08-May-22	08:00 - 17:00	14.4	17:20	2.00	14.3	Surface, bed, evasion

Notes

1. The survey code has the letters CEP, for Clyde Estuary Pontoon
2. The sea water temperature is presented as the average surface temperature measured across the survey
3. The river flow data is taken at Daldowie SEPA gauge and is indicated for the time of mid-point of the survey (UKCEH, 2020b)
4. The tidal range is taken from a harmonic analysis of the Renfrew tide gauge which is located at Latitude 55.875908°N, Longitude 4.360176°4 West (Scottish Environment Protection Agency, 2020b), 3.4km seawards of the survey location
5. The surveys were undertaken across both ebb and flood tides. The tidal range is given for the tide most encompassed in the survey, however there is considerable asymmetry across the semi-diurnal tides on the Clyde.

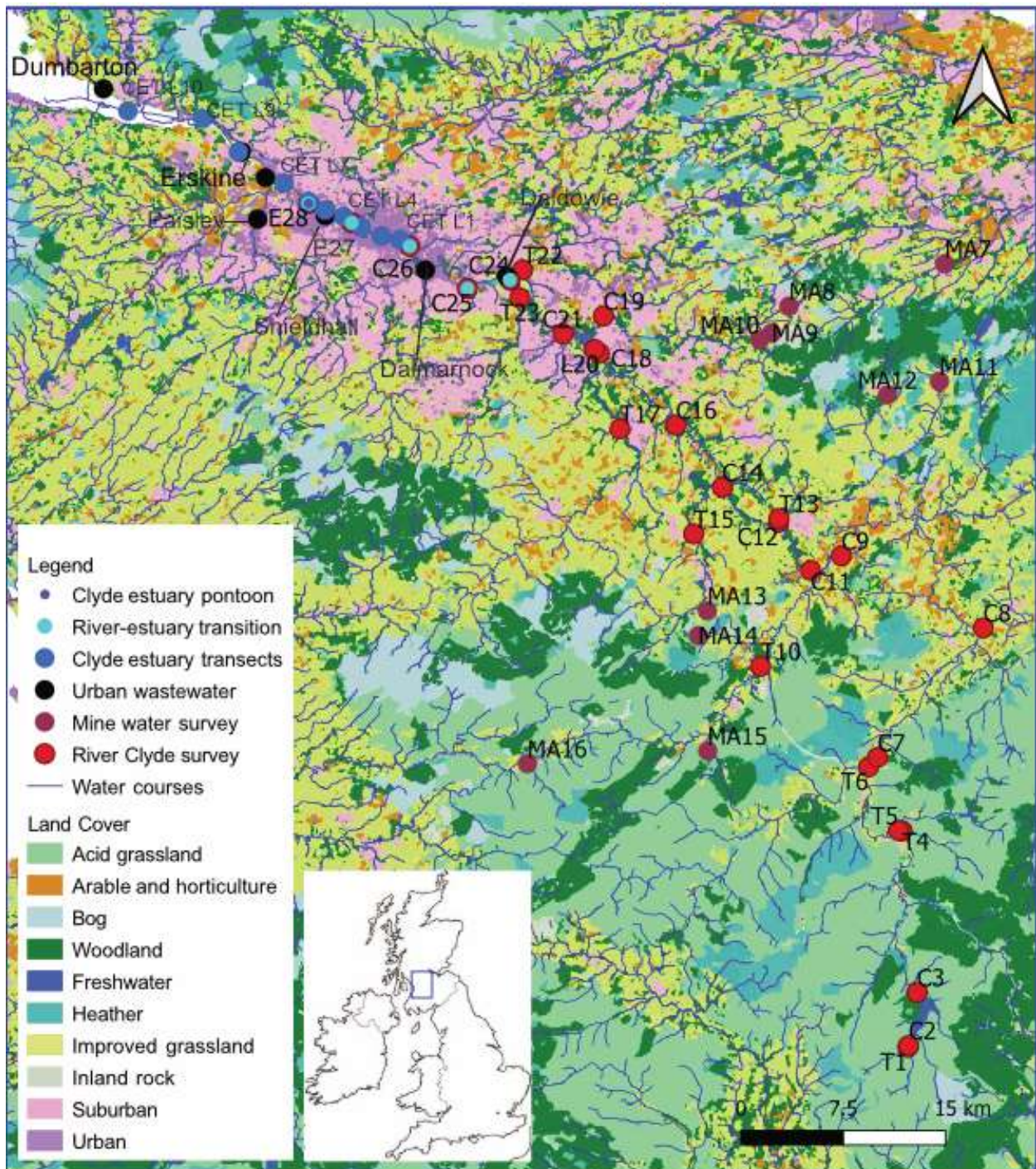


Figure 2.1 - Map of all locations for riverine, estuarine and mine water sampling

Locations of the Clyde source-to-sea survey are numbered 1 to 28 and denoted 'C' for Clyde, 'T' for tributary, 'L' for loch and 'E' for estuary (Chapter 3). Locations denoted MA relate to the mine water survey. MA1 - 6 are not included on this map and further details are provided in Figure 4.2 (Chapter 4). CET1 to CET10 related to the Clyde estuary transect with points going seaward estuary (Chapter 6). CEP related to the Clyde estuary pontoon survey and is the same locations as CET L6, E27 (Chapter 6). The Clyde river-estuary transition CRE1 to 5 (Chapter 6) are the same as C23, C24, C25, E26 and E27.

2.3 Sampling regimes

For all surface locations in the River Clyde, Clyde estuary and for MW, water samples were collected in a ten-litre plastic bucket and no measurements were made directly in the river, stream, outflow or estuary. Samples were either collected from the river bank, pontoon, or side of the boat and in the cases for river locations from a bridge by lowering the bucket. Bridges provided a safe and effective access point. For samples collected near-bed in the estuary both from the power boat and pontoon, samples were collected after first measuring the water depth and then lowering a hand-held water depth sampler to 0.5m above the bed. The sampler was pulled through the water at depth for at least 30 seconds, to ensure the water collected was from the desired depth, before a weight was dropped to trigger the sampler to close. If the sampler hit the bottom the sample was discarded and then retaken to avoid sediment entering the water sampler or sampling near a disturbed bed. These samples were used for all sub-samples.

Dissolved gas samples were collected in triplicate at each location using the headspace method prior to the collected water being disturbed by other measurements together with ambient air samples (Billett and Moore, 2008). While ambient air samples were collected at a consistent height for each location, it was not possible for the height of the ambient air samples above the water surface to be consistent as, for example, some samples were collected from the riverbank while other samples from bridges. Headspace samples were collected using three 200 ml syringes fitted with a 3-way valve, with 100ml of water and 100ml of air being drawn into the syringe and the syringes shaken vigorously for 60 seconds to equilibrate the gas concentrations. The air sample was injected into pre-sealed rubber plugged 20 ml glass vials, using a needle and excess sample being used to flush the vial via an outlet needle. Both needles were removed quickly to prevent any loss from the vial. A 100ml air sample was injected into another rubber plugged 20 ml glass vial. While care was taken to avoid water getting into the glass vials this did sometimes occur.

Dissolved oxygen saturation (DO%), DO, EC and T_w were measured in the sample, taken at 10 cm below the water surface using a HQ40d Multi portable meter (Hach) with a Intellical CDC401 Laboratory 4-Poles Graphite Conductivity Cell, a Intellical LDO101 Laboratory Luminescent / Optical Dissolved Oxygen and a PHC10101 Combined pH electrode. Time was given to ensure sensor equilibrium. A two-litre bottle (plastic) was filled with water from the bucket for later analysis and these were kept in a cool box until they were returned to the lab for processing.

CO₂ and CH₄ evasion data were measured using an ABB Microportable Gas Analyser GLA131 Series (GGA). The GGA was connected via plastics tubes to a floating chamber covered in aluminium foil to prevent warming in a recirculation mode. The floating chamber was deployed on the estuary about 2m from the pontoon and measurements were made in triplicate for 3 minutes at each measurement time for CEP6 and CEP7 (See Appendix 3). The rate of evasion was calculated by accounting for the volume of the chamber and tubes and the surface area of the chamber on the water surface. The period of 3 minutes was selected as it was found that after three minutes the evasion rate decreased, and the relationship became non-linear. It was assumed that this was due to GHG building up in the chamber head space, impacting the head space saturation and equilibrium processes. While the chamber, with a

volume of 6.5 litres and a surface area of 0.071m², was relatively small, it could potentially block the direct effect of wind, reducing evasion rates. However, it was observed that the evasion rate responded rapidly to changes in wind speed, so any shielding was considered minimal. Wind speeds during these surveys were light. In high wind speeds, wind generated waves could cause the chamber to lift releasing any gases collected in the headspace, as such this method was not suitable for measuring evasion rates during high wind and waves. Wind speed measurements at 2m above the pontoon were made to support the evasion data.

Collection of samples for radiogenic and stable carbon isotope analysis of the dissolved CO₂ and CH₄ required processing of between 10 and 70 litres of water, dependent on the CH₄ concentration, to ensure at least 2mg of carbon was available. This was approached by using an accordion water container from which all air was removed, and any CO₂ stripped from the residual air using soda lime. A pump was used to gently fill the container to minimise degassing with between 5 and 6 litres of water and the volume ascertained using a balance. One litre of air, stripped of the CO₂, was added to the water container and the container shaken for 2 minutes to ensure maximum movement of GHGs to the headspace. The air sample was then pumped into gas tight bags for analysis (Garnett et al., 2016).

2.4 Analytical methods

The headspace samples were analysed using an Agilent 7890B gas chromatograph (GC) and 7697A headspace auto-sampler (Agilent, Santa Clara, California). Gas samples were typically run the next day and always within 1 week of collection. The equipment and method were set up to determine concentrations of CO₂, CH₄ and N₂O and concentrations were calculated by running gas vials containing four mixed gas standards prepared in a consistent way to the ambient air samples. The concentrations of the standards gases were: 1.12 to 98.2 ppm for CH₄, 202 to 5253 ppm for CO₂ and 0.208 to 1.04 ppm for N₂O. Typically, five sets of each of the four mixed gas standards were included within each gas chromatography run, and even for a short run a minimum of three sets of mixed gas standards were included.

The water samples were filtered on return to the laboratory on the same day as the samples were collected, except for the pontoon estuary surveys where samples were filtered on the following day. Filtration was through a Whatman GF/F 0.7 µm, 47 mm diameter filter paper, using a Nalgene filtration unit and an electric vacuum pump. These sub-samples were used for analysis of: total dissolved nitrogen (TDN), total dissolved carbon (TDC) dissolved organic carbon (DOC) and for ion chromatography and spectrophotometry and nitrite-N, nitrate-N, and ammonia-N. Total phosphorus (TP) was measured from unfiltered samples. Metals analysis by ICP-MS was applied to both filtered and unfiltered water samples.

Analysis for TDN, TDC and DOC were undertaken using a Shimadzu TOC-L series Total Organic Carbon Analyser. The system was calibrated by running three or four standards for each of TDN, TDC and DOC at the start and end of each machine run. All samples from each survey were run together and samples were run either on the same day or the day after the survey. Where samples were run the following day, they were refrigerated. For the Clyde riverine survey day 1, samples were refrigerated for approximately 24 hours until the samples from day 2 were available. The difference between TDC and DOC was used to calculate dissolved inorganic carbon (DIC). The filtration resulted in out-gassing of gases including CO₂ raising the

pH, such that most DIC measured by this method was in the form of bicarbonate and will underestimate the total DIC (bicarbonate plus CO₂) in the original stream waters.

Absorbance at 254 nm was measured using a Perkin Elmer LAMBDA® 365 UV/Vis Spectrophotometer to evaluate the Specific Ultraviolet Absorbance (SUVA). The SUVA, determined at 254 nm (SUVA₂₅₄) is strongly correlated with percent aromaticity, which is important in assessing the nature or chemical composition of DOC in the water samples. A low SUVA₂₅₄ indicates a smaller portion of aromatic humic matter present and can be used as an indicator of the anthropogenic impact. Land cover linked to nutrient concentrations and the density of humans have been found to impact humic composition (Williams et al., 2016). Sample pH, nitrate, and iron can also influence SUVA measurements (Weishaar et al., 2003).

Ion chromatography using a Metrohm 930 Compact IC Flex was undertaken to determine both anion and cation concentrations in filtered water samples from the river Clyde and mine water locations. This technique was not used for the highly saline estuary samples due to the risk of damage to the column. A mixed ion standard containing 11000ppm chloride (Cl⁻), 5000ppm nitrate (NO₃⁻), 4000ppm sulphate (SO₄⁻), 10000ppm sodium (Na⁺), 5000ppm ammonium (NH₄⁺), 1000ppm potassium (K⁺), 1000ppm calcium (Ca⁺²) and 1000ppm magnesium (Mg⁺²), was diluted to make 7 standard solutions for the calibration. These included dilutions of 0.1:100, 0.5:100, 1:100, 2:100, 5:100, 10:100, and 25:100. For the mine water samples 8 standard solutions were used including an additional dilution of 50:100. Due to the availability of the equipment some samples were frozen and then thawed before they were run while other samples were run after being refrigerated, usually for 24 hours after the survey was completed. All sample points from each survey were run together. In some conditions concentrations exceeded the top standard. These included Cl⁻ and Na⁺ after winter road salting and particularly Ca⁺² and Mg⁺² in the urban tributaries during dry weather, which are influenced by legacy industry and from mine water. When concentrations of Na⁺ were high, the Na⁺ peak dominated the NH₄⁺ peak and no NH₄⁺ concentration data could be obtained.

Total phosphorous (TP) was measured using a SEAL AQ2 analyser. Samples were measured in the unfiltered state, and all had been preserved by freezing before analysis. The samples were prepared by using potassium persulfate (K₂S₂O₈) acid hydrolysis digestion to convert all forms of phosphorous into orthophosphate. Phosphorous concentrations in the digested samples were then determined according to the acid-molybdenum-blue colorimetric method. Colorimetric determination of orthophosphate in water relies on the reaction of orthophosphate with ammonium molybdate ((NH₄)₆Mo₇O₂₄·4H₂O) and potassium antimony tartrate (C₈H₄K₂O₁₂Sb₂) in acid solution (H₂SO₄). The yellow phospho-molybdate complex formed during the reaction is reduced with ascorbic acid (C₆H₈O₆) to a more stable blue complex. The intensity of the blue colour is proportional to the concentration of orthophosphate present in solution and can be measured using colorimetry. Four standards were included in each run for calibration of between 0.025 to 0.20 mg P L⁻¹. Where concentrations exceeded the top standard, the machine diluted and re-measured the sample.

Nitrite-N, nitrate-N, and ammonia-N were measured using a SEAL AQ2 analyser for the estuary samples. Samples were filtered before measurement and had been preserved by freezing before analysis. The nitrite-N was determined through the formation of a redish-purple azo dye produced at pH 2-2.5 by coupling disazotised sulphanimide with *N*- (1-

naphthyl)-ethylenediamine dihydrochloride (NEDD). The absorbance of the resulting compound was measured spectrophotometrically at 520nm. The nitrate-N was measured by mixing the sample with a pH buffer and transferring the sample to a copper coated cadmium coil, where the nitrate was chemically reduced to nitrite. The chemically reduced sample was then mixed with a colour reagent by coupling disazotised sulphanimide with NEDD. The absorbance of the resulting compound was measured spectrophotometrically at 520nm, as for nitrite-N. The amount of nitrate-N was determined by subtracting the original nitrite value determined in the first test. Ammonia-N was measured by increasing the pH of the sample to above pH 12. This enabled any ammonia in the samples to react with hypochlorite to form chloramine. This was then reacted with alkaline phenol in the presence of nitroferricyanide. The sample was incubated to form a blue indophenol dye and the absorbance of the resulting compound was measured spectrophotometrically at 660nm. Where concentrations exceeded the top standard, the machine diluted and re-measured the sample. One possible interference with the determination of ammonia-N by this technique was that dissolved calcium and magnesium may form a precipitation under the alkaline conditions causing a positive bias, which can occur when water salinity approached that of seawater. Stable and radiogenic carbon isotopes were measured as by the National Environmental Isotope Laboratory at East Kilbride (NEIF Grant 2513.0422).

ICP-MS was conducted by Edinburgh University on both filtered and unfiltered samples to determine concentrations of a large range of heavy metals. Samples were acidified with 1% nitric acid prior to measurement. An Agilent 7900 ICP-MS was used to produce a semi-quant scan of each sample in addition to the full quant data for all elements of interest including: Li, Be, B, Na, Mg, Al, Si, P, K, Ca, Ti, V, Cr, Mn, Fe, Co, Ni, Cu, Zn, Ga, As, Se, Rb, Sr, Nb, Mo, Ag, Cd, Sb, Cs, TA, Hg, Pb and U. Multi-element calibrations were run at 6 dilutions at the start of the run and then every 15 samples.

2.5 Gas partial pressures

To calculate dissolved gas concentrations and partial pressures from the headspace equilibration method the following mass-balance equation was applied (Hamilton, 2006).

$$(C_{O_{liq}}).(V_{liq}) + (C_{O_{gas}}).(V_{gas}) = (C_{liq}).(V_{liq}) + (C_{gas}).(V_{gas}) \quad (\text{eq. 1})$$

Where: $C_{O_{liq}}$ and $C_{O_{gas}}$ are the original gas concentration, C_{liq} and C_{gas} are the concentrations in the liquid and gas phases after equilibration (shaking) and V_{liq} and V_{gas} are the volumes of the liquid and gas in the syringe (assumed to be the same before and after shaking). Assuming equilibrium inside the vessel then C_{liq} can be replaced by:

$$C_{liq} = P_{gas} \cdot \beta_T \cdot P_{BAR} \quad (\text{eq. 2})$$

Where: P_{BAR} is the barometric pressure at the measurement time and altitude, P_{gas} is the partial pressure in the gas phase, β_T is the Bunsen solubility coefficient (Wanninkhof, 2014) as a function of temperature. This can be rearranged:

$$(C_{O_{liq}}) = (P_{gas} \cdot \beta_T \cdot P_{BAR}) + (C_{gas} - C_{O_{gas}}).(V_{gas})/(V_{liq}) \quad (\text{eq. 3})$$

This gas concentration in $\mu\text{moles/L}$ can be converted to units of ppmv using the Ideal Gas Law, where $\text{ppmv} = (\mu\text{moles/L}).(RT)$, where R is the gas constant and T temperature in Kelvin.

This method is effective for CH₄ and N₂O but can lead to errors in CO₂ estimates as dissolved CO₂ is in dynamic chemical equilibrium with other carbonate species. The error incurred by headspace analysis of CO₂ is less than 5% for typical samples from boreal systems which have low alkalinity (<900 μmolL⁻¹), with pH <7.5, and high pCO₂ (>1000 μatm). This was the case for 98% of the samples in the River Clyde and tributaries. The lower Clyde tributaries, with both higher alkalinity and pH, were estimated as having errors reaching 10% (Koschorreck et al., 2021). The mine water samples all had pH < 6.5 and high pCO₂ so errors were less than 5% so this method could be applied. The estuary samples had both higher pH and had high alkalinity and while all samples had high pCO₂, CO₂ estimates would be expected to have higher errors in this environment.

2.6 Acknowledgements

- I. Field data collection for the River Clyde, mine water and estuary collected from the pontoon were primarily collected by Alison Brown working alone.
- II. Dr Amy Pickard and Dr Peter Heyes participated in initial surveys on the River Clyde and supported the lone working protocol.
- III. Dr Amy Pickard participated in a survey for the collection radiocarbon and stable carbon isotope samples.
- IV. Estuary transect surveys required three personnel in the power boat and were supported by; Dr Elliot Hurst, Stella White, Mairéad Corr, Dr Amy Pickard, Alanna Grant, Dr Justyna Olszewska and Galina Toteva.
- V. The ICP-MS analysis was undertaken by the Dr Lorna Eades of Edinburgh University
- VI. The radiocarbon work was financially supported by a National Environmental Isotope Facility (Part of the Natural Environmental Research Council), Grant Number 2513.0422 and undertaken by the NEIF Radiocarbon Laboratory, Rankine Ave, East Kilbride, Glasgow. Training for radio carbon sample collection was undertaken by Dr. Mark Garnett.
- VII. Laboratory analysis for all other data was undertaken by Alison Brown. Training and support were provided by; Dr Amy Pickard for the Shimadzu TOC-L series Total Organic Carbon Analyser and spectrophotometry and by Netty van Dijk on the Metrohm 930 Compact IC Flex for the ion chromatography and by Stella White on the SEAL AQ2 analyser and Agilent 7890B gas chromatograph.

3 Urban landscapes and legacy industry provide hotspots for riverine greenhouse gases: A source-to-sea study of the River Clyde

Declaration of authorship: The data in this chapter was collected and analysed by the author of the thesis with Dr. Amy Pickard supporting initial sampling, Co-authors reviewed paper drafts and provided supervision, feedback, and guidance.

The chapter has been published in the Water Research volume 236
<https://www.sciencedirect.com/science/article/pii/S0043135423004050>

with the following DOI - <https://doi.org/10.1016/j.watres.2023.119969>

Graphical Abstract

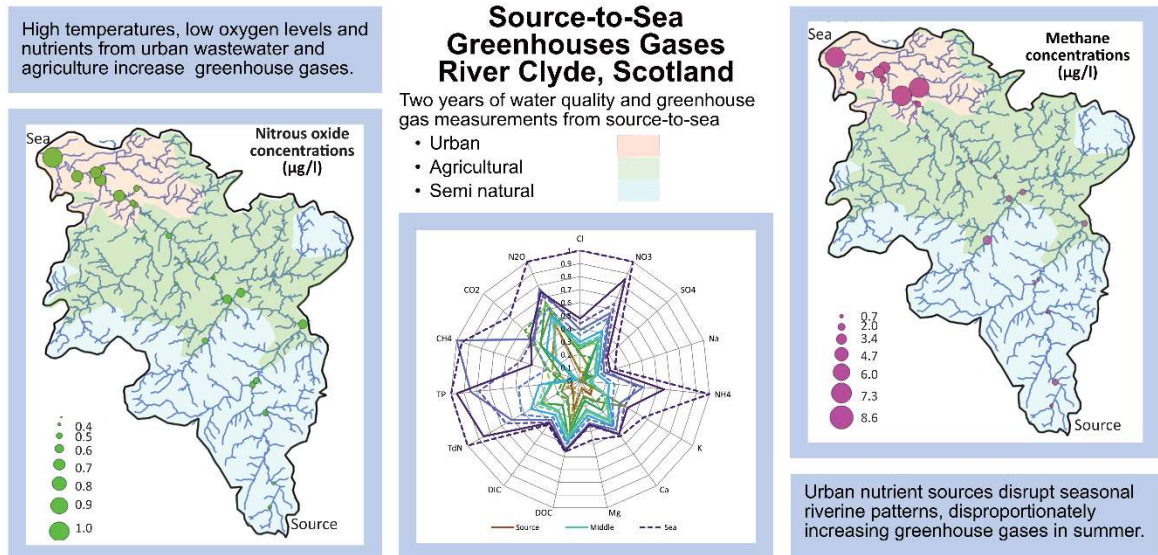


Figure 3.0 - Graphical Abstract - Urban landscapes and legacy industry provide hotspots for riverine greenhouse gases

Highlights

1. Urban wastewater, mine water and agricultural inputs dominated GHG generation.
2. Anthropogenic urban nutrient sources disproportionately increased GHGs in summer.
3. Low oxygen and high riverine residence time increased nutrient impacts on GHGs.
4. A source-to sea methodology enabled easy identification of GHG sources and sinks.
5. Load appointment modelling enabled separation of point and diffuse GHG sources.

Abstract

There is growing global concern that greenhouse gas (GHG) emissions from water bodies are increasing because of interactions between nutrient levels and climate warming. This paper investigates key land-cover, seasonal and hydrological controls of GHGs by comparison of the semi-natural, agricultural and urban environments in a detailed source-to-sea study of the River Clyde, Scotland. Riverine GHG concentrations were consistently oversaturated with respect to the atmosphere. High riverine concentrations of methane (CH₄) were primarily associated with point source inflows from urban wastewater treatment, abandoned coal mines and lakes, with CH₄-C concentrations between 0.1 - 44 µg l⁻¹. Concentrations of carbon dioxide (CO₂) and nitrous oxide (N₂O) were mainly driven by nitrogen concentrations, dominated by diffuse agricultural inputs in the upper catchment and supplemented by point source inputs from urban wastewater in the lower urban catchment, with CO₂-C concentrations between 0.1 - 2.6 mg l⁻¹ and N₂O-N concentrations between 0.3 - 3.4 µg l⁻¹. A significant and disproportionate increase in all GHGs occurred in the lower urban riverine environment in the summer, compared to the semi-natural environment, where GHG concentrations were higher in winter. This increase and change in GHG seasonal patterns, points to anthropogenic impacts on microbial communities. The loss of total dissolved carbon, to the estuary is approximately 48.4 ± 3.6 Gg C yr⁻¹, with the annual inorganic carbon export approximately double that of organic carbon and four times that of CO₂, with CH₄ accounting for 0.03%, with the anthropogenic impact of disused coal mines accelerating DIC loss. The annual loss of total dissolved nitrogen to the estuary is approximately 4.03 ± 0.38 Gg N yr⁻¹ of which N₂O represents 0.06%. This study improves our understanding of riverine GHG generation and dynamics which can contribute to our knowledge of their release to the atmosphere. It identifies where action could support reductions in aquatic GHG generation and emission.

Key Words

Methane; nitrous oxide; carbon dioxide; urban wastewater; agriculture; mine water

Authors

Alison M. Brown^{1,2}; Dr. Adrian M. Bass²; Prof. Ute Skiba¹; Dr. John M. Macdonald²; Dr. Amy E. Pickard¹

1. UK Centre for Ecology & Hydrology, Bush Estate, Penicuik, Midlothian, UK, EH26 0QB.
2. School of Geographical & Earth Science, University of Glasgow, Glasgow, UK, G12 8QQ.

3.1 Introduction

Greenhouse gas (GHG) evasion from inland waters is a significant source of atmospheric GHGs. Global carbon dioxide (CO₂) evasion has been estimated as 1.8 ± 0.25 Pg C yr⁻¹ from streams and rivers, resulting in a global evasion rate from inland waters of 2.1 Pg C yr⁻¹ (Raymond et al., 2013). The contribution from streams and rivers is large relative to their surface area, acting as hotspots for the exchange of gases with the atmosphere. The major sources of CO₂ are direct input via groundwater inflow, which transports CO₂ originating from soil respiration, and in-stream mineralization of organic carbon (OC) often from surface runoff (Winterdahl et al., 2016). Riparian wetlands also contribute disproportionately to CO₂ emissions (Abril and Borges, 2019). The relative importance of these mechanisms changes with stream order as headwater streams have a larger soil-water interface compared to lower reaches, resulting in the proportion of CO₂ produced from aquatic metabolism increasing with stream size (Marx et al., 2017; Hotchkiss et al., 2015). The magnitude of CO₂ riverine emissions is highly dependent on hydrology (Gómez-Gener et al., 2016). In urban areas significantly higher nutrients, organic matter content, and riverine cyanobacteria impact CO₂ variation (Salgado et al., 2022). Global methane (CH₄) evasion from inland waters was estimated at 398.1 ± 79.4 Tg CH₄ yr⁻¹, with rivers evading 30.5 ± 17.1 Tg CH₄ yr⁻¹, with aquatic ecosystems contributing about half of total global CH₄ emissions from anthropogenic and natural sources (Rosentreter et al., 2021). Total CH₄ emissions were found to increase from natural to impacted and from coastal to freshwater ecosystems, with emissions expected to increase due to urbanization, eutrophication and positive climate feedbacks, although there is significant uncertainty in the production, transportation and consumption processes (Rosentreter et al., 2021 ; Stanley et al., 2016). Similarly the production and emission of nitrous oxide (N₂O) from aquatic systems are uncertain (0.3 - 2.1 Tg N₂O-N yr⁻¹) with large spatial and temporal variability in emission estimates (Seitzinger and Kroeze, 1998; Beaulieu et al., 2011; Ciais et al., 2013). However N₂O emissions from rivers, reservoirs and estuaries have been estimated as 148 - 277 Gg N yr⁻¹ with anthropogenic perturbations to river systems resulting in a two to four-fold increase in N₂O emissions from inland waters (Maavara et al., 2019). The dominance of N₂O emissions emanating from nitrification or denitrification in inland waters is partly dependent on residence time (Zarnetske et al., 2011).

Urban rivers and lakes are potential hotspots for GHG emissions and there is an increasing body of literature concerned with quantifying their contribution to aquatic GHG emissions (Zhang et al., 2021; Wang et al., 2021; Gu et al., 2021; Herrero Ortega et al., 2019; Martinez-Cruz et al., 2017 and Garnier et al., 2009). In Mexico City water quality indicators (such as trophic state index and phosphorous level) were positively correlated with CH₄ emissions, suggesting a reduction in untreated wastewater discharge could concurrently reduce GHG emissions. Fluxes of CH₄ were highly variable, both in and across ecosystem locations and seasons (Martinez-Cruz et al., 2017) demonstrating the need for comprehensive studies to understand these temporal dynamics. In water bodies around the city of Berlin, a combination of high nutrient supply and shallow depth produced large CH₄ emissions. However dissolved oxygen and productivity were found to be poor predictors of CH₄ emissions, suggesting a complex combination of factors governed CH₄ fluxes from urban surface waters (Herrero Ortega et al., 2019). Conversely in rivers and lakes within the city of Beijing, high CH₄ emissions were attributed to high dissolved and sediment organic carbon, high aquatic

primary production and shallow water depths, although results were again highly variable (Wang et al., 2021a). In the Chaohu Lake basin in eastern China, diffusive CH₄ and N₂O emissions from rivers were due to large nutrient supply and hypoxic environments, with CO₂ impacted by temperature-dependent rapid decomposition of organic matter (Zhang et al., 2021). Positive correlations between temperature and GHG concentrations have been routinely observed (Wang et al., 2021, Herrero Ortega et al., 2019 and Rosentreter et al., 2021). The presence of ammonia, entering inland water from agriculture or wastewater, can inhibit CH₄ oxidation resulting in elevated CH₄ concentrations compared to low nitrogen systems and high evasion to atmosphere (Dunfield and Knowles, 1995; Bosse et al., 1993; Cotovicz et al., 2021). Conversely in an investigation of N₂O concentrations upstream and downstream of wastewater treatment plants (WWTPs) in an urban river in Japan, lower N₂O concentrations were found in summer (Zhou et al., 2022). Positive correlations between GHGs in surface waters and catchment agricultural land cover linked to higher levels of organic matter and dissolved inorganic nitrogen from the agricultural dominated areas have been found significant, with increases in GHG levels during prolonged low water levels (Borges et al., 2018).

GHG emissions are difficult to attribute to sources due to multiple generation and consumption pathways and high spatial and temporal variability (Rosentreter et al., 2021). Their production results from the interplay of multiple drivers and is influenced by, high between and within-system variation, with the causes of this variation unknown. This variation causes difficulties in up-scaling emissions from local-scale studies resulting in a need for more detailed studies measuring more in-water parameters across a large temporal and spatial scales. It is hypothesised, in this paper, the reasons for the high variation and poor predictability include:

1. GHGs are not conserved like dissolved nutrients but readily out-gas especially in the riverine environment with flow intensity and high stream slopes the primary controls (Long et al., 2015; Maurice et al., 2017; Natchimuthu et al., 2017; Liu and Raymond, 2018; Maurice et al., 2017)
2. The number of different source types within the riverine environment, including: point, diffuse and in-water generation, change with land-use and need to be distinguished.
3. The concentration of nutrients is only one aspect of GHG generation, which changes with availability of electron donors and acceptors, such that mixing of waters may stimulate GHG production (Wrage et al., 2001; Furukawa et al., 2004; Broder et al., 2012; Zhang et al., 2019).
4. Different GHG sources and dynamics dominate in different types and sizes of water body dependent on: land-water interface, depth, hydraulic regime, sediments-water-air interfaces, residence time, land-use, physio-chemical properties, microbial communities, seasonality, and anthropogenic impacts on seasonal patterns of changing water level and temperature.

The concentrations of GHGs in the riverine water column result from the balance between input, consumption, production and output (Fig. 3.1).

Given the potential significance, but inadequate quantification and characterisation of urban catchment fluvial GHG dynamics, further insight into how to quantify and interpret riverine GHG concentration data could support improved estimates. This study addressed the following key objectives: (1) does using a source-to-sea investigative approach allows

quantification of how changes in the nature and size of the riverine environment impact GHG concentrations, (2) can the key controls on GHG generation be determined by comparison of the semi-natural, agricultural and urban environments, including key land-cover, seasonal and hydrological controls, and (3) can point source, diffuse source and in water generation be distinguished for different GHGs. A large temperate catchment was selected for the investigation, where land cover transitioned from semi-natural, through pastoral and arable agricultural to urban (including legacy industrial), as representative of many urbanised catchments globally.

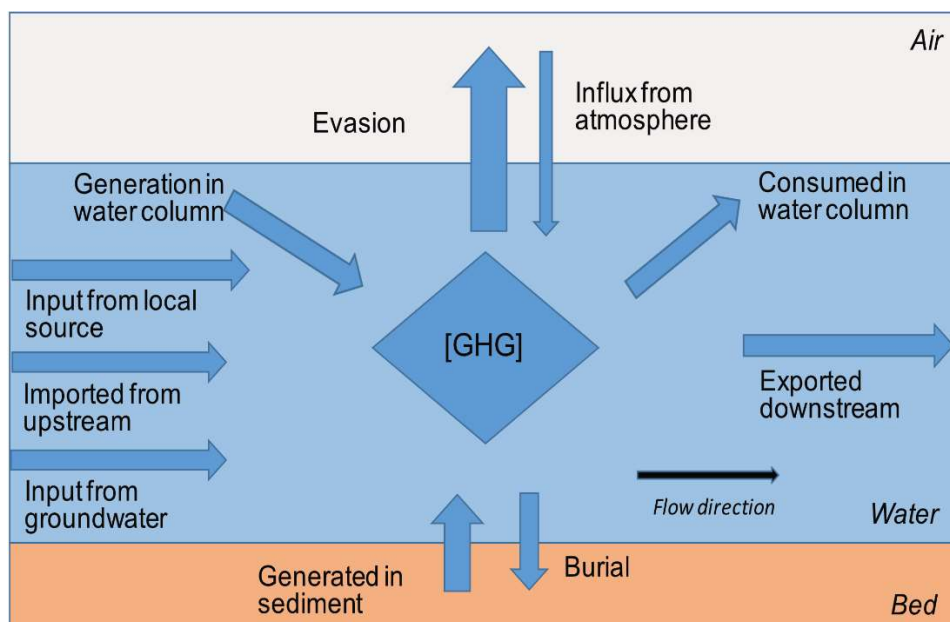


Figure 3.1 - GHG generation, transport and loss - In the schematic the arrows show the direction of GHG movement into/out-from the sediment (brown), water (blue) and air (grey). The balance between the different sources and sinks changes along the river course. Both river slope and hydrology impact this balance as they influence water residence times, sedimentation, out-gassing and nutrient concentrations from point and diffuse sources.

3.2 Materials and methods

3.2.1 Study area

The River Clyde is the third longest river in Scotland (170 km) with a total river network length of 4,244 km and drains an area of 1903 km² (Clyde River Foundation, 2020). The River Clyde together with the rivers Kelvin, White Cart, Black Cart and Leven enter the Clyde estuary, with a catchment area of 3854 km² (Nedwell et al., 2002), which is home to 33.8 % (1.79 million) of Scotland's total population (Clyde River Foundation, 2020). Surface water quality, as assessed in accordance with the European water framework directive (SEPA, 2018 and Natural Scotland, 2015), ranges from 'High' in some small tributaries to 'Bad' in some urban tributaries, with much of the River Clyde rated as 'Moderate'. The groundwater quality is also rated as 'Poor', both in the upper catchment in the Leadhills area and the lower urban catchment. The River Clyde's mean annual flows is 48.3 m³ s⁻¹ with the maximum flow of 560.5 m³ s⁻¹ (24th January 2018) as measured at Daldowie gauging station (supplementary data Table 3.A.1) based on data between 1963 and 2019 (UKCEH, 2020b). The upper moorland catchment consists of steep rough ground with hill pasture and some forestry as the major

land use. In the middle catchment there is mixed farming including arable and pastoral and significant urbanisation in the lower catchment.

3.2.2 Sites description and data collections

Twenty-six measurement locations were selected on the River Clyde and its major tributaries. The locations were distributed along the River Clyde from near the source on Daer Water, above Daer reservoir, to Glasgow Green just above the Clyde tidal weir, which separates two distinct habitats of fresh and salt water. The sample locations are shown spatially against both the water network of the River Clyde and tributaries (Fig. 3.2A) and the catchment land cover (Fig. 3.2B). Full details of the survey locations are provided in the supplementary information Table 3.A.1 with photographs in Appendix 1. Samples were collected monthly between January 2020 and December 2021 at all locations. Twenty-one sampling campaigns were undertaken in total as no sampling was permitted during the period April to June 2020 due to Covid-19 working restrictions. Each sampling campaign was undertaken over two consecutive days with samples collected at the upper catchment sites on day one and in the lower catchment on day two. Sample filtration and processing being undertaken on the same day the samples were collected.

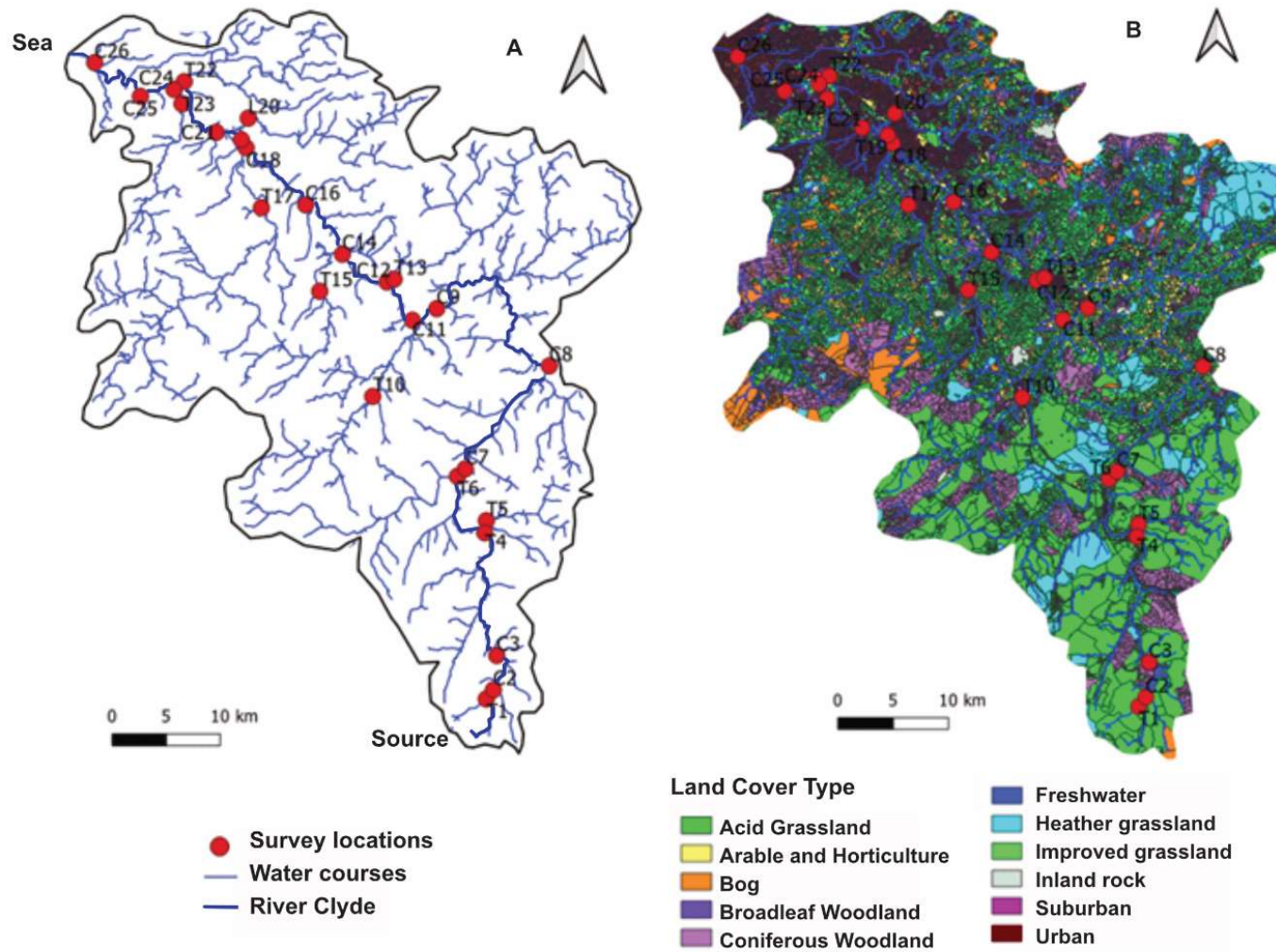


Figure 3.2 - Spatial plots of the River Clyde catchment. Panel A shows the River Clyde and tributaries (Ordnance Survey, 2022) and Panel B shows the land cover (UKCEH, 2020a). The source-to-sea survey locations are denoted with the lowest number near the source of the River Clyde and the highest number near the river-sea interface. The measurements on the River Clyde are indicated by a `C` and the tributaries by a `T` and where the tributary is direct inflow from a loch this is indicated by an `L`.

3.2.3 Field sampling and laboratory measurements

Dissolved gas samples were collected in triplicate at each location using the headspace method, prior to the collected water being disturbed by other measurements, together with ambient air samples (Billett and Moore, 2008). Conductivity (EC), water temperature (T_w), dissolved oxygen concentration (DO) and pH were measured, and a two-litre water sample was retained for later analysis, which was kept in a dark, cool-box until returned to the laboratory for processing, to minimise biological activity. Full details of the data collection and laboratory measurement methodologies are described (Brown et al., 2023a).

Headspace samples were analysed using an Agilent 7890B gas chromatograph (GC) and 7697A headspace auto-sampler (Agilent, Santa Clara, California), with CO_2 , CH_4 and N_2O concentrations determined by running gas vials containing four mixed gas standards prepared in a consistent way to the ambient air samples. The concentrations of the standards gases were: 1.12 to 98.2 ppm for CH_4 ; 202 to 5253 ppm for CO_2 ; and 0.208 to 1.04 ppm for N_2O . Water samples were filtered within 12-hrs of collection through a Whatman GF/F 0.7 μm , under vacuum. Filtrate was then analysed for: total dissolved nitrogen (TDN), total dissolved carbon (TDC) and dissolved organic carbon (DOC), anion & cation concentration, UV-Vis absorbance. Total phosphorus (TP) analysis was undertaken on unfiltered samples. Analysis for TDN, TDC and DOC were undertaken using a Shimadzu TOC-L series Total Organic Carbon Analyser with all samples run within 36-hrs of collection. The difference between TDC and DOC was used to calculate dissolved inorganic carbon (DIC). The filtration resulted in out-gassing of gases including CO_2 raising the pH, such that most DIC measured by this method was in the form of bicarbonate and will underestimate the total DIC in the original stream waters (bicarbonate plus CO_2). Absorbance at 254 nm, indicative of aromaticity, was measured using a Perkin Elmer LAMBDA® 365 UV-Vis Spectrophotometer to evaluate the Specific Ultraviolet Absorbance (SUVA). A low SUVA_{254} indicates a smaller portion of aromatic humic matter present in the water and can be used as an indicator of the anthropogenic impact (Williams et al., 2016). Ion chromatography using a Metrohm 930 Compact IC Flex was undertaken to determine both anion and cation concentrations. A mixed ion standard containing 11000 ppm chloride (Cl^-), 5000 ppm nitrate (NO_3^-), 4000 ppm sulphate (SO_4^{2-}), 10000 ppm sodium (Na^+), 5000 ppm ammonium (NH_4^+), 1000ppm potassium (K^+), 1000ppm calcium (Ca^{2+}) and 1000ppm magnesium (Mg^{2+}), was diluted to make 7 standard solutions for calibration. These included dilutions of 0.1:100, 0.5:100, 1:100, 2:100, 5:100, 10:100, and 25:100. Total phosphorous (TP) was measured using a SEAL AQ2 analyser. Four standards were included in each run for calibration of between 0.025 to 0.20 mg P L^{-1} . Where concentrations exceeded the top standard, the machine diluted and re-measured the sample. For all techniques all sample points from each survey were run together.

3.2.4 Gas partial pressures

To calculate dissolved gas concentrations and partial pressures from the headspace equilibration method the following mass-balance equation was applied (Hamilton, 2006).

$$(C_{\text{liq}}) \cdot (V_{\text{liq}}) + (C_{\text{gas}}) \cdot (V_{\text{gas}}) = (C_{\text{liq}}) \cdot (V_{\text{liq}}) + (C_{\text{gas}}) \cdot (V_{\text{gas}}) \quad (\text{Eq. 1})$$

Where: C_{liq} and C_{gas} are the original gas concentration, C_{liq} and C_{gas} are the concentrations in the liquid and gas phases after equilibration (shaking) and V_{liq} and V_{gas} are the volumes of the

liquid and gas in the syringe (assumed to be the same before and after shaking). Assuming equilibrium inside the vessel then C_{liq} can be replaced by:

$$C_{liq} = P_{gas} \cdot \beta_T \cdot P_{BAR} \quad (\text{Eq. 2})$$

Where: P_{BAR} is the barometric pressure at the measurement time and altitude, P_{gas} is the partial pressure in the gas phase, β_T is the Bunsen solubility coefficient as a function of temperature. This can be rearranged:

$$(C_{Oliq}) = (P_{gas} \cdot \beta_T \cdot P_{BAR}) + (C_{gas} - C_{Ogas}) \cdot (V_{gas}) / (V_{liq}) \quad (\text{Eq. 3})$$

This gas concentration in $\mu\text{moles/L}$ can be converted to units of ppmv using the Ideal Gas Law, where $\text{ppmv} = (\mu\text{moles/L}) \cdot (RT)$, where R is the gas constant and T is the temperature in Kelvin.

This method is effective for CH_4 and N_2O but can lead to errors in CO_2 estimates as dissolved CO_2 is in dynamic chemical equilibrium with other carbonate species. The error incurred by headspace analysis of CO_2 is less than 5% for typical samples from boreal systems which have low alkalinity ($<900 \mu\text{molL}^{-1}$), with $\text{pH} < 7.5$, and high pCO_2 ($>1000 \mu\text{atm}$). This was the case for (98% of the samples here but errors in the lower Clyde tributaries, with both higher alkalinity and pH , were estimated as reaching 10% (Koschorreck et al., 2021).

3.2.5 Data sources and processing

Flow data measured by SEPA at their various gauging stations was used for all hydraulic calculations, details of the data applied at each location are provided in the supplementary information Table 3.A.1 (Scottish Environment Protection Agency, 2020 and (UK Centre of Ecology & Hydrology (UKCEH), 2020). River flow, over the period January 2020 to December 2021, for the Sills of Clyde in the upper catchment ranged between 2.5 and $345 \text{ m}^3 \text{ s}^{-1}$ (the survey captured a range of $3.3 - 113 \text{ m}^3 \text{ s}^{-1}$) and Daldowie in the lower catchment ranged between 4.8 and $522 \text{ m}^3 \text{ s}^{-1}$ (the survey captured a range of $5.6 - 170 \text{ m}^3 \text{ s}^{-1}$) (Fig. 3.3 A & B). The River Clyde experiences significant height loss between 75 and 100 km from source, which would be expected to produce significant out-gassing (Fig. 3.3 C) and significant inputs from urban wastewater treatment (UWWT) and mine water outflows (MW) (Fig. 3.3 D).

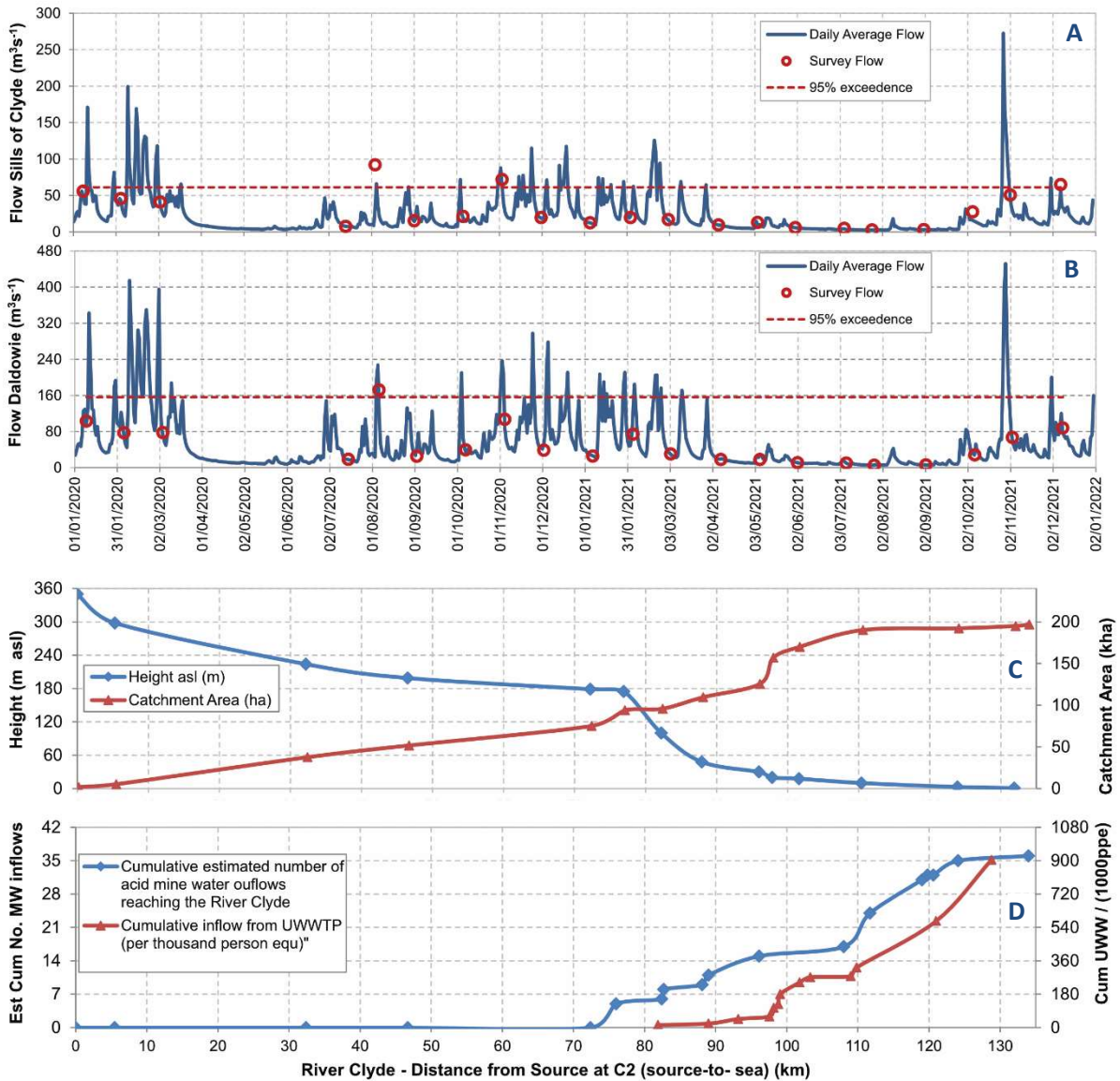


Figure 3.2 - River Clyde volumetric flow and contaminants inputs - Panels A and B show the volumetric flow (Q) for the upper and lower River Clyde relative to the survey dates for the first and second days of the surveys respectively. Effort was made to get consistent riverine flows over the two days of sampling, although during high river flows this was not possible (e.g. August 2020). In the spring and summer of 2021 (from April to September inclusive) a period of very low rainfall persisted, which was twice the duration as for 2020 and resulted in very dry conditions across the Clyde catchment. Panel C shows the height and area of the Clyde catchment compared to distance from source for the different measurement points. Panel D provides information on cumulative point sources entering the River Clyde from both urban wastewater treatment plants (UWWTP) in per 1000 person equivalent (1000ppe) and the cumulative number of known sources for Mine Water (MW) outflows. Note that this provides no information on the volume of MW entering the River Clyde or the degree of treatment. MW volumetric flow varies widely from different sources.

Data was analysed using a combination of approaches. Spatial analysis of all measured parameters was undertaken using Quantum Geographic Information System (QGIS) version 3.22. Land cover analysis was undertaken by generation of the catchment area for each measurement point and applications of a land cover date; (UK Centre for Ecology & Hydrology (UKCEH), 2020) also using QGIS. Pearson's correlation was applied to determine relationships between the GHG concentrations, water physiochemical properties and land cover. Locations

were grouped using K-cluster analysis, to help investigate the impact of seasonality, based on measured water chemical properties (DOC, DIC, TDN, TP, Cl⁻, NO₃⁻, SO₄²⁻, Na⁺, NH₄⁺, K⁺, Ca²⁺ and Mg²⁺). Physical parameters such as temperature (which mainly distinguish sites by elevation) and conductivity (a function of all dissolved ions) were not included.

Load appointment modelling (Bowes et al., 2008) was applied to all the GHG and chemical concentration data at all locations where flow data was available or could be calculated. The difference in the occurrence of point and diffuse sources is linked to the concentration-flow relationship, and can be calculated by using equation 4, where Q is volumetric flow rate and C_P and C_D are the point and diffuse source concentrations respectively. The constants A, B, C and D need to be calculated by iteration for each solute (Bowes et al., 2008). The models for the point and diffuse sources once generated were then applied to the full 2 years of flow data from January 2020 to December 2021 to determine volume transport for each GHG or solute.

$$C_T = C_P + C_D, \text{ where } C_P = A \cdot Q^{(B-1)} \text{ and } C_D = C \cdot Q^{(D-1)} \quad (\text{Eq. 4})$$

3.3 Results

3.3.1 GHG concentrations and water contamination from source-to-sea.

Maximum concentrations for all GHGs occurred in the river urban section during July-September 2021, where concentrations of reached; CH₄-C 44 µg L⁻¹, CO₂-C 2.6 mg L⁻¹ and N₂O-N 3.4 µg L⁻¹, with corresponding saturations of 130400%, 1170% and 1310%, respectively. All GHG concentrations exhibited both strong spatial and temporal variability. Riverine dissolved GHGs (CH₄, CO₂ and N₂O) were typically supersaturated with respect to the atmosphere, with >97% above the theoretical equilibrium value. The lowest saturations occurring in areas of steep slope and high turbulence, which included the head waters of the Clyde (C3) and the areas surrounding the Falls of Clyde (C12, T13, C14, T15, C16 and T17), with CH₄ showing the largest change in concentrations.

Riverine dissolved GHG (CH₄-C, CO₂-C and N₂O-N) and water physiochemical property (TP, TDN, DOC, DIC, Cl⁻, NO₃⁻, SO₄²⁻, Na⁺, NH₄⁺, K⁺, Ca²⁺ and Mg²⁺) concentrations for the different locations measured on the River Clyde (Fig. 3.4 A) and its tributaries (Fig. 3.4 B) all increased from source-to-sea, in line with increasing percentage of both agricultural and urban land cover (Fig. 3.4 C). Average concentrations for all locations are included in supplementary data Tables 3.A.2 and 3.A.3.

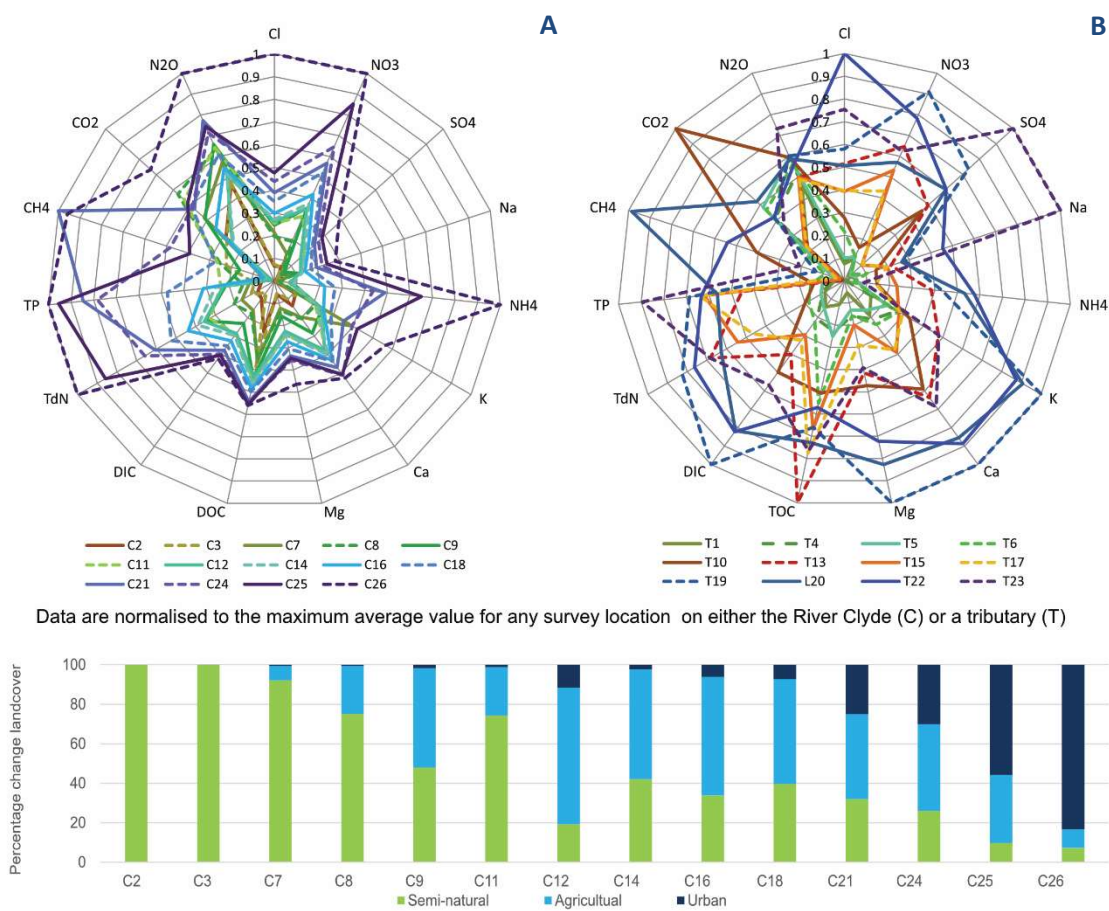


Figure 3.4 - Radar plots of average dissolved GHGs and water chemical properties - Panel A and B are radar plots of average dissolved GHGs (CH₄-C, CO₂-C and N₂O-N) and water chemical properties (TP, TDN, DOC, DIC, Cl⁻, NO₃⁻, SO₄²⁻, Na⁺, NH₄⁺, K⁺, Ca²⁺ and Mg²⁺). The source-to-sea survey locations are denoted with numbers from 1 (source) to 26 (sea), with the River Clyde indicated by a `C` and the tributaries by a `T` or `L`, where direct inflow is from a loch. Panel A is a source-to-sea progression of the River Clyde (coloured brown-green-blue) clearly demonstrating how the concentrations increase downstream. All data are normalised to the maximum average value for any survey location. Panel B is a source-to-sea progression for the Clyde tributaries, with tributaries joining in the upper Clyde (green), the middle Clyde (red-orange) and the lower Clyde (blue) and exhibiting a similar progression of concentrations. All data are normalised to the maximum average value for any survey location. Panel C shows the percentage land cover change between each location from source-to-sea on the River Clyde for comparison with panel A. Semi-natural (acid grassland, heather and forest) is in green, agricultural (arable and improved grassland) in light blue and urban (urban and suburban) in dark blue (UK Centre for Ecology & Hydrology, 2020).

3.3.2 Land cover relationship with and methane and nitrous oxide dynamics

To determine land cover influences on nutrient and GHG concentrations, the land cover was correlated to the measured GHG concentrations and water physio-chemical properties (Table 3.1 and supplementary data Table 3.A.4 and supplementary Figure 3.A.1 and 3.A.2). Analysis was for the tributaries and Clyde headwaters only, to ensure all data was independent and points within the analysis were on a similar spatial scale (catchment area < 250km²). As such the measurements points in the lower urban River Clyde catchments (with the highest GHG concentrations) are not included to avoid confounding of data.

Table 3.1 - Pearson's Correlation Coefficient between nutrients and GHGs (EC, DO%, pH SUVA₂₅₄, TP, DOC, DIC, TDN, CH₄, N₂O and CO₂) and percentage land-cover across Clyde tributaries and headwaters

Land use type	%	CH ₄	CO ₂	N ₂ O	EC	DO%	pH	DOC	DIC	TDN	TP	SUVA ₂₅₄
Acid grassland	21.7%	-0.38	0.06	-0.40	-0.84	0.24	-0.84	-0.88	-0.77	-0.94	-0.93	0.79
Arable & horticulture	3.9%	0.51	-0.05	0.07	0.65	-0.06	0.73	0.48	0.77	0.74	0.67	-0.63
Bog	5.7%	0.04	-0.41	0.02	0.36	0.23	0.63	0.64	0.27	0.61	0.77	-0.41
Coniferous woodland	13.8%	0.05	0.28	0.08	0.16	0.15	0.05	0.61	0.20	0.27	0.30	-0.11
Freshwater	0.7%	0.12	-0.05	-0.10	-0.10	0.13	-0.03	-0.22	-0.09	-0.10	-0.16	-0.04
Heather	2.9%	-0.15	-0.20	-0.01	0.19	-0.01	0.08	0.55	0.08	0.33	0.14	-0.27
Heather grassland	1.4%	-0.03	0.13	0.15	-0.05	-0.21	-0.22	0.10	-0.06	-0.10	-0.07	-0.06
Improved grassland	29.4%	0.21	-0.20	0.38	0.76	-0.18	0.82	0.91	0.64	0.91	0.94	-0.70
Inland rock	0.9%	0.71	0.56	0.55	0.73	-0.55	0.48	0.36	0.85	0.54	0.44	-0.51
Urban & Suburban	7.8%	0.59	0.06	0.49	0.88	-0.56	0.85	0.36	0.84	0.78	0.70	-0.81

Notes

1. Vales are the Pearson's correlations coefficient with the values in bold considered significant with at P-value < 0.05.
2. There is a strong correlation between broadleaf woodland and urban and suburban land-cover within the Clyde catchment (R² =0.91, P-value <0.001), possibly because broadleaf woodland has been planted within the suburban and urban environment. Hence broadleaf woodland has not been included (4.2%).
3. To ensure all data points are independent only tributaries and the upper River Clyde are included. As a result, the lower Clyde points (including the large UWWTP linked to high CH₄ concentrations) are not included to avoid confounding of catchments.

Conductivity, pH, TDN, TP, DIC, DOC, Cl⁻, NO₃⁻, SO₄²⁻, Na⁺, NH₄⁺, K⁺, Ca²⁺, Mg²⁺ and N₂O-N were strongly negatively correlated with percentage cover of acid (semi-natural) grassland and positively correlated with improved (pasture) grassland, suggesting that acid grassland behaved as a nutrient sink while improved grassland behaved as a nutrient source. Arable & horticulture (arable) cover was positively correlated with EC, pH, DIC, TDN, TP, Cl⁻, NO₃⁻, NH₄⁺, K⁺, Ca²⁺, Mg²⁺ and behaved as a nutrient source. The area of arable & horticulture cover is an order of magnitude lower than for improve grassland, but correlations are similar (Table 3.1 and supplementary data Table 3.A.4).

Urban & suburban (urban) cover was strongly positively correlated with EC, pH, TDN, TP, DIC, Cl⁻, NO₃⁻, SO₄²⁻, Na⁺, NH₄⁺, K⁺, Ca²⁺, Mg²⁺, CH₄-C and N₂O-N suggesting that the urban cover acts as both a nutrient and GHG source. Urban land cover was negatively correlated with DO% while other land-cover types had no statistically significant impact of river oxygenation. Improved grassland, urban and arable cover were all negatively correlated with SUVA₂₅₄ suggesting an anthropogenic influence as land cover linked to nutrient concentrations and human density have been found to impact humic composition (Williams et al., 2016). No statistically significant correlations are detected for CO₂ except that of inland rock (Table 3.1 and supplementary data Table 3.A.5).

3.3.3 GHG spatial heterogeneity

The spatial patterns of CH₄, N₂O and CO₂ are similar, with the lower (urban) catchment to the northwest having the highest concentrations (Fig. 3.5). The concentrations of CH₄, N₂O and CO₂ in the middle catchment associated with the Falls of Clyde (C12-C18, 78 to 100 km from source) an area of high turbulence with an elevation drop of 150m are the lowest, and are typically at or near atmospheric equilibrium, likely associated with high evasion due to

increased turbulence. The upper more rural catchment has more variability between the different GHGs. For example, T10 has both high CH₄ and CO₂ but lower relative N₂O concentrations and was observed associated with MW inflows, conversely the C9 has higher N₂O but lower relative CH₄ and CO₂ concentrations and has high agriculture land cover.

Average SUVA₂₅₄ values of 5 (35% aromaticity) occur in the upper catchment dropping to 3 (20% aromaticity) in the lower catchment with the three most urban tributaries (T19, T22 & T23) consistently demonstrate the lowest values characteristic of high anthropogenic impact. The spatial patterns for DIC, SO₄²⁻, Ca²⁺, Mg²⁺ and K⁺ (supplementary data Figure 3.A.3-6) are similar and exhibit high concentrations in the tributaries measurements (T10, T13, T19, T22), all of these catchments are influenced by legacy coal mines and outflow of MW (Fig. 3.3 D). The tributary T23 also exhibits high SO₄²⁻ and Na⁺ compared to other ions suggestive of a different industrial legacy waste history. The ions, Cl⁻, NO₃⁻, Na⁺ and NH₄⁺, all increase with urbanisation of the catchment and are consistent with anthropogenic sources (Herlihy et al., 1998).

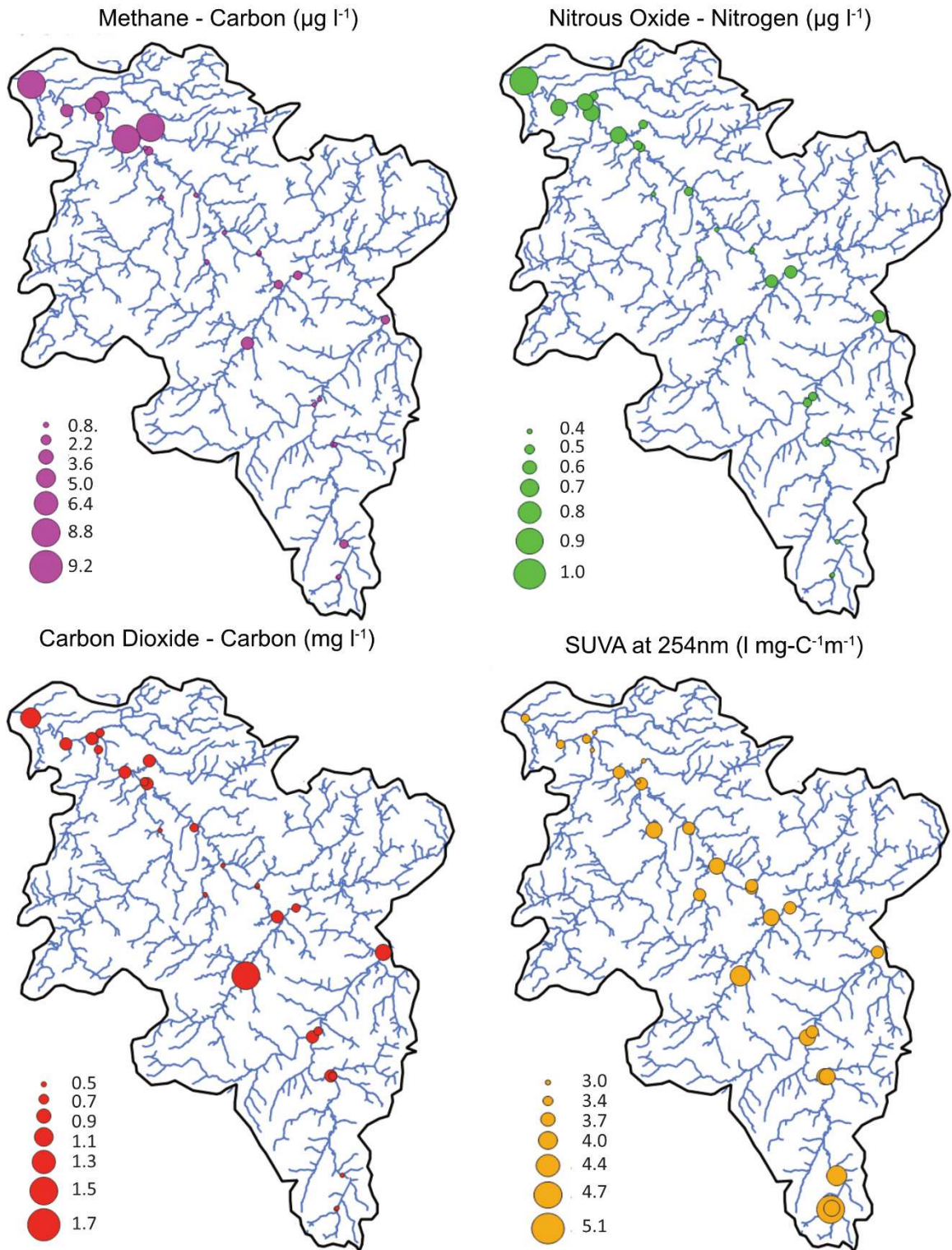


Figure 3.5 - Spatial average of CH_4 , CO_2 , N_2O and SUVA at 254nm across the Clyde catchment - The average concentration data for $\text{CH}_4\text{-C}$, $\text{N}_2\text{O-N}$, $\text{CO}_2\text{-C}$ and SUVA_{254} shown spatially (for T_w , EC, pH, DO, TP, TDN, DOC, DIC, Cl⁻, NO_3^- , SO_4^{2-} , Na^+ , NH_4^+ , K^+ , Ca^{2+} , Mg^{2+} see supplementary information Figure 3.A.3-6). The size of the marker denoting the average concentration / value at each measured location. The concentrations of all three GHGs ($\text{CH}_4\text{-C}$, $\text{CO}_2\text{-C}$ and $\text{N}_2\text{O-N}$) are low in the middle Clyde catchment due to high out-gassing corresponding to regions of high turbulence. Both CH_4 and N_2O concentrations are high in the lower catchment. Both $\text{CH}_4\text{-C}$ and $\text{CO}_2\text{-C}$ concentrations are elevated in tributaries that have significant MW inflow (e.g., at T10). The SUVA_{254} values decrease from the upper to lower catchment.

3.3.4 Seasonal GHG distribution by land use characteristics

Locations were grouped using K-cluster analysis based on measured water chemical properties. The result with six clusters was selected and summarised in Table 3.2.

Table 3.2 - Cluster analyses based on the measured water chemical properties (DOC, DIC, TDN, TP, Cl⁻, NO₃⁻, SO₄²⁻, Na⁺, NH₄⁺, K⁺, Ca²⁺ and Mg²⁺) distinguishes locations by position in the catchment.

No	Cluster Name	Locations	Description
1	Upper Clyde-Agricultural	C7, C8, C9	Upper section of the River Clyde, with both pastoral and arable agriculture
2	Middle Clyde-suburban arable	C11, C12, C14, C16, C18	Middle section of the River Clyde with a mixed signal of suburban, mining and agriculture
3	Lower Clyde-highly urban	C21, C24, C25, C26	Lower section of the River Clyde, dominated by high urban land coverage and increases in Cl ⁻ , TDN and TP
4	Upper tributaries-Semi-natural	T1, C2, T4, T5, T6	Upper Clyde tributaries, flowing from semi-natural or pastoral environments including streams from reservoirs.
5	Middle tributaries-rural plus mining	T10, T14, T15, T17	Middle Clyde tributaries, dominated by pastoral and arable agriculture, disused coal mines and DOC from peat
6	Lower tributaries-urban plus mining	T19, T22, T23	Lower Clyde tributaries, dominated by urban, coal mining and legacy industry with the highest concentrations of all ions.

Notes:

1. K-Cluster analyses based for 6 clusters using measured water chemical properties effectively distinguishes locations on the river Clyde and tributaries by their position in the catchment.
2. C3 (measured below Daer reservoir) and L20 (Strathclyde Loch) were not included in the cluster analysis as these primarily represent lake properties rather than riverine properties.

Seasonal patterns for riverine dissolved GHGs (CH₄, CO₂ and N₂O) and water physiochemical properties (TDN and TP) were investigated using the clustering in Table 3.2 and were found to be inconsistent throughout the catchment (Fig. 3.6). In the upper and middle catchment for both the River Clyde and its tributaries, CH₄ and TP concentrations exhibit low variability by season. However, in the lower urban catchments both the highest mean and maximum concentrations occur in summer and autumn. Concentrations of CH₄ in the lower urban catchment have increased by an order of magnitude and TP by at least four times. Conversely N₂O, CO₂ and TDN exhibit their lowest average values in summer with the highest values in spring and winter in the upper and middle catchments. However, in the lower urban catchment the seasonality pattern changes with the highest concentrations of N₂O, CO₂ and TDN in the summer.

The seasonal change in summer could be driven by temperature or reduced river flow. Temperature is correlated with reduced river flow and this correlation becomes more significant in the lower urban catchment (at C9 (upper catchment); R² = 0.5, p-value <0.03 and at C24 (lower catchment); R² = 0.61, p-value <0.003 (August 20 data excluded and log-linear relationship applied)). The low river flow in summer would impact contaminant and nutrient concentrations particularly where these are linked to point rather than diffuse sources. Thus, this seasonal impact could be driven by temperature and concentrations of nutrients from point sources.

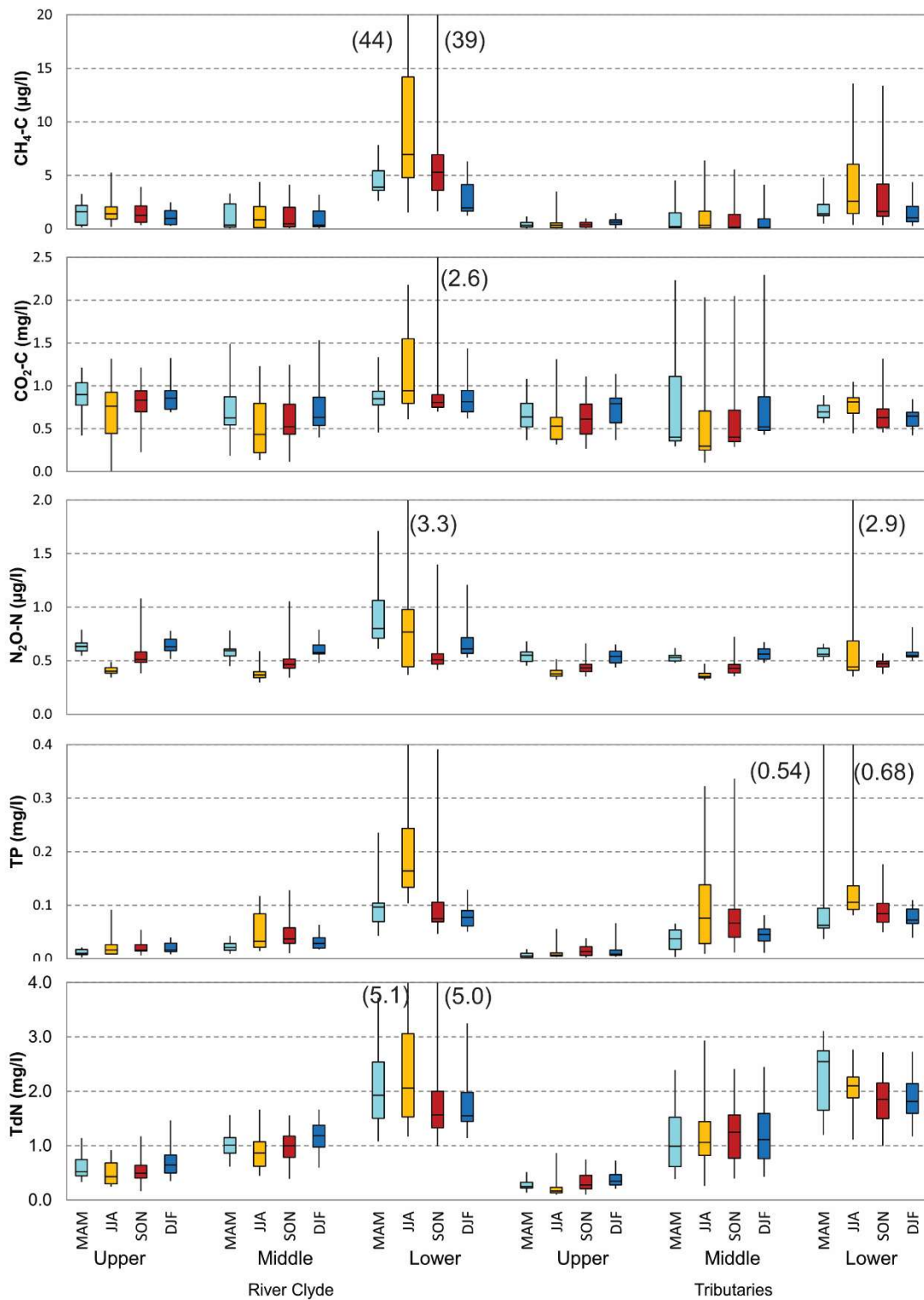


Figure 3.6 - Seasonal analysis of GHGs for the upper, middle and lower River Clyde and tributaries - Box plots of concentrations of dissolved CH₄-C, CO₂-C, N₂O-N, TdN and TP, showing the median, 25% and 75% quantiles, minimum and maximum for a seasonal analysis: spring (March-May) light blue, summer (June to August) yellow, autumn (September to November) red and winter (December to February) blue. The results are grouped by region of measurement on the upper, middle and lower River Clyde and tributaries. Seasonal trends that occur in the upper and middle reaches are impacted in the highly urban lower Clyde and its tributaries.

3.3.5 GHGs, nutrient and contaminants correlations

Correlations over the whole catchment show that both CH₄ and N₂O were significantly positively correlated with TP, TDN, NO₃⁻ and NH₄⁺ with CH₄ also significantly positively correlated with DIC and Mg²⁺ and N₂O significantly positively correlated with Cl⁻. CH₄, CO₂ and N₂O are all negatively correlated with DO%, with CH₄ and CO₂ meeting the significance criteria (Table 3.3 and supplementary data Table 3.A.2). In the urban sector (L20 to C26) DO values are lower (supplementary data Table 3.A.3), suggesting reduced water aeration. Conductivity, DIC, Cl⁻, SO₄²⁻, Na⁺, K⁺, Ca²⁺, Mg²⁺, are all strongly inter-correlated. TDN is strongly correlated with NO₃⁻ but also TP. These correlations are not consistent across the whole the catchment and are investigated using the clustering from Table 3.2. The correlations for clusters 1, 3, 4 and 6 are shown in Fig. 3.7.

Table 3.3 - GHG correlation (Pearson's R) with water physiochemical properties over the whole catchment

GHG	EC	T _w	pH	DO	DO%	DOC	DIC	TDN	TP	SUVA ₂₅₄
CH ₄ -C	0.41	0.34	0.13	-0.47	-0.42	0.03	0.41	0.43	0.45	-0.18
CO ₂ -C	0.23	-0.04	-0.10	-0.28	-0.64	-0.02	0.19	0.23	0.19	0.02
N ₂ O-N	0.49	-0.14	0.12	-0.11	-0.38	0.01	0.16	0.47	0.51	-0.10

There are few significant correlations for GHGs in the upper catchment, especially for CH₄, N₂O is positively correlated with T_w, NO₃⁺ and TDN, and CO₂ negatively correlated with DO% (Fig. 3.7 A and B). However, in the lower urban catchment strong correlations occur between almost all GHGs and physiochemical properties, suggesting high GHG concentrations occur as contaminate concentrations increase and DO% decreases (Fig. 3.7 C and D). The correlation between TDN and TP is high in the urban environment (Pearon's R= 0.76), both linked to UWW. This may result in some correlations which are unlikely to be causal. In the urban area CH₄ is highly correlated with TP and N₂O with TDN (associated with UWW), and CH₄ with the DIC, SO₄²⁻, Ca²⁺ and Mg² grouping (associated with MW), suggesting different mechanisms for CH₄ production compared to the semi-natural environment. In the urban area significant negative correlations occur between DO% and SUVA₂₅₄ with most physiochemical properties and GHG concentrations.

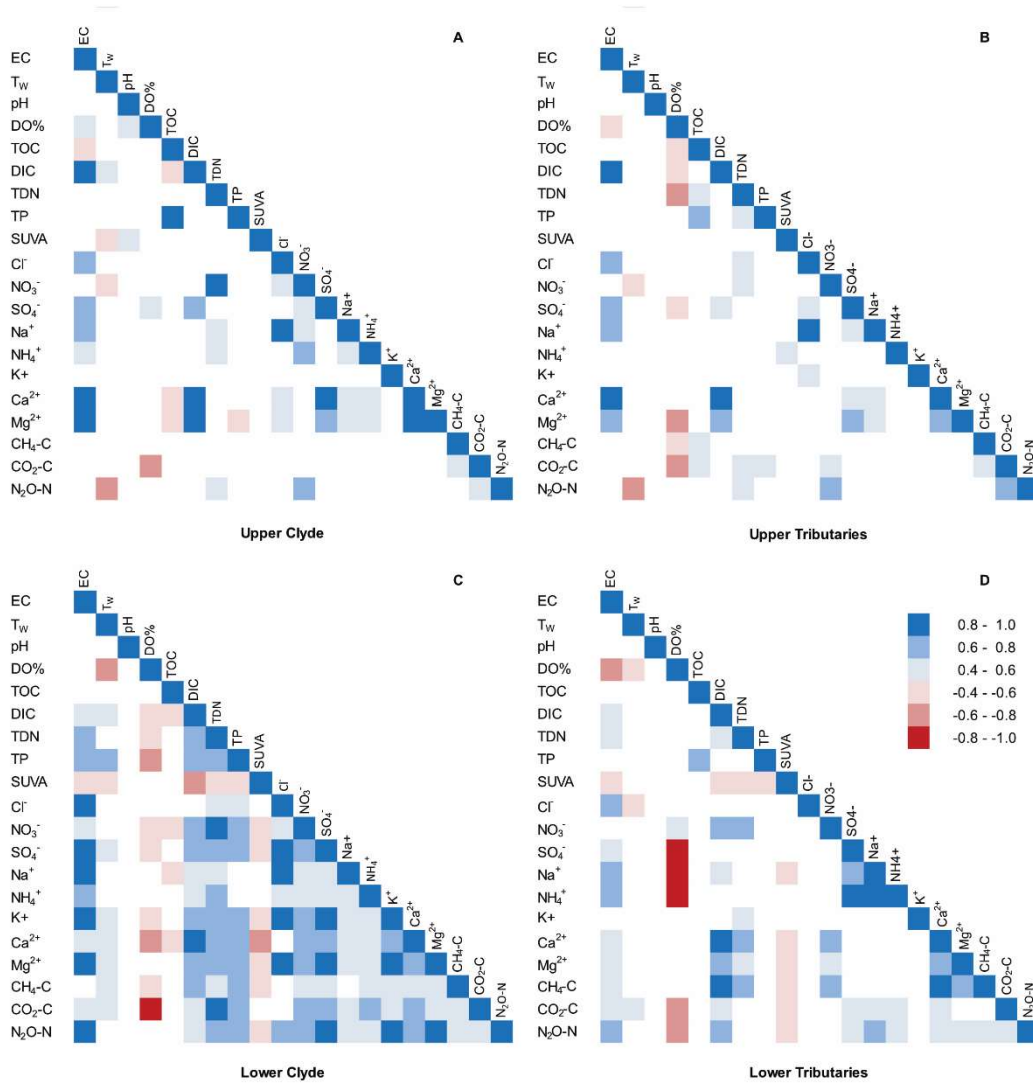


Figure 3.7 - Correlation (Pearson's R) between GHGs and physiochemical water properties
 Correlations are for A) the upper and B) lower River Clyde and C) upper and D) lower Clyde tributaries as selected from the groups in Table 3.2. Positive correlations are depicted in blue and negative correlations in red with the stronger correlations in a darker shade. Positive correlations < 0.4 and negative correlations > -0.4 have been excluded as do not meet this significance criteria (p -value < 0.005) Correlations increases in the lower catchment, with GHGs strongly correlated with contaminants and inversely correlated with DO%.

3.3.6 Drivers for greenhouse gas concentrations

Using a load apportionment model the GHG and solute concentrations can be modelled and the exponents (B and D) from the relationships for concentration as a function of flow (equation 4) can be estimated for point and diffuse sources and used to distinguish four source types: (1) point sources which are fully independent of flow ($B = 0$), (2) point sources where concentration appears influenced by flow or rainfall ($0 < B < 1$), (3) diffuse sources where the concentration increases with flow ($D > 1$) and (4) diffuse sources where concentrations remain constant with flow ($D = 1$). The ions, nutrients and GHGs are categorised for these four source types in Table 3.4 and show different behaviours in the upper and lower catchment.

Table 3.4 - Categorisation of the dominant sources of GHG and nutrients between point and diffuse sources and their dependence on flow in upper and lower Clyde catchment

		Upper catchment dominant source		Lower catchment dominant source	
		Point	Diffuse	Point	Diffuse
Flow	Independent of flow		Cl ⁻ , Na ⁺ ⁽⁴⁾	CH ₄ , TP, NH ₄ ⁺ (TDN, N ₂ O, CO ₂) ⁽¹⁾	Cl ⁻ , Na ⁺ ⁽⁴⁾ NO ₃ ⁻ , N ₂ O, CO ₂
	Influenced by flow	DIC, SO ₄ ²⁻ , Ca ²⁺ , Mg ²⁺ ⁽²⁾	CH ₄ , N ₂ O, CO ₂ ⁽³⁾ , DOC TP, TDN, NO ₃ ⁻ , NH ₄ ⁺ , K ⁺	DIC, SO ₄ ²⁻ , Ca ²⁺ , Mg ²⁺ ⁽²⁾	TDN, K ⁺ , DOC

Notes:

1. Point sources independent of flow are only evident in the lower (urban) catchment and all GHGs are influenced by this type of source. Values in brackets are significant sources not the dominant source.
2. Point sources influenced by flow (DIC, SO₄²⁻, Ca²⁺, Mg²⁺) are related to groundwater inputs. This type of source occurs in both the upper and lower catchment for this group of ions. Ion concentrations increase by an order of magnitude between the upper and lower catchment. This can be attributed (due to extensive further investigation by the authors) to mine water outflows from disused coal mines, which is a feature of the middle and lower Clyde catchment. Rainfall influences both the water residence time within the mine system and source flow rate influence the point source characteristics.
3. Diffuse sources where the concentration increases with flow, such as for DOC are dominated by storm runoff events (Vaughan et al., 2017). GHGs in the upper catchments behave similarly to nutrient suggesting a similar source, however in the lower catchment point sources dominate GHG concentrations to the extent that for CH₄ diffuse generation is difficult to detect.
4. Diffuse sources where the concentrations are independent of flow are exhibited by Cl⁻ and Na⁺, throughout the catchment. Salt in river water is typically found to be damped by the catchment and independent from atmospheric inputs. (Neal and Kirchner, 2000). This type of analysis does not account for period inputs such as those caused by winter road salting.

Mean concentrations together with calculated point and diffuse concentrations for the River Clyde from source-to-sea (Fig. 3.8 and supplementary data Figure 3.A.3-6), show the increasing significance of point source inputs in the lower urban river for both GHGs and nutrients. In the upper catchment GHG concentrations are dominated by diffuse agricultural sources. In the lower, urban catchment point sources become dominant over diffuse sources for CH₄, TP and NH₄⁺ and become significant for N₂O, CO₂, NO₃⁻ and TDN. Additionally, while NO₃⁻, N₂O and CO₂ are still dominated by diffuse flow their concentrations remain constant with flow, suggesting a reduced connection with their catchment and N₂O and CO₂ generation in the water column with in-water generation and out-gassing approximately in balance (N₂O by (de)-nitrification of dissolved nitrogen compounds and CO₂ by in-stream mineralization of DOC rather than direct input via groundwater inflow). The CH₄ concentrations best reflect those of TP (R² = 0.5, P-value <0.005), while TDN concentration are reflected by N₂O (R² = 0.65, P-value <0.0005) and CO₂ (R² = 0.71, P-value <0.0002) concentrations. The locations C21 (112km from source) and C26 (134km) (Fig. 3.8) show the highest concentrations of CH₄ and N₂O, which are within 0.3km and 3.4km of UWWTP outfalls. The tidal weir (400m downstream of this C26) locally reduces flow and increases water residence times, which may act to reduce DO% seen at this location. The major point sources identified in the lower catchment included inflows from UWWTP and MW from abandoned coal mines detailed in Fig. 3.3 D.

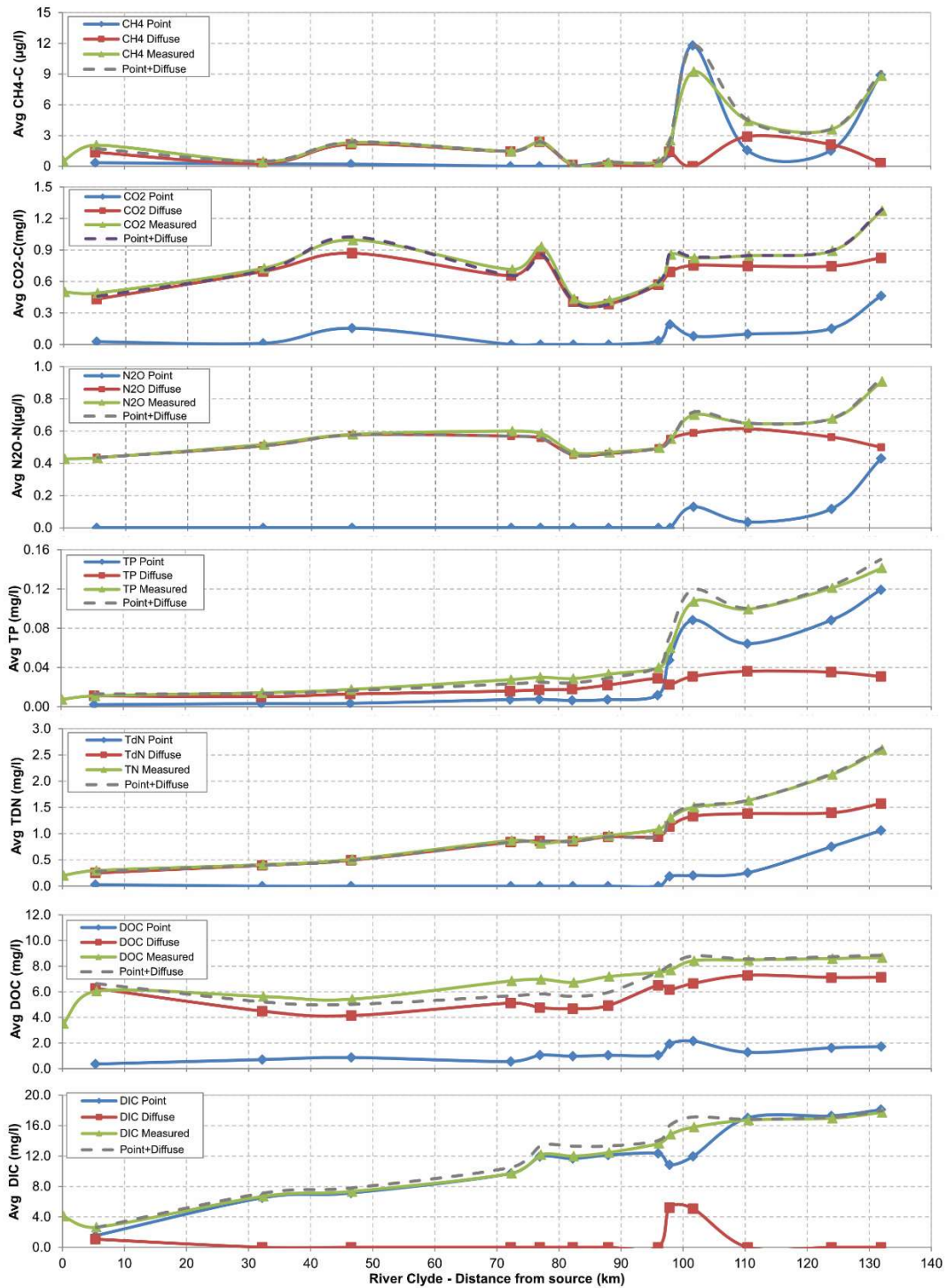


Figure 3.3 - Average concentrations from point source and diffuse sources on the River Clyde
 The concentrations for measured data and determination of point and diffuse sources are shown for: (A) CH₄, (B) CO₂ (C) N₂O (D) TP, (E) TDN (F) DOC, (G) DIC, against distance from source (C2 at 0km to C26 at 134 km). For other ions supplementary data Figure 3.A.7. The measured concentrations are the average values measured across the 21 surveys for each location. The point and diffuse concentrations are the average values based on the 2 year of flow data for the time of the survey (1st January 2020 to 31st December 2021) applied at 15-minute intervals. Considerable input from point sources for both nutrients and GHG occurs after a distance of 95km and is coincident with an increase in urban land cover and the three highly urban tributaries entering the River Clyde.

3.3.7 Carbon and nitrogen exports to the estuary

Data measured at C26, was used to estimate the carbon, nitrogen and other direct riverine exports into the Clyde estuary. The horizontal flux models for these exports of are included in Table 3.5 based on volumetric flow rate (Q) in $\text{m}^3 \text{s}^{-1}$. The annual export, based on flow data for the survey period (1-Jan-20 to 31-Dec-21) is included in the final column of Table 3.5. This estimate only includes fluxes attributed to continuous point or diffuse sources. Sporadic pollution from winter road salting or periodic agricultural fertiliser application is estimated separately.

Storm events dominate riverine loading of DOC and nutrients from agricultural run-off and low water levels dominate inputs from point sources, particularly those near to measurement locations. Variability in this relationship does arise due to hysteresis. For example DOC concentrations during storm events are related to the whether the DOC source is plentiful or exhaustible (Vaughan et al., 2017, Vaughan and Schroth, 2019 and Pohle et al., 2021). In this study continuous measurements were not available, resulting in the inability to quantify any hysteresis.

The annual loss of TDC from DIC, TOC, CO_2 and CH_4 , to the estuary was estimated as $48.39 \pm 3.6 \text{ Gg C yr}^{-1}$, with annual DIC export approximately double that of DOC and four times that of CO_2 , with CH_4 accounting for 0.03%. The annual loss of total nitrogen, from TDN and N_2O , to the estuary was estimated as $4.03 \pm 0.38 \text{ Gg N yr}^{-1}$ of which N_2O represents 0.06%. The largest exports are for TDC, Cl^- , SO_4^{2-} , Ca^{2+} , all exceeding 40 Gg yr^{-1} , with Na^+ exceeding 36 Gg yr^{-1} , with road winter salting contributing an additional 10 Mg yr^{-1} of Cl^- and 5.6 Mg yr^{-1} of Na^+ .

Table 3.5 - Flux of CO_2 , CH_4 , N_2O , TP, TDN, DOC, DIC, Cl^- , NO_3^- , SO_4^{2-} , Na^+ , NH_4^+ , K^+ , Ca^{2+} , Mg^{2+} into the Clyde Estuary

Flux	Concentration equations (Q is in $\text{m}^3 \text{s}^{-1}$) $CT = A \cdot Q^{(B-1)} + C \cdot Q^{(D-1)}$	R ²	P- value	Annual export (tonnes)
$F_{\text{DOC}} (\text{mg l}^{-1})$	$= 36.0526 \cdot Q^{-1} + 0.4979 \cdot Q^{0.6940559}$	0.425	<0.005	13534 ± 1510
$F_{\text{DIC}} (\text{mg l}^{-1})$	$= 60.70614 \cdot Q^{-0.36701}$	0.891	<0.001	27629 ± 1448
$F_{\text{TDN}} (\text{mg l}^{-1})$	$= 22.1784 \cdot Q^{-1} + 1.5727 \cdot Q$	0.819	<0.001	4023 ± 377
$F_{\text{CO}_2} (\text{mg l}^{-1})$	$= 9.66653 \cdot Q^{-1} + 0.825557 \cdot Q$	0.781	<0.001	7213 ± 654
$F_{\text{CH}_4} (\mu\text{g l}^{-1})$	$= 184.1654 \cdot Q^{-1} + 0.000000394 \cdot Q^{2.93923}$	0.798	<0.001	14.4 ± 3.3
$F_{\text{N}_2\text{O}} (\mu\text{g l}^{-1})$	$= 13.291247 \cdot Q^{-1} + 0.07187 \cdot Q^{0.38284}$	0.753	<0.001	2.3 ± 0.14
$F_{\text{TP}} (\text{mg l}^{-1})$	$= 2.490657 \cdot Q^{-1} + 0.000132 \cdot Q^{1.31679}$	0.964	<0.001	229 ± 36
$F_{\text{Cl}^-} (\mu\text{moll}^{-1})$	$= 8303.752 \cdot Q^{-1} + 494.1491 \cdot Q$	0.719 ⁽¹⁾⁽²⁾	<0.001	48273 ± 5186
$F_{\text{NO}_3^-} (\mu\text{moll}^{-1})$	$= 1533.528 \cdot Q^{-1} + 74.2137 \cdot Q$	0.773	<0.001	13978 ± 1543
$F_{\text{SO}_4^{2-}} (\mu\text{moll}^{-1})$	$= 1140.427 \cdot Q^{-0.430324}$	0.744	<0.001	40968 ± 3778
$F_{\text{Na}^+} (\mu\text{moll}^{-1})$	$= 10460.07 \cdot Q^{-1} + 524.7421 \cdot Q$	0.837 ⁽¹⁾⁽²⁾	<0.001	36001 ± 5734
$F_{\text{NH}_4^+} (\mu\text{moll}^{-1})$	$= 139.6026 \cdot Q^{-1} + 11.07243 \cdot Q$	0.342	<0.001	498 ± 62
$F_{\text{K}^+} (\mu\text{moll}^{-1})$	$= 8639982 \cdot Q^{-1} + 55.69099 \cdot Q^{1.00091}$	0.927 ⁽²⁾	<0.001	5805 ± 474
$F_{\text{Ca}^{2+}} (\mu\text{moll}^{-1})$	$= 1986.658 \cdot Q^{-0.31986}$	0.841	<0.001	42040 ± 3376
$F_{\text{Mg}^{2+}} (\mu\text{moll}^{-1})$	$= 1349.282 \cdot Q^{-0.421596}$	0.873 ⁽²⁾	<0.001	12598 ± 1412

Notes:

(1) $CT = CP + CD$, where $CP = A \cdot Q^{(B-1)}$ and $CD = C \cdot Q^{(D-1)}$ (C = concentration, T = Total, P = Point, D = Diffuse)

(2) Two values removed for January 21 and February 21 and assumed due to winter salting, as salt evident on the roads

(3) One value removed for August 2021 due to tidal ingress at Glasgow green, this most influenced K^+ , Mg^{2+} , Na^+ and Cl^- concentrations.

Despite the focus on measuring DOC in rivers, a recent UK modelling study demonstrated that DIC accounted for 80% of the TDC flux from the UK's 7 largest rivers (Jarvie et al., 2017) and a one year study (2017) measured DIC as 78% of the TDC flux for the same rivers (Tye et al., 2022). Table 3.6 provide a ranked comparison of DIC and DOC export from various UK rivers, including the River Clyde from this study, based on river catchment area on a per annum basis, showing the dominance of DIC export over DOC in the UK.

Table 3.6 - Comparison of DIC and DOC export from UK Rivers as a function of catchment area

River	Catchment Size (km ²)	DIC export Mg km ⁻² yr ⁻¹	DOC export Mgkm ⁻² yr ⁻¹	Ratio DIC/DOC	
Halladale	193	1.0	13.06	0.1	(García-Martín et al., 2021), (Tye et al., 2022)
Conwy	340	3.9	12.15	0.3	(García-Martín et al., 2021), (Tye et al., 2022)
Forth	1025	9.4	11.41	0.8	(García-Martín et al., 2021), (Tye et al., 2022)
Tay	5042	5.4	4.91	1.1	(García-Martín et al., 2021), (Tye et al., 2022)
Tamar	956	9.0	7.64	1.2	(García-Martín et al., 2021), (Tye et al., 2022)
Tay	4587	6.8	5	1.4	(Jarvie et al., 2017)
Tyne	2262	9.25	4.93	1.9	(García-Martín et al., 2021), (Tye et al., 2022)
Dart	257	8.9	5.18	1.7	(García-Martín et al., 2021), (Tye et al., 2022)
Kelvin	331	9.25	4.93	1.9	(Gu et al., 2021)
River Clyde	2003	13.78	6.74	2.0	This Study
Clyde	2003	13.5	6.04	2.2	(García-Martín et al., 2021), (Tye et al., 2022)
Clwyd	431	12.7	5.17	2.5	(García-Martín et al., 2021), (Tye et al., 2022)
Tweed	4390	8.3	2.9	2.9	(Jarvie et al., 2017)
Yorkshire Ouse	3315	16.2	4.3	3.8	(Jarvie et al., 2017)
Severn	9895	14	3.3	4.2	(Jarvie et al., 2017)
Trent	8231	17.7	2.4	7.4	(Jarvie et al., 2017)
Humber-Trent	8209	14.6	1.77	8.2	(García-Martín et al., 2021), (Tye et al., 2022)
Ely Ouse	3430	10.6	1.2	8.8	(Jarvie et al., 2017)
Thames	9948	13.4	1.4	9.6	(Jarvie et al., 2017)
Thames	9948	9.3	0.57	16.3	(García-Martín et al., 2021), (Tye et al., 2022)
Avon	1712	18.5	0.86	21.5	(García-Martín et al., 2021), (Tye et al., 2022)
Test	1035	19.3	0.51	37.8	(García-Martín et al., 2021), (Tye et al., 2022)
Average export		11.1	4.9	2.4	
Catchment weighted Average export		12.32	2.98	4.1	

Notes:

- 1 Load of dissolved inorganic carbon (DIC) and dissolved organic carbon (DOC) for the significant British rivers as function of catchment area as a comparator for the river Clyde.
- 2 DOC exports are from (García-Martín et al., 2022) and DIC exports estimated from (Tye et al., 2022), but data in these papers was gathered as part of the same study.

3.4 Discussion

3.4.1 Urban nutrients and climate warming increase GHG emissions

Our study supports the growing global concern that GHG emissions from water bodies are increasing because of the interaction between nutrient levels and climate warming. More specifically our study points to the largest increase in riverine GHGs coming from urban nutrients and the riverine climate stressors of low summer water levels resulting in increased water residence time and reduced river oxygenation. Our source-to-sea methodology showed clearly that seasonal patterns of CH₄, CO₂ and N₂O changed between the semi-natural environment in the upper catchment and urban environment in the lower catchment. In the semi-natural upper catchment GHGs were higher in winter, while in the lower urban catchment, GHG were significantly higher in summer. The GHGs from the urban catchment were dominated by point source inputs and their impact increased during low river flow and high temperature conditions. In the agricultural middle catchment GHG concentrations increased slightly above those of the semi-natural upper catchment but did not exhibit a change in seasonal pattern. This seasonal change in GHG concentrations may be related to changes in microbial community composition and activities, which have been observed downstream of UWWTP (Zhou et al., 2022; Beaulieu et al., 2010). The abundance of sediment microbial community have been found to be correlated with EC, organic matter, TP, DO and TN (Feng et al., 2022). This suggests microbial adaptation to changing conditions.

Riverine dissolved GHG, nutrient and chemical concentrations all increased from source-to-sea, in line with the increasing percentage of urban and agricultural land cover. The increase in GHG concentrations between the semi-natural and urban environment was on average three times higher for N₂O and CO₂, but twenty times higher for CH₄, suggesting the significant nature of CH₄ as an urban marker. While there were few significant correlations for any GHGs in the upper catchment, in the lower urban catchment strong correlations occurred between all GHGs and water physiochemical properties, suggesting that removal of contaminants from river systems, could lower GHG concentrations. Three main anthropogenic sources were identified that increased GHGs these included: (1) UWW outflows as a major point source of both CH₄ linked to TP and TDN, and N₂O linked to TDN; (2) MW outflows as a major point source of CH₄ and CO₂ emanating from groundwater interacting with disused coal mines and (3) agricultural activities as a major diffuse source of N₂O linked to TDN. Additionally, three major hydrological-environmental interactions were found that increased GHG concentrations in addition to those directly attributed to the nutrient increases. These included: (1) low oxygen conditions, (2) higher temperatures and (3) changes in river geometry linked to increased water residence times, and made it challenging to attribute causes absolutely.

3.4.2 High nutrient-residence time interactions promote GHG generation

Once the availability of TDN is accounted for (N₂O/TDN) neither T_w (in the range 0-22°C) or DO% (>90%) have significant effects on N₂O concentration. However, where water residence time increases, T_w and DO% appear significant. In low flow situations, residence time is further increased, decreasing DO% and providing more time for temperatures to increase in summer. Both this increased residence time (Zarnetske et al., 2011) and low oxygen level (Frey et al., 2020; Rosamond et al., 2012) will act to increase N₂O, by promoting denitrification over nitrification and increasing the proportion of N₂O per unit TDN.

In the upper Clyde catchment CH₄ concentrations are low and highly variable, with higher CH₄ observed with elevated DOC occurring in high flow events, suggesting DOC availability may be limiting CH₄. However, in the lower urban catchment CH₄ is strongly positively correlated to T_w, TP, TDN and DIC and negatively correlated with flow and DO%. This point source CH₄ generation is over 20 times higher than the underlying diffuse source. Generation of CH₄ in the lower urban catchment may be linked to eutrophication (nutrient enrichment). Our SUVA₂₅₄ values show a shift in riverine OC sources toward a more microbial and algal origin, as has been found as human disturbance increases (Lambert et al., 2017). High CH₄ in many shallow lakes is produced by eutrophication, mostly driven by TP and TDN enrichment and sediment microbiome (Davidson et al., 2018; Aben et al., 2017; Nijman et al., 2022). This mechanism is less likely in river ecosystem due to continual flushing, but during low water levels, increased residence times in combination with the high nutrient concentrations from UWW appear responsible for eutrophication and significant CH₄ generation. This may be enabled by electron donor availability in the receiving waters. This effect was most exacerbated when water residence times were further increased by the flow restrictions at the tidal weir.

3.4.3 Main uncertainty in the causes of GHG variation

Greenhouse gas concentrations were inversely correlated with river oxygenation. This correlation was influenced by several mechanisms, where the dominance changed with position in the catchment. High turbulence caused oxygenation of the water and out-gassing of the supersaturated GHGs. Respiration, photosynthesis and decomposition can create inverse relationships between oxygen and CO₂ dependent on their balance in the water column (Aho et al., 2021). Low oxygen conditions, result in anaerobic condition which promote both methanogenesis and denitrification, which increase CH₄ and N₂O production respectively, from the available resources. While turbulence out-gasses GHGs to atmosphere it also produces conditions less likely to promote CH₄ and N₂O production making it difficult to fully distinguish the mechanisms. The lower urban river has the highest correlations, with GHGs increasing exponentially with reducing oxygen levels. The oxygen concentration primarily influences CH₄, while CO₂ and N₂O are influenced by the DO% (CH₄ R² = 0.45, CO₂ R² = 0.74, N₂O R² = 0.24 (P-value > 0.001)), suggesting CH₄ generation is less influenced by temperature.

Summer seasonal changes impact both temperature and rainfall, which together impact GHG concentrations. Lower rainfall reduces river flow and diffuse nutrients inputs and increases the impact of point source inputs. Higher temperatures reduce the available oxygen, due to reduced solubility and can increase microbial activity. As flow and temperature are often highly correlated this can make distinguishing these mechanisms difficult. Many researchers suggest temperature is a major effect (Wang et al., 2021, Herrero Ortega et al., 2019 and Rosentreter et al., 2021). However, this study found that the size of the impact of flow and temperature on GHG concentrations is dependent on the location in the catchment and specifically the balance between diffuse and point source inputs. The upper catchment is dominated by diffuse inputs, which increase in higher flow and correspond to an increase in GHG concentrations. The lower urban catchment is dominated by point source inputs and corresponds to an increase in GHG concentrations with low flow. Flow and hence nutrient concentrations being more significant than direct impact of temperature in accounting for

GHG variability. After flow, TP is the major influence on CH₄ and TDN on N₂O. The use of the load appointment model to distinguish between points and diffuse sources of GHGs and nutrients suggests that nutrients, however they are delivered, are dominating GHG production. Fully distinguishing between temperature and flow impacts would require longer data set with more instances of high flow during the summer.

Changes in river geometry that reduce river velocity and increase water residence times also cause deposition of sediments and nutrients and reduce oxygen saturation. River sections with increased residence time exhibited higher GHG concentrations, with the largest increases occurring in low flow conditions. However, proportioning the cause of this increase between; increased residence time, reduced out-gassing due to lower turbulence, lower oxygen conditions, or deposition of sediments and nutrients as a source of GHG production is challenging. These higher residence time river sections act as point source locations for GHG generation compared to the surrounding river with CH₄ concentrations showing the most significant increase suggesting the creation anaerobic sediments may be the most significant impact.

Our results show an increase in GHGs, particularly CH₄, in the receiving river after UWWTPs, with the riverine CH₄ concentrations dominated by point source characteristics, pointing to the UWWTP inflows as causal. UWWTP generate CH₄, in locations such as sewer pipes and primary sedimentation, although CH₄ was not noted as discharged in effluent water (Masuda et al., 2018). We made measurements of GHG concentrations in some UWWTPs outflows, which were low in dissolved GHG including CH₄, and this suggested that CH₄ was generated within the receiving river due to changes in the river physicochemical properties, including nutrient availability, rather than transferred from the UWWTP. However, we made insufficient measurements in UWWTP outflows, due to their inaccessibility, to confirm this absolutely. Unexplained CH₄ concentrations in the stream sections after UWW treatments works in southwest Germany were attributed to in-water generation due to additional organic carbon load in the effluent water (Alshboul et al., 2016). After hydrology was accounted for TP, also dominated by point source characteristics, had the highest correlation with unexplained CH₄ concentrations (TP R² = 0.59 at C26), although this correlation changed by proximity from UWWTP. Other authors indicated correlations between TP and CH₄ concentrations, in urban settings usually by impacting microbial activity (Zhang et al., 2021; Martinez-Cruz et al., 2017; Hao et al., 2021).

3.4.4 Carbon dioxide concentration variability reduced by carbonate buffering.

Concentrations of CO₂ were less variable than those of N₂O and CH₄, mostly driven by diffuse sources, with point source inflows associated with tributaries receiving MW, causing short-term CO₂ increases. In-stream mineralization of DOC, the most likely generation mechanism for the consistent super-saturation of CO₂, would require a constant input of carbon to sustain CO₂ supersaturation levels (Winterdahl et al., 2016). DOC concentrations varied little through the catchment emanating from diffuse input, while DIC increased from source-to-sea, dominated by MW inflows. These MW inflows added significant amounts of DIC from the dissolution of limestone, producing high alkalinity, and many dissolved contaminates. The MW inflows are supersaturated with CO₂, which outgases very rapidly in treatment cascades or headwater streams. This rapid out-gassing was observed to shift the pH upwards creating a

new carbonate equilibrium. This changing equilibration would convert some of the remaining CO₂ to bicarbonate rather than emitting it to the atmosphere, thus reducing the gradient of CO₂ across the air-water interface (Stets et al., 2017). Aquatic primary productivity produces oxygen and consumes CO₂. However, primary productivity can be maintained with diminished CO₂, in high alkalinity waters by converting bicarbonate to CO₂ to support productivity (Aho et al., 2021). Conversely mineralisation of DOC to CO₂ would change the carbonate balance increasing bicarbonate concentrations. It is likely that this significant carbonate buffering available in the Clyde is responsible for the low variability in CO₂ concentrations and the reason why nutrients rather than carbon availability appear to influence CO₂ concentrations.

3.4.5 Acid mine inflows are a major source of GHG and outgas directly to the atmosphere

In the middle and lower catchment tributaries, high concentrations of both CO₂ and CH₄ occurred linked to outflows from disused coal mine adits. Where carbonate rock is present, and much coal bearing strata in the UK is associated with Carboniferous limestone (British Geological Survey, 2022), the sulphuric acid generated in the mine dissolves the calcium carbonate to produce CO₂ (Hedin and Hedin, 2016; Vesper et al., 2016; Jarvis, 2006). Details of CH₄ released in MW have not, to our knowledge, been published. Most GHGs from MW had out-gassed before reaching the River Clyde. However high CO₂ and CH₄ concentrations in T10 were traced back to several WM inflows. These MW inflows had high concentrations of DIC, SO₄²⁻, Ca²⁺, Mg²⁺ and K⁺, which together acted as a marker for legacy coal mining. Many other MW sources were traced in the catchment with this marker, although not included within this publication. Despite the focus on measuring DOC in rivers, our data suggest that for the River Clyde carbon loss is dominated by DIC, with the annual DIC export approximately double that for DOC. Comparison with other riverine studies demonstrated that DIC is the major component of the dissolved carbon in UK Rivers, with DIC accounting for 70 to 80% of carbon loss (Table 3.6). Our results suggest that the anthropogenic impacts of disused coal mines are accelerating carbon loss.

3.4.6 Legacy industry is still detectable in our rivers

Other increases in ion concentrations and pH were identified in the three most urban tributaries (T19, T22 and T23). Urban tributaries T19 and T22, had the highest concentrations of DIC, SO₄²⁻, Ca²⁺, Mg²⁺ and K⁺, attributed to inflows of MW from legacy coal mining. Both tributaries had legacy iron or steel making near to the rivers and may have iron slag buried within the catchment (Historic Environment Scotland, 2022). Steel slag is known to increase pH, alkalinity, and Ca²⁺ concentration (Riley and Mayes, 2015). The urban tributary T23, had the highest concentrations of Na⁺ and SO₄²⁻ probably associated with leachate from legacy paper production (H. J. Skinner, 1939). T22 also experienced the highest Na⁺ and Cl⁻ ion concentrations in the winter likely from winter road salting, as this tributary has the biggest road network, including a motorway. Data suggests that road drainage is entering the river directly adding an estimated 15 Mg yr⁻¹ of NaCl.

3.5 Conclusions

3.5.1 Benefits of a source-to-sea approach in interpreting riverine GHG data

We have used the Clyde catchment, with its transitioning land cover from semi-natural through agricultural and legacy industrial to highly urban as a source-to-sea study to support identification of GHG sources. This source-to-sea investigative approach was found effective in tracing how changes in the nature and size of the riverine environment impacted GHG concentrations, particularly as GHGs were not conserved but out-gassed in turbulent riverine sections. This variable out-gassing makes correlations on a catchment scale misleading and is probably one reason for the high variability in GHG-to-nutrient relationships reported in the literature. A key aspect of GHG source identification included the use of load appointment modelling to distinguish point and diffuse sources by their degree of dependence on flow. This was effective in confirming diffuse GHG sources from agriculture and point GHG sources from UWW and MW. This load appointment modelling approach enabled two main seasonal impacts, high temperature and low water levels, to be distinguished. Analysis suggested that the impact of low water levels dominated over temperature change and failure to account for changing water levels, with their implications for oxygen and residence times, may account for some of the variability in the impact of temperature on GHGs reported in the literature.

Measurement of a high number of water physiochemical properties allowed source fingerprinting of different inflows, which enabled detection even when the inflows were not physically identified, supporting identification of contamination from legacy industry. Results suggested that outflows from UWW treatment plants caused generation of GHG within the riverine water column. Changes in the seasonal pattern of GHG generation associated with urban wastewater inflows could be due to changes in microbial community structure, eutrophication at low water levels and supported by the availability of electron donors and acceptors in receiving waters. This was not confirmed as part of this study, and it is suggested that future surveys should be designed to quantify in-water generation resulting from mixing of UWW and riverine water.

The most important anthropogenic GHG from inland waters is CH₄ (Rosentreter et al., 2021), but CH₄ outgases the most rapidly, due to its high concentration to solubility ratio, as such catchment scale analysis can be misleading. Improved methods to detect and quantify CH₄ concentrations are required. A drone-mounted CH₄ sensor might be effective in identifying point sources while continuous in-situ CH₄ measurements would better define source-flow relationships, although sensor reliability and sensitivity need improvement. Where the source of nutrient pollution is unclear, human tracers such as caffeine could be applied to support understanding of contributions to nutrients (Mizukawa et al., 2019, and Chen et al., 2002).

3.5.2 Implications and ideas for policy makers

To effectively reduce anthropogenic GHGs from the riverine environment it is important to understand their sources. For the River Clyde, UWW outflows were a major point source of both anthropogenic CH₄ and N₂O, MW outflows a major point source of anthropogenic CH₄ and CO₂ and agricultural activities (including field and farmyard run-off and poorly maintained septic tanks (septic tank are not effective in removing nitrogen and phosphorous (O’Keeffe et al., 2015)) were a source of anthropogenic N₂O. All sources of GHGs were associated with

high concentrations of nutrients. Reducing nutrient loading, industrial and legacy contamination and agricultural run-off would ultimately act to reduce GHG within riverine environments. Pollution point sources are easier to tackle as the inflow locations are known.

While many UWWTP in the Clyde have phosphorous removal, our measurements suggest that levels of effectiveness vary between plants, suggesting improvement is possible. Additionally none of the UWWTP in this area have nitrogen removal (European Commission (Directorate General Environment), 2016). Riverine environments with low oxygenation, increased river residence times and high levels of nitrogen, should be prioritised for nitrogen removal from UWWTP to have the largest impact on N₂O reduction. Urban influences may have stimulated adaptation in microbial communities, further increasing GHG production and further studies of microbial activity may support GHG reduction. Nitrogen capture at UWWTP could ultimately act as an important source of fertiliser, avoiding outflows to the environment (van der Hoek et al., 2018). Mine water is more difficult to tackle in terms of GHG generation as GHGs are generated below ground with the generation mechanism poorly understood.

While agricultural pollution was primarily from diffuse sources additional measurements showed a significant proportion entered the Clyde via the numerous field drainage ditches and small streams, which could be treated as point sources. Approaches to reduce run-off may include: (1) use freshwater wetlands for nitrogen and phosphorus removal (Land et al., 2016) and wetlands have been shown as effective for diffuse run-off (Ockenden et al., 2012); (2) use of biochar filtrations, an effective technology for both cleaning of wastewater and run-off water. Its capabilities include removal of pesticides, organic chemicals and nutrients. However, a practical approach for application to small streams is needed. After use the biochar could be redeployed onto farmland supporting carbon sequestration and a circular economy, recycling nutrients and further preventing run-off (Catizzone et al., 2021, Phillips et al., 2022, Kamali et al., 2021); (3) Riparian buffer zones are recommended between crops and rivers. In Scotland, General Binding Rule 20 requires a buffer strip at least 2m wide to be left between surface waters and wetlands and cultivated land (SEPA, 2009). This rule was not set with the objective of reducing nutrient leaching. Further research demonstrates that woody vegetation is more effective than shrubs or grass at preventing nutrient leaching to rivers, with a 60m buffer strip effectively removing all nutrients (Aguar et al., 2015). While this would take considerable agricultural land, approximately 70% of nutrients are removed by a 12m strip, which would also stabilise river banks, reduce erosion and sediment loss, increase biodiversity and provide shade making the riverine system more robust to climate change (Cole et al., 2020).

Declaration of Competing Interest

The authors declare that they have no known competing financial interests or personal relationships that could have appeared to influence the work reported in this paper.

Acknowledgements

This work was financially supported by Natural Environment Research Council (NERC) studentship through the IAPETUS 2 Doctoral Training Partnership Grant No. NE/S007431/1.

The authors would like to thank the three anonymous reviewers who helped improve the quality of the manuscript.

3.6 Supplementary information

Table 3.A.1 - Sample locations on the River Clyde and flow gauging details

Location code ⁽¹⁾	Latitude	Longitude	Distance (km) ⁽²⁾	Sampling - above water surface (aws)	Gauging Stations Applied ⁽³⁾	River Name and location of sample	Comments on location relative to applied gauging
T1	55°19'56.44"N	3°38'08.02"W	<i>0.0</i>	River bank	None	Roger Clench	
C2	55°20'00.96"N	3°38'04.20"W	0.2	River bank	None	Daer Water - reservoir inflow	
C 3	55°22'06.79"N	3°37'34.25"W	5.5	River bank	Scottish water ⁽⁵⁾	Daer Water - reservoir outflow	Compensations flow for Daer Reservoir
T 4	55°28'28.53"N	3°38'52.72"W	<i>23.2</i>	River bank	None	Midlock Water	
T 5	55°28'29.37"N	3°39'07.95"W	<i>23.5</i>	River bank	Scottish water ⁽⁵⁾	Camps Water	Compensations flow for Camps Reservoir
T 6	55°30'58.10"N	3°41'18.84"W	<i>31.5</i>	River bank	Maidencots	Duneaton Water at Maidencots	400m downstream of Maidencots SEPA station
C7	55°31'20.99"N	3°40'42.80"W	32.4	Bridge 10m aws	Abington+Maidencots	Clyde at Abington	Summed flow of Clyde and Duneaton Water
C8	55°36'33.59"N	3°33'32.49"W	46.7	River bank	Abington+Maidencots	Clyde at the Symington	Summed flow of Clyde and Duneaton Water
C9	55°39'16.25"N	3°43'34.40"W	72.4	Bridge 15m aws	Sills of Clyde	Clyde at Sills of Clyde	1.9km downstream of Sills of Clyde SEPA station
T 10	55°34'49.81"N	3°49'00.88"W	<i>76.0</i>	Bridge 15m aws	Happendon	Douglas Water at Happendon	5m downstream of Happendon SEPA station
C 11	55°38'39.72"N	3°45'41.24"W	77.1	River bank	Tulliford Mill	Clyde at Tulliford Mill	200m downstream of Tulliford Mill SEPA station
C 12	55°40'31.87"N	3°48'01.43"W	82.4	Bridge 15m aws	Tulliford Mill	Clyde at Kirkfieldbank	Assumed as for the Clyde at Tulliford Mill
T 13	55°40'40.62"N	3°48'00.19"W	<i>82.7</i>	Bridge 5m aws	None	Mouse Water	
C 14	55°41'51.18"N	3°52'01.15"W	88.1	River bank	Hazelbank	Clyde at Hazelbank	1.4km upstream of Hazelbank SEPA station
T 15	55°39'59.08"N	3°53'55.87"W	<i>89.0</i>	River bank	Kirkmuirhill	Nethan at Kirkmuirhill	950m downstream of Kirkmuirhill SEPA station
C 16	55°44'15.42"N	3°55'22.74"W	96.1	Bridge 15m aws	Hazelbank+Kirkmuirhill	Clyde at Garrion bridge	Summed flow of Clyde and Nethan Water
T 17	55°44'02.77"N	3°59'17.37"W	<i>107.6</i>	River bank	Fairholm	Avon Water at Fairholm	1.5km upstream of Fairholm SEPA station
C 18	55°47'00.03"N	4°00'52.94"W	108.0	River bank	Blairston	Clyde at Hamilton	Assumed as for the Clyde at Blairston
T 19	55°48'28.82"N	4°00'40.44"W	<i>108.2</i>	Bridge 8m aws	Calderpark ⁽⁴⁾	South Calder Water	Assumed relationship with NCW flow
L20	55°47'08.93"N	4°01'13.92"W	<i>108.2</i>	River bank	As for SCW ⁽⁴⁾	Strathclyde Loch	Assumed as inflow from SCW
C 21	55°47'43.72"N	4°03'28.24"W	111.7	River bank 5m aws	Blairston	Clyde at Blairston	700m upstream of Blairston SEPA station
T 22	55°49'05.51"N	4°06'34.46"W	<i>119.0</i>	Bridge 8m aws	Redless	Rotten Calder at Redless	105m upstream of Redless SEPA station
T 23	55°50'12.02"N	4°06'26.31"W	<i>119.8</i>	Bridge 12m aws	Calderpark	North Calder at Calderpark	240m downstream of Calderpark SEPA station
C 24	55°49'47.78"N	4°07'19.11"W	120.6	River bank	Daldowie	Clyde at Daldowie	Measured at Daldowie SEPA station
C 25	55°49'24.01"N	4°10'16.21"W	124.1	Bridge 15m aws	Daldowie	Clyde at Cambuslang	Assumed as for the Clyde at Daldowie
C 26	55°51'00.14"N	4°14'25.07"W	134.0	River bank 3m aws	Daldowie	Clyde at Glasgow Green	Assumed as for the Clyde at Daldowie

Notes

- In the location code 'C' indicates the River Clyde 'T' indicates a tributary and 'L' indicates the tributary is direct inflow from a Loch
- Distance is the distance from the first measurements point nearest the source. Tributary distances are given as the distance at which they enter the River Clyde and are in italics.
- As sites were measured on the River Clyde in addition to those at the gauging stations, in some cases gauging station data has also be applied to a site further downstream. Where a gauged tributary enters the River Clyde in this section of river the gauging data from this tributary has been added to that of the River Clyde station. This is indicated in the gauging column.
- Gauging on South Calder Water at Forgewood was discontinued in 2010 but historical data (UKCEH, 2010) allowed a relationship to be derived with the flow of North Calder Water at Calderpark, the nearest catchment.
- Rotten Calder and North Calder Water enter the Clyde at almost the same point and their influence has not been separated.
- South Calder Water enters the River Clyde through Strathclyde Loch, a man-made lake excavated from a coal mining depression and is the only lake environment sampled in this study.
- Locations L1 and L2 could not be accessed in January and February 2021 due to heavy snow fall and L13 (Mouse water) was only introduced to the sampling campaign in August 2020.

Table 3.A.2 - Average GHG and physiochemical concentrations for each survey location

Location name ⁽¹⁾	CH ₄ -C (µg l ⁻¹)		CO ₂ -C (mg l ⁻¹)		N ₂ O-N (µg l ⁻¹)		DOC-C (mg l ⁻¹)		IC-C (mg l ⁻¹)		TN-N (mg l ⁻¹)		TP (mg l ⁻¹)		SUVA ₍₂₅₄₎ (l mg-C ⁻¹ m ⁻¹)		DO (%)		pH		T _w (°C)	
	Mean	SD	Mean	SD	Mean	SD	Mean	SD	Mean	SD	Mean	SD	Mean	SD	Mean	SD	Mean	SD	Mean	SD	Mean	SD
T1	0.06	0.11	0.38	0.07	0.42	0.06	1.67	1.4	6.01	2.7	0.26	0.08	0.007	0.01	5.09	1.77	98.2	1.3	7.32	0.27	7.3	3.4
C2	0.52	0.19	0.50	0.07	0.43	0.06	3.53	2.6	4.09	2.0	0.20	0.08	0.007	0.01	4.00	0.66	98.7	1.8	7.19	0.22	7.4	4.2
C3	2.07	1.14	0.49	0.12	0.43	0.06	6.05	2.0	2.64	1.0	0.30	0.10	0.011	0.00	4.26	0.42	100.0	3.3	7.24	0.19	7.8	3.8
T4	0.50	0.28	0.84	0.18	0.54	0.09	3.87	2.2	6.37	1.1	0.31	0.13	0.014	0.01	3.89	0.74	95.6	2.4	7.25	0.23	7.1	3.3
T5	0.13	0.08	0.71	0.16	0.47	0.07	3.53	3.9	8.73	2.4	0.28	0.12	0.010	0.01	3.86	1.02	95.1	1.6	7.23	0.28	7.4	3.8
T6	0.85	0.81	0.80	0.21	0.51	0.10	8.55	6.3	9.33	6.1	0.47	0.21	0.021	0.01	3.87	0.63	93.1	3.3	7.12	0.33	7.1	4.5
C7	0.46	0.33	0.73	0.14	0.52	0.09	5.63	4.7	6.70	2.6	0.41	0.14	0.014	0.01	3.69	0.69	93.3	2.5	7.12	0.40	7.6	4.6
C8	2.32	1.05	0.99	0.21	0.58	0.09	5.42	4.7	7.34	2.7	0.51	0.16	0.018	0.01	3.65	0.73	88.2	6.9	7.05	0.42	8.3	4.9
C9	1.48	0.56	0.71	0.33	0.60	0.20	6.86	6.0	9.73	4.1	0.87	0.29	0.028	0.02	3.71	0.58	99.8	9.0	7.30	0.25	9.1	5.6
T10	3.78	1.58	1.74	0.39	0.54	0.10	7.83	5.8	20.99	11.1	0.52	0.18	0.019	0.01	4.40	2.25	91.5	2.3	7.18	0.36	8.4	5.1
C11	2.45	0.76	0.93	0.42	0.58	0.18	6.97	5.8	12.17	5.1	0.81	0.26	0.030	0.03	4.04	1.62	98.6	9.1	7.33	0.25	9.3	5.7
C12	0.13	0.10	0.43	0.15	0.47	0.11	6.73	5.3	11.99	5.5	0.88	0.28	0.029	0.02	3.76	0.62	102.4	4.4	7.46	0.23	9.4	5.6
T13	0.08	0.04	0.38	0.09	0.45	0.08	15.49	9.2	16.88	8.7	1.77	0.37	0.064	0.04	3.59	0.66	99.9	3.1	7.54	0.26	8.7	4.9
C14	0.35	0.35	0.42	0.20	0.47	0.09	7.19	5.5	12.46	5.7	0.96	0.27	0.033	0.02	3.92	1.31	103.7	5.9	7.54	0.22	9.4	5.5
T15	0.19	0.19	0.41	0.14	0.45	0.09	10.35	5.8	12.37	6.4	1.41	0.52	0.088	0.07	3.73	0.68	102.0	4.7	7.61	0.20	8.6	4.6
C16	0.45	0.31	0.60	0.20	0.50	0.09	7.51	5.6	13.66	6.0	1.09	0.22	0.040	0.02	3.73	0.74	93.7	5.6	7.44	0.34	9.3	5.5
T17	0.36	0.30	0.39	0.13	0.44	0.08	12.02	6.0	13.63	7.2	1.22	0.39	0.091	0.07	3.92	0.60	101.92	4.0	7.65	0.22	9.2	5.4
C18	2.53	1.10	0.86	0.17	0.55	0.09	7.71	5.4	14.85	6.7	1.30	0.25	0.060	0.03	3.63	0.64	90.38	6.6	7.63	0.18	9.2	5.6
T19	1.23	0.33	0.72	0.11	0.55	0.11	10.22	5.6	42.10	14.3	2.15	0.47	0.097	0.04	2.99	0.81	97.22	1.6	7.96	0.25	8.7	4.2
L20	9.11	8.22	0.90	0.47	0.53	0.10	11.28	4.8	34.38	9.8	1.63	0.38	0.080	0.03	3.10	0.65	87.93	18.5	7.72	0.29	10.1	5.8
C21	9.25	10.71	0.82	0.15	0.70	0.31	8.43	5.2	15.82	7.0	1.50	0.30	0.107	0.06	3.59	0.71	92.17	5.4	7.61	0.20	9.5	5.7
T22	5.02	2.92	0.73	0.23	0.50	0.52	8.84	9.0	34.62	11.4	1.98	0.46	0.090	0.17	2.82	0.89	90.78	20.8	7.96	0.16	9.0	4.7
T23	1.93	2.99	0.62	0.12	0.67	0.08	11.87	3.0	23.88	11.7	1.78	0.51	0.127	0.02	3.06	0.61	85.68	6.1	7.95	0.17	8.5	4.8
C24	4.45	2.17	0.84	0.24	0.65	0.23	8.49	4.8	16.73	6.9	1.63	0.38	0.099	0.06	3.42	0.70	90.38	9.0	7.73	0.13	9.5	5.7
C25	3.62	1.96	0.89	0.24	0.68	0.22	8.59	4.5	16.96	6.6	2.13	0.82	0.121	0.08	3.38	0.76	91.92	7.6	7.79	0.13	9.7	5.7
C26	8.86	9.57	1.27	0.51	0.91	0.32	8.67	1.4	17.75	6.4	2.60	1.05	0.141	0.08	3.39	0.79	84.78	12.6	7.71	0.11	9.4	3.4

Note

1. The source-to-sea survey locations are denoted with numbers from 1 (source) to 26 (sea) with the River Clyde indicated by a `C` and the tributaries by a `T` or a `L`, where direct inflow is from a loch
2. The highest level of TN-N and TP are in the urban tributaries T19, T22 and T23 and the lower urban River Clyde C25 and C26 and the highest GHG at C26 and C21.
3. The highest variation associated with GHGs is linked to C21 and C26 and particularly evident for CH₄. The highest variation associated with DIC, is linked to the urban tributaries T19, T22 and T23.
4. The Greenhouse gas concentrations, CO₂-C, CH₄-C and N₂O-N, present the concentrations of carbon and nitrogen within the three greenhouse gases only.

Table 3.A.3 - Average dissolved ion concentrations for each survey location

Location name ⁽¹⁾	EC ($\mu\text{S/cm}$)		Chloride (mg l^{-1})		Nitrate (mg l^{-1})		Sulphate (mg l^{-1})		Sodium (mg l^{-1})		Ammonium (mg l^{-1})		Potassium (mg l^{-1})		Calcium (mg l^{-1})		Magnesium (mg l^{-1})	
	Mean	SD	Mean	SD	Mean	SD	Mean	SD	Mean	SD	Mean	SD	Mean	SD	Mean	SD	Mean	SD
T1	75.5	23.3	4.8	1.0	0.89	0.25	2.1	0.3	3.9	0.4	0.02	0.04	1.06	1.0	9.7	3.9	1.2	0.3
C2	57.7	16.9	4.3	0.6	0.58	0.20	1.9	0.4	3.6	0.5	0.00	0.00	0.85	0.6	6.9	2.7	1.3	0.4
C3	47.4	6.8	4.7	0.9	0.56	0.09	2.0	0.9	3.4	0.4	0.00	0.00	0.91	0.9	5.1	0.9	1.2	0.2
T4	83.8	8.4	6.4	2.4	0.97	0.32	3.0	0.4	4.8	0.4	0.02	0.03	1.72	2.9	8.3	1.0	2.9	0.4
T5	101.2	22.9	6.0	3.9	0.91	0.30	3.0	0.7	4.5	0.6	0.00	0.00	2.10	4.7	10.8	2.3	3.5	0.8
T6	141.4	67.0	14.0	8.9	0.99	0.58	3.3	1.1	9.7	6.2	0.01	0.02	2.15	1.4	12.3	5.9	3.5	1.7
C7	115.9	34.7	13.8	5.8	1.12	0.44	3.4	0.8	8.6	4.2	0.00	0.00	3.12	2.8	10.1	3.1	2.7	0.8
C8	118.9	31.0	12.7	4.5	1.60	0.66	3.6	0.9	8.4	2.6	0.01	0.01	1.65	1.0	10.6	2.9	2.9	0.8
C9	156.3	49.1	15.8	5.9	2.95	1.33	4.9	1.5	10.4	3.9	0.02	0.02	1.91	1.3	14.6	4.3	3.5	1.0
T10	313.1	135.1	17.9	13.4	1.34	0.60	38.4	17.2	13.6	11.2	0.05	0.05	2.61	1.0	30.4	11.6	10.4	4.8
C11	198.9	68.9	16.4	7.2	2.64	1.08	14.8	5.5	11.5	5.7	0.02	0.02	1.63	0.3	20.1	7.2	5.3	1.9
C12	195.3	70.5	16.9	7.2	2.93	1.19	13.1	6.4	11.3	5.4	0.02	0.02	1.90	0.9	19.4	7.8	5.0	2.0
T13	340.9	140.3	33.3	24.0	5.43	2.63	41.3	22.8	19.9	13.3	0.12	0.12	3.75	0.7	32.8	13.2	9.1	4.7
C14	207.5	78.0	17.5	7.8	3.14	1.06	14.9	7.6	12.2	5.9	0.03	0.04	1.71	0.4	20.8	7.7	5.3	2.1
T15	218.1	97.6	25.4	18.0	4.47	2.05	8.6	4.2	18.3	17.3	0.07	0.11	2.17	0.6	20.1	7.9	4.4	1.9
C16	226.8	81.2	19.2	8.8	3.52	0.89	16.7	7.7	13.2	7.1	0.07	0.06	1.97	0.5	22.3	8.2	6.0	2.5
T17	229.1	101.9	25.6	11.8	3.63	1.67	8.9	5.1	18.3	9.8	0.04	0.05	2.30	0.8	19.4	8.2	6.4	3.4
C18	248.2	95.9	22.6	11.5	4.40	1.12	18.7	9.3	15.8	8.0	0.08	0.07	2.25	0.7	22.5	8.1	6.7	3.1
T19	580.9	166.0	37.4	20.6	7.66	2.52	61.4	22.0	26.1	8.7	0.14	0.09	7.85	1.9	51.6	15.2	22.0	8.5
L20	490.2	117.8	32.7	11.9	4.79	1.56	50.2	15.0	24.7	7.7	0.16	0.11	7.12	1.1	44.2	8.0	18.2	6.4
C21	271.3	104.0	25.1	12.9	4.77	0.92	19.8	9.8	18.2	9.7	0.15	0.13	2.76	0.8	24.3	8.4	7.4	3.4
T22	602.7	374.5	64.6	40.9	6.58	2.04	50.3	106.1	42.4	158.8	0.18	0.04	6.86	1.2	45.8	11.0	15.9	3.6
T23	578.5	227.2	48.7	51.2	5.24	1.82	83.6	16.0	93.1	16.3	0.03	0.14	3.77	2.0	35.4	11.2	8.6	6.2
C24	293.8	112.4	28.3	15.4	5.44	1.62	21.8	10.0	20.5	11.6	0.14	0.12	3.10	1.1	26.5	8.8	7.8	3.4
C25	313.5	123.0	30.7	17.4	7.17	3.47	23.6	11.4	22.7	13.7	0.20	0.13	3.31	1.3	26.2	8.8	7.6	3.3
C26	321.9	140.6	41.7	42.0	8.40	4.22	26.2	10.8	26.3	16.4	0.31	0.17	3.53	1.4	26.2	8.8	7.7	3.2

Note

1. The source-to-sea survey locations are denoted with numbers from 1 (source) to 26 (sea) with the River Clyde indicated by a 'C' and the tributaries by a 'T' or a 'L', where direct inflow is from a loch.
2. The highest ion concentrations are in the urban tributaries T19, T22 and T23.
3. The highest variation associated with ion concentrations is linked to the urban tributary T22.

Table 3.A.4 - Correlation between nutrients and GHG and percentage land-cover across all tributaries and Clyde headwater sampling points

	CH ₄	CO ₂	N ₂ O	EC	DO%	pH	DOC	DIC	TDN	TP	SUVA ₂₅₄	Cl ⁻	NO ₃ ⁻	SO ₄ ²⁻	Na ⁺	NH ₄ ⁺	K ⁺	Ca ²⁺	Mg ²⁺
Acid grassland	-0.38	0.06	-0.40	-0.84	0.24	-0.84	-0.88	-0.77	-0.94	-0.93	0.79	-0.87	-0.91	-0.72	-0.63	-0.77	-0.75	-0.83	-0.74
Arable / horticulture	0.51	-0.05	0.07	0.65	-0.06	0.73	0.48	0.77	0.74	0.67	-0.63	0.63	0.75	0.41	0.20	0.82	0.80	0.72	0.79
Bog	0.04	-0.41	0.02	0.36	0.23	0.63	0.64	0.27	0.61	0.77	-0.41	0.49	0.58	0.25	0.41	0.33	0.23	0.32	0.23
Coniferous woodland	0.05	0.28	0.08	0.16	0.15	0.05	0.61	0.20	0.27	0.30	-0.11	0.14	0.24	0.08	-0.04	0.22	0.12	0.25	0.24
Freshwater	0.12	-0.05	-0.10	-0.10	0.13	-0.03	-0.22	-0.09	-0.10	-0.16	-0.04	-0.02	-0.08	-0.13	-0.13	0.01	-0.04	-0.13	-0.07
Heather	-0.15	-0.20	-0.01	0.19	-0.01	0.08	0.55	0.08	0.33	0.14	-0.27	0.30	0.29	0.22	0.14	0.28	0.15	0.21	0.09
Heather grassland	-0.03	0.13	0.15	-0.05	-0.21	-0.22	0.10	-0.06	-0.10	-0.07	-0.06	-0.01	-0.13	-0.12	-0.01	-0.13	-0.04	-0.09	-0.09
Improved grassland	0.21	-0.20	0.38	0.76	-0.18	0.82	0.91	0.64	0.91	0.94	-0.70	0.80	0.86	0.70	0.69	0.63	0.60	0.73	0.59
Inland rock	0.71	0.56	0.55	0.73	-0.55	0.48	0.36	0.85	0.54	0.44	-0.51	0.46	0.54	0.71	0.33	0.62	0.79	0.80	0.88
Urban + Suburban	0.59	0.06	0.49	0.88	-0.56	0.85	0.36	0.84	0.78	0.70	-0.81	0.90	0.79	0.76	0.67	0.77	0.85	0.82	0.78

Notes

1. Values in bold are significant at P < 0.05.
2. There is a strong correlation between broadleaf woodland and urban and suburban land-cover within the Clyde catchment (R² =0.91, P-value <0.001), possibly because broadleaf woodland has been planted within the suburban and urban environment. Hence broadleaf woodland has not been included.
3. To ensure all data points are independent only tributaries and the upper River Clyde are included. As a result, the lower Clyde points (including the large UWWTP linked to high CH₄ concentrations) are not included to avoid confounding of catchments.

Table 3.A.5 - GHG correlation with water physiochemical properties dissolved ion concentrations.

	EC	T _w	pH	DO	DO%	DOC	DIC	TDN	TP	SUVA ₂₅₄	Cl ⁻	NO ₃ ⁻	SO ₄ ²⁻	Na ⁺	NH ₄ ⁺	K ⁺	Ca ²⁺	Mg ²⁺
CH ₄ -C	0.41	0.34	0.13	-0.47	-0.42	0.03	0.41	0.43	0.45	-0.18	0.26	0.39	0.33	0.19	0.44	0.38	0.38	0.45
CO ₂ -C	0.23	-0.04	-0.10	-0.28	-0.64	-0.02	0.19	0.23	0.19	0.02	0.17	0.22	0.21	0.11	0.32	0.19	0.20	0.23
N ₂ O-N	0.49	-0.14	0.12	-0.11	-0.38	0.01	0.16	0.47	0.51	-0.10	0.58	0.45	0.29	0.18	0.46	0.30	0.22	0.31

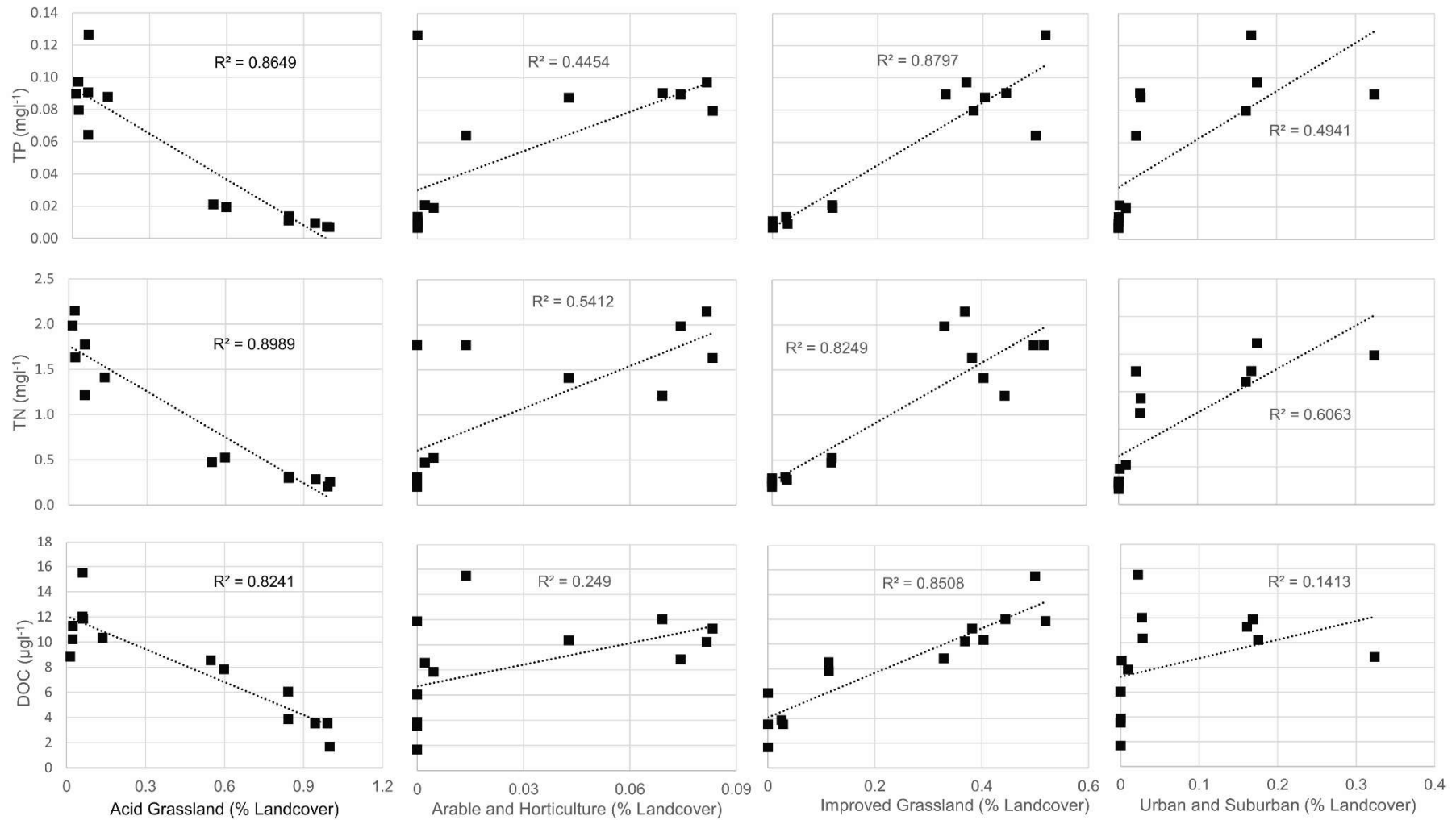


Figure 3.A.1 - Correlation between TP, TDN and DOC, and percentage land-cover across Clyde tributaries and headwaters

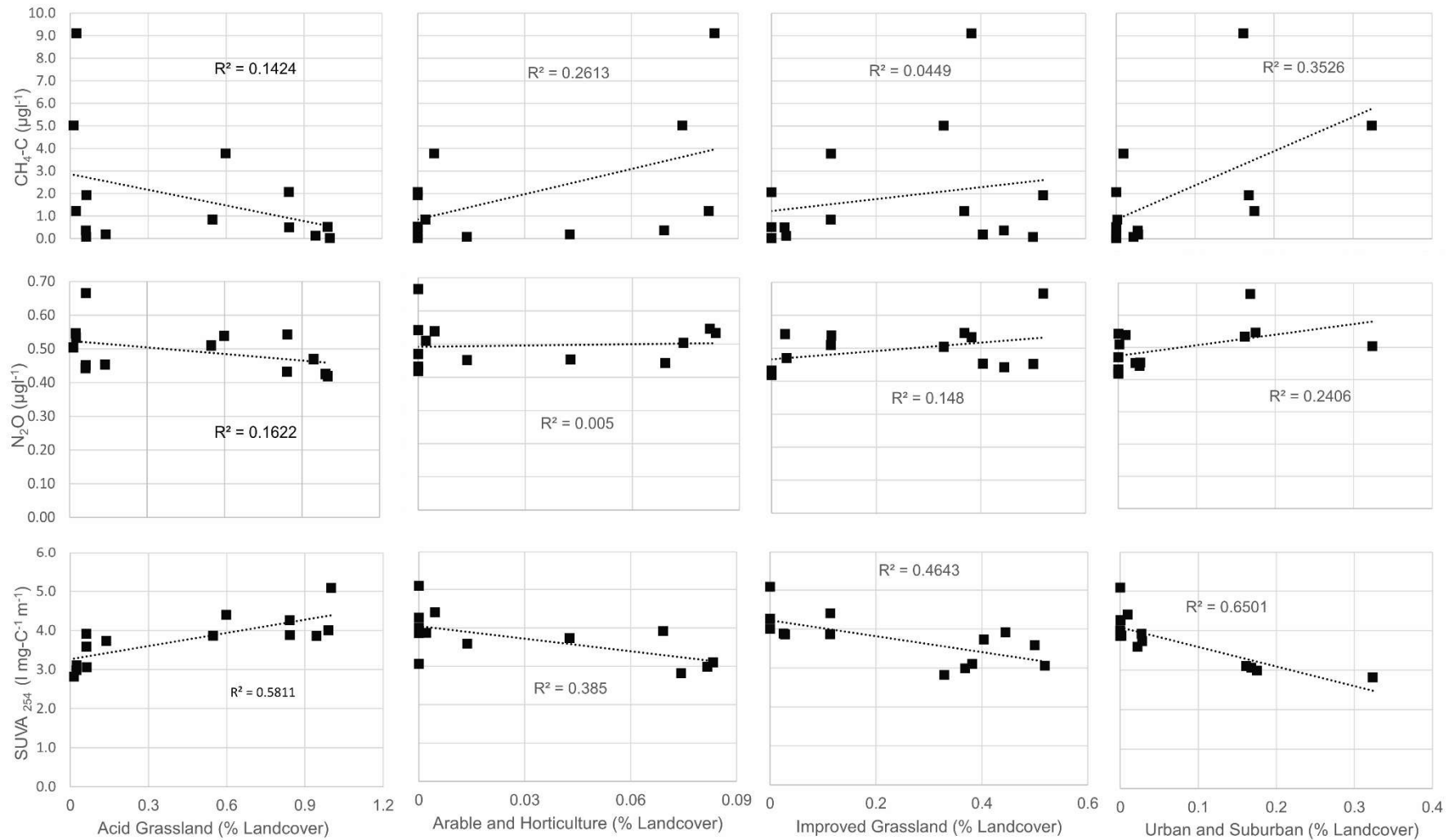


Figure 3.A.2 - Correlation between CH₄, N₂O and SUVA₂₅₄ and percentage land-cover across Clyde tributaries and headwaters

Spatial plots for all physio-chemical properties

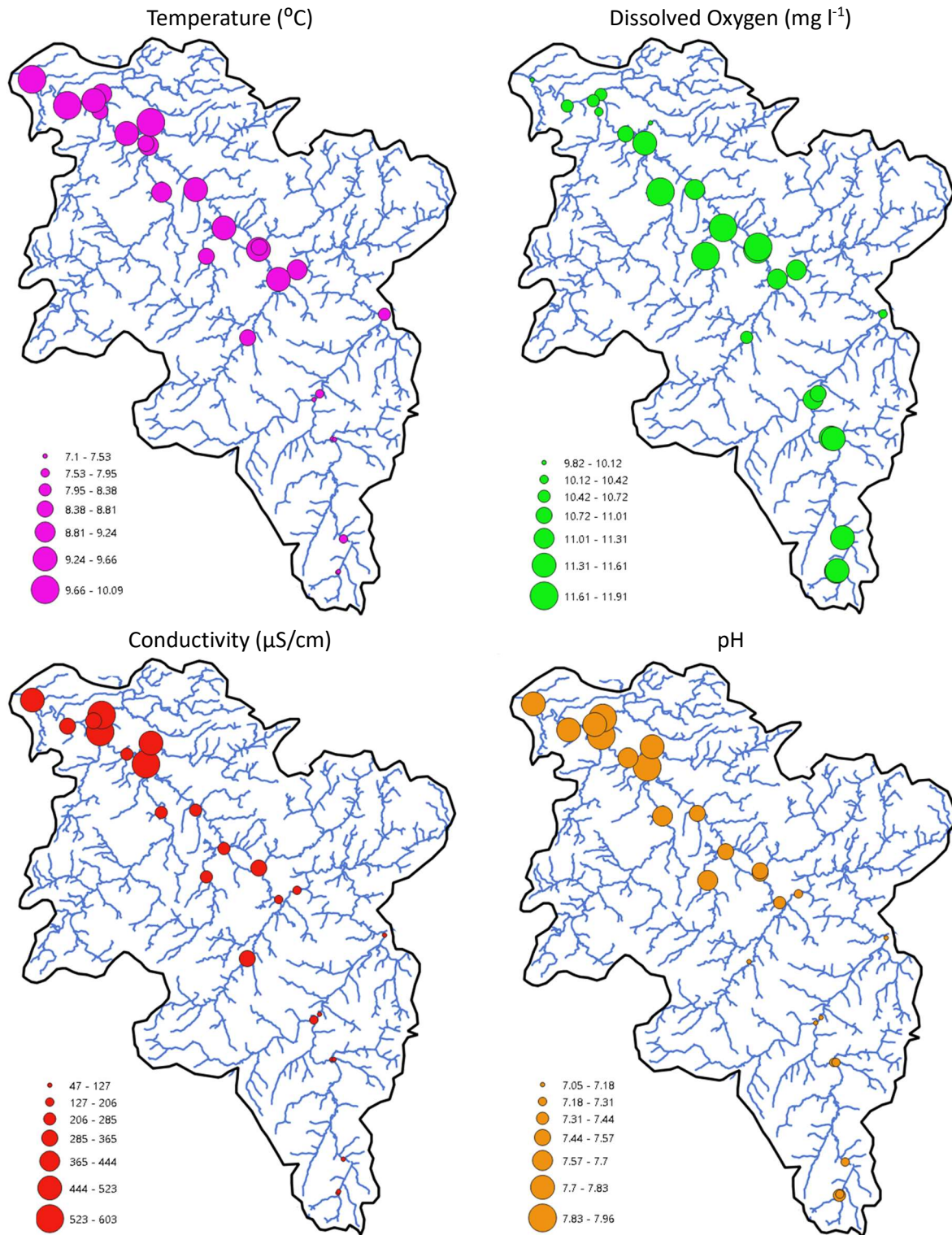


Figure 3.A.3 - Spatial plots for Temperature, Dissolved Oxygen, Conductivity and pH

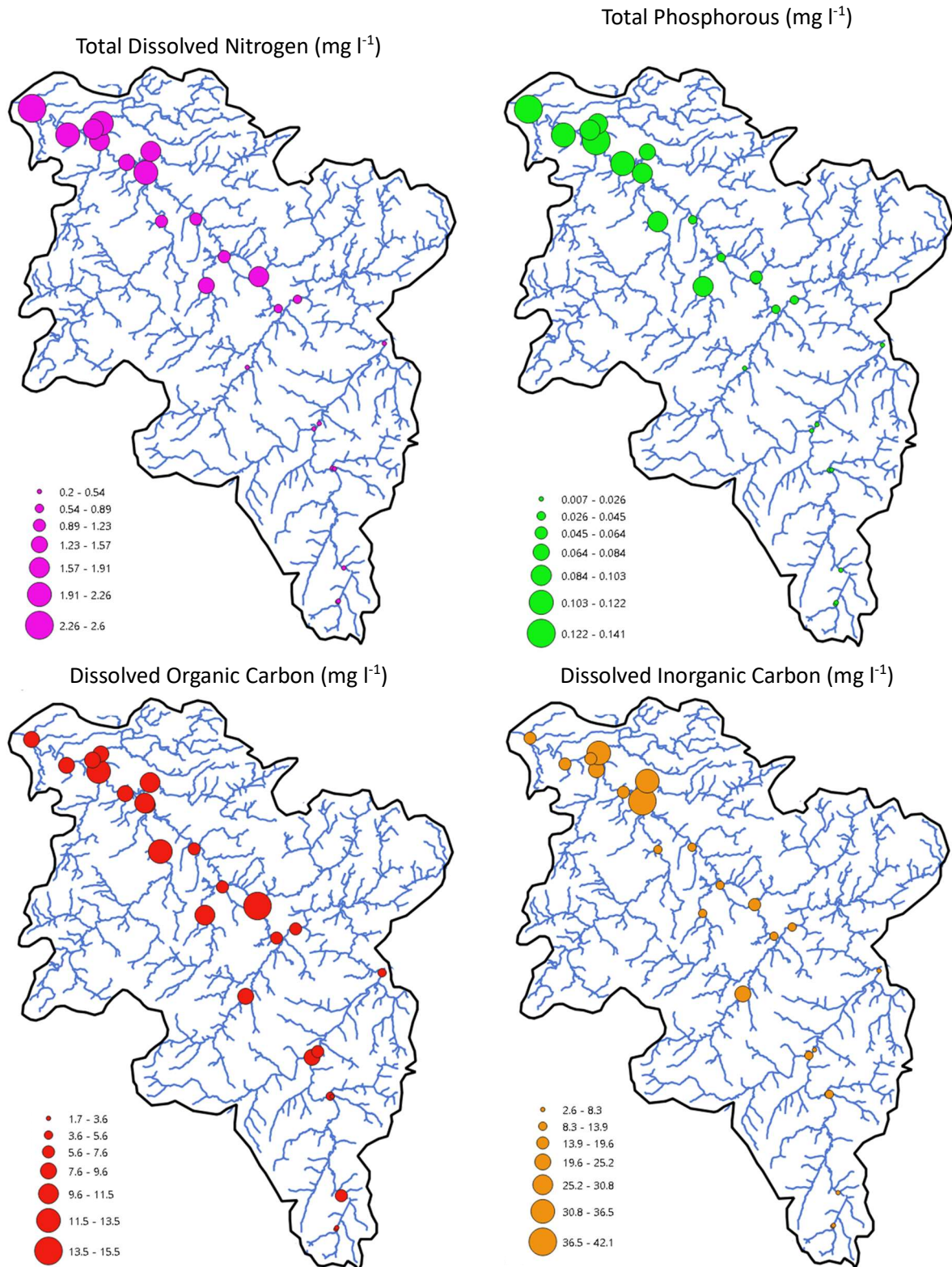


Figure 3.A.4 - Spatial plots for Total Dissolved Nitrogen, Total Phosphorous, Dissolved Organic and Carbon and Dissolved Inorganic Carbon

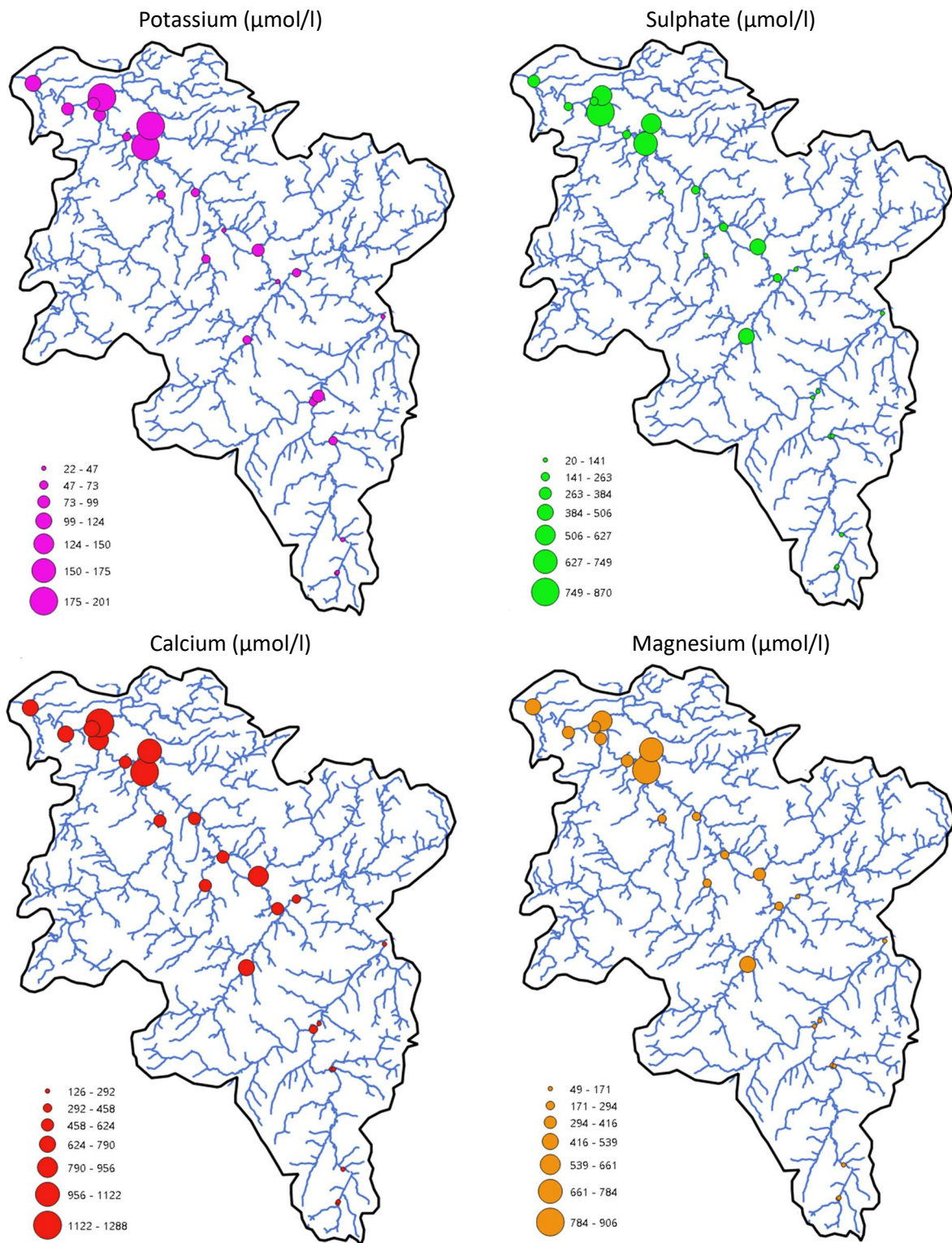


Figure 3.A.5 - Spatial plots for Potassium, Sulphate, and Calcium and Magnesium ions

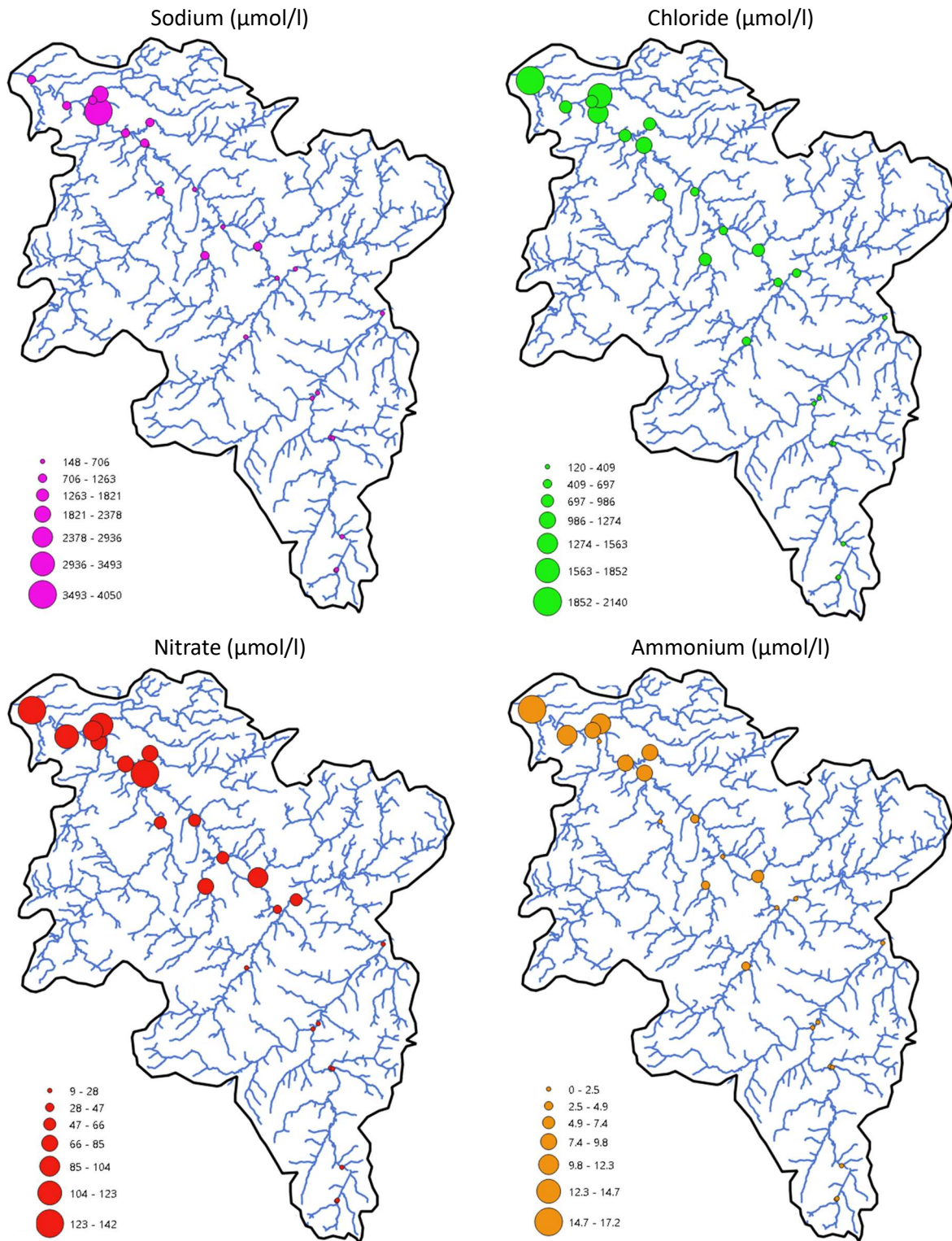


Figure 3.A.6 - Spatial plots for Sodium, Chloride, Nitrate and Ammonium ions

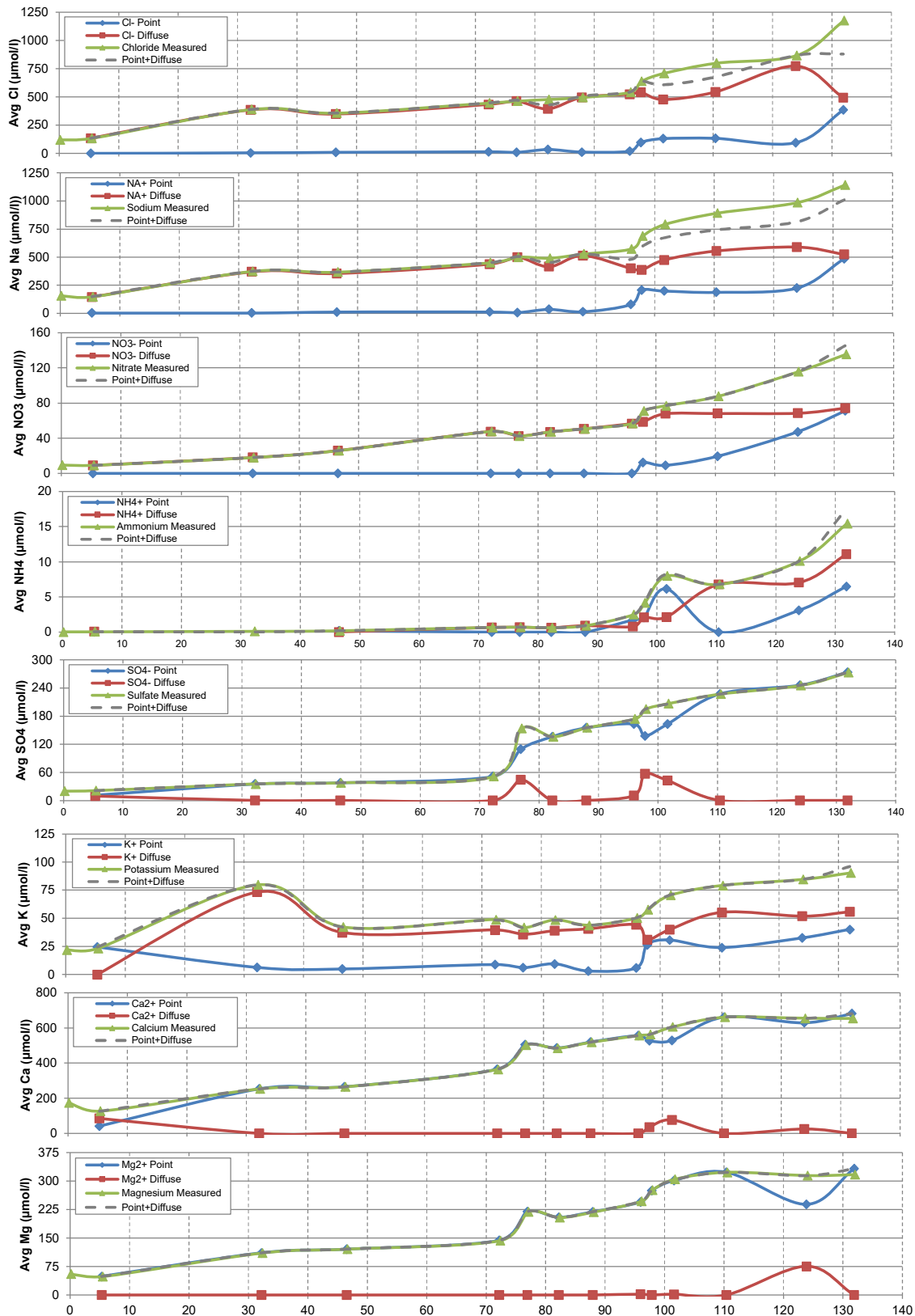


Figure 3.A.7 - River Clyde Average concentrations for ion point source and diffuse sources (a) Cl⁻, (b) Na⁺, (c) NO₃⁻, (d) NH₄⁺, (e) SO₄²⁻, (f) K⁺, (g) Ca²⁺, (h) Mg²⁺ against distance from source to Glasgow Green (132km). Average measured concentrations represent the average of the 21 surveys for each location. The point and diffuse source modelling has been applied to the 2 year of flow data at 15-minute interval. Unattributed relates to the concentrations which cannot be attributed the river Clyde or its measured tributaries.

4 Sources and controls of greenhouse gases and heavy metals in mine water: A continuing climate legacy

Declaration of authorship: The data in this chapter was collected and analysed by the author of the thesis, with Dr. Amy Pickard supporting one sampling campaign. The work was supported by a NEIF grant for radio isotope work which was undertaken by Dr. Mark Garnett. Co-authors reviewed paper drafts and provided supervision, feedback, and guidance.

The chapter has been submitted to the Science of the Total Environment and is under review

Graphical Abstract

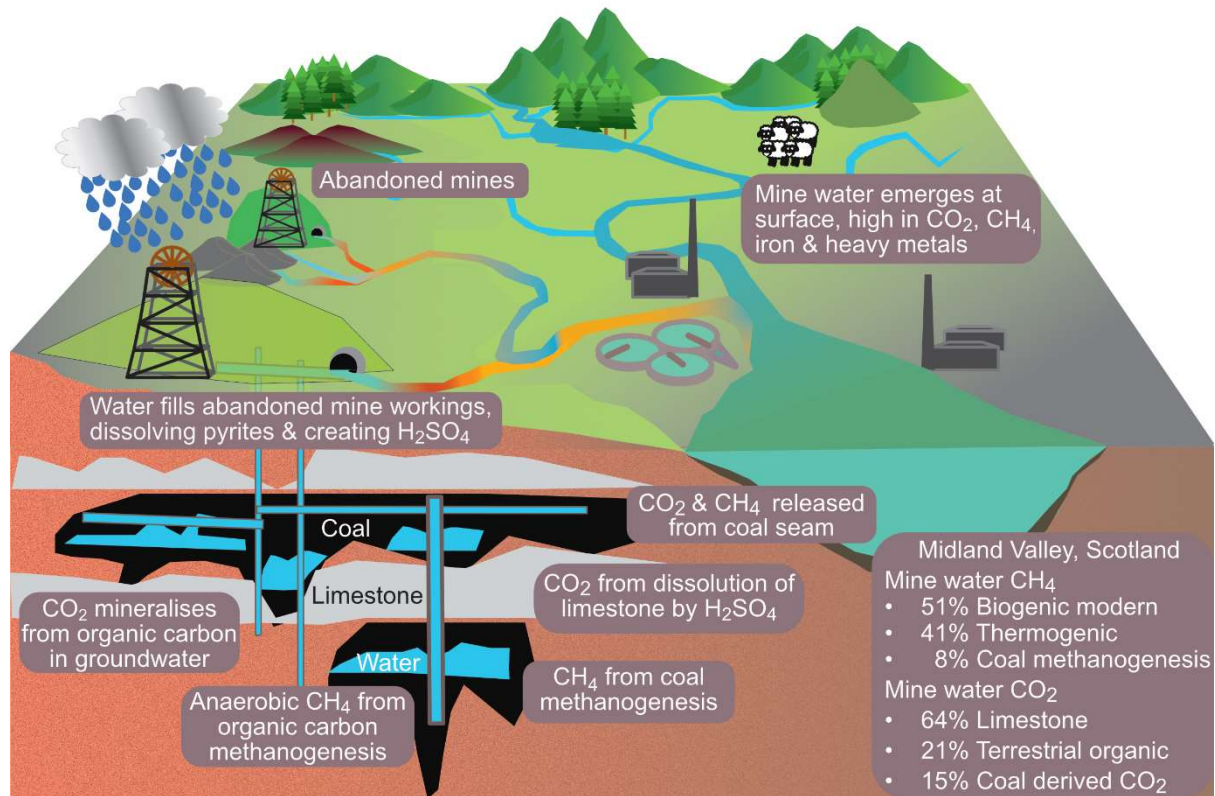


Figure 4.0 - Graphical Abstract - Sources and controls of greenhouse gases and heavy metals in mine water

Highlights

1. Water from abandoned coal mines contains high levels of carbon dioxide and methane.
2. Mine water as a source of GHGs, needs recognition in greenhouse gas budgets.
3. Methane sources were modern biogenic, thermogenic and coal-based hydrogenotrophic.
4. Carbon dioxide sources were limestone, terrestrial organic carbon and coal.
5. Mine water treatment removed Fe and As and partially removed Ni, Co and Mn only.

Abstract

Water pollution arising from abandoned coal mines, is second only to sewage as a source of freshwater pollution in Scotland and in coalfield catchments, mine water can be the dominant pollutant, with oxidised iron smothering the bed of receiving rivers. This study measured greenhouse gases in mine water outflows from sixteen sites across the Midland Valley in Scotland. Radiogenic and stable carbon isotopes measurements ($\Delta^{14}\text{C}$ and $\delta^{13}\text{C}$) were used to determine the sources of both methane (CH_4) and carbon dioxide (CO_2) produced within the flooded mine environment. Concentrations of $\text{CH}_4\text{-C}$ ranged from 20 to 215 $\mu\text{g l}^{-1}$ and $\text{CO}_2\text{-C}$ from 30 to 120 mg l^{-1} , with CO_2 accounting for 97% of the mine water global warming potential. Methane origins included 51% modern biogenic, 41% thermogenic and 8% from hydrogenotrophic methanogenesis of coal. The most significant inverse impact on biogenic CH_4 concentrations was sulphate, most likely due to sulphate reducing bacteria outcompeting methanogens. Carbon dioxide origins included 64% from the dissolution of limestone, 21% from terrestrial organic carbon and 15% from coal. The limestone derived CO_2 was positively correlated with high sulphate concentrations, which resulted in sulphuric acid and caused the dissolution of carbonate from limestone. The mine waters experienced significant carbonate buffering becoming only slightly acidic (pH 6 - 7), but with significant loss of inorganic carbon. The mine waters had low dissolved oxygen (6 - 25%) and high dissolved iron (2 to 65 mg l^{-1}) and manganese (0.5 to 5 mg l^{-1}) concentrations. GHGs from abandoned mines was estimated as 0.36 % of Scotland's Global Warming Potential. This novel work has contributed information about the sources and controls of greenhouse gas fluxes in mine waters and identified the need to quantify and report this emissions term.

Key words

Greenhouse gases; methane; carbon dioxide; mine water; coal.

Authors

Alison M. Brown^{1,2}; Dr. Adrian M. Bass²; Dr. Mark H. Garnett³; Prof. Ute Skiba¹; Dr. John M. Macdonald²; Dr. Amy E. Pickard¹

1. UK Centre for Ecology & Hydrology, Bush Estate, Penicuik, Midlothian, UK, EH26 0QB.
2. School of Geographical & Earth Science, University of Glasgow, Glasgow, UK. G12 8QQ.
3. NEIF Radiocarbon Laboratory, Rankine Ave, East Kilbride, Glasgow, UK. G75 0QF

4.1 Introduction

4.1.1 Acid mine drainage

In recent decades, heavy metal pollution has become a global environmental issue with implications for both environmental and human health, with mine water (MW) outflows from coal and metal mines constituting one of the major sources of heavy metal pollution to the aquatic environment (Fleming et al., 2021, 2022; Schwarzenbach et al., 2010; Voogt, 2020; Wright et al., 2017; Younger, 2001). When in operation, water is pumped from the mine and the mine is ventilated. The introduction of oxygen oxidises pyrites (iron sulphide (FeS_2)) which accumulate on the mine walls. After mine closure, pumps are switched off, and water rises until it reaches the lowest discharge point (the surface via old adits, springs and seepage or an overlying aquifer). This dissolves the accumulated salts, making the initial discharge from abandoned mines of very poor quality. Additionally when exposed coal seams are flooded, microorganisms can greatly accelerate the oxidation of mineral sulphides forming sulphuric acid, which subsequently dissolves metal compounds present, resulting in high concentrations of Fe, Zn, Cu, Pb, Cd, Mn and Al (Dhir, 2018; Alhamed and Wohnlich, 2014; Stearns et al., 2005), with most pollution from deep mines rather than opencast (Younger, 2001).

Mine water from abandoned mines, including coal mines, has been documented as globally, polluting water bodies including groundwater (Acharya and Kharel, 2020; Tomiyama and Igarashi, 2022). These impacts are likely to increase in future and be with us for many hundreds of years (Younger, 1997). China is the biggest producer of coal globally with its national production rising by over 10% in 2020 to reach 4560 million tonnes, equivalent to 52% of global production. Other countries that contribute more than 5% of global coal mining production include the US, India, Australia, Russia and Indonesia (Energy Institute, 2023). While comprehensive figures for abandoned mines do not exist, South Africa has identified 6,152, the United States > 500,000, Australia 50,000 and the United Kingdom 2000 (Thisani et al., 2020). The number of abandoned coal mines in China is expected to reach 12,000 by 2020 (Lyu et al., 2022) with China the most seriously impacted country by mine water (Li, 2018).

In addition to being a source of heavy metals, MWs are supersaturated with greenhouse gases (GHG), including carbon dioxide (CO_2) and methane (CH_4). Where carbonate rock is present, the sulphuric acid generated in the mine dissolves the carbonate to produce CO_2 . Elevated concentrations of CO_2 are common in discharges from abandoned coal mines (Hedin and Hedin, 2016; Vesper et al., 2016; Jarvis, 2006), though its contribution to global GHG budgets remains uncertain. As the carbonate dissolves, the acid is neutralised, the pH typically rises to around pH 6, reducing the environmental impact, and MW becomes supersaturated with CO_2 (of a fossil origin) with high inorganic carbon loading in the form of bicarbonate. Where limestone is not present in the mine, it is often added to the treatment process to aid neutralisation (Dhir, 2018; Watten et al., 2005) also producing CO_2 . Additionally CO_2 may be produced by in-water mineralisation of modern dissolved organic carbon (DOC) in groundwater (Winterdahl et al., 2016), and CO_2 may be associated directly with ancient coal seams which could transfer into the MW (Iram et al., 2017).

Details of CH_4 released in MW are currently poorly constrained. The production mechanisms are not necessarily simple but there are likely two main mechanisms encompassing three sources: thermogenic CH_4 from the coal seams (degradation of coal due to high temperature

and pressure) and biogenic CH₄ from both ancient and modern carbon sources, which may progress via acetoclastic (using acetate) or hydrogenotrophic (using CO₂ and hydrogen (H₂)) methanogenesis (Moguel et al., 2021; Mayumi et al., 2016; Meslé et al., 2013). Thermogenic CH₄ is associated with all coal seams, with deeper and older coal seams typically containing more CH₄ than shallower younger seams (IEA, 2020). Once underground mines flood, the hydrostatic pressure on the coal seams stabilises and CH₄ emissions are estimated to continue until the mines are completely flooded (Fernando, 2011). However CH₄ emissions can continue where workings remain above the recovered water levels and pockets of CH₄ can be trapped by rising waters (Kershaw, 2005). Projections of global coal mine CH₄ emissions to 2100, estimate a 4-fold increase from active underground mines and an 8-fold increase from abandoned mines (Kholod et al., 2020), though this does not account for CH₄ dissolved in the MW which subsequently evades to the surface. The rate of CH₄ emissions from abandoned coal mines was linked to the size of the remaining CH₄ reserve, with CH₄ content increasing with depth (Kershaw, 2005). Hence emissions of CH₄ from MW could be associated with the dissolution of thermogenic CH₄, despite its low solubility, with the concentration dependent on the depth and age of the coal and the size of the remaining CH₄ reservoir. Biogenic CH₄ production may occur because of the presence of methanogenic bacteria in the MW, with anaerobic biodegradation of either coal substrate or modern organic material accumulating in the mines or from groundwater (Gonzalez Moguel et al., 2021). Microbial degradation of coal to produce CH₄ (coal methanogenesis) is another potential source but the irregular structure of coal and the complex microbial consortia, requiring specific conditions, make it unlikely to occur at all locations. This mechanism has been more commonly found in more volatile grade coals (lignite and bituminous) compared to anthracite found in Scotland (Iram et al., 2017), and would necessarily occur before dissolution of Fe²⁺, a strong electron donor, inhibited methanogenesis (Furukawa et al., 2004). All three mechanisms for CH₄ production are plausible and could occur synchronously.

The different CO₂ and CH₄ pathways leading to subsurface GHG generation will result in different isotopic signatures. For example, CO₂ and CH₄ from ancient sources will no longer contain ¹⁴C and the mechanism of production will impact the amount of ¹³C depletion (Lopez et al., 2017). In this context, carbon radiogenic and stable isotope concentrations ($\Delta^{14}\text{C}$ and $\delta^{13}\text{C}$) are powerful tools for understanding CO₂ and CH₄ sources, which could inform measures to reduce emissions to atmosphere either within the mine or treatment process with clear implications for climate.

4.1.2 Mine water treatment approaches

The generation of low pH MW enhances the dissolution of heavy metals (Saria et al., 2006; Florence et al., 2016), with concentrations likely impacted by geology, flow conditions and MW temperatures. However water from abandoned mines often contains a predominance of calcium bicarbonate (Ca(HCO₃)₂) and calcium sulphate (CaSO₄). The dissolution of these minerals increases pH, consumes hydrogen ions and releases calcium (Ca²⁺), magnesium (Mg²⁺) and bicarbonate (HCO₃⁻). The main environmental hazard of MWs in this situation is therefore not low pH but the high concentration of dissolved Fe(II) associated with low oxygen conditions. When the MW reaches the surface the soluble Fe(II) reacts with oxygen to produce insoluble Fe(III) and this process significantly depletes dissolved oxygen from rivers and streams, producing an orange iron precipitate (Johnston et al., 2008). Most treatment

systems are designed to achieve the oxidation and subsequent precipitation as Fe(III) prior to discharge to the environment.

Wetlands are often used to treat MW as they can absorb and bind heavy metals depending on soil, substrate, hydrology and vegetation. This involves: settling, sedimentation, adsorption, oxidation and hydrolysis of metals and precipitation of metal carbonates and sulphates or anaerobic conversion to metal sulphides and biological removal of heavy metal in the wetlands by plant uptake (Sheoran and Sheoran, 2006). There are variations on the standard treatment approach, dependent on space available, site geography and topography and the requirement to minimise energy usage (The Coal Authority, 2017). The process is primarily designed for the removal of Fe and not specifically for removal of heavy metals or GHGs. Different stages may both promote or reduce GHG release to the atmosphere. There are typically three stages in the treatment process with the different treatment options shown schematically in Fig. 4.1.

1. Oxygenation of the water either via a gravity cascade or chemical oxidation, e.g., adding peroxide, primarily to change dissolved soluble Fe^{2+} (ferrous) to insoluble Fe^{3+} (ferric).
2. Passing the water to a deep lagoon where the insoluble Fe^{3+} has time to settle out.
3. Passing the water through a series of reed beds to filter out fine Fe^{3+} particles.

While research on methods to minimise the impact of acid mine drainage have been ongoing for over 50 years (Verburg et al., 2009), MWs from many abandoned mines globally are not treated. This can be dependent on land-use history, climate, topography, hydrogeology, available technology, socio-political outlooks, environmental scientists and regulatory agencies (Acharya and Kharel, 2020). Global data pertaining to treatment are not available, but some data is available at national scale. For example significant MW pollution is reported for the USA, a legacy of how the mining industry has operated, with average flows of 190,000 m^3d^{-1} of contaminated MW, with around 76,000 m^3d^{-1} untreated, entering the environment from 43 mining sites under federal oversight (Brown, 2019).

GHG emissions from MW could be influenced by the treatment approach. For example, the use of chemical oxidation may provide an opportunity for oxygenation of CH_4 by methanotrophs and the absorption of the CO_2 by reeds, whereas direct out-gassing occurs in a gravity cascade. Sediments within the deep anoxic lagoons could support methanogens, whereas methanotrophs could be supported in the water column, with various forms known to be associated with natural gas (Topp and Pattey, 1997). Burial of inorganic and organic carbon may occur within the mud, but how the mud is disposed of will determine potential carbon capture. MW treatment shallow-water reed beds are a wetland environment and may absorb CO_2 and release CH_4 (Laanbroek, 2010) as wetlands are the highest natural source of CH_4 (Gauci et al., 2010; Peng et al., 2022). Conversely reed-bed may act as a conduit for soil-produced CH_4 passing to the atmosphere or support methanotrophs reducing CH_4 evasion (Macdonald et al., 1998). This complex interplay of processes requires further investigation to determine the potential significance of GHGs in MW.

Given the global challenge presented by pollution from MW, but inadequate understanding and quantification of MW GHG dynamics, further insight into their sources and mechanisms could support remediation approaches with multiple benefits including GHG management. This study addressed the following key questions: (1) can the origins of the MW CH_4 and CO_2 be determined from stable and radiogenic isotopes measurement, (2) what controls variation

in MW CH₄ and CO₂ composition and concentration and (3) do different treatment processes, specifically the use of peroxide or cascade, and varied use of pools and reed beds, minimise GHGs release to the atmosphere improve heavy metals removal.

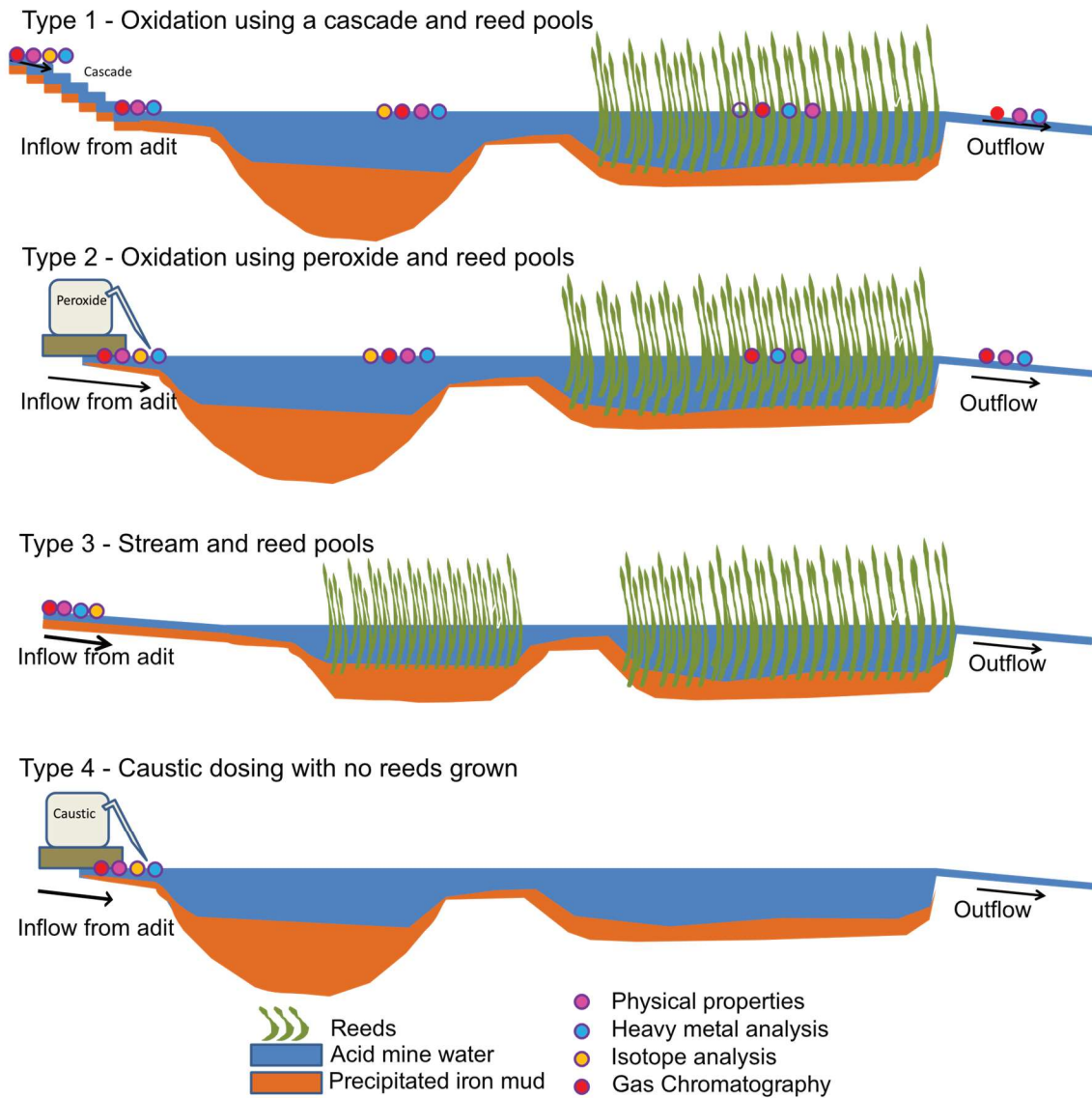


Figure 4.1 - Schematic of main mine water treatment processes for measurement sites.

The pink, blue, yellow and red indicate where different types of measurements were made. Details of which locations used which treatment approach are included in Table 4.1. In type 4 caustic (sodium hydroxide) dosing is used both to oxidise and neutralise the mine waters.

To investigate these questions the Midland Valley in Scotland, a historical coal mining region, was selected for this study. Water pollution arising from abandoned coal mines is second only to sewage as a source of freshwater pollution in Scotland and in many coalfield catchments it is the dominant pollutant source (Younger, 2001). Nine percent of rivers in England and Wales, and two percent in Scotland fail to meet their Water Framework Directive targets of good chemical and ecological status due to abandoned mines and carry high levels of Cd, Fe, Cu and Zn (Johnston et al., 2008). The Coal Authority manages over 75 MW treatment schemes across Britain, treating over 122 billion litres of MW every year (The Coal Authority, 2017), although not all MW is treated at present.

4.2 Materials and methods

4.2.1 Geology and study area

Coal bearing rocks in Scotland date from the Carboniferous and trend from southwest (covering the Ayrshire coast to Glasgow) to the northeast (covering the Edinburgh area and the Fife coast) and identified as the Midland Valley of Scotland. These rocks are bounded by the Highland Boundary Fault to the northwest and the Southern Upland Fault to the southeast (Leslie et al., 2016). Most stages of the Carboniferous are present, with the coal-bearing Namurian strata from the Clackmannan Group. Limestone is both above, below and within the coal measures (Leslie et al., 2016; Dean et al., 2011). Sixteen identified MW outflows were selected from across the Midland Valley, some of which had treatment systems and others which discharged directly into rivers or streams (Fig. 4.2), with full details of the survey locations included in Table 4.1 and additional site information photographs are included in Appendix 2. All of these sites are considered to be in the Limestone Coal Group or the Lower Limestone Coal Group with the exception of MA2 which is considered to be in Productive Coal Measures and MA4 which covers all coal measures from outcrop in the west to the deepest undersea workings in the east (Whitworth et al., 2012). The mines within this survey were closed between 1800 and 1989 (the last being MA6 closing in 1989 and MA4 which closed in 1988 but continued to be pumped until 1995). Many mines closed in the period 1955 to 1974. All the mine locations have been recovering over the last 30-220 years, and assumed to be fully flooded, although at some locations pumping is deployed to prevent the MW from contaminating groundwater.

Between July and September 2022, sixteen MW outflow sites (MA1- MA16) were sampled for dissolved GHG concentrations, water physiochemical properties, carbon stable and radiogenic isotopes of the CO₂ and CH₄ and metal concentrations. At most locations measurements could not be made directly in the outflow and samples were collected via a bucket at the nearest possible access location to the source. Additionally, four treatment locations, two using a cascade (MA7 and MA10) and two using peroxide (MA11 and MA12), were sampled throughout the treatment reed pools to determine the impact of treatment processes on both GHG processing and heavy metal removal. Carbon stable and radiogenic isotopes of the CO₂ and CH₄ were sampled in these reed pool systems for comparison with each source, to determine if retention of CH₄ and CO₂ within the reed pools impacted exchange of carbon between CH₄ and CO₂ or whether additional CH₄ and CO₂ were generated. Use of peroxide instead of a cascade slows the GHG out-gassing to atmosphere. To further understand oxygenation and out-gassing in the cascade systems, one system MA7, which had the most efficient oxygenation cascade, was sampled throughout the cascade. This cascade had 71 steps, each with a length of 0.76m and a drop of 0.16m with the water taking 65 seconds to traverse the cascade. A study of this system, with water sampled every 10 steps enabled the effect of oxygenation and out-gassing to be determined on GHGs concentrations. The outgassing rate of the CH₄, where no CH₄ generation would be expected linked to oxygenation in the cascade, could be used to infer information about the impact of carbonate buffering on CO₂ concentration and the production of N₂O by nitrification on oxygenation of the water. Sample collection in the cascade caused some additional turbulence, but it was assumed to be the same for each measurement point.

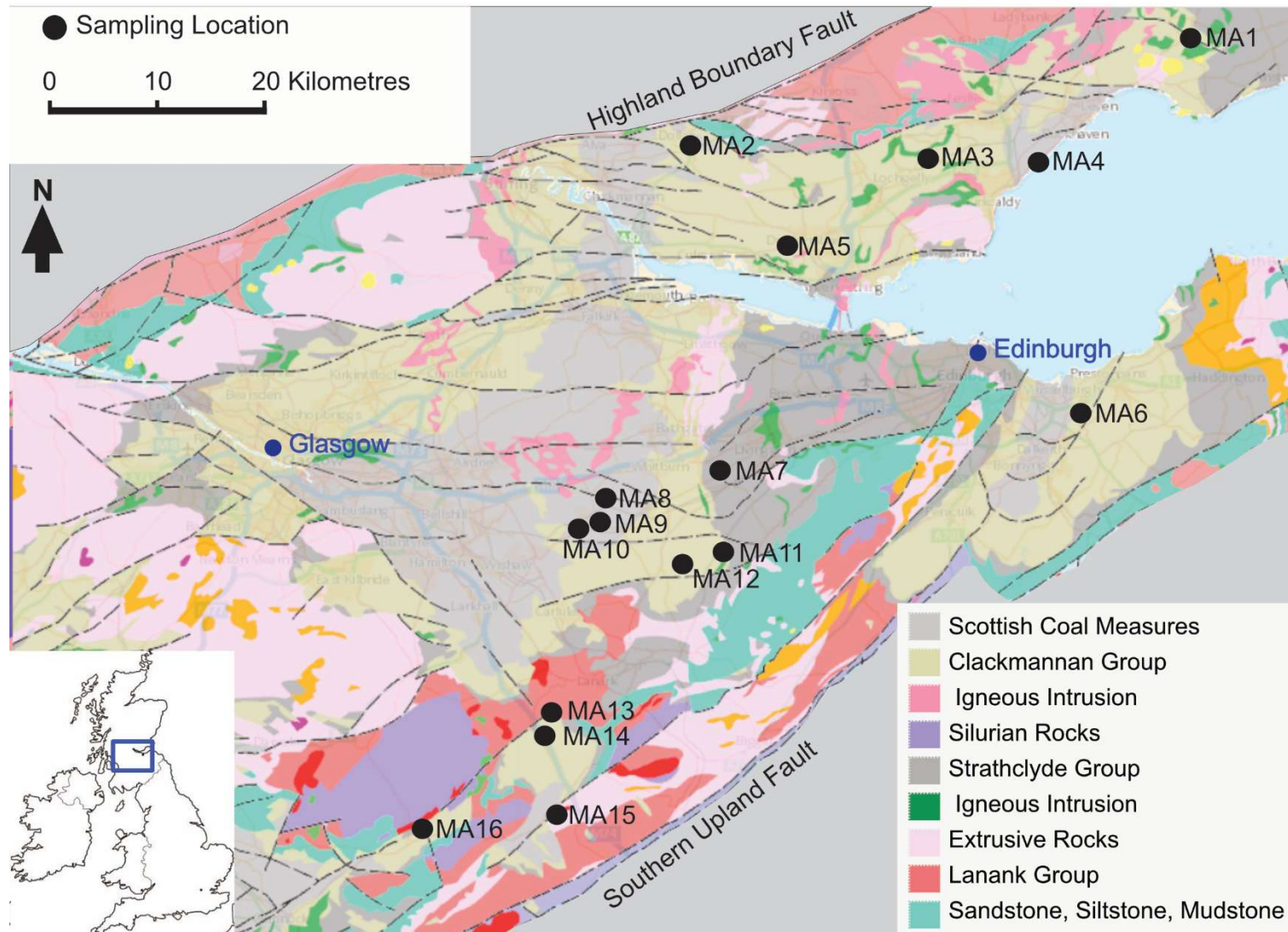


Figure 4.2 - Sample site locations (MA1 to MA16) shown in the relation to the geology of the Midland Valley, Scotland.

Faults and bedrock geology were derived at a scale of 1:625,000 from <https://mapapps2.bgs.ac.uk/geindex/home.html> (British Geological Survey, 2023)

Table 4.2 - Mine water sampling location, treatment, geology and hydrology

No	Location code ⁽¹⁾	Latitude (N)	Longitude (W)	Height (m asl)	Mine or mine water locations name	Treatment ⁽²⁾	Last known mining date ⁽⁴⁾	Source Coal ^{(3) (4)}	Flow (l/s) ⁽⁴⁾	Iron (mg l ⁻¹) ⁽⁴⁾	pH ⁽⁴⁾
1	MA1	56°14'45.06"	2°51'56.68"	145	Lathallan Mill	Treated (3)	Unknown	LCG	12	12.8	N/A
2	MA2	56° 9'30.24"	3°38'36.52"	35	Mains of Blairingone	Treated (3)	1900s - 1954	PCM	5-15	10-25	N/A
3	MA3	56° 8'20.60"	3°16'51.52"	75	Minto	Treated (3)	1967	LCG	40-80	12	N/A
4	MA4	56° 8'1.15"	3° 6'45.45"	50	Frances	Treated (4)	1988, (Pumping stopped 1995)	Multiple	120	40-120	6.2
5	MA5	56° 3'36.90"	3°30'6.14"	40	Pitferrane	Treated (3)	1800, recent opencast	LCG	200-400	3	N/A
6	MA6	55°53'38.10"	3° 3'40.39"	35	Bilston (Junkies Adit)	Discharged	Lady Victoria 1981, Easthouses 1969, Lingerwood 1967 Connected to Bilston 1989	LCG	46	7	N/A
7	MA7	55°50'53.67"	3°36'49.78"	175	Cuthill	Treated (1)	1962	LLCG	5-15	10-30	N/A
8	MA8	55°49'3.96"	3°47'40.92"	200	Shotts	Discharged	1968-1974	LCG	240	1.6	7.1
9	MA9	55°47'59.39"	3°48'50.64"	200	East Allerton	Treated (3)	Unknown, recent opencast	N/A	N/A	N/A	N/A
10	MA10	55°47'43.31"	3°49'40.28"	200	Kingshill	Treated (1)	1974 and 1968	LCG	11.6	11.6	7
11	MA11	55°46'15.03"	3°37'0.78"	240	Pool Farm	Treated (2)	1955	LCG	30-100	10-20	N/A
12	MA12	55°45'40.04"	3°40'36.95"	260	Mousewater	Treated (2)	1955	LCG	30-70	10-30	N/A
13	MA13	55°36'57.91"	3°52'49.97"	210	Johnhill burn	Discharged	Recent opencast - Broken Cross Auchlochan No. 9, 1968,	LCG	N/A	N/A	N/A
14	MA14	55°35'58.21"	3°53'24.73"	225	Muirburn	Discharged	Auchlochan 1968, Coalburn 1962, recent opencast	LCG	N/A	N/A	N/A
15	MA15	55°31'26.18"	3°52'32.54"	225	Glentaggart	Discharged	Glentaggart 1969, recent opencast	N/A	22	4.18	7.12
16	MA16	55°30'43.73"	4° 5'3.35"	215	Kames	Treated (1)	1968	LCG	15-20	15	6.8

Notes

- Locations code: MA- indicates this survey (Mine Adits) and the location code the number from 1 to 16 represents the position on this survey, with 1 furthest north and the 16 furthest south.
- The number in brackets in the treatment column refers to the treatment arrangement as described in Figure 4.1; (1) cascade, (2) peroxide (3) stream and no deep-water pool and (4) caustic with no reeds.
- LCG = Limestone Coal Group, LLCG = Lower Limestone Coal Group, PCM = Productive Coal Measures
- Indicative coal measure, flow, pH and iron concentration is from - The Coal Authority Overview of Mine Water in the UK Coalfields - Advice on Mine Water recovery and Mine Gas (November 2012) (Whitworth et al., 2012), however these values can change with time.
- Johnhill was measured in the receiving stream (Johnhill burn) as mine water pollution was via seepage with the source unidentified. Field sampling and laboratory measurements

Dissolved gas samples were collected in triplicate at each location using the headspace method, together with ambient air samples (Billett and Moore, 2008). Conductivity (Cdt), temperature (T_w), dissolved oxygen concentration (DO), dissolved oxygen saturation (DO%) and pH were measured 0.1 m below the water surface using a HQ40d Multi portable meter (Hach) with a Intellical CDC401 Laboratory 4-Poles Graphite Conductivity Cell, a Intellical LDO101 Laboratory Luminescent / Optical Dissolved Oxygen and a PHC10101 Combined pH electrode. A two-litre water sample was retained for later analysis which was kept in a cool-box until returned to the laboratory for processing. Sample filtration and processing was undertaken on the same day as collection.

Headspace samples were analysed using an Agilent 7890B gas chromatograph (GC) and 7697A headspace auto-sampler (Agilent, Santa Clara, California), with CO_2 , CH_4 and nitrous oxide (N_2O) concentrations determined by running gas vials containing four mixed gas standards prepared in a consistent way to the ambient air samples. The concentrations of the standards gases were: 1.12 to 98.2 ppm for CH_4 ; 202 to 5253 ppm for CO_2 ; and 0.208 to 1.04 ppm for N_2O . Water samples were filtered within 8-hrs of collection through a Whatman GF/F 0.7 μm , under vacuum. Filtrate was then analysed for: total dissolved nitrogen (TDN), total dissolved carbon (TDC) and dissolved organic carbon (DOC) and anion & cation concentration. Analysis for TDN, TDC and DOC were undertaken using a Shimadzu TOC-L series Total Organic Carbon Analyser with all samples run within 24-hrs of collection. The difference between TDC and DOC was used to calculate dissolved inorganic carbon (DIC). The filtration prior to measurement, resulted in out-gassing of any residual GHGs including CO_2 raising the pH, such that most DIC measured by this method was in the form of bicarbonate and will underestimate the total DIC in the original MW sample. TOC measurement accuracy was impacted by high DIC concentrations (Findlay et al., 2010), which was corrected for, but has increased the TOC uncertainty. Ion chromatography using a Metrohm 930 Compact IC Flex was undertaken to determine both anion and cation concentrations. A mixed ion standard containing 11000 ppm chloride (Cl^-), 5000 ppm nitrate (NO_3^-), 4000 ppm sulphate (SO_4^-), 10000 ppm sodium (Na^+), 5000 ppm ammonium (NH_4^+), 1000ppm potassium (K^+), 1000ppm calcium (Ca^{2+}) and 1000ppm magnesium (Mg^{2+}), was diluted to make 8 standard solutions for calibration. These included dilutions of 0.1, 0.5, 1, 2, 5, 10, 25 and 50%. ICP-MS was conducted by Edinburgh University on both filtered and unfiltered samples to determine concentrations of a large range of heavy metals. Agilent 7900 ICP-MS was used to produce a semi-quant scan of each sample in addition to the full quant data for all elements of interest including: Li, Be, B, Na, Mg, Al, Si, P, K, Ca, Ti, V, Cr, Mn, Fe, Co, Ni, Cu, Zn, Ga, As, Se, Rb, Sr, Nb, Mo, Ag, Cd, Sb, Cs, TA, Hg, Pb and U. Concentrations presented are derived from for isotopes with the highest relative abundance. Multi-element calibrations were run at 6 dilutions at the start and then every 15 samples.

4.2.2 Gas partial pressures

To calculate dissolved gas concentrations and partial pressures from the headspace equilibration method the following mass-balance equation was applied (Hamilton, 2006).

$$(C_{0liq}) \cdot (V_{liq}) + (C_{0gas}) \cdot (V_{gas}) = (C_{liq}) \cdot (V_{liq}) + (C_{gas}) \cdot (V_{gas}) \quad (\text{Eq. 1})$$

Where: C_{0liq} and C_{0gas} are the original gas concentration, C_{liq} and C_{gas} are the concentrations in the liquid and gas phases after equilibration (shaking) and V_{liq} and V_{gas} are the volumes of the

liquid and gas in the syringe (assumed to be the same before and after shaking). Assuming equilibrium inside the vessel then C_{liq} can be replaced by:

$$C_{liq} = P_{gas} \cdot \beta_T \cdot P_{BAR} \quad (\text{Eq. 2})$$

Where: P_{BAR} is the barometric pressure at the measurement time and altitude, P_{gas} is the partial pressure in the gas phase, β_T is the Bunsen solubility coefficient as a function of temperature. This can be rearranged:

$$(C_{O_{liq}}) = (P_{gas} \cdot \beta_T \cdot P_{BAR}) + (C_{gas} - C_{O_{gas}}) \cdot (V_{gas}) / (V_{liq}) \quad (\text{Eq. 3})$$

This gas concentration in $\mu\text{moles L}^{-1}$ can be converted to units of ppmv using the Ideal Gas Law, where $\text{ppmv} = (\mu\text{moles L}^{-1}) \cdot (RT)$, where R is the gas constant and T temperature in Kelvin.

This method can lead to errors in CO_2 estimates as dissolved CO_2 is in dynamic chemical equilibrium with other carbonate species. However for these over-saturated MW samples with pH typically < 6.5, the error was estimated to be < 5% and no corrections were applied (Koschorreck et al., 2021). One concern in the study design was that MW GHGs could outgas prior to measurement. This occurred due to the level of supersaturation resulting in observed bubble formation (MA4), turbulence induced by sample collection (MA7 and MA11) and transfer by pipe to the measurement location (MA2 and MA5). The results presented here therefore represent minimum GHG concentrations. Where rapid out-gassing of CO_2 does occur the effect of carbonate buffering resulted in an increase in pH and some of the DIC converting to CO_2 . The known relationships of carbonate chemistry in water can be used to determine if CO_2 out-gassing is occurring before source measurement, allowing the theoretical CO_2 concentration to be determined from the measured pH and DIC concentration (Millero et al., 2006).

4.2.3 Radiogenic and stable carbon isotopes

Collection of samples for the radiogenic and stable carbon isotopes analysis of CO_2 and CH_4 required processing of sufficient water to collect a minimum of 2 mg of carbon for each gas. Evacuated accordion containers were used to collect water for isotopic analysis. A slow pump was used to gently fill the container (to minimise degassing), with between 5 and 6 litres of water. One litre of CO_2 -free air was added to the water container, which was shaken for 2 minutes to equilibrate the headspace. The headspace was subsequently collected in gas tight bags for analysis (Garnett et al., 2016). Stable ($\delta^{13}\text{C}$) and radiogenic ($\Delta^{14}\text{C}$) carbon isotopes were measured at the National Environmental Isotope Facility at East Kilbride. To distinguish between the possible sources of CH_4 and CO_2 , both radiogenic ($\Delta^{14}\text{C}$) and stable ($\delta^{13}\text{C}$) isotope measurements were required and analysis was undertaken by assuming a three-source model (Fig. 4.3) (Gonzalez Moguel et al., 2021; Keith and Weber, 1964; Iram et al., 2017; Lu et al., 2021).

To determine the proportions of the different CH_4 and CO_2 sources the following assumptions were made: (1) any CH_4 from thermogenic or ancient carbon methanogenesis and any CO_2 from limestone or coal would have no measurable ^{14}C , (2) any CH_4 from modern biogenic methanogenesis and any CO_2 from terrestrial DOC mineralisation would be of modern origin and exhibit no significant loss of ^{14}C , (3) the $\delta^{13}\text{C}$ signals from all CH_4 or CO_2 sources were the same across the Midland Valley region and (4) there was no isotopic fractionation of the CO_2 when produced from limestone. However once in the aqueous phase, the CO_2 will fractionate

from the bicarbonate with more ^{13}C in the bicarbonate than the CO_2 . The limestone derived CO_2 has an equilibrium fractional of $\delta^{13}\text{C}$ of -1.26‰ (at 11 °C) (Zhang et al., 1995).

The $\delta^{13}\text{C}$ values from the MW locations for both CH_4 and CO_2 were calculated by iteration and then the $\delta^{13}\text{C}$ confirmed by reference to the literature. The modern biogenic acetoclastic production of CH_4 has a median $\delta^{13}\text{C}$ value of -60‰ , the thermogenic CH_4 has a median $\delta^{13}\text{C}$ value of -30‰ and the hydrogenotrophic production of CH_4 has a median $\delta^{13}\text{C}$ value of -80‰ (Negandhi et al., 2013). The modern terrestrial organic carbon source for CO_2 has a $\delta^{13}\text{C}$ value of -29‰ . The coal carbon source for CO_2 has a $\delta^{13}\text{C}$ value of -23.5‰ (NEIF internal Scottish anthracite standard) with literature values between 23.7‰ and 27.4‰ (Suto and Kawashima, 2016). The limestone source has a $\delta^{13}\text{C}$ value of -6‰ , with the main area of uncertainty around the $\delta^{13}\text{C}$ value for limestone, dependent on the source rock. Literature values ranged between -8.3 to $+2.7\text{‰}$ (Stanienda-pilecki, 2022), -12 to $+4\text{‰}$ (Keith and Weber, 1964) and -4 to $+7\text{‰}$ with European Namurian strata having values -3 to $+6\text{‰}$ (Bruckschen et al., 1999). The $\delta^{13}\text{C}$ for Scottish Carboniferous limestone, to the author's knowledge, has never been measured and the variation in literature values for limestone introduce uncertainty in the CO_2 $\delta^{13}\text{C}$ for this calculation.

4.2.4 Analysis

Pearson's correlation was applied to determine relationships between the GHG concentrations, water physiochemical properties and metal concentrations. Principal component analysis (PCA) was used to determine the level of correlation between the multiple variables within the survey, treating the different locations across the Midland Valley as different data points in a regional study. Values of $p < 0.05$ for correlation and difference tests were considered statistically significant.

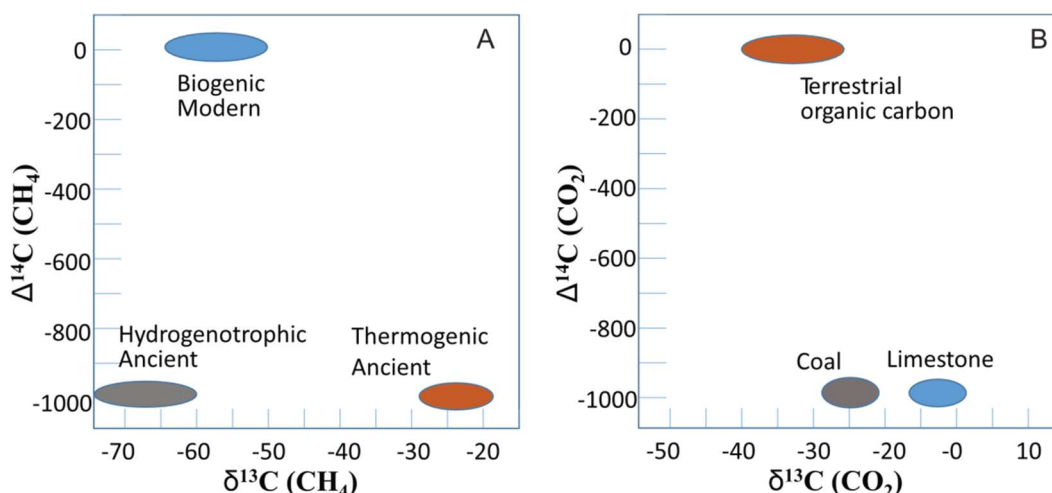


Figure 4.3 - Potential CO_2 and CH_4 sources in terms of their $\delta^{14}\text{C}$ and $\delta^{13}\text{C}$ signature.

Panel A represents signatures for three possible CH_4 sources; modern biogenic, ancient thermogenic and ancient hydrogenotrophic methanogenesis. Panel B represents signatures for three possible CO_2 sources: terrestrial organic carbon, ancient fossil carbon (limestone) and ancient CO_2 from coal. The actual samples will be a mixture of different sources. As both the CH_4 and CO_2 may have a modern or thermogenic/fossil carbon source and have been converted by different processes both $\delta^{14}\text{C}$ and $\delta^{13}\text{C}$ measurements are required (Gonzalez Moguel et al., 2021; Keith and Weber, 1964; Iram et al., 2017; Lu et al., 2021).

4.3 Results

4.3.1 The Midland Valley's mine water physicochemical properties

MW outflows were characterized by high conductivity (400 - 4400 $\mu\text{S cm}^{-1}$), up to two orders of magnitude above that of the receiving river, slightly acidic to near-neutral conditions (pH 6 - 7), a low DO% content (6 - 25%) and surface water temperatures between 9 °C and 16 °C. Compared to receiving rivers MW outflows were high in DIC (40 - 200 mg l^{-1}), Mg^{2+} (10 - 170 mg l^{-1}), Ca^{2+} (50 - 290 mg l^{-1}), K^+ (2.5 - 25 mg l^{-1}) and SO_4^{2-} (25 - 610 mg l^{-1}). The total dissolved nitrogen was between 0.2 and 2.3 mg l^{-1} which most likely reflected the inflowing groundwater and organic carbon values ranged between 0 and 10 mg l^{-1} but most values were close to zero. The MW contained heavy metals with the concentrations ranging between; Fe (2 - 65 ppm), Mn (0.4 - 5.1 ppm), As (0.2 - 3.5 ppb), Co (0.1 - 225 ppb), Zn (1.8 - 125 ppb), Ni (0.5 - 300 ppb), Cu (0.5 - 35 ppb), Al (2.5 - 305 ppb) and B (36 - 1000ppb). Other elements of concern such as Cd and Pb were low, in some cases below the limit of detection for the ICP-MS. Three sites were noted for particularly high concentrations of heavy metals. These were MA4 and MA6, which are outflows from the most recently flooded mines and had the highest concentrations of Fe and Mn and MA2 the only location situated in the Productive Coal Measures (see Table 4.1), which had the highest concentrations of Co, Ni, Se, Hg and Zn. Location MA15 had the highest concentrations of Pb and As.

Due to the high number of variables PCA was undertaken to look at similarities between locations. However, the high metal content of sites, MA2, MA4 and MA6 dominated any analysis, indicating that time since abandonment and coal measure geology are important. To enable other relationships in this regional study to be determined, data from MA2, MA4 and MA6 were removed from the PCA in Fig. 4.4. Mg^{2+} , Ca^{2+} , DIC and CO_2 and SO_4^{2-} are highly correlated, consistent with high acidity from sulphuric acid dissolving the limestone in the coal measures. CH_4 is almost inversely correlated to Mg^{2+} , Ca^{2+} , DIC and CO_2 and SO_4^{2-} suggesting that conditions favourable to CO_2 production may inhibit methanogenesis. Fe is strongly correlated with total TDN and NH_4 and to a lesser extent Na^+ and K^+ . Several metals were positively correlated to SO_4^{2-} and negatively correlated to pH across the range of MWs investigated including Mn, Fe, Co, Ni, Li, B, Zn, Rh, Sr and U. Conversely, Al, Ti, V, As, Cu, Se, Mo, Cs, Hg and Pb show no statistically significant correlations with either SO_4^{2-} or pH. Concentrations of Cd and Pb, often associated with coal measures, were very low.

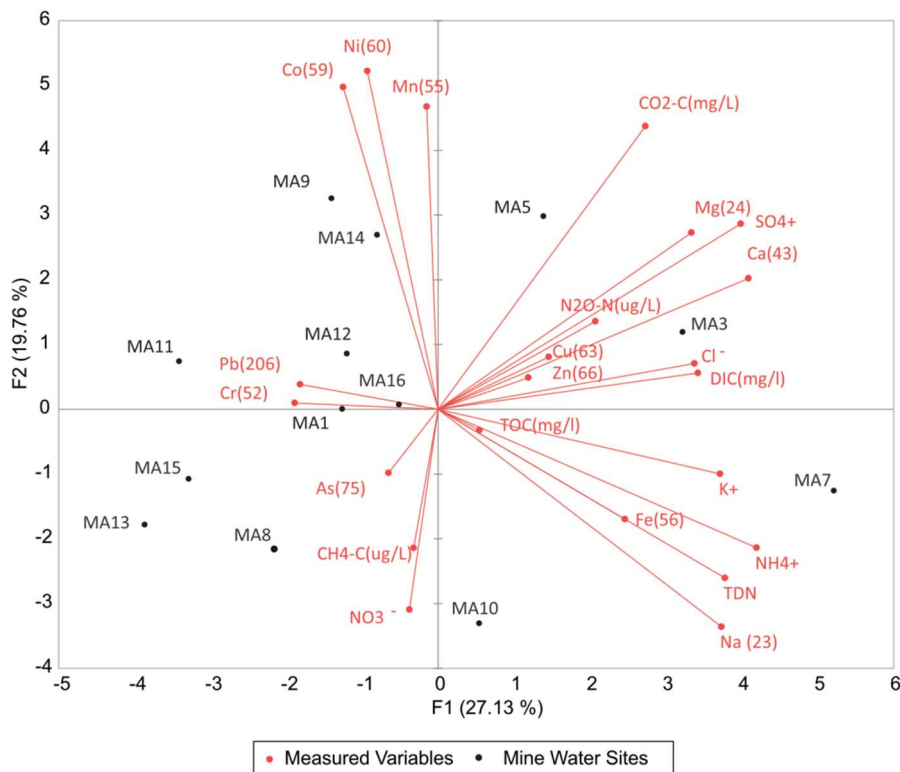


Figure 4.4 - Relationships between greenhouse gases and water chemical properties.

MA1 to MA16 indicate the mine water locations sampled as part of this study (MA 2, 4 and 6 are not included as their high heavy metals concentrations dominate the analysis). Dissolved GHGs include: CO₂-C, CH₄-C and N₂O-N. Water chemical properties include: total dissolved nitrogen (TDN), dissolved organic carbon (DOC) and dissolved inorganic carbon (DIC), Cl⁻, NO₃⁻, SO₄²⁻, Na⁺, NH₄⁺, K⁺, Ca²⁺ and Mg²⁺ Co, Pb, Cr, Mn, As, Ni, Cu, Fe and Zn.

4.3.2 Sources of greenhouse gases in mine water

The GHG concentrations from the MW source locations were high, with [CH₄] and [CO₂] ranging from 20 to 215 µg l⁻¹ and 30 to 120 mg l⁻¹ respectively. Where MW sources were high in DO% and low in GHG, for example at MA2 and MA5, it is likely that some out-gassing has already occurred during transport by underground pipe. The radiogenic and stable isotope data ($\Delta^{14}\text{C}$ and $\delta^{13}\text{C}$) were used to determine the sources of the CH₄ and CO₂, by using a three-source model (Fig. 4.3). Where isotopic characterisation was possible 51% of the [CH₄] were of modern biogenic origin, 41% from thermogenic origin and 8% from hydrogenotrophic origin (Fig. 4.5 A, C and E). Conversely 65% of the CO₂ is derived from limestone, 20% from modern terrestrial organic carbon and 15% from coal related carbon (Fig. 4.5 B, D and F). There is no correlation between the two 'modern carbon' concentrations for CH₄ and CO₂ (Table 4.2). Four locations (MA 8, 11, 14 and 15) appeared to contain no coal-based CH₄ and no coal-based CO₂ as indicated by their $\delta^{13}\text{C}$ values.

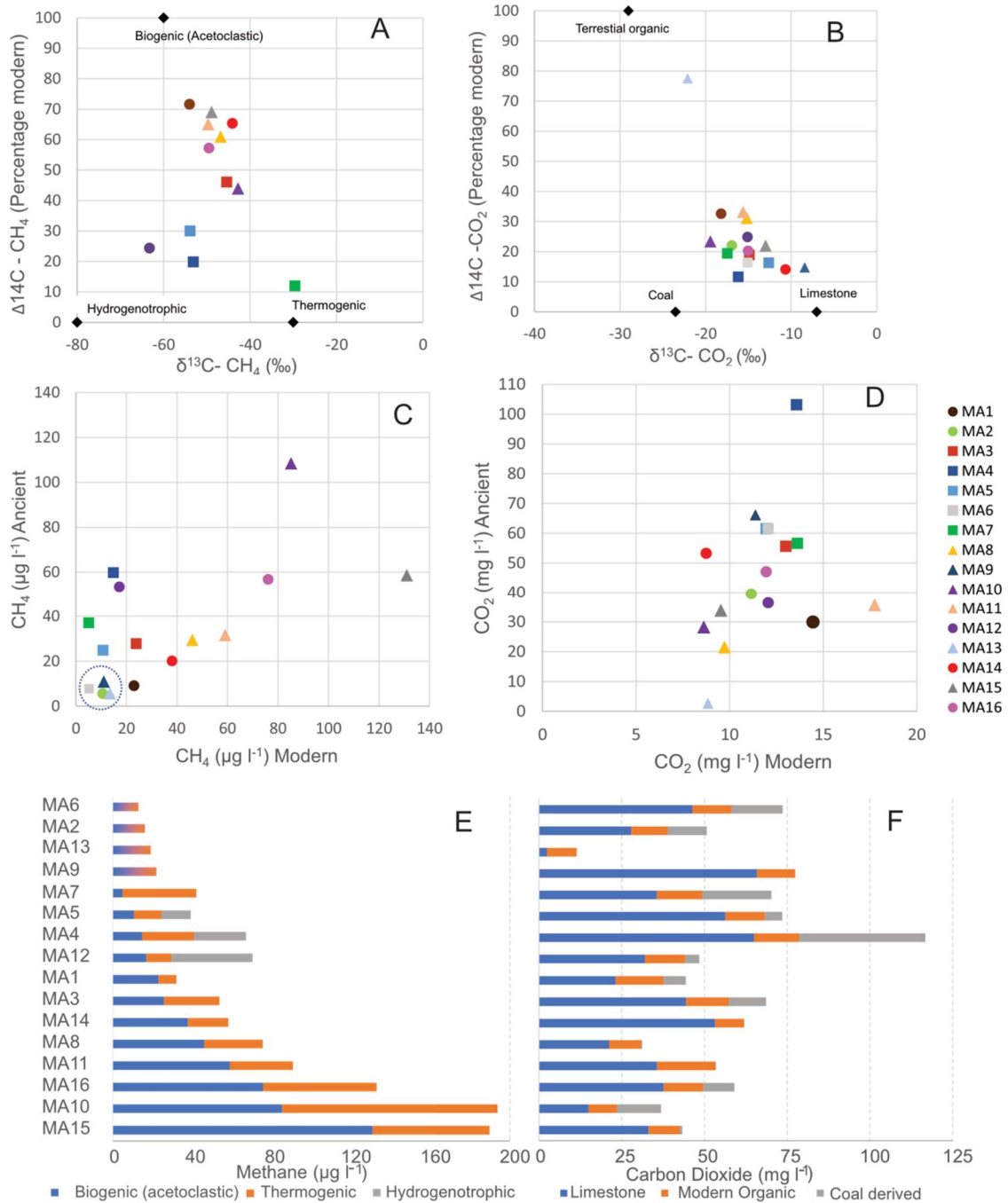


Table 4.2 - Estimated concentrations of methane and carbon dioxide based on radiogenic and stable isotope ratios

Sources		Modern Biogenic CH ₄		Ancient Thermogenic CH ₄		Hydrogenotrophic CH ₄		Modern Biogenic CO ₂		Ancient Limestone CO ₂		Ancient Coal CO ₂	
		Proportion	($\mu\text{g l}^{-1}$)	Proportion	($\mu\text{g l}^{-1}$)	Proportion	($\mu\text{g l}^{-1}$)	Proportion	(mg l^{-1})	Proportion	(mg l^{-1})	Proportion	(mg l^{-1})
MA1S	Lathallum	0.72	22.9	0.23	7.5	0.05	1.6	0.33	14.6	0.52	23.2	0.15	6.7
MA2S	Mains							0.22	11.2	0.55	27.7	0.23	11.9
MA3S	Minto	0.46	23.8	0.51	26.3	0.03	1.6	0.19	13.0	0.65	44.5	0.16	11.1
MA4S	Frances	0.20	14.8	0.46	34.2	0.34	25.6	0.12	13.6	0.56	65.0	0.33	38.2
MA5S	Pitfirrane	0.30	10.7	0.40	14.4	0.30	10.6	0.16	12.0	0.77	56.3	0.07	5.2
MA6S	Bllston							0.16	12.1	0.63	46.2	0.21	15.4
MA7S	Cuthill	0.12	5.0	0.88	37.1	0.00		0.19	13.6	0.51	35.7	0.3	21.0
MA8S	Shotts	0.61	46.1	0.39	29.5	0.00		0.31	9.7	0.68	21.2	0.01	0.3
MA9S	E Allerton							0.15	11.4	0.85	66.1	0.00	
MA10S	Kingshill	0.44	85.1	0.56	108.5	0.00		0.23	8.6	0.41	15.0	0.36	13.3
MA11S	Pool-Farm	0.65	59.0	0.35	31.4	0.00	0.3	0.33	17.8	0.67	35.7	0.00	
MA12S	Mousewater	0.24	17.2	0.24	16.8	0.52	36.7	0.25	12.1	0.66	32.0	0.09	4.4
MA13S	Johnhill							0.78	8.8	0.22	2.6	0.00	
MA14S	Muirburn	0.65	38.0	0.35	20.2	0.00		0.14	8.8	0.86	53.3	0.00	
MA15S	Glentagart	0.69	130.9	0.31	58.7	0.00		0.22	9.5	0.76	33.1	0.02	0.7
MA16S	Kames	0.57	76.1	0.38	50.6	0.05	6.2	0.2	12.0	0.64	37.7	0.16	9.4
Average Source		0.47	44.1	0.42	36.3	0.11	6.9	0.25	11.8	0.62	37.2	0.13	8.6
Weighted average		0.51		0.41		0.08		0.20		0.65		0.15	

Reed Pools		Proportion	($\mu\text{g l}^{-1}$)	Proportion	($\mu\text{g l}^{-1}$)	Proportion	($\mu\text{g l}^{-1}$)	Proportion	Total	Proportion	Total	Proportion	Total
MA10R	Kingshill	0.45	16.8	0.55	20.5	0.00		0.33	8.6	0.67	17.2	0	0
MA11R	PoolFarm	0.66	18.6	0.34	9.6	0.00		0.26	8.2	0.75	24.0	0	0
MA12R	Mousewater	0.31	11.0	0.27	9.8	0.42	15.20	0.23	3.7	0.41	6.3	0.36	5.6

Notes

1. On the location code, S indicates this was a Source location, R indicates this was a reed pool location.
2. The following $\delta^{13}\text{C}$ values have been calculated for CH₄: modern biogenic acetoclastic production = -60 ‰, the thermogenic = -30 ‰ and the hydrogenotrophic production = -80 ‰.
3. The following $\delta^{13}\text{C}$ values have been calculated for CO₂: modern terrestrial organic carbon = -29 ‰. The coal carbon source = -23.5 ‰ and the Scottish Carboniferous limestone = -6 ‰.
4. Both MA13 and MA9 may derive from opencast and appear to have a more positive $\delta^{13}\text{C}$ values for CO₂ from a fossil source (limestone) than at other sites.
5. The [CH₄] was too low at sites MA2 (16.2 $\mu\text{g l}^{-1}$) MA6 (13.1 $\mu\text{g l}^{-1}$) MA9 (22 $\mu\text{g l}^{-1}$) MA13 (19.2 $\mu\text{g l}^{-1}$) to measure the radiogenic and stable isotopes.
6. The average source value is the average across the site and the proportion weighted average is weighted by the concentration of each source.

4.3.3 Greenhouse gas generation or consumption in reed pools

Measurements of $\Delta^{14}\text{C}$ and $\delta^{13}\text{C}$ were made on CH_4 and CO_2 from the reed pools and compared with that at the source (Fig. 4.1), using cascade (MA7 and MA10) and peroxide oxygenation (MA11 and MA12). The cascade at location MA7 was too efficient at outgassing GHGs to enable sufficient sample to be collected for this analysis.

There was no significant change in the $\Delta^{14}\text{C}$ of any reed pool samples compared to the source for CO_2 , however the CO_2 $\delta^{13}\text{C}$ increased. For CH_4 there is a slight increase in percentage modern, particularly for MA12, which has extensive good quality reed pools and a similar increase in the CH_4 $\delta^{13}\text{C}$. This difference was particularly evident for the peroxide systems (MA11 and MA12) where energy is not being supplied by the cascade (Fig. 4.6).

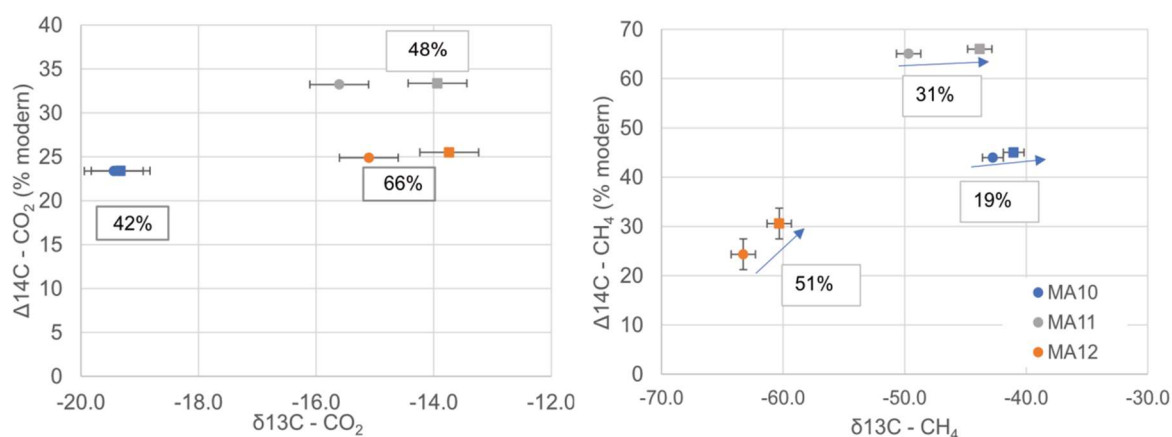


Figure 4.6 - Source to reed pool transition on $\delta^{14}\text{C}$ and $\delta^{13}\text{C}$ composition.

Location MA10 was oxygenated by a cascade system and locations MA11 and MA12 were oxygenated by peroxide. The circle indicates the location source and the square the location reed pool. The arrow showing the direction from source to reed pool. The percentage of the GHG remaining after transfer to the reed pool is indicated in the box for each system.

4.3.4 Impact of oxygenation by cascade on greenhouse gas concentrations

At location MA7 water is pumped 0.25km, from a well (source) site to a location where there is space and height for a 12m gravity cascade to oxygenate the MW. GHGs were measured throughout the cascade, every 10 steps with the final location measured in the reed pool. The cascade increased DO from 17% to 92% and pH from 6.3 to 7.2. The [DIC] (assumed when measured to represent bicarbonate only) decreased from 119 mg l^{-1} to 84 mg l^{-1} . [CH_4] decreased from 482 to 0.2 $\mu\text{g l}^{-1}$ and the [CO_2] from 71 to 6.8 mg l^{-1} . Conversely the N_2O concentrations increased from 0.4 $\mu\text{g l}^{-1}$ to 0.6 $\mu\text{g l}^{-1}$ and then stabilised and further increased in the reed pools. This increase and stabilisation of [N_2O], indicated that N_2O was being produced rapidly within the water, probably stimulated by oxygen availability, with production and outgassing likely in equilibrium. The CH_4 concentration, unaffected by in-water processes could be used to estimate outgassing rate and would suggest that [$\text{N}_2\text{O-N}$] was on average 1.06 $\mu\text{g l}^{-1}$ in the cascade (180% higher than measured). The TDN concentrations in this sample was 1.6 mg l^{-1} , likely derived from groundwater. The outgassing of the CO_2 resulted in a pH change and changed the carbonate balance. Theoretical CO_2

values can be calculated from the pH and [DIC] and indicated that around 38% of the CO₂ had outgassed before measurement.

4.3.5 The effectiveness of reed pools for removing heavy metals

Four treatment systems were selected to examine heavy metal removal, two with a cascade (MA7 and MA11) and two with peroxide treatment (MA12 and MA13) (Fig. 4.1). Measurements were made at each stage of the treatment including; at source, after the cascade (if one was used), after the deep-water pool, in the main reed bed and at the out-flow to the river (or after the second reed bed). Measurements included GHG concentrations and water physicochemical properties in addition to a range of metals. The cascade or peroxide systems increased the DO in the water causing Fe and As to precipitate (Fig. 4.7) demonstrated by the difference in the filtered and unfiltered concentrations. However sufficient time was still required for fine particles of the insoluble Fe (III) and As (v) to settle to the bed. The Co, Ni and Mn are partly removed but do not appear to be precipitated by changes in their oxidations state as there is little difference between the filtered and unfiltered measurements. They may be partly removed by complexing or coagulation and then filtration by reeds or sedimentation. The reed pools had little impact on any other metals, for example Cu was not removed. The residence times within the systems varied, with that estimated for MA7, 11 and 12 in the order of days. At location MA11 there was a significant reduction in treatment residence time, which appeared insufficient for removal of metals, as the second reed bed was by-passed due to maintenance work and water was discharged to the river after the first reed bed.

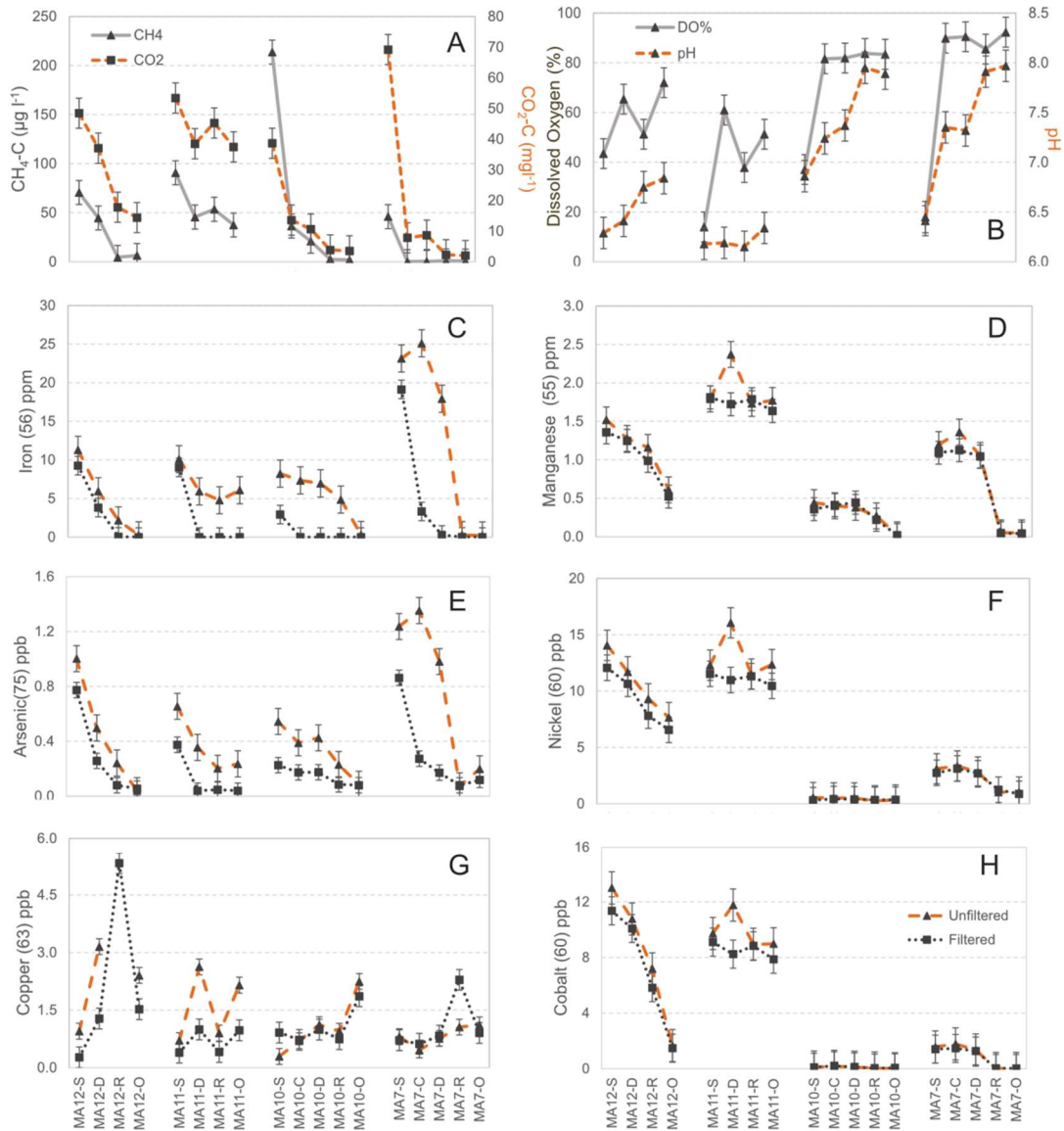


Figure 4.7 - Changes in heavy metal concentrations in treatment reed pools.

Oxygenation is by a cascade for MA7 and MA10 and a peroxide drip for MA11 and MA12. The MA7 cascade is the most efficient oxygenation system. The measurement points through treatment system included: S = source, C = end of cascade, D = exit from deep pool, R = reed pool, O = outflow. At the time of the measurements the second reed pool at MA11 was bypassed reducing the residence time.

4.4 Discussion

4.4.1 Causes of and variation in carbon dioxide and methane in mine water

This study is, to our knowledge, the first to investigate GHGs both in terms of source size and origin in the context of MW outflows. Across the locations in the Midland Valley for which stable and radiogenic isotopes were measured; 51% of the CH₄ was of modern biogenic origin, 41% from thermogenic origin and 8% from hydrogenotrophic methanogenesis of coal origin. Conversely 65% of the CO₂ was derived from limestone, 20% from modern terrestrial organic carbon and 15% from coal related carbon. There was no correlation between the CH₄ and CO₂ ‘modern carbon’ concentrations, suggesting factors other than availability of organic carbon are limiting these concentrations.

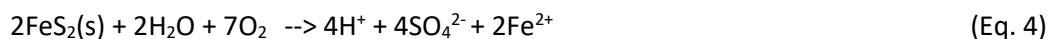
For biogenic CH₄ in MW, 70% of the variation can be accounted for by considering the [SO₄²⁻] and the DO as per the equation in Fig. 4.8 A ($R^2 = 0.78$, p -value < 0.001). Sulphate reducing bacteria (SRB) can outcompete methanogens, with rates of methanogenesis estimated at two orders of magnitude lower than rates of sulphate reduction, indicative of SRB having a higher substrate affinity for H₂ (Lovley and Klug, 1983; Kristjansson and Schönheit, 1983). The inverse relationship with DO may be an indication that anoxic conditions within the mine, increase CH₄ production. Alternatively, it more likely indicates that partial reoxygenation of the MW has occurred prior to measurement. Our results from investigation of a cascade system at MA7 demonstrated that the rate of increase in DO% is proportional to the rate of decrease of GHGs by outgassing. If outgassing rather than mine environment is the main influence on measured DO, this indicates that MW [CH₄] would be higher than measured, with a proportion of CH₄ already lost to the atmosphere. There is no statistically significant correlation between biogenic CH₄ concentration and DOC or time since abandonment, suggesting that time for organic material build up in the mine systems is not a major factor. Several of the deep mine sites have subsequently been mined by opencast including locations MA5, MA10 and MA15, and much of this opencast has undergone land restoration using sewage sludge. This is documented for the area above the MA15 outflow, the location with the highest measured biogenic [CH₄], [Pb] and [As]. It is possible that this contamination is derived not from the mine but from the sewage sludge used in land restoration after 2017 (Eadha Enterprises, 2023; Scottish Power Energy Networks, 2019; Glasgow World, 2017). Sewage sludge could provide a source of modern carbon for biogenic methanogenesis or alternatively the bioavailable heavy metals contained in the sewage sludge could impact microbial metabolism. Metals can act as catalysts for enzymes including methanogens. However high metal concentrations can be toxic to microorganisms (Jarosławiecka and Piotrowska-Seget, 2022). As such adding sewage sludge in land restoration could have multiple, variable impacts on [CH₄] in MW (Paulo et al., 2017).

Thermogenic CH₄ production occurs during coalification as increasing temperature and pressure drive CH₄ from the coal. The CH₄ production increases rapidly with increasing coal rank (based on hardness and volatility) although storage capacity is lower within high rank coals due to their lower porosity (Kholod et al., 2020). The longwall mining approach, often used in the UK, leads to the collapse of overlying strata into the created void, reducing the stress in the overlying 150-200m and underlying 40-70m, with fracturing increasing the permeability of the coal. This together with the reduced pressure from mine ventilation has

resulted in thermogenic CH₄ desorbing from the coal (Jones et al., 2004). Remaining coal seams within the strata, disturbed by mining continue to produce CH₄ at a low rate (Kershaw, 2005). It is hypothesised that once the mine is flooded, water pressure will restrict desorption of thermogenic CH₄, but water moving past the coal dissolved some thermogenic CH₄ probably dependent on the remaining amount of coal and the CH₄ pressure, making up 41% of the CH₄ in this region. Trapped thermogenic CH₄ could also be dissolved, with increasing water pressure. All MW contains thermogenic CH₄, with no statistically significant correlation with time since abandonment, suggesting an equilibrium is reached after flooding, with the amount of CH₄ dissolved, low compared to the size of the CH₄ reservoir. The best predictor of thermogenic CH₄ is pH and T_w as per the equation in Fig. 4.8 B (R²= 0.66, p-value < 0.001).

Hydrogenotrophic methanogenesis is associated with the metabolism of short and long-chain alkanes and polyaromatic hydrocarbon (Gonzalez Moguel et al., 2021). This mechanism was only positively identified at locations MA 4, 5 and 12. Hydrogenotrophic CH₄ production requires CO₂ being produced from coal and reduced with H₂ as the electron donor (Park and Liang, 2016). However, the irregular structure of coal, the need for methoxylated aromatic compounds and complex microbial consortia under specific culture conditions and the more common occurrence in lower rank coals (Iram et al., 2017) are probably the reasons this biodegradation is limited. Hydrogenotrophy has been found to dominate in some low-temperature waters from coal seams with different coals having different methanogens present (Meslé et al., 2013). This mechanism does not appear very important in this region and there is insufficient data to determine causality, but it was found in both the most recent and the oldest abandoned mines.

CO₂ generated from the dissolution of limestone is the major mechanism for production of CO₂ in MW in the Midland Valley Scotland, as all coal measures are associated with limestone. The mechanism involves dissolution of FeS₂ forming sulphuric acid and this acidic environment accelerates the dissolution of limestone forming CO₂ (Eq. 4 and 5). The ratio of dissolved CO₂, carbonic acid (H₂CO₃) and bicarbonate (HCO₃⁻) are dependent on the pH. As the pH increases the percentage of bicarbonate also increases. In this context the strong negative correlation between limestone derived CO₂ and pH is predicted and is improved when the amount of DIC in solution is accounted for (R² = 0.51 and p-value <0.001). The concentration of CO₂ from limestone increased most strongly with [SO₄²⁻] as per the equation in Fig. 4.8 D (R² = 0.66 and p-value <0.001).



The relationship between biogenic CO₂ and pH is also significant as per the equation in Fig. 4.8C (R² = 0.55 and p-value <0.001), with the amount of biogenic CO₂ inversely correlated to pH. The pH is not known to impact DOC decomposition, although decomposition of organic matter leads to the production of acids, these acids are likely to be weak compared to the sulphuric acid produced from FeS₂. T_w was not found to be correlated with biogenic CO₂ although this is usually positively correlated with organic decomposition (Billett et al., 2007). While the proportion of biogenic CO₂ from terrestrial source changes the amount was relatively constant 8 - 18 mg l⁻¹ and probably derived from the DOC in the water entering the mine, resulting in little remaining DOC.

The CO₂ derived from coal may also be the source of the hydrogenotrophic CH₄ found in some MW. Both the CO₂ and CH₄ data are consistent in suggesting that four locations (MA8, MA11, MA14 and MA15) have very little remaining coal and show no evidence for CO₂ from coal. The coal-based [CO₂] is inversely correlated with time since abandonment as in Fig. 4.8 E ($R^2 = 0.73$ and p -value < 0.001), suggesting that less CO₂ from this mechanism was produced with time, reducing to a low stable level (5 mg l⁻¹) after 100-200 years. This is the only identified GHG source to show a statistically significant relationship with time since flooding. This would suggest that loss of dissolved CO₂ is significant compared to the CO₂ reservoir, leading to depletion of this source, probably due to the higher CO₂ solubility compared to that of CH₄. The reduction in coal-based CO₂ suggests hydrogenotrophic methanogenesis is less likely to be significant at new locations in the future.

4.4.2 Causes of heavy metals in mine waters

Heavy metals Fe and Mn had the highest concentrations, and both showed a significant reduction with time from flooding (Fe $R^2 = 0.63$, p -value < 0.001) and (Mn $R^2 = 0.73$, p -value < 0.001 (one value removed)) (Fig. 4.8 F), with reduction to around half the initial concentration after 50-years. Although MA5 had an [Fe] of only 3 mg l⁻¹ (about 5% of the maximum value), the [Mn] was still 2.1 mg l⁻¹ (about 42% of the maximum value) after 230 years. MW outflow receiving rivers were often noted to have high [Mn] (SEPA, 2015). Li, B, K, Rb and Sb, available at much lower concentrations, showed similar significant reductions with time from flooding but this trend is not significant for any other metals in this region. Li, B, Mg, Ca, Mn, Fe, Rh, Sr and Ur showed a positive correlation with [SO₄²⁻] and Co, Ni and Zn a negative correlation with pH, suggesting these are mainly dissolved by the low pH waters. However, there was no evidence that MW pH or [SO₄²⁻] changed with time. Heavy metals are likely to continue to be dissolved if available in the mine. The reed pools were effective at removing Fe and As by oxidation to an insoluble form followed by precipitation. Mn, Co and Ni were also partly removed by the reed pool systems, most likely by adsorption (complexing or coagulation) to particles which subsequently settled, or by precipitation as carbonates and hydroxides which can occur at higher pHs (Nielsen et al., 2013). No other metals were removed. Treatment systems effectiveness was associated with longer residence time and increasing pH and DO, with the high carbonate buffering likely reducing the overall dissolution of heavy metals.

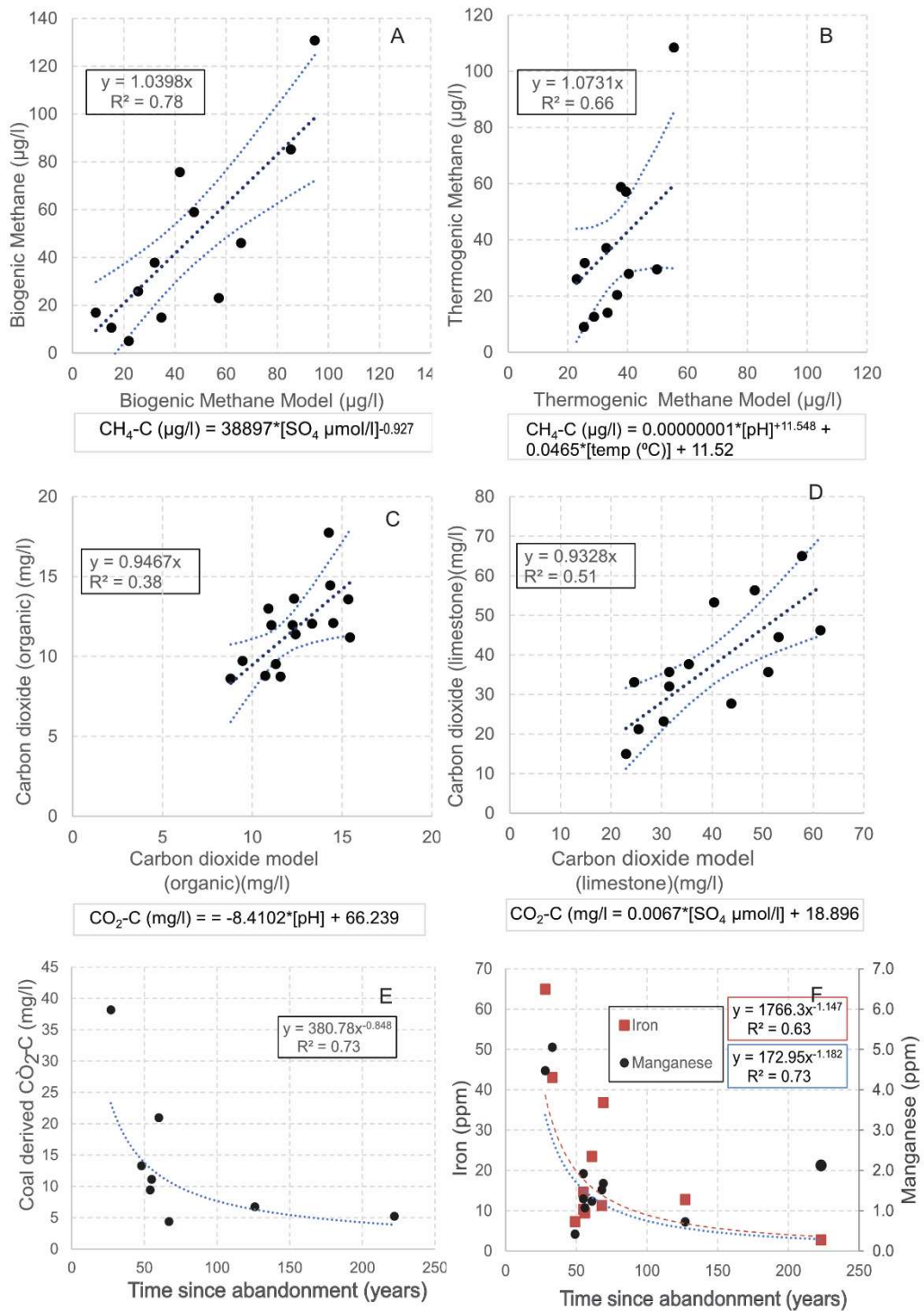


Figure 4.8 - Causal relationship for different CO_2 and CH_4 sources and metal concentration

Panel A - relationship between biogenic CH_4 concentration and sulphate and dissolved oxygen. Panel B - relationship between thermogenic CH_4 concentration and pH and temperature. Panel C - relationship between biogenic CO_2 concentration and pH. Panel D - relationship between CO_2 from limestone and sulphate concentration. Panel E - relationship between CO_2 from coal and time since abandonment. Panel F - relationship between Iron and manganese concentration and time since abandonment. Confidence limits are for 95%. Measurement standard error (σ) for modern CH_4 and CO_2 are in the order of 2% and for the ancient CH_4 and CO_2 sources in the order of 5%.

4.4.3 Greenhouse gases from mine waters are all released to atmosphere

Where cascade systems are used the GHGs in the MW were released directly to atmosphere. The more effective the oxygenation cascade, the more GHGs were released. Where GHGs do enter the reed-pool systems there was little evidence of either CH₄ or CO₂ generation or consumption associated with the wetland environment. The change in the carbonate balance in a cascade resulted in some of the bicarbonate being converted to CO₂ to replace that lost by rapid outgassing increasing carbon loss. In peroxide systems most of the CO₂ is lost to the atmosphere, but 30% less bicarbonate appears to be converted to CO₂, due to slower processing. For CH₄ there is a slight increase in the modern carbon within one treatment system (MA12). This could be indicative of biogenic methanogenesis within the reed pools, but the reed pools are likely to be a weak source for methanogenesis while Fe²⁺ is present. Measurements of CH₄ δ¹³C and CO₂ δ¹³C from the reed pools and compared with that at the source showed an increase in all δ¹³C, which was particularly evident for the peroxide systems where energy is not being supplied by the cascade as was attributed to preferential loss of ¹²C compared to ¹³C during evasion processes.

In the low oxygen conditions in the mine, most of the nitrogen was in a reduced state, as ammonia, and in the presence of Fe²⁺, a strong electron donor. As Fe²⁺ is oxidised to Fe³⁺ it donates electrons enabling nitrification (Wrage et al., 2001). Once oxygenation of the water occurred, N₂O was observed to increase, suggesting nitrification was main mechanism of nitrogen processing, as observed in the cascade at MA7. The N₂O concentration increased through the treatment process provided TDN was available in the MW. Reducing nitrogen in groundwater would reduce this GHG source.

Due to methodological limitations resulting in outgassing prior to measurements, GHG measurements represent a minimum value. The average unweighted measured dissolved CO₂ concentrations across all sites was 58 mg l⁻¹ and the average unweighted theoretical CO₂ concentrations was 91 mg l⁻¹, suggesting that on average 37% of the supersaturated gases may be escaping prior to our measurements. The largest factor dictating the level of gas loss being the CO₂ saturation (R² = 0.51, p-value <0.001). At location MA4, which had the highest CO₂ concentration bubbles were observed in the water as it reached the surface. A secondary factor appears to be distance of transfer, which was evident for locations MA2 and MA5 (Whitworth et al., 2012).

4.4.4 Estimates of the Global Warming Potential in the mine waters

The estimated global warming potential (GWP) of the GHGs from MW are provided in Table 4.3 based on the assumptions: (1) all the GHGs from the MW outgas to atmosphere and are not consumed, (2) the distribution of GHGs across all sites is the same as the distribution measured, (3) the most likely number of potential sites in Scotland is 200 and (4) the average flow volume for all sites is not known, hence flow-weighted average concentrations were used with the average flow volume from the measurement sites (Table 4.3).

Table 4.3 - Global warming potential from mine water in Scotland - High and low estimates are based on ± 3 standard deviations from the mean for concentrations (shown as median)

	High	Median	Low
Number of sources	200	150	100
Average Flow (l/s)	90	70	50
Average CH ₄ - C ($\mu\text{g l}^{-1}$)	77	64	51
Average CO ₂ - C (mg l^{-1})	80	64	46
Average N ₂ O- N ($\mu\text{g l}^{-1}$)	0.73	0.6	0.43
Total GWP (tones / year) (Measured / Calculated)	168334 / 230620	78589/ 107667	26969 / 36940
Percentage of Scotland GWP (%) (Measured / Calculated)	0.42 / 0.58 %	0.20 / 0.27 %	0.07 / 0.09%

Notes

1. GWP for CO₂ = 1, CH₄ = 28 and N₂O =298 (based on a 100-year time horizon) (Myhre et al., 2013))
2. The concentrations are estimated as the flow weighted average values from the survey.
3. 200 mine water sites have been identified (used as the upper estimate) however, the average flow volume for all sites is not known, hence the average flow from the measurement sites was used.
4. Scotland's emissions are 40.0 MtCO₂e as reported for 2020(Scottish Government, 2022)
5. The N₂O estimate is derived from N₂O measured at source but oxidations of the ammonia in MW would enable further N₂O production once the dissolved nitrogen is moved to the reed pools and rivers.
6. The calculated values include the estimated outgassing prior to measurement of 37%.

Our results show the legacy effects of mining related activities and their association with GHG production and climate change in the UK context, where most mining activity has ceased. The UK has over 900 abandoned coal mines (Fernando, 2011) but it is estimated there are over 48,000 in the USA (Manthos, 2016; OSMRE, 2016) and over 1million mines globally (Candeias et al., 2019). Although climate change has prompted many countries to change their coal production strategies, worldwide coal consumption reached 7,585 Mt in 2017, with Asia continuing to expand its coal mining to drive economic development (International Energy Agency, 2018). Global coal consumption rebounded by 6% to 7,929 Mt in 2021 resulting from the energy crisis (International Energy Agency, 2022). Given that mining remains a contemporary pressure, further investigation of GHG release and management within such systems is important to inform closure procedures that minimise legacy emissions.

To enable translation of the MW GWP estimates from this regional study to a global GHG budget significant knowledge gaps need to be filled including: quantification of the total volume of MW from abandoned mines, their associated geology particularly with respect to the occurrence of carbonate and sulphur containing rocks and the impact of mining techniques and coal rank on the GHG sources identified. Additionally GHGs in MW from active mines has not be quantified but may be significant, for example China produces 4.5 billion m³ yr⁻¹ (Wang et al., 2021b). Further research to characterise this potentially highly variable source would help with close the gap between bottom-up and top-down estimates of GHG emissions.

The 2006 IPCC Guidelines for National Greenhouse Gas Inventories includes fugitive emissions from mining, including from abandoned mines (IPCC, 2006). It considers that abandoned mines are significant CH₄ emitters unless flooding inhibits release and allows emissions from completely flooded abandoned mines to be treated as negligible. Emissions related to GHGs dissolved in MW, are not considered including in the 2019 revision (IPCC, 2019). The focus for abandoned mines is on CH₄ emissions to air, while this study confirms that dissolved CO₂ can

be the most significant GHG emission (97% of the MW GWP) with dissolved CH₄ constituting the remainder. A section on future methodological development for fugitive emissions is presented in the Appendix (IPCC, 2019) which could be amended to include GHG dissolved in MW with the focus on mines where limestone and high sulphur rocks are present in the geology. Where carbonate-based rocks are used to treat acid MW, associated CO₂ should also be included as a fugitive emission.

For Scotland the 2020 deep mine abandoned mine methane (AMM) projections were 0.05 MtCO₂e with no AMM utilisation (Fernando, 2011). The annual estimates of GHG emissions from this study for MW in Scotland range from 0.03 to 0.35 MtCO₂e. The median estimate of GHG production from AMW in Scotland derived from this study is 0.1 MtCO₂e, twice that from the AMM, suggesting this term should be accounted for in the fugitive emission calculation towards inventory reporting.

4.5 Conclusions

The origins of the dissolved CH₄ and CO₂ in MW from the abandoned coal mines were effectively determined by the application of $\Delta^{14}\text{C}$ and $\delta^{13}\text{C}$ measurements, with three different sources distinguished for both CH₄ and CO₂. The concentrations of the different CH₄ and CO₂ sources varied considerably dependant on the MW location, with [SO₄²⁻] the biggest factor influencing both [CH₄] and [CO₂]. Sulphate inhibited methanogenesis but increased CO₂ production from the dissolution of limestone. The flooding of the mine enabled dissolution of limestone and conversion of DOC to produce CO₂, whereas CH₄ production was significantly reduced by flooding of the mine, which reduced the escape of thermogenic CH₄ by pressure on the coal seams. The main source of CH₄ was biogenic production from modern carbon in the water, but thermogenic CH₄ was still significant with neither CH₄ nor CO₂ impacted by time since abandonment.

The different treatment processes, specifically the use of peroxide or cascade, and varied use of pools and reed beds had only a small impact on the final GHG emissions to atmosphere. The cascade systems released GHGs more rapidly reducing any opportunity for later removal, and resulting in increased CO₂ emissions (30%) due to the rapid conversion of HCO₃⁻ to CO₂ to restore the carbonate equilibrium. Reed pools could act as a source of biogenic CH₄ although the effect was small likely due to inhibition by metal ions. Configuration of the reed pools had a significant impact on heavy metal removal with residence times in the order of days required to allow settling of precipitated ions. The treatment by oxygenation and reed pools was most effective for the removal of Fe and As, which relies on oxidation and precipitation of higher valence state compounds and to a lesser extent Co, Ni and Mn, but no other metals were removed. The MWs [Fe] and [Mn] decreased by half, typically 50-years after mine inundation although some MWs exhibited persistent residual metal contamination.

In Scotland many MW sites are treated, but this is not be the case globally with contamination from tailings and acid mine drainage a significant cause of global pollution (Carvalho, 2017) and causing significant damage to biodiversity (Ayangbenro et al., 2018). As coal mines are abandoned it is advantageous to utilise AMM, with the most suitable mines having minimal water ingress and the ability to reduce water and air ingress with the largest quantities of

AMM recovered in the first 10 years after abandonment (UNECE, 2019). However, most mines will eventually flood creating MW, although the prevention of air ingress could reduce pyrites oxidation. While mines are often engineered to facilitate AMM production, mines also need to be engineered to prevent significant MW pollution, which would be most effectively done before or as the mine is abandoned. Modifications to inhibit sulphuric acid generation processes would be required and would reduce CO₂ generation and the dissolution of heavy metals but could increase biogenic CH₄. While the latter would be a relatively small GHG impact when compared to any CO₂ reduction it could also support AMM. Dissolved MW CH₄ could perhaps be recovered from the MW, in similar ways to that applied to wastewater (GMI, 2023). Two approaches to reduce sulphuric acid generation include, use of engineered SBRs (Muyzer and Stams, 2008; Ayangbenro et al., 2018), although the isolation of acid tolerant SBRs, may be required (Magowo et al., 2020) to avoid the use of neutralising agency such a calcium carbonate and, coating the pyrites within the mine while in operation as each area is mined and before pyrites oxidation and mine flooding. Coating of mine walls would be viable to reduce acid generation hence preventing the dissolution of both metals and carbonate rock from future abandoned mines (Liu et al., 2017) and could be tested for its compatibility with AMM recovery.

This novel work has contributed information about the sources and controls of GHG fluxes in MW and identified the need to quantify and include this emissions term in GHG budgets.

Acknowledgements

This work was financially supported by Natural Environment Research Council (NERC) studentship through the IAPETUS 2 Doctoral Training Partnership Grant No. NE/S007431/1.

The carbon isotope work was financially supported by a National Environmental Isotope Facility (Part of the Natural Environmental Research Council), Grant Number 2513.0422. The radiogenic and stable isotopes were measured by the NEIF Radiocarbon Laboratory in East Kilbride.

The authors would like to thank The Coal Authority and Severn Trent Services for allowing access to and supporting sampling at their MW treatment sites for the purpose of making these measurements.

The authors would like to thank Edinburgh University for undertaking the ICP-MS analysis

All photographs in the supplementary data were taken by Alison M. Brown.

5 Anthropogenic-estuarine interactions cause disproportionate greenhouse gas production: A review of the evidence base

Declaration of authorship: The data in this chapter was analysed by the author of the thesis. Co-authors reviewed paper drafts and provided supervision, feedback, and guidance.

The chapter has been published in the Marine Pollution Bulletin volume 174
<https://www.sciencedirect.com/science/article/pii/S0025326X21012741>

with the following DOI - <https://doi.org/10.1016/j.marpolbul.2021.113240>

Graphical Abstract

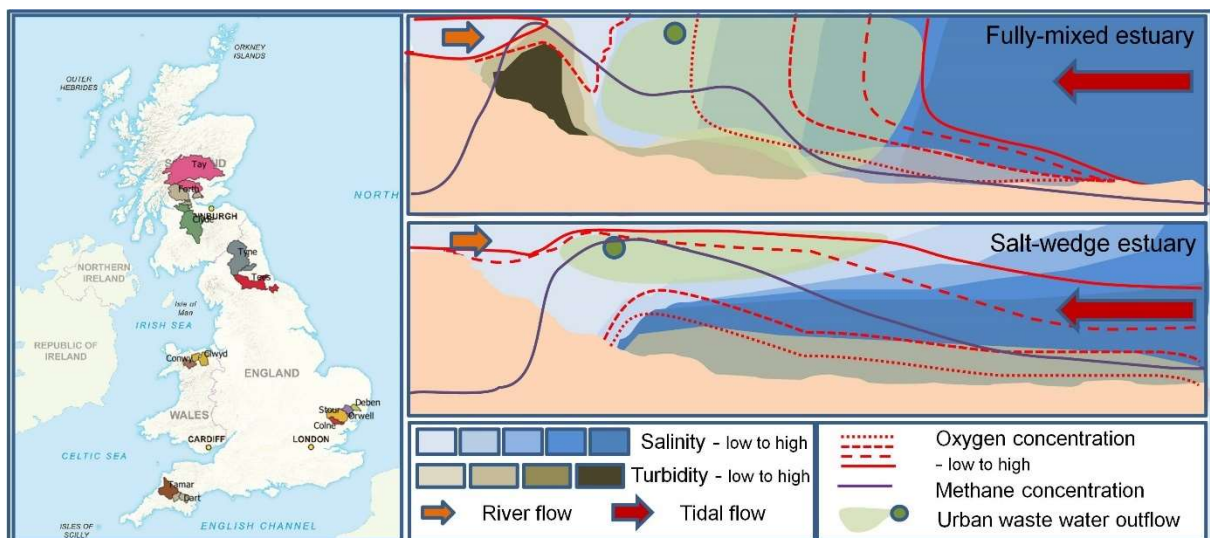


Figure 5.0 - Graphical Abstract - Anthropogenic-estuarine interactions cause disproportionate greenhouse gas production

Highlights

- Urban wastewater and low oxygen levels promote high estuarine greenhouse gases.
- Interactions between estuary type and anthropogenic impact amplify greenhouse gases.
- Urban pressures may make estuaries a hidden source of greenhouse gases globally.
- A conceptual model for estuarine greenhouse gas generation is presented.

Abstract

Biologically productive regions such as estuaries and coastal areas, even though they only cover a small percentage of the world's oceans, contribute significantly to methane and nitrous oxide emissions. This paper synthesises greenhouse gas data measured in UK estuary studies, highlighting that urban wastewater loading is significantly correlated with both methane ($P < 0.001$) and nitrous oxide ($P < 0.005$) concentrations. It demonstrates that specific estuary typologies render them more sensitive to anthropogenic influences on greenhouse gas production, particularly estuaries that experience low oxygen levels due to reduced mixing and stratification or high sediment oxygen demand. Significantly, we find that estuaries with high urban wastewater loading may be hidden sources of greenhouse gases globally. Synthesising available information, a conceptual model for greenhouse gas concentrations in estuaries with different morphologies and mixing regimes is presented. Applications of this model should help identification of estuaries susceptible to anthropogenic impacts and potential hotspots for greenhouse gas emissions.

Key Words

Greenhouse gas; nitrous oxide; methane; estuary; salt-wedge; fully-mixed; nutrients; urban wastewater; ammonium; nitrate; nitrite; phosphate; tidal range; river flow.

Authors

Alison M. Brown^{1,2}; Dr. Adrian M. Bass²; Dr. Amy E. Pickard¹

1. UK Centre for Ecology & Hydrology, Bush Estate, Penicuik, Midlothian, UK, EH26 0QB.
2. School of Geographical & Earth Science, University of Glasgow, Glasgow, UK. G12 8QQ.

5.1 Introduction

The climate is considered unequivocally to have warmed significantly since the 1950s with increasing levels of greenhouse gases (GHGs), with the largest contribution derived from carbon dioxide (CO₂) followed by methane (CH₄) and nitrous oxide (N₂O) (IPCC, 2013). Shelf seas including estuaries and coastal areas, cover approximately 9% of the world's oceans (Harris et al., 2014) and are highly biologically productive, driving between 10 and 30% of marine primary production (Sharples et al., 2019) and contributing about 75% of the oceanic methane emissions (Bange et al., 1994). Shelf seas are a major nitrous oxide source, with European shelf sea (9.4% of total shelf) contributing 26% of global oceanic nitrous oxide (Bange, 2006), largely through denitrification-nitrification cycling from terrestrial runoff. Additionally, the outflows from urban wastewater (UWW) contribute to enhanced nitrous oxide production (McElroy et al., 1978; de Angelis and Gordon, 1985; Seitzinger, 1988; Law et al., 1992).

A review of the literature on estuarine methane emissions from different locations globally (Bange et al., 1994; Bernard, 1978; Oremland et al., 1983; Franklin et al., 1988; Munson et al., 1997; Torres-Alvarado et al., 2013; Bange et al., 1998; Lyu et al., 2018), suggests that estuaries can drive particularly high methane production, despite their varying physical conditions, where they have the following conditions; high levels of organic matter, active sedimentation processes moving both river and estuarine sediments to trap organic matter and low oxygen levels. Similarly, a range of studies (Wrage et al., 2001; Pfenning, 1996; Revsbech et al., 2005; Reay et al., 2003; Pattinson et al., 1998; Beaulieu et al., 2011; Yu et al., 2013; Rosamond et al., 2012) suggests there are several major controls on nitrous oxide production within estuaries in both nitrification and denitrification rates, including ammonium (NH₄⁺) and nitrate (NO₃⁻) concentrations, dissolved oxygen, organic matter availability and temperature. Greenhouse gas fluxes generated within the estuarine environment are often highly variable, as reflected in the considerable range observed in UK, European and global estimates (Upstill-Goddard and Barnes, 2016; Borges et al., 2016; Bange, 2006). European estimates range in the order of 0.007 to 1.6 Mt N₂O yr⁻¹ and 0.03 - 0.7 Mt CH₄ yr⁻¹, with UK estimates accounting for more than 20% of these values. However, there is both a paucity of data for estuaries globally and concerning the drivers of these emissions. There is a clear need for an improved understanding of anthropogenic impacts, largely in the form of urban pollution, as well as the interactive effects associated with tidal, flushing and river regimes, climate, temperature and land-use. In order to increase the confidence in the magnitude of these estuarine GHGs as part of the general IPCC process (IPCC et al., 2006) and the UK government's carbon emission strategy (Institute for Government, 2020), further elucidation of the mechanisms that generate GHG emissions from estuaries is required. Such understanding could inform policies to help reduce emissions in anthropogenically impacted estuaries.

Estuaries have long been considered an effective location for the disposal of urban and industrial waste; resulting in considerable legacy pollution (including metals). Nitrogen and phosphorus compounds are not typically removed from most wastewater discharges to estuaries, although this is dependent on legislation. In the EU and UK removal requirements are related to plant size, the quantity of nutrients and eutrophication risk (EEC, 1991). Where nitrogen compounds are not removed from wastewater, nitrous oxide production may occur

when the treated wastewater is discharged to rivers and estuaries. Ammonia is rapidly oxidised, a process that consumes oxygen and other available electron receptors, which may promote methanogenesis and the presence of ammonium may further inhibit methane oxidation (Dunfield and Knowles, 1995 and Bosse et al., 1993) (Fig. 5.1). Additionally, nitrification processes may deplete oxygen, preventing methane oxidation, and where oxygen concentrations are low or highly variable, as typical in the estuary environment, denitrification may be triggered (Marchant et al., 2017), even with oxygen present, thereby increasing nitrous oxide concentrations. Estuaries with high suspended sediment loads may also support nitrogen processing in the water column (Barnes and Upstill-Goddard, 2011). The effects of temperature, salinity, ammonium concentration and pH can further affect the nitrification rate (Isnansetyo, A., et al., 2014) with a salinity optimum between 12-20ppt, suggesting more nitrogen cycling would occur in an estuary than in either the freshwater or coastal environments. The estuary, therefore, is perhaps the least suitable environment of the land-ocean continuum for the discharge of UWW effluent when considering resultant GHG emissions.

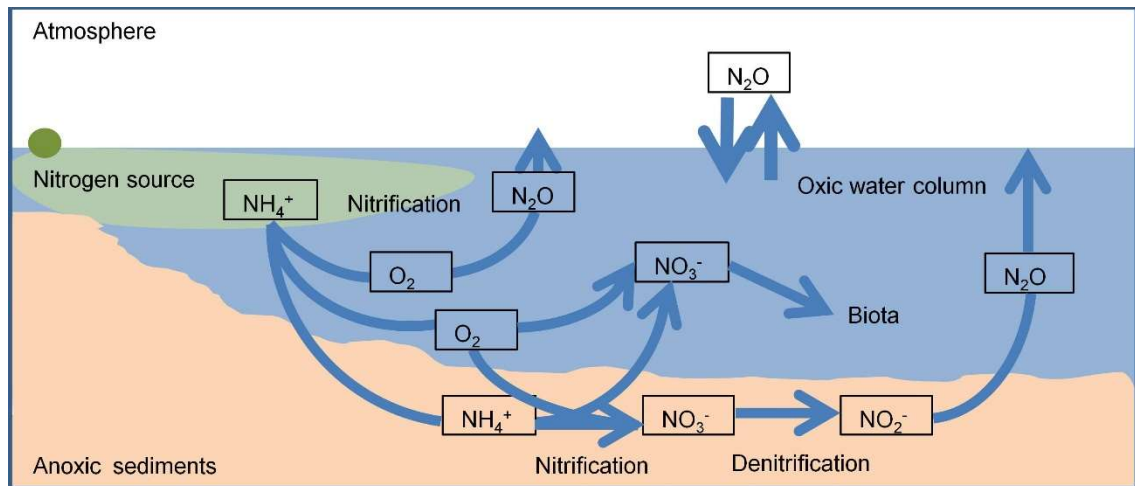


Figure 5.1 - Simplified nitrification-denitrification pathways in estuaries.

Nitrification is shown in the aerobic water-column with oxygen from the water column also used in nitrification in the sediment layer. When insufficient oxygen is present de-nitrification can occur in the anoxic sediment layer. De-nitrification can also occur in the water column linked to sediments, when oxygen levels are low, such as below a pycnocline.

5.1.1 Objectives

Investigations of GHG emissions from estuaries and coastal waters have typically been conducted with the purpose of improving the estimate of GHG emissions from estuaries on a UK, European or global scale. There has been less emphasis on determining the interplay of processes that result in these high GHG emissions and our understanding therefore remains incomplete. As estuaries vary significantly in their physical characteristics and degree of anthropogenic influence, it can be difficult to determine exact causation mechanisms for this globally important source. Existing data to our knowledge, have not been used to distinguish between natural or anthropogenic emissions, nor have opportunities to prevent or reduce these emissions been identified. This paper synthesises published GHG data from UK estuaries in conjunction with other public domain data to address the following objectives. To

determine the: 1) causes of estuarine GHGs, 2) mechanisms that promote high estuarine GHG concentrations and 3) optimum approach for quantifying estuarine GHGs. It employs a series of case studies of UK estuaries examining possible causes of high GHGs and their interaction with different estuary typologies (Fig. 5.2). This results in a conceptual model of GHG concentrations for different estuary typologies and is followed by an overarching synthesis section. This synthesis section also considers how estuary GHG concentrations and estuary typology impact GHG emissions to the atmosphere and whether estuaries are an overall net carbon sink or source.

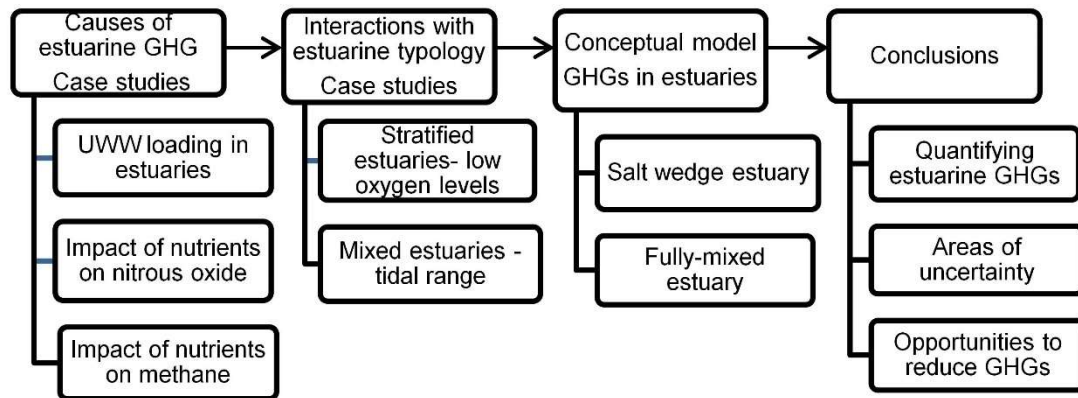


Figure 5.2 - Outline of approach in this paper

5.2 Methods

A literature search containing the following terms was used to select the papers to be considered in this review: 'greenhouse gas' OR 'nitrous oxide' OR 'methane' AND 'estuary'. Only data from measurements made in the UK were applied in the analysis section to limit the variability in terms of geographic, climatic, nutrient and tidal regimes. Some estuarine GHG data from other geographic areas are contrasted in the discussion section. Methane and nitrous oxide concentration values from five studies conducted between 2005 and 2021 (Table 5.1), have been extracted as average values for specific surveys or estuaries (Table 5.2). These data were compared with other physical parameters from publicly available data associated with each estuary, including: estuary area and catchment, tidal range, river flow, oxygen concentration, land cover and the level of urban wastewater entering these estuaries (Table 5.3 and supplementary data Tables 5.A.1 and 5.A.2), together with data on nutrients and legacy pollution typically using linear regression methods. The thirteen estuary systems mainly considered in this analysis (Clyde, Clywd, Colne, Conwy, Dart, Deben, Forth, Orwell, Stour, Tamar, Tay, Tees and Tyne), see Fig. 5.3 for estuary catchment locations, represent 12% of UK estuary systems and 9% and 15% of the UK estuary and catchment areas respectively (Nedwell et al., 2002). While a single survey was available for the Thames (Middelburg et al., 2002) and three for the Humber (see Table 5.1), these estuaries have not been included because of their size and complexity. Different studies use different surveying approaches; comparison between studies is possible but imperfect. The major differences between studies are in the depth of measurements, either surface or at 1m and the phase of the tide on which the studies were conducted, either the ebb or the flood (detailed in Table 5.1). Both of these factors should be less significant for a fully mixed estuary compared to a

salt wedge estuary. Seasonality is also not fully covered in all studies. Consideration of these results and the variances calculated for each estuary suggest that estuarine variability is more significant than the small differences in survey approach.

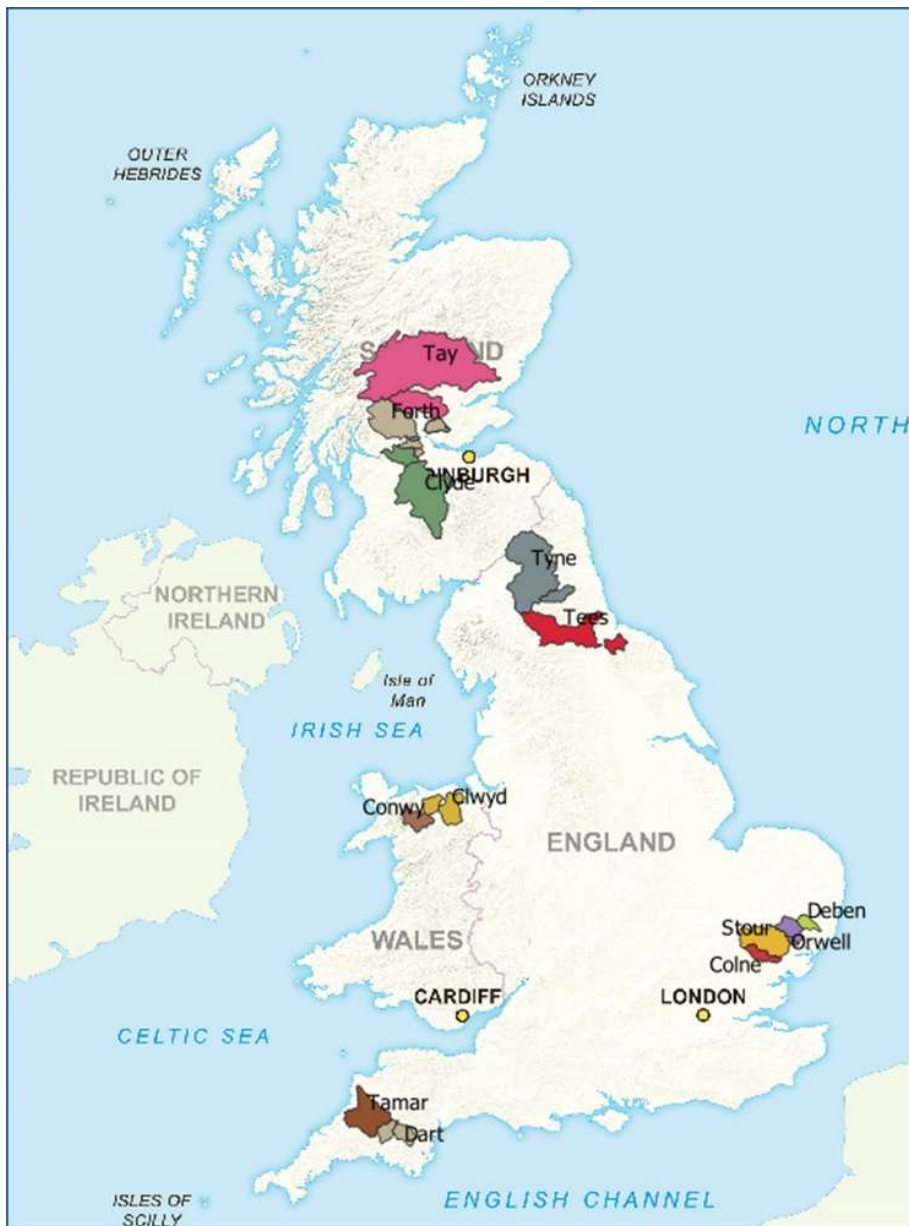


Figure 5.3 - Map showing estuary catchments of the thirteen estuary systems considered

Table 5.1 - Summary of published data applied in this review

	Study scope	GHGs sampled	Sample depth	Sampling durations	Sampling approach	Sampling resolution	Study reference
1	Tay, Forth, Clyde, Tamar, Dart, Conwy & Clywd	CO ₂ , N ₂ O & CH ₄	Surface	Quarterly, usually Jul 2017, Oct 2017, Jan 2018, Apr 2018	Ebb tide starting at high water, sampling downstream	6 sites across a salinity gradient	(Pickard et al., 2021a)
2	Tay	CO ₂ , N ₂ O & CH ₄	Surface	Eight occasions from Apr 2009 - June 2010	Ebb tide starting at high water, sampling downstream	10 sites at fixed locations	(Harley et al., 2015)), (Pickard et al., 2021b)
3	Humber, Forth, Tamar, Tyne, Tees, and Tay	N ₂ O	1m depth	Variable between Feb 2000 - Oct 2002 from 1 and 8 surveys	Flood tide starting after low water, sampling upstream	7 - 20 sites, due to estuary & local conditions	(Barnes and Upstill-Goddard, 2011)
4	Humber, Forth, Tamar, Tyne, Tees, and Tay	CH ₄	1 m depth	Variable between Feb 2000 - Oct 2002 from 1 and 8 surveys	Flood tide starting after low water, sampling upstream	7 - 20 sites, due to estuary & local conditions	(Upstill-Goddard and Barnes, 2016).
5	Colne, Stour, Orwell, Deben, Humber ,Conwy	N ₂ O	Surface	Quarterly, Aug 01, Nov 01, Feb 02, May 02. Conwy - 2002-3	Ebb tide starting at high water, sampling downstream	10-16 sites dependent on estuary	(Dong et al., 2005)

Notes for studies 1-5:

1. No data were available for the Clywd in January, and the Dart and Tamar in October. Target salinities were typically 0.2, 2, 5, 10, 15, 25 psu. Surveys covered different physical extent due to the salinity criteria applied. No CO₂ data was available for the Tamar and Dart.
2. Survey dates were Apr-09, Jun-09, Jul-09, Sep-09, Feb-10, Apr-10, Jun-10 and Aug-10 (final survey not included in publication.)
3. The number of surveys undertaken for N₂O were Tay: 1, Humber: 3, Tees: 3, Forth: 4, Tamar: 4 and Tyne: 8.
4. The number of surveys undertaken for CH₄ were; Tay: 1, Humber: 2, Tamar: 2 Tees: 3, Forth: 4 and Tyne: 6. (Methane surveys are a subset of those for nitrous oxide (3) with one additional survey for the Tyne).
5. The specific dates of the measurements are not provided. The rivers Mawddach and Dovey were measured but data were not provided for the estuaries, so this has not been included.
6. Abbreviations: - Greenhouse Gas (GHG), Methane (CH₄), Nitrous Oxide (N₂O), Carbon Dioxide (CO₂)

Table 5.2 - Summary of average methane and nitrous oxide concentrations measured

Estuary	Year	Reference ⁽¹⁾	No. of surveys	Average CH ₄ (nM/l)	Average N ₂ O (nM/l)	Average CH ₄ (% sat)	Average N ₂ O (% sat)
Conwy	2017-18	1	4	103.2	13.0	2964	130
Clywd	2017-18	1	3	178.6	13.8	5571	140
Tamar	2017-18	1	4	214.6	17.5	7820	164
Dart	2017-18	1	3	187.1	16.0	6415	165
Tay	2017-18	1	4	53.3	12.0	1475	107
Forth	2017-18	1	4	158.3	34.4	4138	262
Clyde	2017-18	1	4	1120.6	32.4	31285	251
Tay	2009-10	2	8	48.2	13.9	2698	118
Humber	2000-02	3 & 4	2-3	55.1	71.4 ⁽²⁾	1546	396
Forth	2000-02	3 & 4	4	178.4	20.1 ⁽²⁾	5067	152
Tamar	2000-02	3 & 4	2-4	132.9	18.5 ⁽²⁾	3047	145
Tay	2000-02	3 & 4	1	24.8	9.9 ⁽²⁾	584	104
Tees	2000-02	3 & 4	3	500.1	68.8 ⁽²⁾	16559	383
Tyne	2000-02	3 & 4	6-8	910.0	14.0 ⁽²⁾	26348	124
Colne	2001-02	5	4	na	197.3	na	993
Stour	2001-02	5	4	na	24.9	na	143
Orwell	2001-02	5	4	na	46.3	na	282
Deben	2001-02	5	4	na	32.6	na	187
Humber (Trent falls - Humber Br)	2001-02	5	4	na	32.1	na	187
Humber (Humber Br - spurn head)	2001-02	5	4	na	24.7	na	149
Conwy	2002-03	5	4	na	18.6	na	114

Notes

1. References see Table 5.1
2. Estimated from concentration data provided in reference 3
3. Abbreviations: - Methane (CH₄), Nitrous Oxide (N₂O)

Table 5.3 - Physical characteristics of the estuarine systems

	Estuary	Estuary catchment Area ⁽¹⁾ (km ²)	Estuary area ⁽¹⁾ (km ²)	Mean freshwater input ⁽²⁾ (m ³ /s)	Tidal range HAT-LAT ⁽³⁾ (m)	UWWT Capacity Estuary ⁽⁴⁾ (pp equ)	UWWT Capacity River ⁽⁴⁾ (pp equ)	UWWT Capacity Total (pp equ)	UWWT Capacity/ Mean freshwater input (per 1000)	Mixing regime
1	Conwy	345	14.9	19.1	9.01	88,731	4,072	92,803	4.86	Macrotidal, well mixed, can stratify on flood and mix on the ebb ⁽⁵⁾
2	Clywd	598	1.2	11.2	9.70	88,248	27,037	115,285	10.28	Macrotidal, well mixed
3	Tamar	1338	39.6	22.7	5.91	358,096	46,641	404,737	17.83	Macrotidal, well mixed, low salinity TMZ, stratification occurs on ebb ⁽⁶⁾
4	Dart	475	8.6	11.3	5.91*	36,084	22,134	58,218	5.16	Macrotidal, stratified neap & low freshwater runoff ⁽⁷⁾
5	Tay	5669	121.3	201.1	6.31*	98,000	99,975	197,975	0.98	Macrotidal, partially mixed, stratified on ebb, longitudinal fronts ⁽⁸⁾
6	Forth	1938	84.0	46.4	6.31	267,700	111,250	378,950	8.17	Macrotidal, well mixed, low salinity TMZ, double high/low waters ⁽⁹⁾
7	Clyde	3854	54.9	57.1	3.90	1,159,202	886,846	2,046,048	35.84	Mesotidal, stratified at neap, channel straightened and deepened ⁽¹⁰⁾
8	Humber	19427	303.5	212.3	7.83				-	Macrotidal, well mixed, low salinity TMZ ⁽¹¹⁾
9	Tees	1930	13.3	22.4	5.99	932,367	10,892	943,259	42.13	Macrotidal, partially mixed, stratified at neaps and on ebb tide ⁽¹²⁾
10	Tyne	2935	7.9	47.5	5.73	1,003,785	104,748	1,108,533	23.27	Macrotidal, partially mixed, low salinity TMZ ⁽¹³⁾
12	Colne	255	23.4	1.1	4.71	144,152	28,675	172,827	161.52	Macrotidal, with extensive mud flat and tidal creaks ⁽¹⁴⁾
13	Stour	578	23.3	3.1	4.71	48,355	55,932	104,287	33.68	Macrotidal with extensive mud flat and tidal creaks ⁽¹⁴⁾
14	Orwell	-	-	1.4	4.71	178,075	11,731	189,806	140.7	Macrotidal with extensive mud flat and tidal creaks ⁽¹⁴⁾
15	Deben	-	-	0.8	4.71	28,630	6,000	34,630	43.78	Macrotidal, ⁽¹⁴⁾

Notes:

- (Nedwell et al., 2002)
- All flow data were derived from CEH (UKCEH, 2020b) and focus on the main rivers entering at the head of the estuary. The mean flow data represent the specific river mentioned unless stated below: Clywd is the sum of the Clywd and Elwy, Tay is the sum of the Tay and Earn, Clyde is the sum of the Clyde and the Kelvin, Humber is the sum of the Aire, Trent, Ouse, Don, Wharfe and Derwent, the Tees is the sum of the Tees and the Leven and the Tyne is the sum of the Tyne and the Derwent.
- (BODC, 2020), (*)Due to the location of standard ports the Forth estuary tidal range is applied to the Tay and the Tamar estuary tidal range is applied to the Dart
- (European Commission (Directorate General Environment), 2016)
- (Robins et al., 2014);
- (Uncles and Stephens, 1993)
- (Thain et al., 2004)
- (Silke F.K. Wewetzera, Robert W. Ducka, Anderson, 1999); (McManus, 2005)
- (Lindsay et al., 1996)
- (Scottish Environment Protection Agency, 2020a)
- (Mitchell et al., 1999), (Mitchell et al., 1998)
- (Environmental Agency, 1999)
- (Upstill-Goddard et al., 2000)
- (Dong et al., 2005)
- Abbreviations: Highest / Lowest Astronomical Tide (H/ LAT) , Urban Wastewater Treatment (UWWT)

5.3 Case studies considering the effect of urban waste and nutrients on GHG production

The relationships between UWW and nutrients on both methane and nitrous oxide concentrations in the estuary environment are considered in the following three case studies: (i) effects of UWW loading on average GHG concentrations, (ii) causes of high estuarine nitrous oxide concentrations and (iii) effects of different nutrients on methane concentrations. Relationships between GHG concentrations and estuary, catchment and land-cover area are reviewed in supplementary data Table 5.A.2 and Fig. 5.A.1.

5.3.1 Wastewater loading is a primary driver of methane and nitrous oxide emissions

The average methane and nitrous oxide concentrations for nine and thirteen estuaries respectively appear highly correlated with urban wastewater loading per mean river flow (Fig.5.4).

River-estuary systems that have higher levels of UWW per unit river flow have both higher methane and nitrous oxide production on average (Fig. 5.4). The correlation coefficients for both methane $R^2= 0.80$ (excluding the Clyde) and nitrous oxide $R^2 =0.78$ (all data) are statistically significant despite the large number of factors that could influence methane and nitrous concentrations including: natural estuarine variability, anthropogenic affects and survey protocols. Natural estuarine variability would include: stratification, tidal range, tidal asymmetry, fresh water flushing time, average particle residence time, river flow, the shape and area of the estuary, area of tidal flats and sedimentation processes. Other significant anthropogenic affects might include the percentage cover and type of agriculture in the catchments, industrial waste, water extraction and legacy pollution. The main variation associated with the survey protocols include the number, seasonal balance and range of methods used. While on average all estuaries fit the relationship between GHG concentrations and UWW loading, the methane to nitrous oxide ratio is higher for the Clyde and Tyne compared to, for example, the Tay, Forth and Humber estuaries (Table 5.2). Here, estuary morphology may be an influencing factor. The large and exposed Tay, Forth and Humber systems may allow for more effective oxygenation of the surface waters resulting in more methane oxidation, in comparison to the physically restricted, narrow estuaries of the Clyde and Tyne. Morphological variation aside, these data underline the potential importance of UWW output on both methane and nitrous oxide concentrations in estuarine environments and undermine the assumption that discharge into estuaries is flushed away without environmental repercussions.

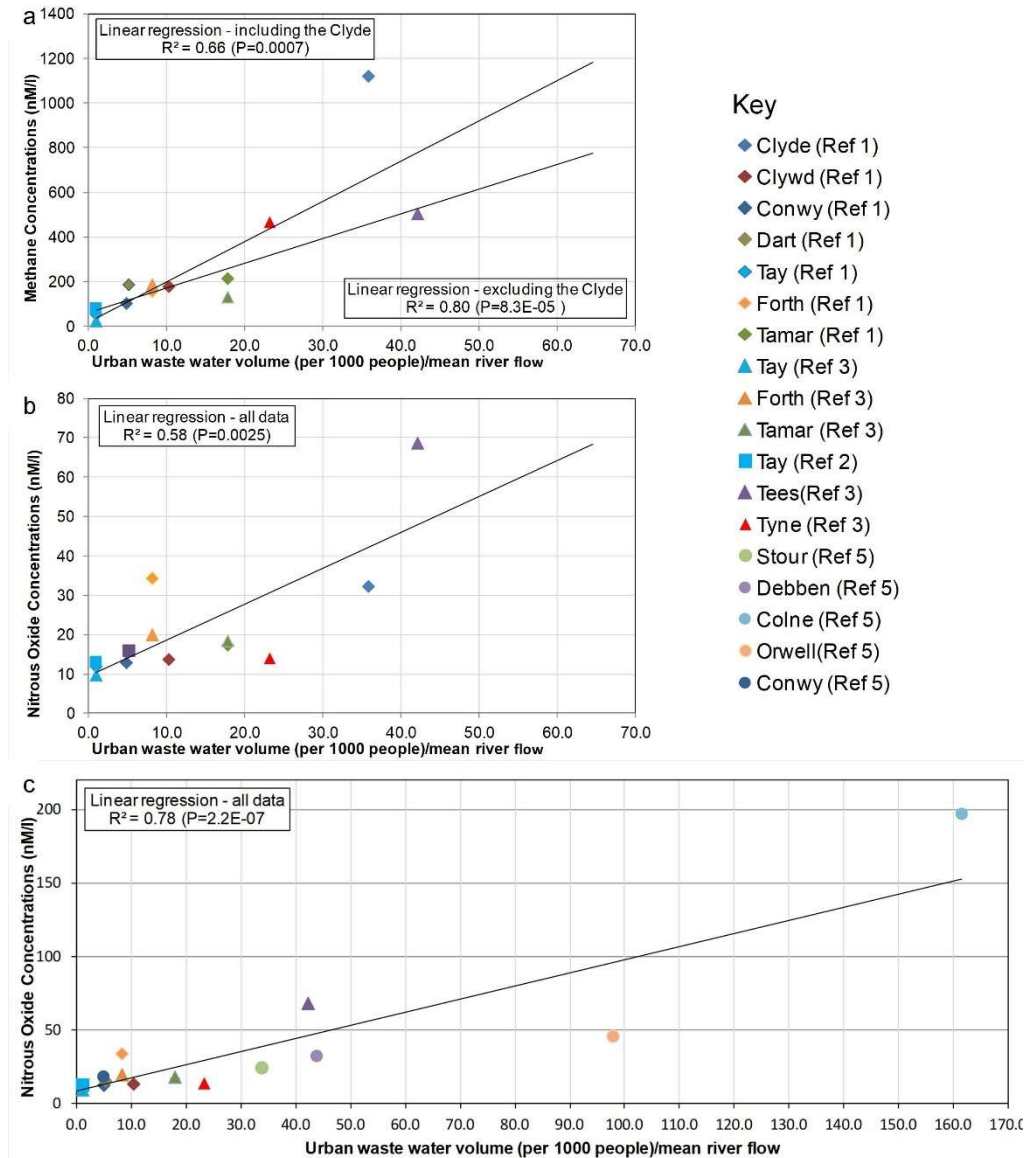


Figure 5.4 - UWW loading compared with GHG concentration data

UWW loading (urban wastewater volume (per 1000 people/mean river flow)) is compared with (a) Average methane concentration (Pickard, 2021 and Barnes and Upstill-Goddard, 2011); (b) Average nitrous oxide concentration data (Pickard et al., 2021a and Upstill-Goddard and Barnes, 2016); (c) Average nitrous oxide concentrations as for (b) but including estuaries from SE England (Dong et al., 2005).

To further investigate the relationship between urban influences and estuarine GHGs, catchment land cover was considered (Morton et al., 2020), (see supplementary data Fig. 5.A.1). These relationships strongly support the inference that high urban populations increase both estuary methane and nitrous oxide but agriculture primarily impacts nitrous oxide concentration. The limited data for carbon dioxide (only available for five estuary systems) has a positive correlation with UWW loading. Bioavailability of anthropogenic derived organic matter may promote microbial production and degradation, rather than carbon sequestration (García-martín et al., 2021).

5.3.2 Nitrous oxide concentrations significantly increased by activation of denitrification

Nitrous oxide emissions from rivers and estuaries have been linked to the dissolved inorganic nitrogen (DIN) concentration for which agriculture and sewage treatments are considered the main sources (Dong et al., 2005; Barnes and Upstill-Goddard, 2011). Fig. 5.5 shows the average nitrous oxide percentage saturation against concentrations of nitrate, nitrite and ammonium respectively from (Dong et al., 2005; Pickard, 2021). While these plots confirm the strong correlations between nitrous oxide and particularly nitrite and ammonium, as previously reported (Dong et al., 2005) and are generally consistent for all authors, there are exceptions, specifically for the Colne, Forth and Clyde (see ringed points in Fig. 5.5 a, b, c) which demonstrate higher nitrous oxide concentrations compared to DIN loading. The relationship between DIN and nitrous oxide percentage saturation for six estuaries also shows higher nitrous oxide concentrations for the Forth (Barnes and Upstill-Goddard, 2011, Fig. 5.6). The river data (Dong et al., 2005), show no exceptions, even for the Colne. Additionally, the relationship between nitrous oxide and ammonium (but not nitrate or nitrite) is different between the rivers and estuaries. Nitrification, which converts ammonium to nitrous oxide, requires oxygen, and rivers are typically more oxygenated than estuaries.

The Colne estuary is muddy and hyper-nutriented (Ogilvie et al., 1997) with strong gradients (increasing up river) of nitrate and ammonium due to inputs from the river and sewage treatment. Sediments located near the tidal limit were found to be major sites of denitrification and correlated with high nitrite concentrations (Robinson et al., 1998; Dolfing et al., 2002). Dissolved oxygen data for the Forth showed a strong negative correlation with nitrous oxide (Barnes and Upstill-Goddard, 2011), and both the Clyde and Forth are known to experience low oxygen conditions under some tidal and river flow regimes (Scottish Environment Protection Agency, 2020a). These are all consistent with a denitrification mechanism for the higher nitrous oxide in the Colne, Forth and Clyde (Fig. 5.5). Uncoupled bacterial denitrification supported by nitrate diffusing into the sediment from the overlying water column and by the sediment organic carbon content, can exhibit faster rates of nitrate reduction (Dong et al., 2000) with organic carbon content determining the potential capacity of denitrification when the nitrate concentration is not limiting with bacterial communities adapting to high nitrate concentrations. Hence when high levels of oxidised nitrogen and ammonium are delivered to an estuary this mechanism is likely to result in high nitrous oxide production. Nitrous oxide concentrations are more significantly impacted by the presence of ammonium compared to nitrate (Fig. 5.5), suggesting nitrification with exceptions for Colne, Forth and Clyde. The dynamic often low oxygen environment within these estuaries may trigger denitrification even with oxygen present (Marchant et al., 2017) and mid-salinity waters and ammonium concentration can further optimise nitrification rates (Isnansetyo, A., et al., 2014). These two observations suggest that more nitrogen cycling can occur in an estuary than in either fresh or coastal waters. This data underlines the importance of preventing both excessive inputs of nitrate and ammonium and the occurrence of low oxygen condition within estuaries.

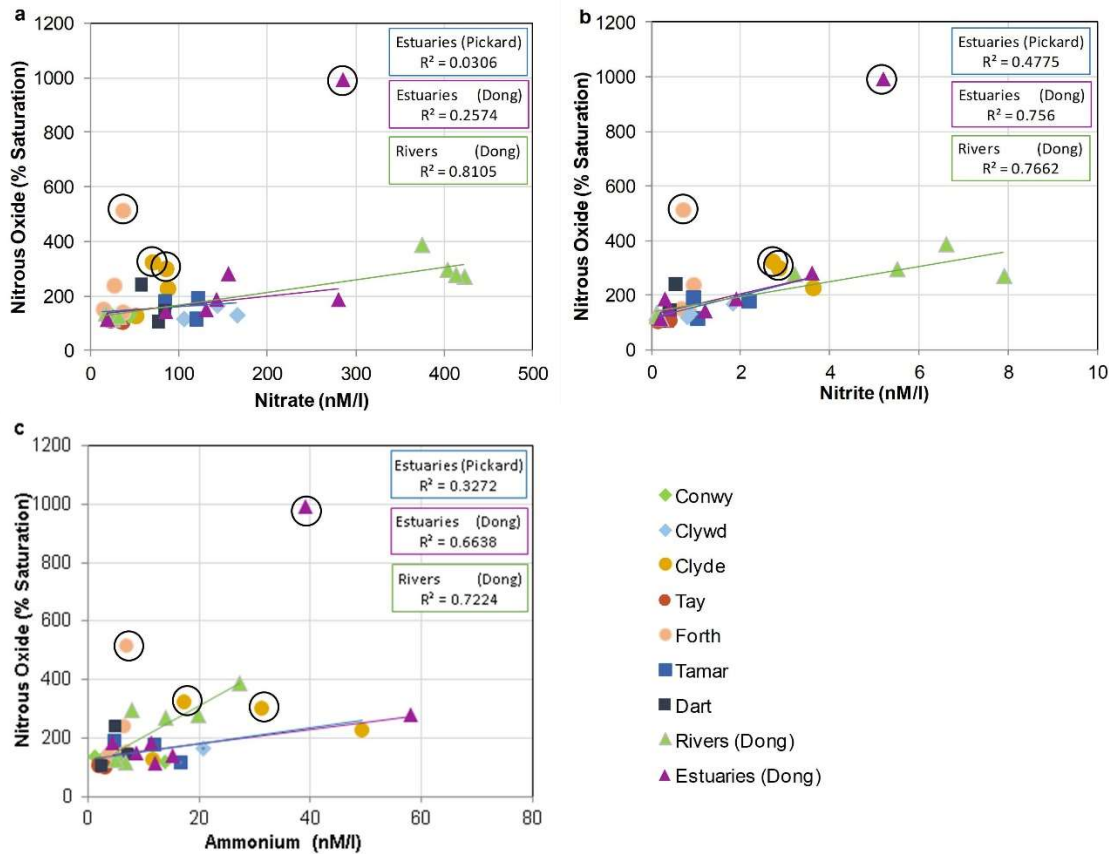


Figure 5.5 - Relative relationships between DIN concentrations and N₂O saturation, Specifically (a) nitrate, (b) nitrite, (c) ammonium with data from (Dong et al., 2005; Pickard, 2021). Note ringed points related to the Colne (ringed purple triangle), Forth and Clyde are not included in the regression lines.

5.3.3 Methane dynamics driven by ammonium concentrations

Average methane concentration data from seven estuaries (Pickard et al., 2021a) appear highly correlated with nutrients, particularly nitrite, ammonium, phosphate and (Fig. 5.6 b, c, d respectively). While causal factors are not clear, the higher correlations with nitrite, ammonium and phosphate ($P < 0.001$) point towards UWW as a contributor to methane production in the estuary. Conversely the poor, not statistically significant, correlation with nitrate concentrations, would not suggest agricultural run-off is significantly affecting estuary methane production. This is consistent with the land-cover data in supplementary data Table 5.A.2 and Fig. 5.A.1. Furthermore, inputs from agriculture typically occur higher in the catchment compared to UWW giving more time for processing to occur prior to water arriving in the estuary.

Methane concentrations can be influenced by DIN indirectly. Nitrification of ammonium requires oxygen, and this process may consume sufficient oxygen to reduce methane oxidation through the water column. Additionally inhibition of methane oxidation by ammonium can occur in the surface layer of a sediment, allowing more methane evasion (Bosse et al., 1993; Dunfield and Knowles, 1995). Conversely if denitrification is the prevalent mechanism of nitrous oxide production, the low oxygen environment that promotes nitrous oxide production would also reduce methane oxidation, resulting in a secondary correlation. These potential mechanisms linked to oxygen levels are also consistent with the poor

correlation with nitrate, which does not require oxygen for further processing. These relationships only hold for each estuary survey as a whole, not for each specific measurement point, suggesting that process timescales are important (Fig. 5.6).

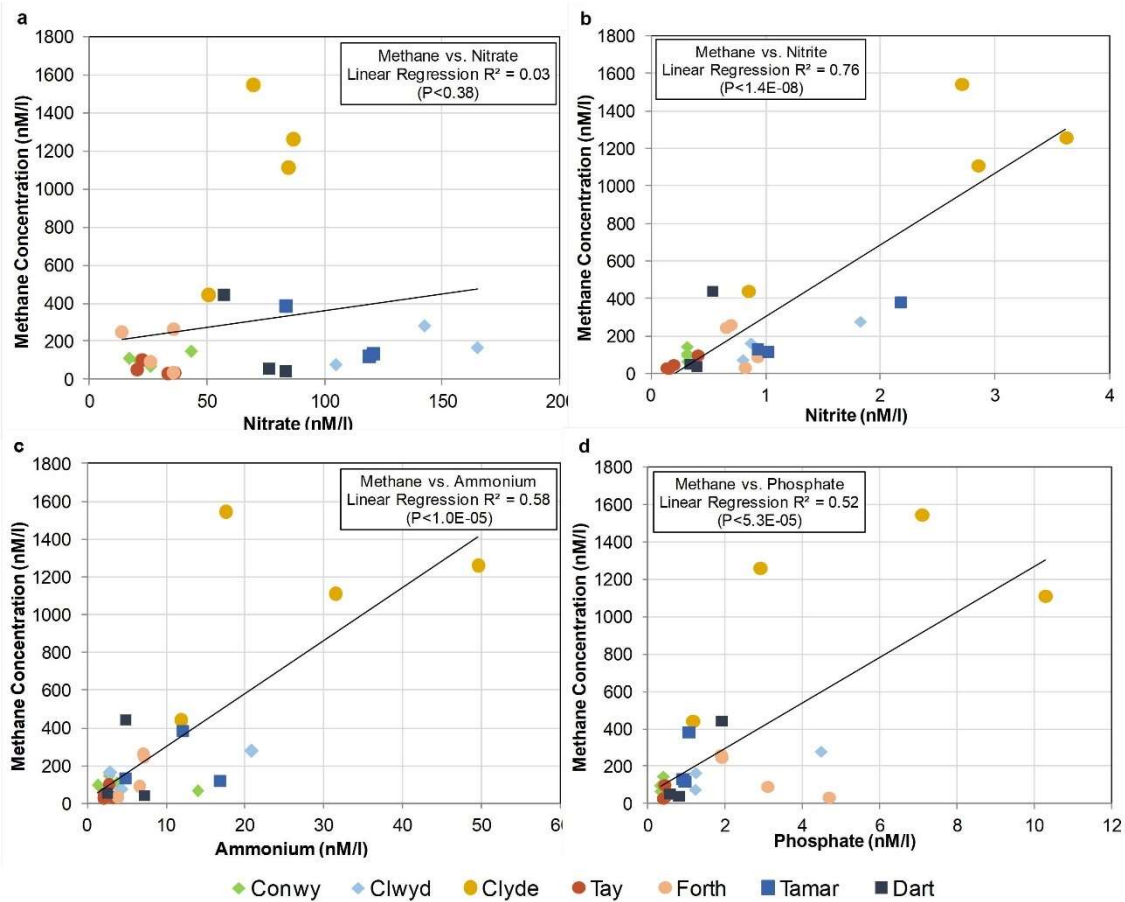


Figure 5.6 - Relationships between average methane concentration for each estuary (a) nitrate, (b) nitrite, (c) ammonium and (d) phosphate concentrations with data from (Pickard et al., 2021a).

5.3.4 Urban waste and nutrients summary

Estuary systems that have higher levels of nutrients from UWW per unit river flow have higher methane and nitrous oxide concentrations and both methane and nitrous oxide concentrations are more strongly correlated to nitrite and ammonium concentrations than nitrate. Analysis on the influence of land-cover (supplementary data Table 5.A.2 and Fig. 5.A.1) strongly support the inference that high urban populations increase both estuary methane and nitrous oxide but agriculture primarily impacts nitrous oxide concentration. Significantly higher levels of nitrous oxide and methane occur in estuaries that experience high urban loading and low oxygen conditions, likely via denitrification and inhibited oxidation pathways respectively. The natural but highly variable conditions in estuaries related to changing oxygen levels and mid-salinity values may act to increase nitrogen cycling rates in estuaries compared to either fresh or coastal waters and suggest that UWW discharge into estuaries has environmental repercussions related to GHGs.

5.4 Estuarine processes as drivers of GHG production

To elucidate the impact and interactions of estuarine processes on GHG production it is useful to consider different types of estuaries, where there is sufficient data for interpretation, as morphology strongly influences estuarine processes. As such two different estuaries with high urban loading: (i) the Clyde (Pickard et al., 2021a), which can be stratified and (ii) the Tyne, (Barnes and Upstill-Goddard, 2011; Upstill-Goddard and Barnes, 2016), which is well mixed with a distinct turbidity maximum, are considered and contrasted with more pristine systems. Note that estuary area was found to have no significant correlation with GHG concentrations.

5.4.1 Estuary stratification leading to near bed anoxia driving GHG production

Very high methane and nitrous oxide concentrations have been observed in the Clyde estuary (Pickard et al., 2021a). This may in part be attributed to the frequent occurrence of near-bed anoxia, as evident in continuously monitored surface and near-bed oxygen data in the upper estuary by Inner Clyde Estuary (ICE) monitoring buoy (Scottish Environment Protection Agency, 2020). Anoxic events are most common when neap tides and low river flows align. The inner Clyde estuary, which is long and narrow, has been anthropogenically constrained with near vertical walls along much of its length and obstacles such as sandbanks removed by dredging. These factors together with the lower tidal range (Table 5.3) reduce turbulence and consequently mixing, in contrast with most UK inner estuaries. When low river flows coincide with neap tides the reduced energy conditions result in a strong pycnocline and low oxygen concentrations particularly associated with the lower portion of the water column. These low oxygen concentrations enhance conditions for GHG production.

Four surveys covering different river flows and tidal ranges, average methane and nitrous oxide concentrations within the Clyde estuary showed considerable temporal variability (Pickard, 2021; Table 5.4). Potential key drivers of this variability include tidal range, river flow, surface and bed salinity, temperature and oxygen levels. While there is insufficient data in four surveys for the mechanisms impacting GHG concentrations to be fully understood, the rank orders for methane and nitrous oxide concentrations are similar suggesting that the estuarine conditions influence both methane and nitrous oxide concentrations. This would suggest reduced methane oxidation and denitrification processing of DIN possibly occurring concurrently under low oxygen conditions. The lowest methane and nitrous oxide concentrations were associated with high river flow and spring tide conditions (January 2018) and associated with a mixed, highly oxygenated estuary and diluted nutrients. The higher methane and nitrous oxide concentrations were recorded when sampling took place during a neap tide that coincided with relatively low river flows, which had resulted in a highly stratified estuary and low oxygen conditions near the bed.

Table 5.4 - Clyde Estuary GHG concentrations associated with tidal, river, salinity and oxygen conditions

	River flow Daldowie ⁽²⁾ (m ³ /s)	Percent of mean flow (%)	Tidal range ⁽³⁾ (m)	Water Temperature Deg C ⁽⁴⁾	Surface / Bed Salinity ⁽¹⁾ (PSU)	Surface / Bed Oxygen ⁽¹⁾ (mg/l)	Survey average ⁽⁴⁾ N ₂ O (nM)	Survey average ⁽⁴⁾ CH ₄ (nM)
July-17	22.6	47	2.53	15.3	2.0 / 15.0	8 / 1	31	1114
Nov-17	53.1	110	2.14	12.1	0.5 / 20.0	11 / 6	51	1460
Jan-18	139.0	287	3.49	5.4	0.1 / 0.1	12 / 12	14	445
Apr-18	20.7	43	3.33	11.8	2.0 / 6.0	8 / 5	30	1263

Note:

(1) (Scottish Environment Protection Agency, 2020a), (2) (NRFA, 2010), (3) (BODC, 2020), (4) (Pickard et al., 2021a)

The Clyde has a high urban loading with UWW treatment plants adding significant volumes of wastewater discharging both directly into the estuary and at 3.5km and 13.3km upstream of the estuary's upper saline extent, without prior nitrate or phosphate removal at the time of this survey (European Commission (Directorate General Environment), 2016). The highest methane and nitrous oxide concentrations correspond to the proximity of the largest estuarine UWW discharge, amplified by its addition to an area often stratified with a pronounced anoxic layer.

The data from the upper Clyde as measured by ICE monitoring buoy also shows that in recent years (2016 to 2019) the May to July period had higher salinity intrusion and lower dissolved oxygen data (Scottish Environment Protection Agency, 2020a). This appears linked to sustained low river flows during this period (UKCEH, 2020b), which would act to increase the saline intrusion and reduce estuary flushing, resulting in longer particle residence times. This together with the physically restricted estuary morphology would further limit the re-oxygenation of incoming saline water between tides. While these low oxygen levels during prolonged low river flow events would also be expected to result in higher GHG concentrations, the low river flow would result in an upward shift in salinity for all locations, effectively shifting the location of the estuarine water upstream impacting the effective estuary area and would need to be accounted for.

Association of near bed anoxia with weak tidal mixing and low river flow can be observed in other estuaries. Flow and stratification data across the Dart estuary showed that two layer flow occurs at neap tides during low water flow (Thain et al., 2004). Methane and nitrous oxide concentration data from the same estuary were collected across a range of river flows. Methane concentrations were an order of magnitude higher when sampling occurred at low river flow (34% of the mean flow), although all measurements occurred during neap tides (Pickard et al., 2021a); Table 5.5).

Table 5.5 - Tide and river condition associated with measurements occasions - Dart estuary

	River flow Austins Bridge ⁽²⁾ (m ³ /s)	Percent of mean flow (%)	Tidal range ⁽³⁾ (m)	Survey average N ₂ O ⁽⁴⁾ (nM)	Survey average CH ₄ ⁽⁴⁾ (nM)
July-17	3.87	34	3.45	21	442
Oct-17	14.37	127	3.46	-	-
Jan-18	53.64	475	3.54	11	54
Apr-18	25.85	229	3.71	15	41

Note:

(2) (NRFA, 2010), (3) (BODC, 2020), (4) (Pickard et al., 2021a)

While fully equivalent oxygen and nutrient data for the estuaries are not available, the urban loading of the Dart is one eighth of the Clyde (Table 5.3). The best estimate of surface oxygen levels for the Dart (Environment Agency, 2020) and the Clyde (Scottish Environment Protection Agency, 2020a) shows that the Clyde has an average surface oxygen level of 82%, and the Dart 97% (Table 5.A.1). This ranking of both oxygen levels and UWW loading is aligned with the methane and nitrous oxide data available. The extent and frequency of stratification and near bed anoxia is not known for the Dart.

Stratified estuaries experiencing low river flows in summer, when oxygen levels may already be low are even more susceptible to high methane concentrations. Higher methane concentrations were observed in four estuaries measured in July (Pickard et al., 2021a); the Clwyd, Tamar, Dart and Conwy, which had river flows between 21% and 40% of the mean flow on the measurement dates (NRFA, 2010) although no oxygen data were available. Overall, this suggests that both tide and river flow interact with urban loading to influence methane concentrations in particular, and that surface oxygen levels may provide an initial indication of likely methane concentrations.

5.4.2 Tidal range impacting sediment oxygen demand driving methane production

The Tyne (together with the Humber, Forth and Tamar) is noted to have flood tide asymmetry, (Barnes and Upstill-Goddard, 2011), which forces marine sediments upstream, when river discharge is slow, resulting in a well-defined Estuary Turbidity Maximum (ETM). High suspended sediments associated with low oxygen levels have been measured on the tidal rivers Trent and Ouse (Mitchell et al., 1999) and attributed to the high sediment oxygen demand (SOD) of the suspended sediment particles. Organic material and metals (for example from industrial legacy waste) can adsorb onto the surface of sediments and lead to increased biochemical oxygen demand (BOD) (Mitchell et al., 1998). Sediments that are re-suspended from anoxic or anaerobic layers in the bed and moved to aerobic locations by river flow or tidal flow can use more oxygen than expected because they are newly exposed to aerobic organisms and contain chemicals or metal ions in a reduced state.

Across six surveys covering different river flows and tidal ranges in the Tyne estuary, average methane concentrations showed considerable temporal variability (Upstill-Goddard and Barnes, 2016). Whilst similar methane concentrations occur across a range of river flows from 35% to 235% of the mean flow (NRFA, 2010), there is a strong correlation ($R^2=82\%$, $P < 0.02$) between methane concentrations and tidal range (using data from the standard port at Whitby at the mouth of the Tyne) (BODC, 2020), see Fig. 5.7. The higher tidal ranges have the potential to increase mixing and re-suspension of sediment, which could reduce oxygen concentrations. However, when high river flow occurs simultaneously with high tidal range, the extent of the tidal intrusion will be reduced, likely causing reduced methane production within the estuary area.

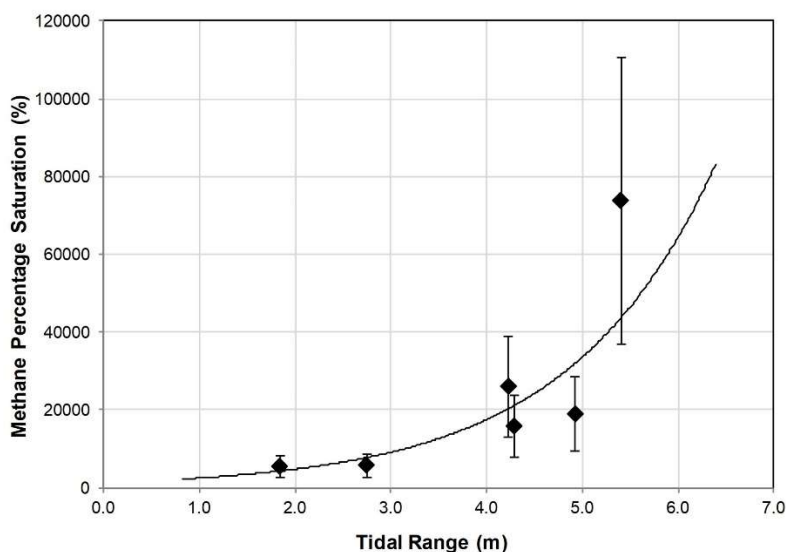


Figure 5.7 - Tyne estuary average relationships between methane concentration and tidal range
Plot uses data derived from (Upstill-Goddard and Barnes, 2016).

Other fully-mixed estuaries also show an increase in methane associated with high tidal range, but the limited number of survey occasions and confounding between potential driving variables means that methane is also correlated with low river flow and high temperature, both of which would reduce oxygen levels. These three possible causes are too strongly correlated to enable firm conclusions, and all may contribute to elevated methane concentrations to some degree.

5.4.3 Estuarine processes summary

The Clyde and Dart estuaries provide examples of stratified systems with weak tidal mixing, frequently experiencing near bed anoxia, which is associated with high methane and nitrous oxide concentrations, particularly during neap tides and low river flows. Conversely, the Tyne estuary which is typically fully-mixed shows a strong correlation between methane concentrations and tidal range, which we consider to be linked to suspended sediments removing oxygen from the water column. The Tyne has considerable legacy pollution (Hall et al., 1996; Lewis, 1990) and hence high SOD may be associated with this condition. These interpretations, while interesting, are based on limited samples from what are highly variable systems and are unlikely to fully characterise the GHG variability and associated mechanisms and should be treated with caution. Additionally, there is insufficient data overall to determine the impact of temperature on nitrous oxide and methane concentrations, which would be expected to be significant. These relationships once established may vary between environments and further improve predictive power.

5.5 Conceptual model for methane and nitrous oxide within the estuary environment

Whilst spatial-temporal variability in estuarine systems is high, evidence collated here indicates the potential for robust conceptual understanding of GHG production pathways in estuaries. Summarising the key processes that have been presented in UK estuary case studies, a conceptual model for methane and nitrous oxide concentrations within the

estuarine environment has been developed. This model aims to capture, as far as possible, the high variability between and within estuarine environments, influenced by the catchment, estuarine shape and dimensions, tidal regime and river flow, together with anthropogenic perturbations. To illustrate this model, four diagrammatic examples are provided relating to the two extremes of estuarine mixing; a salt-wedge estuary with significant stratification (Fig. 5.8) and a fully-mixed estuary (Fig. 5.9), both shown at high tide. The model also incorporates a prediction of how a low nutrient estuary (panel A) is influenced by the introduction of UWW (panel B) and how this change will interact with estuarine processes to increase both the methane and nitrous oxide emissions. Anthropogenic susceptibility can vary in different estuaries or due to different conditions within a particular estuary; for example, variation from spring to neap tides, changes in river flow and changes in temperature, can cause an estuary to change its level of stratification, oxygenation or the amount of suspended sediment. Additionally, flood or ebb tide dominance varies between estuaries with some systems becoming stratified only on the ebb and others only on the flood tide. These physical differences, which occur over varying temporal scales, will impact the interactions with UWW and can, in part, be inferred from our simplified model.

A high level of legacy pollution assimilated into the estuary sediments could further remove oxygen from the lower layer if sediments are disturbed, increasing anoxia and reducing methane oxidation. Conversely high river levels may more rapidly replenish oxygen to the upper layer, reducing the impact of UWW. As a result higher methane concentrations would be expected to increase as oxygen becomes depleted towards high tide and reach a maximum at the extent of the saline intrusion. Methane concentrations would be expected to reduce on the ebb tide as surface waters are replaced by oxygenated riverine waters and nutrient are no longer trapped in the estuary. The longitudinal profile of methane may peak where there is lowest oxygen levels while that of nitrous oxide may peak associated with mid salinity, DIN concentration and low oxygen. The location of these peaks will also be influenced by the river flow and associated with urban inflows which are then diluted seawards on the ebb. Any artificial barrages or weirs (more often found in stratified estuaries as they can remove tidal energy) may be associated with sediment or debris deposition which may act as a carbon source and hence be related to higher GHG production. Periods of drought will likely increase the extent of the saline intrusion and the estuary flushing times, which would change the location of the maximum GHGs and increase nitrous oxide concentrations. The lower estuary turbulence and the typically reduced concentration of GHGs at the surface may act to reduce emissions to atmosphere, although when mixing or overturning of the bottom layer occurs this could cause a dynamic release.

Where there are high levels of legacy pollution, sediment re-suspension in the turbidity maximum leads to high SOD, reducing oxygen levels and increasing methane concentrations and evasion significantly. Higher tides would be expected to suspend more sediment, further reducing oxygen and increasing methane production. Changes in river flows may serve only to move the location of the methane and nitrous oxide production, which on high rivers flow would cause an overall reduction GHG production in the estuary area as water is pushed seaward. In a mixed estuary (with no stratification on the ebb) methane and nitrous oxide production are expected to be similar on the flood and ebb tide. Where stratification does occur on the ebb the lower portion of the estuary stagnates, depleting oxygen and thereby producing more methane when compared to the flood tide. If sediment suspension occurs at

low tide, this could cause a rapid drop in oxygen and be associated with increased nitrous oxide concentrations due to high DIN concentrations and denitrification. The longitudinal profiles of methane and nitrous oxide may exhibit peaks associated with the low salinity turbidity maximum, areas where sediment is routinely deposited and UWW inflows. Nitrous oxide concentrations may be higher in the mid salinity range of the estuary diluting seawards. The higher estuary turbulence and continual mixing of GHGs to the surface will act to increase emissions to atmosphere.

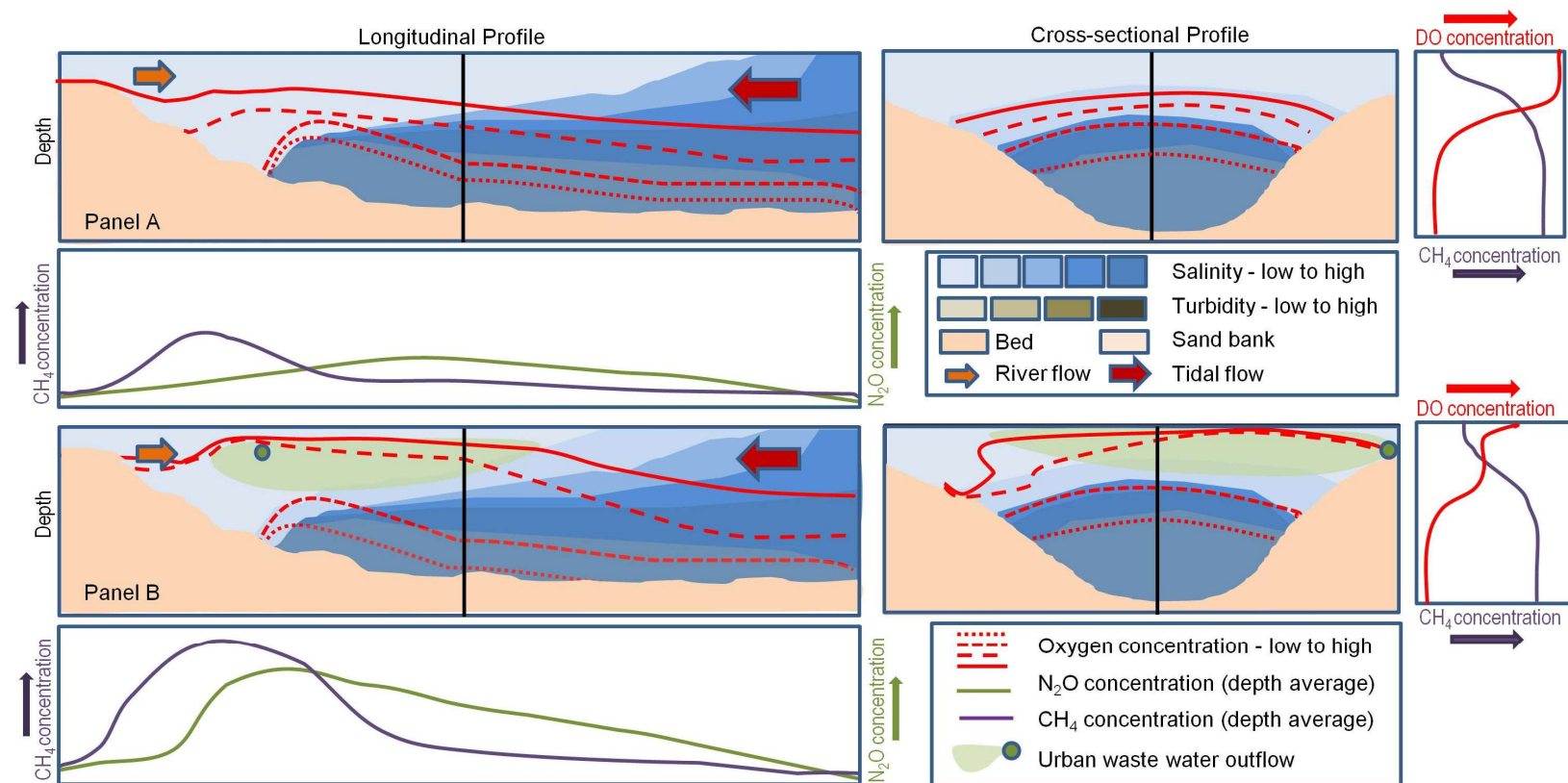


Figure 5.8 - Longitudinal and cross-sectional profiles of a highly stratified salt-wedge

Panel A: - Longitudinal and cross-sectional profiles of a highly stratified salt-wedge estuary at high tide, with the higher salinity water flowing shore-wards underneath the out-flowing river water. The upper layer, from the river, would typically be oxygenated, but the lower layer would become lower in oxygen with no means of replenishment, as the oxygen is depleted with distance from the sea and time from low tide. The degree of stratification will change during the tidal cycle and with river and tidal conditions, but when the estuary is highly stratified, this will reduce diffusion of GHGs from the lower to upper layer trapping GHGs under the pycnocline. Methane generation in the bed is generally associated with the low salinity area of the estuary, significantly reducing when the water becomes highly saline. Oxidic methane may be generated in the upper fresh water layer. Most methane (CH₄) oxidation would occur in the upper layer resulting in methane concentrations that are linked both to the water layer of generation and inversely related to the vertical oxygen profile. The specific relationship and location of the methane maximum is expected to change with river flow, tidal range and state of the tide, with surface methane concentration reducing on the ebb as more river water becomes available. Some dissolved inorganic nitrogen (DIN) may enter the estuary from the river, with DIN loading changing with river flow. Nitrous oxide (N₂O) concentration would be relatively low peaking at mid-salinity, compared to the methane peaking at low salinity, both reducing seawards due to dilution with sea water. Panel B: -

Longitudinal and cross-sectional profiles of a salt-wedge estuary at high tide including the introduction of urban wastewater concentrated in the low salinity upper layer. Introduction of UWW will result in additional nutrients trapped in the upper layer, causing oxygen depletion thereby inhibiting methane oxidation, resulting in higher methane concentrations and additional methane evasion. Ammonium derived from urban wastewater may significantly increase nitrous oxide production, near the source and in the mid salinity range. Most DIN will be trapped in the more oxygenated upper layer making nitrification, driven by DIN concentration, the main N₂O producing mechanism in this layer. N₂O production in the lower layer will be driven by denitrification, with the N₂O concentration increasing with lower oxygen levels further supported in estuaries that have long flushing times allowing DIN to mix or diffuse downwards. Oxygen depletion can result in a switch from nitrification to denitrification even in the surface layer.

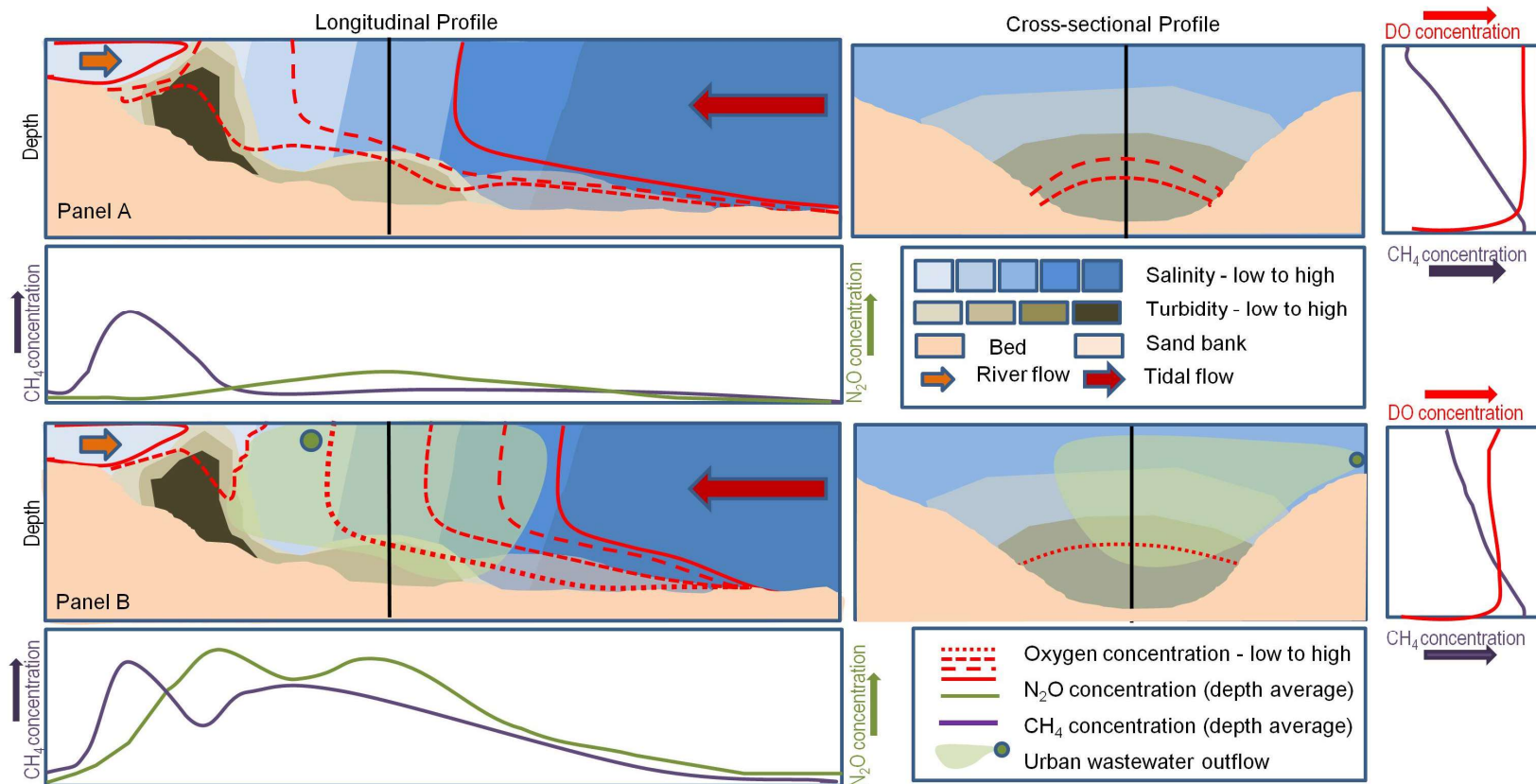


Figure 5.9 - Longitudinal and cross-sectional profiles of a fully-mixed estuary

Panel A: Longitudinal and cross-sectional profiles of a fully-mixed estuary, with salinity and oxygen levels mixed vertically throughout the water column. Estuaries with high tidal mixing typically experience tidal asymmetry and the transport of fine marine sediments into the upper estuary resulting in a turbidity maximum at low salinity. These sediments are moved up the estuary on the flood and down the estuary of the ebb tide and can trap organic matter at the bed. Methane (CH₄) is mixed and oxidised throughout the water column resulting in little methane evasion in the unpolluted scenario. Any dissolved inorganic nitrogen (DIN) will likely be converted by the nitrification route due to the mixing and higher oxygen levels. Panel B: - Longitudinal and cross-sectional profiles of a fully-mixed estuary, including the introduction of urban wastewater which is distributed throughout the water column due to mixing. - Introduction of urban wastewater (UWW) which will be mixed throughout the water column, will result in an interaction between the DIN and suspended sediments, allowing for both processing of nitrogen in the bed and water column, leading to higher nitrous oxide (N₂O) production. Where the UWW is sufficient to deplete oxygen levels through the water column denitrification could occur. This can further act to increase methane if resulting in reduced oxygen levels and subsequent methane oxidation inhibition.

5.6 Discussion and Conclusions

There is convincing evidence from UK estuaries that excesses of nutrients from UWW result in both higher methane and nitrous oxide concentrations and these concentrations link directly to UWW loading per unit river flow. This is supported by estuaries with higher urban land cover having higher methane and nitrous oxide concentrations. Furthermore, methane and nitrous oxide concentrations are more strongly correlated to nitrite and ammonium than nitrate. Where estuaries experience very low oxygen conditions, higher concentrations of both nitrous oxide, most likely generated via denitrification, and methane, in part due to reduced methane oxidation, can be detected. As enhanced nitrogen processing is favourably associated with mid-salinity conditions (Isnansetyo, A., et al., 2014) and methane oxidation may be inhibited either directly or indirectly by higher ammonium concentrations, this makes the estuarine environment an unfortunate location for UWW disposal with respect to GHG emissions. Similarly nitrogen enrichment has been found associated with increased methane and nitrous oxide emissions from tidal flats (Hamilton et al., 2020) and higher methane emissions are now being associated with urban or anthropogenically influenced inland waters (Wang et al., 2021; Hao et al., 2021).

Estuary physio-chemical properties strongly influence methane and nitrous oxide concentrations. Stratified estuaries can experience significant oxygen depletion in the deeper more saline layer, with any legacy waste and associated oxygen sediment demand potentially exacerbating this effect. Additionally, inputs of UWW into a stratified estuary can result in further oxygen depletion in the upper layer due to nitrification of ammonium. Stratified estuaries experiencing low river flow, particularly in summer, when oxygen levels may already be low are even more susceptible to the impacts of UWW, as lower river flows will increase flushing times. Fully mixed estuaries, characterised by a low salinity and high turbidity maximum, can produce high levels of GHGs. The re-suspension of sediments can encourage high SOD (Mitchell et al., 1998), preventing oxidation of methane in the water column. This increase in methane concentration can be linked to tidal range and also possibly to urban or legacy waste.

The conceptual model presented in this paper hypothesises that higher concentrations of both methane and nitrous oxide occurs due to interactions between natural estuarine processes and anthropogenic factors. Low estuarine oxygen levels appear to be significant in causing high methane concentrations within the estuary environment and probably linked to increased methane production and reduced methane oxidation in the surface sediments and water column. Estuarine processes can cause low oxygen levels where they prevent oxygen from being brought to the estuary, for example during low river flows and at high temperatures. Additionally, oxygen may not be replenished in the water column, for example when the estuary is stratified or particle residence times increased. Sediments re-suspension can result in BOD, when oxygen is consumed by mineralization of the degradable organic components in fine sediments. Oxygen can be further depleted by the interaction with anthropogenic factors; for example: the introduction of nutrients from UWW and where legacy pollution is contained in the sediment resulting in high SOD.

Use of this conceptual model enables us to predict that some stratified estuaries may experience elevated methane concentrations at high tide, upstream at the low salinity section of the estuary. It also suggests that fully mixed estuaries with significant SOD would experience elevated methane concentrations during sediment suspension events, which are most often associated with high tidal range. However, these events can also occur at low tide and if sediments are re-suspended in shallow water over estuarine mud, low oxygen and high GHG concentrations may result. The rate of nitrous oxide generation from nitrification is variable, dependent on the availability of electron acceptors and donors (Wrage et al., 2001), the salinity level (with optimum nitrification in the mid salinity range) and temperature (with increased production typical at higher temperatures). Where oxygen concentrations are low or variable, as is often the case in estuarine environments, denitrification may be triggered. This can further significantly increase nitrous oxide concentrations. Estuaries with high suspended sediment concentrations may also support nitrogen processing in the water column as well as at the bed, associated with, for example, a turbidity maximum.

The conceptual model presented here summarises the processes evident in several UK estuaries, but if relationships can be generated for different estuaries and related to both natural processes and anthropogenic perturbations then it may theoretically be applied elsewhere. A study in Chesapeake Bay, the largest estuary in the United States which is eutrophic with near bed hypoxia, also found that methane was associated with low oxygen conditions. Interestingly in this study methane built up under the thermocline and could be released by storm events that induced mixing and overturning (Gelesh et al., 2016). While our conceptual model considers only tidal stratification which lasts in the order of hours, this thermal stratification may last weeks and act to reduce methane diffusion to the surface. The only estuary in this study deep enough to form a thermocline in calm summer weather is the Forth estuary (Black Culm Ltd, 2018). Methane concentrations in the deeper, higher salinity part of the Forth (Upstill-Goddard and Barnes, 2016) were lower in summer, as such it is possible the formation of a thermocline may impact the surface methane signature and methane evasion estimates. GHGs evasion linked to large river plumes may also be dependent on offshore mixing, with higher GHG concentrations found in calm weather. Methane concentrations were measured in nine tidal estuaries in NW Europe including well-mixed, turbid estuaries with long particle residence times (Elbe, Ems, Thames, Scheldt, Loire, Gironde, and Sado) and salt-wedge estuaries with short particle residence times (Rhine and Douro) (Middelburg et al., 2002). While it is not clear how measurements were made relative to the phase of the tide or river flow, it is interesting that the stratified Rhine experienced high and highly variable methane concentrations as would be predicted by the conceptual model dependent on river flow and tidal range and phase. Conversely in well mixed estuaries methane was often highest at the low salinity end consistent with the turbidity maximum being important in methane production (Burgos et al., 2015).

While a single survey was available for the Thames (Middelburg et al., 2002) and some data for the Humber (see Table 5.1), these large complex estuaries with several contributing rivers and many UWW entry points were not included in the analysis and did not fit the model as well as the simpler estuaries. It is suggested that the large number of tributaries, distance between where tributaries enter the estuary and the large number of UWW treatment plants and the distance of these plants from the estuary make the results difficult to interpret. For example, the outflow from 335 and 200 UWW treatment plants eventually enter the Humber

and Thames estuaries respectively, some from over 200km. It is likely that where UWW enters a river far from the estuary, that most nitrogen processing is completed within the typically well oxygenated riverine section reducing its influence within the estuary. Additionally, wide more exposed estuaries are likely to be mixed by wind helping oxygenation and increasing evasion, a process not explicit in this model.

5.6.1 Are estuaries a net carbon source or sink?

The flux of GHGs between estuaries and the atmosphere has been estimated by those authors considered herein. This flux is dependent on the dissolved gas concentrations (under consideration in this paper) and the gas transfer velocity (k), which is in turn dependent on in-water turbulence and wind speed (Wanninkhof, 1992 and Clark et al., 1995). In estuaries the estimation of the gas transfer velocity associated with turbulence is complex, as turbulence is the result of tidal velocity and river flow interacting with friction from the bed bathymetry. As such salt-wedge estuaries, with lower turbulence compared to mixed estuaries may have a lower value of k . Wind speed, found to have the major impact on k (Clark et al., 1995), not only impacts diffusion at the interface but also wind induced waves which increase mixing. Estuaries that are wide and align with the prevailing wind direction and in topographies that increase wind exposure, are likely to evade a higher proportion of their GHGs to the atmosphere. Thus, k -values from a narrow, dredged, salt-wedge estuary may be less than from a fully-mixed, wide and exposed estuary, especially as GHGs in the lower layer will be less accessible. However, when the stratification is overturned or the stratified water becomes mixed, this may result in dynamic release of trapped GHGs to atmosphere. This process would be difficult to observe requiring detailed temporal monitoring, and emissions may be underestimated if only surface concentrations have been measured.

In addition to the direct atmospheric emissions, it is also important to understand whether estuaries are an overall carbon sink or source. The term 'Blue Carbon' is used to highlight the importance of the carbon sequestration capacity of coastal vegetated ecosystems (Santos et al., 2021). While there is currently insufficient data to understand the link between carbon sequestration and GHG concentrations, it has been hypothesised that discharges of high-nutrient but relatively low-carbon water generated by wastewater treatment can enhance carbon uptake from the atmosphere by affecting biogeochemical cycles in these system (Kuwae et al., 2016). While this is yet to be tested, this estimate focuses primarily on carbon dioxide and not nitrous oxide or methane. In contrast arable and (sub)urban estuaries were found to export, on average, 50% more dissolved organic carbon to coastal areas than they receive from rivers due to net anthropogenic derived organic matter inputs within the estuary, with the bioavailability of this dissolved organic matter promoting microbial production and degradation (García-martín et al., 2021). While beyond the scope of this paper, understanding where estuaries could act as carbon sinks and how this is impacted by anthropogenic inputs (in terms of micro-biome communities and bioavailability of nutrients) and activities (e.g. dredging) would be a beneficial area of study. The highly variable estuarine environments are likely to respond differently to enabling carbon sequestration both in terms of anthropogenic influences and estuarine processes.

5.6.2 The impact of survey design and areas of uncertainty

Where estuarine surveys are designed to produce an estimate of GHG concentrations it is important to consider the best approach to capture spatio-temporal variability. Based on data reviewed here we recommend the following approach for future studies:

- a) use of fixed point transects with each point aligned to a particular area within the estuary and measurements taken upstream to the limit of the maximum saline intrusion.
- b) sufficient sampling undertaken to account for tidal range, stage of the tide, river flow and river flow history (for example periods of drought).
- c) sufficient sampling undertaken to account for temperature ranges and seasonality, including the interaction of temperature and river flow.
- d) measurements to quantify the influence of any nutrient and pollution point sources within the estuary and to account for the different mechanisms of GHG production, for examples linked to: stratification, high turbidity and SOD, tidal flats, variation in salinity, legacy pollution and UWW.
- e) measurements of oxygen, turbidity and nutrients in addition to GHG concentrations.
- f) measurements to quantify GHGs in both layers where stratification occurs.

Further measurements designed to quantify the specific impact of stratification, tide, temperature and river flow on GHG concentrations and emissions could help remove uncertainties in the conceptual models and further the objective of this paper in helping to identify and remediate estuaries that have high GHG concentrations, globally.

It can be difficult to distinguish between different anthropogenic factors, because areas which were the centres of past industrial activity still have high urban populations. Population density has been found to be significantly related to enrichment of sedimentary metals (Birch et al., 2015). As referred to previously, high levels of legacy pollution, particularly metals, may play a role in GHG emissions. Impairments to water quality can result in the creation of toxicologically stressful environments that may affect the microbiome community structure (Rodgers et al., 2020). This can have an impact on GHGs; for example methanogens use metals such as nickel within coenzymes (Lyu et al., 2018). At least four of the estuaries considered here have high legacy pollution, particularly heavy metals, including the Clyde (Rodgers et al., 2020; Balls et al., 1997), Forth (Lindsay et al., 1998), Tees and Tyne (Hall et al., 1996; Lewis, 1990). The Clyde and Tyne produce more methane than might be expected compared to the Tees and Forth. While this may be related to the Clyde and Tyne being physically restricted, narrow estuaries, it should be noted that the Clyde and Tyne estuaries are regularly dredged, while the upper Forth estuary has never been dredged and the Tees is only occasionally dredged (Marine Scotland, 2021; The Crown Estate, 2021). Dredging and straightening are likely to reduce bed friction and, hence mixing. Dredging can re-suspend buried sediments associated with legacy heavy-metal pollution making it more available and leading to further anthropogenic interactions. A further uncertainty is the impact of temperature, salinity and nutrient levels on microbiome community structure and hence the balance between methane production and oxidation.

Expected changes in climate will also impact the estuary environment (Robins et al., 2016). This may act to further increase estuary GHG concentrations via a number of mechanisms. Increasing temperatures will reduce oxygen concentrations and increase nitrogen processing rates. Rising sea levels may increase sediment re-suspension and the extent of the saline

intrusion, which could increase access to legacy waste. Changing rainfall patterns may increase the prevalence of drought conditions resulting in lower river flows and consequently lower oxygen and higher nutrient concentrations and reduced estuary flushing. Conversely more extreme rainfall events may lead to flooding which could result in flooding of land affected by legacy waste and nitrogen-rich agricultural land. All of these changes may act to further increase the susceptibility of estuaries to anthropogenic influences increasing GHG production.

5.6.3 Opportunities to reduce estuarine GHG emissions

Given that the estuary environment is a potentially significant source of GHG emissions, opportunities to manage and reduce emissions should be considered. Fundamental to the reduction of both nitrous oxide and methane emissions from estuaries is the lowering of DIN levels and removal of low oxygen conditions. Relating to the former, addition of nitrogen and phosphate removal technologies to existing UWW treatment systems outputting to estuaries should be considered. While estuary oxygenation has been trialled in a eutrophic estuary ((Larsen et al., 2019a) and some reservoirs (Gerling et al., 2014) its impact on the biome community and GHG production is unknown. This type of technology could be beneficial if powered by renewable technology. Our conceptual model may be applied to identify priority estuaries for this intervention. Additionally, an improved understanding of processes associated with GHG generation could, in the interim, support the adoption of changed management practices, for example ensuring that outflows of UWW are not timed with conditions which may exacerbate estuarine GHG production. Applying our model to the Clyde estuary, we would expect the estuary to be well oxygenated (and hence have lower surface methane concentrations) during high river flows and during ebb tides. Hence, managing UWW outflow to avoid low oxygen conditions and timing outflows on the ebb tide rather than the flood tide could help reduce oxygen stress and methane and nitrous oxide emissions.

The annual nutrient loads to estuaries in the UK are comparatively small compared to reported figures for European and North African estuaries (Nedwell et al., 2002). As such, there may be even greater potential for excess GHG emissions, and reduction thereof, from estuaries at the global scale. With twenty two of the thirty two largest cities in the world are located on estuaries (NOAA, 2020), anthropogenically impacted estuaries may be hidden sources of GHG globally. The conceptual model could be applied to other estuaries globally, by considering both natural processes and anthropogenic perturbations. Furthermore, with relatively little extra data, for example nutrients and oxygen (parameters that are often routinely measured) and an understanding of estuary dynamics (tide and river flow), this conceptual model could underpin both effective modelling of estuary GHG production and also provide a route for simpler monitoring of future improvements.

5.6.4 Considerations for policy makers:

Estuaries are highly valuable as they are critical natural habitats and provide a wide range of ecosystem services. However they experience a wide range of anthropogenic stressors (Kennish, 2005). Estuaries have long been considered an effective location for the disposal of urban and industrial waste, because of their proximity to that waste generation and their perceived ability to flush this waste to the sea with its high dilution capability. However, evidence shows that estuaries (both inner and outer) by their very nature: brackish water, low

oxygen, stratification and high sediments loads, can become significant GHG sources, particularly when high levels of urban waste enter the estuary. Additionally seasonal changes in river flow, tide and temperature can further exacerbate this GHG generation.

As such criteria linked to GHG generation (not just eutrophication risk) should be included in legislation to further constrain wastewater disposal. The mechanistic understanding of GHG generation in the estuarine environment and the associated conceptual model presented in this paper can be applied to help in the identification of estuaries which may act as significant GHG sources and also estuaries where interventions and reduction of anthropogenic influence could significantly reduce these emissions. Further research globally into estuary environments as a GHG source, together with research into mechanisms and the effectiveness of mitigations is still required.

Declaration of interests

The authors declare that they have no known competing financial interests or personal relationships that could have appeared to influence the work reported in this paper.

Acknowledgments

The authors would like to thank the authors of the papers and data sets used in this review and the two anonymous reviewers whose comments have helped improve the quality of this paper.

This work was funded by a Natural Environment Research Council (NERC) studentship through the IAPETUS Doctoral Training Partnership. AP's input was funded by the Natural Environment Research Council as part of the LOCATE project. CEH Grant No.: NEC05686, NOC Grant No.: NE/N018087/1.

5.7 Supplementary data

Table 5.A.1 - Average dissolved oxygen (DO) saturation data for several estuaries of interest

	Location	Location	Period	DO sat % range	DO sat % Average
Clyde	Inner estuary (1m surf)	55°52'04.0"N, 4°19'02.8"W	Jan-17 - Sep19	1.5-219%	82%
Clyde	Inner estuary (1m bed)	55°52'04.0"N, 4°19'02.8"W	Jan-17 - Sep19	0.0-100%	67%
Clyde	Dunoon (surf)	55°56'33.6"N, 4°55'08.5"W	Jan-17 - Dec 19	3.1-209%	99%
Forth	South Alloa (surf)	56°06'10.3"N, 3°48'35.5"W	Jan-17 - Dec 19	0.4-100%	78%
Forth	Gunnet Edge (surf)	56°01'41.1"N, 3°10'35.4"W	Jan-17 - Dec 19	81-128%	96%
Tamar	EA - Shellfish	50.428024, -4.200493	Jan-16 - Mar-19	75-127%	92%
Tamar	Westonmill	50.392132, -4.196016	Oct-12 - Jan-20	79-128%	94%
Tamar	Devonport	50.385048, -4.190062	Jul-14 - Mar-19	78-130%	95%
Tyne	Jarrow	54.987489, -1.485819	Jul-12 - Jan-20	63- 96%	84%
Tyne	Whitehall	54.987353, -1.454566	Oct-12 - Mar-20	69-108%	90%
Tees	Billingham Reach	54.575636, -1.260516	Oct-11- Nov-19	56-137%	87%
Tees	Transported Bridge	54.584429, -1.229411	Jul-12 - Feb-20	58-135%	86%
Tees	Teesport	54.605532, -1.159347	Jul-12- Feb-20	70-120%	91%
Dart	Totnes	50.419799, -3.669391	Oct-08 – Nov 18	55-123%	94%
Dart	White Rock	50.397312, -3.629598	Jun-17 to Jan-20	81-130%	98%
Dart	Buoy No 8	50.357851, -3.575835	Jun-17 to Jan-20	88-112%	98%
Humber	Whitgif sands	53.696654, -0.775779	Jun-10 to Oct-18	62-96%	80%
Humber	Flaxfleet	53.703104, -0.692122	Jun-10 to Oct-18	67-88%	79%
Humber	South Ferriby Cliffs	53.686943, -0.49393	Jun-10 to Sep-17	75-93%	82%
Humber	East Clough	53.710544, -0.521769	Sep-11 to Oct-18	67-97%	81%
Humber	Salt End Jetty	53.727559, -0.248249	Sep-10 to Oct-19	58-154%	91%
Humber	Humber at Spurn	53.578975, 0.11181	Jun-10 to Oct-18	83-100%	95%

Notes

- Both the Clyde and Forth estuaries have SEPA monitoring buoys installed measuring water temperature, dissolved oxygen, turbidity, salinity and pH. The buoys were installed because these estuaries are known to experience low oxygen conditions and allow an interesting and detailed case study. Analysis of data from the monitoring buoys (Scottish Environment Protection Agency, 2020a) has enabled an understanding of how different river flows and stages of the tide can impact oxygen levels within the estuaries.
- The Tamar, Tees, Tyne and Dart are measured by the Environment Agency (EA) (Environment Agency, 2020) with sampling typically completed monthly or bimonthly. Dissolved Oxygen percentage saturations are summaries for several locations for each estuary.
- The range from the continuous monitoring buoys would be expected to exceed that sampled monthly by the EA, which is also likely to be nearer surface than the buoy data (impacting the values).

Table 5.A.2 - Percentage land cover for estuaries of interest

	Deciduous woodland	Coniferous woodland	Arable	Improve grassland	Neutral grassland	Calcareous grassland	Acid grassland	Fen	Heather	Heather grassland	Bog	Inland rock	Freshwater	Littoral rock	Littoral sediment	Urban	Suburban
Conwy	6.3%	14.1%	0.0%	14.6%	3.1%	0.0%	42.6%	0.0%	6.5%	2.0%	9.6%	0.5%	0.5%	0.0%	0.0%	0.0%	0.2%
Clywd	8.1%	5.8%	2.0%	59.1%	0.3%	0.0%	18.6%	0.0%	1.3%	0.0%	2.7%	0.2%	0.2%	0.0%	0.0%	0.3%	1.3%
Tamar	9.3%	3.1%	6.3%	69.0%	0.0%	0.0%	6.9%	0.0%	0.2%	0.1%	2.6%	0.0%	0.3%	0.0%	0.0%	0.1%	2.0%
Dart	9.6%	4.3%	2.2%	22.4%	0.6%	0.0%	49.2%	0.0%	1.2%	0.0%	8.5%	0.0%	0.1%	0.0%	0.0%	0.1%	1.7%
Tay	5.9%	11.2%	7.7%	9.0%	0.0%	0.0%	25.2%	0.0%	29.0%	0.8%	2.3%	5.5%	2.6%	0.0%	0.0%	0.0%	0.7%
Forth	11.0%	18.6%	8.1%	18.4%	0.0%	0.0%	30.4%	0.0%	3.8%	1.0%	3.1%	0.5%	2.9%	0.0%	0.0%	0.3%	2.0%
Clyde	7.3%	11.2%	3.2%	34.2%	0.0%		25.2%		1.7%	2.5%	4.1%	1.2%	0.6%			1.2%	7.5%
Tyne	5.6%	19.0%	3.7%	28.3%	0.0%	0.0%	18.2%	0.0%	5.6%	5.6%	11.5%	0.1%	1.0%	0.0%	0.0%	0.1%	1.2%
Humber	6.7%	2.8%	24.7%	30.8%	0.0%	2.6%	5.8%	0.0%	4.7%	3.7%	8.2%	0.1%	0.7%	0.0%	0.0%	2.4%	6.7%
Tees	4.3%	1.6%	27.9%	26.0%	0.4%	1.1%	3.8%	0.0%	1.6%	3.6%	24.4%	0.2%	0.7%	0.0%	0.0%	0.7%	3.9%
Orwell	5.9%	0.1%	68.8%	13.6%	0.3%	0.0%	0.0%	0.0%	0.0%	0.0%	0.0%	0.0%	0.2%	0.0%	0.0%	2.0%	9.1%
Stour	5.8%	0.1%	71.4%	17.1%	0.1%	0.0%	0.0%	0.0%	0.0%	0.0%	0.0%	0.0%	0.2%	0.0%	0.0%	0.6%	4.7%
Debben	4.5%	0.0%	75.3%	15.8%	0.4%	0.0%	0.0%	0.0%	0.0%	0.0%	0.0%	0.0%	0.0%	0.0%	0.0%	0.2%	3.6%
Colne	7.4%	0.2%	63.0%	22.5%	0.0%	0.0%	0.0%	0.0%	0.0%	0.0%	0.0%	0.0%	0.3%	0.0%	0.0%	0.7%	5.9%

Notes:

1. Conway, Dart, Stour, Debben and Colne use only the catchments from the main river.
2. Clywd is the sum of the catchment areas from Clywd and Elwy.
3. Tamar is the sum of the catchment areas from Tamar and the Tavy.
4. Tay is the sum of the catchment areas from Tay and Earn.
5. Forth is the sum of the catchment areas from Forth, Bannock Burn and Devon.
6. Clyde is the sum of the catchment areas from Clyde and the Kelvin.
7. Tyne is the sum of the catchment areas from Tyne and the Derwent.
8. Humber is the sum of the catchment areas from Aire, Trent, Ouse, Don, Wharfe, Derwent, Torne and Foss
9. Tees is the sum of the catchment areas from Tees and the Leven
10. Orwell is the sum of the catchment areas from Gipping and Belstead Brook
11. The catchment areas applied are from the National River Flow Archive (NRFA, 2010)
12. The land cover data applied was from the UKCEH Land Cover Maps (Morton et al., 2020)

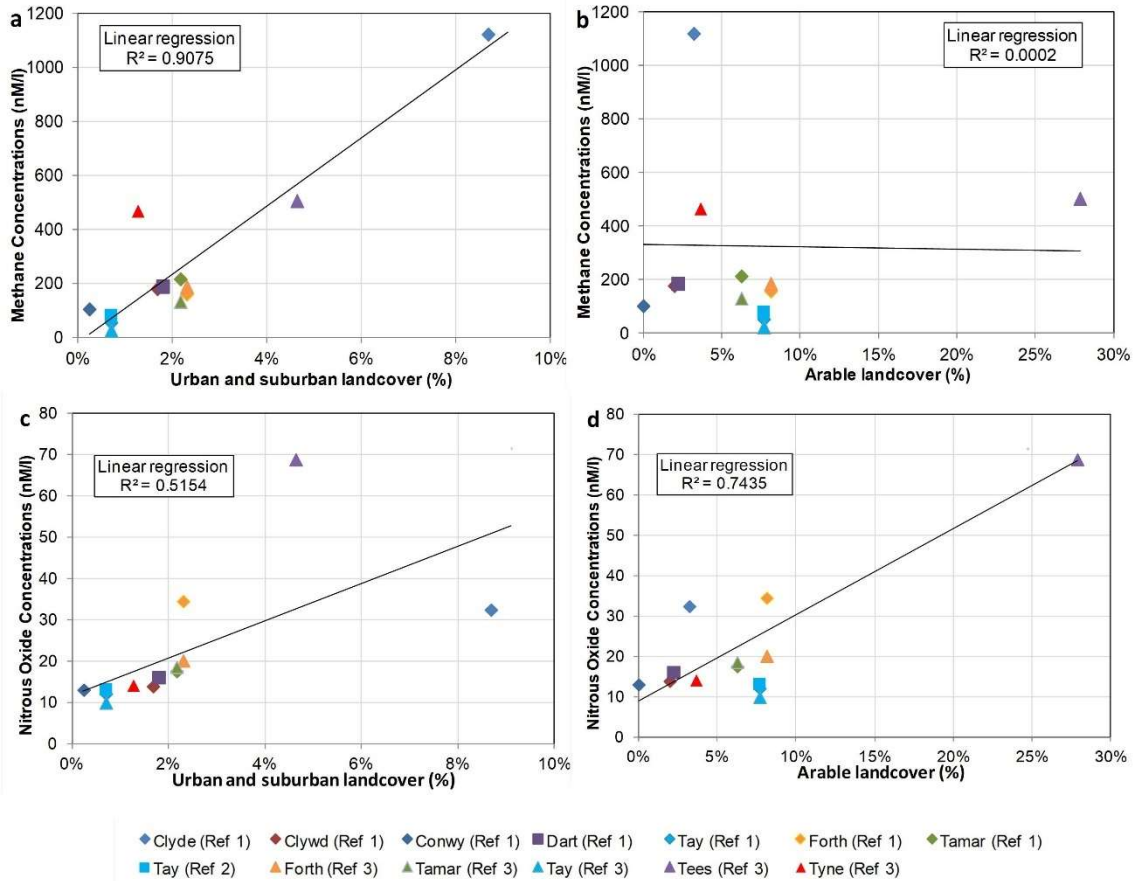


Figure 5.A.1 - Average CH₄ and N₂O concentrations compared to urban and arable land cover

Average methane concentration compared to (a) urban land cover (b) arable land cover and average nitrous oxide concentration compared to (c) urban land cover (d) arable land cover with GHG data from (Pickard et al., 2021 and Upstill-Goddard and Barnes, 2016) and land cover data from (Morton et al., 2020).

1. No significant correlations were found for areas of woodland, grassland, freshwater or other substrate or overall catchment area. The total urban (urban plus suburban) percentage land cover is significantly correlated to estuary methane concentration ($P < 0.001$) and total urban ($P < 0.05$) and arable ($P < 0.001$) percentage land cover are significantly correlated to nitrous oxide concentration.
2. The significant correlation between catchment area and mean river flow ($R^2 = 97\%$, $P < 0.005$) for the selected estuaries, allows sensible use of the percentage land cover (compared to total land cover/mean river flow).

6 The impact of salinity and hypoxia on estuarine Greenhouse gases: A study of the stratified Clyde estuary

Declaration of authorship: The data in this chapter was collected and analysed by the author of the thesis, some co'-authors supported for the power boat surveys including Stella White, Dr. Elliot Hurst; Mairéad Corr and Dr. Amy E. Pickard and as detailed in the acknowledgments. Co-authors reviewed paper drafts and provided supervision, feedback, and guidance.

The chapter has been submitted to the Estuarine, Coastal and Shelf Science and is under review

Graphical Abstract

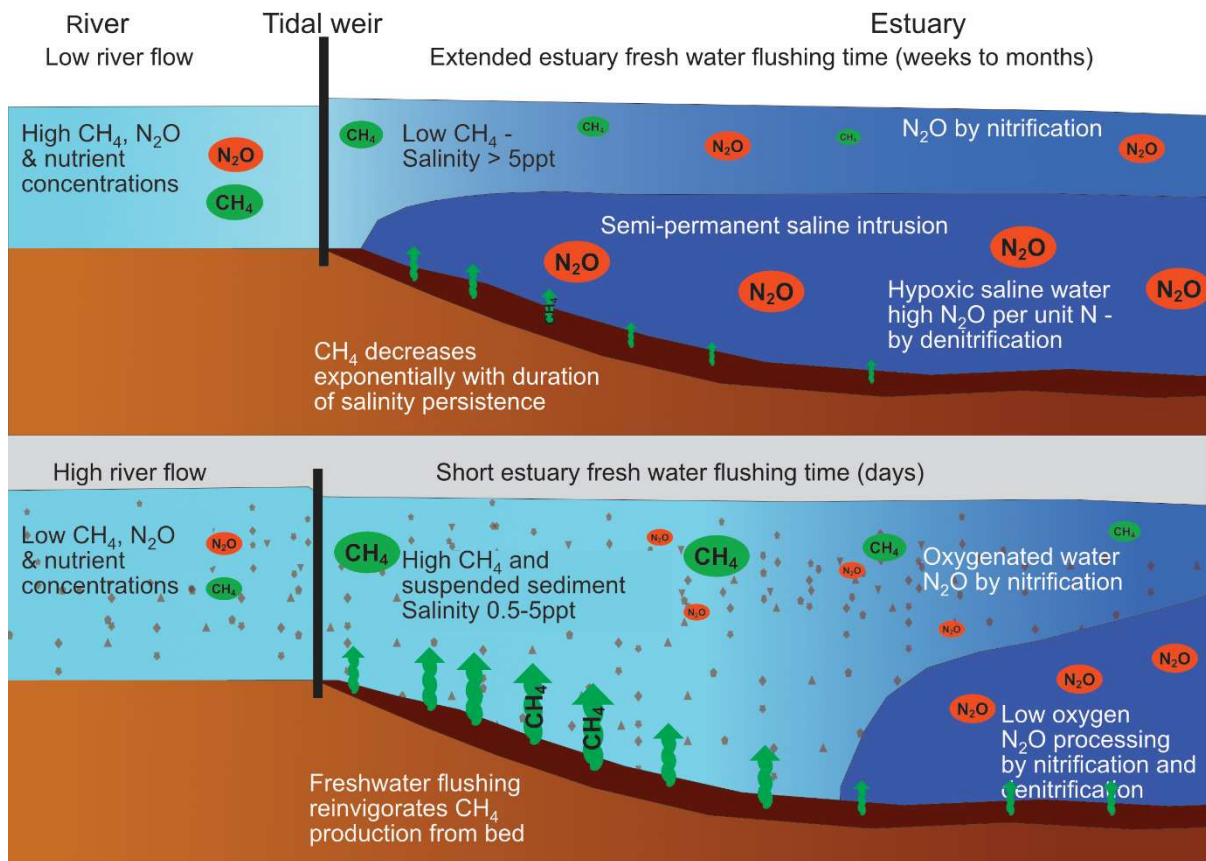


Figure 6.0 - Graphical Abstract - The impact of salinity and hypoxia on estuarine greenhouse gases

Highlights

1. Low dissolved oxygen exponentially increased estuarine N₂O concentration.
2. Urban wastewater entering the estuary was the major contributor to hypoxia.
3. Nitrification dominated the freshwater layer and denitrification the saline layer.
4. CH₄ decreased exponentially with salinity persistence (50% after 10 days).
5. CH₄ production from the estuary bed was reinvigorated by freshwater flushing.

Abstract

Estuaries and coastal waters are sensitive to ecological degradation but receive some of the highest levels of pollutants. One impact of these pollutants is increased greenhouse gas generation, which is significant, but difficult to estimate due to high variability and data paucity. This paper investigates key controls on methane (CH₄) and nitrous oxide (N₂O) in the urban, mesotidal, stratified Clyde estuary, in Scotland, between February 2020 and October 2022. Measurements covered the estuary longitudinally, through tidal cycles and across the river-estuary transition. Dissolved CH₄ and N₂O were always supersaturated relative to air exhibiting strong spatial and temporal variability. Nitrification dominated in the upper freshwater layer, where [N₂O-N] exceeded 4.0 µg l⁻¹, while in the lower saline layer denitrification dominated and [N₂O-N] exceeded 5.9 µg l⁻¹, quadrupling the N₂O per unit available nitrogen. There was a significant inverse exponential correlation between N₂O and dissolved oxygen in the lower layer, with hypoxia driving elevated denitrification. Methanogenesis increased in the estuary surface waters as soon as the waters became slightly saline (>0.5ppt) and [CH₄-C] was positively correlated with turbidity and exceeded 65 µg l⁻¹. Lower saline layer [CH₄-C] exceeded 130 µg l⁻¹ and were highest after freshwater flushing events. The [CH₄-C] decreased exponentially with salinity persistence, reducing by 50% after 10 days of continuously saline water (> 5ppt). Salinity persistence likely provides a tipping point between the dominance of different microbial communities. The impact of small increases in salinity and the persistence of saline conditions, explaining much of the previously reported variability in estuarine CH₄. This study provides unique insights into the conditions that generate greenhouse gases in stratified urban impacted estuaries.

Key words

Estuary; methane; nitrous oxide; hypoxia; salinity; salinity persistence; stratification.

Authors

Alison M. Brown^{1,2}; Dr. Adrian M. Bass², Stella White¹, Dr. Elliot Hurst¹; Mairéad Corr¹; Dr. John M. Macdonald²; Prof. Ute Skiba¹; Dr. Amy E. Pickard¹

1. UK Centre for Ecology & Hydrology, Bush Estate, Penicuik, Midlothian, UK, EH26 0QB.
2. School of Geographical & Earth Science, University of Glasgow, Glasgow, UK. G12 8QQ.

6.1 Introduction

Estuaries and coastal waters are among the most sensitive ecosystems to ecological degradation but receive some of the highest levels of pollutants. The primary pollutants of estuarine and coastal waters include; sewage and other high nutrient oxygen-demanding wastes, organic and inorganic nutrients resulting in progressive enrichment, pathogens and infectious agents, oils, heavy metals, organic chemicals including polynuclear aromatic and chlorinated hydrocarbons and radioactive wastes (Kennish, 1994). The often low-energy environment within estuaries, can result in pollutants being trapped and concentrated, potentially resulting in significant habitat damage. While there have been major improvements in estuarine water quality over the past century resulting from a reduction in raw sewage discharges, this has made other contamination more visible (Matthiessen and Law, 2002). Major changes to the estuarine environment due to industrial and urban development have resulted in excesses of pollution coinciding with changes to estuary geomorphology which can impact flow, sedimentation and other estuarine processes. These physical and chemical changes combined can transform these sensitive ecosystems into hot-spots for GHG generation (Brown et al., 2022).

Evasion of GHGs from the estuarine environment is significant; global methane (CH_4) evasion from the total coastal and open ocean was estimated at $33.2 \pm 37.6 \text{ Tg CH}_4 \text{ yr}^{-1}$, with estuaries evading 0.90 to 5.96 $\text{Tg CH}_4 \text{ yr}^{-1}$ (Rosentreter et al., 2021; Zheng et al., 2022), suggesting estuary emissions are highly uncertain. The large range of uncertainty in estuarine and coastal CH_4 fluxes is attributed to the paucity of data and the high variability of these ecosystems, with human alterations to aquatic ecosystems such as urbanization, eutrophication and positive climate feedbacks acting to increase CH_4 emissions (Rosentreter et al., 2021; Borges and Abril, 2012). Methanogenesis within the estuarine environment is highly dependent on both in-water and in-sediment processes, with methanogens competing for resources. For example, methanogens can be outcompeted by sulphate reducing bacteria (SRB) where the methanogenesis pathway uses hydrogen (H_2) and acetate, with rates of methanogenesis found to be two orders of magnitude lower than rates of sulphate reduction (Euler et al., 2020; Sela-Adler et al., 2017). Conversely the presence of ammonium may inhibit CH_4 oxidation thereby increasing CH_4 evasion (Dunfield and Knowles, 1995; Bosse et al., 1993). In fully mixed estuaries CH_4 concentrations are non-linearly inversely correlated with salinity, with the highest CH_4 concentrations observed at low salinity and associated with the turbidity maximum (Upstill-Goddard et al., 2000; Upstill-Goddard and Barnes, 2016). In salt-wedge estuaries CH_4 concentrations are considerably more variable (Middelburg et al., 2002). Distinct zones of elevated GHG concentrations occur at the tip of salt wedge and in the anaerobic bottom waters, suggesting acetoclastic methane production in fresh surface waters and hydrogenotrophic methane production occurring in the saline bottom waters or sediments (Tait et al., 2017). Decreased CH_4 concentrations have been observed in higher water flows and are linked to dilution under the assumption that the net CH_4 production does not change significantly (Bange et al., 2019). Conversely dissolved oxygen (DO) was the dominant factor influencing CH_4 fluxes, with DO and dissolved organic carbon (DOC) explaining 60% of the variance, although estuarine CH_4 emission patterns need improved understanding (Zheng et al., 2022).

Global emissions of nitrous oxide (N_2O) from estuaries were estimated as 0.06 to 0.40 Tg N_2O yr^{-1} with large spatial and temporal heterogeneity (Maavara et al., 2019; Zheng et al., 2022). Anthropogenic nitrogen perturbations to rivers can result in a two to four-fold increase in N_2O emissions from inland waters (Maavara et al., 2019). N_2O emissions are dependent on the amount of nitrogen entering the estuary primarily from run-off and wastewater (Robinson et al., 1998; de Angelis and Gordon, 1985; Dong et al., 2005; Nguyen et al., 2022; Seitzinger and Kroeze, 1998). The fraction of nitrogen converted to N_2O determines the climate impact of nitrogen in rivers and estuaries, however the production and emission of N_2O from estuarine systems is currently poorly constrained. The balance between nitrification and denitrification, is dependent on residence time, with nitrification dominating during short residence times and denitrification dominating at longer residence times (Zarnetske et al., 2011), and oxygen levels with low oxygen levels supporting denitrification, (Tang et al., 2022; Li et al., 2022; Brase et al., 2017; Rosamond et al., 2012). Nitrification can occur in both sediments and the water column, with water column nitrification dominating particularly when turbidity maximums occur (Beaulieu et al., 2010; Barnes and Upstill-Goddard, 2011; Murray et al., 2015). N_2O production from denitrification in sediments has been measured as a linear function of the nitrate concentration in the overlying water (Revsbech et al., 2005). However spatial and temporal heterogeneity can be significant, with inverse correlations between N_2O and dissolved oxygen acting independently of the dissolved nitrate concentrations (Beaulieu et al., 2010; Rosamond et al., 2012). Denitrification can be stimulated by frequent switches between oxic and anoxic conditions with microbes able to respond rapidly to changing environmental conditions (Marchant et al., 2017). Concentrations of N_2O can vary on a diurnal basis and are highest at night when DO is generally lowest (Rosamond et al., 2012). Mean N_2O concentrations have been shown to increase with rainfall, suggesting enhanced N_2O emissions with runoff and /or higher water tables favouring denitrification (Bange et al., 2019).

Despite the limited surface area of estuaries compared to the open ocean, estuaries undertake considerable biogeochemical cycling and are active filters of dissolved and suspended material entering the ocean from the land (Dürr et al., 2011), processes likely to continue into estuarine plumes, coastal zones and the continental shelf. High nutrient levels in urban estuaries can cause hypoxia, eutrophication and enhanced phytoplankton abundance, leading to increases in GHG concentrations (Nguyen et al., 2022; Cotovicz et al., 2021). Environmental factors, including pollutant and wastewater outflows can impact microbial community structure and diversity (Feng et al., 2022; Zhou et al., 2022). The most sensitive estuarine systems to anthropogenic impacts are likely to be stratified systems due to their limited mixing rendering them prone to hypoxia (Park et al., 2007). This can have a detrimental impact on estuarine biodiversity and severe hypoxic events can result in fish and invertebrate mortality (Breitburg, 2002; Lucchesi et al., 2022; Larsen et al., 2019). Hypoxia can impact biogeochemical processes such as sediment phosphate efflux (Foster and Fulweiler, 2019) and increase GHG emissions (Brown et al., 2023d). GHG concentration in stratified estuaries have been found to be more variable and less well explained compared to fully mixed estuaries (Middelburg et al., 2002) with a paucity of estuarine GHG data, (Zheng et al., 2022; Rosentreter et al., 2021). All of which supports the need to understand anthropogenic interactions within these sensitive systems.

Addressing this gap in understanding is needed to inform improved estimates and remediation approaches with multiple benefits including GHG management. This study addressed the following key questions: (1) what hydro-chemical conditions (tidal regime, level of stratification, salinity, temperature, river flow, mixing, nutrients and sedimentation) drive estuarine N₂O and CH₄ dynamics and (2) how do short- and long-term hydro-chemical changes impact N₂O and CH₄ variability.

6.2 Material and methods

6.2.1 Study Area

The Clyde estuary on the west coast of Scotland (Fig. 6.1), is a temperate, highly urban, mesotidal salt wedge estuary, stratified throughout the 20km of the inner estuary, with a mean spring tidal range of 3.0 m and mean neap tidal range of 1.9 m (Karunaratna, 2011). The inner estuary is long and narrow with friction and turbulence reduced by dredging (over the last 200-years) and the presence of seawalls (Jones and Ahmed, 2000). The rivers flowing into the urban Clyde estuary, (including the Rivers Clyde, Kelvin, White Cart, Black Cart, Gryffe and Leven) have a catchment surface area of 3,200 km² (Clyde River Foundation, 2020). The average combined freshwater flow into the estuary was estimated as 110 m³s⁻¹, with the 50-year extreme flow estimated as 1438 m³s⁻¹ (Bekic et al., 2005). These inflowing rivers can contain high sediment concentrations during high flow events, but the tidal asymmetry (ebb tide velocity > flood tide velocity) acts to move riverine and estuarine sediments downstream preventing a turbidity maximum. As such the Clyde estuary is not an area of active modern sedimentation, with only a thin layer of recent contaminated sediment on top of an earlier layer of glacial and post-glacial origin (Jones et al., 2019). The Clyde estuary is highly contaminated, a legacy from its industrial past and the increasing urban population of the City of Glasgow, and is still at risk from nutrient enhancement and diffuse pollution (Scotland's Environment, 2014). While water quality has improved, estuarine sediments still contain high levels of contamination including heavy metals (Hursthouse et al., 2001), with the highest elemental concentrations of Cu, Pb, Co, Cr, Ni, Sb and Zn occurring in the urban estuary, at concentrations significantly above that of the urban river (Jones et al., 2019; Rodgers et al., 2020; Balls et al., 1997). The Clyde estuary exhibits anomalously high levels of polyaromatic hydrocarbons (PAHs) and polychlorinated biphenyls (PCBs) (Edgar et al., 2003; Edgar et al., 2006; Vane et al., 2007).

6.2.2 Site description and data collection

Estuarine measurements were made using three approaches; (1) longitudinally by power boat (Clyde estuary transects (CET)), (2) from a single location through tidal cycles (Clyde estuary pontoon (CEP)) and (3) across the river estuary transition (CRE). Samples for CET and CEP were collected at the surface and 0.5m above the bed and CRE samples only at the surface.

For the longitudinal surveys, ten measurement locations were selected (Fig. 6.1 and Table 6.1) between the tidal weir, which separates the fresh and salt-water habitats, and the location where the estuary widens as it joins the Irish Sea. Sample locations were selected to provide an understanding of how salinity, river flow and stratification impacted GHG generation. Spacing between sampling locations increased seawards as the estuary homogenised. Samples were collected on eight occasions between September 2021 and May 2022 (Table

6.2) starting at high tide and sampling seawards on the ebb tide. Water depths at the sampling locations typically ranged from 5 - 6 m at the head of the estuary to 10 - 12 m in the outer estuary (Brown et al., 2023c).

The CEP surveys were made from the pontoon adjacent CET L6, 7.9 km from the tidal weir and located on the south bank of the estuary. The water depth at the pontoon varied between 3m and 7m. Samples were collected on seven occasions between August 2020 and May 2022 (Table 6.3) (Brown and Pickard, 2023). Monthly surveys of the river and estuary transition (CRE) were made between January 2020 and December 2021. This involved consecutive surface measurements at three locations in the river and two in the estuary (a pontoon between CET L3 and L4 and the pontoon as for CEP and CET L6) (Brown et al., 2023b), (Fig.6.1 and Table 6.4). Temporal sampling covered a range of discharge conditions, including baseflow and > 95 % exceedance (Fig. 6.2). Figure 1 includes all survey location, together with the locations of urban wastewater treatment plants (UWWTP) discharging to the estuary.

Table 6.3 - Sampling locations for the Clyde estuary transects

No.	Location code	Latitude (N) (WGS84)	Longitude (W) (WGS84)	Distance from tidal weir (km) ⁽¹⁾	Distance between Locations (km)	Location Information
1	L1	55.853931°	-4.251681°	0.43	0.43	Most upstream point
2	L2	55.856082°	-4.273576°	1.85	1.42	Adjacent M8 motorway
3	L3	55.861379°	-4.297750°	3.51	1.66	Restricted point in estuary
4	L4	55.867974°	-4.318569°	5.00	1.49	Adjacent the SEPA Buoy
5	L5	55.868900°	-4.339734°	6.35	1.35	Adjacent Shieldhall UWWTP
6	L6	55.876932°	-4.360132°	7.88	1.53	Adjacent Breahead pontoon
7	L7	55.888767°	-4.390125°	10.20	2.14	Adjacent scrap metal working
8	L8	55.908154°	-4.444381°	14.35	4.14	Adjacent Dalmuir UWWTP
9	L9	55.929253°	-4.487592°	18.00	3.65	Adjacent Bowling old harbour
10	L10	55.932344°	-4.575588°	23.50	5.50	Offshore from River Leven

Notes

1. Distance is from the tidal weir to the measurements point, with distance between locations increasing seawards
2. The River Kelvin enters the estuary between L3 and L4, the Rivers White Cart and Black Cart enter the estuary between L7 and L8 and the River Leven enters the estuary adjacent L10

Table 6.2 - Sampling dates for the Clyde estuary transects

No.	Survey code ⁽¹⁾	Date	Survey start time (GMT)	Surface Water Temperature ⁽²⁾ (°C)	Time of High tide (GMT)	Tidal range (m)	River Flow at high tide (m ³ /s)	Comments ⁽⁴⁾
1	CET1	21-Sep-21	13:00	16.4 - 15.6	13:10	3.86	10.8	All locations
2	CET2	15-Oct-21	08:50	11.7 - 12.1	08:10	1.73	16.0	All locations
3	CET3	21-Oct-21	12:40	11.2 - 11.5	13:20	3.82	29.0	Locations 1 to 9
4	CET4	22-Nov-21	12:51	7.3 - 8.7	14:20	3.45	26.6	All locations
5	CET5	29-Mar-22	10:50	10.4 - 9.8	11:00	3.29	17.4	All locations
6	CET6	13-Apr-22	10:20	9.2 - 10.4	10:30	2.29	22.3	Locations 1 to 8
7	CET7	25-May-22	09:30	14.7 - 15.4	08:50	3.09	13.1	Locations 1 to 4
8	CET8	31-May-22	12:40	15.4 - 14.5	13:30	3.45	10.5	Locations 1 to 8

Notes

1. The water temperature is presented for L1 and then for L10 for the surface data only
2. The river flow is for SEPA's Daldowie gauge for the time of the survey start, (UKCEH, 2020b)
3. The tidal range is taken from harmonic analysis of the tidal data and Renfrew tide gauge which is located at 55.885812°N, 4.3828324 West (Scottish Environment Protection Agency, 2020b). This is closest to location L7.
4. The time of high tide was used as a guide for the start of the survey.
5. In surveys CET3,6,7,and 8 some locations could not be reached due to rough weather.

Table 6.3 - Sampling dates for the Clyde estuary tidal cycle measurements

No.	Survey code ⁽¹⁾	Date	Survey time (GMT)	Average Surface Temperature ⁽²⁾ (°C)	Time of High tide (GMT)	Tidal range (m)	River Flow - mid survey (m ³ /s)	Comments
1	CEP1	13-Aug-20	06:00 - 18:30	18.1	06:30	2.23	33.8	Surface, bed
2	CEP2	25-Feb-21	06:15 - 16:00	7.3	11:50	2.94	106.6	Surface, bed
3	CEP3	28-Mar-21	06:15 - 15:15	8.2	12:50	4.40	56.8	Surface, bed
4	CEP4	29-Jun-21	06:00 - 16:30	19.0	16:10	4.35	8.1	Surface, bed
5	CEP5	24-Aug-21	05:30 - 15:30	17.9	14:10	4.06	10.0	Surface, bed
6	CEP6	15-Mar-22	08:00 - 17:00	7.5	11:20	2.63	99.8	Surface, bed & evasion
7	CEP7	08-May-22	08:00 - 17:00	14.4	17:20	2.00	14.3	Surface, bed & evasion

Notes

1. The sea water temperature is presented as the average surface temperature measured across the survey
2. The river flow is for SEPA's Daldowie gauge for the middle of the survey (UKCEH, 2020b)
3. The tidal range is taken from a harmonic analysis of the tidal data and Renfrew tide gauge which is located at 55.875908°N, 4.360176°W (Scottish Environment Protection Agency, 2020b), 3.4km seawards of the survey location.
4. The tidal range is for the tide most encompassed in the survey. There is considerable asymmetry across the semi-diurnal tides.
5. The estuary is periodically dredged, dredging activity occurred in the summer of 2020, survey CEP1 was impacted by this activity

Table 6.4 - Sampling locations for the Clyde river estuary transition

No.	Location code ⁽¹⁾	Latitude (N) (WGS84)	Longitude (W) (WGS84)	Distance from Tidal weir minus is upstream (km)	Number of surveys	Comments
1	CRE1	55.82994°	-4.121975°	-13.8	20	Surface only
2	CRE2	55.82334°	-4.171169°	-10.3	20	Surface only
3	CRE3	55.85004°	-4.240297°	-0.40	20	Surface only
4	CRE4	55.86416°	-4.308975°	4.28	20	Surface only
5	CRE5	55.87601°	-4.360505°	7.88	20	Surface only

Notes

1. Distance is from the tidal weir increasing seawards, with negative values in the river upstream of the tidal weir
2. Data was measured monthly between Feb 2020 to Dec 2021, with no data measured in the period Apr to Jun 2020.

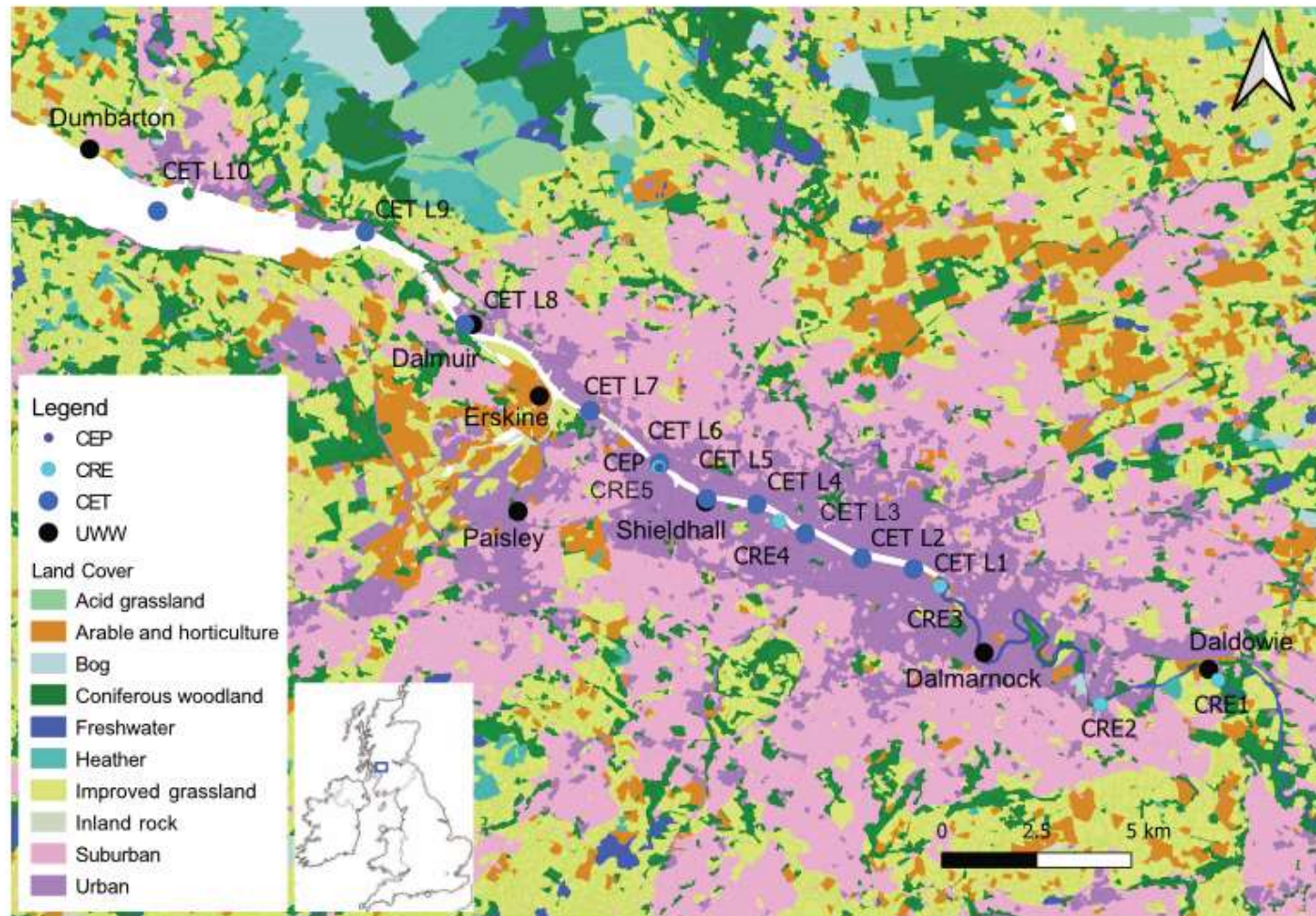


Figure 6.1 - Sampling locations and land cover for the Clyde estuary.

Land cover is from UK Centre for Ecology & Hydrology (UKCEH, 2020a). Locations are for the Clyde estuary transects (CET), Clyde estuary pontoon (CEP) and Clyde estuary river transition (CRE) surveys. The R. Kelvin enters the estuary between CET L3 and L4, the R. White Cart and Black Cart between CET L7 and L8 and the R. Leven adjacent CET L10. The estuary is impacted by urban wastewater including: Shieldhall near CET L5, Paisley and Erskine via the R. Cart seawards of CET L7, Dalmuir near CET L8 and Dumbarton West seawards of CET L10 (Marine Scotland, 2022).

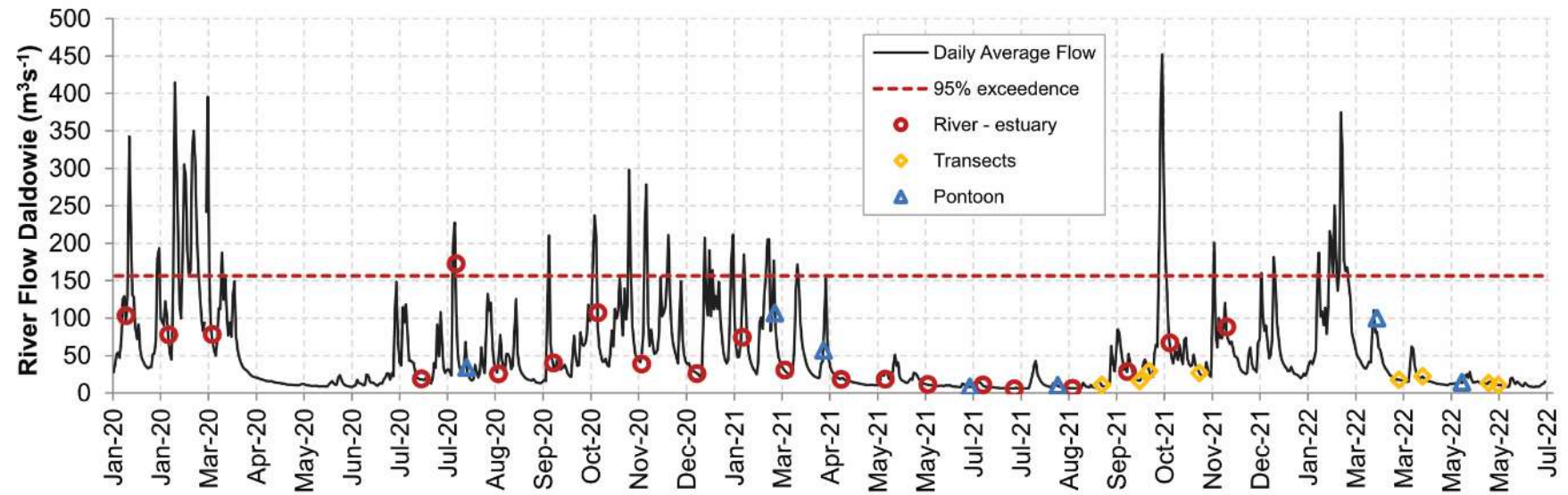


Figure 6.2 - River Clyde flow for survey period -

River flow data is daily average flow for Daldowie on the River Clyde (UKCEH, 2020b). CET surveys are denoted by yellow diamonds, CEP surveys by blue triangles and CRE surveys by red circles. Note the extended period of low river flow from Apr to Sep 2021 which resulted in a semi-permanent saline intrusion in the estuary and increased estuary flushing times.

6.2.3 Field sampling and laboratory measurements

Water samples were collected at the surface using a 10 L bucket and 0.5m above the bed using a 5 L water depth sampler. Dissolved gas samples were collected in triplicate at each location using the headspace method, prior to the collected water being disturbed by other measurements, together with ambient air samples (Billett and Moore, 2008; Kling et al., 1992). Conductivity (EC), water temperature (T_w), dissolved oxygen concentration (DO) and pH were measured with a HQ40d Multi portable meter (Hach) with a Intellical CDC401 Laboratory 4-Poles Graphite Conductivity Cell, a Intellical LDO101 Laboratory Luminescent / Optical Dissolved Oxygen and a PHC10101 Combined pH electrode. A two-litre water sample was retained for later analysis which was kept in a cool-box until returned to the laboratory for processing. Turbidity (T_{UR}) was measured in the water samples using a Thermo Scientific, Orion AQUAfast AQ3010 Turbidity Meter.

Headspace samples for CO_2 , CH_4 and N_2O were analysed using an Agilent 7890B gas chromatograph (GC) and 7697A headspace auto-sampler (Agilent, Santa Clara, California), calibrated against a series of mixed air standards of: 1.12 to 98.2 ppm for CH_4 ; 202 to 5253 ppm for CO_2 ; and 0.208 to 1.04 ppm for N_2O . Gas partial pressures were determined as in (Brown et al., 2023d). Water samples were filtered within 12-hrs of collection through Whatman GF/F 0.7 μm filters. Filtrate was analysed for: total dissolved nitrogen (TDN), total dissolved carbon (TDC) and dissolved organic carbon (DOC), UV-Vis absorbance, nitrite-N (NO_2^-), nitrate-N (NO_3^-) and ammonia-N (NH_4^+). Analysis for TDN, TDC and DOC were undertaken using a Shimadzu TOC-L series Total Organic Carbon Analyser with all samples run within 36-hrs of collection. Absorbance at 254 nm, indicative of aromaticity, was measured using a Perkin Elmer LAMBDA® 365 UV-Vis Spectrophotometer to evaluate the Specific Ultraviolet Absorbance (SUVA). NO_2^- , NO_3^- , and NH_4^+ were measured using a SEAL AQ2 analyser. One possible interference with the determination of ammonia-N by this technique was that dissolved calcium and magnesium may form a precipitate under alkaline conditions causing a positive bias at high salinity. Total phosphorous (TP) was measured from unfiltered digested samples using a SEAL AQ2 analyser. Full details of the data collection and laboratory measurement methodologies for the various survey approaches are detailed separately (Brown et al., 2023c, 2023b; Brown and Pickard, 2023)

6.2.4 Data sources and processing

Discharge data, measured at Daldowie on the River Clyde, 13.8km upstream of the tidal weir was applied (Scottish Environment Protection Agency, 2020; UK Centre of Ecology & Hydrology (UKCEH), 2020). River flow over the measurement period ranged from 4.8 m^3s^{-1} to peak at 522 m^3s^{-1} (daily average of 450 m^3s^{-1}) with the measurement days capturing a range of 5.6 - 170 m^3s^{-1} . SEPA support an Inner Clyde Estuary (ICE) buoy located within the inner Clyde estuary adjacent to the CET L4 sampling location. Data from this buoy were not yet available coincident with these estuary measurements but data from the period 2015 to 2019 were used to provide insights into estuarine processes including river, tidal and seasonal impacts on estuary temperature, oxygen, salinity and turbidity at the surface and near-bed (Scottish Environment Protection Agency, 2020a).

The mechanisms by which an estuary is flushed are related to several factors including, tidal flushing, river discharge and density induced estuarine circulation. Density induced circulation

is significant in fjord-type system with a sill restricting seawater ingress, but unlikely to be important in the Clyde and has been assumed to be negligible. Estuary residence time was defined as the average time an initially existing water parcel resides in the estuary before being flushed out and estuary flushing time was defined as the time required to replace the existing freshwater in the estuary at a rate equal to the river discharge. If all processes were linear the residence time, would be half of the flushing time (Wang et al., 2004). As the Clyde estuary is stratified with river flow dominating, the flushing time was estimated using the fraction of freshwater method (Eq. 1) (Wang et al., 2004). The flushing time of an estuary (T_f) can be estimated by using the low tide estuary volume (V) (the average low tide depth multiplied by the estuary area), the equivalent estuarine outflow (Q_o), the river discharge (R), the sea water salinity (S_o) and the volume-weighted average salinity of the outgoing flow during ebb tide or the upper layer salinity in case there is a two-layered system (S_e).

$$T_f = \frac{V}{Q_o} = \frac{V}{R} * \left(\frac{S_o - S_e}{S_o} \right) \quad (\text{Eq. 1})$$

Flushing time calculations were made using the SEPA ICE buoy data at CET L4, for the different locations measured during the CET survey and for all data from the three surveys measured at the common location of the Breahead pontoon (CET L6, CEP and CRE 5). To ensure all data points were independent, only one (mid ebb-tide) measurement was selected from each CEP survey. Data from the CRE survey were from a range of tidal conditions.

Nutrients (TP and TDN) enter the inner estuary from the rivers, predominantly the River Clyde and directly from UWWTP. The [TP] and [TDN] entering the estuary from riverine diffuse and point sources was calculated using the relationships derived for the Clyde (Brown et al., 2023d). To estimate nutrients entering from the UWWTP adjacent CET L5 it was assumed that: the UWWTP treats wastewater for 600,000ppe (per person equivalent) (SEPA, 2017) and the TP and TDN inputs were TP = 2 g pppd (per person per day) and TN =13 g pppd (Agthe and Pendergast, 1983). This nutrient input from the River Clyde and the UWWTP adjacent L5 were estimated assuming these inflows were mixed into the top 5m of estuary water and the residence time is half the fresh water flushing time (T_{FW}).

The sea-to-air CH_4 and N_2O emissions as a flux (F) ($\text{mol m}^{-2} \text{d}^{-1}$), can be estimated from, the gas specific transfer velocity, k_w (cm h^{-1}), the gas specific solubility L ($\text{mol cm}^{-3} \text{atm}^{-1}$) using (Wiesenburg and Guinasso, 1979) for CH_4 and (Weiss and Price, 1980) for N_2O and the gas specific water-to-air partial pressure difference Δp (Wanninkhof, 2014) (Eq. 2).

$$F = k_w \cdot L \cdot \Delta p \quad (\text{Eq. 2})$$

The gas specific transfer velocity (k_w) can be estimated from the average monthly wind speed (U) (ms^{-1}) and the gas specific Schmidt number (Sc) (Wanninkhof, 2014) (Eq. 3).

$$k_w = 0.251 \cdot U^2 \cdot \left(\frac{Sc}{660} \right)^{-0.5} \quad (\text{Eq. 3})$$

In addition to wind speed, current speed and turbulence, particularly that during overturning and mixing of the stratified layers would increase gas exchange. However, the requirement for measured current speeds precludes the use of this term in this analysis, making the estimate of flux likely a minimum flux. Noting the inherent uncertainties we use Eq. 2 to determine flux, an approach that has been widely applied (Upstill-Goddard and Barnes, 2016).

Average monthly wind speeds were obtained from (Met Office, 2021). The total estuary emissions were calculated by the sum of total emissions for an individual section within the estuary. This resulted in one section for each of the 10 sampling sites from CET surveys, starting and at the tidal weir and ending at longitude -4.667° , with each section divided midway between the two measurement points. This accounted for 26.58 km^2 of the Clyde estuary and not the whole estuary area of 54.85 km^2 (Nedwell et al., 2002), as measurements did not go far enough west to be representative.

Spatial analysis of all measured parameters was undertaken using Quantum Geographic Information System (QGIS) version 3.22. Regression analysis to determine relationships between GHGs and water physiochemical properties was undertaken using Statgraphics version 5. Estuary residence times were calculated using MatLab R2014a. Values of $p < 0.05$ were considered statistically significant for correlation and difference tests.

6.3 Results

6.3.1 Hydrological drivers on estuary flushing

High-resolution (15-min) data from the ICE buoy at CET L4 allowed comprehensive flushing times to be calculated for the period 2015 to 2019. The area of the estuary from the tidal weir to the ICE buoy (adjacent CET L4) is 0.65 km^2 and the maximum flushing time was 12 days at the lowest flow (Fig. 6.3 A). Flushing time decreased exponentially as river flow increased. Tidal range had a larger impact on flushing times during low river flow compared to high river flow (Fig. 6.3 A). Flushing times increased with the area of the estuary, for example at CET L10, with an area of 8.25 km^2 flushing time reached 65 days (Fig. 6.3 B).

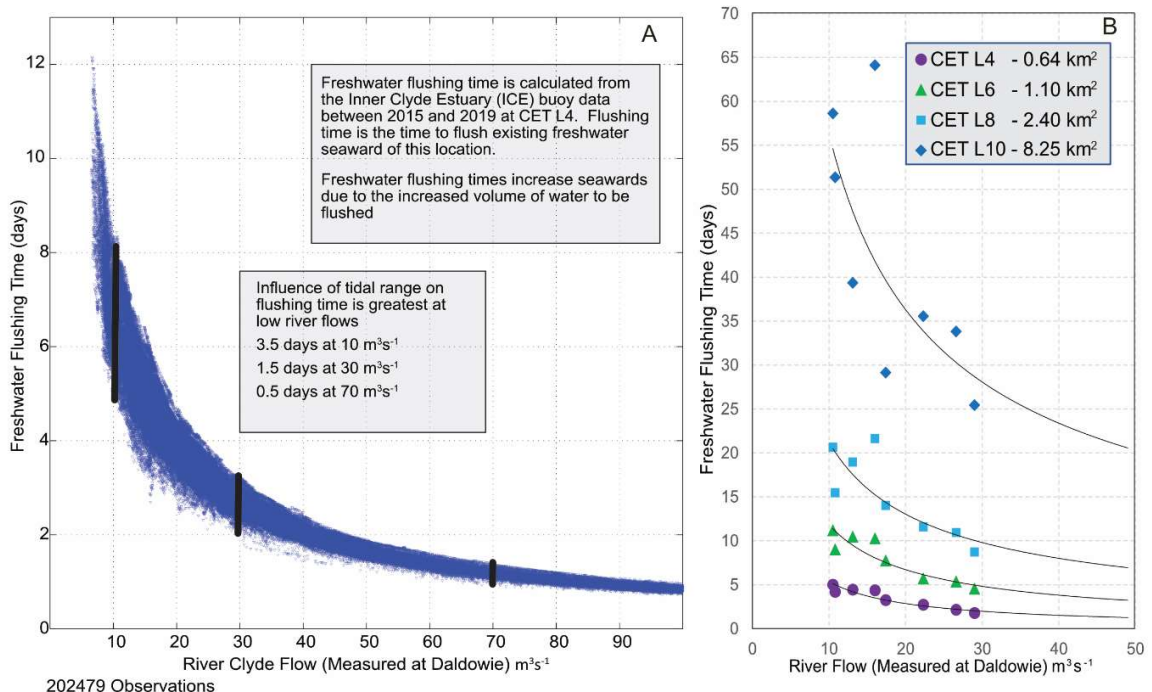


Figure 6.3 - Clyde estuary freshwater flushing time (T_f) - Panel A - T_f for location CET L4 derived from the Inner Clyde Estuary (ICE) Buoy (Scottish Environment Protection Agency, 2020a). T_f ranged from 1 and 12 days for area inshore of L4 (0.65 km^2) (2015 to 2019). River flow had the largest influences on T_f with tide having a larger impact in low river flow. (River flows of $10 \text{ m}^3\text{s}^{-1}$, T_f of 5 - 8.5 days & river flows of $70 \text{ m}^3\text{s}^{-1}$ T_f of 1.0 - 1.5 days). Panel B is T_f for locations CET L4, L6, L8 and L10 from CET survey.

6.3.2 The impact of estuary flushing on nutrients and greenhouse gases

Estuary flushing time was significantly positively correlated with surface water quality data for $[\text{N}_2\text{O}]$, T_w , $[\text{TP}]$, $[\text{TDN}]$, $[\text{DIC}]$, and EC and significantly negatively correlated with surface water SUVA_{254} and DO, with no significant correlation with $[\text{CH}_4]$ and $[\text{DOC}]$ ($n=35$). Estuary flushing time was significantly positively correlated with near-bed data for T_w , $[\text{DIC}]$ and SUVA_{254} ($n=18$) (Fig. 6.4). The lack of a correlation with near-bed nutrient data suggests there is limited penetration of nutrients from the riverine surface layer into the lower layer due to limited mixing. The lack of correlation with near-bed EC suggests the lower layer water properties are more impacted by tidal influences, rather than freshwater flushing (Fig. 6.4). In the lower saline layer, the N:P ratio did not change significantly with DO, T_w , TUR, or $[\text{DOC}]$, but in the surface layer the N:P ratio reduced as DO and DOC were depleted, suggesting significant N and P processing is occurring in the upper layer. Estimates of estuarine inputs of P and N from the river and UWWTPs suggested that for a T_f of 2 days, 45% of the TP and 63% of the TDN were removed and for a T_f of 10 days that 58% of the TP and 84% of the TDN were removed, indicating considerable nutrient processing within the estuary, especially during low river flow, with TDN the limiting nutrient.

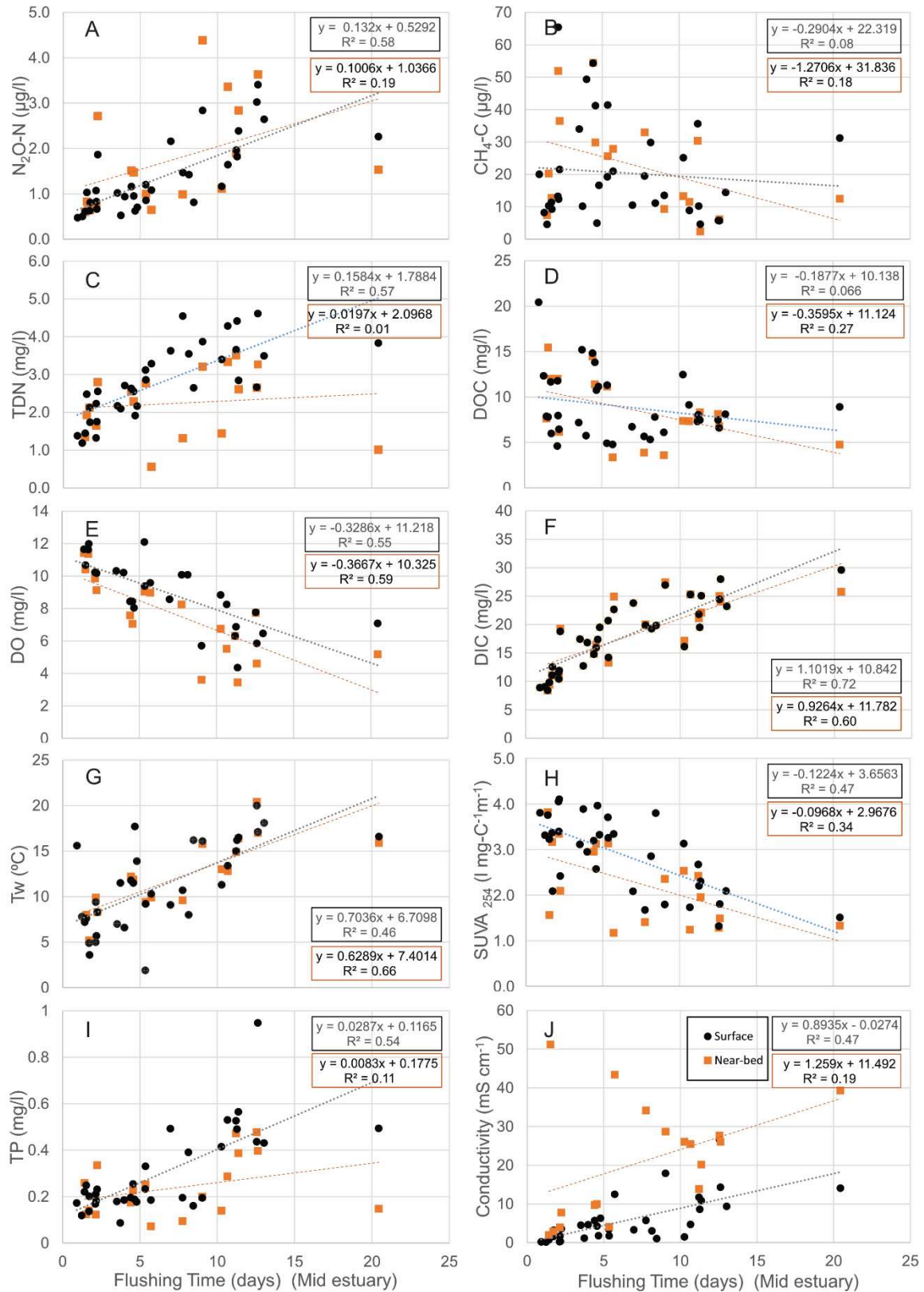


Figure 6.4 - Impact of freshwater flushing time (T_f) on estuary physiochemical properties
 Data for location CET L6 - The surface water is indicated by black circles and the near-bed water by brown squares. T_f was significantly positively correlated with surface N_2O , T_w , TP, TDN, DIC and EC and negatively correlated with DO and $SUVA_{254}$, with no significant correlation with CH_4 and DOC. Near-bed correlations are only significant for DO, DIC, T_w , $SUVA_{254}$.

6.3.3 Greenhouse gases across the riverine to estuary interface

The tidal weir in the Clyde enabled clear river and estuary regions to be distinguished, particularly during low river flows. The transition to the estuary had a negligible impact on [DOC] but the $SUVA_{254}$ indicated an increased anthropogenic signature. EC, [TP] and [TDN] increased in the estuary surface waters and DO% was reduced (Fig. 6.5). Some nutrients entered the estuary from the river but predominantly they entered from the UWWTP upstream of CRE5. N_2O concentrations were highest in both the river and the estuary between April and September 2021, associated with low river flow conditions and high [TDN]. The $[N_2O]$ further increased between the river and the estuary. The correlations between $[N_2O]$ and [TDN] including all data across the river and estuary waters was significant ($R^2= 0.51$ p-value < 0.001), suggesting N_2O is generated in the river and estuary surface water by similar mechanisms.

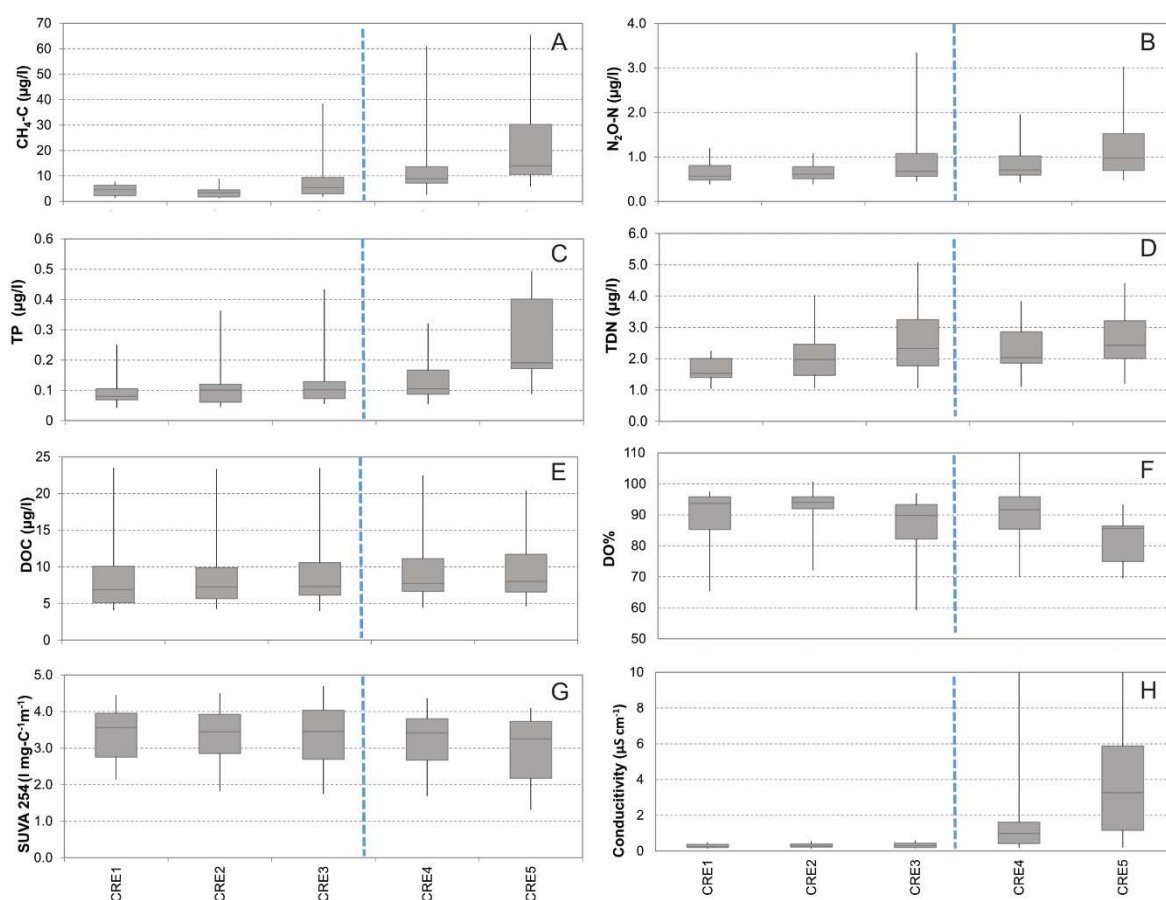


Figure 6.5 - Comparison of river and estuary transition -

Panels A to H show variation in $[CH_4]$, $[N_2O]$, [TP], [TDN], [DOC], DO%, $SUVA_{254}$ and EC across the river estuary transition, defined by the tidal weir (indicated by the blue dashed line). The $[CH_4]$ increased in the estuary, but the highest $[CH_4]$ in the river occurred in summer under low river flow conditions and in the estuary in winter during high river flows. The highest $[N_2O]$ in both the river and estuary occurred in summer under low river flow conditions.

Conversely [CH₄] increased from the river to the estuary, but while the conditions that produced the highest [CH₄] in the river occurred between April and September 2021, associated with low river flow conditions, these conditions did not produce high [CH₄] in the estuary. The highest [CH₄] in the estuary occurred after high river flow events often during winter. Under these conditions additional CH₄ must be generated within the estuary surface waters and not transferred from the river. The highest correlation with [CH₄] in the river environment is with [TP], (R²= 0.76 p-value < 0.001) but this correlation does not persist after the transition to the estuary (R²= 0.009 p-value = 0.69). Differences in water physicochemical properties as per Figure 6.5 (CH₄-C, N₂O-N, TP, TN, DOC, DO% SUVA₂₅₄ and EC) were statistically significant (T-test) between the river and estuary for all parameters. The biggest statistically significant point-to-point difference was between CRE4 and CRE5, which was significant for all variable except DOC. However, the point-to-point difference between CRE3 and CRE4 was not significant, suggesting freshwater dominance was retained at the surface.

6.3.4 Drivers of estuarine nitrous oxide

Both surface and near-bed [N₂O-N] were positively exponentially correlated with T_w and [TDN] and negatively exponentially correlated with [DO] (Fig. 6.6 B, C and A). For the near-bed data only, [N₂O-N] and pH were negatively exponentially correlated (Fig. 6.6 D). For the near-bed, the exponential correlation between [N₂O-N] and [DO] could account for 95% of the variability (R² = 0.95, p-value >0.0001) with none of the residual variability accounted for by T_w and TDN. In the Clyde estuary the DO% is inversely correlated with both T_w (R² = 0.57 p-value < 0.001) and the percentage of reduced nitrogen (NH₄⁺) (R² = 0.47 p-value < 0.001), making it difficult to distinguish individual effects (see supplementary data Fig. 6.A.1 and 2).

The [N₂O-N] was positively linearly correlated with [NH₄⁺] in both surface and near-bed layers, but the correlation with [NO₃⁻] was not significant (Fig. 6.6 E and F). However, if data that were riverine (EC < 500 μS cm⁻¹) were removed from the near-bed layer, the near-bed [N₂O-N] had a significant positive correlation with NO₃⁻ (R² = 0.35, p-value < 0.01), indicating different nitrogen processing in the surface and near-bed layers when the estuary was stratified (Fig. 6.6 F). Relationship between [N₂O-N] and EC, [DOC], [DIC], T_{UR} and other ions were not significant. These distinct differences between the surface and near-bed layers resulted in different linear regression models for each layer. For the surface (S) (R² = 0.82, p-value <0.0001) (Eq. 4) and for the lower layer (B) (R² = 0.93, p-value <0.0001) (Eq. 5), where N₂O is in μg l⁻¹, TOC, TP, TDN are in mg l⁻¹, DO in % saturation and NH₄⁺ in μmol l⁻¹.

For the surface

$$[N_2O - N](S) = 3.53 + 0.5539 \cdot NH_4 - 0.0267 \cdot DO\% - 0.0687 \cdot TOC + 0.531 \cdot TP \quad (\text{Eq. 4})$$

For the near-bed

$$[N_2O - N](B) = -14.27 + 2.60 \cdot pH - 0.0728 \cdot DO\% + 0.463 \cdot TDN \quad (\text{Eq. 5})$$

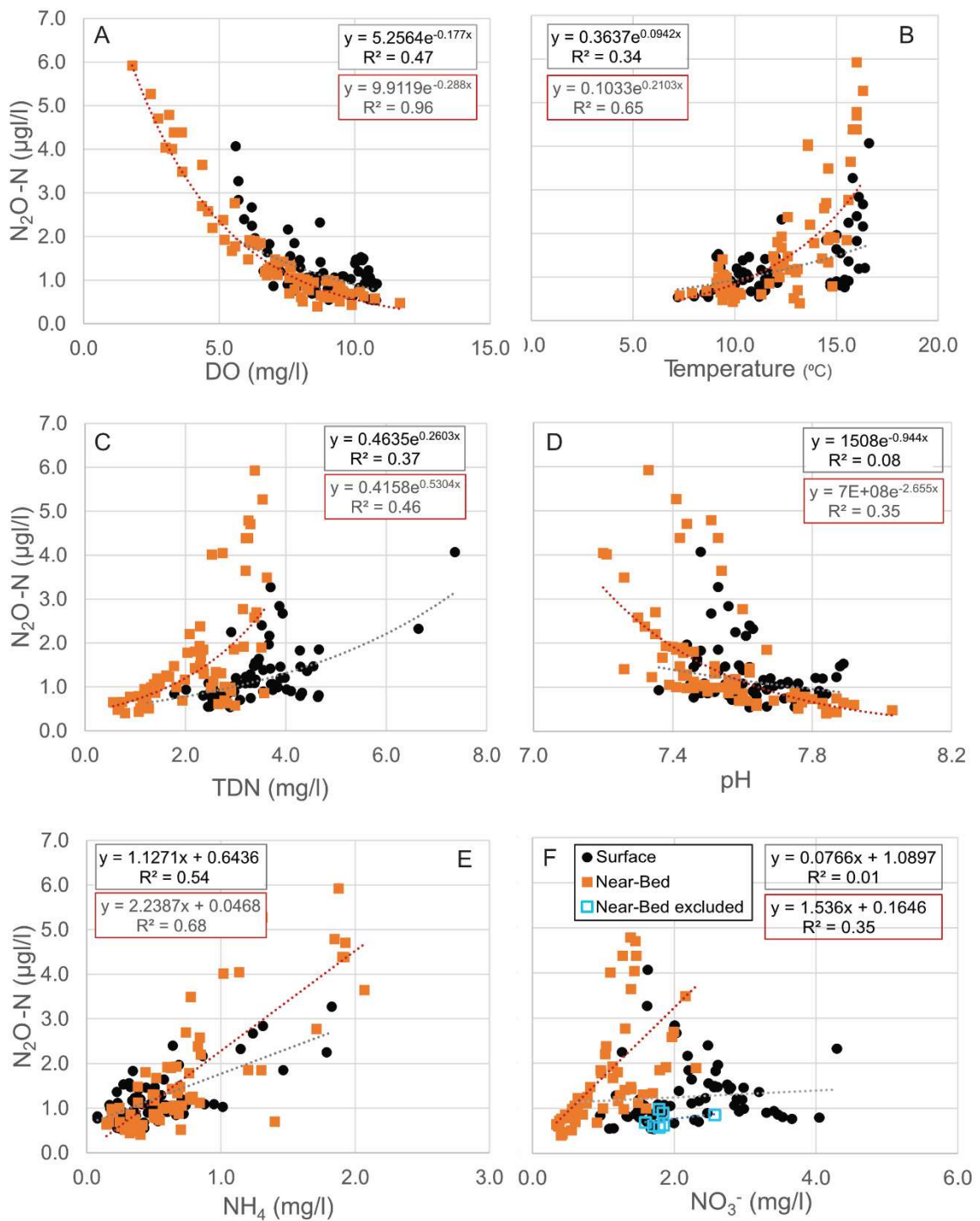


Figure 6.6 - Relationship between $[N_2O-N]$ and water physiochemical properties

Water properties for surface (black circles) and near-bed (brown squares), from CET survey. In plot F the near-bed layer points that are fully riverine, due to a limited saline intrusion, are indicated in open light blue squares and have been removed from the regression resulting in a significant correlation between N_2O-N and NO_3^- ($R^2 = 0.35$).

6.3.5 Estuarine methane generation

The $[CH_4]$ were typically higher in the near-bed layer compared to the surface, especially in the upper estuary (CET L1 to L6). In the near-bed layer there were no significant correlations between $[CH_4]$ with any of the measured parameters, with $[CH_4]$ in the upper estuary highly variable. In the lower estuary (CET L7 to L10) $[CH_4]$ decayed exponentially with distance seawards. The EC was also highly variable in the upper estuary near-bed layer but exceeded 10 mS cm^{-1} throughout the lower estuary (see supplementary data Figure 6.A.1 and 2). The surface layer $[CH_4]$ exhibited weak correlations between T_{UR} , $[DOC]$ and EC (Fig. 6.7 C, A and B). A linear regression equation considering these variables explained 50% of the measured surface-layer (S) variability (Eq. 6), ($R^2 = 0.50$, p-value < 0.001), where $[CH_4-C]$ is in $\mu\text{g l}^{-1}$, T_{UR} in NTU and EC in $\mu\text{S cm}^{-1}$. Indicating that surface $[CH_4]$ is positively associated with suspended sediments and negatively associated with increasing EC. There were two sets of outliers in this relationship. Firstly, surface measurements where the water was fully riverine (during high river flow at CET L1) and had lower $[CH_4]$ than predicted, and secondly measurements where the estuary had become mixed (at CET L10 due to higher tidal mixing at this location).

For the surface

$$[CH_4 - C](S) = 4.415 + 4.19 * T_{UR} - 0.0006589 * EC \quad (\text{Eq. 6})$$

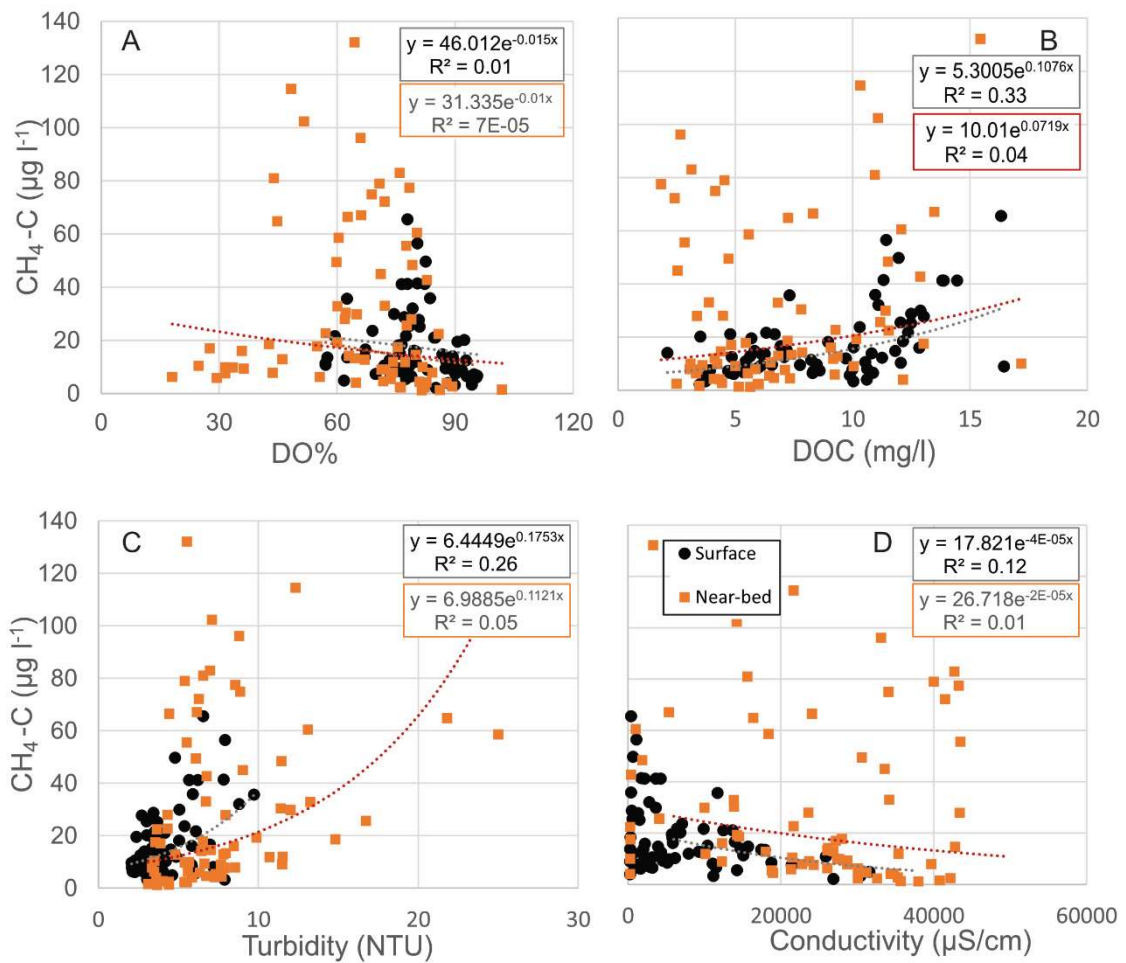


Figure 6.7 - Relationship between $[\text{CH}_4\text{-C}]$ and water physicochemical properties

Water properties for surface (black circles) and near-bed (brown squares), from CET survey. $[\text{CH}_4\text{-C}]$ behave differently between the surface fresh layer and lower saline layer and show a high level of variability.

The near-bed layer $[\text{CH}_4]$ were highly variable with no clear drivers and distinct differences between surveys. Continuous low river flows between April and September 2021 resulted in a semi-permanent saline intrusion in the Clyde estuary. The effects of this semi-permanent intrusion on the lower layer were measured during the CEP4, CEP5 and CET1 surveys. During this period $[\text{CH}_4]$ were observed to be low in the near-bed layer compared to data outside of this period when regular flushing occurred. The time of saline influence or salinity persistence (i.e., the time since the last freshwater flushing event, considering river flows that exceeded $30 \text{ m}^3\text{s}^{-1}$) was significantly correlated with near-bed $[\text{CH}_4\text{-C}]$ (Fig. 6.8). Note that tide (not accounted for here) could influence salinity persistence as during spring tides freshwater flushing could occur at low tide which might not occur during neap tides. Additionally, the fresh water flushing events have different durations and intensity which could impact the level of influence of a fresh water flushing events on near-bed layer $[\text{CH}_4]$.

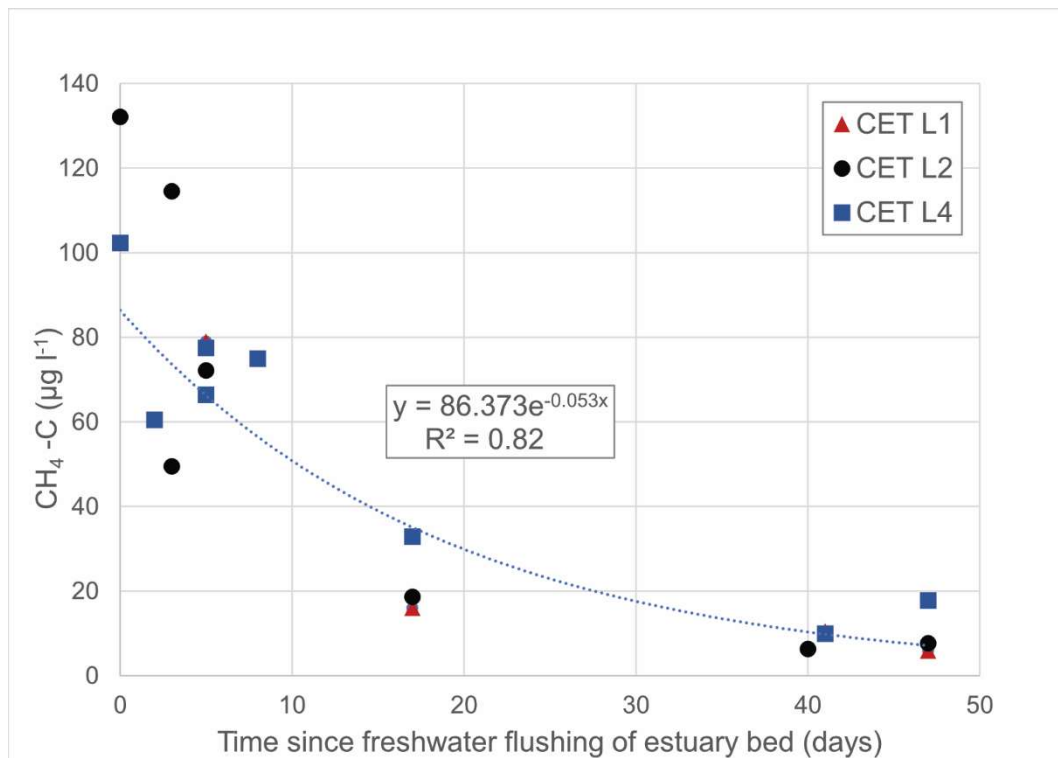


Figure 6.8 - Methane concentrations vs. salinity persistence (time since last freshwater flushing)
Data from location CET L1, L2 and L4, demonstrating the impact of persistent salinity on near-bed [CH₄-C]. Data that were completely riverine in nature (due to higher river flows and occurred during 4 surveys at CET L1 and one survey at CET L2) have been removed.

6.3.6 Short term tidal variability and GHG generation

Measurements through the tidal cycle (CEP) indicated that short-term changes were secondary to the longer-term factors influencing GHG concentrations as observed between surveys. Two CEP surveys, both during spring tides were contrasted in Figure 6.9; CEP3 (March 21) which experienced high river flow, with high dissolved oxygen and low conductivity and had high [CH₄] and CEP4 (June 21) which experienced low river flows, low dissolved oxygen and high conductivity and had low [CH₄], especially at the bed. These surveys showed little change in GHG concentrations across the tidal cycle compared to the difference between the surveys. Higher [N₂O], [TP] and [TDN] were observed on the ebb tide, particularly at the surface and likely linked to both the river and outflow from Shieldhall UWWTP, 1.4km upstream of the CEP location. Conversely increased [CH₄] occurred at high tide when conductivity was low CEP3 (March 21), but [CH₄] were suppressed at the bed for CEP4 (June 21), when river flows had been low over the previous 6-week period.

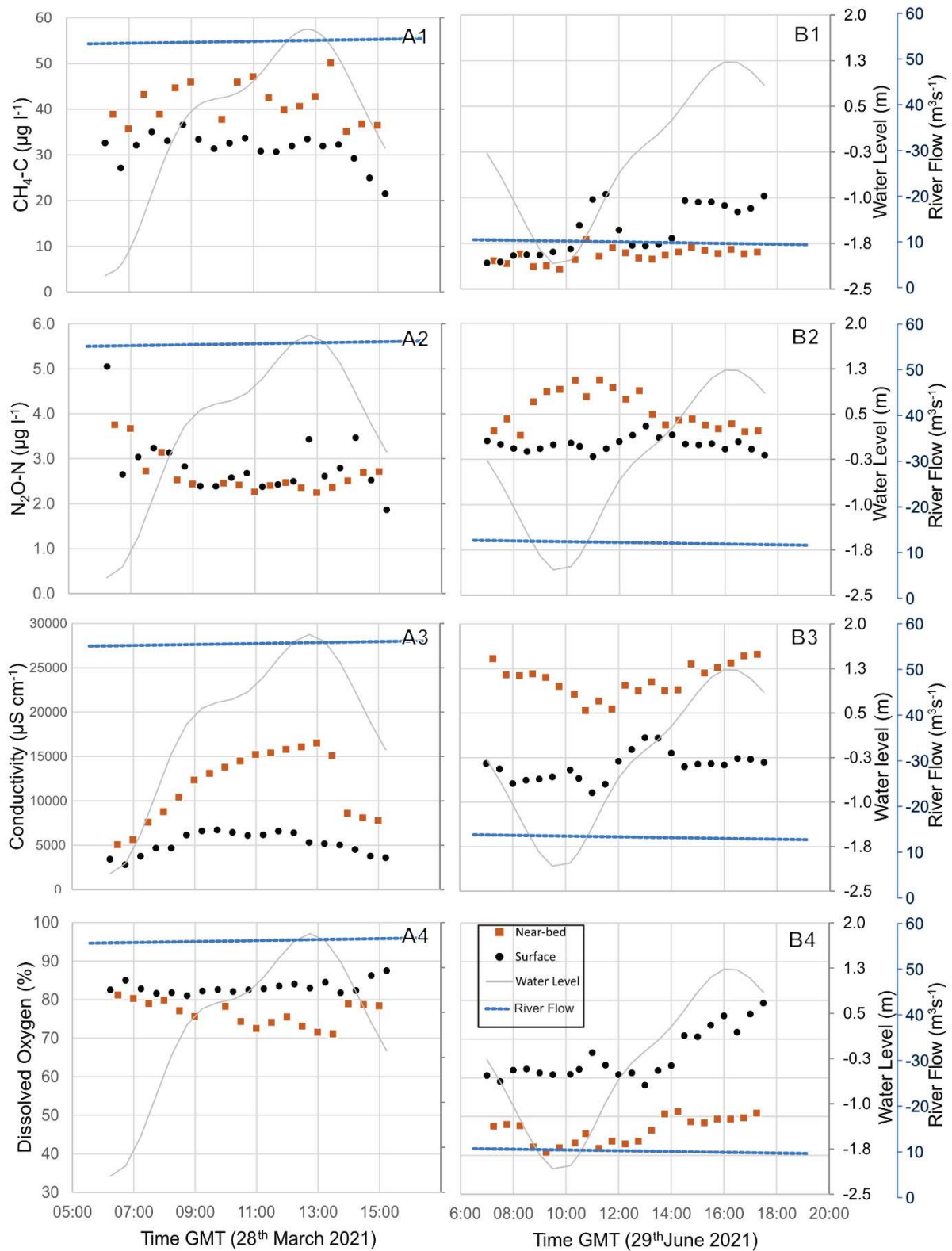


Figure 6.9 - Impact of short-term (tidal) variation on GHG generations

Panel A data is for CEP3 (March 21) and panel B data for CEP 4 (June 21). Items 1 to 4 show [CH₄-C], [N₂O-N], EC and DO. The surface data is represented by black dots and the bed data brown squares. The tidal range was similar for both surveys (grey line), but during CEP3 (A) river flow exceeded 50 m³s⁻¹, while during CEP4 (B) river flow was <11m³s⁻¹ and was preceded by 6 weeks of low river flows (blue dashed line). [CH₄] are suppressed at the bed in CEP4. [N₂O] increased at low tide, likely due to nutrients moving downstream. [N₂O] is higher at the bed compared to the surface in CEP4 likely due to the longer fresh water flushing times (*T_f*) allowing nutrients to penetrate the stratification.

6.3.7 Comparison with other estuaries

The observed maximum dissolved CH₄ percentage saturations were the highest reported for any estuary reaching 308,351% in the near-bed layer and 147,455% in the surface layer. Other temperate estuaries with high reported surface CH₄ percentage saturations include the Tyne, UK (107,725%), the Guadelete, ES (130,358%), the Sado, PT (158,000%) (although this value was from a tidal creek entering the estuary only and not the main estuary) and for tropical estuaries the Adyar, IN (115,655%) (see Table 6.5 for further details and references).

The observed maximum dissolved N₂O percentage saturations were high relative to other reported for estuaries reaching 1949% in the near-bed layer and 1300% in the surface layer. This was exceeded by Guadelete, ES (2174%), Humber, UK (6506%), Tees, UK (2118%), Ems, DE (1794%) and Scheldt, FR (3100%) and for tropical estuaries the Saigon River estuary, VT (3500%) and based on the strong correlations observed in this study, suggests that these estuaries have high nitrogen and low oxygen condition (see Table 6.5 for further details and references).

Table 6.5 - Comparison of annual CH₄ and N₂O emissions in estuaries

Name	Country	Survey year	Type	No	Area (km ²)	Mean % Sat CH ₄	Range % Sat CH ₄	Annual emission (g CH ₄ yr ⁻¹)	Flux density (gCH ₄ m ⁻² yr ⁻¹)	Mean % Sat N ₂ O	Range % Sat N ₂ O	Annual emission (g N ₂ O yr ⁻¹)	Flux density (gN ₂ O m ⁻² yr ⁻¹)	Ref
Temperate														
Clyde, UK (S)		2020-2022	S	8	26.6	41,100	6,202-147,455	5.4 × 10 ⁷	2.04	360	120-1300	6.3 × 10 ⁶	0.24	This study
Clyde, UK (B)		2020-2022	S	8	26.6	76,183	3,343-308,351			513	117-1949			
Conwy, UK		2017- 2018	M	4	14.9	2,964	370-8223	6.7 × 10 ⁶	0.45	130	106-191	7.0 × 10 ⁵	0.05	(2)*
Clywd, UK		2017- 2018	M	4	1.2	5,571	456-15,812	1.0 × 10 ⁶	0.85	140	110-202	7.5 × 10 ⁴	0.06	(2)*
Clyde, UK		2017- 2018	S	4	54.85	31,285	2,161-122,582	2.7 × 10 ⁸	4.90	251	99-970	1.3 × 10 ⁷	0.24	(2)*
Tamar, UK		2017- 2018	M	4	39.62	7,820	111-40,669	4.7 × 10 ⁷	1.19	164	76-236	3.9 × 10 ⁶	0.10	(2)*
Dart, UK		2017- 2018	P	4	8.63	6,415	221-35,098	8.4 × 10 ⁶	0.98	165	67-320	8.8 × 10 ⁵	0.10	(2)*
Tay, UK		2017- 2018	P	4	121.3	1,475	205-7,185	2.6 × 10 ⁷	0.21	107	86-143	1.4 × 10 ⁶	0.01	(2)*
Forth, UK		2017- 2018	M	4	84.0	4,138	554-13,545	5.3 × 10 ⁷	0.63	262	98- 885	2.2 × 10 ⁷	0.26	(2)*
Elbe, DE		2015-2022	M	11	327	-	-	-	-	191	-2.5 -746	2.4 × 10 ⁸	0.64	(17)
Guadelete, ES		2013	M	1	2.3	21,753	1105-130,358	6.6 × 10 ⁶	2.9		96-2174	3.4 × 10 ⁶	1.5	(6)
Tay, UK		2009- 2010	P/M	8	121.3	2600	100-13,100	6.9 × 10 ⁷	1.0	118	69-188	2.2 × 10 ⁶	0.059	(4)
Guadalquivir, ES		2006	M			-	150-1740	-	-	-	-	-	-	(11)
Río San Pedro, ES		2004	M		0.3	-	514-5000	1.5 × 10 ⁵	0.5	-	191-843	2.1 × 10 ⁵	0.7	(9)
Ria de Vigo, ES		2003 - 2004	M		178	1620	101-8500	3.1 × 10 ⁶	0.02	-	-	-	-	(8)
Temmesjoki, FI		2003- 2004	M	1	3	15,400	7,970-29,800	2.7 × 10 ⁷	9.1			3.8 × 10 ⁶	1.26	(7)
Colne, UK		2001 -2002	M		23.3	-	-	-	-	993	-	2.6 × 10 ⁷	5.42	(19)
Stour, UK		2001 -2002	M		24.4	-	-	-	-	143	-	8.1 × 10 ⁶	0.33	(19)
Orwell, UK		2001 -2002	M		17.5	-	-	-	-	282	-	2.5 × 10 ⁷	1.43	(19)
Deben, UK		2001 -2002	M		9.3	-	-	-	-	187	-	5.6 × 10 ⁶	0.60	(19)
Conwy, UK		2002 - 2003	M		5.0	-	-	-	-	114	-	6.9 × 10 ⁵	0.14	(19)
Humber, UK		2001	M	2	303.6	1546	194-5558	6.6 × 10 ⁷	0.2	396	157 -6506	4.0 × 10 ⁸	1.23	(1) (18)
Forth, UK		2000 - 2012	M	4	84.0	5067	627-19,548	7.3 × 10 ⁷	1.3	152	98-313	1.3 × 10 ⁷	0.25	(1) (18)
Tamar, UK		2001	M	2	39.6	3407	452-5837	6.2 × 10 ⁷	1.8	143	99-210	5.8 × 10 ⁶	0.13	(1) (18)
Tyne, UK		2000 - 2002	P/M	6	7.9	26,348	599-107,725	4.0 × 10 ⁷	7.9	124	98-288	5.8 × 10 ⁵	0.12	(1) (18)
Tees, UK		2001 - 2002	P	3	13.5	16,559	1702-52,368	3.1 × 10 ⁷	3.0	383	106 - 2118	1.1 × 10 ⁷	1.11	(1) (18)
Tay, UK		2001	P/M	1	121.3	584	234-1294	3.1 × 10 ⁷	0.3	104	100-118	4.0 × 10 ⁶	0.04	(1) (18)
Douro, PT		1998	M	1	2	-	620-5720	-	-	465	280-650	2.9 × 10 ⁶	1.20	(3) (18)
Elbe, DE		1997	M	1	224	-	130-2980	-	-	202	139-374	1.2 × 10 ⁸	0.54	(3) (18)
Ems, DE		1997	M	1	162	-	920-13,100	-	-	418	181-1794	2.0 × 10 ⁸	1.23	(3) (18)
Gironde, FR		1996- 1998	M	4	442	-	70-13,400	-	-	218	120-463	1.8 × 10 ⁸	0.41	(3) (18)
Loire, FR		1998	M		41	-	340-23,100	-	-	-	-	-	-	(3)
Rhine, NL		1996	S	4	71	-	140-49,700	-	-	-	-	-	-	(3)
Sado, PT		1998	S	1	102	-	940-158,000	-	-	-	-	-	-	(3)
Scheldt, NL		1996 1998	M	4	269	-	380-20,400	-	-	-	-	-	-	(3)
Thames, UK		1999	M	1	225	-	150-6700	-	-	-	-	-	-	(3)
Elbe, DE		1994	M	1	327	-	700-2200	-	-	-	-	-	-	(10)
Elbe, DE			M	2	327	-	-	-	-	201	-	1.8 × 10 ⁸	0.77	(16)
Temmesjoki, FI		2003- 2004	M	1	3	15,400	7,970-29,800	2.7 × 10 ⁷	9.1			3.8 × 10 ⁶	1.26	(7)
Thames, UK		1998	M		47.5	-	-	-	-	321	93-681	5.3 × 10 ⁷	1.11	(21)
Humber, UK		1996	M		303.6	-	248-21,048	4.8 × 10 ⁷	0.2	452	100-4250	4.1 × 10 ⁸	1.35	(20) (5)
Tweed, UK		1996 - 1997	S		2.4	-	-	-	-	100	96-110	8.4 × 10 ⁴	0.05	(20)
Tyne, UK		1996	M		7.9	5,843	450-2000	1.1 × 10 ⁷	1.4	-	-	-	-	(5)
Scheldt, FR		1978 - 1996			262	-	-	-	-	710	100 - 3100	2.8 × 10 ⁸	1.07	(21)
Tropical														
Adyar, IN		2003 - 2004		7	3.2	64840	621- 115,655	3.4 × 10 ⁷	10.7			1.4 × 10 ⁶	0.44	(13)
Lupar, MY		2011	P	2	220	970	168 - 2799	8.0 × 10 ⁷	0.78	112	102-208	6.3 × 10 ⁶	0.03	(23)
Saribas, MY		2011	P	2	102	1000	397 - 3050	4.4 × 10 ⁷	0.43	124	110-592	4.7 × 10 ⁶	0.05	(23)
Rajang, MY		2016-2017	P/M	3	455	-	350- 40,598	1.3 × 10 ⁹	2.79	-	28-390	3.3 × 10 ⁷	0.74	(14)
Maludam, MY		2016-2017	P/M	2	0.36	-	163- 32,998	3.6 × 10 ⁶	8.02	-	62-331	2.0 × 10 ⁵	0.44	(14)
Sebuyau, MY		2016-2017	P/M	2	2.11	-	299 - 50,774	3.5 × 10 ⁶	7.77	-	55-335	2.4 × 10 ⁵	0.54	(14)
Simunjan, MY		2016-2017	P/M	2	4.73	-	106- 57 459	4.3 × 10 ⁷	9.44	-	35-365	3.2 × 10 ⁶	0.69	(14)
Sematan, MY		2016-2017	P/M	2	1.47	-	433 - 47,055	6.0 × 10 ⁶	10.65	-	71-109	-3.0 × 10 ⁴	-0.69	(14)
Samunsam, MY		2016-2017	P/M	2	0.85	-	830 - 43 807	5.0 × 10 ⁶	10.95	-	67-142	3.0 × 10 ⁴	0.07	(14)
Jiaoxi, CN		2019-2020		4	-	-	-	-	-	120	-	-	0.007	(22)
Min, CN		2019-2020		4	-	-	-	-	-	150	-	-	0.014	(22)
Mulan, CN		2019-2020		4	-	-	-	-	-	390	-	-	0.067	(22)
Jin, CN		2019-2020		4	-	-	-	-	-	600	-	-	0.117	(22)
Jiulong, CN		2019-2020		4	-	-	-	-	-	120	-	-	0.122	(22)
Saigon, VN		2019-2020		4	-	-	5,200-33,200	-	11.25		900-3700	-	1.22	(12)

Notes

- Comparison of CH₄ and N₂O saturation mean and range, and annual emission and flux densities
- Estuary references from (1) (Upstill-Goddard and Barnes, 2016), (2) (Pickard et al., 2021a), (3) (Middelburg et al., 2002), (4) (Harley et al., 2015), (5) (Upstill-Goddard et al., 2000), (6) (Burgos et al., 2015), (7) (Silvennoinen et al., 2008), (8) (Silvennoinen et al., 2008), (9) (Ferrón et al., 2007), (10) (Rehder et al., 1998), (11) (Ferrón et al., 2010), (12) (Nguyen et al., 2022), (13), (Rajkumar et al., 2008), (14) (Bange et al., 2019), (15) (Musenze et al., 2014), (16) (Brase et al., 2017), (17) (Schulz et al., 2023), (18) (Barnes and Upstill-Goddard, 2011), (19) (Dong et al., 2005), (20) (Barnes and Owens, 1998), (21), (De Wilde and De Bie, 2000), (22) (Li et al., 2022), (23) (Müller et al., 2016)
- (*) Data from (Pickard et al., 2021a) has been converted to annual emission and flux densities by taking the average estuary concentrations multiplied by the average estuary area. This will likely over-estimate the annual emission and flux densities, as the lower estuaries with high surface area typically have lower GHG concentrations.

6.4 Discussion

6.4.1 Causes and controls of estuarine methane

Significant spatial and temporal variability in $[\text{CH}_4]$ was exhibited within the stratified Clyde estuary. The major influences on this variation were different in the surface and lower layers. The lower layer typically had higher $[\text{CH}_4]$, but conditions did occur when $[\text{CH}_4]$ in the surface layer significantly exceeded that of the lower layer. In the lower layer $[\text{CH}_4\text{-C}]$ reached $> 130 \mu\text{g l}^{-1}$. However near-bed $[\text{CH}_4\text{-C}]$ were $< 10 \mu\text{g l}^{-1}$ after a saline intrusion into the upper estuary had persisted for several months with $[\text{CH}_4]$ declining proportionally with the duration of the saline intrusion. Near-bed $[\text{CH}_4]$ in the upper estuary appeared to be rapidly (< 1 day) reinvigorated by freshwater flushing input, (river flows above $30\text{m}^3\text{s}^{-1}$) and exponentially declined with time since the last freshwater flushing event, with $[\text{CH}_4]$ reduced by about 50% after 10 days. The near-bed $[\text{CH}_4]$ in the lower estuary, which was less impacted by freshwater flushing, except during exceptionally high river flow events, were lower and less variable, declining exponentially seawards and consistent with persistent higher salinity and dilution. Hence accounting for hydrological variation and persistence is important for understanding methane generation in estuaries.

In the surface layer $[\text{CH}_4\text{-C}]$ reached $> 65 \mu\text{g l}^{-1}$, however any high $[\text{CH}_4]$ derived from the river, associated with low river flow and high nutrient conditions, did not persist into the estuary. High $[\text{CH}_4]$ occurred in the surface estuary waters, associated with increased river flow, T_{UR} and $[\text{DOC}]$. This increase in $[\text{CH}_4]$ was only observed after a small increase in salinity had occurred in the surface layer by mixing and $[\text{CH}_4]$ declined once the surface layer salinity increased. The observations that surface layers $[\text{CH}_4]$ could be higher or lower than in the near-bed layer and that influences on $[\text{CH}_4]$ were different in the surface and near-bed layers indicated that diffusion of CH_4 across the pycnocline was not an explanation for surface $[\text{CH}_4]$. These observations support findings in the stratified Yarra estuary, Australia, which found a dominance of acetoclastic CH_4 production in fresh surface waters and hydrogenotrophic CH_4 production in the saline bottom waters (Tait et al., 2017).

Research into methanogenesis in other contexts has found relationships with salinity. The presence of sodium chloride can inhibit the production of CH_4 from food waste in anaerobic digestion (Zhao et al., 2017). In tidal marshes, CH_4 emissions in oligohaline tidal marshes (0.5 - 5 ppt) were the highest and most variable, polyhaline tidal marshes (>18 ppt) had significantly lower CH_4 emissions, with fresh (0 - 0.5 ppt) and mesohaline (5 - 18 ppt) tidal marshes having intermediate emissions (Poffenbarger et al., 2011). These observations support the conclusion from this study that methanogenesis is initially stimulated by slightly saline conditions, but inhibited by salinities > 5 ppt. Inner estuaries with salinity ranges of 1 - 5 ppt are likely hotspots for methane emissions.

In permanently saline waters methanogens are outcompeted for resources by other microbial communities, including SRB with rates of methanogenesis estimated at two orders of magnitude lower than rates of sulphate reduction, probably indicative of SRB having a higher substrate affinity for H_2 (Kristjansson and Schönheit, 1983; Lovley and Klug, 1983). Estuarine conditions can indicate how quickly these microbial communities respond to changes in salinity. The methanogens experience a slow decline linked to increased salinity but a very

rapid reinvigoration after a freshwater flushing event, indicative of both their adaptive capacity and rapid transition between methanogens and SRB.

The time to respond to salinity changes could vary between locations, even in the same estuary due to sediment structure. The time for equilibration between interstitial and overlying water can be rapid in sand but slow (many days) in silts and clays, due to sediment porosity and permeability, with surface sediments more rapidly affected than bottom sediments (Chapman and Wang, 2001). The availability of labile carbon in sediments can influence $[\text{CH}_4]$ (Sha et al., 2011). Flow restrictions in the inner Clyde estuary (CET L3) caused deposition of organic matter, particularly leaves, resulting in bed sediments with high levels of decomposing organic matter. This may have influenced $[\text{CH}_4]$ at CET L3 which had a more variable relationship with salinity persistence. The observed slow decline in $[\text{CH}_4]$ with salinity persistence could be due to varying methanogen salinity tolerance, the time for overlying water to penetrate the bed or other sediment properties such as levels of labile carbon.

6.4.2 Uncertainty in estuarine methane controls

Estuarine $[\text{CH}_4]$ could be influenced by the competing interaction of anaerobic methanogenesis and aerobic methanotrophy, both of which are stimulated by higher temperatures, and different conditions and may result in their changing dominance (Dessandier et al., 2016). Oxygen is the preferred terminal electron acceptor for methanotrophs, which can oxidize 60-90% of the CH_4 produced in wetlands before its emission to atmosphere (Le Mer and Roger, 2001). Low oxygen conditions, as occur in the lower layer, may result in higher $[\text{CH}_4]$, with methanotrophy reducing $[\text{CH}_4]$ in the surface. However no significant correlation was observed between CH_4 and DO in either layer to support methanotroph activity. The diversity and effectiveness of the methanotrophic community decreases with increasing salinity in lake sediments (Zhang et al., 2023) and suggests that salinity might also dominate methanotroph activity above that of oxygen availability.

Several authors observed high $[\text{CH}_4]$ variability both within and between estuaries (Middelburg et al., 2002; Upstill-Goddard et al., 2000; Upstill-Goddard and Barnes, 2016). River-dominated, stratified estuaries were found to be more erratic compared to well mixed estuaries (Middelburg et al., 2002), however measurements were made at the surface only, making the impact of salinity persistence on stratified estuaries impossible to compare. Many of the mixed estuaries (Middelburg et al., 2002; Upstill-Goddard and Barnes, 2016) showed a rapid decline in $[\text{CH}_4]$ with increasing salinity, consistent with the salinity persistence model. Several of the mixed estuaries had high $[\text{CH}_4]$ in the middle of the estuary, often attributed to tidal flats. The Tyne estuary experienced a mid-estuarine $[\text{CH}_4]$ peak (Upstill-Goddard and Barnes, 2016), which was linked to increasing tidal range associated with high suspended particulate matter (SPM) (Brown et al., 2022), consistent with in-water CH_4 production. However, spring tides at low tide would also result in removal of saline water from the estuary providing an opportunity for freshwater flushing which could reinvigorate methanogens in the bed resulting in a mid-estuary $[\text{CH}_4]$ peak. Turbidity, flushing linked to salinity persistence and the influence of tidal flats, which may have different salinity to the main estuary, may all influence mixed estuary $[\text{CH}_4]$. We found no significant impact of temperature on $[\text{CH}_4]$, however climate change models also predict more-frequent flushing

events in winter and longer periods of drought in summer (Robins et al., 2016). Flushing events would reinvigorate methanogenesis while droughts would increase saline intrusions suppressing methanogenesis. As such the overall impact of climate change on estuarine $[\text{CH}_4]$ is unclear.

In the river high $[\text{CH}_4]$ were significantly correlated with TP, however this relationship did not persist into the estuarine waters. While the main reason appears to be the dominating impact of salinity on methanogenesis, TP may be impacted by a variety of other influences. Sediments typically acts as both a sink and source for P with the overlying water (Cheng et al., 2020), with the release of P subject to anthropogenic activities and complex biochemical interactions including coupling with DOC and P (Dong et al., 2022). Inorganic P is adsorbed by a variety of soil minerals (Xiong et al., 2022) and speciation impacted by salinity (Hsu et al., 2022) as such the river estuarine transition could also act to change P availability for biochemical processing. However, this data is not sufficient to interrogate such changes.

This study provides insights into methane generation but does not address the difference between different estuarine environments. The Clyde estuary has one of the highest $[\text{CH}_4]$ despite the low turbidity which has been associated with UWW outflows (Brown et al., 2022). The high level of nutrient processing found in the Clyde estuary could result in a build-up of nutrients within the estuary sediments supporting methanogenesis. Further research into factor impacting the level of methanogenesis from sediments could yield important insights about drivers of GHG production in other estuary typologies.

6.4.3 Causes and controls of estuarine N_2O

This study supports the growing global concern that N_2O emissions from estuaries are increasing because of the elevated nutrient loading and are further exacerbated by the ability of these nutrients to cause hypoxia, observed here to quadruple the N_2O produced per unit available nitrogen. In the Clyde estuary, the UWW directly entering the estuary has neither nitrogen or phosphate removal and is causing eutrophication and oxygen depletion during periods of low river flow (and the resultant longer freshwater flushing times) with most nutrients processed within the estuary, rather than output to the sea. These extended flushing times and low oxygen levels lead directly to more nitrogen processing by denitrification and consequently more N_2O per unit TDN.

Within the stratified Clyde estuary N_2O is produced by two different pathways. Nitrogen processing in the upper layer was primarily via nitrification, as indicated by the significant correlation with NH_4^+ . In the lower layer both nitrification and denitrification occurred, but significant nitrogen processing was via denitrification, prompted by the low oxygen conditions and linked to NO_3^- . When compared with data measured for other UK estuaries (Dong et al., 2005; Barnes and Upstill-Goddard, 2011), N_2O saturation in the Clyde estuary lower layer was 4.4 times higher compared to the available TDN and aligned with that found for the Colne estuary, widely reported for significant denitrification (Dong et al., 2000, 2002) (Fig. 6.10). N_2O saturation in the Clyde estuary surface layer was 1.6 times higher compared to other estuary surface measured compared to the available TDN and experienced low oxygen saturation. All the measurements made in this study in the Clyde were made during daylight and no account has been made for diurnal variation. Other researcher report low $[\text{DO}]$ at night, (Rosamond et al., 2012; Yu et al., 2013) which would likely further increase $[\text{N}_2\text{O}]$.

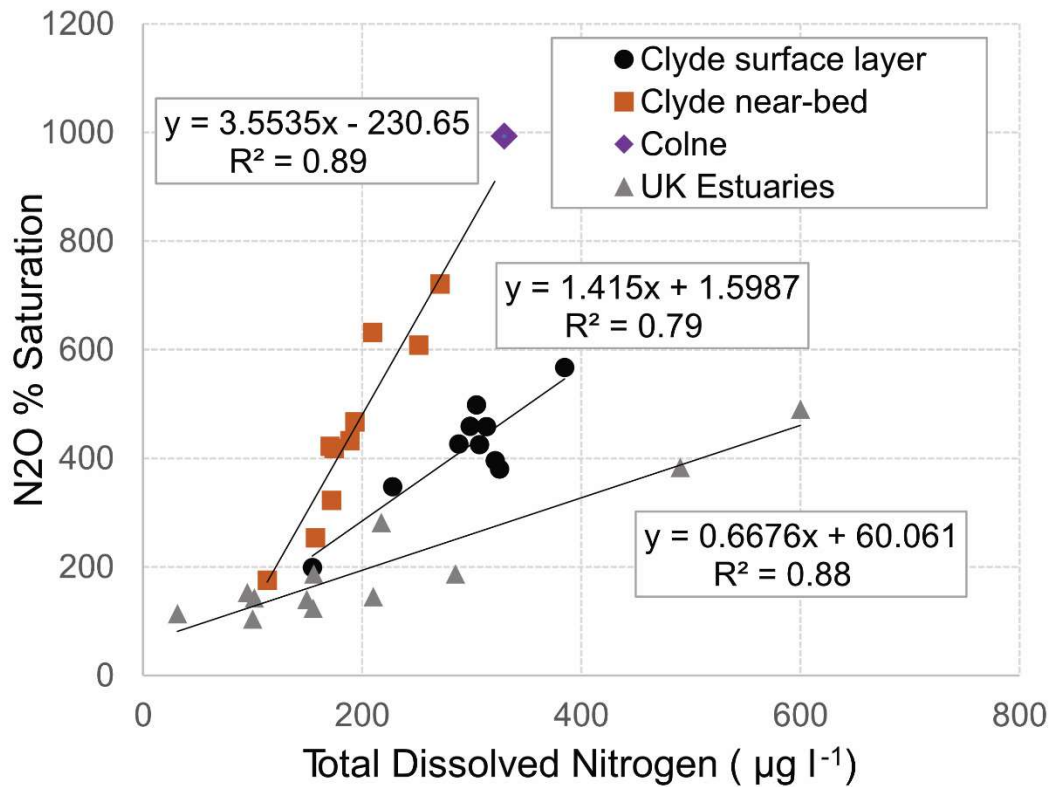


Figure 6.10 - Relationship between observed UK estuarine N₂O saturations and TDN

The Clyde surface data is indicated by black circles and the near-bed by brown squares. Data for other UK estuaries (Humber, Tamar, Tay, Tees, Tyne, Forth, Conwy, Stour, Orwell, Deben), were from (Dong et al., 2005; Barnes and Upstill-Goddard, 2011) and indicated by a grey triangle. Data for the Colne estuary were from (Dong et al., 2002) and indicated by a purple diamond. The N₂O saturation is 4.4 times higher compared to TDN for the Clyde near-bed data compared to the other estuaries and similar to that for the Colne estuary noted for the occurrence of denitrification.

6.4.4 High nutrients and low oxygen are driving N₂O

It is widely reported that in fully mixed estuaries where a turbidity maximum forms, that the SPM supports nitrogen processing by nitrification (or coupled nitrification-denitrification) in the water column (Law et al., 1992; Abril et al., 2000; Barnes and Upstill-Goddard, 2011; Zhu et al., 2018). The Clyde estuary does not experience a turbidity maximum, and turbidity caused by SPM was low. Additionally, there was no correlation between turbidity and N₂O in the estuary but a very strong correlation between N₂O and DO. This result from the Clyde suggests that the positive correlation between turbidity and N₂O may be promoted by high SOD and the movement of nutrients together with the sediment that forms the turbidity maximum, rather than driven by nitrogen processing on the sediment surface. Measurements of DO in the Forth (Barnes and Upstill-Goddard, 2011) showed a strong negative exponential correlation between DO and turbidity and a strong negative linear correlation to between DO and N₂O, although DO was not measured in other estuaries, supporting this possible explanation. Expanding survey methodologies to measure dissolved oxygen and SOD could provide important insights into GHG production mechanisms in estuaries.

The N₂O saturation was shown (Barnes and Upstill-Goddard, 2011) to be a function of estuarine TDN load for the surface waters of six inner estuaries and supports the use of global-scale N₂O models that express N₂O emissions as simple linear functions of river-borne dissolved inorganic nitrogen (DIN). This result is supported by surface measurements in other estuaries (Dong et al., 2005). However the [N₂O] for the lower saline layer in the Clyde and also the Colne (Dong et al., 2002) was over 4 times higher, compared to the TDN load. This indicates that increased production of N₂O can occur under low oxygen and high nutrient conditions. N₂O is a powerful, long-lived GHG, which makes it important to take action to reduce both nitrogen sources and the amount of N₂O produced from these sources (Murray et al., 2015). Taking steps, not only to reduce estuarine nutrient loading but to remove sources of estuarine hypoxia are important not only for estuarine health but to significantly reduce estuarine N₂O production. Strong stratification can cause bottom hypoxia (Park et al., 2007; Muller et al., 2016) making stratified estuaries more susceptible and worthy of further study. In the Clyde [TDN] reached 7.4 mg l⁻¹, higher than reported for most estuaries (Barnes and Owens, 1998), and occurred during a period of low river flow and reduced estuarine flushing. Climate models predict longer periods of drought in summer but estuarine mixing and recovery rates are poorly understood (Robins et al., 2016). These summer droughts will likely increase the number of estuaries susceptible to hypoxia, concentrating nutrients and increasing N₂O evasion.

Total estuary GHG evasion can be difficult to estimate for a stratified estuary, where the GHG in the lower layer are higher than for the surface. The stratification restricted the nutrients and GHGs passing between layers in the inner estuary, although when mixing does occur due to turbulence, high wind or storms, GHG release to atmosphere from the lower layers would be expected (Tait et al., 2017; Gelesh et al., 2016).

6.5 Conclusions

There were two important and unique aspects of this survey approach to identify sources and controls of estuarine GHG in the urban Clyde estuary. Firstly, measuring in both the upper fresh and lower saline layers of a stratified estuary enabled the production processes in each layer to be identified. Secondly use of a three-pronged survey approach which measured over different spatial and temporal scales, including contiguous data from the river to estuary that allowed understanding of the riverine-to-estuary transition zone, data throughout tidal cycles that helped delineate short-term variation, and data longitudinally through the estuary during different river, tidal and seasonal conditions that enabled longer-term changes to be distinguished.

The Clyde estuary exhibited both high [N₂O] with N₂O being produced primarily by nitrification in the upper freshwater layer and denitrification in the lower saline layer. The amount of N₂O in the lower layer was four times higher relative to the available TDN, compared to other UK estuaries (Dong et al., 2005; Barnes and Upstill-Goddard, 2011) and the strong ($R^2 = 0.96$) inverse exponential correlation between N₂O with DO, emphasised the importance of low oxygen conditions associated with high [N₂O]. Our analysis indicates that the UWW directly entering the estuary was a major source of nutrients and a contributor to low oxygen conditions. Low [DO] were exacerbated during low river flow events, increasing estuary flushing times and resulting in the processing of most of the nutrients within the inner

estuary. Emissions of N₂O could be lowered by reducing nutrients from UWW and increasing estuary oxygenation, for example by natural aeration or turbulence. This high level of nutrients processing in the inner estuary could result in a build-up of nutrients within the estuary sediments, resulting in future nutrient release further contributing to hypoxia (Valdemarsen et al., 2015). In the Swan River, Australia, physical oxygenations of the highly stratified estuary was tested to alleviate hypoxia (Larsen et al., 2019b) but in most estuaries removal of anthropogenic nutrient inputs, as UWW inflows add oxygen scavenging nutrients (Conley et al., 2007), would reduce N₂O and restore estuary environments.

Production of CH₄ in the upper estuary was high compared to other UK estuaries (Middelburg et al., 2002; Upstill-Goddard and Barnes, 2016; Harley et al., 2015) but highly variable. This study indicates that salinity above 0.5ppt stimulated methanogenesis, which continued until salinity reached around 5ppt. However, once the salinity was sustained above 5ppt for around 10 days methanogenesis reduced by about 50% and after 30-40 days by about 90%, explaining some of the high CH₄ variability in this and other estuarine studies. This apparent impact of salinity persistence on methanogenesis may be dependent on local factors such as sediment porosity and permeability, which could vary within and between estuaries. Methanogens in the surface waters were associated with suspended sediments and high river flows. While the mechanisms that causes changes in methane production with salinity persistent are not well understood, future studies may benefit from microbial community analysis to help further illicit GHG production controls. Methanogens and SRB coexist and compete for resources and may also exists in a symbiotic system with typically methanogens dominating in fresher waters and SRB outcompeting methanogens in more saline waters (Shi et al., 2020;, Purdy et al., 2003; Dar et al., 2008), with changing salinity impacting the activity within microbial communities.

Acknowledgement

This work was financially supported by Natural Environment Research Council (NERC) studentship through the IAPETUS Doctoral Training Partnership Grant No. NE/S007431/1.

To access the Clyde estuary the authors used Kelvin Harbour. The authors would like to thank The Tall Ship Glenlee Trust, a registered charity limited by guarantee, and the wholly-owned subsidiary of the Trust, the Clyde Maritime Centre, which is responsible for the operation of Kelvin Harbour and supported the researcher in their work (Tall Ship Glenlee Trust, 2022).

The authors would like to thank Intu SGS, Global Mutual and Savills for access to Braehead pontoon for the purpose of making measurements from that location.

The authors would like to thank Glasgow City Council for access to Govan pontoon for the purpose of making measurements from that location.

The authors would like to thank Alanna Grant, Galina Toteva, Dr Justyna Olszewska, Ivan Simmons and Duncan Harvey from UKCEH Edinburgh for their support with measurements.

6.6 Supplementary information

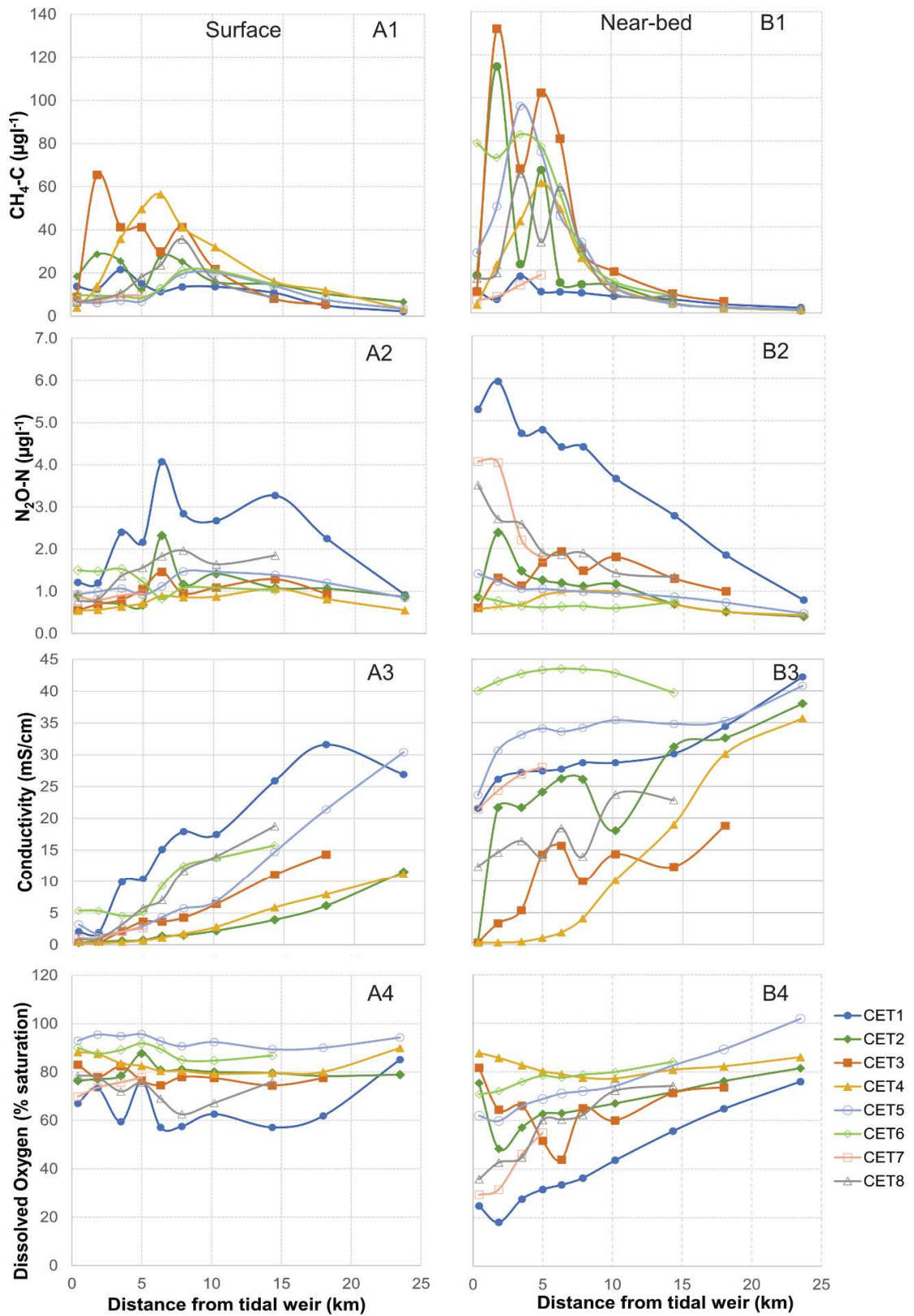


Figure 6.A.1 - Clyde transect data for CET survey CET1 to CET8 for locations L1 to L10
 Panel A indicates Surface data and Panel B Near-bed data. Plot 1 indicates CH₄-C concentration, plot 2 N₂O-N concentration, plot 3 conductivity and plot 4 dissolved oxygen. The tidal weir is the interface between the river and estuary and the distance is seawards.

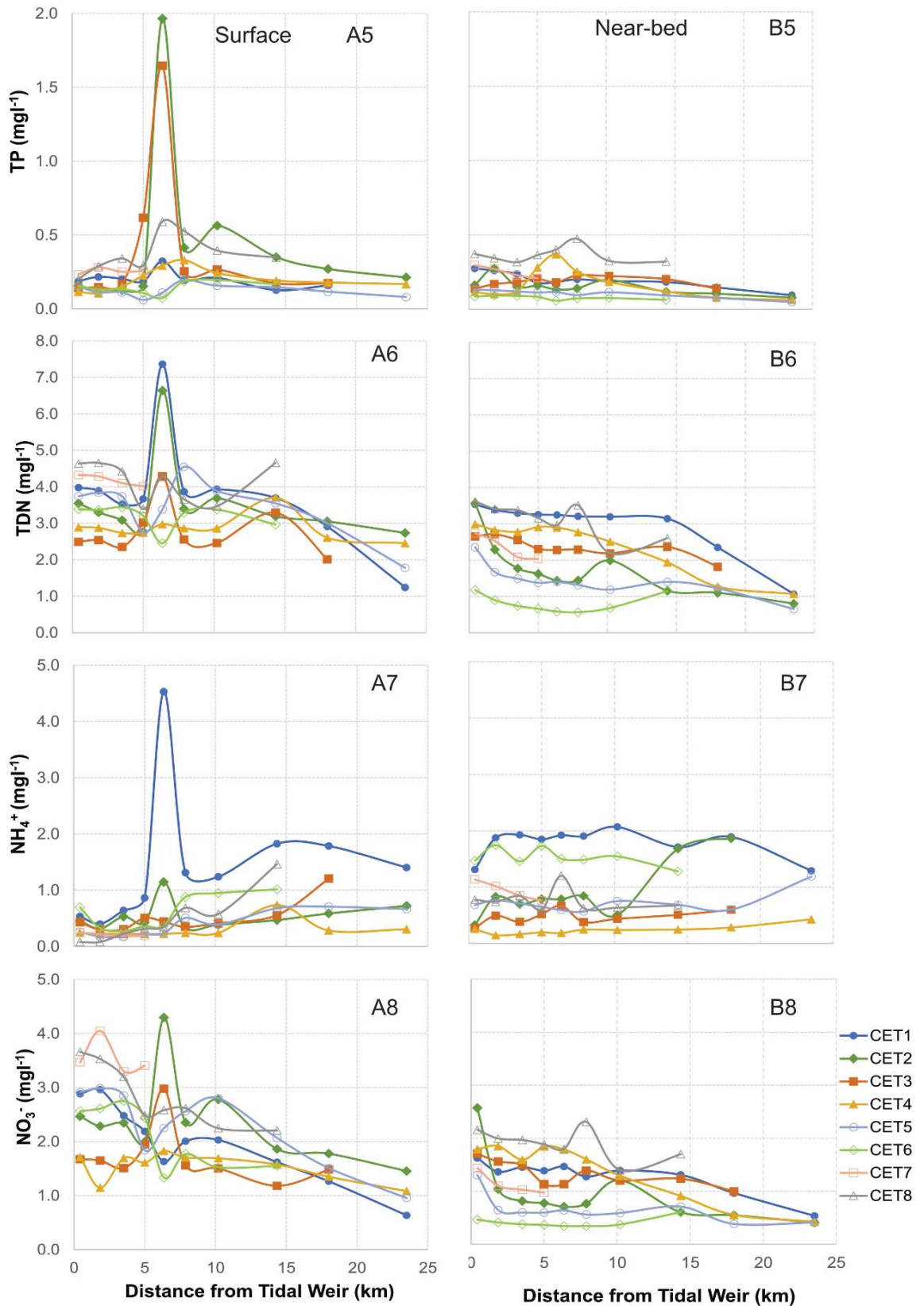


Figure 6.A.2 - Clyde transect data for CET survey CET1 to CET8 for locations L1 to L10
 Panel A indicates Surface data and Panel B Near-bed data. Plot 5 indicates total phosphorous, plot 6 total dissolved nitrogen, plot 7 ammonium and plot 8 nitrate. The tidal weir is the interface between the river and estuary and the distance is seawards.

7 Discussion

7.1 GHG 'hotspots' in the Clyde catchment, river and estuary

Across the human-impacted Clyde catchment, river and estuary, the source-to-sea study methodology helped identify several GHG 'hotspots'. All the identified hotspots were associated with anthropogenic impacts, with GHG concentrations low in the semi-natural environment.

The main sources of GHGs in the riverine catchment associated with nutrient inputs included:

- a) Nutrients entering the water from UWWTP outflows, which resulted in point source in-water generation of CH₄ linked to TP and TDN, and CO₂ and N₂O linked to TDN.
- b) Nutrients entering streams and rivers from agriculture (arable and pastoral) which were a major diffuse source of in-water generation of N₂O and CO₂ linked to TDN.
- c) Nutrients entering streams from badly run septic tanks were a source of N₂O.
- d) Mine water outflows from disused coal mines where DOC probably from groundwater had been converted to CO₂ and CH₄. The CH₄ may have significantly increased where sewage sludge was used for mine land restoration.
- e) Mine water outflows from disused coal mines where TDN probably from groundwater was a source of N₂O generated both in the anaerobic mine environment and on reoxygenation of the MWs at the surface.

There were additional sources of GHGs in the riverine catchment associated hydrological-environmental interactions. These processes often interacted with nutrients to further increase GHGs and occurred:

- a) At locations in the river where physical, chemical and /or biological processes resulted in low riverine DO.
- b) At locations in the river which were deeper, wider and hence slower flowing than the upstream river section, resulting in deposition of sediments and lower oxygen levels including areas associated with the dredging of river gravel.
- c) As a result of higher temperatures.
- d) As a result of high rainfall increasing run-off from the land, increasing levels of nutrients, sediments and DOC entering the rivers and streams and increasing in CO₂, CH₄ and N₂O.
- e) As a result of low water levels concentrating point sources of nutrients leading to eutrophication, low DO and high residence times and increasing CO₂, CH₄ and N₂O.
- f) At MW outflows from disused coal mines, which were point sources of thermogenic CH₄, thermogenic CO₂ and fossil origin CO₂ from the dissolution of limestone. These processes were driven by the water flow through the abandoned mine and the subsequent dissolution of pyrites.

The main sources of GHGs in the Clyde estuary were similar to those in the rivers and streams in the Clyde catchment but exhibited some distinct and interesting differences and included:

- a) High river flow conditions linked to high turbidity and DOC in the surface estuary waters increased [CH₄]. Where high [CH₄] were generated in the river just prior to the estuary associated with high nutrients and low water levels, these did not persist into the estuary.

- b) Salinity increases above 0.5ppt stimulated methanogenesis in the surface waters and could increase the [CH₄] by an order of magnitude. High [CH₄] continued until the salinity exceeded a threshold (around 5ppt).
- c) Salinity persistence, the time the salinity remained above a threshold (in the order of 5 ppt), caused methanogenesis from the bed as measured by near-bed [CH₄] to decline exponentially and was reduced by about 50% after 10 days. Methanogenesis was reinvigorated after fresh water flushing of the bed.
- d) Low oxygen conditions in the estuary's lower saline layer resulted in denitrification and the production of > 4 times the amount of N₂O per unit available nitrogen.
- e) Nutrients entering the estuary from UWWTP outflows resulted in a major point source of in-water generation of N₂O linked to TDN.
- f) Nutrients entering the estuary from UWWTP outflows in conjunction with low river flows resulted in high processing of nutrients within the estuary, eutrophication and increased [N₂O].

Almost all these sources for GHGs correspond to other types of pollution impacting environmental and human health. Mine outflows and sewage sludge add heavy metals to the environment, and agriculture and UWW, including from badly run septic tanks, add nutrients which can contribute to eutrophication in rivers and estuaries. UWW can add pathogens and a wide range of other pollutants and agriculture can add chemicals or chemical fertilisers. Hence actions to reduce aquatic GHGs could also reduce aquatic pollution more broadly.

7.2 GHG sources and controls (process understanding)

One of the key objectives of this work was to elucidate the sources and controls of GHGs over an anthropogenically impacted catchment and compare this with natural sources. However where it was possible to distinguish natural or semi-natural GHG sources, correlations with measured water properties were generally poor. The identified GHG processes are described for fresh, mine and saline waters.

7.2.1 Greenhouse gas processes in freshwater

Riverine dissolved GHG, nutrient and chemical concentrations all increased from source-to-sea, in line with the increasing percentage of urban and agricultural land cover. The increase in GHG concentrations between the semi-natural and urban environment was on average three times higher for N₂O and CO₂, but twenty times higher for CH₄, suggesting the significant nature of CH₄ as an aquatic urban marker. In the lower urban catchment strong correlations occurred between all GHGs and water physiochemical properties, suggesting that removal of contaminants from river systems, could lower GHG concentrations. The anthropogenic sources of UWW and agriculture were identified to increase GHGs. While UWW outflows were a major point source of CH₄ linked to TP and TDN, and N₂O linked to TDN, the results indicated that the CH₄ and the N₂O were not passed from the UWWTP but generated in the river as a result of mixing of the two water streams.

The seasonal patterns of [CH₄], [CO₂] and [N₂O] changed between the semi-natural environment in the upper catchment and urban environment in the lower catchment. In the semi-natural upper catchment GHGs were higher in winter, while in the lower urban catchment, GHG were considerably higher in summer. The GHGs in the urban catchment

were dominated by point source inputs and their impact increased during low river flow and high temperature conditions. This seasonal change in GHG concentrations may be related to changes in microbial community composition and activities, which have been observed downstream of UWWTP (Zhou et al., 2022; Beaulieu et al., 2010). The abundance of sediment microbial community have been found to be correlated with EC, organic matter, TP, DO and TN (Feng et al., 2022). This suggests microbial adaptation to changing conditions. High CH₄ in many shallow lakes is produced by eutrophication, mostly driven by TP and TDN enrichment and sediment microbiome (Davidson et al., 2018; Aben et al., 2017; Nijman et al., 2022). This mechanism is less likely in river ecosystem due to continual flushing, but during low water levels, increased residence times in combination with the high nutrient concentrations from UWW appear responsible for eutrophication and significant CH₄ generation. This may be enabled by electron donor availability in the receiving waters.

Three major hydrological-environmental interactions were found that increased GHG concentrations in addition to those directly attributed to the nutrient increases including low oxygen conditions, higher temperatures and changes in river geometry.

Low oxygen conditions, which can promote both methanogenesis and denitrification, were observed to be correlated with increased [CH₄], [CO₂] and [N₂O]. Respiration, photosynthesis and decomposition can create inverse relationships between DO and CO₂ dependent on their balance in the water column (Aho et al., 2021). The lower urban river had the highest correlations, with GHGs increasing exponentially with reducing oxygen levels. The [CH₄] were more highly correlated to [DO] compared to DO%, while [CO₂] and [N₂O] were more highly correlated with DO% compared to [DO]. This suggests that CH₄ is primarily influenced by the amount of oxygen in the water with temperature having a smaller impact compared to CO₂ and N₂O. High turbulence causes oxygenation of the water and out-gassing of the supersaturated GHGs but it also produced conditions less likely to promote GHG production, making it difficult to fully distinguish mechanisms associated with low oxygen conditions.

In temperate climates higher temperatures are typically correlated with reduced rainfall increased evaporation and higher plant water usage (UKCEH, 2022), all resulting in low river flows making the impact of high temperature and low river flow difficult to distinguish. The use of a load appointment modelling enables the effect of flow to be distinguished. The direct effect of temperature did not have a large impact on GHG concentrations, independent of that associated with low river flows despite the fact that high temperatures are associated with increased microbial activity and often found significant (Wang et al., 2021, Herrero Ortega et al., 2019 and Rosentreter et al., 2021). In the case of CH₄ both methanogenesis and methanotrophy can both increase with temperature and could be in balance, masking the independent effects (Grossart et al., 2011). Studies undertaken in tropical climates where increasing rainfall and temperature are correlated, also do not find temperature a significant driver for GHG concentrations (Yu et al., 2017). Flow and hence nutrient concentrations were more significant than the direct impact of temperature in accounting for GHG variability.

Changes in river geometry that reduced river velocity and increased water residence times compared to the upstream river, resulted in deposition of sediments and nutrients and reduced out-gassing and oxygenation. These slow sections of river exhibited disproportionately higher GHG concentrations, with the largest increases occurring in low flow conditions, which

also resulted in further decreases in DO%. However, proportioning the cause of this increase between; increased residence time, reduced outgassing due to lower turbulence, lower oxygen conditions, or deposition of sediments and nutrients as a source of GHG production is challenging. Their point source behaviour may suggest the creation of anaerobic sediments was the most significant impact. Both the increased residence time (Zarnetske et al., 2011) and low oxygen level (Frey et al., 2020; Rosamond et al., 2012) will act to increase N₂O, by promoting denitrification over nitrification and increasing the proportion of N₂O per unit TDN.

Concentrations of CO₂ were less variable than those of N₂O and CH₄ and were thought to be influenced by carbonate buffering as the MW inflows added significant amounts of DIC from the dissolution of limestone, increasing alkalinity, which masked other influences on [CO₂]. For example, primary productivity can be maintained with diminished CO₂, in high alkalinity waters by converting bicarbonate to CO₂ (Aho et al., 2021) and mineralisation of DOC to CO₂ would change the carbonate balance increasing bicarbonate concentrations. High alkalinity waters are likely to result in increased CO₂ emissions over what might be estimated from the measured CO₂ concentrations, with outgassing events triggering changes in the carbonate balance.

7.2.2 Greenhouse gas processes in mine water

Across the measured MW locations in the Midland Valley 51% of the CH₄ was of modern biogenic origin, 41% from thermogenic origin and 8% from hydrogenotrophic methanogenesis of coal. Conversely 65% of the CO₂ was derived from limestone, 20% from modern terrestrial organic carbon and 15% from coal related carbon probably thermogenic CO₂. Some MW outflows were high in N₂O and N₂O was additionally generated on oxygenation of reduced nitrogen in the MW outflows likely by nitrification. The relationships derived for the six different GHG sources provided insights into the MW GHG generation processes.

Modern biogenic CH₄ was likely produced from modern carbon sources dissolved in the MW. This process was inhibited by increasing [SO₄²⁻] most likely as SRB can outcompete methanogens, by two orders of magnitude for resources, indicative of SRB having a higher substrate affinity (Lovley and Klug, 1983; Kristjansson and Schönheit, 1983). This suggests that methanogenesis occurred after the dissolution of pyrites within the anaerobic mine environment, rather than in the groundwater before the water entered the mine. Alternatively Fe(III) and Mn(IV) reducers can interfere with the metabolism of methanogens by competing for organic carbon, (Magonigal et al., 2004). However, while both Fe and Mn are readily available in the MW, they are only soluble in their reduced state making this mechanism less likely.

Thermogenic CH₄ was present in all MW measured, suggesting that even after a mine was flooded, desorption of thermogenic CH₄ still occurred despite the low solubility of CH₄ (Fernando, 2011). Any remaining thermogenic CH₄ would be in deeper coal seams and may be dissolved due to the higher hydrostatic pressure (Pruteanu et al., 2017). There was no statistically significant correlation with time since abandonment, suggesting an equilibrium is reached after the mine is flooded and that the CH₄ reservoir is large relative to the amount of CH₄ dissolved in the MW. The best predictor for thermogenic CH₄ was pH which may impact the dissolution processes at the mine walls.

Hydrogenotrophic methanogenesis of coal occurs due to metabolism of short and long-chain alkanes and polyaromatic hydrocarbon (Gonzalez Moguel et al., 2021). This mechanism was not common in the Midland Valley and would likely be more common in lower rank coals (Iram et al., 2017). There was insufficient data to understand the mechanism.

Dissolution of limestone to produce CO_2 was the major source of CO_2 in the MW. The mechanism involved dissolution of FeS_2 to form sulphuric acid and this acidic environment accelerated the dissolution of limestone to form CO_2 (Vesper et al., 2016). As limestone was dissolved the ratio of dissolved CO_2 , H_2CO_3 and HCO_3^- changed due to carbonate buffering which acts to increase the pH. When the MW reached the surface, it had typically reached a pH of 6. If the CO_2 was evaded quickly to atmosphere such as in a cascade, some of the HCO_3^- was converted to CO_2 increasing the potential release of the CO_2 to atmosphere before the effect of carbonate buffering resulted in an increase of pH.

The modern terrestrial organic carbon-based CO_2 was likely derived from a terrestrial DOC source. Most MW had low levels of remaining DOC, suggesting that DOC from groundwater had been converted, most likely to CO_2 through soil respiration. This implied biogenic CO_2 was being produced prior to the organic carbon passing into the anaerobic part of the mine. This could be facilitated by the longer mine residence times compared to fluvial systems which would promote this conversion (Winterdahl et al., 2016).

Coal related CO_2 , probably thermogenic, is associated with coal seams (Iram et al., 2017). The coal-based $[\text{CO}_2]$ was inversely correlated with time since abandonment and reduced to a low stable level (5 mg l^{-1}) after 100-200 years. Depletion of the thermogenic CO_2 reservoir probably occurred associated with the higher solubility of CO_2 compared to that of thermogenic CH_4 enabling significant quantities to escape via the MW, depleting the source.

N_2O produced within from MW was probably related to TDN sources within the groundwater and converted to N_2O via denitrification within the anaerobic mine environments, supported by longer residence time. Remaining TDN, in a reduced state, could be converted by nitrification to N_2O on oxygenation of MW at the surface.

There was no correlation between the different GHG sources including CO_2 and CH_4 from modern DOC, suggesting generation of all GHG sources were driven by different factors. Considerable variation in GHG concentrations, did occur over time, particularly for CH_4 and N_2O , likely related to changes in hydrological conditions, which would impact flow rate, MW residence times and DOC and TDN concentrations in the groundwater. However insufficient data were available to understand how sources were impacted by hydrological changes.

7.2.3 Methane processes in estuaries

The biggest factor impacting $[\text{CH}_4]$ within the Clyde estuary was estuarine salinity. This influenced $[\text{CH}_4]$ to such an extent that other potential relationships with, for example, oxygen, temperature and nutrient concentrations were not statistically significant. Comparison of data across UK estuaries suggested that $[\text{CH}_4]$ were impacted by nutrient concentrations from UWW entering the estuary systems. UWW inflows likely contributed to the resources required for methanogenesis over longer timescales (Burgos et al., 2015), by build-up within the estuarine sediments.

In the Clyde estuary upper freshwater layer, methanogenesis was invigorated by salinity increasing above 0.5 ppt and reduced when salinity exceeded 5ppt. The surface [CH₄-C] exceeded 65 µg l⁻¹ with the highest concentrations occurring during high river flow events. Methanogenesis in the surface layer was supported in the water column by DOC and turbidity both associated with high river flows. High [CH₄-C] from the River Clyde, caused by high nutrient concentration, typically occurred during low river flow conditions. The maximum [CH₄-C] concentration measured in the River Clyde was 44 µg l⁻¹, but these occasions of high [CH₄-C] did not persist into the estuary, indicating that transfer of CH₄ from the river was not an explanation for high surface estuarine [CH₄].

In the estuary lower saline layer [CH₄-C] exceeded 130 µg l⁻¹ and were highest after freshwater flushing events. The near-bed [CH₄-C] were significantly impacted by salinity persistence. The increasing duration of saline waters, above a salinity threshold (> 5 ppt), reduced the near-bed [CH₄] and presumably the CH₄ generation exponentially (50% after 10 days). However, the near-bed methanogenesis was rapidly reinvigorated (< 1 day) by freshwater flushing events, presumably by reducing the salinity to more optimum levels.

In the stratified Clyde estuary, the observations that surface freshwater layer [CH₄] could be higher or lower than in the near-bed saline layer and that the influences on [CH₄] were different in the surface and near-bed layers indicated that diffusion across the pycnocline was not an explanation for surface [CH₄] and the surface and near-bed [CH₄] were independent and likely impacted by different processes. Studies of methanogenesis in the temperate south of Australia in a stratified estuary suggested acetoclastic production occurred in the fresh surface waters and hydrogenotrophic production in the saline bottom waters (Tait et al., 2017). Alternatively investigation of methanogenesis in sediments in a tropical estuary in India, found that acetoclastic methanogens were abundant at bottom layers of the sediments and methylotrophic methanogens in top layers of the sediments (Reshmi et al., 2015).

It is likely that in permanently saline waters, methanogens are outcompeted for resources by other microbial communities, the most likely being SRB with rates of methanogenesis estimated at two orders of magnitude lower than rates of sulphate reduction, probably indicative of sulphate-reducing bacteria having a higher substrate affinity for H₂ (Kristjansson and Schönheit, 1983; Lovley and Klug, 1983; Sela-Adler et al., 2017). In estuaries the frequent changes between semi-permanent saline intrusions and freshwater influxes may act to alternate dominance between methanogens and SRB. Acetoclastic methanogens have been found to favour higher salinity and methylotrophic methanogens favour highly reducing conditions and higher pH (Reshmi et al., 2015). Conversely mesophilic, hydrogenotrophic and methylotrophic methanogens have been found to show high-salinity tolerances, but acetoclastic methanogens much lower tolerance (Blake et al., 2020). While these results do not provide a consistent or complete picture, they suggest that different methanogens have different salinity tolerances and may inhabit different areas of the bed. This could result in the slow decrease of methanogenesis with increasing salinity persistence, as the interstitial waters in estuarine muds, which have low porosity and permeability, may take days to equilibrate with the overlying waters (Chapman and Wang, 2001). Rapid reinvigoration of methanogenesis could occur on fresh water flushing if methanogens in surface sediments favoured lower salinity conditions. As these methanogen communities may vary by climate and sediment types, the relationship with salinity might be expected to vary on a similar basis.

High variability in $[\text{CH}_4]$ have been reported within and between estuarine systems (Middelburg et al., 2002; Upstill-Goddard et al., 2000; Upstill-Goddard and Barnes, 2016; Bange et al., 1998; Bange, 2006) although this had often been attributed to the presence of mud flats (Rosentreter et al., 2021; Upstill-Goddard and Barnes, 2016), seasonal changes (Harley et al., 2015; Bange et al., 1998; Burgos et al., 2015) and methanotroph activity (Middelburg et al., 2002), with little change over the tidal cycle (Li et al., 2021). River-dominated, stratified estuaries were found to be more erratic compared to well mixed estuaries (Middelburg et al., 2002). However, the limited data available for some surveys makes the impact of salinity persistence in stratified estuaries impossible to compare. Many of the mixed estuaries (Middelburg et al., 2002; Upstill-Goddard and Barnes, 2016) showed a rapid decline in $[\text{CH}_4]$ with increasing salinity, consistent with the salinity persistence model. However, several of the mixed estuaries had high $[\text{CH}_4]$ in the middle of the estuary, often attributed to tidal flats. The Tyne estuary experienced a mid-estuarine $[\text{CH}_4]$ peak (Upstill-Goddard and Barnes, 2016), which was linked herein to increasing tidal range associated with high SPM (Brown et al., 2022). However, spring tides at low tide could result in removal of saline water from the estuary providing an opportunity for freshwater flushing which could reinvigorate methanogens resulting in a mid-estuary $[\text{CH}_4]$ peak. Turbidity, flushing linked to salinity persistence and tidal flats, which may have different salinity to the main estuary, may all influence mixed estuary $[\text{CH}_4]$.

The availability of labile carbon concentrations in the bed-soil could influence $[\text{CH}_4]$ (Sha et al., 2011). Carbon was measured from sediments taken by sediments grabs during CET6 and the total organic matter (including OC and labile and recalcitrant organic matter) increased from L1 to L4 where it reached >10% and it remained >8% until L6 and then declined. This pattern could have occurred due to the interaction of saline and freshwater flows on the output of the large UWWTP at L5 resulting in an area of deposition. It was observed that a restriction in the inner Clyde estuary at L3 caused deposition of organic matter, particularly leaves, and resulted in bed sediments high in decomposing organic matter, suggesting L3 is the location for river-sourced deposition. However, correlations between $[\text{CH}_4]$ and labile carbon concentrations in the bed are secondary to salinity gradient and not statistically significant in this data.

There was no significant impact of temperature on $[\text{CH}_4]$, however climate change models also predict more-frequent flushing events in winter and longer periods of drought in summer (Robins et al., 2016). Flushing events would reinvigorate methanogenesis and provide SPM, while droughts would increase saline intrusions suppressing methanogenesis. As such the overall impact of climate change on estuarine CH_4 is unclear.

7.2.4 Nitrous oxide processes in estuaries

The biggest factors influencing N_2O emissions from the stratified Clyde estuary were low oxygen conditions and elevated nutrient loading. Untreated storm water entering the Clyde estuary has been significantly reduced by a storm water storage system called the Shieldhall tunnel, made operational in 2018 (Kling et al., 1991). However, UWWTP outflows for over 600,000 ppe entered the estuary directly and have neither nitrogen nor phosphate removal, with this water primarily entering the estuary's upper layer. Within the stratified Clyde estuary $[\text{N}_2\text{O-N}]$ exceeded $4.0 \mu\text{g l}^{-1}$ in the upper freshwater layer and $5.9 \mu\text{g l}^{-1}$ in the lower

saline layer, with some differences in the processes impacting N₂O in the surface and lower layer.

The N₂O emissions from the Clyde estuary were high linked to the elevated nutrient loading, eutrophication and oxygen depletion and further exacerbated by the ability of these nutrients to cause hypoxia. During periods of medium to low river flow most of the nutrients were processed within the estuary, rather than output to the sea. Nitrogen processing in the upper layer was primarily via nitrification, as indicated by the significant correlation with NH₄⁺. In the lower-saline layer / bed both nitrification and denitrification occurred, but significant nitrogen processing was via denitrification, prompted by the low oxygen conditions and linked to NO₃⁻. There was a significant inverse exponential correlation between N₂O and dissolved oxygen in the lower layer, with hypoxia driving elevated denitrification. When compared with data measured for other UK estuaries (Dong et al., 2005; Barnes and Upstill-Goddard, 2011), N₂O saturations were 4.4 times higher in the lower layer and 1.6 times higher in the surface layer compared to the available TDN.

The Clyde estuary does not experience a turbidity maximum, and turbidity caused by SPM was low. Additionally, there was no correlation between turbidity and N₂O in the Clyde estuary but a very strong correlation between N₂O and DO ($R^2 = 0.96$). This result is in contrast with data from estuaries with TMZs, where it has been assumed that the SPM supports nitrogen processing by nitrification (or coupled nitrification-denitrification) in the water column (Law et al., 1992; Abril et al., 2000; Barnes and Upstill-Goddard, 2011; Zhu et al., 2018). The data from the Clyde suggests that this positive correlation between turbidity and N₂O may be promoted by high SOD and the movement of nutrients together with sediments, rather than driven by nitrogen processing on the sediment surface. This was supported by measurements of DO in the Forth (Barnes and Upstill-Goddard, 2011) which showed a strong negative exponential correlation between DO and turbidity and a strong negative linear correlation to between DO and N₂O. Expanding survey methodologies to measure dissolved oxygen and SOD could provide important insights into GHG production mechanisms in estuaries. Other researcher reported lower [DO] at night, (Rosamond et al., 2012; Yu et al., 2013) which would likely further increase [N₂O] above those measured in daylight for the Clyde estuary.

7.3 Implications for policy makers

To effectively reduce anthropogenic GHGs from the riverine and estuarine environments it is important to understand their sources. For the River Clyde, all significant sources of GHGs were associated with high concentrations of nutrients and were influenced by anthropogenic factors. Hence reducing nutrient loading, industrial and legacy contamination and agricultural run-off would ultimately act to reduce GHG emissions. While many UWWTP in the River Clyde have phosphorous removal, our measurements suggest that levels of effectiveness vary between plants, suggesting improvement is possible. Additionally none of the UWWTP in this area had nitrogen removal (European Commission (Directorate General Environment), 2016). Riverine environments with low oxygenation, increased river residence times and high levels of nitrogen, should be prioritised for nitrogen removal from UWWTP to have the largest impact on N₂O reduction. Higher GHG concentrations were associated with both low and high river flow. Low river flows due to increased residence times, reduced oxygen levels and increased concentrations of point source nutrient inputs, and high river flows due to increased

run-off adding nitrogen and carbon to rivers. Actions, particularly nature-based solutions, to increase upland water retention and ground penetration have been investigated to mediate both flooding and drought (Hewett et al., 2020). These approaches include activities such as installation of leaky dams, peatland restoration and woodland creation, and could reduce both hydro-meteorological hazards and in-water GHG generation.

Across the UK there was a significant correlation between UWW inputs and estuarine GHG production. For the Clyde estuary, a significant source of GHGs was associated with high concentrations of nutrients coming from UWW output directly into the estuary. These nutrients are primarily processed within the estuarine environment and not dispersed as sea, due to the extended flushing times. In the Clyde [TDN] reached 7.4 mg l^{-1} , higher than reported for most estuaries (Barnes and Owens, 1998), which occurred during a period of low river flow and reduced estuarine flushing. High nutrient processing within the Clyde estuary likely contributed to in-water generation of GHG, and nutrient build up within the estuary bed increasing methanogenesis and denitrification. Reducing direct nutrient inputs would support estuarine recovery, but full recovery may take time due to the likely high levels of nutrient storage within the bed. Taking steps, not only to reduce estuarine nutrient loading but to remove sources of estuarine hypoxia are important not only for estuarine health but to significantly reduce estuarine N_2O production. Strong stratification, which occurred in the Clyde, can cause bottom hypoxia (Park et al., 2007; Muller et al., 2016) making stratified estuaries a larger source of GHGs per unit nutrient availability. Climate models predict longer periods of drought in summer but estuarine mixing and recovery rates are poorly understood (Robins et al., 2016). These summer droughts will likely increase the number of estuaries susceptible to hypoxia, concentrating nutrients and increasing N_2O evasion across estuaries making it even more important to tackle direct estuarine UWW nutrients inputs.

Agricultural run-off caused significant increases in GHGs, primarily from diffuse sources. Additional measurements showed a large proportion of agricultural run-off entered the Clyde via the numerous field drainage ditches and small streams, which could be treated as point sources to make remediation easier. Approaches to reduce run-off and pollution via drainage ditches could include: (1) use freshwater wetlands for nitrogen and phosphorus removal (Land et al., 2016) as wetlands have been shown as effective for diffuse run-off (Ockenden et al., 2012) and could be effectively deployed on streams and ditches; (2) use of biochar filtrations, an effective technology for both cleaning of wastewater and run-off water. Its capabilities include removal of pesticides, organic chemicals and nutrients. However, a practical approach for application to small streams is needed to reduce the required residence times. After use the biochar could be redeployed onto farmland supporting carbon sequestration and a circular economy, recycling nutrients and further preventing run-off (Catizzone et al., 2021, Phillips et al., 2022, Kamali et al., 2021); (3) Riparian buffer zones are recommended between crops and rivers and help reduce run-off during high rainfall. In Scotland, General Binding Rule 20 requires a buffer strip at least 2m wide to be left between surface waters and wetlands and cultivated land (SEPA, 2009). This rule was not set with the objective of reducing nutrient leeching. Further research demonstrates that woody vegetation is more effective than shrubs or grass at preventing nutrient leaching to rivers, with a 60m buffer strip effectively removing all nutrients (Aguiar et al., 2015). While this would take considerable agricultural land, approximately 70% of nutrients are removed by a 12m strip. This could stabilise river banks,

reduce erosion and sediment loss, increase biodiversity and wildlife areas and provide shade making the riverine system more robust to climate change (Cole et al., 2020).

Mine water pollution from both active and abandoned mines is a global pollution problem both impacting environmental and human health and requires more government intervention globally at the planning, operational and restoration stages to ensure pollution does not occur (Carvalho, 2017). Monitoring of MW discharges is required which should include not only physiochemical water properties and heavy metals but also GHG emissions. However preventative technologies such as coating the walls of the mines and hence the pyrites while in operation, as each area is mined and before allowing flooding, could be the most viable option for preventing dissolution of both metals and GHGs from future abandoned mines (Liu et al., 2017). Mines could be filled with biochar from appropriate waste sources. A flooded repository for carbon storage would reduce the water flow in abandoned mines, may prevent any degradations of the biochar and could help with absorption of metals (Gopinath et al., 2021) that do leach into the water but is unlikely to be effective for remove of all metal contaminations from mines, unless concentrations can be reduced.

8 Conclusions

8.1 Significance of this research

8.1.1 Novel research approaches

Several of the research approaches used within this investigation were novel or different from those previously reported in the literature and were highly beneficial to understanding the processes and mechanisms of GHG generation, these included:

1. The source-to-sea study approach used to support identification of GHG sources was very effective in the Clyde catchment, with its transitioning land cover from semi-natural through agricultural and legacy industrial to highly urban. As GHGs were not conserved but out-gassed in turbulent riverine sections this method was effective at tracing changes and identifying GHG sources and sinks. It showed how correlations on a catchment scale can be misleading due to variable outgassing and residence times which likely contributed to the high variability in GHG-to-nutrient relationships reported in the literature.
2. The use of load appointment modelling to distinguish point and diffuse sources by their degree of dependence on flow was effective in confirming diffuse GHG sources from agriculture and point GHG sources from UWW and MW. This approach enabled the two main, but highly correlated, seasonal impacts of high temperature and low water levels that commonly occur in temperate latitudes to be distinguished. Not accounting for the correlation between temperature and water level or rainfall may account for the high reported variability on the impact of temperature on CH₄, reported in the literature.
3. The measurement of a high number of water physiochemical properties allowed source fingerprinting of different inflows, which enabled detection of contaminant sources even when the inflows were not physically identified. This approach supported identification of contamination from legacy industry, including mine water, steel slag and paper making and other active land management activities including road salting and the addition of potassium-based fertilisers.
4. The application of radiogenic and stable carbon isotope ($\Delta^{14}\text{C}$ and $\delta^{13}\text{C}$) measurements to CH₄ and CO₂ dissolved in water flowing from abandoned mine adits enabled three different sources of both CH₄ (modern biogenic, thermogenic and coal-based hydrogenotrophic) and CO₂ (limestone, coal-based and from modern terrestrial organic carbon) to be distinguished. The [CH₄] and [CO₂] varied considerably dependant on the MW location and the ability to distinguish the different sources enabled drivers for each source to be identified. This showed that [SO₄²⁻] was the biggest factor negatively influencing [CH₄] by inhibiting biogenic methanogenesis and positively influencing [CO₂] by increasing the dissolution of limestone. This novel work has contributed information about the sources and controls of GHG from MW and identified the need to quantify and report this emissions term.
5. The measurement of all species including metals throughout MW reed pools treatment systems, enabled the effectiveness of the different reed pool systems to be quantified for elements other than iron. This work could be extended to cover more treatment systems across the UK which could help optimise removal of other heavy metals. Coal can be high in heavy metals (Li et al., 2018; McConnell and Edwards, 2008) and heavy metal removal options are required globally to reduce environmental impact from MW.
6. The selection of the Clyde river and estuary system with its tidal weir, which separated the two distinct habitats of salt and fresh water, allowed clear differentiation of what were riverine and estuarine processes. The extent of the saline intrusion into most estuaries

changes daily, based on river flow and tidal conditions, making the impact and interaction between in-sediment and in-water processes in both the river and estuary difficult to distinguish. These data across the river to estuary transition demonstrated how factors that dominated CH₄ production changed between the estuarine and riverine environment. This previous lack of clarity between river and estuary likely contributed to the variable interpretations of the causes of surface estuarine CH₄ concentrations reported in the literature.

7. Measurements of estuary waters both at surface and near-bed, not previously reported, enabled the processes within the upper fresh and lower saline layers in a stratified estuary to be distinguished and data from the lower layer supported identification of the impact of salinity persistence on methanogenesis. Most estuarine studies to date have only measured the surface layer, even in stratified estuaries. While surface measurements might be expected to be sufficient to account for GHG losses to atmosphere, when mixing occurs GHGs from the near-bed layers would be released.
8. The investigations of estuary processes over both short-term (tidal cycle) and longer-term (weeks to months) timescales and longitudinally throughout the estuary enabled process timescales that particularly impacted anaerobic methanogenesis to be distinguished and provided a mechanism (salinity persistence) that has the potential to explain the highly variable CH₄ measurements from estuaries previously reported in the literature.

8.1.2 Increased process understanding

Several of the findings in this research have increased knowledge of anthropogenically influenced GHG generation in the aquatic environment, which may ultimately help to reduce GHG generation, these findings include:

1. The largest increase in riverine GHGs was derived from urban nutrients and the riverine climate stressors of low summer water levels resulting in increased water residence times and reduced river oxygenation. These stressors dominated over the direct impact of temperature, although often highly correlated in temperate latitudes. The removal of these stressors may enable riverine systems to be more resilient to climate change.
2. Seasonal patterns of CH₄, CO₂ and N₂O changed between the semi-natural environment in the upper catchment and urban environment in the lower catchment, with GHG concentrations higher in winter in the semi-natural upper catchment but higher in summer in the lower urban catchment. This result suggested that urban inputs, particularly UWW may be impacting microbiological community composition.
3. Hydrological-environmental interactions were found that increased GHG concentrations including: low oxygen conditions, higher temperatures and changes in river geometry linked to increased water residence times and resulted in increased sedimentation, with the possibility of nutrient disposition associated with this sedimentation.
4. Concentrations of CO₂ were less variable than those of N₂O and CH₄ where significant amount of DIC were in the water, from the dissolution of limestone, which produced high alkalinity and significant carbonate buffering. This carbonate buffering was likely responsible for the lower variability in CO₂ concentrations and the reason why nutrients rather than carbon availability appear to influence CO₂ concentrations. However, carbonate buffering may make estimates of CO₂ released to atmosphere less accurate.
5. The sources and processes of GHG generations in mine water have not before been determined. The split of CH₄ between modern biogenic, thermogenic and hydrogenotrophic methanogenesis of coal and that of CO₂ between limestone, modern

terrestrial organic carbon and coal related carbon, and hence some understanding of the generations processes allows a better understand of how these GHGs could be reduced.

6. The high level of CH₄ and CO₂ derived from mine waters, possibly making up to about 1% of Scotland GWP and is not currently accounted for in emission reporting including that from fugitive emissions.
7. The MW outflows are causing a significant loss of rock carbon to atmosphere by dissolution of limestone, which was primarily linked to sulphate concentrations. There was no evidence that dissolution of limestone had reduced linked to time since mine abandonment and it is having a significant negative and likely continuing impact on climate change. DIC rather than DOC may dominate CO₂ release from riverine environments in the UK.
8. All researchers have previously reported highly variable CH₄ measurements from estuaries, with no consistent explanations. The impact of salinity and salinity persistence on CH₄ estuarine processes is a new insight. CH₄ generation was invigorated by a small increase (0.5ppt) in salinity and inhibited when salinity exceeded around 5ppt. CH₄ generation at the bed was significantly impacted by salinity persistence with [CH₄] decreasing exponentially with duration the salinity remained above about 5ppt. A 50% reduction in [CH₄] occurred after 10 days but methanogenesis was reinvigorated after high river flow events transporting fresh water over the estuary bed.
9. The high level of GHGs derived from estuaries was linked to two factors. These included the lack of N and P removal from UWW entering estuarine waters, due to the assumed flushing and supposed lack of eutrophication, and the low oxygen conditions induced by low mixing and high stratification. Many estuaries have high freshwater flushing times, resulting in most nutrients being processed within the estuary. Where estuarine mixing is low this can result in hypoxia and significant increases in GHG generation. These processes were further exacerbated by low river flow, more likely in our changing climate.

8.2 Suggestions for future work

The main questions remaining around GHGs from urban impacted rivers and estuaries identified as part of this research include:

1. What are the mechanisms for riverine GHG generation associated with the inflow of UWW?

From this research it was identified that GHGs particularly CH₄ and N₂O increased because of UWW inflows with the inference that the mixing of the high nutrient UWW with electron donors and acceptors in receiving waters could facilitate GHG generation with the highest correlation to nutrient concentrations. Further investigation including measurements of both inflows and the combined outflow, including parameters to determine the degree of mixing and relative flows would enable mechanisms to be fully understood and help quantify which aspects inhibit and promote in-water generation of GHGs resulting from mixing of UWW and riverine water.

2. What are the changes to microbial communities around UWWTP outflow and could this contribute to the generation of antimicrobial resistance?

From this research it was identified that seasonal changes in the patterns of GHG generation altered from the upstream semi-natural environment to the downstream urban environment, suggesting possible anthropogenic impact on microbial communities. This is of high concern especially as the River Clyde and estuary have been reported to have the highest levels of waste pharmaceuticals pollution within the UK (Wilkinson et al.,

2022). High metal concentrations, may also contribute to the promotion of antibiotic resistance through co-selection when both antibiotics and metals are co-located conferring resistance to both antibiotics and metals, leading to co-selection of bacterial strains, or mobile genetic elements that they carry (Pal et al., 2017). The River Clyde and estuary are also reported to have high levels of heavy metals contamination (Hursthouse et al., 2003; Jones et al., 2019; Rodgers et al., 2019). These three factors together could increase the risk of antibiotic resistant bacteria and could make this a priority location in the UK for the investigation of changes in microbial species around UWW outflows.

3. Can passive MW treatment be optimised to further remove heavy metals?

From this research it was identified that different MW reed pool treatment systems had different effectiveness. The measurement of all species throughout a larger range of MW treatment facilities including reed pools, to understand seasonal impacts; including reed die-back, temperature, residence time and relative flow rates, could enable the quantification of the effectiveness of the different reed pool systems and help optimise this type of passive treatment for different heavy metals, reducing environmental impact.

4. To determine how salinity persistence impacted estuary bed CH₄ production?

From this research it was identified that salinity and salinity persistence impacted methanogenesis in the water column and in the bed. However, the exact mechanisms of these processes are not clear and could be related to; the time to equilibrium of overlaying and interstitial waters, sediment composition and carbon profile, nutrient processing within the bed sediments, the type of methanogens and their salinity tolerance or the competing interests of methanogens, sulphate reducing bacteria and methanotrophs in the estuary environment. Further investigations to support the quantification of these processes could yield important insights about drivers of GHG production in other estuary typologies and improve modelling of estuary GHG generation and budgets which are highly uncertain.

5. To determine relationships between urban ebullitive and diffusive fluxes?

From this research considerable insights were gained into diffusive fluxes, with CH₄ identified as a significant urban maker. However diffusion may be the minor cause of CH₄ emissions from urban environments as ebullition can contribute up to 62 - 84% of total CH₄ fluxes across all inland waters (Zheng et al., 2022). GHG fluxes can be observed directly using flux chambers or using micrometeorological techniques for which the eddy covariance method has become the default approach (Levy et al., 2022). These could be used to quantify which environments have significant ebullitive fluxes. Additionally continuous concentration sensors have evolved significantly and could help diffusive estimates to capture temporal changes. These sensors are effective for aquatic CO₂ concentrations (Pro-oceanus, 2023), but there are still challenges in making continuous sensors work for the lower aquatic concentrations of CH₄ and N₂O. Further development and deployment of these measurement processes could allow more effective GHG emission estimates.

6. To determine how diurnal variation in estuaries and rivers impact GHG generation?

From this research several GHG sources, sinks and generation mechanisms were identified. However, all the measurements made in the river Clyde and estuary were made during daylight and no account has been made for diurnal variation. Other researchers report low [DO] during the night, (Rosamond et al., 2012; Yu et al., 2013) which would likely further increase all GHGs but particularly [N₂O] and [CO₂]. Quantifications of diurnal changes in GHG generation are relatively few, due to research

practicalities, and could improve modelling of river and estuary GHG generation and budgets.

7. To determine N₂O generation mechanism associated with turbidity maximum zones?

From this research estuarine N₂O generation was not found to be linked to turbidity, as suggested by several researcher considering TMZ. It is possible that high [N₂O] may be linked to high SOD rather than nitrogen processing on the sediment surface. Expanding survey methodologies to measure dissolved oxygen, SOD and sediment carbon loading, to help distinguish sediment-supported nitrogen processing from high N₂O production in low oxygen or hypoxic conditions could provide important insights into GHG production mechanisms in estuaries.

8. Can mine environments be modified to reduce GHG production and the dissolution of heavy metals and fossil carbon (limestone)?

Many researchers have demonstrated that MW forms a serious threat to human health and the environment and can directly increase GHGs. However, because the GHG generation processes occur underground they are difficult to tackle. Investigation of processes and approaches that could reduce dissolution limestone and metals in flooded mine environments, particularly by reducing sulphuric acid generation would have a beneficial impact to reduced GHG generation, particularly CO₂ from limestone and could reduce pollution sources globally.

References

- Aben, R. C. H., Barros, N., Van Donk, E., Frenken, T., Hilt, S., Kazanjian, G., Lamers, L. P. M., Peeters, E. T. H. M., Roelofs, J. G. M., De Senerpont Domis, L. N., Stephan, S., Velthuis, M., Van De Waal, D. B., Wik, M., Thornton, B. F., Wilkinson, J., Delsontro, T. and Kosten, S.: Cross continental increase in methane ebullition under climate change, *Nat. Commun.*, 8(1), 1–8, doi:10.1038/s41467-017-01535-y, 2017.
- Abril, G. and Borges, A. V.: Carbon Dioxide and Methane Emissions from Estuaries, , 187–207, doi:10.1007/978-3-540-26643-3_8, 2005.
- Abril, G. and Borges, A. V.: Ideas and perspectives: Carbon leaks from flooded land: Do we need to replumb the inland water active pipe?, *Biogeosciences*, 16(3), 769–784, doi:10.5194/bg-16-769-2019, 2019.
- Abril, G. and Iversen, N.: Methane dynamics in a shallow non-tidal estuary (Randers Fjord, Denmark), *Mar. Ecol. Prog. Ser.*, 230, 171–181, doi:10.3354/meps230171, 2002.
- Abril, G., Riou, S. A., Etcheber, H., Frankignoulle, M., De Wit, R. and Middelburg, J. J.: Transient, tidal time-scale, nitrogen transformations in an estuarine turbidity maximum - Fluid mud system (the Gironde, South-West France), *Estuar. Coast. Shelf Sci.*, 50(5), 703–715, doi:10.1006/ecss.1999.0598, 2000.
- Acharya, B. S. and Kharel, G.: Acid mine drainage from coal mining in the United States – An overview, *J. Hydrol.*, 588(April), 125061, doi:10.1016/j.jhydrol.2020.125061, 2020.
- Agthe, K. E. and Pendergast, K. J.: Bhumi putra: What is it? And why do i need it?, *Bus. Horiz.*, 26(6), 60–68, doi:10.1016/0007-6813(83)90050-2, 1983.
- Aguiar, T. R., Asera, K., Parron, L. M., Brito, A. G. and Ferreira, M. T.: Nutrient removal effectiveness by riparian buffer zones in rural temperate watersheds : The impact of no-till crops practices, *Agric. Water Manag.*, 149, 74–80, doi:10.1016/j.agwat.2014.10.031, 2015.
- Aho, K. S., Hosen, J. D., Logozzo, L. A., McGillis, W. R. and Raymond, P. A.: Highest rates of gross primary productivity maintained despite CO₂ depletion in a temperate river network, *Limnol. Oceanogr. Lett.*, 6(4), 200–206, doi:10.1002/lol2.10195, 2021.
- Alhamed, M. and Wohnlich, S.: Environmental impact of the abandoned coal mines on the surface water and the groundwater quality in the south of Bochum, Germany, *Environ. Earth Sci.*, 72(9), 3251–3267, doi:10.1007/s12665-014-3230-9, 2014.
- Alshboul, Z., Encinas-Fernández, J., Hofmann, H. and Lorke, A.: Export of Dissolved Methane and Carbon Dioxide with Effluents from Municipal Wastewater Treatment Plants, *Environ. Sci. Technol.*, 50(11), 5555–5563, doi:10.1021/acs.est.5b04923, 2016.
- de Angelis, M. A. and Gordon, L. I.: Upwelling and river runoff as sources of dissolved nitrous oxide to the Alsea estuary, Oregon, *Estuar. Coast. Shelf Sci.*, 20(4), 375–386, doi:10.1016/0272-7714(85)90082-4, 1985.
- Ayangbenro, A. S., Olanrewaju, O. S. and Babalola, O. O.: Sulfate-reducing bacteria as an effective tool for sustainable acid mine bioremediation, *Front. Microbiol.*, 9(AUG), 1–10, doi:10.3389/fmicb.2018.01986, 2018.
- Balls, P. W., Hull, S., Miller, B. S., Pirie, J. M. and Proctor, W.: Trace metal in Scottish estuarine and coastal sediments, *Mar. Pollut. Bull.*, 34(1), 42–50, doi:10.1016/S0025-326X(96)00056-2, 1997.

- Bange, H. W.: Nitrous oxide and methane in European coastal waters, *Estuar. Coast. Shelf Sci.*, 70, 361–374, 2006.
- Bange, H. W., Bartell, U. H., Rapsomanikis, S. and Andreae, M. O.: computed with two different exchange models lie in the range of 11-18 Tg CH₄ TM (phosphorus, North, 8(4), 465–480, 1994.
- Bange, H. W., Dahlke, S., Ramesh, R., Meyer-Reil, L. A., Rapsomanikis, S. and Andreae, M. O.: Seasonal study of methane and nitrous oxide in the coastal waters of the southern Baltic Sea, *Estuar. Coast. Shelf Sci.*, 47(6), 807–817, doi:10.1006/ecss.1998.0397, 1998.
- Bange, H. W., Sim, C. H., Bastian, D., Kallert, J., Kock, A., Mujahid, A. and Müller, M.: Nitrous oxide (N₂O) and methane (CH₄) in rivers and estuaries of northwestern Borneo, *Biogeosciences*, 16, 4321–4335, 2019.
- Bansal, S., Johnson, O. F., Meier, J. and Zhu, X.: Vegetation Affects Timing and Location of Wetland Methane Emissions, *J. Geophys. Res. Biogeosciences*, 125(9), doi:10.1029/2020JG005777, 2020.
- Barnes, J. and Owens, N. J. P.: Denitrification and Nitrous Oxide Concentrations in the Humber Estuary, UK, and Adjacent Coastal Zones, *Mar. Pollut. Bull. Vol.*, 37(3–7), 247–260 [online] Available from: papers3://publication/uuid/E6815FA8-6C68-4B06-82C1-97838E9A1946, 1998.
- Barnes, J. and Upstill-Goddard, R. C.: N₂O seasonal distributions and air-sea exchange in UK estuaries: Implications for the tropospheric N₂O source from European coastal waters, *J. Geophys. Res. Biogeosciences*, 116(1), doi:10.1029/2009JG001156, 2011.
- Bass, A. M., O'Grady, D., Berkin, C., Leblanc, M., Tweed, S., Nelson, P. N. and Bird, M. I.: High diurnal variation in dissolved inorganic C, $\delta^{13}\text{C}$ values and surface efflux of CO₂ in a seasonal tropical floodplain, *Environ. Chem. Lett.*, 11(4), 399–405, doi:10.1007/s10311-013-0421-7, 2013.
- Beaulieu, J. J., Arango, C. P., Hamilton, S. K. and Tank, J. L.: The production and emission of nitrous oxide from headwater streams in the Midwestern United States, *Glob. Chang. Biol.*, 14(4), 878–894, doi:10.1111/j.1365-2486.2007.01485.x, 2008.
- Beaulieu, J. J., Shuster, W. D. and Rebholz, J. A.: Nitrous oxide emissions from a large, impounded river: The Ohio river, *Environ. Sci. Technol.*, 44(19), 7527–7533, doi:10.1021/es1016735, 2010.
- Beaulieu, J. J., Tank, J. L., Hamilton, S. K., Wollheim, W. M., Hall, R. O., Bernot, M. J., Burgin, A. J., Crenshaw, C. L., Helton, A. M., Johnson, L. T., Brien, J. M. O., Potter, J. D., Sheibley, R. W., Sobota, D. J. and Thomas, S. M.: Nitrous oxide emission from denitrification in stream and river networks, *PNAS*, 108(1), doi:10.1073/pnas.1011464108, 2011a.
- Beaulieu, J. J., Tank, J. L., Hamilton, S. K., Wollheim, W. M., Hall, R. O., Mulholland, P. J., Peterson, B. J., Ashkenas, L. R., Cooper, L. W., Dahm, C. N., Dodds, W. K., Grimm, N. B., Johnson, S. L., McDowell, W. H., Poole, G. C., Maurice Valett, H., Arango, C. P., Bernot, M. J., Burgin, A. J., Crenshaw, C. L., Helton, A. M., Johnson, L. T., O'Brien, J. M., Potter, J. D., Sheibley, R. W., Sobota, D. J. and Thomas, S. M.: Nitrous oxide emission from denitrification in stream and river networks, *Proc. Natl. Acad. Sci. U. S. A.*, 108(1), 214–219, doi:10.1073/pnas.1011464108, 2011b.
- Beaulieu, J. J., Tank, J. L., Hamilton, S. K., Wollheim, W. M., Hall, R. O., Mulholland, P. J., Peterson, B. J., Ashkenas, L. R., Cooper, L. W., Dahm, C. N., Dodds, W. K., Grimm, N. B., Johnson, S. L., McDowell, W. H., Poole, G. C., Maurice Valett, H., Arango, C. P., Bernot, M. J., Burgin, A. J., Crenshaw, C. L., Helton, A. M., Johnson, L. T., O'Brien, J. M., Potter, J. D., Sheibley, R. W., Sobota, D. J. and Thomas, S. M.: Nitrous oxide emission from denitrification in stream and river networks, *Proc. Natl. Acad. Sci. U. S. A.*, 108(1), 214–219, doi:10.1073/pnas.1011464108, 2011c.

Bekic, D., Ervine, D. A. and Lardet, P.: A COMPARISON OF ONE- AND TWO-DIMENSIONAL MODEL SIMULATION OF THE CLYDE ESTUARY HYDRODYNAMICS, in 7th Conference on Hydrosience and Engineering, Philadelphia, USA., 2005.

Bernard, B. B.: Methane in marine sediments, *Deep Sea Res.*, 26A(1966), 429–443, doi:0011-7471/9/0401-0429 502.00.0, 1978.

Billett, M. F. and Moore, T. R.: Supersaturation and evasion of CO₂ and CH₄ in surface waters at Mer Bleue peatland, Canada, *Hydrological Process.*, 22(November 2008), 2044–2054, doi:10.1002/hyp, 2008.

Billett, M. F., Garnett, M. H. and Harvey, F.: UK peatland streams release old carbon dioxide to the atmosphere and young dissolved organic carbon to rivers, *Geophys. Res. Lett.*, 34(23), 2–7, doi:10.1029/2007GL031797, 2007.

Birch, G. F., Gunns, T. J. and Olmos, M.: Sediment-bound metals as indicators of anthropogenic change in estuarine environments, *Mar. Pollut. Bull.*, 101(1), 243–257, doi:10.1016/j.marpolbul.2015.09.056, 2015.

Black Culm Ltd: VisitMyHarbour.com, [online] Available from: https://www.visitmyharbour.com/harbours/east-and-north-scotland/port_edgar/chart/9115A8E6D3D61/chart-of-port-edgar-and-approaches (Accessed 28 April 2021), 2018.

Blake, L. I., Sherry, A., Mejeha, O. K., Leary, P., Coombs, H., Stone, W., Head, I. M. and Gray, N. D.: An unexpectedly broad thermal and salinity-tolerant estuarine methanogen community, *Microorganisms*, 8(10), 1–10, doi:10.3390/microorganisms8101467, 2020.

BODC: National Oceanography Centre: British Oceanographic Data Centre, [online] Available from: <https://www.bodc.ac.uk/> (Accessed 23 December 2020), 2020.

Bogard, M. J., Kuhn, C. D., Johnston, S. E., Striegl, R. G., Holtgrieve, G. W., Dornblaser, M. M., Spencer, R. G. M., Wickland, K. P. and Butman, D. E.: Negligible cycling of terrestrial carbon in many lakes of the arid circumpolar landscape, *Nat. Geosci.*, 12(3), 180–185, doi:10.1038/s41561-019-0299-5, 2019.

Borges, A. V. and Abril, G.: *Carbon Dioxide and Methane Dynamics in Estuaries*, Elsevier Inc., 2012.

Borges, A. V., Champenois, W., Gypens, N., Delille, B. and Harlay, J.: Massive marine methane emissions from near-shore shallow coastal areas, *Sci. Rep.*, 6(June), 2–9, doi:10.1038/srep27908, 2016.

Borges, A. V., Darchambeau, F., Lambert, T., Bouillon, S., Morana, C., Brouyère, S., Hakoun, V., Jurado, A., Tseng, H. C., Descy, J. P. and Roland, F. A. E.: Effects of agricultural land use on fluvial carbon dioxide, methane and nitrous oxide concentrations in a large European river, the Meuse (Belgium), *Sci. Total Environ.*, 610–611, 342–355, doi:10.1016/j.scitotenv.2017.08.047, 2018.

Borges, A. V., Darchambeau, F., Lambert, T., Morana, C., Allen, G. H., Tambwe, E., Toengaho Sembaito, A., Mambo, T., Wabakhangazi, J. N., Descy, J. P., Teodoru, C. R. and Bouillon, S.: Variations in dissolved greenhouse gases (CO₂, CH₄, N₂O) in the Congo River network overwhelmingly driven by fluvial-wetland connectivity, *Biogeosciences*, 16(19), 3801–3834, doi:10.5194/bg-16-3801-2019, 2019.

Bosse, U., Frenzel, P. and Conrad, R.: Inhibition of methane oxidation by ammonium in the surface layer of a littoral sediment, *FEMS Microbiol. Ecol.*, 13(2), 123–134, doi:10.1016/0168-

6496(93)90030-B, 1993.

Bowes, M. J., Smith, J. T., Jarvie, H. P. and Neal, C.: Modelling of phosphorus inputs to rivers from diffuse and point sources, *Sci. Total Environ.*, 395(2–3), 125–138, doi:10.1016/j.scitotenv.2008.01.054, 2008.

Brase, L., Bange, H. W., Lendt, R., Sanders, T. and Dähnke, K.: High resolution measurements of nitrous oxide (N₂O) in the Elbe estuary, *Front. Mar. Sci.*, 4(MAY), 1–11, doi:10.3389/fmars.2017.00162, 2017.

Breitburg, D.: Effects of hypoxia, and the balance between hypoxia and enrichment, on coastal fishes and fisheries, *Estuaries*, 25(4b), 767–781, 2002.

British Geological Survey: BGS Geology Viewer, 2022.

British Geological Survey: Geindex Onshore, Geindex Onshore - MapApps2 [online] Available from: <https://mapapps2.bgs.ac.uk/geindex/home.html>, 2023.

Broder, T., Blodau, C., Biester, H. and Knorr, K. H.: Peat decomposition records in three pristine ombrotrophic bogs in southern Patagonia, *Biogeosciences*, 9(4), 1479–1491, doi:10.5194/bg-9-1479-2012, 2012.

Brown, A. ., Van Dijk, N. and Pickard, A. E.: Greenhouse gas and water chemistry measurements for the Clyde river, tributaries and estuary, 2021-2022, *Environ. Inf. Data Cent.*, doi:<https://doi.org/10.5285/c3527258-c9ab-40d9-af0c-ddedabbd67a1>, 2023a.

Brown, A. M. and Pickard, A. E.: Physico-chemical water properties and greenhouse gas measurements across a tidal cycle, Clyde estuary, Scotland, 2020-2022, *Environ. Inf. Data Cent.*, 2023.

Brown, A. M., Bass, A. M. and Pickard, A. E.: Anthropogenic-estuarine interactions cause disproportionate greenhouse gas production: A review of the evidence base, *Mar. Pollut. Bull.*, 174(July 2021), 113240, doi:10.1016/j.marpolbul.2021.113240, 2022.

Brown, A. M., van Dijk, N. and Pickard, A. E.: Greenhouse gas and water chemistry measurements for the Clyde river, tributaries and estuary, 2021-2022, *Environ. Inf. Data Cent.* [online] Available from: <https://doi.org/10.5285/c3527258-c9ab-40d9-af0c-ddedabbd67a1>, 2023b.

Brown, A. M., While, S., Hurst, E., Corr, M., Grant, A., Olszewska, J., Toteva, G. and Pickard, A. E.: Physico-chemical water properties and greenhouse gas measurements along a longitudinal estuary transect, Clyde estuary, Scotland, 2020-2022, NERC EDS *Environ. Inf. Data* [online] Available from: <https://doi.org/10.5285/a22b495e-b2cd-43cd-95b7-8712b64dc0da>, 2023c.

Brown, A. M., Bass, A. M., Skiba, U., MacDonald, J. M. and Pickard, A. E.: Urban landscapes and legacy industry provide hotspots for riverine greenhouse gases: A source-to-sea study of the River Clyde, *Water Res.*, 236(April), 119969, doi:10.1016/j.watres.2023.119969, 2023d.

Brown, M.: U.S. mining sites dump 50 million gallons of fouled wastewater daily, *Public Broadcast. Serv.* [online] Available from: <https://www.pbs.org/newshour/nation/u-s-mining-sites-dump-50-million-gallons-of-fouled-wastewater-daily>, 2019.

Bruckschen, P., Oesmann, S. and Veizer, J.: Isotope stratigraphy of the European Carboniferous: Proxy signals for ocean chemistry, climate and tectonics, *Chem. Geol.*, 161(1), 127–163, doi:10.1016/S0009-2541(99)00084-4, 1999.

Burgos, M., Sierra, A., Ortega, T. and Forja, J. M.: Anthropogenic effects on greenhouse gas (CH₄ and N₂O) emissions in the Guadalete River Estuary (SW Spain), *Sci. Total Environ.*, 503–504, 179–189, doi:10.1016/j.scitotenv.2014.06.038, 2015.

Campeau, A. and Del Giorgio, P. A.: Patterns in CH₄ and CO₂ concentrations across boreal rivers: Major drivers and implications for fluvial greenhouse emissions under climate change scenarios, *Glob. Chang. Biol.*, 20(4), 1075–1088, doi:10.1111/gcb.12479, 2014.

Candeias, C., Ávila, P., Coelho, P. and Teixeira, J. P.: Mining activities: Health impacts, *Encycl. Environ. Heal.*, 415–435, doi:10.1016/B978-0-12-409548-9.11056-5, 2019.

Canmore: Ravenscraig Steelworks, Motherwell, Natl. Rec. Hist. environment [online] Available from: https://canmore.org.uk/site/70181/motherwell-ravenscraig-steelworks?display=image&images_page=3, 2022.

Carvalho, F. P.: Mining industry and sustainable development: Time for change, *Food Energy Secur.*, 6(2), 61–77, doi:10.1002/fes3.109, 2017.

Catizzone, E., Sposato, C., Romanelli, A., Barisano, D., Cornacchia, G., Marsico, L., Cozza, D. and Migliori, M.: Purification of Wastewater from Biomass-Derived Syngas Scrubber Using Biochar and Activated Carbons, *Int. J. Environ. Res. Public Health*, 2021.

Chapman, P. M. and Wang, F.: Assessing sediment contamination in estuaries, *Environ. Toxicol. Chem.*, 20(1), 3–22, doi:10.1002/etc.5620200102, 2001.

Chen, Z., Pavelic, P., Dillon, P. and Naidu, R.: Determination of caffeine as a tracer of sewage effluent in natural waters by on-line solid-phase extraction and liquid chromatography with diode-array detection, *Water Res.*, 36, 4830–4838, 2002.

Cheng, X., Huang, Y., Li, R., Pu, X., Huang, W. and Yuan, X.: Impacts of water temperature on phosphorus release of sediments under flowing overlying water, *J. Contam. Hydrol.*, 235(24), 103717, doi:10.1016/j.jconhyd.2020.103717, 2020.

Ciais, P., Sabine, C., Bala, G., Bopp, L., Brovkin, V., Canadell, J., Chhabra, A., DeFries, R., Galloway, J., Heimann, M., Jones, C., Quéré, C. Le, Myneni, R. B., Piao, S. and Thornton, P.: Carbon and Other Biogeochemical Cycles. In: *Climate Change 2013; in The Physical Science Basis. Contribution of Working Group I to the Fifth Assessment Report of the Intergovernmental Panel on Climate Change*, edited by V. B. and P. M. M. (eds.). [Stocker, T.F., D. Qin, G.-K. Plattner, M. Tignor, S.K. Allen, J. Boschung, A. Nauels, Y. Xia, Cambridge University Press, Cambridge, United Kingdom and New York, NY, USA., 2013.

Clark, J. F., Schlosser, P., Simpson, H. J., Stute, M., Wanninkhof, R. and Ho, D. T.: Relationship between gas transfer velocities and wind speeds in the tidal Hudson River determined by dual tracer technique, *Air-water gas Transf.*, 785–800 [online] Available from: http://hci.iwr.uni-heidelberg.de/publications/dip/1995/AWGT1995/CHAPTERS/6_11.PDF, 1995.

Clyde River Foundation: The Clyde catchment, [online] Available from: <https://www.clyderiverfoundation.org/clyde-catchment/>, 2020.

Cole, L. J., Stockan, J. and Helliwell, R.: Agriculture , Ecosystems and Environment Managing riparian buffer strips to optimise ecosystem services : A review, *Agric. Ecosyst. Environ.*, 296(April), 106891, doi:10.1016/j.agee.2020.106891, 2020.

Conley, D. J., Carstensen, J., Ærtebjerg, G., Christensen, P. B., Dalsgaard, T., Hansen, J. L. S. and Josefson, A. B.: Long-term changes and impacts of hypoxia in Danish coastal waters, *Ecol. Appl.*, 17(5

SUPPL.), 165–184, doi:10.1890/05-0766.1, 2007.

Cooper, M. D. A., Estop-Aragonés, C., Fisher, J. P., Thierry, A., Garnett, M. H., Charman, D. J., Murton, J. B., Phoenix, G. K., Treharne, R., Kokelj, S. V., Wolfe, S. A., Lewkowicz, A. G., Williams, M. and Hartley, I. P.: Limited contribution of permafrost carbon to methane release from thawing peatlands, *Nat. Clim. Chang.*, 7(7), 507–511, doi:10.1038/nclimate3328, 2017.

Cotovicz, L. C., Ribeiro, R. P., Régis, C. R., Bernardes, M., Sobrinho, R., Vidal, L. O., Tremmel, D., Knoppers, B. A. and Abril, G.: Greenhouse gas emissions (CO₂ and CH₄) and inorganic carbon behavior in an urban highly polluted tropical coastal lagoon (SE, Brazil), *Environ. Sci. Pollut. Res.*, 28(28), 38173–38192, doi:10.1007/s11356-021-13362-2, 2021.

Dai, X., Zhou, Y., Ma, W. and Zhou, L.: Influence of spatial variation in land-use patterns and topography on water quality of the rivers inflowing to Fuxian Lake, a large deep lake in the plateau of southwestern China, *Ecol. Eng.*, 99, 417–428, doi:10.1016/j.ecoleng.2016.11.011, 2017.

Dar, S. A., Kleerebezem, R., Stams, A. J. M., Kuenen, J. G. and Muyzer, G.: Competition and coexistence of sulfate-reducing bacteria, acetogens and methanogens in a lab-scale anaerobic bioreactor as affected by changing substrate to sulfate ratio, *Appl. Microbiol. Biotechnol.*, 78(6), 1045–1055, doi:10.1007/s00253-008-1391-8, 2008.

Davidson, T. A., Audet, J., Jeppesen, E., Landkildehus, F., Lauridsen, T. L., Søndergaard, M. and Syväranta, J.: Synergy between nutrients and warming enhances methane ebullition from experimental lakes, *Nat. Clim. Chang.*, 8(2), 156–160, doi:10.1038/s41558-017-0063-z, 2018.

Dean, M. T., Browne, M. A. E., Waters, C. N. and Powell, J. H.: A lithostratigraphical framework for the Carboniferous successions of northern Great Britain (onshore), *Br. Geol. Surv. Res. Rep. RR/09/01*, 174, 2011.

Dessandier, P.-A., Bonnin, J., Kim, J.-H., Bichon, S., Deflandre, B., Gremare, A. and Sinninghe Damste, J. S.: *Journal of Geophysical Research: Biogeosciences*, *J. Geophys. Res. Biogeosciences*, 1689–1714, doi:10.1002/2016JG003328. Received, 2016.

Dhir, B.: *Biotechnological Tools for Remediation of Acid Mine Drainage (Removal of Metals From Wastewater and Leachate)*, Elsevier Inc., 2018.

Dinsmore, K. J., Billett, M. F. and Dyson, K. E.: Temperature and precipitation drive temporal variability in aquatic carbon and GHG concentrations and fluxes in a peatland catchment, *Glob. Chang. Biol.*, 19(7), 2133–2148, doi:10.1111/gcb.12209, 2013.

Dong, L. F., Thornton, D. C. O., Nedwell, D. B. and Underwood, G. J. C.: Denitrification in sediments of the River Colne estuary, England, *Mar. Ecol. Prog. Ser.*, 203, 109–122, doi:10.3354/meps203109, 2000.

Dong, L. F., Nedwell, D. B., Underwood, G. J. C., Thornton, D. C. O. and Rusmana, I.: Nitrous oxide formation in the Colne estuary in England: The central role of nitrite, *Appl. Environ. Microbiol.*, 68(3), 1240–1249, doi:10.1128/AEM.68.10.5202-5204.2002, 2002a.

Dong, L. F., Nedwell, D. B., Underwood, G. J. C., Thornton, D. C. O. and Rusmana, I.: Nitrous oxide formation in the Colne estuary in England: The central role of nitrite, *Appl. Environ. Microbiol.*, 68(3), 1240–1249, doi:10.1128/AEM.68.10.5202-5204.2002, 2002b.

Dong, L. F., Nedwell, D. B., Colbeck, I. and Finch, J.: Nitrous oxide emission from some English and Welsh rivers and estuaries, *Water, Air, Soil Pollut. Focus*, 4(6), 127–134, doi:10.1007/s11267-005-3022-z, 2005.

Dong, X. M., Ma, S. N., Wang, H. J., Li, Y. Y., Li, Y. and Xu, J. L.: Dissolved Organic Carbon Loading Stimulates Sediment Phosphorus Mobilization and Release: Preliminary Evidence From Xiangshan Port, East China Sea, *Front. Environ. Sci.*, 9(January), 1–10, doi:10.3389/fenvs.2021.782701, 2022.

Drake, T. W., Raymond, P. A. and Spencer, R. G. M.: Terrestrial carbon inputs to inland waters: A current synthesis of estimates and uncertainty, *Limnol. Oceanogr. Lett.*, 3(3), 132–142, doi:10.1002/lol2.10055, 2018.

Dunfield, P. and Knowles, R.: Kinetics of inhibition of methane oxidation by nitrate, nitrite, and ammonium in a humisol, *Appl. Environ. Microbiol.*, 61(8), 3129–3135, doi:10.1128/aem.61.8.3129-3135.1995, 1995.

Dürr, H. H., Laruelle, G. G., van Kempen, C. M., Slomp, C. P., Meybeck, M. and Middelkoop, H.: Worldwide Typology of Nearshore Coastal Systems: Defining the Estuarine Filter of River Inputs to the Oceans, *Estuaries and Coasts*, 34(3), 441–458, doi:10.1007/s12237-011-9381-y, 2011.

Eadha Enterprises: Glentaggart Opencast Mine Woodland Project, [online] Available from: http://www.eadha.co.uk/projects/331_glentaggart_opencast_mine_woodland_project, 2023.

Edgar, P. J., Hursthouse, A. S., Matthews, J. E. and Davies, I. M.: An investigation of geochemical factors controlling the distribution of PCBs in intertidal sediments at a contamination hot spot, the Clyde Estuary, UK, *Appl. Geochemistry*, 18(2), 327–338, doi:10.1016/S0883-2927(02)00128-2, 2003.

Edgar, P. J., Hursthouse, A. S., Matthews, J. E., Davies, I. M. and Hillier, S.: Sediment influence on congener-specific PCB bioaccumulation by *Mytilus edulis*: A case study from an intertidal hot spot, Clyde Estuary, UK, *J. Environ. Monit.*, 8(9), 887–896, doi:10.1039/b606960f, 2006.

EEC: 1991b Council Directive 91/271/EEC Concerning Urban Waste Water Treatment, L 135, *Official Journal of the European Community*, Brussels, , 34(May 1991), 1–16 [online] Available from: <https://eur-lex.europa.eu/LexUriServ/LexUriServ.do?uri=CONSLEG:1991L0271:20081211:EN:PDF>, 1991.

Energy Institute: *Statistical Review of World Energy.*, 2023.

Environment Agency: Water quality data archive, [online] Available from: <https://environment.data.gov.uk/water-quality/view/landing> (Accessed 23 December 2020), 2020.

Environmental Agency: *State of the Tees Estuary environment, and strategy into the millennium, 1999.*

Euler, S., Jeffrey, L. C., Maher, D. T., Mackenzie, D. and Tait, D. R.: Shifts in methanogenic archaea communities and methane dynamics along a subtropical estuarine land use gradient, *PLoS One*, 15(11 November), doi:10.1371/journal.pone.0242339, 2020.

European Commission (Directorate General Environment): *European Commission Urban Waste Water Website: United Kingdom*, [online] Available from: <https://uwatd.eu/United-Kingdom/> (Accessed 23 December 2020), 2016.

Feng, W., Gao, J., Wei, Y., Liu, D., Yang, F., Zhang, Q. and Bai, Y.: Pattern changes of microbial communities in urban river affected by anthropogenic activities and their environmental driving mechanisms, *Environ. Sci. Eur.*, 34(1), 1–13, doi:10.1186/s12302-022-00669-1, 2022.

Fernando, S.: *Update of Estimated Methane Emissions from UK Abandoned Coal Mines*, , (May) [online] Available from: www.wspenvironmental.com, 2011.

- Ferrón, S., Ortega, T., Gómez-Parra, A. and Forja, J. M.: Seasonal study of dissolved CH₄, CO₂ and N₂O in a shallow tidal system of the bay of Cádiz (SW Spain), *J. Mar. Syst.*, 66(1–4), 244–257, doi:10.1016/j.jmarsys.2006.03.021, 2007.
- Ferrón, S., Ortega, T. and Forja, J. M.: Temporal and spatial variability of methane in the north-eastern shelf of the Gulf of Cádiz (SW Iberian Peninsula), *J. Sea Res.*, 64(3), 213–223, doi:10.1016/j.seares.2010.02.007, 2010.
- Findlay, S., McDowell, W. H., Fischer, D., Pace, M. L., Caraco, N., Kaushal, S. S. and Weathers, K. C.: Total carbon analysis may overestimate organic carbon content of fresh waters in the presence of high dissolved inorganic carbon, *Limnol. Oceanogr. Methods*, 8(MAY), 196–201, doi:10.4319/lom.2010.8.196, 2010.
- Fleming, C., Morrison, K., Robba, L., Reynolds, J. and Wright, I. A.: 14-Month Water Quality Investigation of Coal Mine Discharge on Two Rivers in NSW, Australia: Implications for Environmental Regulation, *Water. Air. Soil Pollut.*, 232(3), doi:10.1007/s11270-021-05020-7, 2021.
- Fleming, C., Belmer, N., Reynolds, J. K., Robba, L., Davies, P. J. and Wright, I. A.: Legacy Contamination of River Sediments from Four Decades of Coal Mine Effluent Inhibits Ecological Recovery of a Polluted World Heritage Area River, *Water. Air. Soil Pollut.*, 233(1), doi:10.1007/s11270-021-05487-4, 2022.
- Florence, K., Sapsford, D. J., Johnson, D. B., Kay, C. M. and Wolkersdorfer, C.: Iron-mineral accretion from acid mine drainage and its application in passive treatment, *Environ. Technol. (United Kingdom)*, 37(11), 1428–1440, doi:10.1080/09593330.2015.1118558, 2016.
- Fordyce, F. ., Everett, P. ., Bearcock, J. ., Lister, T. ., Gowing, C., Watts, M. and Ellen, R.: Soil geochemical atlas of the Clyde Basin. [online] Available from: <http://nora.nerc.ac.uk/id/eprint/519195/>, 2017.
- Foster, S. Q. and Fulweiler, R. W.: Estuarine Sediments Exhibit Dynamic and Variable Biogeochemical Responses to Hypoxia, *J. Geophys. Res. Biogeosciences*, 124(4), 737–758, doi:10.1029/2018JG004663, 2019.
- Franklin, M. J., Wiebe, W. J. and Whitman, W. B.: Populations of Methanogenic Bacteria in a Georgia Salt Marsh, *Appl. Environ. Microbiol.*, 54(5), 1151–1157, doi:10.1128/aem.54.5.1151-1157.1988, 1988.
- Frey, C., Bange, H. W., Achterberg, E. P., Jayakumar, A., Löscher, C. R., Arévalo-martínez, D. L., León-palmero, E., Sun, M., Sun, X. and Xie, R. C.: Regulation of nitrous oxide production in low-oxygen waters off the coast of Peru, *Biogeosciences*, 17, 2263–2287, 2020.
- Furukawa, Y., Inubushi, K. and Furukawa, Y.: Effect of application of iron materials on methane and nitrous oxide emissions from two types of paddy soils, *Soil Sci. Plant Nutr.*, 50(6), 917–924, doi:10.1080/00380768.2004.10408554, 2004.
- Gao, Y., Jia, J., Lu, Y., Sun, K., Wang, J. and Wang, S.: Carbon transportation, transformation, and sedimentation processes at the land-river-estuary continuum, *Fundam. Res.*, (xxxx), doi:10.1016/j.fmre.2022.07.007, 2022.
- García-martín, E. E., Sanders, R., Evans, C. D. and Kitidis, V.: Contrasting Estuarine Processing of Dissolved Organic Matter Derived From Natural and Human-Impacted Landscapes, *Global Biogeochem. Cycles*, (C), 1–17, doi:10.1029/2021GB007023, 2021.
- García-Martín, E. E., Sanders, R., Evans, C. D., Kitidis, V., Lapworth, D. J., Rees, A. P., Spears, B. M.,

Tye, A., Williamson, J. L., Balfour, C., Best, M., Bowes, M., Breimann, S., Brown, I. J., Burden, A., Callaghan, N., Felgate, tacey L., Fishwick, J., Fraser, M., Gibb, S. W., Gilbert, P. J., Godsell, N., Gomez-Castillo, A. P., Hargreaves, G., Jones, O., Kennedy, P., Lichtschlag, A., Martin, A., May, R., Mawji, E., Mounteney, I., Nightingale, hilip D., Olszewska, J. P., Painter, S. C., Pearce, C. R., Pereira, M. G., Peel, K., Pickard, A., Stephens, J. A., Stinchcombe, M., Williams, P., Woodward, M. S., Yarrow, D. and Mayor, D. J.: Contrasting Estuarine Processing of Dissolved Organic Matter Derived From Natural and Human-Impacted Landscapes, *Glob. Biogeochem. Cycles*, (2393175), 2021.

Garnett, M. H., Billett, M. F., Gulliver, P. and Dean, J. F.: A new field approach for the collection of samples for aquatic $^{14}\text{CO}_2$ analysis using headspace equilibration and molecular sieve traps: the super headspace method, *Ecohydrology*, 9(8), 1630–1638, doi:10.1002/eco.1754, 2016.

Garnier, J., Billen, G., Vilain, G., Martinez, A., Silvestre, M., Mounier, E. and Toche, F.: Nitrous oxide (N_2O) in the Seine river and basin: Observations and budgets, *Agric. Ecosyst. Environ.*, 133(3–4), 223–233, doi:10.1016/j.agee.2009.04.024, 2009.

Gauci, V., Gowing, D. J. G., Hornibrook, E. R. C., Davis, J. M. and Dise, N. B.: Woody stem methane emission in mature wetland alder trees, *Atmos. Environ.*, 44(17), 2157–2160, doi:10.1016/j.atmosenv.2010.02.034, 2010.

Gelesh, L., Marshall, K., Boicourt, W. and Lapham, L.: Methane concentrations increase in bottom waters during summertime anoxia in the highly eutrophic estuary, Chesapeake Bay, U.S.A., *Limnol. Oceanogr.*, 61, S253–S266, doi:10.1002/lno.10272, 2016.

Gerling, A. B., Browne, R. G., Gantzer, P. A., Mobley, M. H., Little, J. C. and Carey, C. C.: First report of the successful operation of a side stream supersaturation hypolimnetic oxygenation system in a eutrophic, shallow reservoir, *Water Res.*, 67, 129–143, doi:10.1016/j.watres.2014.09.002, 2014.

Glasgow World: Human sewage sludge plan for Dalquhandy opencast site, *Glas. World* [online] Available from: <https://www.glasgowworld.com/news/human-sewage-sludge-plan-for-dalquhandy-opencast-site-2083872>, 2017.

GMI: Global Methane Initiative (GMI) - Municipal Wastewater Technical Group, 2023 [online] Available from: <https://www.globalmethane.org/biogas/ww.aspx>, 2023.

Gómez-Gener, L., von Schiller, D., Marcé, R., Arroita, M., Casas-Ruiz, J. P., Staehr, P. A., Acuña, V., Sabater, S. and Obrador, B.: Low contribution of internal metabolism to carbon dioxide emissions along lotic and lentic environments of a Mediterranean fluvial network, *J. Geophys. Res. Biogeosciences*, 121(12), 3030–3044, doi:10.1002/2016JG003549, 2016.

Gong, C., Yan, W., Zhang, P., Yu, Q., Li, Y., Li, X., Wang, D. and Jiao, R.: Effects of stream ecosystem metabolisms on CO_2 emissions in two headwater catchments, Southeastern China, *Ecol. Indic.*, 130, 108136, doi:10.1016/j.ecolind.2021.108136, 2021.

Gonzalez Moguel, R., Vogel, F., Ars, S., Schaefer, H., Turnbull, J. and Douglas, P.: Using carbon-14 and carbon-13 measurements for source attribution of atmospheric methane in the Athabasca Oil Sands Region, *Atmos. Chem. Phys. Discuss.*, (August), 1–21, doi:10.5194/acp-2021-622, 2021.

Gopinath, A., Divyapriya, G., Srivastava, V., Laiju, A. R., Nidheesh, P. V and Kumar, M. S.: Conversion of sewage sludge into biochar : A potential resource in water and wastewater treatment, *Environ. Res.*, 194(December 2020), 110656, doi:10.1016/j.envres.2020.110656, 2021.

Grossart, H. P., Frindte, K., Dziallas, C., Eckert, W. and Tang, K. W.: Microbial methane production in oxygenated water column of an oligotrophic lake, *Proc. Natl. Acad. Sci. U. S. A.*, 108(49), 19657–19661, doi:10.1073/pnas.1110716108, 2011.

- Gu, C., Waldron, S. and Bass, A. M.: Carbon dioxide, methane, and dissolved carbon dynamics in an urbanized river system, *Hydrol. Process.*, 35(9), 1–17, doi:10.1002/hyp.14360, 2021.
- Gulshin, I. and Gogina, E.: Global importance of methane emissions from drainage ditches and canals OPEN ACCESS Global importance of methane emissions from drainage ditches and canals, 2021.
- H. J. Skinner: Waste Problems in the Pulp and Paper Industry, *Ind. Eng. Chem.*, 31(11), 1331–1335 [online] Available from: <https://pubs.acs.org/doi/pdf/10.1021/ie50359a006#>, 1939.
- Hall, J. A., Frid, C. L. J. and Proudfoot, R. K.: Effects of metal contamination on macrobenthos of two North Sea estuaries, *ICES J. Mar. Sci.*, 53(6), 1014–1023, doi:10.1006/jmsc.1996.0127, 1996.
- Hamilton, D. J., Bulmer, R. H., Schwendenmann, L. and Lundquist, C. J.: Nitrogen enrichment increases greenhouse gas emissions from emerged intertidal sandflats, *Sci. Rep.*, 10(1), 1–14, doi:10.1038/s41598-020-62215-4, 2020.
- Hamilton, S.: Prediction of dissolved gas concentrations in water at atmospheric equilibrium, , 3–6 [online] Available from: https://lter.kbs.msu.edu/docs/linx/linx2/linx2_dissolved_gas_headspace_equilibration_calcs.pdf, 2006.
- Hao, X., Ruihong, Y., Zhuangzhuang, Z., Zhen, Q., Xixi, L., Tingxi, L. and Ruizhong, G.: Greenhouse gas emissions from the water–air interface of a grassland river: a case study of the Xilin River, *Sci. Rep.*, 11(1), 1–14, doi:10.1038/s41598-021-81658-x, 2021.
- Harley, J. F., Carvalho, L., Dudley, B., Heal, K. V., Rees, R. M. and Skiba, U.: Spatial and seasonal fluxes of the greenhouse gases N₂O, CO₂ and CH₄ in a UK macrotidal estuary, *Estuar. Coast. Shelf Sci.*, 153, 62–73, doi:10.1016/j.ecss.2014.12.004, 2015.
- Harris, P. T., Macmillan-Lawler, M., Rupp, J. and Baker, E. K.: Geomorphology of the oceans, *Mar. Geol.*, 352, 4–24, doi:10.1016/j.margeo.2014.01.011, 2014.
- Hedin, R. S. and Hedin, B. C.: The complicated role of CO₂ in mine water treatment, *Proc. IMWA 2016, Freiberg/Germany*, 3(TU), 844–849, 2016.
- Herlihy, A. T., Stoddard, J. L. and Johnson, C. B.: The relationship between stream chemistry and watershed land cover data in the mid-atlantic region, U.S., *Water. Air. Soil Pollut.*, 105(1–2), 377–386, doi:10.1023/A:1005028803682, 1998.
- Herrero Ortega, S., Romero González-Quijano, C., Casper, P., Singer, G. A. and Gessner, M. O.: Methane emissions from contrasting urban freshwaters: Rates, drivers, and a whole-city footprint, *Glob. Chang. Biol.*, 25(12), 4234–4243, doi:10.1111/gcb.14799, 2019.
- Hewett, C. J. M., Wilkinson, M. E., Jonczyk, J. and Quinn, P. F.: Catchment systems engineering: An holistic approach to catchment management, *Wiley Interdiscip. Rev. Water*, 7(3), 1–14, doi:10.1002/wat2.1417, 2020.
- Historic Environment Scotland: Canmore - Clyde Iron Works, Canmore [online] Available from: <https://canmore.org.uk/site/162565/glasgow-clyde-iron-works>, 2022.
- Ho, L., Jerves-Cobo, R., Barthel, M., Six, J., Bode, S., Boeckx, P. and Goethals, P.: Greenhouse gas dynamics in an urbanized river system: influence of water quality and land use, *Environ. Sci. Pollut. Res.*, 29(25), 37277–37290, doi:10.1007/s11356-021-18081-2, 2022.
- van der Hoek, J. P., Duijff, R. and Reinstra, O.: Nitrogen recovery from wastewater: Possibilities,

competition with other resources, and adaptation pathways, *Sustain.*, 10(12), doi:10.3390/su10124605, 2018.

Hope, D., Palmer, S. M., Billett, M. F. and Dawson, J. J. C.: Carbon dioxide and methane evasion from a temperate peatland stream, *Limnol. Oceanogr.*, 46(4), 847–857, doi:10.4319/lo.2001.46.4.0847, 2001.

Hotchkiss, E. R., Hall, R. O., Sponseller, R. A., Butman, D., Klaminder, J., Laudon, H., Rosvall, M. and Karlsson, J.: Sources of and processes controlling CO₂ emissions change with the size of streams and rivers, *Nat. Geosci.*, 8(9), 696–699, doi:10.1038/ngeo2507, 2015.

Hsu, L. C., Tzou, Y. M., Liao, W. H., Teah, H. Y. and Liu, Y. T.: Transformation of sedimentary and colloidal phosphorus across the land–sea margin received effluents from agricultural and municipal activities, *J. Clean. Prod.*, 379(P2), 134686, doi:10.1016/j.jclepro.2022.134686, 2022.

Hursthouse, A. S., Matthews, J., Figures, J., Iqbal-Zahid, P., Davies, I. M. and Vaughan, D. H.: Chromium Behaviour in Intertidal Sediments and Pore Waters, R, Clyde, UK, *Environ. Geochem. Health*, 23, 253–259, 2001.

Hursthouse, A. S., Matthews, J. M., Figures, J. E., Iqbal-Zahid, P., Davies, I. M. and Vaughan, D. H.: Chromium in intertidal sediments of the Clyde, UK: Potential for remobilisation and bioaccumulation, *Environ. Geochem. Health*, 25(2), 171–203, doi:10.1023/A:1023201827528, 2003.

IEA: Methane Tracker 2020. [online] Available from: www.iea.org/reports/methane-tracker-2020, 2020.

Institute for Government: UK net zero target, [online] Available from: <https://www.instituteforgovernment.org.uk/explainers/net-zero-target>, 2020.

International Energy Agency: Market Report Series: Coal 2018. [online] Available from: www.iea.org/t&c/, 2018.

International Energy Agency: Coal 2022. [online] Available from: <https://iea.blob.core.windows.net/assets/91982b4e-26dc-41d5-88b1-4c47ea436882/Coal2022.pdf>, 2022.

IPCC: IPCC Guidelines for National Greenhouse Gas Inventories - Volume 2 Energy - Chapter 4 Fugitive Emissions., 2006.

IPCC: Summary for Policymakers, *Clim. Chang. 2013 Phys. Sci. Basis. Contrib. Work. Gr. I to Fifth Assess. Rep. Intergov. Panel Clim. Chang.* [Stocker T.F., D. Qin, G.-K. Plattner, M. Tignor, S.K. Allen, J. Boschung, A. Nauels, Y. Xia, , 2013.

IPCC: 2019 Refinement to the 2006 IPCC Guidelines for National Greenhouse Gas Inventories - Volume 2 Energy - Chapter 4 Fugitive Emissions, *IPCC Natl. Greenh. Gas Invent. Program. Calvo Buendia, E., Tanabe, K., Kranjc, A., Baasansuren, J., Fukuda, M., Ngarize S., Osako, A., Pyrozhenko, Y., Shermanau, P. Federici, S. (eds).*, 2, 56–74, doi:10.1007/978-1-4939-6911-1, 2019.

IPCC: Summary for Policymakers., 2021a.

IPCC: The Physical Science Basis. Contribution of Working Group I to the Sixth Assessment Report of the Intergovernmental Panel on Climate Change, *Clim. Chang. 2021* [Masson-Delmotte, V., P. Zhai, A. Pirani, S.L. Connors, C. Péan, S. Berger. N. Caud, Y. Chen, L. Goldfarb, M.I. Gomis, M. Huang, K. Leitzell, E. Lonnoy, J.B.R. Matthews, T.K. Maycock, T. Waterfield, O. Yelekçi, R. Yu, B. Zhou, 2391, doi:doi:10.1017/9781009157896, 2021b.

IPCC: Summary for Policymakers - Longer report: Synthesis Report. A Report of the Intergovernmental Panel on Climate Change. Contribution of Working Groups I, II and III to the Sixth Assessment Report of the Intergovernmental Panel on Climate Change, Clim. Chang. [Core Writ. Team, H. Lee J. Romero (eds.)] [online] Available from: https://www.ipcc.ch/report/ar6/syr/downloads/report/IPCC_AR6_SYR_SPM.pdf, 2023a.

IPCC: Synthesis report: Summary for Policy makers I. [online] Available from: <https://eur-lex.europa.eu/legal-content/PT/TXT/PDF/?uri=CELEX:32016R0679&from=PT%0Ahttp://eur-lex.europa.eu/LexUriServ/LexUriServ.do?uri=CELEX:52012PC0011:pt:NOT>, 2023b.

IPCC, (Netherlands), M. R. J. D., (Thailand), S. T., (Brazil), S. M. M. V., (USA), W. I., (Canada), C. P., (Finland), R. P. and (China), C. W.: Volume 5: Waste - Chapter 6 Wastewater Treatment and. [online] Available from: www.ipcc-nggip.iges.or, 2006.

Iram, A., Akhtar, K. and Ghauri, M. A.: Coal methanogenesis: a review of the need of complex microbial consortia and culture conditions for the effective bioconversion of coal into methane, *Ann. Microbiol.*, 67(3), 275–286, doi:10.1007/s13213-017-1255-5, 2017.

Isnansetyo, A., Getsu, S., Segeguchi, M. and Koriyama, M.: Independent Effects of Temperature, Salinity, Ammonium Concentration and pH on Nitrification Rate of the Ariake Seawater Above Mud Sediment, *HAYATI J. Biosci.*, 21(1), 21–30, doi:10.4308/hjb.21.1.21, 2014.

Jarosławiecka, A. K. and Piotrowska-Seget, Z.: The Effect of Heavy Metals on Microbial Communities in Industrial Soil in the Area of Piekary Śląskie and Bukowno (Poland), *Microbiol. Res. (Pavia)*, 13(3), 626–642, doi:10.3390/microbiolres13030045, 2022.

Jarvie, H. P., King, S. M. and Neal, C.: Inorganic carbon dominates total dissolved carbon concentrations and fluxes in British rivers: Application of the THINCARB model – Thermodynamic modelling of inorganic carbon in freshwaters, *Sci. Total Environ.*, 575(October), 496–512, doi:10.1016/j.scitotenv.2016.08.201, 2017.

Jarvis, A. P.: The role of dissolved carbon dioxide in governing deep coal mine water quality and determining treatment process selection, 7th Int. Conf. Acid Rock Drain. 2006, ICARD - Also Serves as 23rd Annu. Meet. Am. Soc. Min. Reclam., 1, 833–843, doi:10.21000/jasmr06020833, 2006.

Johnston, D., Potter, H., Jones, C., Rolley, S., Watson, I. and Pritchard, J.: Abandoned mines and the water environment., 2008.

Jones, D. G., Vane, C. H., Lass-Evans, S., Chenery, S., Lister, B., Cave, M., Gafeira, J., Jenkins, G., Leslie, A., Breward, N., Freeborough, K., Harrison, I., Kim, A. W., Lacinska, A., Milodowski, T., Ridgway, J., Riding, J., Strutt, M., Wagner, D. and Wilkinson, I.: Geochemistry and related studies of Clyde Estuary sediments, *Earth Environ. Sci. Trans. R. Soc. Edinburgh*, 108(2–3), 269–288, doi:10.1017/S1755691018000348, 2019.

Jones, G. and Ahmed, S.: The impact of coastal flooding on conservation areas: A study of the Clyde Estuary, Scotland, *J. Coast. Conserv.*, 6(2), 171–180, doi:10.1007/BF02913813, 2000.

Jones, N. S., Holloway, S., Creedy, D. P., Garner, K., Smith, N. J. P., Browne, M. A. E. and Durucan, S.: UK Coal Resource for New Exploitation Technologies Final Report UK Coal Resource for New Exploitation Technologies Final Report., 2004.

Kamali, M., Appels, L., Kwon, E. E., Aminabhavi, T. M. and Dewil, R.: Biochar in water and wastewater treatment - a sustainability assessment, *Chem. Eng. J.*, 420(P1), 129946, doi:10.1016/j.cej.2021.129946, 2021.

- Karunaratna, H.: Modelling the long-term morphological evolution of the Clyde Estuary, Scotland, UK, *J. Coast. Conserv.*, 15(4), 499–507, doi:10.1007/s11852-010-0138-8, 2011.
- Keith, M. L. and Weber, J. N.: Carbon and oxygen isotopic composition of selected limestones and fossils, *Geochim. Cosmochim. Acta*, 28(10–11), 1787–1816, doi:10.1016/0016-7037(64)90022-5, 1964.
- Kennish, M. J.: Pollution in Estuaries and Coastal Marine Waters, *J. Coast. Res.*, (12), 27–49 [online] Available from: http://www.jstor.orghttp://www.jstor.org/stable/25735588http://www.jstor.org/stable/25735588?seq=1&cid=pdf-reference#references_tab_contents, 1994.
- Kennish, M. J.: Estuaries, anthropogenic impacts, *Encycl. Earth Sci. Ser.*, 14, 434–436, doi:10.1007/1-4020-3880-1_140, 2005.
- Kershaw, S.: Development of a Methodology for Estimating Methane Emissions from Abandoned Coal Mines in the UK, , IMC White, 109 [online] Available from: [file://tsn.tno.nl/Data/SV/sv-066092/Refworks/Kershaw \(2005\).pdf](file://tsn.tno.nl/Data/SV/sv-066092/Refworks/Kershaw%20(2005).pdf), 2005.
- Kholod, N., Evans, M., Pilcher, R. C., Roshchanka, V., Ruiz, F., Coté, M. and Collings, R.: Global methane emissions from coal mining to continue growing even with declining coal production, *J. Clean. Prod.*, 256(February), 120489, doi:10.1016/j.jclepro.2020.120489, 2020a.
- Kholod, N., Evans, M., Pilcher, R. C., Roshchanka, V., Ruiz, F., Coté, M. and Collings, R.: Global methane emissions from coal mining to continue growing even with declining coal production, *J. Clean. Prod.*, 256, doi:10.1016/j.jclepro.2020.120489, 2020b.
- Kling, G. W., Kipphut, G. W. and Miller, M. C.: Arctic lakes and streams as gas conduits to the atmosphere: Implications for tundra carbon budgets, *Science (80-.)*, 251(4991), 298–301, doi:10.1126/science.251.4991.298, 1991.
- Kling, G. W., Kipphut, G. W. and Miller, M. C.: The flux of CO₂ and CH₄ from lakes and rivers in arctic Alaska, *Hydrobiologia*, 240(1–3), 23–36, doi:10.1007/BF00013449, 1992.
- Koschorreck, M., Prairie, Y. T., Kim, J. and Marcé, R.: Technical note: CO₂ is not like CH₄- Limits of and corrections to the headspace method to analyse pCO₂ in fresh water, *Biogeosciences*, 18(5), 1619–1627, doi:10.5194/bg-18-1619-2021, 2021.
- Kristjansson, J. K. and Schönheit, P.: Why do sulfate-reducing bacteria outcompete methanogenic bacteria for substrates?, *Oecologia*, 60(2), 264–266, doi:10.1007/BF00379530, 1983.
- Kuwa, T., Kanda, J., Kubo, A., Nakajima, F., Ogawa, H., Sohma, A. and Suzumura, M.: Blue carbon in human-dominated estuarine and shallow coastal systems, *Ambio*, 45(3), 290–301, doi:10.1007/s13280-015-0725-x, 2016.
- Laanbroek, H. J.: Methane emission from natural wetlands : interplay between emergent macrophytes and soil microbial processes . A mini-review, *Ann. Bot.*, 105, 141–153, doi:10.1093/aob/mcp201, 2010.
- Lambert, T., Bouillon, S., Darchambeau, F., Morana, C., Roland, F. A. E., Descy, J. P. and Borges, A. V.: Effects of human land use on the terrestrial and aquatic sources of fluvial organic matter in a temperate river basin (The Meuse River, Belgium), *Biogeochemistry*, 136(2), 191–211, doi:10.1007/s10533-017-0387-9, 2017.
- Land, M., Granéli, W., Grimvall, A., Hoffmann, C. C., Mitsch, W. J., Tonderski, K. S. and Verhoeven, J.

T. A.: How effective are created or restored freshwater wetlands for nitrogen and phosphorus removal? A systematic review, *Environ. Evid.*, 5(1), 1–26, doi:10.1186/s13750-016-0060-0, 2016.

Larsen, S. J., Kilminster, K. L., Mantovanelli, A., Goss, Z. J., Evans, G. C., Bryant, L. D. and McGinnis, D. F.: Artificially oxygenating the Swan River estuary increases dissolved oxygen concentrations in the water and at the sediment interface, *Ecol. Eng.*, 128(December 2018), 112–121, doi:10.1016/j.ecoleng.2018.12.032, 2019a.

Larsen, S. J., Kilminster, K. L., Mantovanelli, A., Goss, Z. J., Evans, G. C., Bryant, L. D. and McGinnis, D. F.: Artificially oxygenating the Swan River estuary increases dissolved oxygen concentrations in the water and at the sediment interface, *Ecol. Eng.*, 128(January), 112–121, doi:10.1016/j.ecoleng.2018.12.032, 2019b.

Law, C. S., Rees, A. P. and Owens, N. J. P.: Nitrous oxide: Estuarine sources and atmospheric flux, *Estuar. Coast. Shelf Sci.*, 35(3), 301–314, doi:10.1016/S0272-7714(05)80050-2, 1992.

Leslie, A. G., Browne, M. A. E., Cain, T. and Ellen, R.: From threat to future asset—The legacy of opencast surface-mined coal in Scotland, *Int. J. Coal Geol.*, 164, 123–133, doi:10.1016/j.coal.2016.06.017, 2016.

Levy, P., Clement, R., Cowan, N., Keane, B., Myrgiotis, V., van Oijen, M., Smallman, T. L., Toet, S. and Williams, M.: Challenges in Scaling Up Greenhouse Gas Fluxes: Experience From the UK Greenhouse Gas Emissions and Feedbacks Program, *J. Geophys. Res. Biogeosciences*, 127(5), doi:10.1029/2021JG006743, 2022.

Lewis, R. E.: The nature of outflows from the north-east estuaries, *Hydrobiologia*, 195(1), 1–11, doi:10.1007/BF00026809, 1990.

Li, F., Li, X., Hou, L. and Shao, A.: Impact of the Coal Mining on the Spatial Distribution of Potentially Toxic Metals in Farmland Tillage Soil, *Sci. Rep.*, 8(1), 1–10, doi:10.1038/s41598-018-33132-4, 2018.

Li, P.: Mine Water Problems and Solutions in China, *Mine Water Environ.*, 37(2), 217–221, doi:10.1007/s10230-018-0543-z, 2018.

Li, S., Gu, S., Tan, X. and Zhang, Q.: Water quality in the upper Han River basin, China: The impacts of land use/land cover in riparian buffer zone, *J. Hazard. Mater.*, 165(1–3), 317–324, doi:10.1016/j.jhazmat.2008.09.123, 2009.

Li, X., Qi, M., Gao, D., Liu, M., Sardans, J., Peñuelas, J. and Hou, L.: Nitrous oxide emissions from subtropical estuaries: Insights for environmental controls and implications, *Water Res.*, 212(November 2021), doi:10.1016/j.watres.2022.118110, 2022.

Li, Y., Wang, D., Chen, Z., Chen, J., Hu, H. and Wang, R.: Methane emissions during the tide cycle of a yangtze estuary salt marsh, *Atmosphere (Basel)*, 12(2), 1–14, doi:10.3390/atmos12020245, 2021.

Lindsay, P., Balls, P. W. and West, J. R.: Influence of tidal range and river discharge on suspended particulate matter fluxes in the Forth estuary (Scotland), *Estuar. Coast. Shelf Sci.*, 42(1), 63–82, doi:10.1006/ecss.1996.0006, 1996.

Lindsay, P., Bell, F. G. and Hytiris, N.: Contamination of sediments in the Forth Estuary, Scotland, *Geol. Soc. Eng. Geol. Spec. Publ.*, 14, 179–187, doi:10.1144/GSL.ENG.1998.014.01.21, 1998.

Liu, S. and Raymond, P. A.: Hydrologic controls on pCO₂ and CO₂ efflux in US streams and rivers, *Limnol. Oceanogr. Lett.*, 3(6), 428–435, doi:10.1002/lol2.10095, 2018.

- Liu, Y., Hu, X. and Xu, Y.: PropS-SH/SiO₂ nanocomposite coatings for pyrite oxidation inhibition to control acid mine drainage at the source, *J. Hazard. Mater.*, 338, 313–322, doi:10.1016/j.jhazmat.2017.05.043, 2017.
- Long, H., Vihermaa, L., Waldron, S., Hoey, T., Quemain, S. and Newton, J.: Hydraulics are a first-order control on CO₂ efflux from fluvial systems, *Geophys. Res. Biogeosciences*, 1912–1922, doi:10.1002/2015JG002955. Received, 2015.
- Looman, A., Maher, D. T., Pendall, E., Bass, A. and Santos, I. R.: The carbon dioxide evasion cycle of an intermittent first-order stream: contrasting water–air and soil–air exchange, *Biogeochemistry*, 132(1–2), 87–102, doi:10.1007/s10533-016-0289-2, 2017.
- Lopez, M., Sherwood, O. A., Dlugokencky, E. J., Kessler, R., Giroux, L. and Worthy, D. E. J.: Isotopic signatures of anthropogenic CH₄ sources in Alberta, Canada, *Atmos. Environ.*, 164, 280–288, doi:10.1016/j.atmosenv.2017.06.021, 2017.
- Lovley, D. R. and Klug, M. J.: Sulfate Reducers Can Outcompete Methanogens at Freshwater Sulfate Concentrations, *Appl. Environ. Microbiol.*, 45(1), 187–192, 1983.
- Lu, X., Harris, S. J., Fisher, R. E., France, J. L., Nisbet, E. G., Lowry, D., Röckmann, T., Van Der Veen, C., Menoud, M., Schwietzke, S. and Kelly, B. F. J.: Isotopic signatures of major methane sources in the coal seam gas fields and adjacent agricultural districts, Queensland, Australia, *Atmos. Chem. Phys.*, 21(13), 10527–10555, doi:10.5194/acp-21-10527-2021, 2021.
- Lucchini, D. O., Chipps, S. R. and Schumann, D. A.: Effects of seasonal hypoxia on macroinvertebrate communities in a small reservoir, *Lakes Reserv. Res. Manag.*, 27(1), 1–14, doi:10.1111/lre.12395, 2022.
- Lyu, X., Yang, K. and Fang, J.: Science of the Total Environment Utilization of resources in abandoned coal mines for carbon neutrality, *Sci. Total Environ.*, 822, 153646, doi:10.1016/j.scitotenv.2022.153646, 2022.
- Lyu, Z., Shao, N., Akinyemi, T. and Whitman, W. B.: Methanogenesis, *Curr. Biol.*, 28(13), R727–R732, doi:10.1016/j.cub.2018.05.021, 2018.
- Maavara, T., Lauerwald, R., Laruelle, G. G., Bouskill, N. J., Cappellen, P. Van and Regnier, P.: Nitrous oxide emissions from inland waters : Are IPCC estimates too high ?, *Glob. Chang. Biol.*, (July 2018), doi:10.1111/gcb.14504, 2019.
- Macdonald, J. A., Fowler, D., Hargreaves, K. J., Skiba, U., Leith, I. D. and Murray, M. B.: Methane emission rates from a northern wetland; Response to temperature, water table and transport, *Atmos. Environ.*, 32(19), 3219–3227, 1998.
- Macias, D., Garcia-gorriz, E., Piroddi, C. and Stips, A.: Global Biogeochemical Cycles, *Global Biogeochem. Cycles*, 5, 1–11, doi:10.1002/2013GB004715. Received, 2014.
- Magowo, W. E., Sheridan, C. and Rumbold, K.: Global Co-occurrence of Acid Mine Drainage and Organic Rich Industrial and Domestic Effluent: Biological sulfate reduction as a co-treatment-option, *J. Water Process Eng.*, 38(September), 101650, doi:10.1016/j.jwpe.2020.101650, 2020.
- Manthos, D.: Mapping Abandoned Coal Mines, Sky Truth [online] Available from: <https://skytruth.org/2015/10/mapping-abandoned-coal-mines/>, 2016.
- Marchant, H. K., Ahmerkamp, S., Lavik, G., Tegetmeyer, H. E., Graf, J., Klatt, J. M., Holtappels, M., Walpersdorf, E. and Kuypers, M. M. M.: Denitrifying community in coastal sediments performs

aerobic and anaerobic respiration simultaneously, *ISME J.*, 11(8), 1799–1812, doi:10.1038/ismej.2017.51, 2017.

Marine Scotland: Marine Scotland Information - Dredging, [online] Available from: <http://marine.gov.scot/application-type/dredging>, 2021.

Marine Scotland: Marine Scotland - Waste Water Treatment and Industrial Outfalls, [online] Available from: <https://marinescotland.atkinsgeospatial.com/nmpi/default.aspx?layers=1880>, 2022.

Martinez-Cruz, K., Gonzalez-Valencia, R., Sepulveda-Jauregui, A., Plascencia-Hernandez, F., Belmonte-Izquierdo, Y. and Thalasso, F.: Methane emission from aquatic ecosystems of Mexico City, *Aquat. Sci.*, 79(1), 159–169, doi:10.1007/s00027-016-0487-y, 2017.

Marx, A., Dusek, J., Jankovec, J., Sanda, M., Vogel, T., van Geldern, R., Hartmann, J. and Barth, J. A. C.: A review of CO₂ and associated carbon dynamics in headwater streams: A global perspective, *Rev. Geophys.*, 55(2), 560–585, doi:10.1002/2016RG000547, 2017.

Masuda, S., Sano, I., Hojo, T., Li, Y. Y. and Nishimura, O.: The comparison of greenhouse gas emissions in sewage treatment plants with different treatment processes, *Chemosphere*, 193, 581–590, doi:10.1016/j.chemosphere.2017.11.018, 2018.

Matthiessen, P. and Law, R. J.: Contaminants and their effects on estuarine and coastal organisms in the United Kingdom in the late twentieth century, *Environ. Pollut.*, 120(3), 739–757, doi:10.1016/S0269-7491(02)00175-6, 2002.

Maurice, L., Rawlins, B. G., Farr, G., Bell, R. and Goody, D. C.: The Influence of Flow and Bed Slope on Gas Transfer in Steep Streams and Their Implications for Evasion of CO₂, *J. Geophys. Res. Biogeosciences*, 122(11), 2862–2875, doi:10.1002/2017JG004045, 2017.

Mayumi, D., Mochimaru, H., Tamaki, H., Yamamoto, K., Yoshioka, H., Suzuki, Y., Kamagata, Y. and Sakata, S.: Methane production from coal by a single methanogen, *Sci. - Res. reports*, 354(6309), 222–225, 2016.

McConnell, J. R. and Edwards, R.: Coal burning leaves toxic heavy metal legacy in the Arctic, *Proc. Natl. Acad. Sci. U. S. A.*, 105(34), 12140–12144, doi:10.1073/pnas.0803564105, 2008.

McElroy, M. B., Elkins, J. W., Wofsy, S. C., Kolb, C. E., Durán, A. P. and Kaplan, W. A.: Production and release of N₂O from the Potomac Estuary, *Limnol. Oceanogr.*, 23(6), 1168–1182, doi:10.4319/lo.1978.23.6.1168, 1978.

McManus, J.: Salinity and suspended matter variations in the Tay estuary, *Cont. Shelf Res.*, 25, 729–747, 2005.

Megonigal, J. P., Hines, M. E. and Visscher, P. T.: Linkages to Trace Gases and Aerobic Processes, *Treatise on Geochemistry*, 8, 350–362 [online] Available from: https://repository.si.edu/bitstream/handle/10088/15579/Megonigal_Hines_Visscher_2004.pdf?sequence=1&isAllowed=y, 2004.

Mendonça, R., Müller, R. A., Tranvik, L. J., Sobek, S., Clow, D., Verpoorter, C. and Raymond, P.: Organic carbon burial in global lakes and reservoirs, *Nat. Commun.*, 1–6, doi:10.1038/s41467-017-01789-6, 2017.

Le Mer, J. and Roger, P.: Production, oxidation, emission and consumption of methane by soils: A review, *Eur. J. Soil Biol.*, 37(1), 25–50, doi:10.1016/S1164-5563(01)01067-6, 2001.

Meslé, M., Dromart, G. and Oger, P.: Microbial methanogenesis in subsurface oil and coal, *Res. Microbiol.*, 164(9), 959–972, doi:10.1016/j.resmic.2013.07.004, 2013.

Met Office: UK Climate Averages, Met Off. Clim. Res. [online] Available from: <https://www.metoffice.gov.uk/research/climate/maps-and-data/uk-climate-averages>, 2021.

Middelburg, J. J., Nieuwenhuize, J., Iversen, N., Høgh, N., DeWilde, H., Helder, W., Seifert, R. and Christof, O.: Methane distribution in European tidal estuaries, *Biogeochemistry*, 59, 95–119, 2002a.

Middelburg, J. J., Nieuwenhuize, J., Iversen, N., Høgh, N., De Wilde, H., Helder, W., Seifert, R. and Christof, O.: Methane distribution in European tidal estuaries, *Biogeochemistry*, 59(1–2), 95–119, doi:10.1023/A:1015515130419, 2002b.

Middelburg, J. J., Nieuwenhuize, J., Iversen, N., Høgh, N., De, H., Middelburg, J. J., Nieuwenhuize, J., Iversen, N., Hogh, N., Wilde, H. D. E. and Helder, W. I. M.: Methane Distribution in European Tidal Estuaries, *Biogeochemistry*, 59(1), 95–119, 2002c.

Millero, F. J., Graham, T. B., Huang, F., Bustos-Serrano, H. and Pierrot, D.: Dissociation constants of carbonic acid in seawater as a function of salinity and temperature, *Mar. Chem.*, 100(1–2), 80–94, doi:10.1016/j.marchem.2005.12.001, 2006.

Mitchell, S. B., West, J. R., Arundale, A. M. W., Guymer, I. and Couperthwaite, J. S.: Dynamics of the Turbidity Maxima in the Upper Humber Estuary System, UK, *Mar. Pollut. Bull.*, 37(3–7), 190–205 [online] Available from: <https://www.sciencedirect.com/science/article/pii/S0025326X98001787>, 1998.

Mitchell, S. B., West, J. R. and Guymer, I.: Dissolved - Oxygen / Suspended -Solids Concentration Relationships in the Upper Humber Estuary, *Journnal CIWEM*, 13(11), 327–337, 1999.

Mizukawa, A., Filipp, T. C., Peixoto, L. O. M., Scipioni, B., Leonardi, I. R. and de Azevedo, J. C. R.: Caffeine as a chemical tracer for contamination of urban rivers, *Brazilian J. Water Resour.*, 2019.

Morton, R. D., Marston, C. G., O’Neil, A. W. and Rowland, C. S.: Land Cover Map 2019 (land parcels, GB) [Dataset]., NERC Environ. Inf. Data Centre. [online] Available from: <https://doi.org/10.5285/44C23778-4A73-4A8F-875F-89B23B91ECF8>, 2020.

Muller, A. C., Muller, D. L. and Muller, A.: Resolving spatiotemporal characteristics of the seasonal hypoxia cycle in shallow estuarine environments of the Severn River and South River, MD, Chesapeake Bay, USA, *Heliyon*, 2(9), doi:10.1016/j.heliyon.2016.e00157, 2016.

Müller, D., Bange, H. W., Warneke, T., Rixen, T., Müller, M., Mujahid, A. and Notholt, J.: Nitrous oxide and methane in two tropical estuaries in a peat-dominated region of northwestern Borneo, , (April), doi:10.5194/bg-13-2415-2016, 2016.

Munson, M. A., Nedwell, D. B. and Embley, T. M.: Phylogenetic diversity of Archaea in sediment samples from a coastal salt marsh, *Appl. Environ. Microbiol.*, 63(12), 4729–4733, doi:10.1128/aem.63.12.4729-4733.1997, 1997.

Murray, R. H., Erler, D. V. and Eyre, B. D.: Nitrous oxide fluxes in estuarine environments: Response to global change, *Glob. Chang. Biol.*, 21(9), 3219–3245, doi:10.1111/gcb.12923, 2015.

Musenze, R. S., Werner, U., Grinham, A., Udy, J. and Yuan, Z.: Methane and nitrous oxide emissions from a subtropical estuary (the Brisbane River estuary, Australia), *Sci. Total Environ.*, 472, 719–729, doi:10.1016/j.scitotenv.2013.11.085, 2014.

- Muyzer, G. and Stams, A. J. M.: The ecology and biotechnology of sulphate-reducing bacteria, *Nat. Rev. Microbiol.*, 6(6), 441–454, doi:10.1038/nrmicro1892, 2008.
- Myhre, G., Shindell, D., Bréon, F., Collins, W., Fuglestedt, J., Huang, J., Koch, D., Lamarque, J., Lee, D., Mendoza, B., Nakajima, T., Robock, A., Stephens, G., Takemura, T. and Zhang, H.: Anthropogenic and Natural Radiative Forcing. In: *Climate Change 2013: The Physical Science Basis. Contribution of Working Group I to the Fifth Assessment Report of the Intergovernmental Panel on Climate Change*, Cambridge University Press, Cambridge, United Kingdom and New York, NY, USA., 2013.
- Natchimuthu, S., Wallin, M. B., Klemetsson, L. and Bastviken, D.: Spatio-temporal patterns of stream methane and carbon dioxide emissions in a hemiboreal catchment in Southwest Sweden, *Sci. Rep.*, 7(November 2016), 1–12, doi:10.1038/srep39729, 2017.
- Natural Scotland: The river basin management plan for the Scotland river basin district 2009–2015. [online] Available from: <https://www.sepa.org.uk/media/163445/the-river-basin-management-plan-for-the-scotland-river-basin-district-2015-2027.pdf>, 2015.
- Neal, C. and Kirchner, J. W.: Sodium and chloride levels in rainfall, mist, streamwater and groundwater at the Plynlimon catchments, mid-Wales: inferences on hydrological and chemical controls, *Hydrol. Earth Syst. Sci.*, 4(2), 2000.
- Nedwell, D. B., Dong, L. F., Sage, A. and Underwood, G. J. C.: Variations of the nutrients loads to the mainland U.K. estuaries: Correlation with catchment areas, urbanization and coastal eutrophication, *Estuar. Coast. Shelf Sci.*, 54(6), 951–970, doi:10.1006/ecss.2001.0867, 2002.
- Negandhi, K., Laurion, I., Whitticar, M. J., Galand, P. E., Xu, X. and Lovejoy, C.: Small thaw ponds: An unaccounted source of methane in the Canadian high Arctic, *PLoS One*, 8(11), doi:10.1371/journal.pone.0078204, 2013.
- Nguyen, A. T., Némery, J., Gratiot, N., Dao, T. S., Le, T. T. M., Baduel, C. and Garnier, J.: Does eutrophication enhance greenhouse gas emissions in urbanized tropical estuaries?, *Environ. Pollut.*, 303(January), doi:10.1016/j.envpol.2022.119105, 2022.
- Nielsen, E., Greve, K. and Ladefoged, O.: Cobalt(II), inorganic and soluble salts - Evaluation of health hazards and proposal of a health based quality criterion for drinking water., 2013.
- Nijman, T. P. A., Amado, A. M., Bodelier, P. L. E. and Veraart, A. J.: Relief of Phosphate Limitation Stimulates Methane Oxidation, *Front. Environ. Sci.*, 10(April), 1–8, doi:10.3389/fenvs.2022.804512, 2022.
- Nisbet, E. G.: Climate feedback on methane from wetlands, *Nat. Clim. Chang.*, 13(5), 421–422, doi:10.1038/s41558-023-01634-3, 2023.
- NOAA: Estuary Habitat, *Habitata Conserv.* [online] Available from: <https://www.fisheries.noaa.gov/national/habitat-conservation/estuary-habitat> (Accessed 9 March 2021), 2020.
- NRFA: National River Flow Archive, *Cent. Ecol. Hydrol.*, <http://www.ceh.ac.uk/data/nrfa/> [online] Available from: <https://nrfa.ceh.ac.uk/> (Accessed 5 September 2020), 2010.
- O’Keeffe, J., Akunna, J., Olszewska, J., Bruce, A., May, L. and Allan, R.: Practical measures for reducing phosphorus and faecal microbial loads from onsite wastewater treatments systems discharged to the environment. A review., , 52, 2015.
- Ockenden, M. C., Deasy, C., Quinton, J. N., Bailey, A. P., Surridge, B. and Stoate, C.: Evaluation of field

- wetlands for mitigation of diffuse pollution from agriculture: Sediment retention, cost and effectiveness, *Environ. Sci. Policy*, 24, 110–119, doi:10.1016/j.envsci.2012.06.003, 2012.
- Ogilvie, B., Nedwell, D. B., Harrison, R. M., Robinson, A. and Sage, A.: High nitrate, muddy estuaries as nitrogen sinks: the nitrogen budget of the River Colne estuary (United Kingdom), *Mar. Ecol. Prog. Ser.*, 150, 217–228, 1997.
- Ordnance Survey: OS Open Rivers, OS Open Rivers [online] Available from: <https://www.ordnancesurvey.co.uk/business-government/products/open-map-rivers>, 2022.
- Oremland, R. S., Polcin, S., Survey, U. S. G. and Park, M.: Methanogenesis and sulfate reduction: competitive and noncompetitive substrates in estuarine sediments, *Deep Sea Res. Part B. Oceanogr. Lit. Rev.*, 30(6), 470, doi:10.1016/0198-0254(83)90262-5, 1983.
- OSMRE: Abandoned mine land inventory system, U.S. Dep. Inter. [online] Available from: <https://amlis.osmre.gov/Summaries.aspx>, 2016.
- Pal, C., Asiani, K., Arya, S., Rensing, C., Stekel, D. J., Larsson, D. G. J. and Hobman, J. L.: Metal Resistance and Its Association With Antibiotic Resistance, 1st ed., Elsevier Ltd., 2017.
- Park, K., Kim, C. K. and Schroeder, W. W.: Temporal variability in summertime bottom hypoxia in shallow areas of Mobile Bay, Alabama, *Estuaries and Coasts*, 30(1), 54–65, doi:10.1007/BF02782967, 2007.
- Park, S. Y. and Liang, Y.: Biogenic methane production from coal: A review on recent research and development on microbially enhanced coalbed methane (MECBM), *Fuel*, 166, 258–267, doi:10.1016/j.fuel.2015.10.121, 2016.
- Pattinson, S. N., García-Ruiz, R. and Whitton, B. A.: Spatial and seasonal variation in denitrification in the Swale-Ouse system, a river continuum, *Sci. Total Environ.*, 210–211, 289–305, doi:10.1016/S0048-9697(98)00019-9, 1998.
- Paulo, L. M., Ramiro-Garcia, J., van Mourik, S., Stams, A. J. M. and Sousa, D. Z.: Effect of nickel and cobalt on methanogenic enrichment cultures and role of biogenic sulfide in metal toxicity attenuation, *Front. Microbiol.*, 8(JUL), 1–12, doi:10.3389/fmicb.2017.01341, 2017.
- Peng, S., Lin, X., Thompson, R. L., Xi, Y., Liu, G., Hauglustaine, D., Lan, X., Poulter, B., Ramonet, M., Saunois, M., Yin, Y., Zhang, Z., Zheng, B. and Ciais, P.: Wetland emission and atmospheric sink changes explain methane growth in 2020, *Nature*, 612(7940), 477–482, doi:10.1038/s41586-022-05447-w, 2022.
- Pfenning, K. S. and P. B. M.: Effect of nitrate, organic carbon, and temperature on potential denitrification rates in nitrate-rich riverbed sediments, *J. Hydrol.*, 187, 283–295, 1996.
- Phillips, B. M., Mccalla Fuller, L. B., Siegler, K., Deng, X. and Tjeerdema, R. S.: Treating Agricultural Runoff with a Mobile Carbon Filtration Unit, *Arch. Environ. Contam. Toxicol.*, 82(4), 455–466, doi:10.1007/s00244-022-00925-8, 2022.
- Pickard, A. E., Brown, I., Burden, A., Callaghan, N., Evans, C. D., Kitidis, V., Mayor, D., Olszewska, J., Pereira, G., Spears, B. M., Williamson, J., Woodward, M. and Rees, A. P.: Greenhouse gas and nutrient data measured across estuaries in the UK, 2017-2018, NERC Environ. Inf. Data Cent., 2021a.
- Pickard, A. E., Skiba, U. M., Carvalho, L., Brown, A. M., Heal, K. V., Rees, R. M. and Harley, J. F.: Greenhouse gas and water chemistry data measured across the Tay estuary, Scotland, from 2009-2011, NERC Environ. Inf. Data Cent., 2021b.

- Poffenbarger, H. J., Needelman, B. A. and Megonigal, J. P.: Salinity influence on methane emissions from tidal marshes, *Wetlands*, 31(5), 831–842, doi:10.1007/s13157-011-0197-0, 2011.
- Pohle, I., Baggaley, N., Palarea-albaladejo, J., Stutter, M. and Glendell, M.: A Framework for Assessing Concentration-Discharge Catchment Behavior From Low-Frequency Water Quality Data, *Water Resour. Res.*, doi:10.1029/2021WR029692, 2021.
- Pro-oceanus: Mini CO₂ Submersible pCO₂ Sensor, [online] Available from: <https://pro-oceanus.com/products/mini-series/mini-co2>, 2023.
- Pruteanu, C. G., Ackland, G. J., Poon, W. C. K. and Loveday, J. S.: When immiscible becomes miscible- Methane in water at high pressures, *Sci. Adv.*, 3(8), 1–6, doi:10.1126/sciadv.1700240, 2017.
- Purdy, K. J., Nedwell, D. B. and Embley, T. M.: Analysis of the sulfate-reducing bacterial and methanogenic archaeal populations in contrasting antarctic sediments, *Appl. Environ. Microbiol.*, 69(6), 3181–3191, doi:10.1128/AEM.69.6.3181-3191.2003, 2003.
- Rajkumar, A. N., Barnes, J., Ramesh, R., Purvaja, R. and Upstill-goddard, R. C.: Methane and nitrous oxide fluxes in the polluted Adyar River and estuary , SE India, *Mar. Pollut. Bull.*, 56(12), 2043–2051, doi:10.1016/j.marpolbul.2008.08.005, 2008.
- Raymond, P. A., Hartmann, J., Lauerwald, R., Sobek, S., McDonald, C., Hoover, M., Butman, D., Striegl, R., Mayorga, E., Humborg, C., Kortelainen, P., Dürr, H., Meybeck, M., Ciais, P. and Guth, P.: Global carbon dioxide emissions from inland waters, *Nature*, 503(7476), 355–359, doi:10.1038/nature12760, 2013.
- Reay, D. S., Smith, K. A. and Edwards, A. C.: Nitrous oxide emission from agricultural drainage waters, *Glob. Chang. Biol.*, 9(2), 195–203, doi:10.1046/j.1365-2486.2003.00584.x, 2003.
- Rehder, G., Keir, R. S., Suess, E. and Pohlmann, T.: The multiple sources and patterns of methane in North Sea waters, *Aquat. Geochemistry*, 4(3–4), 403–427, doi:10.1023/a:1009644600833, 1998.
- Reshmi, R. R., Deepa Nair, K., Zachariah, E. J. and Vincent, S. G. T.: Methanogenesis: Seasonal changes in human impacted regions of Ashtamudi estuary (Kerala, South India), *Estuar. Coast. Shelf Sci.*, 156(1), 144–154, doi:10.1016/j.ecss.2014.11.031, 2015.
- Revsbech, N. P., Jacobsen, J. P. and Nielsen, L. P.: Nitrogen transformations in microenvironments of river beds and riparian zones, *Ecol. Eng.*, 24(5 SPEC. ISS.), 447–455, doi:10.1016/j.ecoleng.2005.02.002, 2005.
- Riley, A. L. and Mayes, W. M.: Long-term evolution of highly alkaline steel slag drainage waters, *Environ. Monit. Assess.*, 187(7), doi:10.1007/s10661-015-4693-1, 2015.
- Robins, P. E., Lewis, M. J., Simpson, J. H. and Malham, S. K.: Future variability of solute transport in a macrotidal estuary, *Estuar. Coast. Shelf Sci.*, 151(November), 88–99, doi:10.1016/j.ecss.2014.09.019, 2014.
- Robins, P. E., Davies, A. G., Skov, M. W., Lewis, M. J., Gim, L., Malham, S. K., Neill, S. P., McDonald, J. E., Whitton, T. A., Jackson, S. E. and Jago, C. F.: Estuarine , Coastal and Shelf Science Impact of climate change on UK estuaries : A review of past trends and potential projections, , 169, doi:10.1016/j.ecss.2015.12.016, 2016.
- Robinson, A. D., Nedwell, D. B., Harrison, R. M. and Ogilvie, B. G.: Hypernutriented estuaries as sources of N₂O emission to the atmosphere: The estuary of the River Colne, Essex, UK, *Mar. Ecol. Prog. Ser.*, 164(1994), 59–71, doi:10.3354/meps164059, 1998.

Robison, A. L., Wollheim, W. M., Perryman, C. R., Cotter, A. R., Mackay, J. E., Varner, R. K., Clarizia, P. and Ernakovich, J. G.: Dominance of Diffusive Methane Emissions From Lowland Headwater Streams Promotes Oxidation and Isotopic Enrichment, *Front. Environ. Sci.*, 9(January), 1–14, doi:10.3389/fenvs.2021.791305, 2022.

Rodgers, K., McLellan, I., Peshkur, T., Williams, R., Tonner, R., Knapp, C. W., Henriquez, F. L. and Hursthouse, A. S.: The legacy of industrial pollution in estuarine sediments: spatial and temporal variability implications for ecosystem stress, *Environ. Geochem. Health*, 4, doi:10.1007/s10653-019-00316-4, 2019.

Rodgers, K., McLellan, I., Peshkur, T., Williams, R., Tonner, R., Knapp, C. W., Henriquez, F. L. and Hursthouse, A. S.: The legacy of industrial pollution in estuarine sediments: spatial and temporal variability implications for ecosystem stress, *Environ. Geochem. Health*, 42(4), 1057–1068, doi:10.1007/s10653-019-00316-4, 2020.

Rosamond, M. S., Thuss, S. J. and Schiff, S. L.: Dependence of riverine nitrous oxide emissions on dissolved oxygen levels, *Nat. Geosci.*, 5(10), 715–718, doi:10.1038/ngeo1556, 2012.

Rosentreter, J. A., Borges, A. V., Deemer, B. R., Holgerson, M. A., Liu, S., Song, C., Melack, J., Raymond, P. A., Duarte, C. M., Allen, G. H., Olefeldt, D., Poulter, B., Battin, T. I. and Eyre, B. D.: Half of global methane emissions come from highly variable aquatic ecosystem sources, *Nat. Geosci.*, 14(4), 225–230, doi:10.1038/s41561-021-00715-2, 2021.

Salgado, J., Duc, T. A., Nga, D. T., Panizzo, V. N., Bass, A. M., Zheng, Y., Taylor, S., Roberts, L. R., Lacey, J. H., Leng, M. J. and McGowan, S.: Urbanization and seasonality strengthens the CO₂ capacity of the Red River Delta, Vietnam, *Environ. Res. Lett.*, 17(10), doi:10.1088/1748-9326/ac9705, 2022.

Santos, I. R., Burdige, D. J., Jennerjahn, T. C., Bouillon, S., Cabral, A., Serrano, O., Wernberg, T., Filbee-Dexter, K., Guimond, J. A. and Tamborski, J. J.: The renaissance of Odum's outwelling hypothesis in "Blue Carbon" science, *Estuar. Coast. Shelf Sci.*, 255(April), 107361, doi:10.1016/j.ecss.2021.107361, 2021.

Saria, L., Shimaoka, T. and Miyawaki, K.: Leaching of heavy metals in acid mine drainage, *Waste Manag. Res.*, 24(2), 134–140, doi:10.1177/0734242X06063052, 2006.

Saunio, M., Bousquet, P., Poulter, B., Peregon, A., Ciais, P., Canadell, J. G., Dlugokencky, E. J., Etiope, G., Bastviken, D., Houweling, S., Janssens-Maenhout, G., Tubiello, F. N., Castaldi, S., Jackson, R. B., Alexe, M., Arora, V. K., Beerling, D. J., Bergamaschi, P., Blake, D. R., Brailsford, G., Brovkin, V., Bruhwiler, L., Crevoisier, C., Crill, P., Covey, K., Curry, C., Frankenberg, C., Gedney, N., Höglund-Isaksson, L., Ishizawa, M., Ito, A., Joos, F., Kim, H. S., Kleinen, T., Krummel, P., Lamarque, J. F., Langenfelds, R., Locatelli, R., Machida, T., Maksyutov, S., McDonald, K. C., Marshall, J., Melton, J. R., Morino, I., Naik, V., O'Doherty, S., Parmentier, F. J. W., Patra, P. K., Peng, C., Peng, S., Peters, G. P., Pison, I., Prigent, C., Prinn, R., Ramonet, M., Riley, W. J., Saito, M., Santini, M., Schroeder, R., Simpson, I. J., Spahni, R., Steele, P., Takizawa, A., Thornton, B. F., Tian, H., Tohjima, Y., Viovy, N., Voulgarakis, A., Van Weele, M., Van Der Werf, G. R., Weiss, R., Wiedinmyer, C., Wilton, D. J., Wiltshire, A., Worthy, D., Wunch, D., Xu, X., Yoshida, Y., Zhang, B., Zhang, Z. and Zhu, Q.: The global methane budget 2000–2012, *Earth Syst. Sci. Data*, 8(2), 697–751, doi:10.5194/essd-8-697-2016, 2016.

Saunio, M., Stavert, A. R., Poulter, B., Bousquet, P., Canadell, J. G., Jackson, R. B., Raymond, P. A., Dlugokencky, E. J., Houweling, S., Patra, P. K., Ciais, P., Arora, V. K., Bastviken, D., Bergamaschi, P., Blake, D. R., Brailsford, G., Bruhwiler, L., Carlson, K. M., Carrol, M., Castaldi, S., Chandra, N., Crevoisier, C., Crill, P. M., Covey, K., Curry, C. L., Etiope, G., Frankenberg, C., Gedney, N., Hegglin, M. I., Höglund-Isaksson, L., Hugelius, G., Ishizawa, M., Ito, A., Janssens-Maenhout, G., Jensen, K. M.,

Joos, F., Kleinen, T., Krummel, P. B., Langenfelds, R. L., Laruelle, G. G., Liu, L., Machida, T., Maksyutov, S., McDonald, K. C., McNorton, J., Miller, P. A., Melton, J. R., Morino, I., Müller, J., Murguia-Flores, F., Naik, V., Niwa, Y., Noce, S., O'Doherty, S., Parker, R. J., Peng, C., Peng, S., Peters, G. P., Prigent, C., Prinn, R., Ramonet, M., Regnier, P., Riley, W. J., Rosentreter, J. A., Segers, A., Simpson, I. J., Shi, H., Steven J. Smith, S. J. S., Steele, L. P., Thornton, B. F., Tian, H., Tohjima, Y., Tubiello, F. N., Tsuruta, A., Viovy, N., Apostolos Voulgarakis, A. V., Weber, T. S., Weele, M. van, Werf, G. R. van der, Weiss, R. F., Worthy, D., Wunch, D., Yi Yin, Y. Y., Yoshida, Y., Zhang, W., Zhang, Z., Zhao, Y., Zheng, B., Zhu, Q., Zhu, Q. and Zhuang, Q.: Overview of Greenhouse Gases | US EPA, *Earth Syst. Sci. Data*, 12(3), 1561–1623 [online] Available from: <https://www.epa.gov/ghgemissions/overview-greenhouse-gases>, 2020.

Schulz, G., Sanders, T., Voynova, Y. G., Bange, H. W. and Dähnke, K.: Seasonal variability of nitrous oxide concentrations and emissions along the Elbe estuary, , (February), 1–21, 2023.

Schwarzenbach, R. P., Egli, T., Hofstetter, T. B., Von Gunten, U. and Wehrli, B.: Global water pollution and human health, *Annu. Rev. Environ. Resour.*, 35, 109–136, doi:10.1146/annurev-environ-100809-125342, 2010.

Scotland's Environment: Estuaries. [online] Available from: <https://www.environment.gov.scot/media/1175/water-estuaries.pdf>, 2014.

Scottish Environment Protection Agency: Inner Clyde Estuary monitoring buoy, Firth of Clyde, [online] Available from: <https://www.sepa.org.uk/environment/environmental-data/monitoring-buoys-network/inner-clyde-estuary/> (Accessed 23 April 2020a), 2020.

Scottish Environment Protection Agency: SEPA Water Level Data, [online] Available from: <https://www2.sepa.org.uk/WaterLevels/> (Accessed 23 April 2020b), 2020.

Scottish Government: Scottish Greenhouse Gas Statistics 2020, An Off. Stat. Publ. Scotl. [online] Available from: <https://www.gov.scot/news/scottish-greenhouse-gas-statistics-2020/>, 2022.

Scottish Power Energy Networks: Kennoxhead to Coalburn Overhead Line Minerals Report., 2019.

Seitzinger, S. P.: Denitrification in freshwater and coastal marine ecosystems: Ecological and geochemical significance, *Limnol. Oceanogr.*, 33(4part2), 702–724, doi:10.4319/lo.1988.33.4part2.0702, 1988.

Seitzinger, S. P. and Kroeze, C.: Global distribution of nitrous oxide production and N inputs in freshwater and coastal marine ecosystems, *Glob. Biogeochemical Cycles*, 12(1), 93–113, 1998.

Sela-Adler, M., Ronen, Z., Herut, B., Antler, G., Vigderovich, H., Eckert, W. and Sivan, O.: Co-existence of methanogenesis and sulfate reduction with common substrates in sulfate-rich estuarine sediments, *Front. Microbiol.*, 8(MAY), 1–11, doi:10.3389/fmicb.2017.00766, 2017.

SEPA: Riparian Vegetation Management, Engineering in the Water Environment, Good Practice Guide, , 2, 1–47, 2009.

SEPA: Water classification hub, Crown Copyright. SEPA Licens. Number 100016991 [online] Available from: <https://www.sepa.org.uk/data-visualisation/water-classification-hub/>, 2015.

SEPA: Delivering river basin planning in the Clyde catchment. [online] Available from: <https://www.sepa.org.uk/media/306627/delivering-river-basin-planning-in-the-clyde-catchment-may-2017.pdf>, 2017.

SEPA: Water Environment Hub, [online] Available from: <https://www.sepa.org.uk/data->

visualisation/water-environment-hub/?riverbasindistrict=Scotland, 2018.

Sha, C., Mitsch, W. J., Mander, Ü., Lu, J., Batson, J., Zhang, L. and He, W.: Methane emissions from freshwater riverine wetlands, *Ecol. Eng.*, 37(1), 16–24, doi:10.1016/j.ecoleng.2010.07.022, 2011.

Sharples, J., Mayor, D. J., Poulton, A. J., Rees, A. P. and Robinson, C.: Shelf Sea Biogeochemistry: Nutrient and carbon cycling in a temperate shelf sea water column, *Prog. Oceanogr.*, 177, doi:10.1016/j.pocean.2019.102182, 2019.

Sheoran, A. S. and Sheoran, V.: Heavy metal removal mechanism of acid mine drainage in wetlands: A critical review, *Miner. Eng.*, 19(2), 105–116, doi:10.1016/j.mineng.2005.08.006, 2006.

Shi, X., Gao, G., Tian, J., Wang, X. C., Jin, X. and Jin, P.: Symbiosis of sulfate-reducing bacteria and methanogenic archaea in sewer systems, *Environ. Int.*, 143(June), 105923, doi:10.1016/j.envint.2020.105923, 2020.

Sieczko, A. K., Schenk, J., Rudberg, D., Duc, N. T., Pajala, G., Sawakuchi, H. O. and Bastviken, D.: Minor impacts of rain on methane flux from hemiboreal, boreal, and subarctic lakes, *Sci. Total Environ.*, 895(June), 164849, doi:10.1016/j.scitotenv.2023.164849, 2023.

Silke F.K. Wewetzera, Robert W. Ducka, Anderson, J. M.: Acoustic Doppler current profiler measurements in coastal and estuarine environments: examples from the Tay Estuary, Scotland, *Geomorphology*, 29, 21–30, 1999.

Silvennoinen, H., Liikanen, A., Rintala, J. and Martikainen, P. J.: Greenhouse gas fluxes from the eutrophic Temmesjoki River and its Estuary in the Liminganlahti Bay (the Baltic Sea), *Biogeochemistry*, 90(2), 193–208, doi:10.1007/s10533-008-9244-1, 2008.

Stanienda-pilecki, K.: Stable Isotopes Carbon C 13 and Oxygen O 18 as Indicators of Triassic Limestone Sedimentation Environment and Diagenesis, *Res. Sq.*, 1–21, 2022.

Stanley, E. H., Casson, N. J., Christel, S. T., Crawford, J. T., Loken, L. C. and Oliver, S. K.: The ecology of methane in streams and rivers: Patterns, controls, and global significance, *Ecol. Monogr.*, 86(2), 146–171, doi:10.1890/15-1027, 2016.

Stanley, E. H., Loken, L. C., Casson, N. J., Oliver, S. K., Marcus, R. A. S., Liwei, B. W. and Gerard, Z.: GRiMeDB : The global river database of methane concentrations and fluxes, *Earth Sci. Data*, (October), 2022.

Stearns, M., Tindall, J. A., Cronin, G., Friedel, M. J. and Bergquist, E.: Effects of coal-bed methane discharge waters on the vegetation and soil ecosystem in Powder River Basin, Wyoming, *Water, Air, Soil Pollut.*, 168(1–4), 33–57, doi:10.1007/s11270-005-0588-z, 2005.

Stets, E. G., Butman, D., McDonald, C. P., Stackpoole, S. M., DeGrandpre, M. D. and Striegl, R. G.: Carbonate buffering and metabolic controls on carbon dioxide in rivers, *Global Biogeochem. Cycles*, 31(4), 663–677, doi:10.1002/2016GB005578, 2017.

Suto, N. and Kawashima, H.: Global mapping of carbon isotope ratios in coal, *J. Geochemical Explor.*, 167, 12–19, doi:10.1016/j.gexplo.2016.05.001, 2016.

Tait, D. R., Maher, D. T., Wong, W., Santos, I. R., Sadat-noori, M., Holloway, C. and Cook, P. L. M.: Greenhouse Gas Dynamics in a Salt-Wedge Estuary Revealed by High Resolution Cavity Ring-Down Spectroscopy Observations, *Environmental Sci. Technol.*, 51, 13771–13778, doi:10.1021/acs.est.7b04627, 2017.

Tall Ship Glenlee Trust: The Tall Ship Glenlee, [online] Available from: <https://thetallship.com/>, 2022.

Tang, W., Jayakumar, A., Sun, X., Tracey, J. C., Carroll, J., Wallace, E., Lee, J. A., Nathan, L. and Ward, B.: Nitrous Oxide Consumption in Oxygenated and Anoxic Estuarine Waters, *Geophys. Res. Lett.*, 49(21), 1–11, doi:10.1029/2022GL100657, 2022.

Thain, R. H., Priestley, A. D. and Davidson, M. A.: The formation of a tidal intrusion front at the mouth of a macrotidal, partially mixed estuary: a field study of the Dart estuary, UK., *Estuar. Coast. Shelf Sci.*, 61, 161–172, 2004.

The Coal Authority: Coal mine water treatment, [online] Available from: <https://www.gov.uk/government/collections/coal-mine-water-treatment> (Accessed 20 May 2020), 2017.

The Crown Estate: Minerals and Dredging, [online] Available from: <https://www.thecrownestate.co.uk/en-gb/what-we-do/on-the-seabed/minerals-dredging/>, 2021.

Thisani, S. K., Kallon, D. V. Von and Byrne, P.: Geochemical classification of global mine water drainage, *Sustain.*, 12(24), 1–16, doi:10.3390/su122410244, 2020.

Tian, M., Yang, X., Ran, L., Su, Y., Li, L., Yu, R., Hu, H. and Lu, X. X.: Impact of land cover types on riverine CO₂ outgassing in the Yellow River source region, *Water*, 11, doi:10.3390/w11112243, 2019.

Tittel, J., Hüls, M. and Koschorreck, M.: Terrestrial Vegetation Drives Methane Production in the Sediments of two German Reservoirs, *Sci. Rep.*, 1–10, doi:10.1038/s41598-019-52288-1, 2019.

Tomiyaama, S. and Igarashi, T.: ScienceDirect The potential threat of mine drainage to groundwater resources, *Environ. Sci. Heal.*, 27, 100347, doi:10.1016/j.coesh.2022.100347, 2022.

Tonina, D., Marzadri, A., Bellin, A., Dee, M. M., Bernal, S. and Tank, J. L.: Nitrous Oxide Emissions From Drying Streams and Rivers, *Geophys. Res. Lett.*, 48(24), 1–10, doi:10.1029/2021GL095305, 2021.

Topp, E. and Pattey, E.: Soils as sources and sinks for atmospheric methane, *Can. J. Soil Sci.*, 77(2), 167–178, doi:10.4141/s96-107, 1997.

Torres-Alvarado, M. D. R., Fernández, F. J., Ramírez Vives, F. and Varona-Cordero, F.: Dynamics of the methanogenic archaea in tropical estuarine sediments, *Archaea*, 2013, doi:10.1155/2013/582646, 2013.

Tye, A. M., Williamson, J. L., Jarvie, H. P., Dise, N. B., Lapworth, D. J., Monteith, D., Sanders, R., Mayor, D. J., Bowes, M. J., Burden, A., Callaghan, N., Farr, G., Felgate, S. L., Gibb, S., Gilbert, P. J., Hargreaves, G., Keenan, P., Kitidis, V., Jürgens, M. D., Martin, A., Mounteney, I., Nightingale, P. D., Pereira, M. G., Olszewska, J., Pickard, A., Rees, A. P., Spears, B., Stinchcombe, M., White, D., Williams, P., Worrall, F. and Evans, C. D.: Dissolved inorganic carbon export from rivers of Great Britain : Spatial distribution and potential catchment-scale controls, *J. Hydrol.*, 615(PA), 128677, doi:10.1016/j.jhydrol.2022.128677, 2022.

UKCEH: National River Flow Archive, UK Cent. Ecol. Hydrol. [online] Available from: <https://nrfa.ceh.ac.uk/data/station/info/84007>, 2010.

UKCEH: Land Cover Map 2015, UK Cent. Ecol. Hydrol. [online] Available from: <https://www.ceh.ac.uk/services/land-cover-map-2015>, 2020a.

UKCEH: National River Flow Archive, UK Cent. Ecol. Hydrol. [online] Available from:

<https://nrfa.ceh.ac.uk/> (Accessed 5 September 2020b), 2020.

UKCEH: UK River and Flow Regimes, [online] Available from: <https://nrfa.ceh.ac.uk/uk-river-flow-regimes>, 2022.

Uncles, R. J. and Stephens, J. A.: The freshwater-saltwater interface and its relationship to the turbidity maximum in the Tamar Estuary, United Kingdom, *Estuaries*, 16(1), 126–141, doi:10.2307/1352770, 1993.

UNECE: Best Practice Guidance for Effective Methane Recovery and Use from Abandoned Coal Mines., 2019.

Upstill-Goddard, R. C. and Barnes, J.: Methane emissions from UK estuaries: Re-evaluating the estuarine source of tropospheric methane from Europe, *Mar. Chem.*, 180, 14–23, doi:10.1016/j.marchem.2016.01.010, 2016a.

Upstill-Goddard, R. C. and Barnes, J.: Methane emissions from UK estuaries: Re-evaluating the estuarine source of tropospheric methane from Europe, *Mar. Chem.*, 180, 14–23, doi:10.1016/j.marchem.2016.01.010, 2016b.

Upstill-Goddard, R. C., Barnes, J., Frost, T. and Punshon, S.: Methane in the southern North Sea: Low-salinity inputs, estuarine removal, and atmospheric flux, *Global Biogeochem. Cycles*, 14(4), 1205–1217, doi:10.1029/1999GB001236, 2000.

Vachon, D., Sponseller, R. A. and Karlsson, J.: Integrating carbon emission, accumulation and transport in inland waters to understand their role in the global carbon cycle, *Glob. Chang. Biol.*, (August 2020), 719–727, doi:10.1111/gcb.15448, 2021.

Valdemarsen, T., Quintana, C. O., Flindt, M. R. and Kristensen, E.: Organic N and P in eutrophic fjord sediments - Rates of mineralization and consequences for internal nutrient loading, *Biogeosciences*, 12(6), 1765–1779, doi:10.5194/bg-12-1765-2015, 2015.

Vane, C. H., Harrison, I. and Kim, A. W.: Assessment of polyaromatic hydrocarbons (PAHs) and polychlorinated biphenyls (PCBs) in surface sediments of the Inner Clyde Estuary, UK, *Mar. Pollut. Bull.*, 54(8), 1301–1306, doi:10.1016/j.marpolbul.2007.04.005, 2007.

Vaughan, M. C. H. and Schroth, A. W.: Shining light on the storm : in-stream optics reveal hysteresis of dissolved organic matter character, *Biogeochemistry*, 143(3), 275–291, doi:10.1007/s10533-019-00561-w, 2019.

Vaughan, M. C. H., Bowden, W. B., Shanley, J. B., Vermilyea, A., Sleeper, R., Gold, A. J., Pradhanang, S. M., Inamdar, S. P., Levia, D. F., Andres, A. S., Birgand, F. and Schroth, A. W.: High-frequency dissolved organic carbon and nitrate measurements reveal differences in storm hysteresis and loading in relation to land cover and seasonality, *Water Resour. Res.*, 5345–5363, doi:10.1002/2017WR020491. Received, 2017.

Vesper, D. J., Moore, J. E. and Adams, J. P.: Inorganic carbon dynamics and CO₂ flux associated with coal-mine drainage sites in Blythedale PA and Lambert WV, USA, *Environ. Earth Sci.*, 75(4), 1–14, doi:10.1007/s12665-015-5191-z, 2016.

Voogt, P. De: *Reviews of Contamination and Toxicology.*, 2020.

Wan, R., Cai, S., Li, H., Yang, G., Li, Z. and Nie, X.: Inferring land use and land cover impact on stream water quality using a Bayesian hierarchical modeling approach in the Xitiao River Watershed, China, *J. Environ. Manage.*, 133, 1–11, doi:10.1016/j.jenvman.2013.11.035, 2014.

Wang, C. F., Hsu, M. H. and Kuo, A. Y.: Residence time of the Danshuei River estuary, Taiwan, *Estuar. Coast. Shelf Sci.*, 60(3), 381–393, doi:10.1016/j.ecss.2004.01.013, 2004.

Wang, G., Xia, X., Liu, S., Zhang, L., Zhang, S., Wang, J., Xi, N. and Zhang, Q.: Intense methane ebullition from urban inland waters and its significant contribution to greenhouse gas emissions, *Water Res.*, 189, 116654, doi:10.1016/j.watres.2020.116654, 2021a.

Wang, X., Gao, Y., Jiang, X., Zhang, Q. and Liu, W.: Analysis on the Characteristics of Water Pollution Caused by Underground Mining and Research Progress of Treatment Technology, *Adv. Civ. Eng.*, doi:https://doi.org/10.1155/2021/9984147, 2021b.

Wanninkhof, R.: Relationship Between Wind Speed and Gas Exchange Over the Ocean, *J. Geophys. Res.*, 97(C5), 7373–7382, 1992.

Wanninkhof, R.: Relationship between wind speed and gas exchange over the ocean revisited, *Limnol. Oceanogr. Methods*, 12(JUN), 351–362, doi:10.4319/lom.2014.12.351, 2014.

Watten, B. J., Sibrell, P. L. and Schwartz, M. F.: Acid neutralization within limestone sand reactors receiving coal mine drainage, *Environ. Pollut.*, 137(2), 295–304, doi:10.1016/j.envpol.2005.01.026, 2005.

Weishaar, J. L., Aiken, G. R., Bergamaschi, B. A., Fram, M. S., Fujii, R. and Mopper, K.: Evaluation of specific ultraviolet absorbance as an indicator of the chemical composition and reactivity of dissolved organic carbon, *Environ. Sci. Technol.*, 37(20), 4702–4708, doi:10.1021/es030360x, 2003.

Weiss, R. F. and Price, B. A.: Nitrous oxide solubility in water and seawater, *Mar. Chem.*, 8(4), 347–359, doi:[doi:10. 1016/ 0304- 4203(80)90024-9]., 1980.

Whitworth, K., England, A. and Parry, D.: Overview of Mine Water in the UK Coalfields Project: Advice on Mine Water recovery and Mine Gas. [online] Available from: www.wyg.com, 2012.

Wiesenburg, D. A. and Guinasso, N. L.: Equilibrium Solubilities of Methane , Carbon Monoxide , and Hydrogen in Water and Sea Water, *J. Chem. Eng. Data*, 24(4), 356–360, 1979.

De Wilde, H. P. J. and De Bie, M. J. M.: Nitrous oxide in the Schelde estuary: Production by nitrification and emission to the atmosphere, *Mar. Chem.*, 69(3–4), 203–216, doi:10.1016/S0304-4203(99)00106-1, 2000.

Wilkinson, J. L., Boxall, A. B. A., Kolpin, D. W., Leung, K. M. Y., Lai, R. W. S., Wong, D., Ntchantcho, R., Pizarro, J., Mart, J., Echeverr, S., Garric, J., Chaumot, A., Gibba, P., Kunchulia, I., Seidensticker, S., Lyberatos, G., Morales-salda, J. M. and Kang, H.: Pharmaceutical pollution of the world's rivers, *PNAS*, 119(8), 1–10, doi:10.1073/pnas.2113947119/-/DCSupplemental.Published, 2022.

Williams, C. J., Frost, P. C., Morales-williams, A. M., Larson, J. H., Richardson, W. B., Chiandet, A. S. and Xenopoulos, M. A.: Human activities cause distinct dissolved organic matter composition across freshwater ecosystems, *Glob. Chang. Biol.*, 613–626, doi:10.1111/gcb.13094, 2016.

Winterdahl, M., Wallin, M. B., Karlsen, R. H., Laudon, H., Öquist, M. and Lyon, S. W.: Decoupling of carbon dioxide and dissolved organic carbon in boreal headwater streams, *J. Geophys. Res. Biogeosciences*, 121(10), 2630–2651, doi:10.1002/2016JG003420, 2016.

Wrage, N., Velthof, G. L., Van Beusichem, M. L. and Oenema, O.: Role of nitrifier denitrification in the production of nitrous oxide, *Soil Biol. Biochem.*, 33(12–13), 1723–1732, doi:10.1016/S0038-0717(01)00096-7, 2001.

- Wright, I. A., Belmer, N. and Davies, P. J.: Coal Mine Water Pollution and Ecological Impairment of One of Australia's Most 'Protected' High Conservation-Value Rivers, *Water, Air, Soil Pollut.*, 228(3), doi:10.1007/s11270-017-3278-8, 2017.
- Xia, Y., Li, Y., Li, X., Guo, M., She, D. and Yan, X.: Diurnal pattern in nitrous oxide emissions from a sewage-enriched river, *Chemosphere*, 92(4), 421–428, doi:10.1016/j.chemosphere.2013.01.038, 2013.
- Xiong, J., Liu, Z., Yan, Y., Xu, J., Liu, D., Tan, W. and Feng, X.: Role of clay minerals in controlling phosphorus availability in a subtropical Alfisol, *Geoderma*, 409(June 2021), 115592, doi:10.1016/j.geoderma.2021.115592, 2022.
- Younger, P. L.: The longevity of minewater pollution : a basis for decision making, *Sci. Total Environ.*, 194/195, 1997.
- Younger, P. L.: Mine water pollution in Scotland: Nature, extent and preventative strategies, *Sci. Total Environ.*, 265(1–3), 309–326, doi:10.1016/S0048-9697(00)00673-2, 2001.
- Yu, Z., Deng, H., Wang, D., Ye, M., Tan, Y., Li, Y., Chen, Z. and Xu, S.: Nitrous oxide emissions in the Shanghai river network: Implications for the effects of urban sewage and IPCC methodology, *Glob. Chang. Biol.*, 19(10), 2999–3010, doi:10.1111/gcb.12290, 2013.
- Yu, Z., Wang, D., Li, Y., Deng, H., Hu, B., Ye, M., Zhou, X., Da, L., Chen, Z. and Xu, S.: Carbon dioxide and methane dynamics in a human- dominated lowland coastal river network (Shanghai, China), *J. Geophys. Res. Biogeosciences*, 1738–1758, doi:10.1002/2017JG003798, 2017.
- Zarnetske, J. P., Haggerty, R., Wondzell, S. M. and Baker, M. A.: Dynamics of nitrate production and removal as a function of residence time in the hyporheic zone, *J. Geophys. Res.*, 116(March 2010), 1–12, doi:10.1029/2010JG001356, 2011.
- Zhang, J., Quay, P. D. and Wilbur, D. O.: Carbon isotope fractionation during gas-water exchange and dissolution of CO₂, *Geochim. Cosmochim. Acta*, 59(1), 107–114, doi:10.1016/0016-7037(95)91550-D, 1995.
- Zhang, S., Yan, L., Cao, J., Wang, K., Luo, Y., Hu, H., Wang, L., Yu, R., Pan, B., Yu, K., Zhao, J. and Bao, Z.: Salinity significantly affects methane oxidation and methanotrophic community in Inner Mongolia lake sediments, *Front. Microbiol.*, 13(January), doi:10.3389/fmicb.2022.1067017, 2023.
- Zhang, W., Yan, C., Shen, J., Wei, R., Gao, Y., Miao, A., Xiao, L. and Yang, L.: Characterization of aerobic denitrifying bacterium *Pseudomonas mendocina* strain GL6 and its potential application in wastewater treatment plant effluent, *Int. J. Environ. Res. Public Health*, 16(3), doi:10.3390/ijerph16030364, 2019.
- Zhang, W., Li, H., Xiao, Q. and Li, X.: Urban rivers are hotspots of riverine greenhouse gas (N₂O, CH₄, CO₂) emissions in the mixed-landscape chaohu lake basin, *Water Res.*, 189, 116624, doi:10.1016/j.watres.2020.116624, 2021.
- Zhao, J., Liu, Y., Wang, D., Chen, F., Li, X., Zeng, G. and Yang, Q.: Potential impact of salinity on methane production from food waste anaerobic digestion, *Waste Manag.*, 67, 308–314, doi:10.1016/j.wasman.2017.05.016, 2017.
- Zheng, Y., Wu, S., Xiao, S., Yu, K., Fang, X., Xia, L., Wang, J., Liu, S., Freeman, C. and Zou, J.: Global methane and nitrous oxide emissions from inland waters and estuaries, *Glob. Chang. Biol.*, 28(15), 4713–4725, doi:10.1111/gcb.16233, 2022a.

Zheng, Y., Wu, S., Xiao, S., Yu, K., Fang, X., Xia, L., Wang, J., Liu, S., Freeman, C. and Zou, J.: Global methane and nitrous oxide emissions from inland waters and estuaries, , (February), 4713–4725, doi:10.1111/gcb.16233, 2022b.

Zhou, Y., Toyoda, R., Suenaga, T., Aoyagi, T. and Hori, T.: Low nitrous oxide concentration and spatial microbial community transition across an urban river affected by treated sewage, *Water Res.*, 216(February), 118276, doi:10.1016/j.watres.2022.118276, 2022a.

Zhou, Y., Toyoda, R., Suenaga, T., Aoyagi, T. and Hori, T.: Low nitrous oxide concentration and spatial microbial community transition across an urban river affected by treated sewage, *Water Res.*, 216(February), 118276, doi:10.1016/j.watres.2022.118276, 2022b.

Zhu, W., Wang, C., Hill, J., He, Y., Tao, B. and Mao, Z.: A missing link in the estuarine nitrogen cycle?: Coupled mediated by suspended particulate matter, *Sci. Rep.*, (January), 1–10, doi:10.1038/s41598-018-20688-4, 2018.

Appendices

Appendix 1 - Clyde river survey locations

Sample site 1: L1-T-RCRoger Clench

*Semi-natural landscape with some sheep grazing, stream is steep sloped with waterfalls
Sampled from stream bank, no gauging available*



View upstream from sampling location



View of sampling location

Sample site 2: L2-C-DRI- Daer Water - reservoir inflow

*Semi-natural landscape with some sheep grazing, stream flows into Daer reservoir
Sampled from stream bank, no gauging available*



View of sampling location



Flow into Daer reservoir in very dry conditions

Sample site 3: L3-C-DO - Daer Water - reservoir outflow

*Semi-natural landscape with sheep grazing, stream is controlled flow out of Daer reservoir
Sampled from stream bank. Gauging: compensation flow from Daer Reservoir*



View downstream from sampling location



View upstream from sampling location

Sample site 4: L4-T-MW- Midlock Water

Semi-natural landscape with established farming and extensive sheep and cattle grazing. Sampled from stream bank, no gauging available



View upstream from sampling location



View upstream to sampling location

Sample site 5: L5-T-CW- Camps Water

Semi-natural landscape with established farming and sheep and cattle grazing, Sampled from stream bank. Gauging: compensation flow from Camps Reservoir



View upstream from sampling location



View downstream from sampling location

Sample site 6: L6-T-DW- Duneaton Water at Maidencots

Semi-natural landscape with farming moor and forestry Sampled from stream bank 400m downstream of SEPA gauge.



View upstream from sampling location



View of Duneaton Water joining River Clyde

Sample site 7: L7-C-AB - Clyde at Abington

Semi-natural landscape with establish farm and sheep and cattle grazing and forestry
Sampled from bridge over river, 4m downstream from Abington SEPA station



View upstream from sampling location



View downstream from sampling location

Sample site 8: L8-C-SY - Clyde at the Symington

Rural landscape with establish farm and sheep and cattle grazing adjacent river,
Sampled from river bank by bridge (Note 4km downstream from Lamington quarry)



View downstream from sampling location



View of sampling location

Sample site 9: L9-C-SL- Clyde at Sills of Clyde

Flat pastoral and arable agricultural landscape with small towns and extensive farm land
Sampled from bridge 1.9km meters downstream of Sills of Clyde SEPA gauge



View downstream from sampling location



View upstream from sampling location

Sample site 10: L10-T-DW- Douglas Water at Happendon

*Pastoral and agricultural landscape with small towns, Mining outflow entering river
Sampled from bridge 5m downstream of Douglas water SEPA gauge (weir type)*



View upstream from sampling location



View of sampling locations and SEPA weir

Sample site 11: L11-C-TM - Clyde at Tulliford Mill

*Pastoral and agricultural landscape with small towns (Last stations before falls of Clyde)
Sampled from river bank 200m downstream of Tulliford Mill SEPA gauge*



View upstream in low flow conditions



View downstream from sampling location

Sample site 12: L12-C-KB - Clyde at Kirkfieldbank

Pastoral and agricultural landscape with more small towns. Sampled prior to Mouse Water entering and 120m upstream of Kirkfieldbank gauge (mostly non-operational)



View downstream from sampling location



View upstream from sampling location

Sample site 13: L13-T-MW- Mouse Water

Pastoral and agricultural landscape with more small towns. Mostly agricultural catchment with Peat. Sampled from bridge directly before entering River Clyde, no gauge.



View downstream from sampling location

Bridge used for sampling

Sample site 14: L14-C-HB - Clyde at Hazelbank

*Suburban landscape with more towns covering more area
Sampled from bank 1.4km downstream from SEPA river gauge*



View of sampling location

View of outfalls on bank

Sample site 15: L15-T-NW - Nethan at Kirkmuirhill

*Suburban and rural landscape near town, sampling locations between two UWWTP
Sampled from bank, 950m downstream from SEPA river gauge*



View of sampling location

View downstream from sampling location

Sample site 16: - L16- C-GB - Clyde at Garrion bridge

Suburban landscape with significant road network in this area
 Sample from Garrion Bridge, flow assumed summed flow of Clyde and Nethan Water



View downstream during low flow

Sample site 17: L17-T AW - Avon Water at Fairholm

Suburban and agricultural landscape near town, sampling locations below UWWTP
 Samples from bank below weir, which did cause out-gassing of dissolved gases



Sampling locations during low flow



Sampling locations during high flow

Sample site 18: L18-C-HA - Clyde at Hamilton

Suburban location adjacent to parkland after Avon Water but before Strathclyde loch joined
 Samples from River Bank



View upstream from sampling location



View downstream from sampling location

Sample site 19: L19-T-SC- South Calder Water

Suburban river with three UWWTP above sampling location
 Sampled from foot bridge 1.6km downstream from old gauging station



View upstream – showing debris and foam

View downstream from sampling location

Sample site 20: L20-T-SL - Strathclyde Loch

Suburban location, partly built from excavated mining depression but now parkland
 Inflow from South Calder Water and gauging assumed to be as for South Calder Water

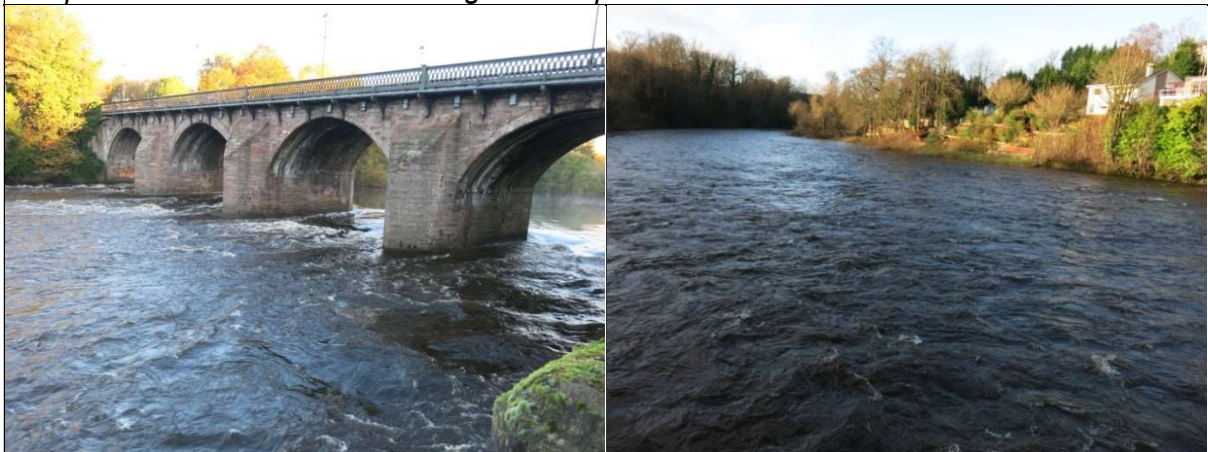


Sampling location - Frozen during winter

Sampling location in summer -low water level

Sample site 21: L21-C-BS - Clyde at Blairston

Suburban location, 300m below UWWTP outfall from Hamilton Sewage works
 Sampled from walled bank foot bridge 700m upstream of Blairston SEPA station



View upstream from sampling location

View downstream from sampling location

Sample site 22: L22-T-RC - Rotten Calder at Redless

Suburban location with some agriculture but also old landfill in catchment and downstream of UWWTP. Sampled 105m upstream of Redless SEPA station



View downstream from sampling location

View of sampling location looking upstream

Sample site 23: L23-T-NC - North Calder at Calderpark

Suburban location, with significant road network in catchment including M8 and M74

Sampled 240m downstream of Calderpark SEPA station



View upstream from sampling location

View downstream from sampling location

Sample site 24: L24-C-DD – Clyde at Daldowie

Suburban location, Sampled 400m upstream of Daldowie UWWTP

Sampled from river bank at Daldowie SEPA Gauging station



View downstream from sampling location

Sampling location during low flow

Sample site 25: L25- C-CL- Clyde at Cambuslang

Highly urban location, 3.1km downstream of Daldowie UWWTP
Sample from foot bridge over river Clyde; Gauging assumed as Daldowie



View upstream showing second foot bridge



View downstream during low flow conditions

Sample site 26: L26- C-GG - Clyde at Glasgow Green

Highly urban location, 2.5km downstream of Dalmarnock UWWTP
Sample from platform on bank of river; Gauging assumed as Daldowie



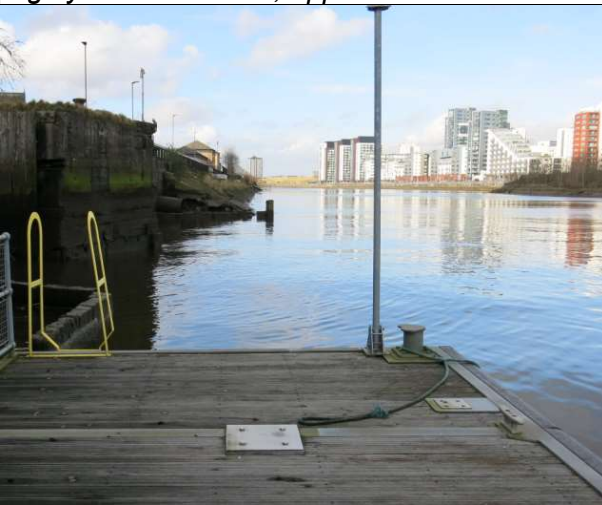
View downstream to tidal weir



View upstream to brewery

Sample site 27: L27-C-GV – Clyde Estuary at Govan Pontoon

Highly urban location, opposite entrance to Kelvin river – Sampled from pontoon



View looking west from Govan pontoon



View looking east from Govan pontoon

Sample site 28: L28-C-BH – Clyde Estuary at Braehead Pontoon

Urban location 1.5km west of the outflow from the Shieldhall UWWTP and adjacent smaller outflows - Sampled from pontoon



View of pontoon looking east towards Glasgow



Outflow entering estuary adjacent pontoon

Examples of visible pollution sources in Clyde Tributaries



Pollution in high flow on Avon water



Acid mine inflow entering South Calder water

Examples of visible pollution sources in Clyde Tributaries



Scum building up on South Calder Water



Outflow from Strathclyde Loch

Appendix 2 - Mine water survey locations

Sample site MA1- Lathallan Mill



View of outflow stream



View of reed beds

Sample site MA2- Mains of Blairingone



View of aerations cascade



View of reed beds

Sample site MA3- Minto



View of outflow from shaft



View of cascade

Sample site MA4- Frances



Aeration cascade at frances

View of one of the setting pools

Sample site MA5- Pitfirrane



Pitfirrane outflow

Aeration at treatment facility

Sample site MA6- Bilston (Junkie's Adit)



View of Junkie's Adit

View of South Esk after inflow from Adit

Sample site MA7- Cuthill



View

View

Sample site MA9- Shotts



View of outflow

Mine water mixing with South Calder Water

Sample site MA10- East Allerton



View of pool below adit

View of reed pools in Spring

Sample site MA11- Kingshill



View of outflow



View of tope of Cascade



Reed pools in winter

Sample site MA12- Poolfarm



View



View

Sample site MA13- Mousewater



View of deepwater pool



View of reed beds

Sample site MA14- CoalBurn



Aerial view of adit coming to surface

Stream flowing under bridge

Sample site MA15- Glespin



Glespin Adit

Adit flowing into Glespin burn

Sample site MA16- Kames



View of treatment for flow from shaft

Shaft now overgrown

Appendix 3 - Estuarine survey locations

Figure A.1. Braehead pontoon at low tide looking west



Figure A.2. Dredging vessel involved in dredging of King George V dock inland of the Braehead pontoon in August 2020



Figure A.3. Braehead pontoon at high tide



Figure A.4. Braehead pontoon at low tide





Figure A.5a. Outflow to estuary at low tide during a spring tide adjacent to and photographed from the Braehead pontoon



Figure A.5b. Outflow to estuary on an incoming tide at mid-tide adjacent to and photographed from the Braehead pontoon



Figure A.5c. Outflow to estuary near to high tide adjacent to and photographed from the Braehead pontoon

Figure A.6. Survey equipment



Bottom Sampler

Floating chamber on Clyde estuary

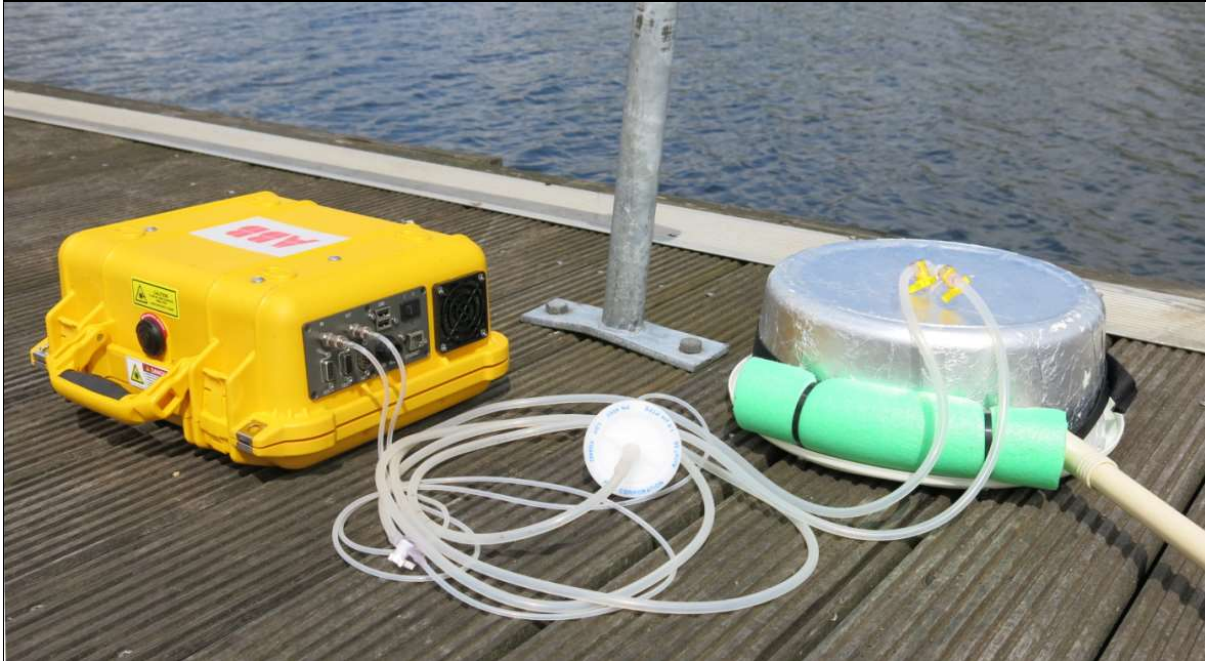


ABB GHG analyser and floating chamber

Addendum 1 - Urban landscapes and legacy industry provide hotspots for riverine greenhouse gases: A source-to-sea study of the River Clyde

The paper has been published in the Water Research volume 236

<https://www.sciencedirect.com/science/article/pii/S0043135423004050>

with the following DOI - <https://doi.org/10.1016/j.watres.2023.119969>



Urban landscapes and legacy industry provide hotspots for riverine greenhouse gases: A source-to-sea study of the River Clyde

Alison M. Brown^{a,b,*}, Adrian M. Bass^b, Ute Skiba^a, John M. MacDonald^b, Amy E. Pickard^a

^a UK Centre for Ecology & Hydrology (Edinburgh), Bush Estate, Pentlands, Midlothian, EH26 0QB, UK

^b University of Glasgow, College of Science and Engineering, School of Geographical and Earth Sciences, University Avenue, Glasgow, G12 8QQ, UK

ARTICLE INFO

Keywords:

Methane
Nitrous oxide
Carbon dioxide
Urban wastewater
Agriculture
Mine water

ABSTRACT

There is growing global concern that greenhouse gas (GHG) emissions from water bodies are increasing because of interactions between nutrient levels and climate warming. This paper investigates key land-cover, seasonal and hydrological controls of GHGs by comparison of the semi-natural, agricultural and urban environments in a detailed source-to-sea study of the River Clyde, Scotland. Riverine GHG concentrations were consistently oversaturated with respect to the atmosphere. High riverine concentrations of methane (CH₄) were primarily associated with point source inflows from urban wastewater treatment, abandoned coal mines and lakes, with CH₄-C concentrations between 0.1 - 44 µg l⁻¹. Concentrations of carbon dioxide (CO₂) and nitrous oxide (N₂O) were mainly driven by nitrogen concentrations, dominated by diffuse agricultural inputs in the upper catchment and supplemented by point source inputs from urban wastewater in the lower urban catchment, with CO₂-C concentrations between 0.1 - 2.6 mg l⁻¹ and N₂O-N concentrations between 0.3 - 3.4 µg l⁻¹. A significant and disproportionate increase in all GHGs occurred in the lower urban riverine environment in the summer, compared to the semi-natural environment, where GHG concentrations were higher in winter. This increase and change in GHG seasonal patterns points to anthropogenic impacts on microbial communities. The loss of total dissolved carbon, to the estuary is approximately 48.4 ± 3.6 Gg C yr⁻¹, with the annual inorganic carbon export approximately double that of organic carbon and four times that of CO₂ with CH₄ accounting for 0.03%, with the anthropogenic impact of disused coal mines accelerating DIC loss. The annual loss of total dissolved nitrogen to the estuary is approximately 4.03 ± 0.38 Gg N yr⁻¹ of which N₂O represents 0.06%. This study improves our understanding of riverine GHG generation and dynamics which can contribute to our knowledge of their release to the atmosphere. It identifies where action could support reductions in aquatic GHG generation and emission.

1. Introduction

Greenhouse gas (GHG) evasion from inland waters is a significant source of atmospheric GHGs. Global carbon dioxide (CO₂) evasion has been estimated as 1.8 ± 0.25 Pg C yr⁻¹ from streams and rivers, resulting in a global evasion rate from inland waters of 2.1 Pg C yr⁻¹ (Raymond et al., 2013). The contribution from streams and rivers is large relative to their surface area, acting as hotspots for the exchange of gases with the atmosphere. The major sources of CO₂ are direct input via groundwater inflow, which transports CO₂ originating from soil respiration, and in-stream mineralization of organic carbon (OC) often from surface run-off (Winterdahl et al., 2016). Riparian wetlands also contribute disproportionately to CO₂ emissions (Abril and Borge, 2019). The relative importance of these mechanisms changes with

stream order as headwater streams have a larger soil-water interface compared to lower reaches, resulting in the proportion of CO₂ produced from aquatic metabolism increasing with stream size (Marx et al., 2017; Hotchkiss et al., 2015). The magnitude of CO₂ riverine emissions is highly dependant on hydrology (Gomez-Gener et al., 2016). In urban areas significantly higher nutrients, organic matter content, and riverine cyanobacteria impact CO₂ variation (Salgado et al., 2022). Global methane (CH₄) evasion from inland waters was estimated at 390.1 ± 79.4 Tg CH₄ yr⁻¹, with rivers evading 30.5 ± 17.1 Tg CH₄ yr⁻¹, with aquatic ecosystems contributing about half of total global CH₄ emissions from anthropogenic and natural sources (Roentzner et al., 2021). Total CH₄ emissions were found to increase from natural to impacted and from coastal to freshwater ecosystems, with emissions expected to increase due to urbanization, eutrophication and positive climate feedbacks,

* Corresponding author at: -UK Centre for Ecology & Hydrology.
E-mail address: albrown52@ceh.ac.uk (A.M. Brown).

<https://doi.org/10.1016/j.watres.2023.119969>

Received 11 December 2022; Received in revised form 1 April 2023; Accepted 9 April 2023

Available online 12 April 2023

0043-1354/© 2023 The Authors. Published by Elsevier Ltd. This is an open access article under the CC BY license (<http://creativecommons.org/licenses/by/4.0/>).

although there is significant uncertainty in the production, transportation and consumption processes (Rosentreter et al., 2021; Stanley et al., 2016). Similarly the production and emission of nitrous oxide (N_2O) from aquatic systems are uncertain ($0.3 - 2.1 \text{ Tg } N_2O-N \text{ yr}^{-1}$) with large spatial and temporal variability in emission estimates (Geitzinger and Kroese, 1990; Beaulieu et al., 2011; Clois et al., 2013). However N_2O emissions from rivers, reservoirs and estuaries have been estimated as $140 - 277 \text{ Gg } N \text{ yr}^{-1}$ with anthropogenic perturbations to river systems resulting in a two to four-fold increase in N_2O emissions from inland waters (Maavara et al., 2019). The dominance of N_2O emissions emanating from nitrification or denitrification in inland waters is partly dependant on residence time (Zarnetske et al., 2011).

Urban rivers and lakes are potential hotspots for GHG emissions and there is an increasing body of literature concerned with quantifying their contribution to aquatic GHG emissions (Zhang et al., 2021; Wang et al., 2021; Gu et al., 2021; Herrero Ortega et al., 2019; Martinez-Cruz et al., 2017 and Garnier et al., 2009). In Mexico City water quality indicators (such as trophic state index and phosphorous level) were positively correlated with CH_4 emissions, suggesting a reduction in untreated wastewater discharge could concurrently reduce GHG emissions. Fluxes of CH_4 were highly variable, both in and across ecosystem locations and seasons (Martinez-Cruz et al., 2017) demonstrating the need for comprehensive studies to understand these temporal dynamics. In water bodies around the city of Berlin, a combination of high nutrient supply and shallow depth produced large CH_4 emissions. However dissolved oxygen and productivity were found to be poor predictors of CH_4 emissions, suggesting a complex combination of factors governed CH_4 fluxes from urban surface waters (Herrero Ortega et al., 2019). Conversely in rivers and lakes within the city of Beijing, high CH_4 emissions were attributed to high dissolved and sediment organic carbon, high aquatic primary production and shallow water depths, although results were again highly variable (Wang et al., 2021). In the Chaohu Lake basin in eastern China, diffusive CH_4 and N_2O emissions from rivers were due to large nutrient supply and hypoxic environments, with CO_2 impacted by temperature-dependant rapid decomposition of organic matter (Zhang et al., 2021). Positive correlations between temperature and GHG concentrations have been routinely observed (Wang et al., 2021; Herrero Ortega et al., 2019 and Rosentreter et al., 2021). The presence of ammonia, entering inland water from agriculture or wastewater, can inhibit CH_4 oxidation resulting in elevated CH_4 concentrations compared to low nitrogen systems and high evasion to atmosphere (Dunfield and Knowles, 1995; Boese et al., 1993; Cotovic et al., 2021). Conversely in an investigation of N_2O concentrations upstream and downstream of wastewater treatment plants (WWTPs) in an urban river in Japan, lower N_2O concentrations were found in summer (Y. Zhou et al., 2022). Positive correlations between GHGs in surface waters and catchment agricultural landcover linked to higher levels of organic matter and dissolved inorganic nitrogen from the agricultural dominated areas have been found significant, with increases in GHG levels during prolonged low water levels (Borges et al., 2018).

GHG emissions are difficult to attribute to sources due to multiple generation and consumption pathways and high spatial and temporal variability (Rosentreter et al., 2021). Their production results from the interplay of multiple drivers and is influenced by, high between and within-system variation, with the causes of this variation unknown. This variation causes difficulties in upscaling emissions from local-scale studies resulting in a need for more detailed studies measuring more in-water parameters across a large temporal and spatial scales. It is hypothesised, in this paper, the reasons for the high variation and poor predictability include:

- 1 GHGs are not conserved like dissolved nutrients but readily out-gas especially in the riverine environment with flow intensity and high stream slopes the primary controls (Long et al., 2015; Maurice et al., 2017; Natchimuthu et al., 2017; Liu and Raymond, 2018).

- 2 The number of different source types within the riverine environment, including: point, diffuse and in-water generation, change with land-use and need to be distinguished.
- 3 The concentration of nutrients is only one aspect of GHG generation, which changes with availability of electron donors and acceptors, such that mixing of waters may stimulate GHG production (Wrage et al., 2001; Furukawa et al., 2004; Broder et al., 2012; Zhang et al., 2019).
- 4 Different GHG sources and dynamics dominate in different types and sizes of water body dependant on: land-water interface, depth, hydraulic regime, sediments-water-air interfaces, residence time, land-use, physio-chemical properties, microbial communities, seasonality, and anthropogenic impacts on seasonal patterns of changing water level and temperature.

The concentrations of GHGs in the riverine water column result from the balance between input, consumption, production and output (Fig. 1).

Given the potential significance, but inadequate quantification and characterisation of urban catchment fluvial GHG dynamics, further insight into how to quantify and interpret riverine GHG concentration data could support improved estimates. This study addressed the following key objectives: (1) does using a source-to-sea investigative approach allows quantification of how changes in the nature and size of the riverine environment impact GHG concentrations, (2) can the key controls on GHG generation be determined by comparison of the semi-natural, agricultural and urban environments, including key landcover, seasonal and hydrological controls, and (3) can point source, diffuse source and in water generation be distinguish for different GHGs. A large temperate catchment was selected for the investigation, where landcover transitioned from semi-natural, through pastoral and arable agricultural to urban (including legacy industrial), as representative of many urbanised catchments globally.

2. Materials and method

2.1. Study area

The River Clyde is the third longest river in Scotland (170 km) with a total river network length of 4244 km and drains a of 1903 km^2 (Clyde River Foundation, 2020). The River Clyde together with the rivers Kelvin, White Cart, Black Cart and Leven enter the Clyde estuary, with a catchment area of 3854 km^2 (Nedwell et al., 2002), which is home to 33.8% (1.79 million) of Scotland's total population (Clyde River Foundation, 2020). Surface water quality, as assessed in accordance with the European water framework directive (SEPA, 2018 and Natural Scotland, 2015), ranges from 'High' in some small tributaries to 'Bad' in some urban tributaries, with much of the River Clyde rated as 'Moderate'. The groundwater quality is also rated as 'Poor', both in the upper catchment in the Leadhills area and the lower urban catchment. The River Clyde's mean annual flows is $48.3 \text{ m}^3 \text{ s}^{-1}$ with the maximum flow of $560.5 \text{ m}^3 \text{ s}^{-1}$ (24th January 2018) as measured at Daldowie gauging station (supplementary data Table A1.1) based on data between 1963 and 2019 (UK Centre of Ecology & Hydrology (UKCEH), 2020). The upper moorland catchment consists of steep rough ground with hill pasture and some forestry as the major land use. In the middle catchment there is mixed farming including arable and pastoral and significant urbanisation in the lower catchment.

2.2. Sites description and data collections

Twenty-six measurement locations were selected on the River Clyde and its major tributaries. The locations were distributed along the River Clyde from near the source on Daer Water, above Daer reservoir, to Glasgow Green just above the Clyde tidal weir, which separates two distinct habitats of fresh and salt water. The sample locations are shown

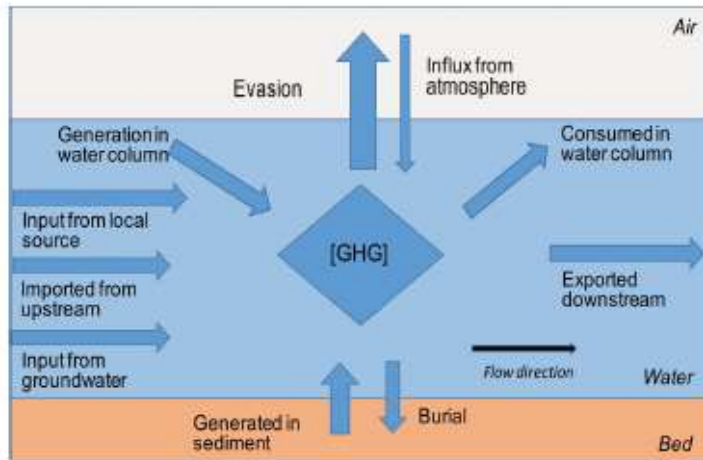


Fig. 1. GHG generation, transport and loss. In the schematic the arrows show the direction of GHG movement into/out from the sediment (brown), water (blue) and air (grey). The balance between the different sources and sinks changes along the river course. Both river slope and hydrology impact this balance as they influence water residence times, sedimentation, out-gassing and nutrient concentrations from point and diffuse sources. (For interpretation of the references to colour in this figure legend, the reader is referred to the web version of this article.)

spatially against both the water network of the River Clyde and tributaries (Fig. 2A) and the catchment land cover (Fig. 2B). Full details of the survey locations are provided in the supplementary information Table A1.1 with photographs in Figure A2. Samples were collected monthly between January 2020 and December 2021 at all locations. Twenty-one sampling campaigns were undertaken as no sampling was permitted during the period April to June 2020 due to Covid-19 working restrictions. Each sampling campaign was undertaken over two

consecutive days with samples collected at the upper catchment sites on day one and in the lower catchment on day two. Sample filtration and processing was undertaken on the same day as sample collection.

2.3. Field sampling and laboratory measurements

Dissolved gas samples were collected in triplicate at each location using the headspace method, prior to the collected water being

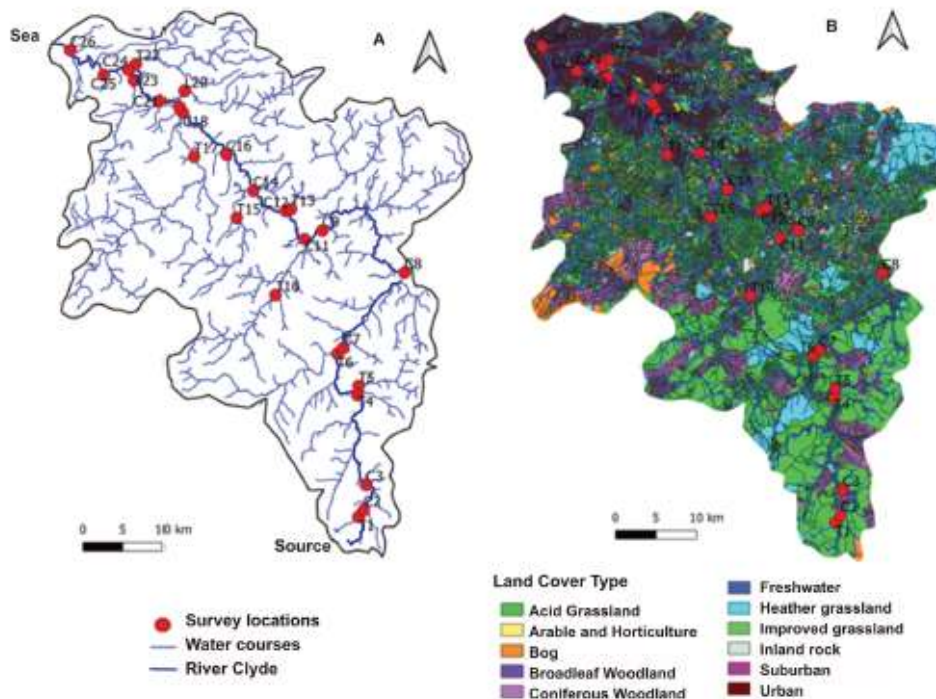


Fig. 2. Spatial plots of the River Clyde catchment. Panel A shows the River Clyde and tributaries (Ordnance Survey, 2022) and Panel B shows the land cover (UK Centre for Ecology & Hydrology (UKCEH), 2020). The source-to-sea survey locations are denoted with the lowest number near the source of the River Clyde and the highest number near the river-sea interface. The measurements on the River Clyde are indicated by a 'C' and the tributaries by a 'T' and where the tributary is direct inflow from a loch this is indicated by an 'L'.

disturbed by other measurements, together with ambient air samples (Billett and Moore, 2000). Conductivity (EC), water temperature (T_w), dissolved oxygen concentration (DO) and pH were measured, and a two-litre water sample was retained for later analysis, which was kept in a dark, cool-box until returned to the laboratory for processing, to minimise biological activity. Full details of the data collection and laboratory measurement methodologies are described (Brown et al., 2023).

Headspace samples were analysed using an Agilent 7890B gas chromatograph (GC) and 7697A headspace auto-sampler (Agilent, Santa Clara, California), with CO_2 , CH_4 and N_2O concentrations determined by running gas vials containing four mixed gas standards prepared in a consistent way to the ambient air samples. The concentrations of the standards gases were: 1.12 to 98.2 ppm for CH_4 ; 202 to 5253 ppm for CO_2 ; and 0.208 to 1.04 ppm for N_2O . Water samples were filtered within 12-hrs of collection through a Whatman GF/F 0.7 μm , under vacuum. Filtrate was then analysed for: total dissolved nitrogen (TDN), total dissolved carbon (TDC) and dissolved organic carbon (DOC), anion & cation concentration, UV-Vis absorbance. Total phosphorus (TP) analysis was undertaken on unfiltered samples. Analysis for TDN, TDC and DOC were undertaken using a Shimadzu TOC-L series Total Organic Carbon Analyser with all samples run within 36-hrs of collection. The difference between TDC and DOC was used to calculate dissolved inorganic carbon (DIC). The filtration resulted in outgassing of gases including CO_2 raising the pH, such that most DIC measured by this method was in the form of bicarbonate and will underestimate the total DIC in the original stream waters (bicarbonate plus CO_2). Absorbance at 254 nm, indicative of aromaticity, was measured using a Perkin Elmer LAMBDA# 365 UV-Vis Spectrophotometer to evaluate the Specific Ultraviolet absorbance (SUVA). A low SUVA_{254} indicates a smaller portion of aromatic humic matter present in the water and can be used as an indicator of the anthropogenic impact (Williams et al., 2016). Ion chromatography using a Metrohm 930 Compact IC Flex was undertaken to determine both anion and cation concentrations. A mixed ion standard containing 11,000 ppm chloride (Cl^-), 5000 ppm nitrate (NO_3^-), 4000 ppm sulphate (SO_4^{2-}), 10,000 ppm sodium (Na^+), 5000 ppm ammonium (NH_4^+), 1000 ppm potassium (K^+), 1000 ppm calcium (Ca^{2+}) and 1000 ppm magnesium (Mg^{2+}), was diluted to make 7 standard solutions for calibration. These included dilutions of 0.1:100, 0.5:100, 1:100, 2:100, 5:100, 10:100, and 25:100. Total phosphorus (TP) was measured using a SEAL AQ2 analyser. Four standards were included in each run for calibration of between 0.025 to 0.20 mg P L^{-1} . Where concentrations exceeded the top standard, the machine diluted and re-measured the sample. For all techniques all sample points from each survey were run together.

2.4. Gas partial pressures

To calculate dissolved gas concentrations and partial pressures from the headspace equilibration method the following mass-balance equation was applied (Hamilton, 2006).

$$(C_{\text{liq}}) \cdot (V_{\text{liq}}) + (C_{\text{gas}}) \cdot (V_{\text{gas}}) = (C_{\text{liq}}) \cdot (V_{\text{liq}}) + (C_{\text{gas}}) \cdot (V_{\text{gas}}) \quad (1)$$

Where: C_{liq} and C_{gas} are the original gas concentration, C_{liq} and C_{gas} are the concentrations in the liquid and gas phases after equilibration (shaking) and V_{liq} and V_{gas} are the volumes of the liquid and gas in the syringe (assumed to be the same before and after shaking). Assuming equilibrium inside the vessel then C_{liq} can be replaced by:

$$C_{\text{liq}} = P_{\text{gas}} \cdot \beta_T \cdot P_{\text{BAR}} \quad (2)$$

Where: P_{BAR} is the barometric pressure at the measurement time and altitude, P_{gas} is the partial pressure in the gas phase, β_T is the Bunsen solubility coefficient as a function of temperature. This can be rearranged:

$$(C_{\text{liq}}) = (P_{\text{gas}} \cdot \beta_T \cdot P_{\text{BAR}}) + (C_{\text{gas}} - C_{\text{liq}}) \cdot (V_{\text{gas}}) / (V_{\text{liq}}) \quad (3)$$

This gas concentration in $\mu\text{moles/L}$ can be converted to units of ppmv using the Ideal Gas Law, where $\text{ppmv} = (\mu\text{moles/L}) \cdot (RT)$, where R is the gas constant and T is the temperature in Kelvin.

This method is effective for CH_4 and N_2O but can lead to errors in CO_2 estimates as dissolved CO_2 is in dynamic chemical equilibrium with other carbonate species. The error incurred by headspace analysis of CO_2 is less than 5% for typical samples from boreal systems which have low alkalinity ($<900 \mu\text{molL}^{-1}$), with $\text{pH} < 7.5$, and high pCO_2 ($>1000 \mu\text{atm}$). This was the case for (90% of the samples here but errors in the lower Clyde tributaries, with both higher alkalinity and pH, were estimated as reaching 10% (Koschorreck et al., 2021).

2.5. Data sources and processing

Flow data measured by SEPA at their various gauging stations was used for all hydraulic calculations, details of the data applied at each location are provided in the supplementary information Table A1.1 (Scottish Environment Protection Agency, 2020 and UK Centre of Ecology & Hydrology (UKCEH), 2020). River flow, over the period January 2020 to December 2021, for the Sills of Clyde in the upper catchment ranged between 2.5 and $345 \text{ m}^3 \text{ s}^{-1}$ (the survey captured a range of $3.3 - 113 \text{ m}^3 \text{ s}^{-1}$) and Daldowie in the lower catchment ranged between 4.8 and $522 \text{ m}^3 \text{ s}^{-1}$ (the survey captured a range of $5.6 - 170 \text{ m}^3 \text{ s}^{-1}$) (Fig. 3A & B). The River Clyde experiences significant height loss between 75 and 100 km from source, which would be expected to produce significant outgassing (Fig. 3C), and significant inputs from urban wastewater treatment (UWWT) and mine water outflows (MW) (Fig. 3D).

Data was analysed using a combination of approaches. Spatial analysis of all measured parameters was undertaken using Quantum Geographic Information System (QGIS) version 3.22. Land cover analysis was undertaken by generation of the catchment area for each measurement point and applications of a land cover date; (UK Centre for Ecology & Hydrology (UKCEH), 2020) also using QGIS. Pearson's correlation was applied to determine relationships between the GHG concentrations, water physiochemical properties and land cover. Locations were grouped using K-cluster analysis, to help investigate the impact of seasonality, based on measured water chemical properties (DOC, DIC, TDN, TP, Cl^- , NO_3^- , SO_4^{2-} , Na^+ , NH_4^+ , K^+ , Ca^{2+} and Mg^{2+}). Physical parameters such as temperature (which mainly distinguish sites by elevation) and conductivity (a function of all dissolved ions) were not included.

Load appointment modelling (Bowes et al., 2008) was applied to all the GHG and chemical concentration data at all locations where flow data was available or could be calculated. The difference in the occurrence of point and diffuse sources is linked to the concentration-flow relationship, and can be calculated by using Eq. (4), where Q is volumetric flow rate and C_p and C_D are the point and diffuse source concentrations respectively. The constants A , B , C and D need to be calculated by iteration for each solute (Bowes et al., 2008). The models for the point and diffuse sources once generated were then applied to the full 2 years of flow data from January 2020 to December 2021 to determine volume transport for each GHG or solute.

$$C_T = C_p + C_D, \text{ where } C_T = A \cdot Q^{B-1} \text{ and } C_D = C \cdot Q^{D-1} \quad (4)$$

3. Results

3.1. GHG concentrations and water contamination from source-to-sea

Maximum concentrations for all GHGs occurred in the river urban section during July-September 2021, where concentrations reached; $\text{CH}_4\text{-C}$ $44 \mu\text{gL}^{-1}$, $\text{CO}_2\text{-C}$ 2.6 mg L^{-1} and $\text{N}_2\text{O-N}$ $3.4 \mu\text{gL}^{-1}$, with corresponding saturations of 130,400%, 1170% and 1310%, respectively. All GHG concentrations exhibited both strong spatial and temporal variability. Riverine dissolved GHGs (CH_4 , CO_2 and N_2O) were typically

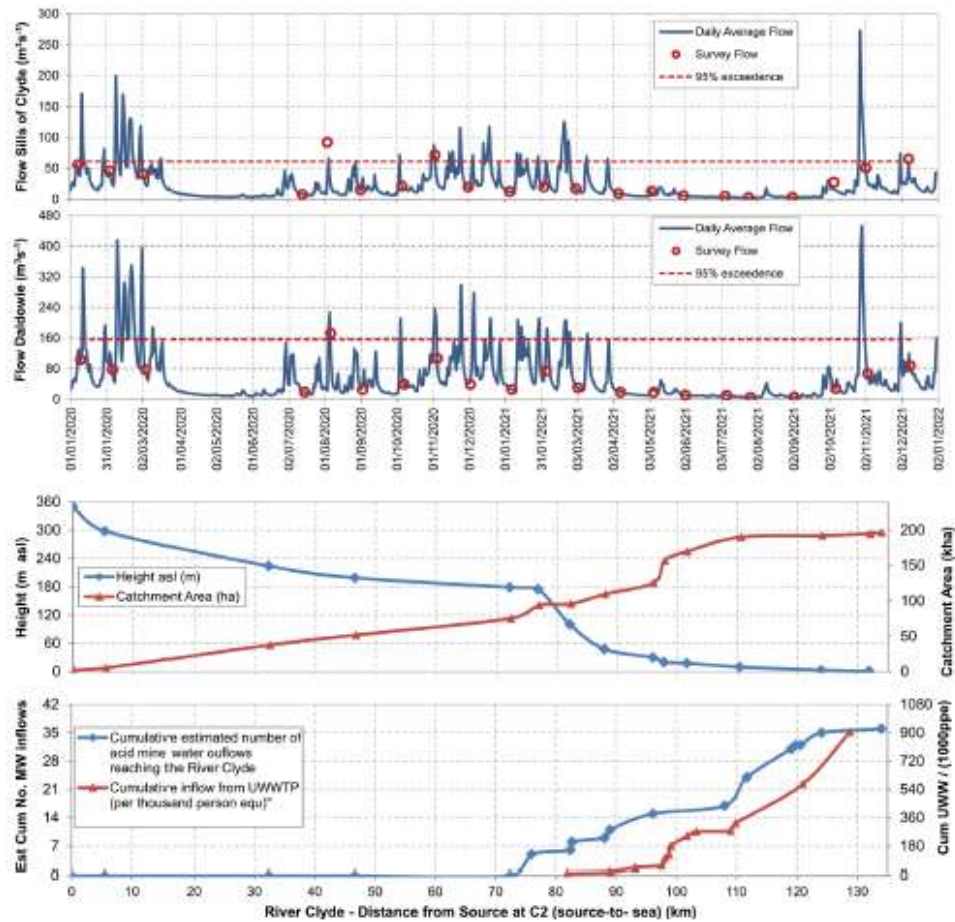


Fig. 3. River Clyde volumetric flow and contaminant inputs. The first two panels show the volumetric flow (Q) for the upper (Sills of Clyde) (A) and lower (Daldowie) (B) River Clyde relative to the survey dates for the first and second days of the surveys respectively. Effort was made to get consistent riverine flows over the two days of sampling, although during high river flows this was not possible (e.g. August 2020). In the spring and summer of 2021 (from April to September inclusive) a period of very low rainfall persisted, which was twice the duration as for 2020 and resulted in very dry conditions across the Clyde catchment. The third panel (C) shows the height and area of the Clyde catchment compared to distance from source for the different measurement points. The final panel (D) provides information on cumulative point sources entering the River Clyde from both urban wastewater treatment plants (UWWTP) in per 1000 person equivalent (1000ppe) and the cumulative number of known sources for Mine Water (MW) outflows. Note that this provides no information on the volume of MW entering the River Clyde or the degree of treatment. MW volumetric flow varies widely from different sources.

supersaturated with respect to the atmosphere, with $>97\%$ above the theoretical equilibrium value. The lowest saturations occurred in areas of steep slope and high turbulence, which included the head waters of the Clyde (C3) and the areas surrounding the Falls of Clyde (C12, T13, C14, T15, C16 and T17), with CH_4 showing the largest change in concentrations.

Riverine dissolved GHG ($\text{CH}_4\text{-C}$, $\text{CO}_2\text{-C}$ and $\text{N}_2\text{O-N}$) and water physiochemical property (TP, TDN, DOC, DIC, Cl^- , NO_3^- , SO_4^{2-} , Na^+ , NH_4^+ , K^+ , Ca^{2+} and Mg^{2+}) concentrations for the different locations measured on the River Clyde (Fig. 4A) and its tributaries (Fig. 4B) all increased from source-to-sea, in line with increasing percentage of both agricultural and urban land cover (Fig. 4C). Average concentrations for all locations are included in supplementary data Tables A3.1 and A3.2.

3.2. Land cover relationship with and methane and nitrous oxide dynamics

To determine land cover influences on nutrient and GHG concentrations, the land cover was correlated to the measured GHG concentrations and water physio-chemical properties (Table 1 and supplementary data Table A4.1). Analysis was for the tributaries and Clyde headwaters only, to ensure all data was independent and points within the analysis were on a similar spatial scale (catchment area $< 250\text{km}^2$). The measurements points in the lower urban River Clyde catchments (with the highest GHG concentrations) are not included to avoid confounding of data.

Conductivity, pH, TDN, TP, DIC, DOC, Cl^- , NO_3^- , SO_4^{2-} , Na^+ , NH_4^+ , K^+ , Ca^{2+} , Mg^{2+} and $\text{N}_2\text{O-N}$ were strongly negatively correlated with percentage cover of acid (semi-natural) grassland and positively correlated with improved (pasture) grassland, suggesting that acid grassland behaved as a nutrient sink while improved grassland behaved as a

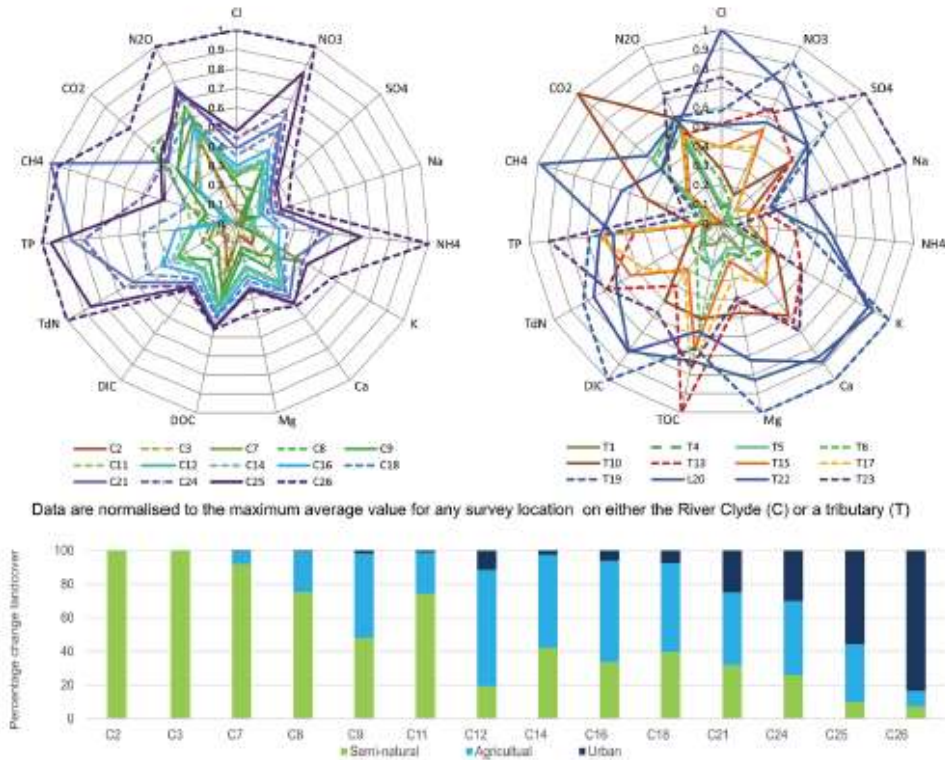


Fig. 4. Radar plots of average dissolved GHGs and water chemical properties. The top panels are radar plots of average dissolved GHGs (CH₄-C, CO₂-C and N₂O-N) and water chemical properties (TP, TDN, DOC, DIC, Cl⁻, NO₃⁻, SO₄²⁻, Na⁺, NH₄⁺, K⁺, Ca²⁺ and Mg²⁺). The source-to-sea survey locations are denoted with numbers from 1 (source) to 26 (sea), with the River Clyde indicated by a 'C' and the tributaries by a 'T' or 'L', where direct inflow is from a loch. The top left panel (A) is a source-to-sea progression of the River Clyde (coloured brown-green-blue) clearly demonstrating how the concentrations increase downstream. All data are normalised to the maximum average value for any survey location. The top right panel (B) is a source-to-sea progression for the Clyde tributaries, with tributaries joining in the upper Clyde (green), the middle Clyde (red-orange) and the lower Clyde (blue) and exhibiting a similar progression of concentrations. All data are normalised to the maximum average value for any survey location. The lower panel (C) shows the percentage land cover change between each location from source-to-sea on the River Clyde for comparison with panel A. Semi-natural (acid grassland, heather and forest) is in green, agricultural (arable and improved grassland) in light blue and urban (urban and suburban) in dark blue (UK Centre for Ecology & Hydrology, 2020). (For interpretation of the references to colour in this figure legend, the reader is referred to the web version of this article.)

Table 1
Pearson's Correlation Coefficient between nutrients and GHGs (EC, DO%, pH SUVA₂₅₄, TP, DOC, DIC, TDN, CH₄, N₂O and CO₂) and percentage land-cover across all Clyde tributaries and headwaters.

	CH ₄	CO ₂	N ₂ O	EC	DO%	pH	DOC	DIC	TDN	TP	SUVA ₂₅₄
Acid grassland	-0.38	0.06	-0.40	-0.84	0.24	-0.84	-0.88	-0.77	-0.94	-0.93	0.79
Arable & horticulture	0.51	-0.05	0.07	0.65	-0.06	0.73	0.48	0.77	0.74	0.67	-0.63
Bog	0.04	-0.41	0.02	0.36	0.23	0.63	0.64	0.27	0.61	0.77	-0.41
Coniferous woodland	0.05	0.28	0.08	0.16	0.15	0.05	0.61	0.20	0.27	0.30	-0.11
Freshwater	0.12	-0.05	-0.10	-0.10	0.13	-0.03	-0.22	-0.09	-0.10	-0.16	-0.04
Heather	-0.15	-0.20	-0.01	0.19	-0.01	0.08	0.55	0.08	0.33	0.14	-0.27
Heather grassland	-0.03	0.13	0.15	-0.05	-0.21	-0.22	0.10	-0.06	-0.10	-0.07	-0.06
Improved grassland	0.21	-0.20	0.38	0.76	-0.18	0.82	0.91	0.64	0.91	0.94	-0.70
Inland rock	0.71	0.56	0.55	0.73	-0.55	0.48	0.36	0.85	0.54	0.44	-0.51
Urban & Suburban	0.59	0.06	0.49	0.88	-0.56	0.85	0.36	0.84	0.78	0.70	-0.81

Notes
¹ Values are the Pearson's correlations coefficient with the values in bold considered significant with a P-value < 0.05.
² There is a strong correlation between broadleaf woodland and urban and suburban land-cover within the Clyde catchment (R² = 0.91, P-value < 0.001), possibly because broadleaf woodland has been planted within the suburban and urban environment. Hence broadleaf woodland has not been included.
³ To ensure all data points are independent only tributaries and the upper River Clyde are included. As a result the lower Clyde points (including the large UWWTP linked to high CH₄ concentrations) are not included to avoid confounding of catchments.

nutrient source. Arable & horticulture (arable) cover was positively correlated with EC, pH, DIC, TDN, TP, Cl^- , NO_3^- , NH_4^+ , K^+ , Ca^{2+} , Mg^{2+} and behaved as a nutrient source. The area of arable & horticulture cover is an order of magnitude lower than for improved grassland, but correlations are similar (Table 1 and supplementary data Table A.4.1).

Urban & suburban (urban) cover was strongly positively correlated

with EC, pH, TDN, TP, DIC, Cl^- , NO_3^- , SO_4^{2-} , Na^+ , NH_4^+ , K^+ , Ca^{2+} , Mg^{2+} , $\text{CH}_4\text{-C}$ and $\text{N}_2\text{O-N}$ suggesting that the urban cover acts as both a nutrient and GHG source. Urban land cover was negatively correlated with DO% while other land-cover types had no statistically significant impact of river oxygenation. Improved grassland, urban and arable cover were all negatively correlated with SUVA_{254} suggesting an anthropogenic

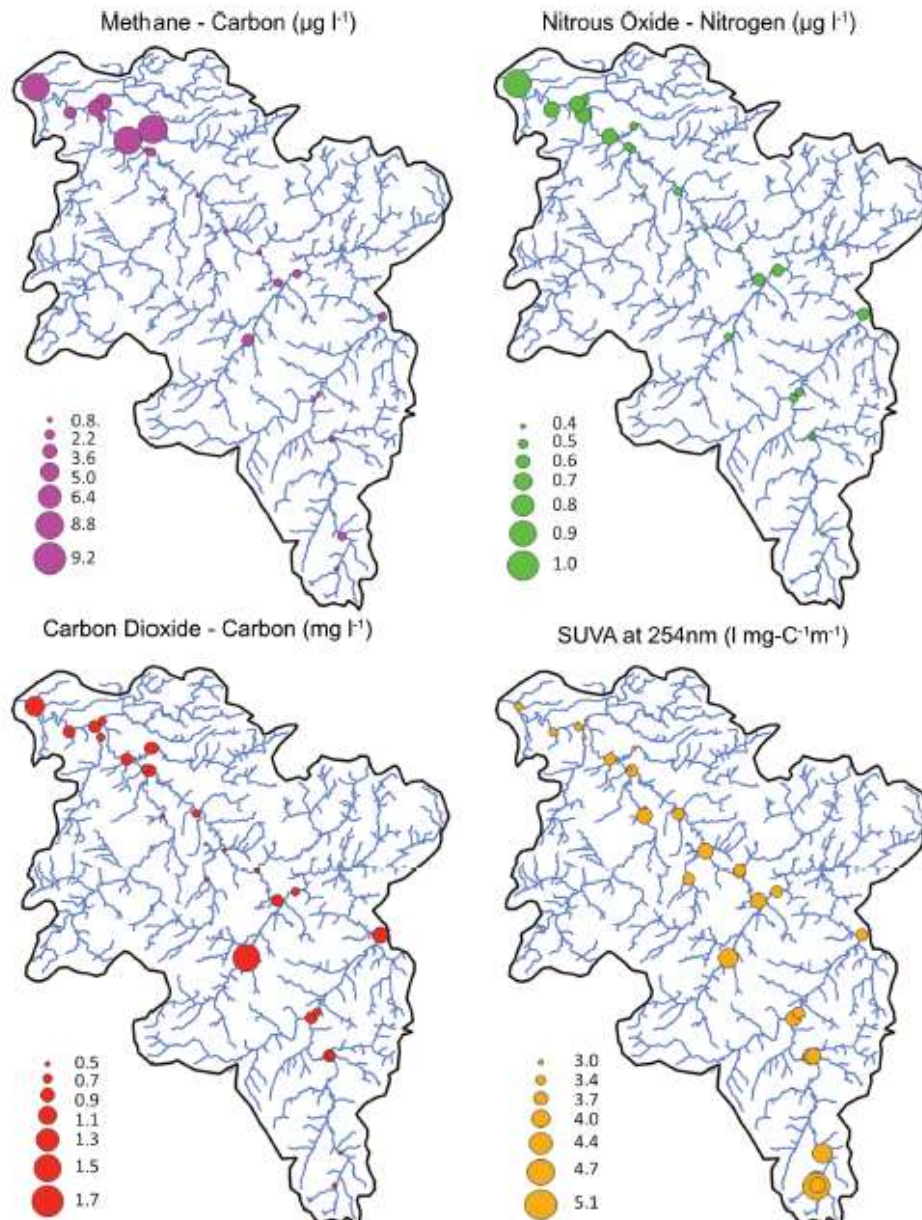


Fig. 5. Spatial average of CH_4 , CO_2 , N_2O and SUVA at 254 nm across the Clyde catchment. The average concentration data for $\text{CH}_4\text{-C}$, $\text{N}_2\text{O-N}$, $\text{CO}_2\text{-C}$ and SUVA_{254} shown spatially (for T_{30} , EC, pH, DO, TP, TDN, DOC, DIC, Cl^- , NO_3^- , SO_4^{2-} , Na^+ , NH_4^+ , K^+ , Ca^{2+} , Mg^{2+} ; see supplementary information Figure A5). The size of the marker denoting the average concentration / value at each measured location. The concentrations of all three GHGs ($\text{CH}_4\text{-C}$, $\text{CO}_2\text{-C}$ and $\text{N}_2\text{O-N}$) are low in the middle Clyde catchment due to high out-gassing corresponding to regions of high turbulence. Both CH_4 and N_2O concentrations are high in the lower catchment. Both $\text{CH}_4\text{-C}$ and $\text{CO}_2\text{-C}$ concentrations are elevated in tributaries that have significant MW inflow (e.g., at T10). The SUVA_{254} values decrease from the upper to lower catchment.

influence as land cover linked to nutrient concentrations and human density have been found to impact humic composition (Williams et al., 2016). No statistically significant correlations are detected for CO₂ (Table 1 and supplementary data Table A4.2).

3.3. GHG spatial heterogeneity

The spatial patterns of CH₄, N₂O and CO₂ are similar, with the lower (urban) catchment to the northwest having the highest concentrations (Fig. 5). The concentrations of CH₄, N₂O and CO₂ in the middle catchment associated with the Falls of Clyde (C12-C18, 78 to 100 km from source), an area of high turbulence with an elevation drop of 150 m, were the lowest and are typically at or near atmospheric equilibrium, likely associated with high evasion due to increased turbulence. The upper more rural catchment has more variability between the different GHGs. For example, T10 has both high CH₄ and CO₂ but lower relative N₂O concentrations and was observed associated with MW inflows, conversely the C9 has higher N₂O but lower relative CH₄ and CO₂ concentrations and has high agriculture land cover.

Average SUVA₂₅₄ values of 5 (35% aromaticity) occurred in the upper catchment dropping to 3 (20% aromaticity) in the lower catchment. The three most urban tributaries (T19, T22 & T23) consistently demonstrated the lowest SUVA₂₅₄ values, characteristic of high anthropogenic impact. The spatial patterns for DIC, SO₄²⁻, Ca²⁺, Mg²⁺ and K⁺ (supplementary data Figure A5) are similar and exhibit high concentrations in the tributary measurements (T10, T13, T19, T22), all of these catchments are influenced by legacy coal mines and outflows of MW (Fig. 3D). The tributary T23 also exhibited high SO₄²⁻ and Na⁺ compared to other ions suggestive of a different industrial legacy waste history. The ions, Cl⁻, NO₃⁻, Na⁺ and NH₄⁺, all increase with urbanisation of the catchment and are consistent with anthropogenic sources (Herlihy et al., 1998).

Table 2
Cluster analyses based on the measured water chemical properties (DOC, DIC, TDN, TP, Cl⁻, NO₃⁻, SO₄²⁻, Na⁺, NH₄⁺, K⁺, Ca²⁺ and Mg²⁺) distinguishes locations by position in the catchment.

No	Cluster Name	Locations	Description
1	Upper Clyde-Agricultural	C7, C8, C9	Upper section of the River Clyde, with both pastoral and arable agriculture
2	Middle Clyde-suburban arable	C11, C12, C14, C16, C18	Middle section of the River Clyde with a mixed signal of suburban, mining and agriculture
3	Lower Clyde-highly urban	C21, C24, C25, C26	Lower section of the River Clyde, dominated by high urban land coverage and increases in Cl ⁻ , TDN and TP
4	Upper tributaries-Semi-natural	T1, C2, T4, T5, T6	Upper Clyde tributaries, flowing from semi-natural or pastoral environments including streams from reservoirs
5	Middle tributaries-rural plus mining	T10, T14, T15, T17	Middle Clyde tributaries, dominated by pastoral and arable agriculture, disused coal mines and DOC from peat
6	Lower tributaries-urban plus mining	T19, T22, T23	Lower Clyde tributaries, dominated by urban, coal mining and legacy industry with the highest concentrations of all ions.

Note:

¹K-Cluster analyses based for 6 clusters using measured water chemical properties effectively distinguishes locations on the river Clyde and tributaries by their position in the catchment.

²C3 (measured below Daer reservoir) and L20 (Strathclyde Loch) were not included in the cluster analysis as these primarily represent lake properties rather than riverine properties.

3.4. Seasonal GHG distribution by land use characteristics

Locations were grouped using K-cluster analysis based on measured water chemical properties. The result with six clusters was selected and summarised in Table 2.

Seasonal patterns for riverine dissolved GHGs (CH₄, CO₂ and N₂O) and water physiochemical properties (TDN and TP) were investigated using the clustering in Table 2 and were found to be inconsistent throughout the catchment (Fig. 6). In the upper and middle catchment for both the River Clyde and its tributaries, CH₄ and TP concentrations exhibited low variability by season. However, in the lower urban catchments both the highest mean and maximum concentrations occurred in summer and autumn. Concentrations of CH₄ in the lower urban catchment increased by an order of magnitude and TP by at least four times. Conversely N₂O, CO₂ and TDN exhibited their lowest average values in summer with the highest values in spring and winter in the upper and middle catchments. However, in the lower urban catchment the seasonality pattern changes with the highest concentrations of N₂O, CO₂ and TDN in the summer.

The seasonal change in summer could be driven by temperature or reduced river flow. Temperature is correlated with reduced river flow and this correlation becomes more significant in the lower urban catchment (at C9 (upper catchment); R² = 0.5, p-value < 0.03 and at C24 (lower catchment); R² = 0.61, p-value < 0.003 (August 20 data excluded and log-linear relationship applied)). The low river flow in summer would impact contaminant and nutrient concentrations particularly where these are linked to point rather than diffuse sources. Thus this seasonal impact could be driven by temperature and concentrations of nutrients from point sources.

3.5. GHG, nutrient and contaminant correlations

Correlations over the whole catchment show that both CH₄ and N₂O were significantly positively correlated with TP, TDN, NO₃⁻ and NH₄⁺ with CH₄ also significantly positively correlated with DIC and Mg²⁺ and N₂O significantly positively correlated with Cl⁻, CH₄, CO₂ and N₂O are all negatively correlated with DO% (Table 3 and supplementary data Table A4.2). In the urban sector (L20 to C26) DO values are lower (supplementary data Table A3.1), suggesting reduced water aeration. Conductivity, DIC, Cl⁻, SO₄²⁻, Na⁺, K⁺, Ca²⁺, Mg²⁺, are all strongly inter-correlated. TDN is strongly correlated with NO₃⁻ but also TP. These correlations are not consistent across the whole the catchment and are investigated using the clustering from Table 2. The correlations for clusters 1, 3, 4 and 6 are shown in Fig. 7.

There are few significant correlations for GHGs in the upper catchment, especially for CH₄, N₂O is positively correlated with T_{air}, NO₃⁻ and TDN, and CO₂ negatively correlated with DO% (Fig. 7A and B). However, in the lower urban catchment strong correlations occurred between almost all GHGs and physiochemical properties, suggesting high GHG concentrations occurred as contaminate concentrations increased and DO% decreased (Fig. 7C and D). The correlation between TDN and TP is high in the urban environment (R² = 0.76), both linked to UWW. This may result in some correlations which are unlikely to be causal. In the urban area CH₄ is highly correlated with TP and N₂O with TDN (associated with UWW), and CH₄ with the DIC, SO₄²⁻, Ca²⁺ and Mg²⁺ grouping (associated with MW), suggesting different mechanisms for CH₄ production compared to the semi-natural environment. In the urban area significant negative correlations occurred between both DO% and SUVA₂₅₄, and most physiochemical properties and GHG concentrations.

3.6. Drivers for greenhouse gas concentrations

A load apportionment model was used to model the GHG and solute concentrations and the exponents (B and D) from the relationships for concentration as a function of flow (Eq. (4)) were estimated for point and diffuse sources and used to distinguish four source types: (1) point

A.M. Brown et al.

Water Research 236 (2023) 119969

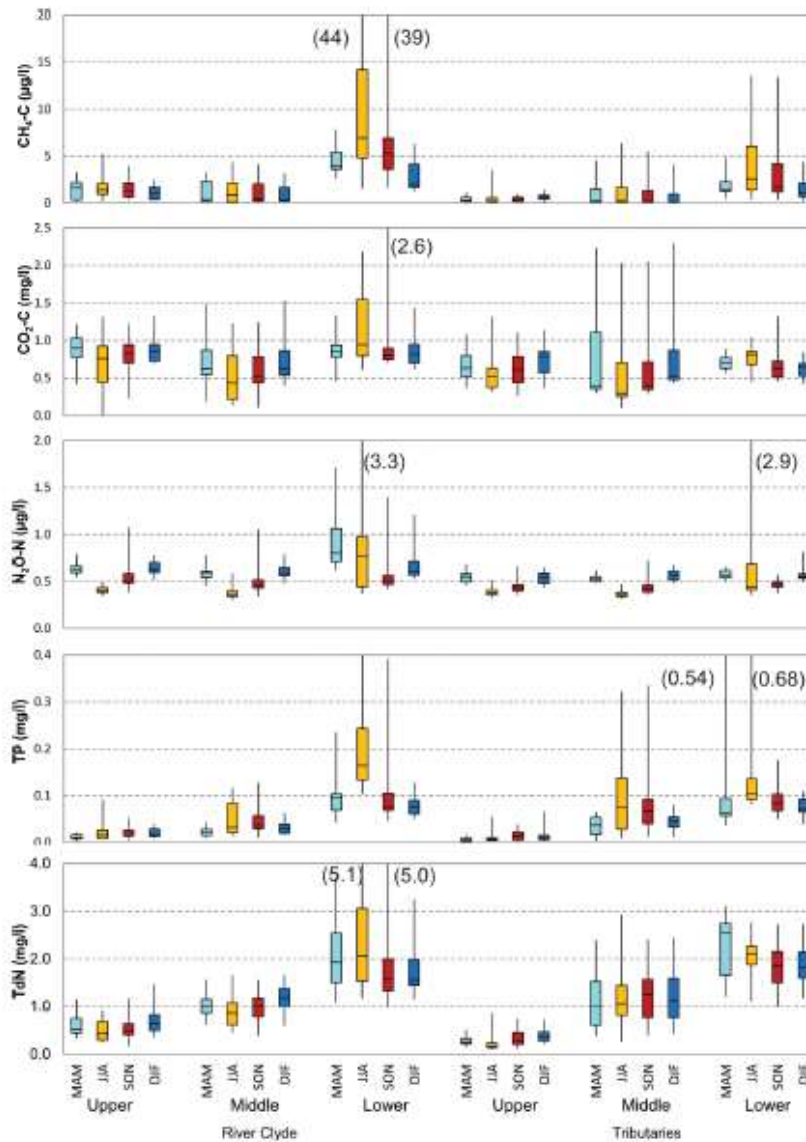


Fig. 6. Seasonal analysis of GHGs for the upper, middle and lower River Clyde and tributaries. Box plots of concentrations of dissolved CH₄-C, CO₂-C, N₂O-N, TDN and TP in the Clyde catchment, showing the median, 25% and 75% quantiles, minimum and maximum for a seasonal analysis: spring (March-May) in light blue, summer (June to August) in yellow, autumn (September to November) in red and winter (December to February) in blue. The results are grouped by six different regions of measurements on the upper, middle and lower River Clyde and tributaries that enter the River Clyde in the upper, middle and lower reaches. Seasonal trends that occur in the upper and middle catchment are changed when the Clyde enters the highly urban lower catchment. (For interpretation of the references to colour in this figure legend, the reader is referred to the web version of this article.)

Table 3
GHG correlation with water physiochemical properties over the whole Clyde catchment.

GHG	EC	T _w	pH	DO	DO%	DOC	DIC	TDN	TP	SUV ₂₅₄
CH ₄ -C	0.41	0.34	0.13	-0.47	-0.42	0.03	0.41	0.43	0.45	-0.18
CO ₂ -C	0.23	-0.04	-0.10	-0.28	-0.64	-0.02	0.19	0.23	0.19	0.02
N ₂ O-N	0.49	-0.14	0.12	-0.11	-0.38	0.01	0.16	0.47	0.51	-0.10

Notes:

- (1) Additional GHG correlations with water physiochemical properties over the whole Clyde catchment are included in supplementary data - Table A4.2.
- (2) Correlation significance increases when the catchment is divided between semi-natural, agricultural and urban.

sources which are fully independent of flow ($B = 0$), (2) point sources where concentration appears influenced by flow or rainfall ($0 < B < 1$), (3) diffuse sources where the concentration increases with flow ($D > 1$) and (4) diffuse sources where concentrations remain constant with flow

($D = 1$). The ions, nutrients and GHGs are categorized for these four source types in Table 4 and show different behaviours in the upper and lower catchment.

Mean concentrations together with calculated point and diffuse

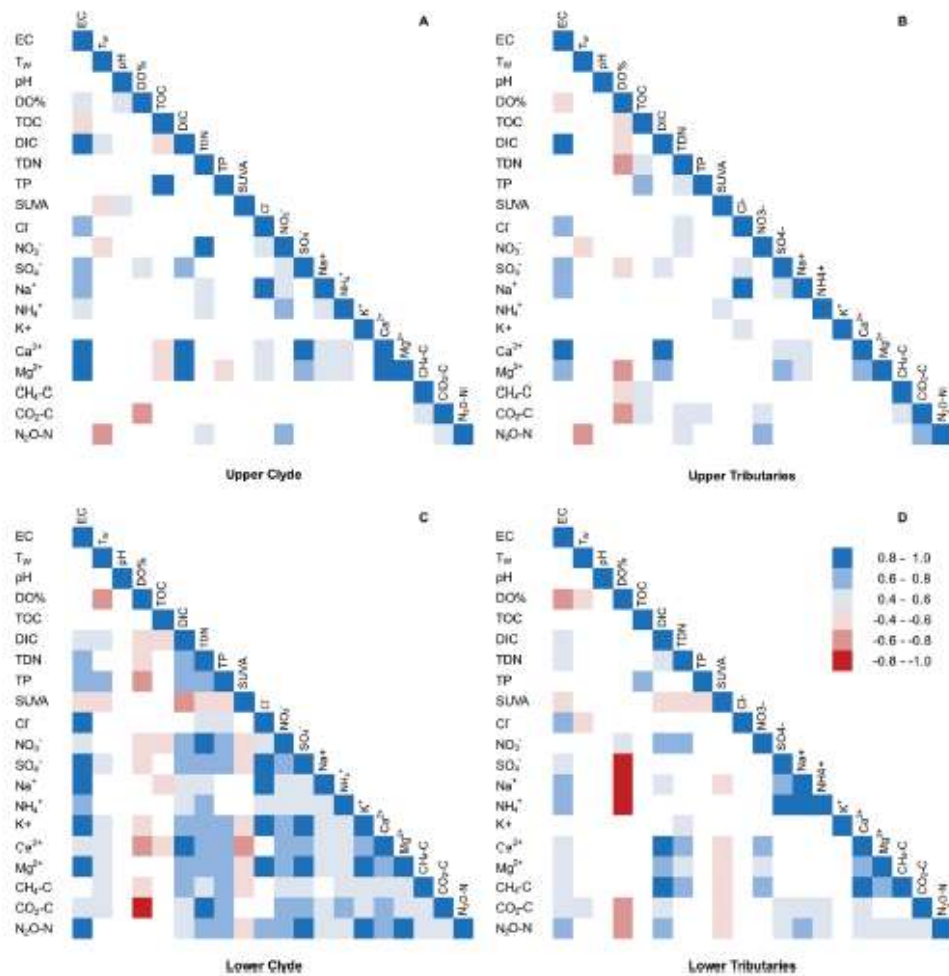


Fig. 7. Correlation between GHGs and physicochemical water properties. Correlations are for A) the upper and B) lower River Clyde and C) upper and D) lower Clyde tributaries as selected from the groups in Table 2. Positive correlations are depicted in blue and negative correlations in red with the stronger correlations in a darker shade. Positive correlations (0.4 and negative correlations) -0.4 have been excluded as do not meet this significance criteria (p -value < 0.005). Correlation increases in the lower catchment, with GHGs strongly correlated with contaminants and inversely correlated with DO%.

concentrations for the River Clyde from source-to-sea (Fig. 3 and supplementary data Figure A6), show the increasing significance of point source inputs in the lower urban river for both GHGs and nutrients. In the upper catchment GHG concentrations were dominated by diffuse agricultural sources. In the lower, urban catchment point sources became dominant over diffuse sources for CH_4 , TP and NH_4^+ and became significant for N_2O , CO_2 , NO_3^- and TDN. Additionally, while NO_3^- , N_2O and CO_2 are dominated by diffuse flows their concentrations remain constant with flow, suggesting a reduced connection with their catchment. Generation of N_2O and CO_2 would be in the water column, with in-water generation and out-gassing approximately in balance (N_2O by (de)nitritification of dissolved nitrogen compounds and CO_2 by in-stream mineralisation of DOC rather than input via groundwater). The CH_4 concentrations best reflect those of TP ($R^2 = 0.5$, P -value < 0.005), while TDN concentrations are reflected in N_2O ($R^2 = 0.65$, P -value < 0.0005) and CO_2 ($R^2 = 0.71$, P -value < 0.0002) concentrations. The locations C21 (112 km from source) and C26 (134 km) (Fig. 3) show the highest concentrations of CH_4 and N_2O , which are within 0.3 km and 3.4 km of

UWWTP outfalls. The tidal weir (400 m downstream of this C26) locally reduces flow and increases water residence times, which may act to reduce DO% seen at this location. The major point sources identified in the lower catchment included inflows from UWWTP and MW from abandoned coal mines (Fig. 3D).

3.7. Carbon and nitrogen exports to the estuary

Data measured at C26, was used to estimate the carbon, nitrogen and other direct riverine exports into the Clyde estuary. The horizontal flux models for these exports are included in Table 5 based on volumetric flow rate (Q) in $\text{m}^3 \text{s}^{-1}$. The annual export, based on flow data for the survey period (1-Jan-20 to 31-Dec-21) is included in the final column of Table 5. This estimate only includes fluxes attributed to continuous point or diffuse sources. Sporadic pollution from winter road salting or periodic agricultural fertiliser application is estimated separately.

Storm events dominated riverine loading of DOC and nutrients from agricultural run-off and low water levels dominated inputs from point

Table 4
Categorisation of the dominant sources of GHG and nutrients between point and diffuse sources and their dependence on flow in upper and lower Clyde catchment.

		Upper catchment dominant source		Lower catchment dominant source	
		Point	Diffuse	Point	Diffuse
Flow	Independent of flow		Cl ⁻ , Na ⁺ ⁽¹⁾	CH ₄ , TP, NH ₄ ⁺ (TDN, N ₂ O, CO ₂) ⁽²⁾	Cl ⁻ , Na ⁺ ⁽¹⁾ , NO ₃ ⁻ , N ₂ O, CO ₂
	Influenced by flow	DIC, SO ₄ ²⁻ , Ca ²⁺ , Mg ²⁺ ⁽³⁾	CH ₄ , N ₂ O, CO ₂ ⁽²⁾ , DOC, TP, TDN, NO ₃ ⁻ , NH ₄ ⁺ , K ⁺	DIC, SO ₄ ²⁻ , Ca ²⁺ , Mg ²⁺ ⁽³⁾	TDN, K ⁺ , DOC

Notes.

¹ Point sources independent of flow are only evident in the lower (urban) catchment and all GHGs are influenced by this type of source. Values in brackets are significant sources not the dominant source.

² Point sources influenced by flow (DIC, SO₄²⁻, Ca²⁺, Mg²⁺) are related to groundwater inputs. This type of source occurs in both the upper and lower catchment for this group of ions. Ion concentrations increase by an order of magnitude between the upper and lower catchment. This can be attributed (due to extensive further investigation by the authors) to mine water outflows from disused coal mines, which is a feature of the middle and lower Clyde catchment. Rainfall influences both the water residence time within the mine system and source flow rate influence the point source characteristics.

³ Diffuse sources where the concentration increases with flow, such as for DOC are dominated by storm runoff events (Vaughan et al., 2017). GHGs in the upper catchments behave similarly to nutrient suggesting a similar source, however in the lower catchment point sources dominate GHG concentrations to the extent that for CH₄ diffuse generation is difficult to detect.

⁴ Diffuse sources where the concentrations are independent of flow are exhibited by Cl⁻ and Na⁺, throughout the catchment. Salt in river water is typically found to be damped by the catchment and independent from atmospheric inputs (Neal and Kirchner, 2000). This type of analysis does not account for period inputs such as those caused by winter road salting.

sources, particularly those near to measurement locations. Variability in this relationship does arise due to hysteresis. For example DOC concentrations during storm events are related to the whether the DOC source is plentiful or exhaustible (Vaughan et al., 2017; Vaughan and Schroth, 2019 and Pohle et al., 2021). In this study continuous measurements were not available, resulting in the inability to quantify any hysteresis.

The annual loss of TDC from DIC, TOC, CO₂ and CH₄, to the estuary was estimated as 48.39 ± 3.6 Gg C yr⁻¹, with annual DIC export approximately double that of DOC and four times that of CO₂ with CH₄ accounting for 0.03%. The annual loss of total nitrogen, from TDN and N₂O, to the estuary was estimated as 4.03 ± 0.38 Gg N yr⁻¹ of which N₂O represents 0.06%. The largest exports are for TDC, Cl⁻, SO₄²⁻, Ca²⁺, all exceeding 40 Gg yr⁻¹, with Na⁺ exceeding 36 Gg yr⁻¹, with road winter salting contributing an additional 10 Mg yr⁻¹ of Cl⁻ and 5.6 Mg yr⁻¹ of Na⁺.

Despite the focus on measuring DOC in rivers, a recent UK modelling study demonstrated that DIC accounted for 80% of the TDC flux from the UK's 7 largest rivers (Jarvie et al., 2017) and a one-year study (2017) measured DIC as 73% of the TDC flux for the same rivers (Tye et al., 2022). Table 6 provides a ranked comparison of DIC and DOC export from various UK rivers, including the River Clyde from this study, based on river catchment area on a per annum basis, showing the dominance of DIC export over DOC in the UK.

4. Discussion

4.1. Urban nutrients and climate warming increase GHG emissions

Our study supports the growing global concern that GHG emissions from water bodies are increasing because of the interaction between nutrient levels and climate warming. More specifically our study points to the largest increase in riverine GHGs coming from urban nutrients and the riverine climate stressors of low summer water levels resulting in increased water residence times and reduced river oxygenation. Our source-to-sea methodology showed clearly that seasonal patterns of CH₄, CO₂ and N₂O changed between the semi-natural environment in the upper catchment and urban environment in the lower catchment. In the semi-natural upper catchment GHGs were higher in winter, while in the lower urban catchment, GHG were significantly higher in summer. The GHGs from the urban catchment were dominated by point source inputs and their impact increased during low river flow and high temperature conditions. In the agricultural middle catchment GHG concentrations increased slightly above those of the semi-natural upper catchment but did not exhibit a change in seasonal pattern. This seasonal change in GHG concentrations may be related to changes in microbial community composition and activities, which have been observed downstream of UWWTP (Y. Zhou et al., 2022; Beaulieu et al., 2010). The abundance of sediment microbial community have been found to be correlated with EC, organic matter, TP, DO and TN (Feng et al., 2022). This suggests microbial adaptation to changing conditions.

Riverine dissolved GHG, nutrient and chemical concentrations all increased from source-to-sea, in line with the increasing percentage of urban and agricultural land cover. The increase in GHG concentrations between the semi-natural and urban environment was on average three times higher for N₂O and CO₂, but twenty times higher for CH₄, suggesting the significant nature of CH₄ as an urban marker. While there were few significant correlations for any GHGs in the upper catchment, in the lower urban catchment strong correlations occurred between all GHGs and water physiochemical properties, suggesting that removal of contaminants from river systems, could lower GHG concentrations. Three main anthropogenic sources were identified that increased GHGs these included: (1) UWW outflows as a major point source of both CH₄ linked to TP and TDN, and N₂O linked to TDN; (2) MW outflows as a major point source of CH₄ and CO₂ emanating from groundwater interacting with disused coal mines and (3) agricultural activities as a major diffuse source of N₂O linked to TDN. Additionally, three major hydrological-environmental interactions were found that increased GHG concentrations in addition to those directly attributed to the nutrient increases. These included: (1) low oxygen conditions, (2) higher temperatures and (3) changes in river geometry linked to increased water residence times, and made it challenging to attribute causes absolutely.

4.2. High nutrient-residence time interactions promote GHG generation

Once the availability of TDN is accounted for (N₂O/TDN) neither T_w (in the range 0–22°C) or DO% (>90%) have significant effects on N₂O concentration. However where water residence time increases, T_w and DO% appear significant. In low flow situations, residence time is further increased, decreasing DO% and providing more time for temperatures to increase in summer. Both this increased residence time (Zarnetske et al., 2011) and low oxygen level (Frey et al., 2020; Rocamond et al., 2012) will act to increase N₂O, by promoting denitrification and increasing the proportion of N₂O per unit TDN.

In the upper Clyde catchment CH₄ concentrations are low and highly variable, with higher CH₄ observed with elevated DOC occurring in high flow events, suggesting DOC availability may be limiting CH₄. However in the lower urban catchment CH₄ is strongly positively correlated to T_w, TP, TDN and DIC and negatively correlated with flow and DO%. This point source CH₄ generation is over 20 times higher than that derived

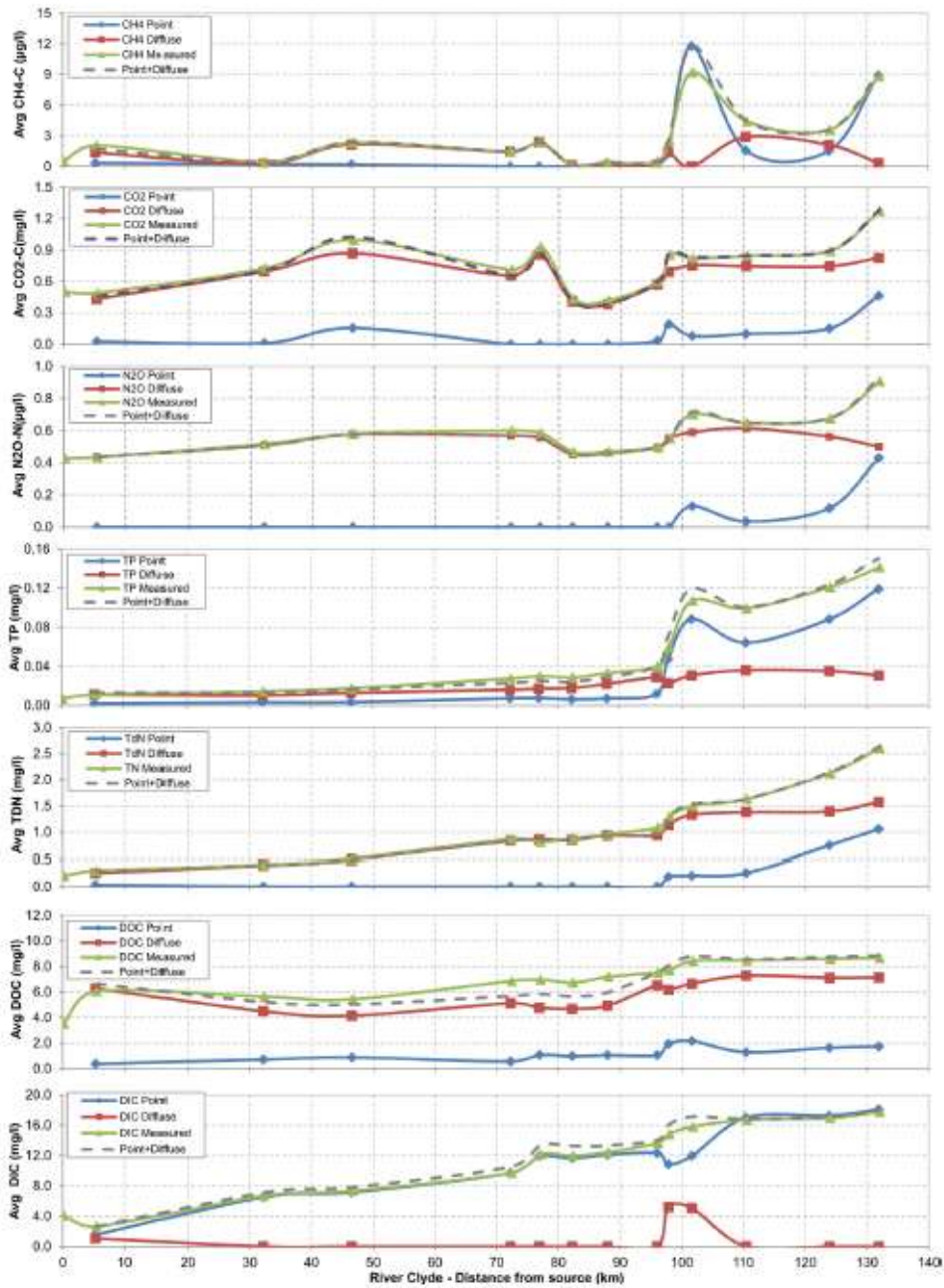


Fig. 8. Average concentrations from point source and diffuse sources on the River Clyde. The concentrations for measured data and determination of point and diffuse sources are shown for: CH₄, CO₂, N₂O, TP, TDN, DOC and DIC, against distance from source (C2 at 0 km to C26 at 134 km). For other ions supplementary data Figure A6. The measured concentrations are the average values measured across the 21 surveys for each location. The point and diffuse concentrations are the average values based on the 2 year of flow data for the time of the survey (1st January 2020 to 31st December 2021) applied at 15-minute intervals. Considerable input from point sources for both nutrients and GHG occurs after a distance of 95 km and is coincident with an increase in urban land cover and the three highly urban tributaries entering the River Clyde.

Table 5
Flux of CO₂, CH₄, N₂O, TP, TDN, DOC, DIC, Cl⁻, NO₃⁻, SO₄²⁻, Na⁺, NH₄⁺, K⁺, Ca²⁺, Mg²⁺ into the Clyde Estuary.

Flux	Concentration equations (Q is in m ³ s ⁻¹) CT = A . Q ^(P-1) + C . Q ^(D-1)	R ²	P- value	Annual export (tonnes)
F _{DOC} (mg l ⁻¹)	- 36.0526 . Q ⁻¹ + 0.4979 . Q ^{0.6940259}	0.425	<0.005	13,534 ± 1510
F _{DOC} (mg l ⁻¹)	- 60.70614 . Q ^{-0.36701}	0.891	<0.001	27,629 ± 1448
F _{TDN} (mg l ⁻¹)	- 22.1784 . Q ⁻¹ + 1.5727	0.819	<0.001	4023 ± 377
F _{DOC,C} (mg l ⁻¹)	- 9.66653 . Q ⁻¹ + 0.825557	0.781	<0.001	7213 ± 654
F _{CH₄,C} (μg l ⁻¹)	- 184.1654 . Q ⁻¹ + 0.00000394 . Q ^{2.409923}	0.798	<0.001	14.4 ± 3.3
F _{NO₃,H} (μg l ⁻¹)	- 13.291247 . Q ⁻¹ + 0.07187 . Q ^{0.36294}	0.753	<0.001	2.3 ± 0.14
F _{TP} (mg l ⁻¹)	- 2.490657 . Q ⁻¹ + 0.000132 . Q ^{1.31079}	0.964	<0.001	229 ± 36
F _{Cl} (μmol l ⁻¹)	- 8303.752 . Q ⁻¹ + 494.1491	0.719 ^{(1),(2)}	<0.001	48,273 ± 5186
F _{NO₃} (μmol l ⁻¹)	- 1533.528 . Q ⁻¹ + 74.2137	0.773	<0.001	13,978 ± 1543
F _{SO₄} (μmol l ⁻¹)	- 1140.427 . Q ^{-0.430224}	0.744	<0.001	40,968 ± 3778
F _{Na} (μmol l ⁻¹)	- 10,460.07 . Q ⁻¹ + 524.7421	0.837 ^{(1),(2)}	<0.001	36,001 ± 5734
F _{NO₃} (μmol l ⁻¹)	- 139.6026 . Q ⁻¹ + 11.07243	0.342	<0.001	498 ± 62
F _K (μmol l ⁻¹)	- 863.9982 . Q ⁻¹ + 55.69099 . Q ^{1.06091}	0.927 ⁽²⁾	<0.001	5805 ± 474
F _{Ca} (μmol l ⁻¹)	- 1986.658 . Q ^{-0.31966}	0.841	<0.001	42,040 ± 3376
F _{Mg} (μmol l ⁻¹)	- 1349.282 . Q ^{-0.411966}	0.873 ⁽²⁾	<0.001	12,598 ± 1412

Notes:

⁽¹⁾ CT = CP + CD, where CP = A . Q^(P-1) and CD = C . Q^(D-1) (C = concentration, T = Total, P = Point, D = Diffuse).

⁽²⁾ Two values removed for January 21 and February 21 and assumed due to winter salting, as salt evident on the roads

⁽³⁾ One value removed for August 2021 due to tidal ingress at Glasgow green, this most influenced K⁺ Mg²⁺ Na⁺ and Cl⁻ concentrations.

from diffuse sources. Generation of CH₄ in the lower urban catchment may be linked to eutrophication (nutrient enrichment). Our SUVA₂₅₄ values show a shift in riverine OC sources toward a more microbial and algal origin, as has been found as human disturbance increases (Lambert et al., 2017). High CH₄ in many shallow lakes is produced by eutrophication, mostly driven by TP and TDN enrichment and sediment microbiome (Davidson et al., 2018; Aben et al., 2017; Nijman et al., 2022). This mechanism is less likely in river ecosystem due to continual flushing, but during low water levels, increased residence times in combination with the high nutrient concentrations from UWW appear responsible for eutrophication and significant CH₄ generation. This may be enabled by electron donor availability in the receiving waters. This effect was most exacerbated when water residence times were further increased by the flow restriction at the tidal weir.

4.3. Main uncertainty in the causes of GHG variation

Greenhouse gas concentrations were inversely correlated with river oxygenation. This correlation was influenced by several mechanisms, where the dominance changed with position in the catchment. High turbulence caused oxygenation of the water and outgassing of the super-saturated GHGs. Respiration, photosynthesis and decomposition can create inverse relationships between oxygen and CO₂ dependant on their balance in the water column (Aho et al., 2021). Low oxygen conditions can result in anaerobic condition, promoting both methanogenesis and denitrification, which increase CH₄ and N₂O production respectively, from the available resources. While turbulence outgasses GHGs to

Table 6
Comparison of DIC and DOC export from UK Rivers as a function of catchment area.

River	Catchment Size (km ²)	DIC export Mg km ⁻² yr ⁻¹	DOC export Mgkm ⁻² yr ⁻¹	Ratio DIC/ DOC	
Halladale	193	1.0	13.06	0.1	(García-Martín et al., 2021), (Tye et al., 2022)
Couwy	340	3.9	12.15	0.3	(García-Martín et al., 2021), (Tye et al., 2022)
Forth	1025	9.4	11.41	0.8	(García-Martín et al., 2021), (Tye et al., 2022)
Tay	5042	5.4	4.91	1.1	(García-Martín et al., 2021), (Tye et al., 2022)
Tamar	956	9.0	7.64	1.2	(García-Martín et al., 2021), (Tye et al., 2022)
Tay	4587	6.8	5	1.4	(Jarvie et al., 2017)
Tyne	2262	9.25	4.93	1.9	(García-Martín et al., 2021), (Tye et al., 2022)
Dart	257	8.9	5.18	1.7	(García-Martín et al., 2021), (Tye et al., 2022)
Kelvin	331	9.25	4.93	1.9	(Gu et al., 2021)
River Clyde	2003	13.78	6.74	2.0	This Study
Clyde	2003	13.5	6.04	2.2	(García-Martín et al., 2021), (Tye et al., 2022)
Clwyd	431	12.7	5.17	2.5	(García-Martín et al., 2021), (Tye et al., 2022)
Tweed	4390	8.3	2.9	2.9	(Jarvie et al., 2017)
Yorkshire Ouse	3315	16.2	4.3	3.8	(Jarvie et al., 2017)
Seven	9895	14	3.3	4.2	(Jarvie et al., 2017)
Trent	8231	17.7	2.4	7.4	(Jarvie et al., 2017)
Humber-Trent	8209	14.6	1.77	8.2	(García-Martín et al., 2021), (Tye et al., 2022)
Ely Ouse	3430	10.6	1.2	8.8	(Jarvie et al., 2017)
Thames	9948	13.4	1.4	9.6	(Jarvie et al., 2017)
Thames	9948	9.3	0.57	16.3	(García-Martín et al., 2021), (Tye et al., 2022)
Avon	1712	18.5	0.86	21.5	(García-Martín et al., 2021), (Tye et al., 2022)
Test	1035	19.3	0.51	37.8	(García-Martín et al., 2021), (Tye et al., 2022)

(continued on next page)

Table 6 (continued)

River	Catchment Size (km ²)	DIC export Mg km ⁻² yr ⁻¹	DOC export Mg km ⁻² yr ⁻¹	Ratio DIC/DOC
				Tye et al., 2022)
Average export		11.1	4.9	2.4
Catchment weighted		12.32	2.98	4.1
Average export				

Note

¹Load of dissolved inorganic carbon (DIC) and dissolved organic carbon (DOC) for the significant British rivers as function of catchment area as a comparator for the river Clyde.

²DOC exports are from (García-Martín et al., 2021) and DIC exports estimated from (Tye et al., 2022), but data in these papers was gathered as part of the same study.

atmosphere it also produces conditions less likely to promote CH₄ and N₂O production making it difficult to fully distinguish the mechanisms. The lower urban river has the highest correlations, with GHGs increasing exponentially with reducing oxygen levels. The oxygen concentration primarily influences CH₄, while CO₂ and N₂O are influenced by the DO% (CH₄ R² = 0.45, CO₂ R² = 0.74, N₂O R² = 0.24 (P-value > 0.001)), suggesting CH₄ generation is less influenced by temperature.

Summer seasonal changes impact both temperature and rainfall, which together impact GHG concentrations. Lower rainfall reduces river flow and diffuse nutrients inputs and increases the impact of point source inputs. Higher temperatures reduce the available oxygen, due to reduced solubility and can increase microbial activity. As flow and temperature are often highly correlated this can make distinguishing these mechanisms difficult. Many researchers suggest temperature is a major effect (Wang et al., 2021; Herrero Ortega et al., 2019 and Rosestretzer et al., 2021). However, this study found that the size of the impact of flow and temperature on GHG concentrations is dependant on the location in the catchment and specifically the balance between diffuse and point source inputs. The upper catchment is dominated by diffuse inputs, which increase in higher flow and correspond to an increase in GHG concentrations. The lower urban catchments is dominated by point source inputs and corresponds to an increase in GHG concentrations with low flow. Flow and hence nutrient concentrations being more significant than direct impact of temperature in accounting for GHG variability. After flow, TP is the major influence on CH₄ and TDN on N₂O. The use of the load appointment model to distinguish between points and diffuse sources of GHGs and nutrients suggests that nutrients, however they are delivered, are dominating GHG production. Fully distinguishing between temperature and flow impacts would require longer data set with more instances of high flow during the summer.

Changes in river geometry that reduce river velocity and increase water residence times also cause deposition of sediments and nutrients and reduce oxygen saturation. River sections with increased residence time exhibited higher GHG concentrations, with the largest increases occurring in low flow conditions. However, proportioning the cause of this increase between; increased residence time, reduced outgassing due to lower turbulence, lower oxygen conditions, or deposition of sediments and nutrients as a source of GHG production is challenging. These higher residence time river sections act as point source locations for GHG generation compared to the surrounding river with CH₄ concentrations showing the most significant increase suggesting the creation of anaerobic sediments may be the most significant impact.

Our results show an increase in GHGs, particularly CH₄, in the receiving river after UWWTPs, with the riverine CH₄ concentrations dominated by point source characteristics, pointing to the UWWTP inflows as causal. UWWTP generate CH₄, in locations such as sewer pipes

and primary sedimentation, although CH₄ was not noted as discharged in effluent water (Mazuda et al., 2018). We made measurements of GHG concentrations in some UWWTPs outflows, which were low in dissolved GHG including CH₄, and this suggested that CH₄ was generated within the receiving river due to changes in the river physicochemical properties, including nutrient availability, rather than transferred from the UWWTP. However, we made insufficient measurements in UWWTP outflows, due to their inaccessibility, to confirm this absolutely. Unexplained CH₄ concentrations in the stream sections after UWW treatments works in southwest Germany were attributed to in-water generation due to additional organic carbon load in the effluent water (Alabboul et al., 2016). After hydrology was accounted for TP, also dominated by point source characteristics, had the highest correlation with unexplained CH₄ concentrations (TP R² = 0.59 at C26), although this correlation changed with proximity to UWWTP. Other authors indicated correlations between TP and CH₄ concentrations, in urban settings usually by impacting microbial activity (Zhang et al., 2021; Martinez-Cruz et al., 2017; Hao et al., 2021).

4.4. Carbon dioxide concentration variability reduced by carbonate buffering

Concentrations of CO₂ were less variable than those of N₂O and CH₄, mostly driven by diffuse sources, with point source inflows associated with tributaries receiving MW, causing short-term CO₂ increases. In-stream mineralization of DOC, the most likely generation mechanism for the consistent super-saturation of CO₂, would require a constant input of carbon to sustain CO₂ supersaturation levels (Winterdahl et al., 2016). DOC concentrations varied little through the catchment emanating from diffuse input, while DIC increased from source-to-sea, dominated by MW inflows. These MW inflows added significant amounts of DIC from the dissolution of limestone, producing high alkalinity, and many dissolved contaminants. The MW inflows are supersaturated with CO₂, which outgases very rapidly in treatment cascades or headwater streams. This rapid outgassing was observed to shift the pH upwards creating a new carbonate equilibrium. This changing equilibration would convert some of the remaining CO₂ to bicarbonate rather than emitting it to the atmosphere, thus reducing the gradient of CO₂ across the air-water interface (Stets et al., 2017). Aquatic primary productivity produces oxygen and consumes CO₂. However, primary productivity can be maintained with diminished CO₂, in high alkalinity water by converting bicarbonate to CO₂ to support productivity (Aho et al., 2021). Conversely mineralization of DOC to CO₂ would change the carbonate balance increasing bicarbonate concentrations. It is likely that this significant carbonate buffering available in the Clyde is responsible for the low variability in CO₂ concentrations and the reason why nutrients rather than carbon availability appear to influence CO₂ concentrations.

4.5. Acid mine inflows are a major source of GHG

In the middle and lower catchment tributaries, high concentrations of both CO₂ and CH₄ occurred linked to outflows from disused coal mine adits. Where carbonate rock is present, and much coal bearing strata in the UK is associated with Carboniferous limestone (British Geological Survey, 2022), the sulphuric acid generated in the mine dissolves the calcium carbonate to produce CO₂ (Hedin and Hedin, 2016; Vesper et al., 2016; Jarvis, 2006). Details of CH₄ released in MW have not, to our knowledge, been published. Most GHGs from MW had out-gassed before reaching the River Clyde. However high CO₂ and CH₄ concentrations in T10 were traced back to several MW inflows. These MW inflows had high concentrations of DIC, SO₄²⁻, Ca²⁺, Mg²⁺ and K⁺, which together acted as a marker for legacy coal mining. Many other MW sources were traced in the catchment with this marker, although not included within this publication. Despite the focus on measuring DOC in rivers, our data suggest that for the River Clyde carbon loss is dominated

by DIC, with the annual DIC export approximately double that for DOC. Comparison with other riverine studies demonstrated that DIC is the major component of the dissolved carbon in UK Rivers, with DIC accounting for 70 to 80% of carbon loss (Table 6). Our results suggest that the anthropogenic impacts of disused coal mines are accelerating carbon loss.

4.6. Legacy industry is still detectable in our rivers

Other increases in ion concentrations and pH were identified in the three most urban tributaries (T19, T22 and T23). Urban tributaries T19 and T22, had the highest concentrations of DIC, SO_4^{2-} , Ca^{2+} , Mg^{2+} and K^+ , attributed to inflows of MW from legacy coal mining. Both tributaries had legacy iron or steel making near to the rivers and may have iron slag buried within the catchment (Historic Environment Scotland, 2022). Steel slag is known to increase pH, alkalinity, and Ca^{2+} concentration (Riley and Mayes, 2015). The urban tributary T23, had the highest concentrations of Na^+ and SO_4^{2-} probably associated with leachate from legacy paper production (Skinner, 1939). T22 also experienced the highest Na^+ and Cl^- ion concentrations in the winter likely from winter road salting, as this tributary has the biggest road network, including a motorway. Data suggests that road drainage is entering the river directly adding an estimated 15 Mg yr^{-1} of NaCl.

5. Conclusions

5.1. Benefits of a source-to-sea approach in interpreting riverine GHGs

We have used the Clyde catchment, with its transitioning land cover from semi-natural through agricultural and legacy industrial to highly urban as a source-to-sea study to support identification of GHG sources. This source-to-sea investigative approach was found effective in tracing how changes in the nature and size of the riverine environment impacted GHG concentrations, particularly as GHGs were not conserved but outgassed in turbulent riverine sections. This variable outgassing makes correlations on a catchment scale misleading and is probably one reason for the high variability in GHG-to-nutrient relationships reported in the literature. A key aspect of GHG source identification included the use of load appointment modelling to distinguish point and diffuse sources by their degree of dependence on flow. This was effective in confirming diffuse GHG sources from agriculture and point GHG sources from UWW and MW. This load appointment modelling approach enabled two main seasonal impacts, high temperature and low water levels, to be distinguished. Analysis suggested that the impact of low water levels dominated over temperature change and failure to account for changing water levels, with their implications for oxygen and residence times, may account for some of the variability in the impact of temperature on GHG generation reported in the literature.

Measurement of a high number of water physiochemical properties allowed source fingerprinting of different inflows, which enabled detection even when the inflows were not physically identified, supporting identification of contamination from legacy industry. Results suggested that outflows from UWW treatment plants caused generation of GHG within the riverine water column. Changes in the seasonal pattern of GHG generation associated with urban wastewater inflows could be due to changes in microbial community structure, eutrophication at low water levels and supported by the availability of electron donors and acceptors in receiving waters. This was not confirmed as part of this study, and it is suggested that future surveys should be designed to quantify in-water generation resulting from mixing of UWW and riverine water.

The most important anthropogenic GHG from inland waters is CH_4 (Rosentreter et al., 2021), but CH_4 outgases the most rapidly, due to its high concentration to solubility ratio, as such catchment scale analysis can be misleading. Improved methods to detect and quantify CH_4 concentrations are required. A drone-mounted CH_4 sensor might be

effective in identifying point sources while continuous in-situ CH_4 measurements would better define source-flow relationships, although sensor reliability and sensitivity needs improvement. Where the source of nutrient pollution is unclear, human tracers such as caffeine could be applied to support understanding of contributions to nutrient pollution (Mizukawa et al., 2019, and Chen et al., 2002).

5.2. Implications and ideas for policy makers

To effectively reduce anthropogenic GHGs from the riverine environment it is important to understand their sources. For the River Clyde, UWW outflows were a major point source of both anthropogenic CH_4 and N_2O , MW outflows a major point source of anthropogenic CH_4 and CO_2 and agricultural activities (including field and farmyard run-off and poorly maintained septic tanks (septic tanks are not effective in removing nitrogen and phosphorus (O'Keefe et al., 2015))) were a source of anthropogenic N_2O . All sources of GHGs were associated with high concentrations of nutrients. Hence reducing nutrient loading, industrial and legacy contamination and agricultural run-off would ultimately act to reduce GHGs within riverine environments. Pollution point sources are easier to tackle as the location of the inflows are known.

While many UWWTP in the Clyde have phosphorus removal, our measurements suggest that levels of effectiveness vary between plants, suggesting improvement is possible. Additionally none of the UWWTP in this area have nitrogen removal (European Commission (Directorate General Environment), 2016). Riverine environments with low oxygenation, increased river residence times and high levels of nitrogen, should be prioritized for nitrogen removal from UWWTP to have the largest impact on N_2O reduction. Urban influences may have stimulated adaptation in microbial communities, further increasing GHG production, and further studies of microbial activity may support GHG reduction. Nitrogen capture at UWWTP could ultimately act as an important source of fertiliser, avoiding outflows to the environment (van der Hoek et al., 2018). Mine water is more difficult to tackle in terms of GHG generation as GHGs are generated below ground with the generation mechanism poorly understood.

While agricultural pollution was primarily from diffuse sources additional measurements showed a significant proportion entered the Clyde via the numerous field drainage ditches and small streams, which could be treated as point sources. Approaches to reduce run-off may include: (1) use freshwater wetlands for nitrogen and phosphorus removal (Land et al., 2016) and wetlands have been shown as effective for diffuse run-off (Ockenden et al., 2012); (2) use of biochar filtration, an effective technology for both cleaning of wastewater and run-off water. Its capabilities include removal of pesticides, organic chemicals and nutrients. However, a practical approach for application to small streams is needed. After use the biochar could be redeployed onto farmland supporting carbon sequestration and a circular economy, recycling nutrients and further preventing run-off (Catinzone et al., 2021; Phillips et al., 2022; Kamali et al., 2021); (3) Riparian buffer zones are recommended between crops and rivers. In Scotland, General Binding Rule 20 requires a buffer strip at least 2 m wide to be left between surface waters and wetlands and cultivated land (SEPA, 2009). This rule was not set with the objective of reducing nutrient leeching. Further research demonstrates that woody vegetation is more effective than shrubs or grass at preventing nutrient leaching to rivers, with a 60 m buffer strip effectively removing all nutrients (Aguilar et al., 2015). While this would take considerable agricultural land, approximately 70% of nutrients are removed by a 12 m strip, which would also stabilize river banks, reduce erosion and sediment loss, increase biodiversity and provide shade making the riverine system more robust to climate change (Cole et al., 2020).

Declaration of Competing Interest

The authors declare that they have no known competing financial

interests or personal relationships that could have appeared to influence the work reported in this paper.

Data availability

The data used for this manuscript has been published by the Environmental Information Data Centre at <https://eidc.ac.uk/> (Brown et al., 2023).

Acknowledgements

This work was financially supported by a Natural Environment Research Council (NERC) studentship through the IAPETUS 2 Doctoral Training Partnership, Grant No. NE/S007431/1.

The authors would like to thank the three anonymous reviewers who helped improve the quality of the manuscript.

Supplementary materials

Supplementary material associated with this article can be found, in the online version, at [doi:10.1016/j.watres.2023.119969](https://doi.org/10.1016/j.watres.2023.119969).

References

- Aben, R.C.H., Barros, N., Van Donk, E., Frenken, T., Hilt, S., Kazanjian, G., Lamers, L.P.M., Peeters, E.T.H.M., Roelofs, J.G.M., De Senerpont Domis, L.N., Stephan, S., Velthuis, M., Van De Waal, D.B., Wik, M., Thornton, R.F., Wilkinson, J., Delontro, T., Koster, S., 2017. Cross continental increase in methane ebullition under climate change. *Nat. Commun.* 8 (1), 1–8. <https://doi.org/10.1038/s41467-017-01535-y>.
- Abril, G., Borges, A.V., 2019. Ideas and perspectives: carbon leaks from flooded land: do we need to replumb the inland water active pipe? *Biogeosciences* 16 (3), 769–784. <https://doi.org/10.5194/bg-16-769-2019>.
- Aguiar, T.R., Azen, K., Farron, L.M., Brito, A.G., Ferreira, M.T., 2015. Nutrient removal effectiveness by riparian buffer zones in rural temperate watersheds: the impact of no-till crops practices. *Agric. Water Manag.* 149, 74–80. <https://doi.org/10.1016/j.agwat.2014.10.031>.
- Aho, K.S., Hosen, J.D., Logozzo, L.A., McGillis, W.R., Raymond, P.A., 2021. Highest rates of gross primary productivity maintained despite CO₂ depletion in a temperate river network. *Limnol. Oceanogr. Lett.* 6 (4), 200–206. <https://doi.org/10.1002/lol2.10195>.
- Alshboul, Z., Encinas-Fernández, J., Hofmann, H., Lorke, A., 2016. Export of dissolved methane and carbon dioxide with effluents from municipal wastewater treatment plants. *Environ. Sci. Technol.* 50 (11), 5555–5563. <https://doi.org/10.1021/acs.est.5b04923>.
- Beaulieu, J.J., Shuster, W.D., Rebolz, J.A., 2010. Nitrous oxide emissions from a large, impounded river: the Ohio river. *Environ. Sci. Technol.* 44 (19), 7527–7533. <https://doi.org/10.1021/es101675v>.
- Beaulieu, J.J., Tank, J.L., Hamilton, S.K., Wohlheim, W.M., Hall, R.O., Mulholland, P.J., Peterson, B.J., Ashkenas, L.R., Cooper, L.W., Dahm, C.N., Dodds, W.K., Grimm, N.B., Johnson, S.L., McDowall, W.H., Poole, G.C., Maurice Valett, H., Arango, C.P., Bernot, M.J., Burgin, A.J., Cresshaw, C.L., Helton, A.M., Johnson, L.T., O'Brien, J. M., Potter, J.D., Sheibley, R.W., Sobota, D.J., Thomas, S.M., 2011. Nitrous oxide emission from denitrification in streams and river networks. *Proc. Natl. Acad. Sci. U. S. A.* 108 (1), 214–219. <https://doi.org/10.1073/pnas.1011464108>.
- Borges, A.V., Darchambeau, F., Lambert, T., Bouillon, S., Morana, C., Broutyère, S., Hakoun, V., Jurado, A., Tseng, H.C., Descy, J.P., Roland, F.A.E., 2018. Effects of agricultural land use on fluvial carbon dioxide, methane and nitrous oxide concentrations in a large European river, the Meuse (Belgium). *Sci. Total Environ.* 610–611, 342–355. <https://doi.org/10.1016/j.scitotenv.2017.08.047>.
- Bosse, U., Frenzel, P., Conrad, R., 1993. Inhibition of methane oxidation by ammonium in the surface layer of a littoral sediment. *FEMS Microbiol. Ecol.* 13 (2), 123–134. [https://doi.org/10.1016/0168-6496\(93\)90030-B](https://doi.org/10.1016/0168-6496(93)90030-B).
- Bowes, M.J., Smith, J.T., Jarvie, H.P., Neal, C., 2008. Modelling of phosphorus inputs to rivers from diffuse and point sources. *Sci. Total Environ.* 395 (2–3), 125–138. <https://doi.org/10.1016/j.scitotenv.2008.01.054>.
- British Geological Survey: BGS geology viewer, 2022.
- Broder, T., Blodau, C., Biester, H., Knorr, K.H., 2012. Peat decomposition records in three pristine ombrotrophic bogs in southern Patagonia. *Biogeosciences* 9 (4), 1479–1491. <https://doi.org/10.5194/bg-9-1479-2012>.
- Brown, A., Van Dijk, N., Pickard, A.E., 2023. Greenhouse gas and water chemistry measurements for the Clyde river, tributaries and estuary, 2021–2022. *Environ. Inf. Data Cent.* <https://doi.org/10.5285/c3527258-c9ab-4069-af0c-d6edabb67a1>.
- Cattizoon, E., Sposato, C., Romanello, A., Barisano, D., Comacchia, G., Marasco, L., Cozza, D., Migliorini, M., 2021. Purification of wastewater from biomass-derived syngas scrubber using biochar and activated carbons. *Int. J. Environ. Res. Public Health*.
- Chen, Z., Pavelli, P., Dillon, P., Najdu, R., 2002. Determination of caffeine as a tracer of sewage effluent in natural waters by on-line solid-phase extraction and liquid chromatography with diode-array detection. *Water Res.* 36, 4830–4838.
- Clair, P., Sabine, C., Sala, G., Bopp, L., Brovkin, V., Canadell, J., Chahra, A., DePina, R., Galloway, J., Heimann, M., Jones, C., Quéré, C.L., Myrnes, R.B., Piao, S., Thornton, P., 2013. Carbon and other biogeochemical cycles. In: *Climate Change 2013*. In: Stocker, T.F., Qin, D., Plattner, G.-K., Tignor, M., Allen, S.K., Boschung, J., Nauels, A., Xia, Y. (Eds.), *The Physical Science Basis. Contribution of Working Group I to the Fifth Assessment Report of the Intergovernmental Panel on Climate Change*, edited by V. B. and P. M. M. Cambridge University Press, Cambridge, United Kingdom/New York, NY, USA.
- Clyde River Foundation: The Clyde catchment, [online] Available from: <https://www.clyderiverfoundation.org/clyde-catchment/>, 2020.
- Cole, L.J., Stockan, J., Hellwell, R., 2020. Agriculture, Ecosystems and Environment Managing riparian buffer strips to optimise ecosystem services: a review. *Agric. Ecosyst. Environ.* 296 (April), 106891 <https://doi.org/10.1016/j.agee.2020.106891>.
- Cotovic, L.C., Ribeiro, R.P., Rêgia, C.R., Bernardes, M., Sobrinho, R., Vidal, L.O., Tremmel, D., Knoppers, B.A., Abril, G., 2021. Greenhouse gas emissions (CO₂ and CH₄) and inorganic carbon behavior in an urban highly polluted tropical coastal lagoon (SE, Brazil). *Environ. Sci. Pollut. Res.* 28 (28), 38173–38192. <https://doi.org/10.1007/s11356-021-13363-2>.
- Davidson, T.A., Audet, J., Jeppesen, E., Landkildehus, F., Lauridsen, T.L., Splidegaard, M., Syväranta, J., 2018. Synergy between nutrients and warming enhances methane ebullition from experimental lakes. *Nat. Clim. Chang.* 8 (2), 156–160. <https://doi.org/10.1038/s41558-017-0063-z>.
- Dunfield, F., Knowles, R., 1995. Kinetics of inhibition of methane oxidation by nitrate, nitrite, and ammonium in a humicol. *Appl. Environ. Microbiol.* 61 (8), 3129–3135. <https://doi.org/10.1128/aem.61.8.3129-3135.1995>.
- European Commission (Directorate General Environment): European commission urban waste water website: United Kingdom, [online] Available from: <https://www.wwf.eu/United-Kingdom/> (Accessed 23 December 2020), 2016.
- Feng, W., Gao, J., Wei, Y., Liu, D., Yang, F., Zhang, Q., Bai, Y., 2022. Pattern changes of microbial communities in urban river affected by anthropogenic activities and their environmental driving mechanisms. *Environ. Sci. Eur.* 34 (1), 1–13. <https://doi.org/10.1186/s12302-022-00669-1>.
- Frey, C., Sänge, H.W., Achterberg, E.P., Jayakumar, A., Löscher, C.R., Arévalo-martínez, D.L., León-palmero, E., Sun, M., Sun, X., Xie, R.C., 2020. Regulation of nitrous oxide production in low-oxygen waters off the coast of Peru. *Biogeosciences* 17, 2263–2287.
- Furukawa, Y., Inubushi, K., Furukawa, Y., 2004. Effect of application of iron materials on methane and nitrous oxide emissions from two types of paddy soils. *Soil Sci. Plant Nutr.* 50 (6), 917–924. <https://doi.org/10.1080/00380768.2004.10408554>.
- García-Martín, E.F., Sanders, R., Evans, C.D., Kildis, V., Lapworth, D.J., Rees, A.F., Spears, B.M., Tye, A., Williamson, J.L., Balfour, C., Rest, M., Howes, M., Breinann, S., Brown, L.J., Burden, A., Callaghan, N., Felgate, Tacey, L., Fishwick, J., Fraser, M., Gibb, S.W., Gilbert, P.J., Goddard, N., Gomez-Castillo, A.P., Hargreaves, G., Jones, O., Kennedy, T., Lichtschlag, A., Martin, A., May, E., Mawji, F., Mountney, I., Nightingale, J., Pickard, A., Stephens, J.A., Stinchcombe, M., Pearce, C.R., Pereira, M.G., Peed, K., Pickard, A., Stephens, J.A., Stinchcombe, M., Williams, P., Woodward, M.S., Yarrow, D., Mayor, D.J., 2021. Contrasting estuarine processing of dissolved organic matter derived from natural and human-impacted landscapes. *Glob. Biogeochem. Cycles* (2393775).
- Garnier, J., Billen, G., Vilain, G., Martinez, A., Silvestre, M., Mounier, E., Toche, F., 2009. Nitrous oxide (N₂O) in the Seine river and basin: observations and budgets. *Agric. Ecosyst. Environ.* 133 (3–4), 223–233. <https://doi.org/10.1016/j.agee.2009.04.024>.
- Gómez-Gener, L., von Schiller, D., Maró, R., Arroita, M., Casas-Ruiz, J.P., Staehr, P.A., Acuña, V., Sabater, S., Obregón, B., 2016. Low contribution of internal metabolism to carbon dioxide emissions along lotic and lentic environments of a Mediterranean fluvial network. *J. Geophys. Res. Biogeosciences* 121 (12), 3030–3044. <https://doi.org/10.1002/2016JG003548>.
- Gu, C., Waldron, S., Bass, A.M., 2021. Carbon dioxide, methane, and dissolved carbon dynamics in an urbanized river system. *Hydrol. Process.* 35 (9), 1–17. <https://doi.org/10.1002/hyp.14360>.
- Skinner, H.J., 1939. Waste problems in the pulp and paper industry. *Ind. Eng. Chem.* 31 (11), 1331–1335 [online] Available from: <https://pubs.acs.org/doi/pdf/10.1021/ie50359a006#>.
- Hamilton, S., Prediction of dissolved gas concentrations in water at atmospheric equilibrium, 3–6 [online] Available from: https://tr.kbs.msu.edu/docs/inx/inx2/inx2_dissolved_gas_headspace_equilibration_calcs.pdf, 2006.
- Hao, X., Ruihong, Y., Zhuangzhuang, Z., Zhen, Q., Xizi, L., Tingxi, L., Ruihong, G., 2021. Greenhouse gas emissions from the water–air interface of a grassland river: a case study of the Xilin River. *Sci. Rep.* 11 (1), 1–14. <https://doi.org/10.1038/s41598-021-81658-z>.
- Hedin, R.S., Hedin, B.C., 2016. The complicated role of CO₂ in mine water treatment. In: *Proc. IMWA 2016, Freiberg/Germany*, 3(TU), pp. 844–849.
- Herlihy, A.T., Stoddard, J.L., Johnson, C.B., 1998. The relationship between stream chemistry and watershed land cover data in the mid-atlantic region. *U.S. Water. Air. Soil Pollut.* 105 (1–2), 377–386. <https://doi.org/10.1023/A:1005028863682>.
- Herrero Ortega, S., Romero González-Quijano, C., Casper, P., Singer, G.A., Gesmer, M.O., 2019. Methane emissions from contrasting urban freshwaters: rates, drivers, and a whole-city footprint. *Glob. Chang. Biol.* 25 (12), 4234–4243. <https://doi.org/10.1111/gcb.14799>.
- Historic Environment Scotland: Cannore – clyde iron works, Cannore [online] Available from: <https://cannore.org.uk/site/162565/glasgow-clyde-iron-works>, 2022.

- van der Hoek, J.P., Duijff, R., Reinstad, O., 2018. Nitrogen recovery from wastewater: possibilities, competition with other resources, and adaptation pathways. *Sustain* 10 (12). <https://doi.org/10.3390/su10124605>.
- Hotchkiss, E.R., Hall, R.O., Sponseller, R.A., Butman, D., Klaminder, J., Laudon, H., Rosvall, M., Karlsson, J., 2015. Sources of and processes controlling CO₂ emissions change with the size of streams and rivers. *Nat. Geosci.* 8 (9), 696–699. <https://doi.org/10.1038/ngeo2507>.
- Jarvie, H.P., King, S.M., Neal, C., 2017. Inorganic carbon dominates total dissolved carbon concentrations and fluxes in British rivers: application of the THINCARS model – Thermodynamic modelling of inorganic carbon in freshwaters. *Sci. Total Environ.* 575 (October), 496–512. <https://doi.org/10.1016/j.scitotenv.2016.08.201>.
- Jarvis, A.P., 2006. The role of dissolved carbon dioxide in governing deep coal mine water quality and determining treatment process selection. In: 7th Int. Conf. Acid Rock Drain. 2006, ICARD - Also Serves as 23rd Annu. Meet. Am. Soc. Min. Reclam., 1, pp. 833–843. <https://doi.org/10.21000/jaamr06020833>.
- Kamali, M., Appels, L., Kwon, E.E., Aminabhavi, T.M., Dewil, R., 2021. Biochar in water and wastewater treatment - a sustainability assessment. *Chem. Eng. J.* 420 (P1), 129946. <https://doi.org/10.1016/j.cej.2021.129946>.
- Koschorreck, M., Prairie, Y.T., Kim, J., Marcé, R., 2021. Technical note: CO₂ is not like CH₄ - Limits of and corrections to the headspace method to analyse pCO₂ in fresh water. *Biogeosciences* 18 (5), 1619–1627. <https://doi.org/10.5194/bg-18-1619-2021>.
- Lambert, T., Bouillon, S., Darchambeau, F., Morana, C., Roland, F.A.E., Descy, J.P., Borges, A.V., 2017. Effects of human land use on the terrestrial and aquatic sources of fluvial organic matter in a temperate river basin (The Meuse River, Belgium). *Biogeochemistry* 136 (2), 191–211. <https://doi.org/10.1007/s10533-017-0387-9>.
- Land, M., Grandt, W., Grimvall, A., Hoffmann, C.C., Mitch, W.J., Tondowski, K.S., Verhoeven, J.T.A., 2016. How effective are created or restored freshwater wetlands for nitrogen and phosphorus removal? A systematic review. *Environ. Evid.* 5 (1), 1–26. <https://doi.org/10.1186/s13750-016-0060-0>.
- Liu, S., Raymond, P.A., 2018. Hydrologic controls on pCO₂ and CO₂ efflux in US streams and rivers. *Limnol. Oceanogr. Lett.* 3 (6), 428–435. <https://doi.org/10.1002/lol2.10095>.
- Long, H., Vihersmaa, L., Waldron, S., Hoey, T., Quinnen, S., Newton, J., 2015. Hydraulics are a first-order control on CO₂ efflux from fluvial systems. *Geophys. Res. Biogeosciences* 1912–1922. <https://doi.org/10.1002/2015JG002955>. Received.
- Marvaia, T., Lauerwald, R., Larudde, G.G., Bouskill, N.J., Cappellen, P.Van, Regnier, P., 2019. Nitrous oxide emissions from inland waters: are IPCC estimates too high? *Glob. Chang. Biol.* (July 2018) <https://doi.org/10.1111/gcb.14504>.
- Martinez-Cruz, K., Gonzalez-Valencia, R., Sepulveda-Jauregui, A., Plascencia-Hernandez, F., Belmonte-Izquierdo, Y., Thalasso, F., 2017. Methane emission from aquatic ecosystems of Mexico City. *Aquat. Sci.* 79 (1), 159–169. <https://doi.org/10.1007/s00027-016-0487-y>.
- Marx, A., Dusek, J., Janoušek, J., Sunda, M., Vogel, T., van Geldern, R., Hartmann, J., Barth, J.A.C., 2017. A review of CO₂ and associated carbon dynamics in headwater streams: a global perspective. *Rev. Geophys.* 55 (2), 560–585. <https://doi.org/10.1002/2016RG000547>.
- Masuda, S., Sano, I., Hojo, T., Li, Y.Y., Nishimura, O., 2018. The comparison of greenhouse gas emissions in sewage treatment plants with different treatment processes. *Chemosphere* 193, 581–590. <https://doi.org/10.1016/j.chemosphere.2017.11.018>.
- Maurice, L., Rawlins, B.G., Farr, G., Bell, R., Gooddy, D.C., 2017. The Influence of Flow and Red Slope on Gas Transfer in Steep Streams and Their Implications for Evasion of CO₂. *J. Geophys. Res. Biogeosciences* 122 (11), 2862–2875. <https://doi.org/10.1002/2017JG004045>.
- Mizukawa, A., Filipp, T.C., Peixoto, L.O.M., Scipioni, B., Lenardi, L.R., de Azevedo, J.C.R., 2019. Caffeine as a chemical tracer for contamination of urban rivers. *Brazilian J. Water Resour.*
- Natchimuthu, S., Wallin, M.B., Klemetsson, L., Bastviken, D., 2017. Spatio-temporal patterns of stream methane and carbon dioxide emissions in a hemiboreal catchment in Southwest Sweden. *Sci. Rep.* 7 (November 2016), 1–12. <https://doi.org/10.1038/srep39729>.
- Natural Scotland: The river basin management plan for the Scotland river basin district 2009–2015. [online] Available from: <https://www.sepa.org.uk/media/163445/the-river-basin-management-plan-for-the-scotland-river-basin-district-2009-2015.pdf>, 2015.
- Neal, C., Kirchner, J.W., 2000. Sodium and chloride levels in rainfall, mist, streamwater and groundwater at the Plynlimon catchments, mid-Wales: inferences on hydrological and chemical controls. *Hydrol. Earth Syst. Sci.* 4 (2).
- Nedwell, D.B., Dong, L.F., Sage, A., Underwood, G.J.C., 2002. Variations of the nutrients loads to the mainland UK estuaries: correlation with catchment areas, urbanization and coastal eutrophication. *Estuar. Coast. Shelf Sci.* 54 (6), 951–970. <https://doi.org/10.1006/ecss.2001.0867>.
- Nijman, T.P.A., Amado, A.M., Bodelier, P.L.E., Vernaert, A.J., 2022. Relief of phosphate limitation stimulates methane oxidation. *Front. Environ. Sci.* 10 (April), 1–8. <https://doi.org/10.3389/fenvs.2022.804512>.
- O’Keefe, J., Akumaa, J., Olszewska, J., Bruce, A., May, L., Allan, S., 2015. Practical measures for reducing phosphorus and faecal microbial loads from onsite wastewater treatment systems discharged to the environment. *A Rev.* 52.
- Ockenden, M.C., Deasy, C., Quinton, J.N., Bailey, A.P., Surridge, B., Stoate, C., 2012. Evaluation of field wetlands for mitigation of diffuse pollution from agriculture: sediment retention, cost and effectiveness. *Environ. Sci. Policy* 24, 110–119. <https://doi.org/10.1016/j.envsci.2012.06.003>.
- Ordnance Survey: OS open rivers, OS open rivers [online] Available from: <https://www.ordnancesurvey.co.uk/business-government/products/open-map-rivers>, 2022.
- Phillips, B.M., Mecalla Fuller, L.B., Siegler, K., Deng, X., Tjoerdema, R.S., 2022. Treating agricultural runoff with a mobile carbon filtration unit. *Arch. Environ. Contam. Toxicol.* 82 (4), 455–466. <https://doi.org/10.1007/s00244-022-00925-8>.
- Pohle, I., Baggaley, N., Palarea-albaladejo, J., Stutter, M., Glendell, M., 2021. A framework for assessing concentration-discharge catchment behavior from low-frequency water quality data. *Water Resour. Res.* <https://doi.org/10.1029/2021WR029692>.
- Raymond, P.A., Hartmann, J., Lauerwald, R., Sobek, S., McDonald, C., Hoover, M., Butman, D., Striegl, R., Mayorga, E., Humborg, C., Kortelainen, P., Diaz, H., Meybeck, M., Clois, P., Guth, P., 2013. Global carbon dioxide emissions from inland waters. *Nature* 503 (7476), 355–359. <https://doi.org/10.1038/nature12760>.
- Riley, A.L., Mayes, W.M., 2015. Long-term evolution of highly alkaline steel slag drainage waters. *Environ. Monit. Assess.* 187 (7) <https://doi.org/10.1007/s10661-015-4693-1>.
- Rosmond, M.S., Thusa, S.J., Schiff, S.L., 2012. Dependence of riverine nitrous oxide emissions on dissolved oxygen levels. *Nat. Geosci.* 5 (10), 715–718. <https://doi.org/10.1038/ngeo1556>.
- Rosenzweig, J.A., Borges, A.V., Deemer, B.R., Holgerson, M.A., Liu, S., Song, C., Melack, J., Raymond, P.A., Duarte, C.M., Allen, G.H., Oleffridt, D., Poulsen, B., Barin, T.J., Eyre, R.D., 2021. Half of global methane emissions come from highly variable aquatic ecosystem sources. *Nat. Geosci.* 14 (4), 225–230. <https://doi.org/10.1038/s41561-021-00715-2>.
- Salgado, J., Duc, T.A., Nga, D.T., Panizzo, V.N., Bass, A.M., Zheng, Y., Taylor, S., Roberts, L.R., Lacey, J.H., Leng, M.J., McGowan, S., 2022. Urbanization and seasonality strengthens the CO₂ capacity of the red river delta, Vietnam. *Environ. Res. Lett.* 17 (10) <https://doi.org/10.1088/1748-9336/ab9705>.
- Scottish Environment Protection Agency: SEPA water level data. [online] Available from: [https://www2.sepa.org.uk/WaterLevels/Accessed 23 April 2020](https://www2.sepa.org.uk/WaterLevels/Accessed%2023%20April%202020), 2020.
- Seitzinger, S.P., Krause, C., 1998. Global distribution of nitrous oxide production and N inputs in freshwater and coastal marine ecosystems. *Glob. Biogeochem. Cycles* 12 (1), 93–113.
- SEPA: Riparian vegetation management, engineering in the water environment, Good Practice Guide, 2, 1–47, 2009.
- SEPA: Water environment hub, [online] Available from: <https://www.sepa.org.uk/data-visualisation/water-environment-hub/riverbasindistrict-scotland>, 2018.
- Stets, E.G., Butman, D., McDonald, C.P., Stackpole, S.M., DeGrandpre, M.D., Striegl, R.G., 2017. Carbonate buffering and metabolic controls on carbon dioxide in rivers. *Global Biogeochem. Cycles* 31 (4), 663–677. <https://doi.org/10.1002/2016GB005578>.
- Tye, A.M., Williamson, J.L., Jarvie, H.P., Dise, N.B., Lapworth, D.J., Monteith, D., Sanders, R., Mayor, D.J., Bowes, M.J., Bowes, M., Burden, A., Callaghan, N., Farr, G., Felgate, S.L., Gibb, S., Gilbert, P.J., Hargreaves, G., Keenan, P., Kiriakos, V., Jürgens, M.D., Martin, A., Mountney, I., Nightingale, P.D., Pereira, M.G., Olszewska, J., Pickard, A., Rees, A.P., Spears, B., Stinchcombe, M., White, D., Williams, P., Worrall, F., Evans, C.D., 2022. Dissolved inorganic carbon export from rivers of Great Britain: spatial distribution and potential catchment-scale controls. *J. Hydrol.* 615 (PA), 128677. <https://doi.org/10.1016/j.jhydrol.2022.128677>.
- UK Centre for Ecology & Hydrology (UKCEH): National river flow archive, [online] Available from: <https://urfa.ceh.ac.uk/data/station/info/84007>, 2010.
- UK Centre for Ecology & Hydrology (UKCEH): Land cover map 2015, [online] Available from: <https://www.ceh.ac.uk/services/land-cover-map-2015>, 2020.
- UK Centre for Ecology & Hydrology (UKCEH): National river flow archive, [online] Available from: [https://urfa.ceh.ac.uk/Accessed 5 September 2020](https://urfa.ceh.ac.uk/Accessed%205%20September%202020), 2020.
- Vaughan, M.C.H., Schroth, A.W., 2019. Shining light on the storm: in-stream optics reveal hysteresis of dissolved organic matter character. *Biogeochemistry* 143 (3), 275–291. <https://doi.org/10.1007/s10533-019-00661-w>.
- Vaughan, M.C.H., Bowden, W.B., Shansley, J.B., Vermilyea, A., Sleeper, R., Gold, A.J., Pradhanang, S.M., Inamdar, S.P., Levia, D.F., Andres, A.S., Birgand, F., Schroth, A.W., 2017. High-frequency dissolved organic carbon and nitrate measurements reveal differences in storm hysteresis and loading in relation to land cover and seasonality. *Water Resour. Res.* 5345–5363. <https://doi.org/10.1002/2017WR020491>. Received.
- Vesper, D.J., Moore, J.E., Adams, J.P., 2016. Inorganic carbon dynamics and CO₂ flux associated with coal-mine drainage sites in Blythedale PA and Lambert WV, USA. *Environ. Earth Sci.* 75 (4), 1–14. <https://doi.org/10.1007/s12665-015-5191-z>.
- Wang, G., Xia, X., Liu, S., Zhang, L., Zhang, S., Wang, J., Xi, N., Zhang, Q., 2021. Intense methane ebullition from urban inland waters and its significant contribution to greenhouse gas emissions. *Water Res.* 189, 116654. <https://doi.org/10.1016/j.watres.2020.116654>.
- Williams, C.J., Frost, P.C., Morales-williams, A.M., Larson, J.H., Richardson, W.B., Chandra, A.S., Xenopoulos, M.A., 2016. Human activities cause distinct dissolved organic matter composition across freshwater ecosystems. *Glob. Chang. Biol.* 613–626. <https://doi.org/10.1111/gcb.13594>.
- Winterdahl, M., Wallin, M.B., Karlson, R.H., Laudon, H., Öquist, M., Lyon, S.W., 2016. Decoupling of carbon dioxide and dissolved organic carbon in boreal headwater streams. *J. Geophys. Res. Biogeosciences* 121 (10), 2630–2651. <https://doi.org/10.1002/2016JG003420>.
- Wrage, N., Velthof, G.L., Van Beusichem, M.L., Oenema, O., 2001. Role of nitrifier denitrification in the production of nitrous oxide. *Soil Biol. Biochem.* 33 (12–13), 1723–1732. [https://doi.org/10.1016/S0038-0717\(01\)00096-7](https://doi.org/10.1016/S0038-0717(01)00096-7).
- Zarnetske, J.P., Haggerty, R., Woodzell, S.M., Baker, M.A., 2011. Dynamics of nitrate production and removal as a function of residence time in the hyporheic zone. *J. Geophys. Res.* 116 (March 2010), 1–12. <https://doi.org/10.1029/2010JG0001356>.
- Zhang, W., Yan, C., Shen, J., Wei, R., Gao, Y., Miao, A., Xiao, L., Yang, L., 2019. Characterization of aerobic denitrifying bacterium *Pseudomonas mendocina* strain

- GL6 and its potential application in wastewater treatment plant effluent. *Int. J. Environ. Res. Public Health* 16 (3). <https://doi.org/10.3390/ijerph16030364>.
- Zhang, W., Li, H., Xiao, Q., Li, X., 2021. Urban rivers are hotspots of riverine greenhouse gas (N₂O, CH₄, CO₂) emissions in the mixed-landscape chaobai lake basin. *Water Res* 189, 116624. <https://doi.org/10.1016/j.watres.2020.116624>.
- Zhou, Y., Toyoda, R., Suenaga, T., Aoyagi, T., Hori, T., 2022a. Low nitrous oxide concentration and spatial microbial community transition across an urban river affected by treated sewage. *Water Res* 216 (February), 118276. <https://doi.org/10.1016/j.watres.2022.118276>.
- Zhou, Y., Toyoda, R., Suenaga, T., Aoyagi, T., Hori, T., 2022b. Low nitrous oxide concentration and spatial microbial community transition across an urban river affected by treated sewage. *Water Res* 216 (February), 118276. <https://doi.org/10.1016/j.watres.2022.118276>.
- Stanley, E.H., Casson, N.J., Christel, S.T., Crawford, J.T., Loken, L.C., Oliver, S.K., 2016. The ecology of methane in streams and rivers: Patterns, controls, and global significance. *Ecol. Monogr.* 86 (2), 146–171. <https://doi.org/10.1890/15-1027>.
- Billet, M.F., Moore, T.R., 2008. Supersaturation and evasion of CO₂ and CH₄ in surface waters at Mer Bleue peatland, Canada. *Hydrological Process* 22, 2044–2054. <https://doi.org/10.1002/hyp>.

Addendum2 - Anthropogenic-estuarine interactions cause disproportionate greenhouse gas production: A review of the evidence base

The chapter has been published in the Marine Pollution Bulletin volume 174

<https://www.sciencedirect.com/science/article/pii/S0025326X21012741>

with the following DOI - <https://doi.org/10.1016/j.marpolbul.2021.113240>



Review

Anthropogenic-estuarine interactions cause disproportionate greenhouse gas production: A review of the evidence base

Alison M. Brown^{a,*}, Adrian M. Bass^b, Amy E. Pickard^a^a UK Centre for Ecology & Hydrology (Edinburgh), Bush Estate, Penicuik, Midlothian EH26 0QJ, United Kingdom^b University of Glasgow, College of Science and Engineering, School of Geographical and Earth Sciences, University Avenue, Glasgow, G12 8QQ, United Kingdom

ARTICLE INFO

Keywords:
Greenhouse gas
Nitrous oxide
Methane
Estuary
Salt-wedge
Fully-mixed
Nutrients
Urban wastewater
Ammonium
Nitrate
Nitrite
Phosphate
Tidal range
River flow

ABSTRACT

Biologically productive regions such as estuaries and coastal areas, even though they only cover a small percentage of the world's oceans, contribute significantly to methane and nitrous oxide emissions. This paper synthesises greenhouse gas data measured in UK estuary studies, highlighting that urban wastewater loading is significantly correlated with both methane ($P < 0.001$) and nitrous oxide ($P < 0.005$) concentrations. It demonstrates that specific estuary typologies render them more sensitive to anthropogenic influences on greenhouse gas production, particularly estuaries that experience low oxygen levels due to reduced mixing and stratification or high sediment oxygen demand. Significantly, we find that estuaries with high urban wastewater loading may be hidden sources of greenhouse gases globally. Synthesising available information, a conceptual model for greenhouse gas concentrations in estuaries with different morphologies and mixing regimes is presented. Applications of this model should help identification of estuaries susceptible to anthropogenic impacts and potential hotspots for greenhouse gas emissions.

1. Introduction

The climate is considered unequivocally to have warmed significantly since the 1950s with increasing levels of greenhouse gases (GHGs), with the largest contribution derived from carbon dioxide (CO₂) followed by methane (CH₄) and nitrous oxide (N₂O) (IPCC, 2013). Shelf seas including estuaries and coastal areas, cover approximately 9% of the world's oceans (Harris et al., 2014) and are highly biologically productive, driving between 10 and 30% of marine primary production (Sharples et al., 2019) and contributing about 75% of the oceanic methane emissions (Bange et al., 1994). Shelf seas are a major nitrous oxide source, with European shelf sea (9.4% of total shelf) contributing 26% of global oceanic nitrous oxide (Bange, 2006), largely through denitrification-nitrification cycling from terrestrial runoff. Additionally, the outflows from urban wastewater (UWW) contribute to enhanced nitrous oxide production (McElroy et al., 1978; de Angelis and Gordon, 1985; Seitzinger, 1988; Law et al., 1992).

A review of the literature on estuarine methane emissions from different locations globally (Bange et al., 1994; Bernard, 1978;

Oremland et al., 1983; Franklin et al., 1988; Munson et al., 1997; Torres-Alvarado et al., 2013; Bange et al., 1998; Lyu et al., 2018), suggests that estuaries can drive particularly high methane production, despite their varying physical conditions, where they have the following conditions; high levels of organic matter, active sedimentation processes moving both river and estuarine sediments to trap organic matter and low oxygen levels. Similarly, a range of studies (Wrage et al., 2001; Pfenning, 1996; Revsbech et al., 2005; Reay et al., 2003; Pattinson et al., 1998; Beaulieu et al., 2011; Yu et al., 2013; Rosamond et al., 2012) suggests there are several major controls on nitrous oxide production within estuaries in both nitrification and denitrification rates, including ammonium (NH₄⁺) and nitrate (NO₃⁻) concentrations, dissolved oxygen, organic matter availability and temperature. Greenhouse gas fluxes generated within the estuarine environment are often highly variable, as reflected in the considerable range observed in UK, European and global estimates (Upotill-Goddard and Barnes, 2016; Borges et al., 2016; Bange, 2006). European estimates range in the order of 0.007 to 1.6 Mt N₂O yr⁻¹ and 0.03–0.7 Mt CH₄ yr⁻¹, with UK estimates accounting for more than 20% of these values. However, there is both a paucity of data for

* Corresponding author at: UK Centre for Ecology & Hydrology Penicuik, Midlothian, United Kingdom.

E-mail addresses: allbrown52@ceh.ac.uk (A.M. Brown), adrian.bass@glasgow.ac.uk (A.M. Bass), amyec92@ceh.ac.uk (A.E. Pickard).<https://doi.org/10.1016/j.marpolbul.2021.113240>

Received 30 July 2021; Received in revised form 3 December 2021; Accepted 4 December 2021

Available online 14 January 2022

0025-326X/© 2022 The Authors. Published by Elsevier Ltd. This is an open access article under the CC BY license (<http://creativecommons.org/licenses/by/4.0/>).

estuaries globally and concerning the drivers of these emissions. There is a clear need for an improved understanding of anthropogenic impacts, largely in the form of urban pollution, as well as the interactive effects associated with tidal, flushing and river regimes, climate, temperature and land-use. In order to increase the confidence in the magnitude of these estuarine GHGs as part of the general IPCC process (IPCC et al., 2006) and the UK government's carbon emission strategy (Institute for Government, 2020), further elucidation of the mechanisms that generate GHG emissions from estuaries is required. Such understanding could inform policies to help reduce emissions in anthropogenically impacted estuaries.

Estuaries have long been considered an effective location for the disposal of urban and industrial waste; resulting in considerable legacy pollution (including metals). Nitrogen and phosphorus compounds are not typically removed from most wastewater discharges to estuaries, although this is dependent on legislation. In the EU and UK removal requirements are related to plant size, the quantity of nutrients and eutrophication risk (EEC, 1991). Where nitrogen compounds are not removed from wastewater, nitrous oxide production may occur when the treated wastewater is discharged to rivers and estuaries. Ammonia is rapidly oxidised, a process that consumes oxygen and other available electron receptors, which may promote methanogenesis and the presence of ammonium may further inhibit methane oxidation (Dunfield and Knowles, 1995; Boussé et al., 1993) (Fig. 1). Additionally, nitrification processes may deplete oxygen, preventing methane oxidation, and where oxygen concentrations are low or highly variable, as typical in the estuary environment, denitrification may be triggered (Marchant et al., 2017), even with oxygen present, thereby increasing nitrous oxide concentrations. Estuaries with high suspended sediment loads may also support nitrogen processing in the water column (Barnes and Upphill-Goddard, 2011). The effects of temperature, salinity, ammonium concentration and pH can further affect the nitrification rate (Janasetyo et al., 2014) with a salinity optimum between 12 and 20 ppt, suggesting more nitrogen cycling would occur in an estuary than in either the freshwater or coastal environments. The estuary, therefore, is perhaps the least suitable environment of the land-ocean continuum for the discharge of UWW effluent when considering resultant GHG emissions.

2. Objectives

Investigations of GHG emissions from estuaries and coastal waters have typically been conducted with the purpose of improving the

estimate of GHG emissions from estuaries on a UK, European or global scale. There has been less emphasis on determining the interplay of processes that result in these high GHG emissions and our understanding therefore remains incomplete. As estuaries vary significantly in their physical characteristics and degree of anthropogenic influence, it can be difficult to determine exact causation mechanisms for this globally important source. Existing data to our knowledge, have not been used to distinguish between natural or anthropogenic emissions, nor have opportunities to prevent or reduce these emissions been identified. This paper synthesises published GHG data from UK estuaries in conjunction with other public domain data to address the following objectives. To determine the: 1) causes of estuarine GHGs, 2) mechanisms that promote high estuarine GHG concentrations and 3) optimum approach for quantifying estuarine GHGs. It employs a series of case studies of UK estuaries examining possible causes of high GHGs and their interaction with different estuary typologies (Fig. 2). This results in a conceptual model of GHG concentrations for different estuary typologies and is followed by an overarching synthesis section. This synthesis section also considers how estuary GHG concentrations and estuary typology impact GHG emissions to the atmosphere and whether estuaries are an overall net carbon sink or source.

3. Methods

A literature search containing the following terms was used to select the papers to be considered in this review: 'greenhouse gas' OR 'nitrous oxide' OR 'methane' AND 'estuary'. Only data from measurements made in the UK were applied in the analysis section to limit the variability in terms of geographic, climatic, nutrient and tidal regimes. Some estuarine GHG data from other geographic areas are contrasted in the discussion section. Methane and nitrous oxide concentration values from five studies conducted between 2005 and 2021 (Table 1), have been extracted as average values for specific surveys or estuaries (Table 2). These data were compared with other physical parameters from publicly available data associated with each estuary, including: estuary area and catchment, tidal range, river flow, oxygen concentration, land cover and the level of urban wastewater entering these estuaries (Table 3 and supplementary data Tables A1 and A2), together with data on nutrients and legacy pollution typically using linear regression methods. The thirteen estuary systems mainly considered in this analysis (Clyde, Clywd, Colne, Conwy, Dart, Deben, Forth, Orwell, Stour, Tamar, Tay, Tees and Tyne), see Fig. 3 for estuary catchment locations, represent

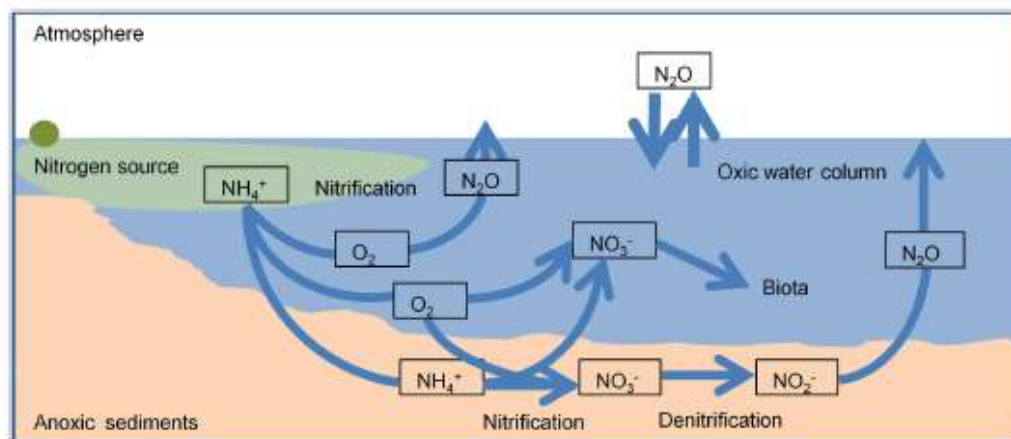


Fig. 1. Simplified nitrification-denitrification pathways in estuaries. Nitrification is shown in the aerobic water-column with oxygen from the water column also used in nitrification in the sediment layer. When insufficient oxygen is present denitrification can occur in the anoxic sediment layer. Denitrification can also occur in the water column linked to sediments, when oxygen levels are low, such as below a pycnocline.

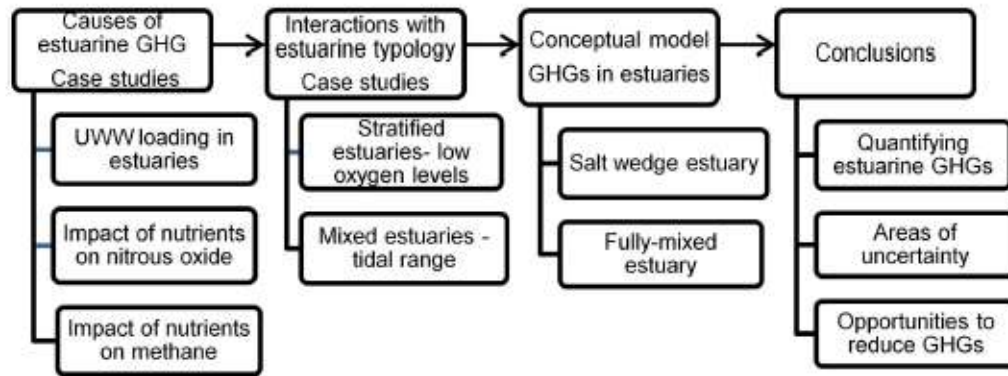


Fig. 2. Outline of approach in this paper.

Table 1
Summary of published data applied in this review.

Study scope	GHGs sampled	Sample depth	Sampling durations	Sampling approach	Sampling resolution	Study reference
1 Tay, Forth, Clyde, Tamar, Dart, Conway & Clywd	CO ₂ , N ₂ O & CH ₄	Surface	Quarterly, usually Jul 2017, Oct 2017, Jan 2018, Apr 2018	Ebb tide starting at high water, sampling downstream	6 sites across a salinity gradient	(Pickard et al., 2022)
2 Tay	CO ₂ , N ₂ O & CH ₄	Surface	Eight occasions from Apr 2009 - June 2010	Ebb tide starting at high water, sampling downstream	10 sites at fixed locations	(Harley et al., 2015), (Pickard et al., 2021)
3 Humber, Forth, Tamar, Tyne, Tees, and Tay	N ₂ O	1 m depth	Variable between Feb 2000 - Oct 2002 from 1 and 8 surveys	Flood tide starting after low water, sampling upstream	7-20 sites, due to estuary & local conditions	(Barnes and Upstill-Goddard, 2011)
4 Humber, Forth, Tamar, Tyne, Tees, and Tay	CH ₄	1 m depth	Variable between Feb 2000 - Oct 2002 from 1 and 8 surveys	Flood tide starting after low water, sampling upstream	7-20 sites, due to estuary & local conditions	(Upstill-Goddard and Barnes, 2016).
5 Colne, Stour, Orwell, Deben, Humber, Conway	N ₂ O	Surface	Quarterly, Aug 01, Nov 01, Feb 02, May 02. Conway - 2002-3	Ebb tide starting at high water, sampling downstream	10-16 sites dependent on estuary	(Dong et al., 2005)

Notes for studies 1-5:

- No data were available for the Clywd in January, and the Dart and Tamar in October. Target salinities were typically 0.2, 2, 5, 10, 15, 25 psu. Surveys covered different physical extent due to the salinity criteria applied. No CO₂ data was available for the Tamar and Dart.
- Survey dates were Apr-09, Jun-09, Jul-09, Sep-09, Feb-10, Apr-10, Jun-10 and Aug-10 (final survey not included in publication.)
- The number of surveys undertaken for N₂O were Tay: 1, Humber: 3, Tees: 3, Forth: 4, Tamar: 4 and Tyne: 8.
- The number of surveys undertaken for CH₄ were; Tay: 1, Humber: 2, Tamar: 2 Tees: 3, Forth: 4 and Tyne: 6. (Methane surveys are a subset of those for nitrous oxide (3) with one additional survey for the Tyne).
- The specific dates of the measurements are not provided. The rivers Mawddach and Dovey were measured but data were not provided for the estuaries, so this has not been included.
- Abbreviations: - Greenhouse Gas (GHG), Methane (CH₄), Nitrous Oxide (N₂O), Carbon Dioxide (CO₂)

12% of UK estuary systems and 9% and 15% of the UK estuary and catchment areas respectively (Nedwell et al., 2002). While a single survey was available for the Thames (Middelburg et al., 2002) and three for the Humber (see Table 1), these estuaries have not been included because of their size and complexity. Different studies use different surveying approaches; comparison between studies is possible but imperfect. The major differences between studies are in the depth of measurements, either surface or at 1 m and the phase of the tide on which the studies were conducted, either the ebb or the flood (detailed in Table 1). Both of these factors should be less significant for a fully mixed estuary compared to a salt wedge estuary. Seasonality is also not fully covered in all studies. Consideration of these results and the variances calculated for each estuary suggest that estuarine variability is more significant than the small differences in survey approach.

4. Case studies considering the effect of urban waste and nutrients on GHG production

The relationships between UWW and nutrients on both methane and nitrous oxide concentrations in the estuary environment are considered

in the following three case studies: (i) effects of UWW loading on average GHG concentrations, (ii) causes of high estuarine nitrous oxide concentrations and (iii) effects of different nutrients on methane concentrations. Relationships between GHG concentrations and estuary, catchment and land-cover area are reviewed in supplementary data Table A2 and Fig. A1.

4.1. Wastewater loading is a primary driver of both methane and nitrous oxide emissions

The average methane and nitrous oxide concentrations for nine and thirteen estuaries respectively appear highly correlated with urban wastewater loading per mean river flow (Fig. 4).

River-estuary systems that have higher levels of UWW per unit river flow have both higher methane and nitrous oxide production on average (Fig. 4). The correlation coefficients for both methane $R^2 = 0.80$ (excluding the Clyde) and nitrous oxide $R^2 = 0.78$ (all data) are statistically significant despite the large number of factors that could influence methane and nitrous concentrations including: natural estuarine variability, anthropogenic affects and survey protocols. Natural

Table 2
Summary of average methane and nitrous oxide concentrations measured.

Estuary	Year	Reference ^a	No. of surveys	Average CH ₄ (nM/l)	Average N ₂ O (nM/l)	Average CH ₄ (% sat)	Average N ₂ O (% sat)	CH ₄ :N ₂ O ratio
Conwy	2017-18	1	4	103.2	13.0	2964	130	7.9
Clywed	2017-18	1	3	178.6	13.8	5571	140	12.9
Tamar	2017-18	1	4	214.6	17.5	7820	164	12.3
Dart	2017-18	1	3	187.1	16.0	6415	165	11.7
Tay	2017-18	1	4	53.3	12.0	1475	107	4.4
Forth	2017-18	1	4	158.3	34.4	4138	262	4.6
Clyde	2017-18	1	4	1120.6	32.4	31,285	251	34.6
Tay	2009-10	2	8	48.2	13.9	2698	118	3.5
Humber	2000-02	3 & 4	2-3	55.1	71.4 ^b	1546	396	0.8
Forth	2000-02	3 & 4	4	178.4	20.1 ^b	5067	152	8.9
Tamar	2000-02	3 & 4	2-4	132.9	18.5 ^b	3047	145	7.2
Tay	2000-02	3 & 4	1	24.8	9.9 ^b	584	104	2.5
Tees	2000-02	3 & 4	3	500.1	68.8 ^b	16,559	383	7.3
Tyne	2000-02	3 & 4	6-8	910.0	14.0 ^b	26,348	124	65.0
Colne	2001-02	5	4	na	197.3	na	993	na
Stour	2001-02	5	4	na	24.9	na	143	na
Orwell	2001-02	5	4	na	46.3	na	282	na
Deben	2001-02	5	4	na	32.6	na	187	na
Humber (Trent falls - Humber Br)	2001-02	5	4	na	32.1	na	187	na
Humber (Humber Br - spurn head)	2001-02	5	4	na	24.7	na	149	na
Conwy	2002-03	5	4	na	18.6	na	114	na

Abbreviations: - Methane (CH₄), Nitrous Oxide (N₂O)

^a References see Table 1

^b Estimated from concentration data provided in reference 3

estuarine variability would include: stratification, tidal range, tidal asymmetry, fresh water flushing time, average particle residence time, river flow, the shape and area of the estuary, area of tidal flats and sedimentation processes. Other significant anthropogenic affects might include the percentage cover and type of agriculture in the catchments, industrial waste, water extraction and legacy pollution. The main variation associated with the survey protocols include the number, seasonal balance and range of methods used. While on average all estuaries fit the relationship between GHG concentrations and UWW loading, the methane to nitrous oxide ratio is higher for the Clyde and Tyne compared to, for example, the Tay, Forth and Humber estuaries (Table 2). Here, estuary morphology may be an influencing factor. The large and exposed Tay, Forth and Humber systems may allow for more effective oxygenation of the surface waters resulting in more methane oxidation, in comparison to the physically restricted, narrow estuaries of the Clyde and Tyne. Morphological variation aside, these data underline the potential importance of UWW output on both methane and nitrous oxide concentrations in estuarine environments and undermine the assumption that discharge into estuaries is flushed away without environmental repercussions.

To further investigate the relationship between urban influences and estuarine GHGs, catchment land cover was considered (Morton et al., 2020), (see supplementary data Fig. A1). These relationships strongly support the inference that high urban populations increase both estuary methane and nitrous oxide but agriculture primarily impacts nitrous oxide concentration. The limited data for carbon dioxide (only available for five estuary systems) has a positive correlation with UWW loading. Bioavailability of anthropogenic derived organic matter may promote microbial production and degradation, rather than carbon sequestration (García-martín et al., 2018).

4.2. Nitrous oxide concentrations significantly increased by activation of denitrification

Nitrous oxide emissions from rivers and estuaries have been linked to the dissolved inorganic nitrogen (DIN) concentration for which agriculture and sewage treatments are considered the main sources (Dong et al., 2005; Barnes and Upstill-Goddard, 2011). Fig. 5 shows the

average nitrous oxide percentage saturation against concentrations of nitrate, nitrite and ammonium respectively from (Dong et al., 2005; Pickard et al., 2022). While these plots confirm the strong correlations between nitrous oxide and particularly nitrite and ammonium, as previously reported (Dong et al., 2005) and are generally consistent for all authors, there are exceptions, specifically for the Colne, Forth and Clyde (see ringed points in Fig. 5 a, b, c) which demonstrate higher nitrous oxide concentrations compared to DIN loading. The relationship between DIN and nitrous oxide percentage saturation for six estuaries also shows higher nitrous oxide concentrations for the Forth (Barnes and Upstill-Goddard, 2011, Fig. 6). The river data (Dong et al., 2005), show no exceptions, even for the Colne. Additionally the relationship between nitrous oxide and ammonium (but not nitrate or nitrite) is different between the rivers and estuaries. Nitrification, which converts ammonium to nitrous oxide, requires oxygen, and rivers are typically more oxygenated than estuaries.

The Colne estuary is muddy and hyper-nutriented (Ogilvie et al., 1997) with strong gradients (increasing up river) of nitrate and ammonium due to inputs from the river and sewage treatment. Sediments located near the tidal limit were found to be major sites of denitrification and correlated with high nitrite concentrations (Robinson et al., 1990; Dolfing et al., 2002). Dissolved oxygen data for the Forth showed a strong negative correlation with nitrous oxide (Barnes and Upstill-Goddard, 2011), and both the Clyde and Forth are known to experience low oxygen conditions under some tidal and river flow regimes (Scottish Environment Protection Agency, 2020). These are all consistent with a denitrification mechanism for the higher nitrous oxide in the Colne, Forth and Clyde (Fig. 5). Uncoupled bacterial denitrification supported by nitrate diffusing into the sediment from the overlying water column and by the sediment organic carbon content, can exhibit faster rates of nitrate reduction (Dong et al., 2000) with organic carbon content determining the potential capacity of denitrification when the nitrate concentration is not limiting with bacterial communities adapting to high nitrate concentrations. Hence when high levels of oxidised nitrogen and ammonium are delivered to an estuary this mechanism is likely to result in high nitrous oxide production. Nitrous oxide concentrations are more significantly impacted by the presence of ammonium compared to nitrate (Fig. 5), suggesting nitrification with exceptions for

Table 3
Physical characteristics of the estuarine systems.

	Estuary	Estuary catchment Area ^a (km ²)	Estuary area ^a (km ²)	Mean freshwater input ^b (m ³ /s)	Tidal range HAT-LAT ^c (m)	UWWT Capacity Estuary ^d (pp eqs)	UWWT Capacity River ^e (pp eqs)	UWWT Capacity Total (pp eqs)	UWWT Capacity/ Mean freshwater input (per 1000)	Mixing regime
1	Coway	345	14.9	19.1	9.01	88,731	4072	92,803	4.86	Macrotidal, well mixed, can stratify on flood and mix on the ebb ^f
2	Clywd	598	1.2	11.2	9.70	88,248	27,057	115,285	10.28	Macrotidal, well mixed
3	Tamar	1338	39.6	22.7	5.91	358,096	46,641	404,737	17.83	Macrotidal, well mixed, low salinity TMZ, stratification occurs on ebb ^f
4	Dart	475	8.6	11.3	5.91*	36,084	22,134	58,218	5.16	Macrotidal, stratified neap & low freshwater runoff ^f
5	Tay	5669	121.3	201.1	6.31*	98,000	99,975	197,975	0.98	Macrotidal, partially mixed, stratified on ebb, longitudinal fronts ^g
6	Forth	1938	84.0	46.4	6.31	267,700	111,250	378,950	8.17	Macrotidal, well mixed, low salinity TMZ, double high/low waters ^h
7	Clyde	3854	54.9	57.1	3.90	1,159,202	886,846	2,046,048	35.84	Mesotidal, stratified at neap, channel straightened and deepened ^f
8	Humber	19,427	303.5	212.3	7.83				-	Macrotidal, well mixed, low salinity TMZ ^f
9	Tees	1980	13.3	22.4	5.99	932,367	10,892	943,259	42.13	Macrotidal, partially mixed, stratified at neaps and on ebb tide ^f
10	Tyne	2935	7.9	47.5	5.73	1,003,785	104,748	1,108,533	23.27	Macrotidal, partially mixed, low salinity TMZ ^h
12	Colne	255	23.4	1.1	4.71	144,152	28,675	172,827	161.52	Macrotidal, with extensive mud flat and tidal creeks ⁱ
13	Stour	578	23.3	3.1	4.71	48,355	55,932	104,287	33.68	Macrotidal with extensive mud flat and tidal creeks ^j
14	Orwell	-	-	1.4	4.71	178,075	11,731	189,806	140.7	Macrotidal with extensive mud flat and tidal creeks ^j
15	Deben	-	-	0.8	4.71	28,630	6000	34,630	43.78	Macrotidal ^k

Abbreviations: Highest / Lowest Astronomical Tide (H/ LAT), Urban Wastewater Treatment (UWWT)

^a (Nedwell et al., 2002)

^b All flow data were derived from CEH (UK Centre for Ecology and Hydrology (UKCEH), 2020) and focus on the main rivers entering at the head of the estuary. The mean flow data represent the specific river mentioned unless stated below: Clywd is the sum of the Clywd and Elwy, Tay is the sum of the Tay and Earn, Clyde is the sum of the Clyde and the Kelvin, Humber is the sum of the Aire, Trent, Ouse, Don, Wharfe and Derwent, the Tees is the sum of the Tees and the Leven and the Tyne is the sum of the Tyne and the Derwent.

^c (BODC, 2020), (*)Due to the location of standard ports the Forth estuary tidal range is applied to the Tay and the Tamar estuary tidal range is applied to the Dart

^d (European Commission (Directorate General Environment), 2016)

^e (Robins et al., 2014)

^f (Uncles and Stephens, 1993)

^g (Thain et al., 2004)

^h (Wewetzer et al., 1999); (McMannus, 2005)

ⁱ (Lindsay et al., 1996)

^j (Scottish Environment Protection Agency, 2020)

^k (Mitchell et al., 1999), (Mitchell et al., 1998)

^l (Environmental Agency, 1999)

^m (Upstill-Goddard et al., 2000)

ⁿ (Dong et al., 2005)

Colne, Forth and Clyde. The dynamic often low oxygen environment within these estuaries may trigger denitrification even with oxygen present (Marchant et al., 2017) and mid-salinity waters and ammonium concentration can further optimise nitrification rates (Imanetsyo et al., 2014). These two observations suggest that more nitrogen cycling can occur in an estuary than in either fresh or coastal waters. This data underlines the importance of preventing both excessive inputs of nitrate and ammonium and the occurrence of low oxygen condition within estuaries.

4.3. Methane dynamics driven by ammonium concentrations

Average methane concentration data from seven estuaries (Pickard et al., 2022) appear highly correlated with nutrients, particularly nitrite, ammonium, phosphate and (Fig. 6 b, c, d respectively). While causal factors are not clear, the higher correlations with nitrite, ammonium and phosphate ($P < 0.001$) point towards UWW as a contributor to methane production in the estuary. Conversely the poor, not statistically significant, correlation with nitrate concentrations, would not suggest agricultural run-off is significantly affecting estuary methane production. This is consistent with the land-cover data in supplementary data Table A2 and Fig. A1. Furthermore inputs from agriculture typically



Fig. 3. Map showing estuary catchments of the thirteen estuary systems mainly considered in this analysis.

occur higher in the catchment compared to UWW giving more time for processing to occur prior to water arriving in the estuary.

Methane concentrations can be influenced by DIN indirectly. Nitrification of ammonium requires oxygen and this process may consume sufficient oxygen to reduce methane oxidation through the water column. Additionally inhibition of methane oxidation by ammonium can occur in the surface layer of a sediment, allowing more methane evasion (Boose et al., 1993; Dunfield and Knowles, 1995). Conversely if denitrification is the prevalent mechanism of nitrous oxide production, the low oxygen environment that promotes nitrous oxide production would also reduce methane oxidation, resulting in a secondary correlation. These potential mechanisms linked to oxygen levels are also consistent with the poor correlation with nitrate, which does not require oxygen for further processing. These relationships only hold for each estuary survey as a whole, not for each specific measurement point, suggesting that process timescales are important (Fig. 6).

4.4. Urban waste and nutrients summary

Estuary systems that have higher levels of nutrients from UWW per

unit river flow have higher methane and nitrous oxide concentrations and both methane and nitrous oxide concentrations are more strongly correlated to nitrite and ammonium concentrations than nitrate. Analysis on the influence of land-cover (supplementary data Table A2 and Fig. A1) strongly support the inference that high urban populations increase both estuary methane and nitrous oxide but agriculture primarily impacts nitrous oxide concentration. Significantly higher levels of nitrous oxide and methane occur in estuaries that experience high urban loading and low oxygen conditions, likely via denitrification and inhibited oxidation pathways respectively. The natural but highly variable conditions in estuaries related to changing oxygen levels and mid-salinity values may act to increase nitrogen cycling rates in estuaries compared to either fresh or coastal waters and suggest that UWW discharge into estuaries has environmental repercussions related to GHGs.

5. Estuarine processes as drivers of GHG production

To elucidate the impact and interactions of estuarine processes on GHG production it is useful to consider different types of estuaries,

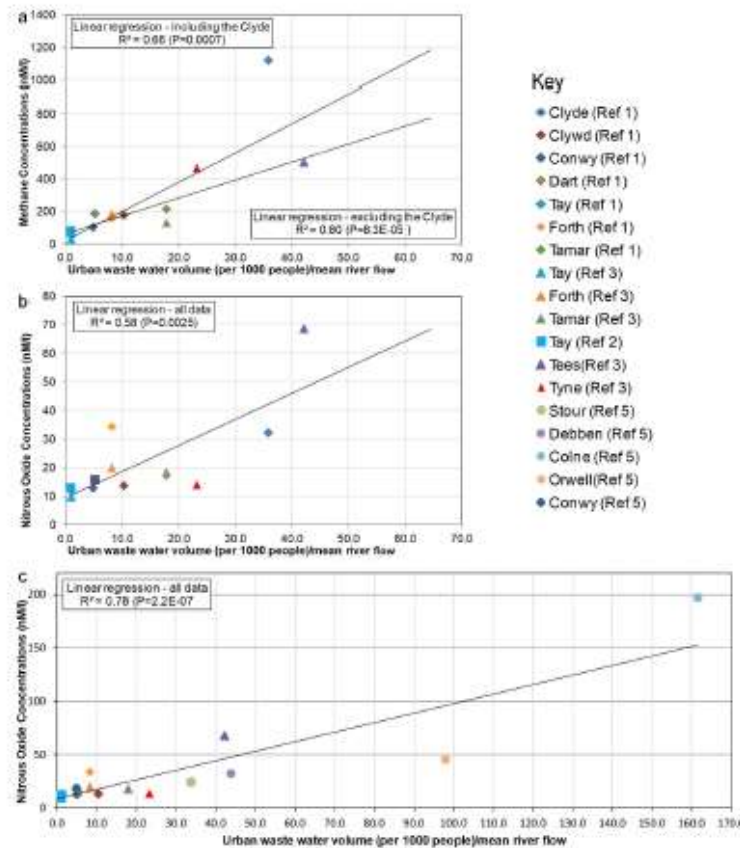


Fig. 4. UWW loading (urban wastewater volume (per 1000 people/mean river flow)) is compared with (a) Average methane concentration (Pickard et al., 2021, 2022 and Barnes and Upsill-Goddard, 2011); (b) Average nitrous oxide concentration data (Pickard et al., 2021, 2022; Upsill-Goddard and Barnes, 2016); (c) Average nitrous oxide concentrations as for (b) but including estuaries from SE England (Dong et al., 2005).

where there is sufficient data for interpretation, as morphology strongly influences estuarine processes. As such two different estuaries with high urban loading: (i) the Clyde (Pickard et al., 2022), which can be stratified and (ii) the Tyne, (Barnes and Upsill-Goddard, 2011; Upsill-Goddard and Barnes, 2016), which is well mixed with a distinct turbidity maximum, are considered and contrasted with more pristine systems. Note that estuary area was found to have no significant correlation with GHG concentrations.

5.1. Estuary stratification leading to near bed anoxia driving GHG production

Very high methane and nitrous oxide concentrations have been observed in the Clyde estuary (Pickard et al., 2022). This may in part be attributed to the frequent occurrence of near-bed anoxia, as evident in continuously monitored surface and near-bed oxygen data in the upper estuary by Inner Clyde Estuary (ICE) monitoring buoy (Scottish Environment Protection Agency, 2020). Anoxic events are most common when neap tides and low river flows align. The inner Clyde estuary, which is long and narrow, has been anthropogenically constrained with near vertical walls along much of its length and obstacles such as sandbanks removed by dredging. These factors together with the lower tidal range (Table 3) reduce turbulence and consequently mixing, in contrast with most UK inner estuaries. When low river flows coincide with neap tides the reduced energy conditions result in a strong

pycnocline and low oxygen concentrations particularly associated with the lower portion of the water column. These low oxygen concentrations enhance conditions for GHG production.

Four surveys covering different river flows and tidal ranges, average methane and nitrous oxide concentrations within the Clyde estuary showed considerable temporal variability (Pickard et al., 2022; Table 4). Potential key drivers of this variability include tidal range, river flow, surface and bed salinity, temperature and oxygen levels. While there is insufficient data in four surveys for the mechanisms impacting GHG concentrations to be fully understood, the rank orders for methane and nitrous oxide concentrations are similar suggesting that the estuarine conditions influence both methane and nitrous oxide concentrations. This would suggest reduced methane oxidation and denitrification processing of DIN possibly occurring concurrently under low oxygen conditions. The lowest methane and nitrous oxide concentrations were associated with high river flow and spring tide conditions (January 2018) and associated with a mixed, highly oxygenated estuary and diluted nutrients. The higher methane and nitrous oxide concentrations were recorded when sampling took place during a neap tide that coincided with relatively low river flows, which had resulted in a highly stratified estuary and low oxygen conditions near the bed.

The Clyde has a high urban loading with UWW treatment plants adding significant volumes of wastewater discharging both directly into the estuary and at 3.5 km and 13.3 km upstream of the estuary's upper saline extent, without prior nitrate or phosphate removal at the time of

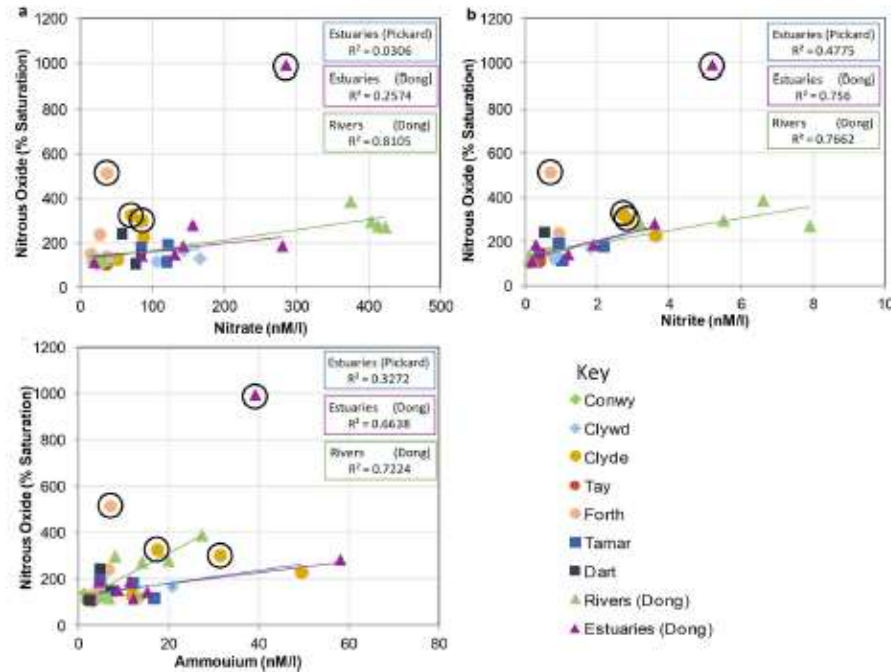


Fig. 5. Relative relationships between various DIN concentrations and average nitrous oxide percentage saturation, specifically (a) nitrate, (b) nitrite, (c) ammonium with data from (Dong et al., 2005; Pickard et al., 2022). Note ringed points related to the Colne, Forth and Clyde are not included in the regression lines.

this survey (European Commission (Directorate General Environment), 2016). The highest methane and nitrous oxide concentrations correspond to the proximity of the largest estuarine UWW discharge, amplified by its addition to an area often stratified with a pronounced anoxic layer.

The data from the upper Clyde as measured by ICE monitoring buoy also shows that in recent years (2016 to 2019) the May to July period had higher salinity intrusion and lower dissolved oxygen data (Scottish Environment Protection Agency, 2020). This appears linked to sustained low river flows during this period (UK Centre for Ecology and Hydrology (UKCEH), 2020), which would act to increase the saline intrusion and reduce estuary flushing, resulting in longer particle residence times. This together with the physically restricted estuary morphology would further limit the re-oxygenation of incoming saline water between tides. While these low oxygen levels during prolonged low river flow events would also be expected to result in higher GHG concentrations, the low river flow would result in an upward shift in salinity for all locations, effectively shifting the location of the estuarine water upstream impacting the effective estuary area and would need to be accounted for.

Association of near bed anoxia with weak tidal mixing and low river flow can be observed in other estuaries. Flow and stratification data across the Dart estuary showed that two layer flow occurs at neap tides during low water flow (Thain et al., 2004). Methane and nitrous oxide concentration data from the same estuary were collected across a range of river flows. Methane concentrations were an order of magnitude higher when sampling occurred at low river flow (34% of the mean flow), although all measurements occurred during neap tides (Pickard et al., 2022; Table 5).

While fully equivalent oxygen and nutrient data for the estuaries are not available, the urban loading of the Dart is one eighth of the Clyde (Table 3). The best estimate of surface oxygen levels for the Dart (Environment Agency, 2020) and the Clyde (Scottish Environment Protection Agency, 2020) shows that the Clyde has an average surface

oxygen level of 82%, and the Dart 97% (Table A1). This ranking of both oxygen levels and UWW loading is aligned with the methane and nitrous oxide data available. The extent and frequency of stratification and near bed anoxia is not known for the Dart.

Stratified estuaries experiencing low river flows in summer, when oxygen levels may already be low are even more susceptible to high methane concentrations. Higher methane concentrations were observed in four estuaries measured in July (Pickard et al., 2022) the Clwyd, Tamar, Dart and Conwy, which had river flows between 21% and 40% of the mean flow on the measurement dates (NRPA, 2010) although no oxygen data were available. Overall this suggests that both tide and river flow interact with urban loading to influence methane concentrations in particular, and that surface oxygen levels may provide an initial indication of likely methane concentrations.

5.2. Tidal range impacting sediment oxygen demand driving methane production

The Tyne (together with the Humber, Forth and Tamar) is noted to have flood tide asymmetry, (Barnes and Upstill-Goddard, 2011), which forces marine sediments upstream, when river discharge is slow, resulting in a well-defined Estuary Turbidity Maximum (ETM). High suspended sediments associated with low oxygen levels have been measured on the tidal rivers Trent and Ouse (Mitchell et al., 1999) and attributed to the high sediment oxygen demand (SOD) of the suspended sediment particles. Organic material and metals (for example from industrial legacy waste) can adsorb onto the surface of sediments and lead to increased biochemical oxygen demand (BOD) (Mitchell et al., 1990). Sediments that are re-suspended from anoxic or anaerobic layers in the bed and moved to aerobic locations by river flow or tidal flow can use more oxygen than expected because they are newly exposed to aerobic organisms and contain chemicals or metal ions in a reduced state.

Across six surveys covering different river flows and tidal ranges in

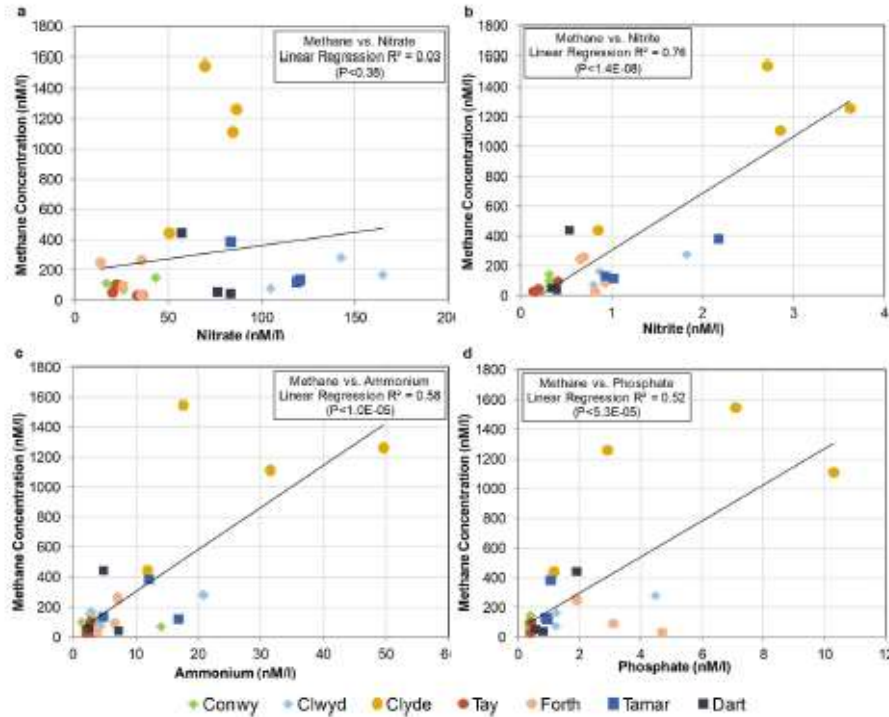


Fig. 6. Relationships between average methane concentration for each estuary and (a) nitrate, (b) nitrite, (c) ammonium and (d) phosphate concentrations with data from (Pickard et al., 2022).

Table 4
Clyde Estuary GHG concentrations associated with tidal, river, salinity and oxygen conditions.

	River flow Daldowie ^b (m ³ /s)	Percent of mean flow (%)	Tidal range ^c (m)	Water Temperature Deg C ^d	Surface / Bed Salinity ^a (PSU)	Surface / Bed Oxygen ^a (mg/l)	Survey average ^d N ₂ O (nM)	Survey average ^d CH ₄ (nM)
July-17	22.6	47	2.53	15.3	2.0 / 15.0	8 / 1	31	1114
Nov-17	53.1	110	2.14	12.1	0.5 / 20.0	11 / 6	51	1460
Jan-18	139.0	287	3.49	5.4	0.1 / 0.1	12 / 12	14	445
Apr-18	20.7	43	3.33	11.8	2.0 / 6.0	8 / 5	30	1263

^a (Scottish Environment Protection Agency, 2020).

^b (NRFA, 2010).

^c (BODC, 2020).

^d (Pickard et al., 2022).

the Tyne estuary, average methane concentrations showed considerable temporal variability (Upstill-Goddard and Barnes, 2016). Whilst similar methane concentrations occur across a range of river flows from 35% to 235% of the mean flow (NRFA, 2010), there is a strong correlation ($R^2 = 82\%$, $P < 0.02$) between methane concentrations and tidal range (using data from the standard port at Whitby at the mouth of the Tyne) (BODC, 2020), see Fig. 7. The higher tidal ranges have the potential to increase mixing and re-suspension of sediment, which could reduce oxygen concentrations. However, when high river flow occurs simultaneously with high tidal range, the extent of the tidal intrusion will be reduced, likely causing reduced methane production within the estuary area.

Other fully-mixed estuaries also show an increase in methane associated with high tidal range, but the limited number of survey occasions and confounding between potential driving variables means that methane is also correlated with low river flow and high temperature, both of which would reduce oxygen levels. These three possible causes

are too strongly correlated to enable firm conclusions and all may contribute to elevated methane concentrations to some degree.

5.3. Estuarine processes summary

The Clyde and Dart estuaries provide examples of stratified systems with weak tidal mixing, frequently experiencing near bed anoxia, which is associated with high methane and nitrous oxide concentrations, particularly during neap tides and low river flows. Conversely, the Tyne estuary which is typically fully-mixed shows a strong correlation between methane concentrations and tidal range, which we consider to be linked to suspended sediments removing oxygen from the water column. The Tyne has considerable legacy pollution (Hall et al., 1996; Lewis, 1990) and hence high sediment oxygen demand may be associated with this condition. These interpretations, while interesting, are based on limited samples from what are highly variable systems and are unlikely

Table 5
Tide and River Condition associated with measurements occasions - Dart estuary.

	River flow Austins Bridge ^a (m ³ /s)	Percent of mean flow (%)	Tidal range ^b (m)	Survey average N ₂ O ^c (nM)	Survey average CH ₄ ^c (nM)
July-17	3.87	34	3.45	21	442
Oct-17	14.37	127	3.46	–	–
Jan-18	53.64	475	3.54	11	54
Apr-18	25.85	229	3.71	15	41

^a (NRFA, 2010).

^b (BOC, 2020).

^c (Pickard et al., 2022).

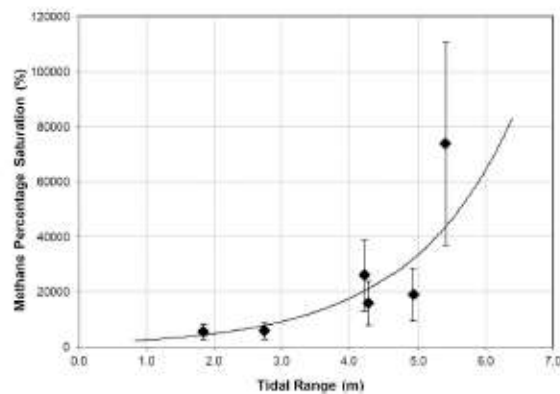


Fig. 7. Tyne Estuary average relationships between methane concentration and tidal range. Methane data from *Upstill-Goddard and Barnes (2016)* and tidal data from *BOC (2020)*.

to fully characterize the OHG variability and associated mechanisms and should be treated with caution. Additionally there is insufficient data overall to determine the impact of temperature on nitrous oxide and methane concentrations, which would be expected to be significant. These relationships once established may vary between environments and further improve predictive power.

6. Conceptual model for methane and nitrous oxide within the estuary environment

Whilst spatial-temporal variability in estuarine systems is high, evidence collated here indicates the potential for robust conceptual understanding of OHG production pathways in estuaries. Summarising the key processes that have been presented in UK estuary case studies, a conceptual model for methane and nitrous oxide concentrations within the estuarine environment has been developed. This model aims to capture, as far as possible, the high variability between and within estuarine environments, influenced by the catchment, estuarine shape and dimensions, tidal regime and river flow, together with anthropogenic perturbations. To illustrate this model, four diagrammatic examples are provided relating to the two extremes of estuarine mixing; a salt-wedge estuary with significant stratification (*Fig. 3*) and a fully-mixed estuary (*Fig. 9*), both shown at high tide. The model also incorporates a prediction of how a low nutrient estuary (panel A) is influenced by the introduction of UWW (panel B) and how this change will interact with estuarine processes to increase both the methane and nitrous oxide emissions. Anthropogenic susceptibility can vary in different estuaries or due to different conditions within a particular estuary; for example,

variation from spring to neap tides, changes in river flow and changes in temperature, can cause an estuary to change its level of stratification, oxygenation or the amount of suspended sediment. Additionally, flood or ebb tide dominance varies between estuaries with some systems becoming stratified only on the ebb and others only on the flood tide. These physical differences, which occur over varying temporal scales, will impact the interactions with UWW and can, in part, be inferred from our simplified model.

A high level of legacy pollution assimilated into the estuary sediments could further remove oxygen from the lower layer if sediments are disturbed, increasing anoxia and reducing methane oxidation. Conversely high river levels may more rapidly replenish oxygen to the upper layer, reducing the impact of UWW. As a result higher methane concentrations would be expected to increase as oxygen becomes depleted towards high tide and reach a maximum at the extent of the saline intrusion. Methane concentrations would be expected to reduce on the ebb tide as surface waters are replaced by oxygenated riverine waters and nutrient are no longer trapped in the estuary. The longitudinal profile of methane may peak where there is lowest oxygen levels while that of nitrous oxide may peak associated with mid salinity, DIN concentration and low oxygen. The location of these peaks will also be influenced by the river flow and associated with urban inflows which are then diluted seawards on the ebb. Any artificial barrages or weirs (more often found in stratified estuaries as they can remove tidal energy) may be associated with sediment or debris deposition which may act as a carbon source and hence be related to higher GHG production. Periods of drought will likely increase the extent of the saline intrusion and the estuary flushing times, which would change the location of the maximum GHGs and increase nitrous oxide concentrations. The lower estuary turbulence and the typically reduced concentration of GHGs at the surface may act to reduce emissions to atmosphere, although when mixing or overturning of the bottom layer occurs this could cause a dynamic release.

Where there are high levels of legacy pollution, sediment re-suspension in the turbidity maximum leads to high sediments oxygen demand, reducing oxygen levels and increasing methane concentrations and evasion significantly. Higher tides would be expected to suspend more sediment, further reducing oxygen and increasing methane production. Changes in river flows may serve only to move the location of the methane and nitrous oxide production, which on high rivers flow would cause an overall reduction GHG production in the estuary area as water is pushed seaward. In a mixed estuary (with no stratification on the ebb) methane and nitrous oxide production are expected to be similar on the flood and ebb tide. Where stratification does occur on the ebb the lower portion of the estuary stagnates, depleting oxygen and thereby producing more methane when compared to the flood tide. If sediment suspension occurs at low tide, this could cause a rapid drop in oxygen and be associated with increased nitrous oxide concentrations due to high DIN concentrations and denitrification. The longitudinal profiles of methane and nitrous oxide may exhibit peaks associated with the low salinity turbidity maximum, areas where sediment is routinely deposited and UWW inflows. Nitrous oxide concentrations may be higher in the mid salinity range of the estuary diluting seawards. The higher estuary turbulence and continual mixing of GHGs to the surface will act to increase emissions to atmosphere.

7. Discussion and conclusions

There is convincing evidence from UK estuaries that excesses of nutrients from UWW result in both higher methane and nitrous oxide concentrations and these concentrations link directly to UWW loading per unit river flow. This is supported by estuaries with higher urban land cover having higher methane and nitrous oxide concentrations. Furthermore, methane and nitrous oxide concentrations are more strongly correlated to nitrite and ammonium than nitrate. Where estuaries experience very low oxygen conditions, higher concentrations of

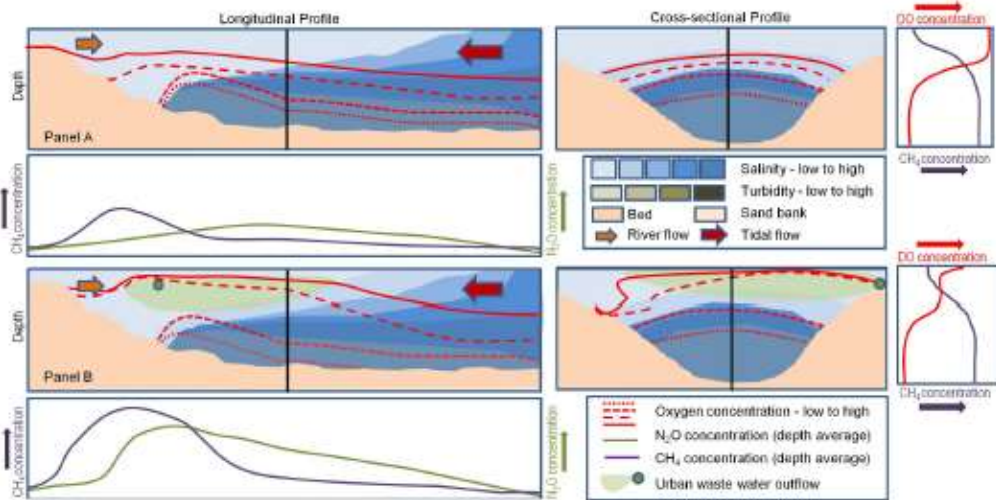


Fig. 8. Panel A: - Longitudinal and cross-sectional profiles of a highly stratified salt-wedge estuary at high tide, with the higher salinity water flowing shore-wards underneath the out-flowing river water.

The upper layer, from the river, would typically be oxygenated, but the lower layer would become lower in oxygen with no means of replenishment, as the oxygen is depleted with distance from the sea and time from low tide. The degree of stratification will change during the tidal cycle and with river and tidal conditions, but when the estuary is highly stratified, this will reduce diffusion of GHGs from the lower to upper layer trapping GHGs under the pycnocline. Methane generation in the bed is generally associated with the low salinity area of the estuary, significantly reducing when the water becomes highly saline. Oxidic methane may be generated in the upper fresh water layer. Most methane (CH_4) oxidation would occur in the upper layer resulting in methane concentrations that are linked both to the water layer of generation and inversely related to the vertical oxygen profile. The specific relationship and location of the methane maximum is expected to change with river flow, tidal range and state of the tide, with surface methane concentration reducing on the ebb as more river water becomes available. Some dissolved inorganic nitrogen (DIN) may enter the estuary from the river, with DIN loading changing with river flow. Nitrous oxide (N_2O) concentration would be relatively low peaking at mid-salinity, compared to the methane peaking at low salinity, both reducing seawards due to dilution with sea water.

Panel B: - Longitudinal and cross-sectional profiles of a salt-wedge estuary at high tide including the introduction of urban wastewater concentrated in the low salinity upper layer due to limited mixing.

Introduction of UWW will result in additional nutrients trapped in the upper layer, causing oxygen depletion thereby inhibiting methane oxidation, resulting in higher methane concentrations and additional methane evasion. Ammonium derived from urban wastewater may significantly increase nitrous oxide production, near the source and in the mid salinity range. Most DIN will be trapped in the more oxygenated upper layer making nitrification, driven by DIN concentration, the main N_2O producing mechanism in this layer. N_2O production in the lower layer will be driven by denitrification, with the N_2O concentration increasing with lower oxygen levels further supported in estuaries that have long flushing times allowing DIN to mix or diffuse downwards. Oxygen depletion can result in a switch from nitrification to denitrification even in the surface layer.

both nitrous oxide, most likely generated via denitrification, and methane, in part due to reduced methane oxidation, can be detected. An enhanced nitrogen processing is favourably associated with mid-salinity conditions (Imanetyo et al., 2014) and methane oxidation may be inhibited either directly or indirectly by higher ammonium concentrations, this makes the estuarine environment an unfortunate location for UWW disposal with respect to GHG emissions. Similarly nitrogen enrichment has been found associated with increased methane and nitrous oxide emissions from tidal flats (Hamilton et al., 2020) and higher methane emissions are now being associated with urban or anthropogenically influenced inland waters (Wang et al., 2021; Hao et al., 2021).

Estuary physio-chemical properties strongly influence methane and nitrous oxide concentrations. Stratified estuaries can experience significant oxygen depletion in the deeper more saline layer, with any legacy waste and associated oxygen sediment demand potentially exacerbating this effect. Additionally, inputs of UWW into a stratified estuary can result in further oxygen depletion in the upper layer due to nitrification of ammonium. Stratified estuaries experiencing low river flow, particularly in summer, when oxygen levels may already be low are even more susceptible to the impacts of UWW, as lower river flows will increase flushing times. Fully mixed estuaries, characterised by a low salinity and high turbidity maximum, can produce high levels of GHGs. The re-suspension of sediments can encourage high sediment oxygen demand

(Mitchell et al., 1998), preventing oxidation of methane in the water column. This increase in methane concentration can be linked to tidal range and also possibly to urban or legacy waste.

The conceptual model presented in this paper hypothesises that higher concentrations of both methane and nitrous oxide occurs due to interactions between natural estuarine processes and anthropogenic factors. Low estuarine oxygen levels appear to be significant in causing high methane concentrations within the estuary environment and probably linked to increased methane production and reduced methane oxidation in the surface sediments and water column. Estuarine processes can cause low oxygen levels where they prevent oxygen from being brought to the estuary, for example during low river flows and at high temperatures. Additionally oxygen may not be replenished in the water column, for example when the estuary is stratified or particle residence times increased. Sediments re-suspension can result in BOD, when oxygen is consumed by mineralization of the degradable organic components in fine sediments. Oxygen can be further depleted by the interaction with anthropogenic factors; for example: the introduction of nutrients from UWW and where legacy pollution is contained in the sediment resulting in high SOD.

Use of this conceptual model enables us to predict that some stratified estuaries may experience elevated methane concentrations at high tide, upstream at the low salinity section of the estuary. It also suggests that fully mixed estuaries with significant SOD would experience

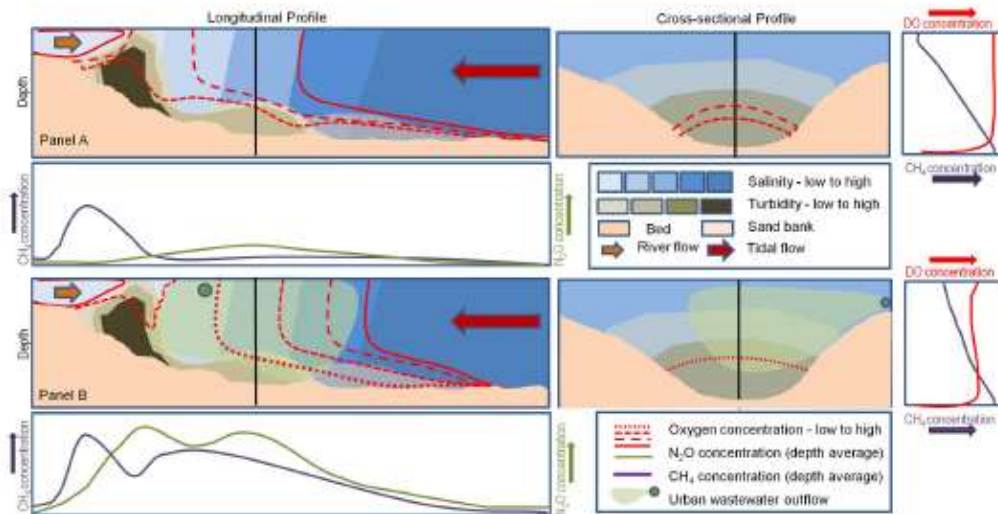


Fig. 9. Panel A - Longitudinal and cross-sectional profiles of a fully-mixed estuary, with salinity and oxygen levels mixed vertically throughout the water column. Estuaries with high tidal mixing typically experience tidal asymmetry and the transport of fine marine sediments into the upper estuary resulting in a turbidity maximum at low salinity. These sediments are moved up the estuary on the flood and down the estuary of the ebb tide and can trap organic matter at the bed. Methane (CH₄) is mixed and oxidised throughout the water column resulting in little methane evasion in the unpolluted scenario. Any dissolved inorganic nitrogen (DIN) will likely be converted by the nitrification route due to the mixing and higher oxygen levels.

Panel B - Longitudinal and cross-sectional profiles of a fully-mixed estuary, including the introduction of urban wastewater which is distributed throughout the water column due to effective mixing.

Introduction of urban wastewater (UWW) which will be mixed throughout the water column, will result in an interaction between the DIN and suspended sediments, allowing for both processing of nitrogen in the bed and water column, leading to higher nitrous oxide (N₂O) production. Where the UWW is sufficient to deplete oxygen levels through the water column denitrification could occur. This can further act to increase methane if resulting in reduced oxygen levels and subsequent methane oxidation inhibition.

elevated methane concentrations during sediment suspension events, which are most often associated with high tidal range. However these events can also occur at low tide and if sediments are re-suspended in shallow water over estuarine mud, low oxygen and high GHG concentrations may result. The rate of nitrous oxide generation from nitrification is variable, dependent on the availability of electron acceptors and donors (Wraga et al., 2001), the salinity level (with optimum nitrification in the mid salinity range) and temperature (with increased production typical at higher temperatures). Where oxygen concentrations are low or variable, as is often the case in estuarine environments, denitrification may be triggered. This can further significantly increase nitrous oxide concentrations. Estuaries with high suspended sediment concentrations may also support nitrogen processing in the water column as well as at the bed, associated with, for example, a turbidity maximum.

The conceptual model presented here summarises the processes evident in several UK estuaries, but if relationships can be generated for different estuaries and related to both natural processes and anthropogenic perturbations then it may theoretically be applied elsewhere. A study in Chesapeake Bay, the largest estuary in the United States which is eutrophic with near bed hypoxia, also found that methane was associated with low oxygen conditions. Interestingly in this study methane built up under the thermocline and could be released by storm events that induced mixing and overturning (Gelesh et al., 2016). While our conceptual model considers only tidal stratification which lasts in the order of hours, this thermal stratification may last weeks and act to reduce methane diffusion to the surface. The only estuary in this study deep enough to form a thermocline in calm summer weather is the Forth estuary (Black Culm Ltd., 2015). Methane concentrations in the deeper, higher salinity part of the Forth (Upstill-Goddard and Barnes, 2016) were lower in summer, as such it is possible the formation of a

thermocline may impact the surface methane signature and methane evasion estimates. GHG evasion linked to large river plumes may also be dependent on offshore mixing, with higher GHG concentrations found in calm weather. Methane concentrations were measured in nine tidal estuaries in NW Europe including well-mixed, turbid estuaries with long particle residence times (Elbe, Ems, Thames, Scheldt, Loire, Gironde, and Sado) and salt-wedge estuaries with short particle residence times (Rhine and Douro) (Middelburg et al., 2002). While it is not clear how measurements were made relative to the phase of the tide or river flow, it is interesting that the stratified Rhine experienced high and highly variable methane concentrations as would be predicted by the conceptual model dependent on river flow and tidal range and phase. Conversely in well mixed estuaries methane was often highest at the low salinity end consistent with the turbidity maximum being important in methane production (Burgos et al., 2015).

While a single survey was available for the Thames (Middelburg et al., 2002) and some data for the Humber (see Table 1), these large complex estuaries with several contributing rivers and many UWW entry points were not included in the analysis and did not fit the model as well as the simpler estuaries. It is suggested that the large number of tributaries, distance between where tributaries enter the estuary and the large number of UWW treatment plants and the distance of these plants from the estuary make the results difficult to interpret. For example the outflow from 335 and 200 UWW treatment plants eventually enter the Humber and Thames estuaries respectively, some from over 200 km. It is likely that where UWW enters a river far from the estuary, that most nitrogen processing is completed within the typically well oxygenated riverine section reducing its influence within the estuary. Additionally, wide more exposed estuaries are likely to be mixed by wind helping oxygenation and increasing evasion, a process not explicit in this model.

8. Are estuaries a net carbon source or sink?

The flux of GHGs between estuaries and the atmosphere has been estimated by those authors considered herein. This flux is dependent on the dissolved gas concentrations (under consideration in this paper) and the gas transfer velocity (k), which is in turn dependent on in-water turbulence and wind speed (Wanninkhof, 1992; Clark et al., 1995). In estuaries the estimation of the gas transfer velocity associated with turbulence is complex, as turbulence is the result of tidal velocity and river flow interacting with friction from the bed bathymetry. As such salt-wedge estuaries, with lower turbulence compared to mixed estuaries may have a lower value of k . Wind speed, found to have the major impact on k (Clark et al., 1995), not only impacts diffusion at the interface but also wind induced waves which increase mixing. Estuaries that are wide and align with the prevailing wind direction and in topographies that increase wind exposure, are likely to evade a higher proportion of their GHGs to the atmosphere. Thus, k -values from a narrow, dredged, salt-wedge estuary may be less than from a fully-mixed, wide and exposed estuary, especially as GHGs in the lower layer will be less accessible. However, when the stratification is overturned or the stratified water becomes mixed, this may result in dynamic release of trapped GHGs to atmosphere. This process would be difficult to observe requiring detailed temporal monitoring, and emissions may be underestimated if only surface concentrations have been measured.

In addition to the direct atmospheric emissions, it is also important to understand whether estuaries are an overall carbon sink or source. The term 'Blue Carbon' is used to highlight the importance of the carbon sequestration capacity of coastal vegetated ecosystems (Santos et al., 2021). While there is currently insufficient data to understand the link between carbon sequestration and GHG concentrations, it has been hypothesised that discharges of high-nutrient but relatively low-carbon water generated by wastewater treatment can enhance carbon uptake from the atmosphere by affecting biogeochemical cycles in these system (Kuwae et al., 2016). While this is yet to be tested, this estimate focuses primarily on carbon dioxide and not nitrous oxide or methane. In contrast arable and (sub)urban estuaries were found to export, on average, 50% more dissolved organic carbon to coastal areas than they receive from rivers due to net anthropogenic derived organic matter inputs within the estuary, with the bioavailability of this dissolved organic matter promoting microbial production and degradation (García-martín et al., 2018). While beyond the scope of this paper, understanding where estuaries could act as carbon sinks and how this is impacted by anthropogenic inputs (in terms of micro-biome communities and bioavailability of nutrients) and activities (e.g. dredging) would be a beneficial area of study. The highly variable estuarine environments are likely to respond differently to enabling carbon sequestration both in terms of anthropogenic influences and estuarine processes.

9. The impact of survey design and areas of uncertainty

Where estuarine surveys are designed to produce an estimate of GHG concentrations it is important to consider the best approach to capture spatio-temporal variability. Based on data reviewed here we recommend the following approach for future studies:

- use of fixed point transects with each point aligned to a particular area within the estuary and measurements taken upstream to the limit of the maximum saline intrusion
- sufficient sampling undertaken to account for tidal range, stage of the tide, river flow and river flow history (for example periods of drought)
- sufficient sampling undertaken to account for temperature ranges and seasonality, including the interaction of temperature and river flow

- measurements to quantify the influence of any nutrient and pollution point sources within the estuary and to account for the different mechanisms of GHG production, for examples linked to: stratification, high turbidity and sediment oxygen demand, tidal flats, variation in salinity, legacy pollution and UWW
- measurements of oxygen, turbidity and nutrients in addition to GHG concentrations
- measurements to quantify GHGs in both layers where stratification occurs

Further measurements designed to quantify the specific impact of stratification, tide, temperature and river flow on GHG concentrations and emissions could help remove uncertainties in the conceptual models and further the objective of this paper in helping to identify and remediate estuaries that have high GHG concentrations, globally.

It can be difficult to distinguish between different anthropogenic factors, because areas which were the centres of past industrial activity still have high urban populations. Population density has been found to be significantly related to enrichment of sedimentary metals (Birch et al., 2015). As referred to previously, high levels of legacy pollution, particularly metals, may play a role in GHG emissions. Impairments to water quality can result in the creation of toxicologically stressful environments that may affect the microbiome community structure (Rodgers et al., 2020). This can have an impact on GHGs; for example methanogens use metals such as nickel within coenzymes (Lyu et al., 2018). At least four of the estuaries considered here have high legacy pollution, particularly heavy metals, including the Clyde (Rodgers et al., 2020; Balls et al., 1997), Forth (Lindsay et al., 1998), Tees and Tyne (Hall et al., 1996; Lewis, 1990). The Clyde and Tyne produce more methane than might be expected compared to the Tees and Forth. While this may be related to the Clyde and Tyne being physically restricted, narrow estuaries, it should be noted that the Clyde and Tyne estuaries are regularly dredged, while the upper Forth estuary has never been dredged and the Tees is only occasionally dredged (Marine Scotland, 2021; The Crown Estate, 2021). Dredging and straitening are likely to reduce bed friction and hence mixing. Dredging can re-suspend buried sediments associated with legacy heavy-metal pollution making it more available and leading to further anthropogenic interactions. A further uncertainty is the impact of temperature, salinity and nutrient levels on microbiome community structure and hence the balance between methane production and oxidation.

Expected changes in climate will also impact the estuary environment (Robins et al., 2016). This may act to further increase estuary GHG concentrations via a number of mechanisms. Increasing temperatures will reduce oxygen concentrations and increase nitrogen processing rates. Rising sea levels may increase sediment re-suspension and the extent of the saline intrusion, which could increase access to legacy waste. Changing rainfall patterns may increase the prevalence of drought conditions resulting in lower river flows and consequently lower oxygen and higher nutrient concentrations and reduced estuary flushing. Conversely more extreme rainfall events may lead to flooding which could result in flooding of land affected by legacy waste and nitrogen-rich agricultural land. All of these changes may act to further increase the susceptibility of estuaries to anthropogenic influences increasing GHG production.

10. Opportunities to reduce estuarine GHG emissions

Given that the estuary environment is a potentially significant source of GHG emissions, opportunities to manage and reduce emissions should be considered. Fundamental to the reduction of both nitrous oxide and methane emissions from estuaries is the lowering of DIN levels and removal of low oxygen conditions. Relating to the former, addition of nitrogen and phosphate removal technologies to existing UWW treatment systems outputting to estuaries should be considered. While estuary oxygenation has been trialled in a eutrophic estuary ((Larsen et al.,

2019) and some reservoirs (Gerling et al., 2014) its impact on the biome community and GHG production is unknown. This type of technology could be beneficial if powered by renewable technology. Our conceptual model may be applied to identify priority estuaries for this intervention. Additionally an improved understanding of processes associated with GHG generation could, in the interim, support the adoption of changed management practices, for example ensuring that outflows of UWW are not timed with conditions which may exacerbate estuarine GHG production. Applying our model to the Clyde estuary, we would expect the estuary to be well oxygenated (and hence have lower surface methane concentrations) during high river flows and during ebb tides. Hence, managing UWW outflow to avoid low oxygen conditions and timing outflows on the ebb tide rather than the flood tide could help reduce oxygen stress and methane and nitrous oxide emissions.

The annual nutrient loads to estuaries in the UK are comparatively small compared to reported figures for European and North African estuaries (Nedwell et al., 2002). As such, there may be even greater potential for excess GHG emissions, and reduction thereof, from estuaries at the global scale. With twenty two of the thirty two largest cities in the world are located on estuaries (NOAA, 2020), anthropogenically impacted estuaries may be hidden sources of GHG globally. The conceptual model could be applied to other estuaries globally, by considering both natural processes and anthropogenic perturbations. Furthermore with relatively little extra data, for example nutrients and oxygen (parameters that are often routinely measured) and an understanding of estuary dynamics (tide and river flow), this conceptual model could underpin both effective modelling of estuary GHG production and also provide a route for simpler monitoring of future improvements.

11. Considerations for policy makers

Estuaries are highly valuable as they are critical natural habitats and provide a wide range of ecosystem services. However they experience a wide range of anthropogenic stressors (Kennish, 2005). Estuaries have long been considered an effective location for the disposal of urban and industrial waste, because of their proximity to that waste generation and their perceived ability to flush this waste to the sea with its high dilution capability. However evidence shows that estuaries (both inner and outer) by their very nature: brackish water, low oxygen, stratification and high sediments loads, can become significant GHG sources, particularly when high levels of urban waste enter the estuary. Additionally seasonal changes in river flow, tide and temperature can further exacerbate this GHG generation.

As such criteria linked to GHG generation (not just eutrophication risk) should be included in legislation to further constrain waste water disposal. The mechanistic understanding of GHG generation in the estuarine environment and the associated conceptual model presented in this paper can be applied to help in the identification of estuaries which may act as significant GHG sources and also estuaries where interventions and reduction of anthropogenic influence could significantly reduce these emissions. Further research globally into estuary environments as a GHG source, together with research into mechanisms and the effectiveness of mitigations is still required.

Declaration of competing interest

The authors declare that they have no known competing financial interests or personal relationships that could have appeared to influence the work reported in this paper.

Acknowledgments

The authors would like to thank the authors of the papers and data sets used in this review and the two anonymous reviewers whose comments have helped improve the quality of this paper.

This work was funded by a Natural Environment Research Council (NERC) studentship through the IAPETUS Doctoral Training Partnership Grant No.: NE/S007431/1. AP's input was funded by the Natural Environment Research Council as part of the LOCATE project. CEH Grant No.: NEC05686, NOC Grant No.: NE/N019037/1.

Appendix A. Supplementary data

Supplementary data to this article can be found online at <https://doi.org/10.1016/j.marpolbul.2021.113240>.

References

- de Angelis, M.A., Gordon, L.L., 1985. Upwelling and river runoff as sources of dissolved nitrous oxide to the Alsea estuary, Oregon. *Estuar. Coast. Shelf Sci.* 20 (4), 375–386. [https://doi.org/10.1016/0272-7714\(85\)90682-4](https://doi.org/10.1016/0272-7714(85)90682-4).
- Balla, P.W., Hall, S., Miller, B.S., Flirie, J.M., Proctor, W., 1997. Trace metal in Scottish estuarine and coastal sediments. *Mar. Pollut. Bull.* 34 (1), 43–50. [https://doi.org/10.1016/S0025-326X\(96\)00056-2](https://doi.org/10.1016/S0025-326X(96)00056-2).
- Bange, H.W., 2006. Nitrous oxide and methane in European coastal waters. *Estuar. Coast. Shelf Sci.* 70, 361–374.
- Bange, H.W., Bartell, U.H., Rapsomanikis, S., Andreae, M.O., 1994. Computed with two different exchange models lie in the range of 11–18 Tg CH₄ TM (phosphorus). *North 8* (4), 465–480.
- Bange, H.W., Dahlke, S., Ramesh, R., Meyer-Reil, L.A., Rapsomanikis, S., Andreae, M.O., 1998. Seasonal study of methane and nitrous oxide in the coastal waters of the southern Baltic Sea. *Estuar. Coast. Shelf Sci.* 47 (6), 807–817. <https://doi.org/10.1006/ecsaa.1998.0397>.
- Barnes, J., Upstill-Goddard, R.C., 2011. N₂O seasonal distributions and air-sea exchange in UK estuaries: implications for the tropospheric N₂O source from European coastal waters. *J. Geophys. Res. Biogeosciences* 116 (1). <https://doi.org/10.1029/2009JG001156>.
- Beaulieu, J.J., Tank, J.L., Hamilton, S.K., Wollheim, W.M., Hall, R.O., Mulholland, P.J., Peterson, B.J., Ashkenas, L.R., Cooper, L.W., Dahm, C.N., Dodds, W.K., Grimm, N.B., Johnson, S.L., McDowell, W.H., Poole, G.C., Maurice Valett, H., Arango, C.P., Bernot, M.J., Burgin, A.J., Crenshaw, C.L., Helton, A.M., Johnson, L.T., O'Brien, J.M., Potter, J.D., Shibles, R.W., Sobota, D.J., Thomas, S.M., 2011. Nitrous oxide emission from denitrification in stream and river networks. *Proc. Natl. Acad. Sci. U. S. A.* 108 (1), 214–219. <https://doi.org/10.1073/pnas.1011464108>.
- Bernard, B.E., 1978. Methane in marine sediments. *Deep Sea Res.* 26A (1966), 429–443. [doi:0011-7471\(78\)90401-0](https://doi.org/10.1016/0011-7471(78)90401-0).
- Birch, G.F., Gunna, T.J., Olmos, M., 2015. Sediment-bound metals as indicators of anthropogenic change in estuarine environments. *Mar. Pollut. Bull.* 101 (1), 243–257. <https://doi.org/10.1016/j.marpolbul.2015.09.056>.
- Black Cairn Ltd, 2018. VisitMyHarbour.com, [online]. <https://www.visitmyharbour.com/harbours/east-and-north-scotland/port-edgar/chart/9115A8E6D3D61/chart-of-port-edgar-and-approaches>, (Accessed 28 April 2021).
- BODC, 2020. National Oceanography Centre: British Oceanographic Data Centre, [online]. Available from: <https://www.bodc.ac.uk/>, (Accessed 23 December 2020).
- Borges, A.V., Champenois, W., Gypens, N., Deille, B., Harlay, J., 2016. Massive marine methane emissions from near-shore shallow coastal areas. *Sci. Rep.* 6 (June), 2–9. <https://doi.org/10.1038/srep27908>.
- Bose, U., Frenzel, P., Conrad, R., 1993. Inhibition of methane oxidation by ammonium in the surface layer of a littoral sediment. *FEMS Microbiol. Ecol.* 13 (2), 123–134. [https://doi.org/10.1016/0168-6496\(93\)9020-B](https://doi.org/10.1016/0168-6496(93)9020-B).
- Burgos, M., Sierra, A., Ortega, T., Forja, J.M., 2015. Anthropogenic effects on greenhouse gas (CH₄ and N₂O) emissions in the Guadalete River Estuary (SW Spain). *Sci. Total Environ.* 503–504, 179–189. <https://doi.org/10.1016/j.scitotenv.2014.06.038>.
- Clark, J.F., Schlosser, P., Simpson, H.J., Stute, M., Wanninkhof, R., Ho, D.T., 1995. Relationship between gas transfer velocities and wind speeds in the tidal Hudson River determined by dual tracer technique. *Air-water gas Transf.* 785–800 [online]. Available from: <http://hel.iwr.uni-heidelberg.de/publications/dtp/1995/AWG1995/CHAPTERS/6.31.PDF>.
- <collab>IPCC, Netherlandscollab, M. R. J. D., Thailand, S. T., Brazil, S. M. M. V., U.S.A., W. I., Canada, C. P., Finland, R. P. and (China), C.W., 2006. Volume 5: Waste - Chapter 6 Wastewater Treatment and. [online]. Available from: www.ipcc-nggip.iges.or.
- Dolfig, J., Nedwell, D.B., Dong, L.F., 2002. Nitrous oxide formation in the Colne estuary in England: the central role of nitrite [1] (multiple letters). *Appl. Environ. Microbiol.* 68 (10), 5202–5204. <https://doi.org/10.1128/AEM.68.10.5202-5204.2002>.
- Dong, L.F., Thornton, D.C.O., Nedwell, D.B., Underwood, G.J.C., 2000. Denitrification in sediments of the River Colne estuary, England. *Mar. Ecol. Prog. Ser.* 203, 109–122. <https://doi.org/10.3354/meps203109>.
- Dong, L.F., Nedwell, D.B., Colbeck, I., Finch, J., 2005. Nitrous oxide emission from some English and Welsh rivers and estuaries. *Water Air Soil Pollut. Focus* 4 (6), 127–134. <https://doi.org/10.1007/s11367-005-3022-z>.
- Dunfield, P., Knowles, R., 1995. Kinetics of inhibition of methane oxidation by nitrate, nitrite, and ammonium in a humicol. *Appl. Environ. Microbiol.* 61 (8), 3129–3135. <https://doi.org/10.1128/aem.61.8.3129-3135.1995>.
- EEC, 1991b. Council Directive 91/271/EEC concerning urban waste water treatment, L 135 [online]. Available from: Official Journal of the European Community, Brussels

- 34 (May 1991), 1–16, 1991. <https://eur-lex.europa.eu/LexUriServ/LexUriServ.do?uri=CONSLEG:1991L0271:20081211:EN:PDF>.
- Environment Agency, 2020. Water quality data archive, [online]. <https://environment.data.gov.uk/water-quality/view/landing>. (Accessed 23 December 2020).
- Environmental Agency, 1999. State of the Tees Estuary Environment, and Strategy into the Millennium.
- European Commission (Directorate General Environment), 2016. European Commission Urban Waste Water Website: United Kingdom, [online]. Available from: <http://www.wtd.eu/United-Kingdom/>. (Accessed 23 December 2020).
- Franklin, M.J., Wiebe, W.J., Whitman, W.B., 1988. Populations of methanogenic bacteria in a Georgia salt marsh. *Appl. Environ. Microbiol.* 54 (5), 1151–1157. <https://doi.org/10.1128/aem.54.5.1151-1157.1988>.
- García-muñoz, E.E., Sanders, R., Evans, C.D., Kitidis, V., 2018. Contrasting estuarine processing of dissolved organic matter derived from natural and human-impacted landscapes. *Global Biogeochemical Cycles* (C), 1–17. <https://doi.org/10.1029/2021GB007023>.
- Gelesh, L., Marshall, K., Boicourt, W., Lapham, L., 2016. Methane concentrations increase in bottom waters during summertime anoxia in the highly eutrophic estuary, Chesapeake Bay, U.S.A. *Limnol. Oceanogr.* 61, S253–S266. <https://doi.org/10.1002/lno.10272>.
- Gerling, A.B., Browne, R.G., Gantzer, P.A., Mobley, M.H., Little, J.C., Carey, C.C., 2014. First report of the successful operation of a side stream supersaturation hypolimnetic oxygenation system in a eutrophic, shallow reservoir. *Water Res.* 67, 129–143. <https://doi.org/10.1016/j.watres.2014.09.002>.
- Hall, J.A., Frid, C.L.J., Proudfoot, R.K., 1996. Effects of metal contamination on macrobenthos of two North Sea estuaries. *ICES J. Mar. Sci.* 53 (6), 1014–1023. <https://doi.org/10.1006/jmasc.1996.0127>.
- Hamilton, D.J., Bulmer, R.H., Schwendenmann, L., Lundquist, C.J., 2020. Nitrogen enrichment increases greenhouse gas emissions from emergent intertidal sandflats. *Sci. Rep.* 10 (1), 1–14. <https://doi.org/10.1038/s41598-020-62215-4>.
- Hao, X., Ruihong, Y., Zhuangzhuang, Z., Zhen, Q., Xidi, L., Tingxi, L., Ruihong, G., 2021. Greenhouse gas emissions from the water-air interface of a grassland river: a case study of the Xilin River. *Sci. Rep.* 11 (1), 1–14. <https://doi.org/10.1038/s41598-021-81658-z>.
- Harley, J.F., Carvalho, L., Dudley, S., Heal, K.V., Rees, R.M., Skiba, U., 2015. Spatial and seasonal fluxes of the greenhouse gases N₂O, CO₂ and CH₄ in a UK macrotidal estuary. *Estuar. Coast. Shelf Sci.* 153, 62–73. <https://doi.org/10.1016/j.ecs.2014.12.004>.
- Harris, P.T., Macmillan-Lawler, M., Rupp, J., Baker, E.K., 2014. Geomorphology of the ocean. *Mar. Geol.* 352, 4–24. <https://doi.org/10.1016/j.margeo.2014.01.011>.
- Institute for Government, 2020. UK net zero target, [online]. Available from: <https://www.instituteforgovernment.org.uk/explainers/net-zero-target>.
- IPCC, 2013. Summary for policymakers. In: Stocker, T.F., Qin, D., Plattner, G.-K., Tignor, M., Allen, S.K., Boschung, J., Nauels, A., Xia, Y., Midgley, V., Wehner, M. (Eds.), *Climate Change 2013: The Physical Science Basis. Contribution of Working Group I to the Fifth Assessment Report of the Intergovernmental Panel on Climate Change*. Cambridge Univ. Press, Cambridge, United Kingdom New York, NY, USA.
- Imanuyeto, A., Getso, S., Segeguchi, M., Koriyama, M., 2014. Independent effects of temperature, salinity, ammonium concentration and pH on nitrification rate of the Ariake seawater above mud sediment. *HAYATI J. Biosci.* 21 (1), 21–30. <https://doi.org/10.4308/hjb.21.1.21>.
- Kemish, M.J., 2005. Estuaries, anthropogenic impacts. *Encycl. Earth Sci. Ser.* 14, 434–436. <https://doi.org/10.1007/s1-4020-3880-1-140>.
- Kiwa, T., Kanda, J., Kubo, A., Nakajima, F., Ogawa, H., Sohma, A., Sumimura, M., 2016. Blue carbon in human-dominated estuarine and shallow coastal systems. *Ambio* 45 (3), 290–301. <https://doi.org/10.1007/s13280-015-0725-z>.
- Larsen, S.J., Kilmister, K.L., Mantovani, A., Goss, Z.J., Evans, G.C., Bryant, L.D., McGinnis, D.F., 2019. Artificially oxygenating the Swan River estuary increases dissolved oxygen concentrations in the water and at the sediment interface. *Ecol. Eng.* 128 (December 2018), 112–121. <https://doi.org/10.1016/j.ecoleng.2018.12.032>.
- Law, C.S., Rees, A.P., Owens, N.J.P., 1992. Nitrous oxide: estuarine sources and atmospheric flux. *Estuar. Coast. Shelf Sci.* 35 (3), 301–314. [https://doi.org/10.1016/0272-7714\(05\)80050-2](https://doi.org/10.1016/0272-7714(05)80050-2).
- Lewis, R.E., 1990. The nature of outflows from the north-east estuaries. *Hydrobiologia* 195 (1), 1–11. <https://doi.org/10.1007/BF00026809>.
- Lindsay, P., Balls, P.W., West, J.R., 1996. Influence of tidal range and river discharge on suspended particulate matter fluxes in the Forth estuary (Scotland). *Estuar. Coast. Shelf Sci.* 42 (1), 63–82. <https://doi.org/10.1006/ecs.1996.0006>.
- Lindsay, P., Bell, F.G., Hytiris, N., 1998. Contamination of sediments in the Forth Estuary, Scotland. *Geol. Soc. Eng. Geol. Spec. Publ.* 14, 179–187. <https://doi.org/10.1144/GSL.SP.1998.014.01.21>.
- Lyu, Z., Shao, N., Akiyoshi, T., Whitman, W.B., 2018. Methanogenesis. *Curr. Biol.* 28 (13), R727–R732. <https://doi.org/10.1016/j.cub.2018.05.021>.
- Marchant, H.K., Ahmerkamp, S., Lavis, G., Tegetmeyer, H.E., Graf, J., Klatt, J.M., Holtappels, M., Walpersdorf, E., Kuyper, M.M.M., 2017. Denitrifying community in coastal sediments performs aerobic and anaerobic respiration simultaneously. *ISME J.* 11 (8), 1799–1812. <https://doi.org/10.1038/ismej.2017.51>.
- Marine Scotland, 2021. Marine Scotland Information - Dredging [online]. Available from: <https://marine.gov.scot/application-type/dredging>.
- McElroy, M.B., Elkins, J.W., Wofsy, S.C., Kolb, C.E., Durán, A.F., Kaplan, W.A., 1978. Production and release of N₂O from the Potomac Estuary. *Limnol. Oceanogr.* 23 (6), 1168–1182. <https://doi.org/10.4319/lno.1978.23.6.1168>.
- McManus, J., 2005. Salinity and suspended matter variations in the Tay estuary. *Cont. Shelf Res.* 25, 729–747.
- Middelburg, J.J., Niemeijer, J., Iversen, N., Høj, N., De Wilde, H., Heider, W., Seifert, R., Christof, O., 2002. Methane distribution in European tidal estuaries. *Biogeochemistry* 59 (1–2), 95–119. <https://doi.org/10.1023/A:1015515130419>.
- Mitchell, S.B., West, J.R., Arundale, A.M.W., Guymer, I., Coupethwaite, J.S., 1998. Dynamics of the turbidity maxima in the Upper Humber Estuary System, UK. *Mar. Pollut. Bull.* 37 (3–7), 190–205. <https://www.sciencedirect.com/science/article/pii/S0025326X98001787>.
- Mitchell, S.B., West, J.R., Guymer, I., 1999. Dissolved - oxygen/suspended-solids concentration relationships in the Upper Humber Estuary. *J. CWEM* 13 (11), 327–337.
- Morton, R.D., Marston, C.G., O’Neil, A.W., Rowland, C.S., 2020. Land Cover Map 2019 (Land Parcels, GB) [Dataset]. NERC Environ. Inf. Data Centre. <https://doi.org/10.5285/44C23778-4A73-4A8F-875F-80823B91E9F3> [online]. Available from.
- Munson, M.A., Nedwell, D.B., Ensbly, T.M., 1997. Phylogenetic diversity of Archaea in sediment samples from a coastal salt marsh. *Appl. Environ. Microbiol.* 63 (12), 4729–4733. <https://doi.org/10.1128/aem.63.12.4729-4733.1997>.
- Nedwell, D.B., Dong, L.F., Sage, A., Underwood, G.J.C., 2002. Variations of the nutrients loads to the mainland U.K. estuaries: Correlation with catchment areas, urbanization and coastal eutrophication. *Estuar. Coast. Shelf Sci.* 54 (6), 951–970. <https://doi.org/10.1006/ecs.2001.0867>.
- NOAA, 2020. Estuary Habitat, Habitata Conserv. [online]. Available from: <https://www.fisheries.noaa.gov/national/habitat-conservation/estuary-habitat>. (Accessed 3 September 2021).
- NRFA, 2010. National River Flow Archive, Cent. Ecol. Hydrol., <http://www.ceh.ac.uk/data/nrfa/> [online]. <http://nrfa.ceh.ac.uk/>. (Accessed 9 May 2020).
- Ogilvie, S., Nedwell, D.B., Harrison, R.M., Robinson, A., Sage, A., 1997. High nitrate, muddy estuaries as nitrogen sinks: the nitrogen budget of the River Colne estuary (United Kingdom). *Mar. Ecol. Prog. Ser.* 150, 217–228.
- Oremland, R.S., Polcin, S., Survey, U.S.G., Park, M., 1983. Methanogenesis and sulfate reduction: competitive and noncompetitive substrates in estuarine sediments. *Deep Sea Res Part B. Oceanogr. Lit. Rev.* 30 (6), 470. [https://doi.org/10.1016/0198-0254\(83\)90262-5](https://doi.org/10.1016/0198-0254(83)90262-5).
- Pattinson, S.N., García-Ruiz, R., Whitton, B.A., 1998. Spatial and seasonal variation in denitrification in the Swale-Ouse system, a river continuum. *Sci. Total Environ.* 210–211, 289–305. [https://doi.org/10.1016/S0048-9697\(98\)00191-9](https://doi.org/10.1016/S0048-9697(98)00191-9).
- Pennings, K.S., P. B. M., 1996. Effect of nitrate, organic carbon, and temperature on potential denitrification rates in nitrate-rich riverbed sediments. *J. Hydrol.* 187, 283–295.
- Pickard, A.E., Skiba, U.M., Carvalho, L., Brown, A.M., Heal, K.V., Rees, R.M., Harley, J.F., 2021. Greenhouse Gas and Water Chemistry Data Measured Across the Tay Estuary, Scotland, From 2009–2011. NERC Environ. Inf. Data Cent. <https://doi.org/10.5285/ec78b74e-631d-4bef-8c28-618b4dc0ff0>.
- Pickard, A.E., Brown, L., Burden, A., Callaghan, N., Evans, C.D., Kitidis, V., Mayor, D., Olanrewaju, J., Pereira, G., Spears, R.M., Williamson, J., Woodward, M., Rees, A.P., 2022. Greenhouse Gas and Nutrient Data Measured Across Estuaries in the UK, 2017–2018. NERC Environ. Inf. Data Cent.
- Reay, D.S., Smith, K.A., Edwards, A.C., 2003. Nitrous oxide emission from agricultural drainage waters. *Glob. Chang. Biol.* 9 (2), 195–203. <https://doi.org/10.1046/j.1365-2486.2003.00584.x>.
- Revsbech, N.P., Jacobsen, J.P., Nielsen, L.P., 2005. Nitrogen transformations in microenvironments of river beds and riparian zones. *Ecol. Eng.* 24 (5 SPEC. ISS.), 447–455. <https://doi.org/10.1016/j.ecoleng.2005.02.002>.
- Robins, P.E., Lewis, M.J., Simpson, J.H., Malham, S.K., 2014. Future variability of solute transport in a macrotidal estuary. *Estuar. Coast. Shelf Sci.* 151 (November), 88–99. <https://doi.org/10.1016/j.ecs.2014.09.019>.
- Robins, P.E., Davies, A.G., Skov, M.W., Lewis, M.J., Gim, L., Malham, S.K., Neill, S.P., McDonald, J.E., Whitton, T.A., Jackson, S.E., Jago, C.F., 2016. Impact of climate change on UK estuaries: a review of past trends and potential projections. *Estuarine, Coastal and Shelf Science* 169. <https://doi.org/10.1016/j.ecs.2015.12.016>.
- Robinson, A.D., Nedwell, D.B., Harrison, R.M., Ogilvie, B.G., 1998. Hypenitrified estuaries as sources of N₂O emission to the atmosphere: the estuary of the River Colne, Essex, UK. *Mar. Ecol. Prog. Ser.* 164 (1994), 59–71. <https://doi.org/10.3354/meps164059>.
- Rodgers, K., McLellan, I., Peshkar, T., Williams, R., Tonner, R., Knapp, C.W., Henriquez, F.L., Hursthouse, A.S., 2020. The legacy of industrial pollution in estuarine sediments: spatial and temporal variability implications for ecosystem stress. *Environ. Geochem. Health* 42 (4), 1057–1068. <https://doi.org/10.1007/s10653-019-00316-4>.
- Rosamond, M.S., Thuss, S.J., Schiff, S.L., 2012. Dependence of riverine nitrous oxide emissions on dissolved oxygen levels. *Nat. Geosci.* 5 (10), 715–718. <https://doi.org/10.1038/ngeo1556>.
- Santos, I.R., Burdige, D.J., Jennerjahn, T.C., Bouillon, S., Cabral, A., Serrano, O., Wernberg, T., Filbee-Dexter, K., Gulmord, J.A., Tamborski, J.J., 2021. The renaissance of Odum’s outwelling hypothesis in “Blue Carbon” science. *Estuar. Coast. Shelf Sci.* 255 (April), 107361. <https://doi.org/10.1016/j.ecs.2021.107361>.
- Scottish Environment Protection Agency, 2020. Inner Clyde Estuary monitoring buoy, Firth of Clyde, [online]. <https://www.sepa.gov.uk/environment/environmental-data/monitoring-buoys-network/inner-clyde-estuary/>. (Accessed 23 April 2020).
- Seitzinger, S.P., 1988. Denitrification in freshwater and coastal marine ecosystems: ecological and geochemical significance. *Limnol. Oceanogr.* 33 (4part2), 702–724. <https://doi.org/10.4319/lno.1988.33.4part2.0702>.
- Sharples, J., Mayor, D.J., Foulton, A.J., Rees, A.P., Robinson, C., 2019. Shelf Sea biogeochemistry: nutrient and carbon cycling in a temperate shelf sea water column. *Prog. Oceanogr.* 177. <https://doi.org/10.1016/j.poc.2019.102182>.

- Thain, R.H., Priestley, A.D., Davidson, M.A., 2004. The formation of a tidal intrusion front at the mouth of a macrotidal, partially mixed estuary: a field study of the Dart estuary, UK. *Estuar. Coast. Shelf Sci.* 61, 161–172.
- The Crown Estate, 2021. Minerals and Dredging [online]. Available from: <https://www.thecrownestate.co.uk/en-gh/what-we-do/on-the-seabed/minerals-dredging/>.
- Torres-Alvarado, M.D.R., Fernández, F.J., Ramírez Vives, F., Varona-Cordero, F., 2013. Dynamics of the methanogenic archaea in tropical estuarine sediments. *Archaea* 2013. <https://doi.org/10.1155/2013/582646>.
- UK Centre for Ecology & Hydrology (UKCEH), 2020. National River Flow Archive, [online]. Available from: <https://nra.ceh.ac.uk/>. (Accessed 9 May 2020).
- Uncles, R.J., Stephens, J.A., 1993. The freshwater-saltwater interface and its relationship to the turbidity maximum in the Tamar Estuary, United Kingdom. *Estuaries* 16 (1), 126–141. <https://doi.org/10.2307/1352770>.
- Upstill-Goddard, R.C., Barnes, J., 2016. Methane emissions from UK estuaries: re-evaluating the estuarine source of tropospheric methane from Europe. *Mar. Chem.* 180, 14–23. <https://doi.org/10.1016/j.marchem.2016.01.010>.
- Upstill-Goddard, R.C., Barnes, J., Frost, T., Punshon, S., 2000. Methane in the southern North Sea: low-salinity inputs, estuarine removal, and atmospheric flux. *Glob. Biogeochem. Cycles* 14 (4), 1205–1217. <https://doi.org/10.1029/1999GB001286>.
- Wang, G., Xia, X., Liu, S., Zhang, L., Zhang, S., Wang, J., Xi, N., Zhang, Q., 2021. Intense methane ebullition from urban inland waters and its significant contribution to greenhouse gas emissions. *Water Res.* 189, 116654. <https://doi.org/10.1016/j.watres.2020.116654>.
- Wanninkhof, R., 1992. Relationship between wind speed and gas exchange over the ocean. *J. Geophys. Res.* 97 (C5), 7373–7382.
- Wewetzera, Silke F.K., Ducka, Robert W., Anderson, J.M., 1999. Acoustic Doppler current profiler measurements in coastal and estuarine environments: examples from the Tay Estuary, Scotland. *Geomorphology* 29, 21–30.
- Wrage, N., Velthof, G.L., Van Beusichem, M.L., Oenema, O., 2001. Role of nitrifier denitrification in the production of nitrous oxide. *Soil Biol. Biochem.* 33 (12–13), 1723–1732. [https://doi.org/10.1016/S0038-0717\(01\)00096-7](https://doi.org/10.1016/S0038-0717(01)00096-7).
- Yu, Z., Deng, H., Wang, D., Ye, M., Tan, Y., Li, Y., Chen, Z., Xu, S., 2013. Nitrous oxide emissions in the Shanghai river network: implications for the effects of urban sewage and IPCC methodology. *Glob. Chang. Biol.* 19 (10), 2999–3010. <https://doi.org/10.1111/gcb.12290>.